

---

# ANALYTICA CHIMICA ACTA

---

An international journal devoted to all branches of analytical chemistry

**Editors:** Harry L. Pardue (West Lafayette, IN, USA)  
Alan Townshend (Hull, Great Britain)  
J.T. Clerc (Berne, Switzerland)  
Willem E. van der Linden (Enschede, Netherlands)  
Paul J. Worsfold (Plymouth, Great Britain)

**Associate Editor:** Sarah C. Rutan (Richmond, VA, USA)

# 300

# ANALYTICA CHIMICA ACTA

**Scope.** *Analytica Chimica Acta* publishes original papers, rapid publication letters and reviews dealing with every aspect of modern analytical chemistry. Reviews are normally written by invitation of the editors, who welcome suggestions for subjects. Letters can be published within **four months** of submission. For information on the Letters section, see inside back cover.

## Submission of Papers

### Americas

Prof. Harry L. Pardue  
Department of Chemistry  
1393 BRWN Bldg, Purdue University  
West Lafayette, IN 47907-1393  
USA  
  
Tel: (+1-317) 494 5320  
Fax: (+1-317) 496 1200

Prof. J.T. Clerc  
Universität Bern  
Pharmazeutisches Institut  
Baltzerstrasse 5, CH-3012 Bern  
Switzerland  
  
Tel: (+41-31) 6314191  
Fax: (+41-31) 6314198

Prof. Sarah C. Rutan  
Department of Chemistry  
Virginia Commonwealth University  
P.O. Box 2006  
Richmond, VA 23284-2006  
USA  
  
Tel: (+1-804) 367 7517  
Fax: (+1-804) 367 8599

### Computer Techniques

### Other Papers

Prof. Alan Townshend  
Department of Chemistry  
The University  
Hull HU6 7RX  
Great Britain  
  
Tel: (+44-482) 465027  
Fax: (+44-482) 466410

Prof. Willem E. van der Linden  
Laboratory for Chemical Analysis  
Department of Chemical Technology  
Twente University of Technology  
P.O. Box 217, 7500 AE Enschede  
The Netherlands  
  
Tel: (+31-53) 892629  
Fax: (+31-53) 356024

Prof. Paul Worsfold  
Dept. of Environmental Sciences  
University of Plymouth  
Plymouth PL4 8AA  
Great Britain  
  
Tel: (+44-752) 233006  
Fax: (+44-752) 233009

Submission of an article is understood to imply that the article is original and unpublished and is not being considered for publication elsewhere. *Anal. Chim. Acta* accepts papers in English only. There are no page charges. Manuscripts should conform in layout and style to the papers published in this issue. See inside back cover for "Information for Authors".

**Publication.** *Analytica Chimica Acta* appears in 18 volumes in 1995 (Vols. 297-314). *Vibrational Spectroscopy* appears in 2 volumes in 1995 (Vols. 8 and 9). Subscriptions are accepted on a prepaid basis only, unless different terms have been previously agreed upon. It is possible to order a combined subscription (*Anal. Chim. Acta* and *Vib. Spectrosc.*).

Our p.p.h. (postage, packing and handling) charge includes surface delivery of all issues, except to subscribers in the U.S.A., Canada, Australia, New Zealand, China, India, Israel, South Africa, Malaysia, Thailand, Singapore, South Korea, Taiwan, Pakistan, Hong Kong, Brazil, Argentina and Mexico, who receive all issues by air delivery (S.A.L.—Surface Air Lifted) at no extra cost. For Japan, air delivery requires 25% additional charge of the normal postage and handling charge; for all other countries airmail and S.A.L. charges are available upon request.

**Subscription orders.** Subscription prices are available upon request from the publisher. Subscription orders can be entered only by calendar year and should be sent to: Elsevier Science B.V., Journals Department, P.O. Box 211, 1000 AE Amsterdam, The Netherlands. Tel: (+31-20) 4853 642, Telex: 18582, Telefax: (+31-20) 4853 598, to which requests for sample copies can also be sent. Claims for issues not received should be made within six months of publication of the issues. If not they cannot be honoured free of charge. Readers in the U.S.A. and Canada can contact the following address: Elsevier Science Inc., Journal Information Center, 655 Avenue of the Americas, New York, NY 10010, U.S.A. Tel: (+1-212) 633 3750, Telefax: (+1-212) 633 3990, for further information, or a free sample copy of this or any other Elsevier Science journal.

**Advertisements.** Advertisement rates are available from the publisher on request.

**US mailing notice – *Analytica Chimica Acta*** (ISSN 0003-2670) is published 3 times a month (total 54 issues) by Elsevier Science B.V. (Molenwerf 1, Postbus 211, 1000 AE Amsterdam). Annual subscription price in the USA US\$ 3677.75 (valid in North, Central and South America), including air speed delivery. Second class postage paid at Jamaica, NY 11431. *USA Postmasters:* Send address changes to *Anal. Chim. Acta*, Publications Expediting, Inc., 200 Meacham Av., Elmont, NY 11003. Airfreight and mailing in the USA by Publication Expediting.

# ANALYTICA CHIMICA ACTA

An international journal devoted to all branches of analytical chemistry

(Full texts are incorporated in *CJELSEVIER*, a file in the *Chemical Journals Online* database available on *STN International*; Abstracted, indexed in: *Aluminum Abstracts*; *Anal. Abstr.*; *Biol. Abstr.*; *BIOSIS*; *Chem. Abstr.*; *Curr. Contents Phys. Chem. Earth Sci.*; *Engineered Materials Abstracts*; *Excerpta Medica*; *Index Med.*; *Life Sci.*; *Mass Spectrom. Bull.*; *Material Business Alerts*; *Metals Abstracts*; *Sci. Citation Index*)

VOL. 300 NO. 1-3

CONTENTS

JANUARY 20, 1995

## Letter

- Simple reversible staining of proteins transferred from polyacrylamide gels onto nitrocellulose membranes  
H. Bloemendal and M. Satijn (Nijmegen, Netherlands) . . . . . 1

## Electroanalytical Chemistry and Sensors

- Electrochemical characteristics of conductive carbon cement as matrix for chemically modified electrodes  
X. Huang, J.J. Pot and W.Th. Kok (Amsterdam, Netherlands) . . . . . 5
- Impedance analysis of the transport of counter ions at polypyrrole-Nafion composite electrodes  
C.-M. Chang and H.-J. Huang (Kaohsiung, Taiwan) . . . . . 15
- Application of enzyme-field effect transistor sensor arrays as detectors in a flow-injection analysis system for simultaneous monitoring of medium components. Part II. Monitoring of cultivation processes  
T. Kullick, U. Bock, J. Schubert (Hannover, Germany), T. Scheper (Münster, Germany) and K. Schügerl (Hannover, Germany) . . . . . 25
- Role of axial ligation on potentiometric response of Co(III) tetraphenylporphyrin-doped polymeric membranes to nitrite ions  
E. Malinowska and M.E. Meyerhoff (Ann Arbor, MI, USA) . . . . . 33
- Ion-selective electrode measurements for the determination of formation constants of alkali and alkaline earth metals with low-molecular-weight ligands  
A. De Robertis, P. Di Giacomo and C. Foti (S. Agata di Messina, Italy) . . . . . 45
- Amperometric determination of oxidizable solutes in water with a solution exchange technique  
C. Gartske and C.O. Huber (Milwaukee, WI, USA) . . . . . 53
- Amperometric glucose-sensing electrode based on carbon paste containing poly(ethylene glycol)-modified glucose oxidase and cobalt octaethoxyphthalocyanine  
F. Mizutani, S. Yabuki and S. Iijima (Ibaraki, Japan) . . . . . 59
- Amperometric glucose sensor using tetrathiafulvalene in Nafion gel as electron shuttle  
H. Liu and J. Deng (Shanghai, China) . . . . . 65
- Competitive amperometric morphine sensor based on an agarose immobilised molecularly imprinted polymer  
D. Kriz and K. Mosbach (Lund, Sweden) . . . . . 71
- Diamond like carbon coated films for enzyme electrodes; characterization of biocompatibility and substrate diffusion limiting properties  
S.P.J. Higson and P.M. Vadgama (Salford, UK) . . . . . 77
- Diamond like carbon films for enzyme electrodes: characterisation of novel overlying permselective barriers  
S.P.J. Higson and P.M. Vadgama (Salford, UK) . . . . . 85
- Thin-film biosensor for the measurement of glucose concentration in human serum and urine  
P. Yu and D. Zhou (Harbin, China) . . . . . 91
- Latex piezoelectric immunoassay: effect of interfacial properties  
H.O. Ghourchian and N. Kamo (Sapporo, Japan) . . . . . 99
- Catalytic method for the determination of traces of tungsten by linear scan voltammetry  
Z.-L. Jiang, L.-X. Liao and M.-D. Liu (Guilin, China) . . . . . 107

(Continued overleaf)

Screen-printed amperometric biosensors for glucose and alcohols based on ruthenium-dispersed carbon inks J. Wang, Q. Chen, M. Pedrero (Las Cruces, NM, USA) and J.M. Pingarrón (Madrid, Spain) . . . . .	111
<i>Flow Injection</i>	
Characterisation of inhibitors of acetylcholinesterase by an automated amperometric flow-injection system A. Günther and U. Bilitewski (Braunschweig, FRG) . . . . .	117
Gradient flow-injection amperometry based on induced retention by the detector coating J. Wang, L. Chen and H. Wu (Las Cruces, NM, USA) . . . . .	127
Chalcogenide based all-solid-state thin electroplated ion-selective membrane for Hg(II) flow-injection determinations M. Neshkova and E. Pancheva (Sofia, Bulgaria) . . . . .	133
Continuous flow-injection–atomic absorption spectrometric method for the determination of Ondansetron L. Lahuerta Zamora (Moncada, Spain) and J. Martínez Calatayud (València, Spain) . . . . .	143
✓ Turbidimetric determination of sulphate in waters employing flow injection and lead sulphate formation R. Erthal Santelli, P.R. Salgado Lopes, R.C. Leme Santelli (Niterói, Brazil) and A. De Luca Rebello Wagener (Rio de Janeiro, Brazil) . . . . .	149
<i>Chromatography</i>	
Determination of mono- <i>ortho</i> substituted chlorobiphenyls by multidimensional gas chromatography and their contribution to TCDD equivalents J. De Boer, Q.T. Dao, P.G. Wester (Ijmuiden, Netherlands), S. Bøwadt (Ispra, Italy) and U.A.Th. Brinkman (Amsterdam, Netherlands) . . . . .	155
✗ Size exclusion chromatography of aluminium species in natural waters L. Zernichow and W. Lund (Oslo, Norway) . . . . .	167
Assessing chromatographic peak purity using condition index and singular value evolving profiles G.A. Bakken and J.H. Kalivas (Pocatello, ID, USA) . . . . .	173
Indirect conductimetric detection of amino acids after liquid chromatographic separation O.-W. Lau and C.-S. Mok (Shatin, Hong Kong) . . . . .	183
Study of the responses of a gas chromatography–reduction gas detector system to gaseous hydrocarbons under different conditions X.-L. Cao, C.N. Hewitt and K.S. Waterhouse (Lancaster, UK) . . . . .	193
Studies on the behaviour of $\alpha$ -, $\beta$ - and $\gamma$ -cyclodextrins and some derivatives under reversed-phase liquid chromatographic conditions A. Bielejewska, M. Koźbiał, R. Nowakowski, K. Duszczyk and D. Sybilska (Warsaw, Poland) . . . . .	201
Ion chromatographic determination of traces of some oxoanions with direct spectrophotometric detection Y.S. Fung and K.L. Dao (Hong Kong) . . . . .	207
<i>Chemiluminescence</i>	
Peroxidatic activity of metalloporphyrin binding to serum albumin: enhancement effect of serum albumin on metalloporphyrin catalyzed luminol chemiluminescence reaction J.-K. Tie, W.-B. Chang and Y.-X. Ci (Beijing, China) . . . . .	215
<i>NMR</i>	
Analysis and characterisation of nitroglycerine based explosives by proton magnetic resonance spectrometry D.T. Burns (Belfast, UK) and R.J. Lewis (Carrickfergus, UK) . . . . .	221
<i>Fluorimetry</i>	
Kinetic analysis of aluminum complex formation with different soil fulvic acids B.J. Plankey (Quincy, CA, USA), H.H. Patterson and C.S. Cronan (Orono, ME, USA) . . . . .	227
Simple, rapid and sensitive spectrofluorimetric determination of diflunisal in serum and urine based on its ternary complex with terbium and EDTA P.C. Ioannou, E.S. Lianidou and D.G. Konstantianos (Athens, Greece) . . . . .	237
2-(5-Hydrazinocarbonyl-2-thienyl)-5,6-methylenedioxybenzofuran and 2-(5-hydrazinocarbonyl-2-furyl)-5,6-methylenedioxybenzofuran as novel fluorescence derivatisation reagents for carboxylic acids in liquid chromatography M. Saito, T. Ushijima, K. Sasamoto, K. Yakata, Y. Ohkura and K. Ueno (Kumamoto, Japan) . . . . .	243
Fluorescence reaction and complexation equilibria between norfloxacin and aluminium(III) ion in chloride medium P.T. Djurdjevic (Kragujevac, Yugoslavia), M. Jelkic-Stankov and D. Stankov (Belgrade, Yugoslavia) . . . . .	253
Instrument for Hadamard transform three-dimensional fluorescence microscope image analysis G. Chen, E. Mei, W. Gu, X. Zeng and Y. Zeng (Wuhan, China) . . . . .	261



### *Enzymatic Methods*

Enzymatic–spectrophotometric determination of phytic acid with phytase from <i>Aspergillus ficuum</i> J.G. March, A.I. Villacampa and F. Grases (Palma de Mallorca, Spain) . . . . .	269
Application of a mimetic enzyme for the enzyme immunoassay for $\alpha$ -1-fetoprotein Y.-X. Ci, Y. Qin, W.-B. Chang and Y.-Z. Li (Beijing, China) . . . . .	273
On-line monitoring of D-lactic acid during a fermentation process using immobilized D-lactate dehydrogenase in a sequential injection analysis system H.-C. Shu, H. Håkanson and B. Mattiasson (Lund, Sweden) . . . . .	277
Microcalorimetric study of the enzymatic hydrolysis of starch: an $\alpha$ -amylase catalyzed reaction G. Salieri, G. Vinci and M.L. Antonelli (Rome, Italy) . . . . .	287

### *Spectrophotometry*

Spectrophotometric determination of catecholamines with metaperiodate by flow-injection analysis J.J. Berzas Nevado, J.M. Lemus Gallego and P. Buitrago Laguna (Ciudad Real, Spain) . . . . .	293
Spectrophotometric cell comprising parallel rotating and stationary bioreactors: application to the determination of glucose in serum samples J. Raba (San Luis, Argentina), S. Li and H.A. Mottola (Stillwater, OK, USA) . . . . .	299
Kinetic spectrophotometric determination of hydrazine A. Safavi and A.A. Ensafi (Shiraz, Iran) . . . . .	307

### *Other Topics*

Age estimation of old carpets based on cystine and cysteic acid content J. Csapó, Z. Csapó-Kiss (Kaposvár, Hungary), T.G. Martin (West Lafayette, IN, USA), S. Folestad, O. Orwar, A. Tivesten and S. Némethy (Göteborg, Sweden) . . . . .	313
Simultaneous determination of arsenic, antimony and selenium by gas-phase diode array molecular absorption spectrometry, after preconcentration in a cryogenic trap S. Cabredo Pinillos, J. Sanz Asensio (Logroño, Spain) and J. Galbán Bernal (Zaragoza, Spain) . . . . .	321
Comparison of two methods for coating piezoelectric crystals M.T. Gomes, A.C. Duarte and J.P. Oliveira (Aveiro, Portugal) . . . . .	329

<i>Book Reviews</i> . . . . .	335
-------------------------------	-----

<i>Author Index</i> . . . . .	341
-------------------------------	-----

ANALYTICA CHIMICA ACTA  
VOL. 300 (1995)

# ANALYTICA CHIMICA ACTA

*An international journal devoted to all branches of analytical chemistry  
Revue internationale consacrée à tous les domaines de la chimie analytique  
Internationale Zeitschrift für alle Gebiete der analytischen Chemie*

**Editors: Harry L. Pardue (West Lafayette, IN, USA)  
Alan Townshend (Hull, Great Britain)  
J.T. Clerc (Berne, Switzerland)  
Willem E. van der Linden (Enschede, Netherlands)  
Paul J. Worsfold (Plymouth, Great Britain)**

**Associate Editor: Sarah C. Rutan (Richmond, VA, USA)**

## Editorial Advisers:

F.C. Adams, Antwerp  
M. Aizawa, Yokohama  
W.R.G. Baeyens, Ghent  
C.M.G. van den Berg, Liverpool  
A.M. Bond, Bundoora, Vic.  
M. Bos, Enschede  
J. Buffle, Geneva  
R.G. Cooks, West Lafayette, IN  
P.R. Coulet, Lyon  
S.R. Crouch, East Lansing, MI  
R. Dams, Ghent  
P.K. Dasgupta, Lubbock, TX  
Z. Fang, Shenyang  
P.J. Gemperline, Greenville, NC  
W. Heineman, Cincinnati, OH  
G.M. Hieftje, Bloomington, IN  
G. Horvai, Budapest  
T. Imasaka, Fukuoka  
D. Jagner, Gothenburg  
G. Johansson, Lund  
D.C. Johnson, Ames, IA  
A.M.G. Macdonald, Birmingham

D.L. Massart, Brussels  
P.C. Meier, Schaffhausen  
M. Meloun, Pardubice  
M.E. Meyerhoff, Ann Arbor, MI  
H.A. Mottola, Stillwater, OK  
M. Otto, Freiberg  
D. Pérez-Bendito, Córdoba  
A. Sanz-Medel, Oviedo  
T. Sawada, Tokyo  
K. Schügerl, Hannover  
M.R. Smyth, Dublin  
R.D. Snook, Manchester  
J.V. Sweedler, Urbana, IL  
M. Thompson, Toronto  
G. Tölg, Dortmund  
Y. Umezawa, Tokyo  
J. Wang, Las Cruces, NM  
H.W. Werner, Eindhoven  
O.S. Wolfbeis, Graz  
Yu.A. Zolotov, Moscow  
J. Zupan, Ljubljana



ELSEVIER

*Anal. Chim. Acta*, Vol. 300 (1995)

Amsterdam – Lausanne – New York – Oxford – Shannon – Tokyo

No part of this publication may be reproduced, stored in a retrieval system or transmitted in any form or by any means, electronic, mechanical, photocopying, recording or otherwise, without the prior written permission of the publisher, Elsevier Science B.V., Copyright and Permissions Dept., P.O. Box 521, 1000 AM Amsterdam, The Netherlands.

Upon acceptance of an article by the journal, the author(s) will be asked to transfer copyright of the article to the publisher. The transfer will ensure the widest possible dissemination of information.

Special regulations for readers in the U.S.A. – This journal has been registered with the Copyright Clearance Center, Inc. Consent is given for copying of articles for personal or internal use, or for the personal use of specific clients. This consent is given on the condition that the copier pays through the Center the per-copy fee stated in the code on the first page of each article for copying beyond that permitted by Sections 107 or 108 of the US Copyright Law. The appropriate fee should be forwarded with a copy of the first page of the article to the Copyright Clearance Center, Inc., 222 Rosewood Drive, Danvers, MA 01923, U.S.A. If no code appears in an article, the author has not given broad consent to copy and permission to copy must be obtained directly from the author. The fee indicated on the first page of an article in this issue will apply retroactively to all articles in the journal, regardless of the year of publication. This consent does not extend to other kinds of copying, such as for general distribution, resale, advertising and promotion purposes, or for creating new collective works. Special written permission must be obtained from the publisher for such copying.

No responsibility is assumed by the publisher for any injury and/or damage to persons or property as a matter of products liability, negligence or otherwise, or from any use or operation of any methods, products, instructions or ideas contained in the material herein.

Although all advertising material is expected to conform to ethical (medical) standards, inclusion in this publication does not constitute a guarantee or endorsement of the quality or value of such product or of the claims made of it by its manufacturer.

☺ The paper used in this publication meets the requirements of ANSI/NISO 239.48-1992 (Permanence of Paper).





ELSEVIER

Analytica Chimica Acta 300 (1995) 1-3

ANALYTICA  
CHIMICA  
ACTA

Letter

## Simple reversible staining of proteins transferred from polyacrylamide gels onto nitrocellulose membranes

Hans Bloemendal<sup>\*</sup>, Monique Satijn

*Department of Biochemistry, University of Nijmegen, P.O. Box 9101, 6500 HB Nijmegen, Netherlands*

Received 7 July 1994

---

### Abstract

A rapid picture of the extent of protein transfer from one- or two-dimensional polyacrylamide gels onto nitrocellulose membranes prior to immunodetection can be obtained by a rapid and reversible Amido Black staining procedure.

*Keywords:* Reversible protein staining; Immunoblotting

---

### 1. Amido Black staining of proteins prior to immunoblotting

In the course of our studies on normal versus cataractous human lens proteins a primary goal was to construct reproducible two-dimensional crystallin maps. Crystallins are the water-soluble proteins in vertebrate eye lenses and represent about 90% of the total soluble lenticular proteins [1,2].

A major difficulty encountered in such studies is the fact that crystallins in the human lens, which are primary gene products, undergo a variety of post-translational modifications, such as deamidation, truncation, phosphorylation, glycosylation, carbamylation and oxidation, particularly upon aging [3]. These modified gene products complicate the human gel map tremendously as compared, for instance, to the corresponding map of calf lens proteins [4].

In order to verify the reproducibility of the gel patterns, localization and identification of one or few proteins was carried out by immunoblotting. For a complete map this localization had to be established in respect to all other protein components that did not react with the antibody. Therefore a combination of immunoblotting and staining of the proteins was necessary. Both staining prior to and after immunoblotting were tested. Several difficulties were encountered. For instance, it appeared with Ponceau S post-staining [5] that the whole blot resisted complete destaining and individual protein spots were hardly visible. Application of the sensitive colloidal gold staining [6] had the same negative result. The blot kept a violet background. Therefore we searched for a reversible pre-staining method which allows the application of preincubation with a protein like bovine serum albumin (BSA), a blocking agent that prevents background staining in immunoblotting. Pre-staining with Ponceau S failed due to the low amount of lens proteins required for immunoblotting

---

<sup>\*</sup> Corresponding author.

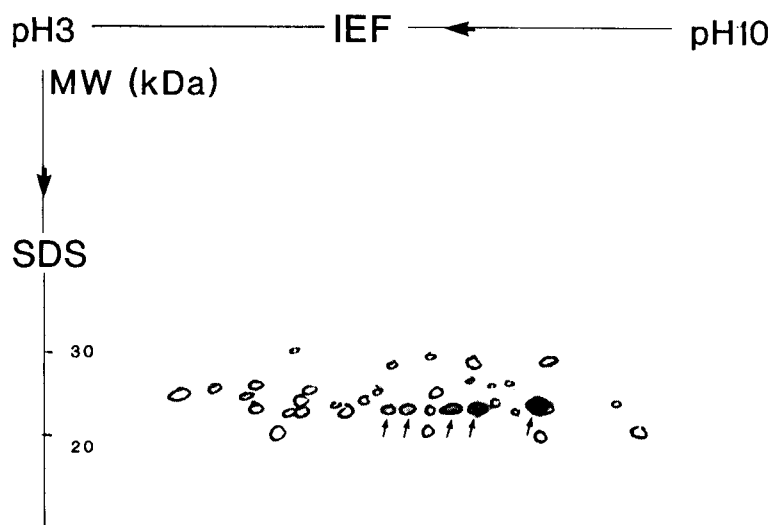


Fig. 1. Two-dimensional immunoblot of human water-soluble lens proteins, prestained with Amido Black. Immunodetection with anti- $\alpha$ B-crystallin (arrows), other crystallins marked with indelible ink.

(20  $\mu$ g of protein to be separated into about 150 spots with a variation of 5–300 ng per individual spot). Gold staining gave unsatisfactory results too in that, only a spotty pattern was obtained. Only Amido Black staining appeared to be a reversible and satisfactory method (compare Table 1). Previously, Syu and Kahan [7] described a staining procedure for nitrocellulose membranes with Amido Black. However, their method differs in that the membranes were blocked with gelatin before immunoblotting. Moreover blue background protein spots not reacting with the antibodies remain on the membrane next to those which have reacted and appeared in purple. This can lead to erroneous evaluation if the immuno-positive spots are faint and hard to distin-

guish from the blue-stained non immuno-reactive spots.

## 2. The protocol

- (1) Proteins are transferred from the 2D-gels onto nitrocellulose membranes according to standard methods for electroblotting.
- (2) The blot is immersed in an Amido Black solution (2.5 g Amido Schwarz (Merck, Darmstadt); 250 ml methanol; 215 ml deionized, distilled water; 35 ml acetic acid) while shaking for 3–6 s, followed by immediate removal of the stain.

Table 1

Advantages and disadvantages of different staining methods for proteins on nitrocellulose membranes

Staining method	Advantage	Disadvantage
Ponceau S	Rapid, cheap, reversible	Not sensitive enough
Colloidal Gold	Sensitive	Slow, expensive, spotty pattern
Amido Black	Sensitive, rapid, cheap, reversible	

Longer contact with the stain would interfere with the destaining procedure.

- (3) Destaining is carried out for 3–5 min by rinsing with running deionized water. The spots then become visible against a faint blue background.
- (4) The localization of the spots can be marked either by photography or careful encircling with indelible ink without damaging the membrane (see Fig. 1).
- (5) Thereafter the blot is further destained by shaking for another 30 min in deionized water, followed by incubation in 1% BSA in PBS/Tween for 1 h. This step is required for immuno-detection.

All remaining stain, including that coupled to proteins, vanishes and the antibody can react with its corresponding antigen. The background appears virtually white.

### 3. Conclusion

This extremely simple method, which appeared to be not damaging to nitrocellulose blots in approxi-

mately hundred experiments, gives a very rapid picture of the extent of protein transfer from the gel and allows correlation of the mutual positions of proteins with those detected with the aid of antibodies.

### Acknowledgements

This work has been supported by an Alcon grant.

### References

- [1] H. Bloemendal, *Science*, 197 (1977) 127.
- [2] H. Bloemendal, *Crit. Rev. Biochem.*, 12 (1982) 1.
- [3] P.J.T.A. Groenen, K.B. Merck, W.W. de Jong and H. Bloemendal, *Eur. J. Biochem.*, 225 (1994) 1.
- [4] G.A.M. Berbers, W.A. Hoekman, H. Bloemendal, W.W. de Jong, T. Kleinschmidt and G. Braunitzer, *Eur. J. Biochem.*, 139 (1984) 467.
- [5] O. Salinovich and R.C. Montelaro, *Anal. Biochem.*, 156 (1986) 341.
- [6] M. Moeremans, G. Daneels and J. de Mey, *Anal. Biochem.*, 145 (1985) 315.
- [7] W.-I. Syu and L. Kahan, *J. Immunol. Methods*, 103 (1987) 247.

# Electrochemical characteristics of conductive carbon cement as matrix for chemically modified electrodes

Xinjian Huang, J.J. Pot, W.Th. Kok \*

*Laboratory for Analytical Chemistry, University of Amsterdam, Nieuwe Achtergracht 166, 1018 WV Amsterdam, Netherlands*

Received 18 March 1994; revised manuscript received 1 August 1994

## Abstract

Conductive carbon cement (CCC) was evaluated as matrix material for the preparation of electrodes bulk-modified with electrocatalysts. For pure CCC electrodes the background current characteristics were examined. In acidic or neutral phosphate buffers the useful electrode potential range was from  $-0.3$  to  $+1.0$  V vs. SCE, while in  $0.1 \text{ mol l}^{-1}$  NaOH it was from  $-0.3$  to  $+0.7$  V. The electrochemical reversibility of CCC electrodes was examined by measuring the standard rate constants for the reduction of hexacyanoferrate(III) and the oxidation of hydroquinone, using cyclic voltammetry (CV) and rotating disk experiments. The reversibility of a CCC electrode was comparable with that of a freshly polished glassy carbon electrode and better than that of carbon paste electrodes. CCC was used as matrix for the preparation of electrodes bulk-modified with cuprous oxide and cobalt phthalocyanine (CoPC). With a  $\text{Cu}_2\text{O}$ -CCC electrode the oxidation potential of glucose, which shows sluggish kinetics at unmodified carbon electrodes, was strongly reduced. The kinetics of the mediated glucose oxidation has been studied with a rotating disk electrode. It was shown that at glucose concentrations higher than approximately  $1 \text{ mmol l}^{-1}$  the electrochemical regeneration of the catalyst becomes rate-determining. The  $\text{Cu}_2\text{O}$ -CCC modified electrode has been applied with a constant potential in flow-injection analysis for the determination of glucose. The long-term stability of the electrode was studied; repeated injections of a glucose solution during a period of 6 h yielded a relative standard deviation of the peak height of 1.8% ( $n=57$ ). In CV experiments the electrocatalytic activity of CoPC was shown for the oxidation of various compounds such as penicillamine, hydrazine and bile acids. Application of the CoPC-CCC electrode for the detection of bile acids in flow-through detection with a constant or pulsed potential failed, due to a rapid deactivation of the electrode.

**Keywords:** Cyclic voltammetry; Chemically modified electrodes; Conductive carbon cement; Cuprous oxide; Cobalt phthalocyanine; Carbohydrates; Bile acids

## 1. Introduction

Carbon is the most widely used electrode material for amperometric detection in flowing solutions, for instance in flow injection analysis (FIA) and liquid chromatography (LC) [1]. Apart from the well known glassy carbon, various carbon composite materials have been used for this purpose. These materials consist of

a mixture of a carbon material with an insulator, such as carbon paste [2], graphite/silicone rubber [3], carbon powder/epoxy resin [4,5], graphite/PTFE [6], reticulated vitreous carbon/epoxy resin [7,8], graphite/polythene [9,10], graphite/Kel-F [11–20] or carbon powder/polystyrene [21–25]. The reason to use these carbon composite materials instead of glassy carbon was usually either to facilitate the construction or the renewal of the electrode, or to obtain improved

\* Corresponding author.



signal-to-noise ratios. More recently, however, the incorporation of electrocatalysts in the composite materials has been studied.

One of the problems encountered in electrochemical detection with carbon electrodes is the low reversibility of the electrochemical reaction of many organic compounds, necessitating the application of high overpotentials for detection. Several techniques have been developed to improve the reversibility of carbon electrodes by pretreatment of the electrode surface, for instance by polishing, heat treatment or electrochemical activation [26]. With these techniques a non-selective improvement of the electrode kinetics can be realised. A more selective improvement of the electrode reversibility can be obtained by modification of the electrode surface with an electrocatalyst, mediating in the electron transfer between the electrode and certain types of compounds in the solution. One of the approaches for this modification is to apply a monomolecular layer or a three-dimensional film containing the electrocatalyst on the surface of the carbon electrode [27–31]. However, it is often difficult to prepare a homogeneous, mechanically stable film with an electrocatalyst.

Another approach to electrode modification is to prepare bulk-modified electrode materials. For this, a solid electrocatalyst is mixed with a carbon composite matrix such as carbon paste or carbon powder/epoxy resin [32–36]. It has been shown that bulk modification is flexible and easy to perform. When the electrode surface has become inactive by, e.g., poisoning of the catalyst by impurities, a fresh surface layer containing the catalyst is easily obtained by polishing.

In previous work [37] we have shown that conductive carbon cement (CCC) can be used as matrix material to prepare an electrode bulk-modified with cobalt phthalocyanine (CoPC). The modified CCC electrode was used for the detection of cysteine compounds in body fluids after separation by LC. CCC, a mixture of carbon particles with a polyacrylic resin, is readily available and easy to use for the preparation of modified electrodes. The CCC matrix was shown to have a high mechanical stability and compatibility with organic modifiers in the solution. This resulted in a better reproducibility and a longer lifetime of the electrode than with a carbon paste matrix.

For the functioning of bulk-modified electrodes, the electrochemical characteristics of the matrix material

are of importance. The useful potential range of a modified electrode is limited by the solvent decomposition on the matrix. Furthermore, at some stage in the mediated electrochemical process, electron transfer with the conducting matrix particles has to take place. In the work presented here, modified and unmodified CCC electrodes have been studied. Charge transfer rates for common analytes on unmodified CCC have been compared with those on carbon paste and glassy carbon electrodes. The kinetics of the oxidation of glucose on a CCC electrode modified with cuprous oxide has been studied in detail, using rotating disk electrode (RDE) experiments and FIA. Some applications of CoPC-modified CCC electrodes will also be presented.

## 2. Experimental

### 2.1. Apparatus

Cyclic voltammetry (CV) experiments were conducted using a computerized Autolab electrochemical analyzer (ECO Chemie, Utrecht) with a platinum auxiliary electrode and a SCE reference electrode. RDE experiments were carried out with a 626 Polarecord and a 663 VA Stand (Metrohm, Herisau). For FIA a peristaltic pump (Gilson) was used, with a Rheodyne 7010 injection valve with a 30  $\mu$ l sample loop. For amperometric detection a Model 1049A programmable electrochemical detector (Hewlett Packard) was operated in the constant potential mode with a Metrohm wall-jet electrochemical cell containing a Ag/AgCl reference electrode and a glassy carbon counter electrode.

The working electrodes in CV, RDE, and FIA experiments were standard Metrohm glassy carbon disk electrodes (3 mm diameter, mounted in PTFE) and carbon paste electrode bases (PTFE body, 3 mm diameter cavity). The latter were packed with either carbon paste or conductive carbon cement, with or without modifiers.

### 2.2. Chemicals and solutions

Cobalt phthalocyanine (Aldrich) and cuprous oxide (Fluka) were used as received. Carbon paste was from Metrohm (E287) and conductive carbon cement (CCC) from Gerhard Neubauer (Münster). Bile acid sodium salts were purchased from Fluka (deoxycholic,

chenodeoxycholic, ursodeoxycholic, glycocholic, taurocholic and taurodeoxycholic acid) or Sigma (cholic, taurochenodeoxycholic, tauroursodeoxycholic, glycodeoxycholic and glycochenodeoxycholic acid). Other chemicals used were A.R. grade. The standard solutions of analytes were prepared daily. Solutions were deaerated with helium before use.

### 2.3. Preparation of the electrodes

Glassy carbon electrodes were polished with 0.05  $\mu\text{m}$  alumina particles (Buehler) on a polishing pad (Buehler) and ultrasonicated for 2 min. Modified carbon paste electrodes were prepared by mixing 5% CoPC (w/w) or 20%  $\text{Cu}_2\text{O}$  (w/w) with carbon paste and pressing the mixture into the cavity of the electrode body. The excess of carbon paste was removed by polishing on a piece of clean smooth paper.

To prepare modified CCC electrodes, CCC was mixed with 5% CoPC (w/w) or 20%  $\text{Cu}_2\text{O}$  (w/w) in the following way. About 300 mg of CCC was transferred into a 1 ml glass vial with a stirrer inside, and the desired amount of modifier was added. Then 300  $\mu\text{l}$  of acetone was added. When necessary, a few  $\mu\text{l}$  of CCC thinner was added. Mixing was achieved on a magnetic stirrer while acetone was allowed to evaporate until a thick paste formed. The vial was closed until use. First, pure CCC was packed in the cavity of carbon paste electrode body and allowed to dry. The excess of CCC was polished off with dry emery paper (grade 2/0, Oakey) and the surface layer of CCC was removed with an acetone-soaked tissue. At this stage, modified CCC paste was packed into the resulting shallow cavity and allowed to dry overnight. The excess of the dried mixture was first polished off with dry emery paper (grade 2/0), then subsequently with 3  $\mu\text{m}$  and 0.3  $\mu\text{m}$  imperial micro finishing film sheets (3M). The final polish was achieved with 0.05  $\mu\text{m}$  alumina particles on a Buehler pad and ultrasonication for 2 min in subboiled water. A fresh surface of the electrode could be obtained in two ways. One way was to repeat the polishing procedure beginning with a 3  $\mu\text{m}$  polishing sheet. The second method was by removing the top layer with an acetone-soaked tissue and repacking with modified CCC. Unmodified CCC electrodes were prepared in the same fashion. After preparation the electrodes were washed with sub-boiled water and dried with compressed air before use.

### 2.4. Kinetic data analysis

Heterogeneous rate constants  $k^0$  were evaluated from the peak separation  $\Delta E_p$  in CV according to the method of Nicholson [38]. From the peak separation a value of the parameter  $\psi$  was obtained which is related to  $k^0$  by [39]:

$$\psi = \frac{(D_0/D_R)^{\alpha/2} \cdot k^0}{[D_0 \pi \nu (nF/RT)]^{1/2}} \quad (1)$$

where  $\nu$  is the scan rate,  $D_0$  and  $D_R$  are the diffusion coefficients of the oxidized and reduced forms of the substrate, respectively, and the other symbols have their usual meaning. The value of  $k^0$  for the hexacyanoferrate couple was also determined by RDE experiments using the Koutecky-Levich equation, which can be written as:

$$\frac{1}{i} = \frac{1}{i_k} + \frac{1}{i_d} \quad (2)$$

where  $i$  is the current measured,  $i_k$  the kinetic current representing the kinetic control process and  $i_d$  the diffusion current. The diffusion current for a RDE is given by:

$$i_d = nFA \cdot D_0^{2/3} \cdot \nu^{-1/6} \cdot \omega^{1/2} \cdot c_0 \quad (3)$$

where  $A$  is the electrode surface area,  $D_0$  is the diffusion coefficient of the substrate,  $\nu$  the hydrodynamic viscosity of the solution,  $\omega$  the rotation rate of the electrode and  $c_0$  the substrate concentration. From the intercept of the Koutecky-Levich plot ( $i^{-1}$  vs.  $\omega^{-1/2}$ ),  $i_k$  was obtained and the forward rate constant  $k_f$  calculated according to:

$$i_k = nFA \cdot k_f \cdot c_0 \quad (4)$$

Since the forward rate constant at a certain potential is given by:

$$k_f = k^0 \cdot \exp\left[\frac{-\alpha nF(E - E_0)}{RT}\right] \quad (5)$$

$k^0$  could be evaluated from a plot of  $\ln k_f$  vs.  $E$ .

It has been recognized [40] that in mediated electrocatalysis three current-controlling factors should be taken into account: (1) the mass transport of the analyte to the electrode surface, as manifest in the limiting current  $i_d$ ; (2) the rate of electron transfer between the analyte and the active sites of the mediator; (3) the

self-electron exchange rate of the mediator at the applied potential. The rate for the chemical step in an oxidative mediated electrode process can be expressed as:

$$i_{\text{ch}} = nFA \cdot k_{\text{ch}} \cdot \Gamma_{\text{ox}} \cdot c_e \quad (6)$$

where  $k_{\text{ch}}$  is the rate constant for the electron transfer,  $\Gamma_{\text{ox}}$  the surface concentration of the active form of the mediator, and  $c_e$  the analyte concentration at the electrode surface. The kinetic equation for the reactivation of the mediator reaction can be expressed as:

$$i_s = nFA \cdot k_s \cdot \Gamma_{\text{red}} \quad (7)$$

where  $k_s$  is the self-exchange rate constant and  $\Gamma_{\text{red}}$  the surface concentration of the inactive form of the mediator. The sum of the surface concentrations of the mediator in the oxidized and reduced form is a constant:

$$\Gamma_{\text{ox}} + \Gamma_{\text{red}} = \Gamma \quad (8)$$

In the steady state, the currents calculated from Eqs. 6 and 7 are equal, and an expression for the kinetic current  $i_k$  can be found by combining Eqs. 6–8 [41–43]:

$$\frac{1}{i_k} = \frac{1}{nFAk_{\text{ch}}\Gamma c_e} + \frac{1}{nFAk_s\Gamma} \quad (9)$$

In mediated electrocatalytic measurements the Koutecky-Levich approach is not valid. Plots of  $1/i$  vs.  $1/\omega^{1/2}$  are curved, and observed slopes do not represent the convective diffusion in the solution. Still, when the kinetics of the electrode reactions are relatively slow, the intercepts of such plots at high rotation speed give a good indication of the kinetic current, with  $c_e$  equal to the bulk analyte concentration  $c_0$ . By measuring  $i_k$  for different analyte concentrations and the construction of a plot of  $1/i_k$  vs.  $1/c_0$ , the values of  $k_{\text{ch}}$  and  $k_s$  can be obtained from the slope and the intercept, respectively.

### 3. Results and discussion

#### 3.1. Background current characteristics of CCC

In 0.1 mol l<sup>-1</sup> phosphate buffer of pH 7.0, with cyclic voltammetry no peaks were observed in a potential range from -0.3 to +1.2 V, except for a higher background at the positive end. However, when the

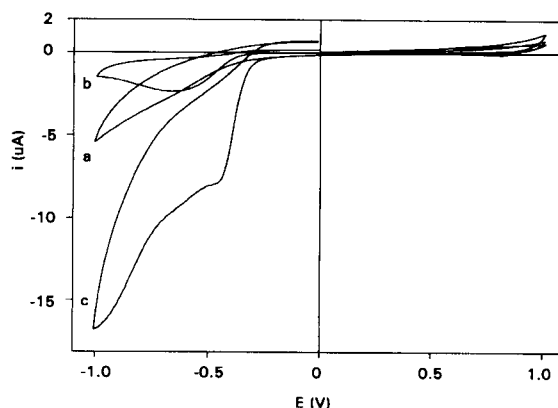


Fig. 1. Cyclic voltammetric background signals with (a) polished GC and (b) CCC electrode in degassed 0.1 mol l<sup>-1</sup> phosphate buffer (pH 7.0), and (c) CCC electrode in air saturated buffer. Scan rate: 10 mV s<sup>-1</sup>.

potential was extended to more negative values, a wave appeared which decreased somewhat in successive scans (see Fig. 1). A similar phenomenon in the negative scan was observed with 0.1 mol l<sup>-1</sup> phosphate buffer of pH 2.0 and with 0.1 mol l<sup>-1</sup> NaOH. The nature of this wave is difficult to establish, since its onset-potential (-0.3 V) is in the range of oxygen reduction. Although it could be characteristic for the CCC electrode surface, a contribution of traces of oxygen trapped in the CCC material can not be excluded. Carbon electrodes normally show a high cathodic background current. For example, similar cathodic residual waves characterize carbon electrodes [2,44], while the applied potential range has a dramatic influence on the background characteristics of carbon-epoxy electrodes [4]. This effect was not observed with CCC electrodes. High cathodic residual currents generally make carbon electrodes unsuitable for reductive detection, for which mercury electrodes are preferably used. The useful electrochemical window for bare CCC electrodes, as determined by CV techniques, can be estimated as -0.3 to +1.0 V vs. SCE in a phosphate buffer of pH 2.0 or 7.0 and -0.3 to +0.7 V in 0.1 mol l<sup>-1</sup> NaOH. Since the main goal of the development of electrocatalytic CMEs is to reduce the overpotential of electrode reactions, this potential range can fulfil the requirements.

#### 3.2. Reversibility of electrode reactions on CCC

The reduction of hexacyanoferrate(III) was studied as a well known example of an outer-sphere, one-electron

tron process. Data obtained in CV experiments with different carbon materials are given in Table 1. The cathodic peak current with CCC electrodes was proportional to the square root of the scan rate from 5 to 200  $\text{mV s}^{-1}$ , which is characteristic for a diffusion controlled process. At higher scan rates, this relationship tailed off and an increase of the peak separation and a decrease of the  $i_a/i_c$  ratio were observed. The standard rate constant  $k^0$  for the hexacyanoferrate redox couple was evaluated from the peak separation  $\Delta E_p$ . Rates of electron transfer for the CCC electrodes and conventionally polished glassy carbon electrodes were similar. It must be noted, however, that the reversibility of glassy carbon electrodes strongly depends on the history and treatment of the surface. For this same electrochemical process standard rate constants from  $10^{-4}$  to  $7 \times 10^{-2} \text{ cm s}^{-1}$  have been reported [26,45,46]. The lower  $k^0$  values obtained with the carbon paste electrodes may be caused by the influence of a thin film of pasting oil on the carbon surface [47]. The formal potential  $E^{\circ'}$ , taken as the average of the oxidation and reduction peak potentials, was the same for all electrode materials. The value found (+0.23 V vs. SCE) is in agreement with literature data [46–48].

A slight aging-effect of the CCC electrode was observed as has been found with carbon paste [47] and pretreated glassy carbon electrodes [26,45]. In a series of 30 CV scans, the signal was almost constant after a few scans. Subsequently the electrode was taken out and washed with water, and another CV scan was conducted. Compared with the original first scan, the peak separation increased by 10 mV and cathodic current decreased by 4%. No obvious memory effect was observed when a blank solution was measured with a CCC electrode which was first used in a solution of hexacyanoferrate(III).

To further explore the electrode kinetics, RDE experiments were also carried out. Voltammograms were

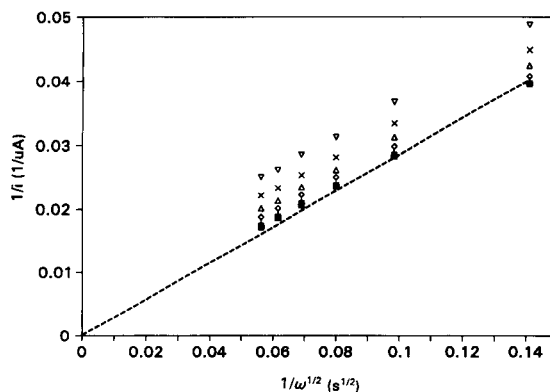


Fig. 2. Koutecky-Levich plots for the reduction of hexacyanoferrate(III) obtained with a CCC electrode at different potentials. (▽) +0.05 V; (×) 0.0 V; (△) -0.05 V; (◇) -0.10 V; (+) -0.15 V; (■) -0.20 V; (-----) theoretical diffusion current.

recorded at several rotation rates and Koutecky-Levich plots were constructed (Fig. 2). The slopes of the plots are in good agreement with the theoretical value calculated from the Levich equation (Eq. 3) using a value for  $D$  of  $0.763 \times 10^{-5} \text{ cm}^2 \text{ s}^{-1}$ . From the intercepts rate constants at different potentials could be calculated. The standard rate constant at  $E^{\circ'} = 0.275 \text{ V vs. Ag/AgCl/sat. KCl}$  can be estimated as  $4.3 \pm 0.5 \times 10^{-3} \text{ s}^{-1}$ , which is in reasonable agreement with the value obtained by CV experiments.

Fig. 3a shows cyclic voltammograms of hydroquinone at several scan rates  $\nu$  with the CCC electrode. The relationship between  $i_p$  and  $\nu^{1/2}$  was linear between 5 and 100  $\text{mV s}^{-1}$ . At higher scan rates this relationship tailed off which suggested that the electron transfer became the rate determining process (Fig. 3b). This was confirmed by a shift of  $E_p$  to more positive values and a decrease of  $i_c/i_a$  with increasing  $\nu$ . After a few scans at the same scan rate, the peak separation remained unchanged, while the anodic peak current decreased by 1.6%, possibly due to the adsorption of oxidation products at the electrode surface. Table 2 lists

Table 1  
Cyclic voltammetric reduction of hexacyanoferrate(III)

Electrode material	$n^a$	$E_{p,c}$ (V)	$\Delta E_p$ (V)	$i_c$ ( $\mu\text{A}$ )	$k^0$ ( $10^{-3} \text{ cm s}^{-1}$ )
CCC	9	$0.185 \pm 0.004$	$0.088 \pm 0.007$	$5.3 \pm 0.2$	$3.3 \pm 0.3$
Glassy carbon	3	$0.183 \pm 0.003$	$0.090 \pm 0.003$	$5.0 \pm 0.1$	$2.5 \pm 0.1$
Carbon paste	5	$0.120 \pm 0.035$	$0.208 \pm 0.044$	$4.6 \pm 0.2$	$0.3 \pm 0.1$

Solution:  $10^{-3} \text{ mol l}^{-1} \text{ K}_3\text{Fe}(\text{CN})_6$  in  $1 \text{ mol l}^{-1} \text{ KCl}$ . Scan rate  $10 \text{ mV s}^{-1}$ . Potentials against SCE.

<sup>a</sup> Number of different electrodes tested.



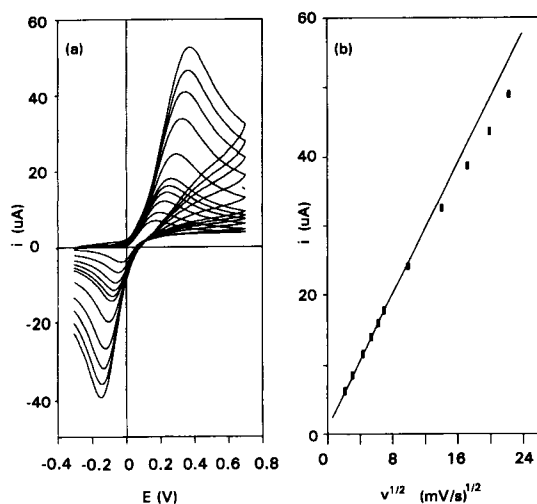


Fig. 3. (a) Cyclic voltammograms of the oxidation of  $10^{-3} \text{ mol l}^{-1}$  hydroquinone in  $0.1 \text{ mol l}^{-1}$  phosphate buffer (pH 7.0) with a CCC electrode at different scan rates. (b) Dependency of the peak current on the scan rate.

the results of the CV experiments on the oxidation of hydroquinone with CCC, glassy carbon and carbon paste electrodes. The standard rate constant  $k^0$  was evaluated with Nicholson's method using a value for  $D$  of  $0.661 \times 10^{-5} \text{ cm}^2 \text{ s}^{-1}$  [49]. It is seen that also for this anodic oxidation process, the electrode reversibility of CCC was better than that of carbon paste.

An explanation for the reversibility difference between CCC and carbon paste electrodes may be found in the surface topology of the materials. With carbon paste electrodes the carbon platelets are oriented parallel to the surface, forming a relatively compressed material, covered by a thin layer of pasting oil which hinders electron transfer [47]. In the case of CCC electrodes, scanning electron microscopy shows no preferential alignment of the carbon particles but rather a random distribution. More carbon with edge orientation is exposed to the solution, on which electron transfer occurs more readily than on basal plane orientation carbon [50].

### 3.3. Oxidation of glucose on $\text{Cu}_2\text{O}$ modified CCC

Metal oxide modified electrodes for the catalysis of redox processes have drawn considerable attention of electroanalytical chemists (e.g., [51]), yet only a few applications in flowing solutions have been described [33,35,52]. Following the work of Xie and Huber

[52], who developed carbon paste electrodes bulk modified with cuprous oxide, we have modified the CCC matrix with  $\text{Cu}_2\text{O}$  for the determination of carbohydrates.

In cyclic voltammetry in blank sodium hydroxide solutions, in the first anodic scan with a freshly prepared  $\text{Cu}_2\text{O}$ -CCC electrode, an irreversible peak is observed with a peak potential of  $+0.20 \text{ V}$ . In later scans this peak did not show. The anodic peak may be related to the oxidation of  $\text{Cu(I)}$  to  $\text{Cu(II)}$  on the electrode surface. Its area corresponds to approximately  $6.9 \times 10^{-9} \text{ mol Cu cm}^{-2}$ .

Cyclic voltammograms of glucose on  $\text{Cu}_2\text{O}$  modified CCC in  $0.1 \text{ mol l}^{-1}$  NaOH show one irreversible anodic wave at  $+0.55 \text{ V}$  (Fig. 4). The height of this peak remained stable in successive scans within 5%. The anodic process on  $\text{Cu}_2\text{O}$ -CCC was not influenced by the hydroxide concentration above a certain value ( $\geq 0.1 \text{ mol l}^{-1}$ ), as has also been observed by others [52]. The appearance of only one anodic wave in CV indicates that the oxidation reaction is different from that on gold electrodes, where two waves are observed at  $-0.53$  and  $+0.15 \text{ V}$  [53,54], attributed to the oxidation of the aldehyde group and the alcohols groups of glucose, respectively. Similar CV behaviour has been observed with copper electrodes and various other copper containing CMEs in alkaline solutions [55–58]. Both  $\text{Cu(II)}$  and  $\text{Cu(III)}$  have been suggested to act as an electron transfer mediator for the oxidation of aldehyde groups [59]. However, since the oxidation of carbohydrates occurs at or near the oxidation wave of the  $\text{Cu(III)/Cu(II)}$  redox couple, although the actual mechanism of glucose oxidation remains uncer-

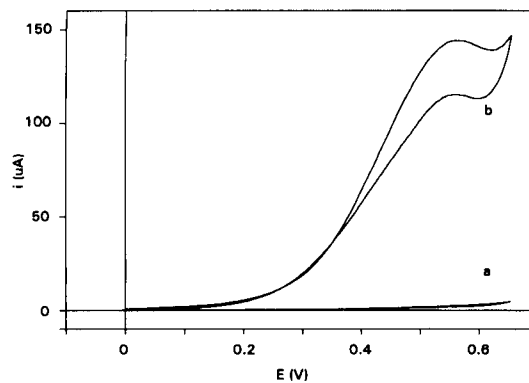


Fig. 4. Cyclic voltammograms of  $5 \times 10^{-3} \text{ mol l}^{-1}$  glucose in  $0.1 \text{ mol l}^{-1}$  NaOH with (a) bare CCC and (b)  $\text{Cu}_2\text{O}$ -CCC electrodes. Scan rate:  $50 \text{ mV s}^{-1}$ .

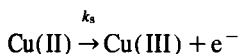
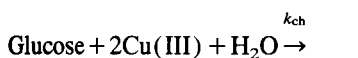
Table 2  
Cyclic voltammetric oxidation of hydroquinone

Electrode material	$n^a$	$E_{p,a}$ (V)	$\Delta E_p$ (V)	$i_a$ ( $\mu\text{A}$ )	$k^0$ ( $10^{-4} \text{ cm s}^{-1}$ )
CCC	5	$0.162 \pm 0.027$	$0.193 \pm 0.037$	$9.1 \pm 0.6$	$3.7 \pm 0.3$
Glassy carbon	5	$0.181 \pm 0.026$	$0.228 \pm 0.042$	$9.4 \pm 0.3$	$2.4 \pm 0.1$
Carbon paste	5	$0.251 \pm 0.024$	$0.355 \pm 0.043$	$9.9 \pm 0.6$	$0.5 \pm 0.1$

Solution:  $10^{-3} \text{ mol l}^{-1}$  hydroquinone in  $0.1 \text{ mol l}^{-1}$  phosphate buffer (pH 7.0). Scan rate  $10 \text{ mV s}^{-1}$ . Potentials against SCE.

<sup>a</sup> Number of different electrodes tested.

tain, it is generally accepted that Cu(III) actively participates in the catalytic oxidation of the carbohydrates. Therefore, the following general scheme of the mediated electrocatalytic oxidation of glucose may be representative:



In RDE experiments it was found that the oxidation current for glucose, measured at  $+0.60 \text{ V}$ , hardly depended on the rotation rate of the electrode. Plots of  $1/i$  vs.  $1/\omega^{1/2}$  yielded straight lines, but with slopes much lower than calculated from the Koutecky-Levich equation (Eqs. 2 and 3). Such behaviour is expected for mediated electrode processes when the electrode kinetics are relatively slow. From the intercepts of the plots obtained, the kinetic current  $i_k$  was estimated for different glucose concentrations. Interestingly, the kinetic current was not proportional to the glucose concentration  $c_0$ . This was already predicted in Eq. 9 with  $c_e$  equal to  $c_0$  for slow electrode process. In Fig. 5,  $1/i_k$  is plotted against  $1/c_0$ . The data points were obtained

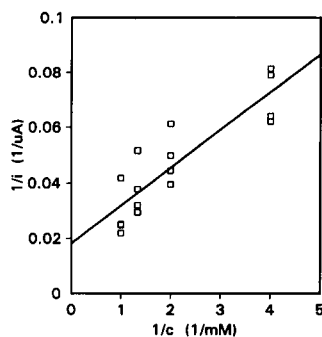


Fig. 5. Dependency of the kinetic current in RDE experiments on the glucose concentration with  $\text{Cu}_2\text{O}$ -CCC electrodes.

in 4 series of measurements, with polishing of the electrode in between. Before rotation rates were varied, a few pre-scans were carried out to obtain a stable baseline. Although the experimental scatter in the plot is rather large, it is clear that an intercept exists. From the slope of the plot a value for  $k_{\text{ch}}\Gamma$  of  $5.4 \pm 0.8 \times 10^{-3} \text{ cm s}^{-1}$  is found, and from the intercept a value for  $k_s\Gamma$  of  $4.1 \pm 1.1 \times 10^{-9} \text{ mol cm}^{-2} \text{ s}^{-1}$ . Combination of these two values gives, as  $k_s/k_{\text{ch}}$ , a 'saturation concentration' for glucose of  $0.76 \text{ mmol l}^{-1}$ . Below this concentration the catalytic oxidation of glucose controls the overall process, while at higher glucose concentrations the regeneration of the mediator is rate determining. For the latter process a heterogeneous rate constant can be calculated, with the surface concentration of the catalyst as determined earlier, of  $0.6 \text{ s}^{-1}$ .

The characteristics of the  $\text{Cu}_2\text{O}$ -CCC electrode were further examined in flow-injection (FIA) experiments. Fig. 6 shows the hydrodynamic voltammogram for glucose oxidation. A maximum sensitivity is obtained at  $+0.50 - +0.55 \text{ V}$ , which is in agreement with the results of the CV experiments. The decrease of the sensitivity at higher potentials seems to be a common

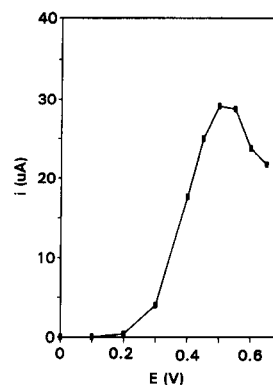


Fig. 6. Hydrodynamic voltammogram of  $10^{-3} \text{ mol l}^{-1}$  glucose with a  $\text{Cu}_2\text{O}$ -CCC electrode. Carrier:  $0.1 \text{ mol l}^{-1}$  NaOH; flow rate:  $1 \text{ ml min}^{-1}$ .

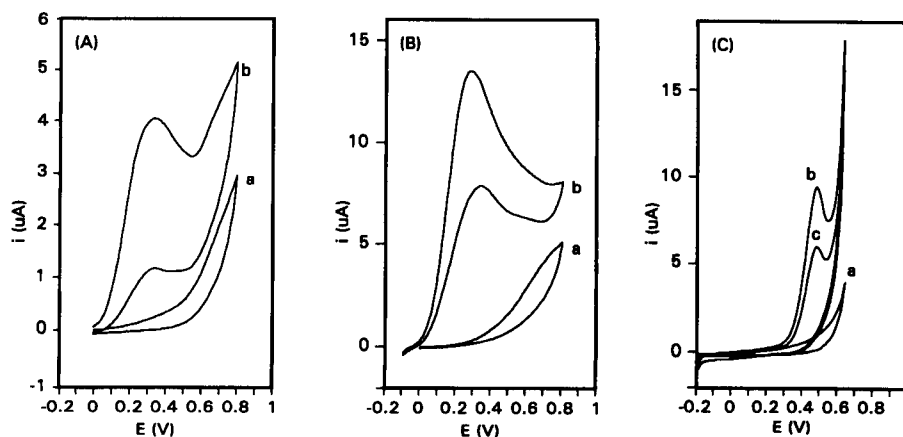


Fig. 7. Cyclic voltammetry with CoPC-CCC electrodes. (A)  $10^{-3}$  mol  $l^{-1}$  penicillamine in 0.1 mol  $l^{-1}$  phosphate buffer (pH 7.0) with (a) bare CCC and (b) CoPC-CCC electrodes. (B)  $0.5 \times 10^{-3}$  mol  $l^{-1}$  hydrazine in 0.1 mol  $l^{-1}$  phosphate buffer (pH 7.0) with (a) bare CCC and (b) CoPC-CCC electrodes. (C)  $10^{-3}$  mol  $l^{-1}$  cholate in 0.1 M NaOH with (a) bare CCC, (b) CoPC-CCC electrode for the first scan and (c) the second scan. Scan rate: 10 (A, B) or 20 (C)  $mV s^{-1}$ .

characteristic of electrocatalytic CMEs, related to the deactivation of the catalyst. The original activity of the electrode could be restored by applying a lower potential again.

When the flow rate of the solution was varied (from 0.2 to 2 ml/min), it was found that the area of the glucose peak obtained, expressed in coulombs, was inversely proportional to the flow rate. This supports the conclusion from the RDE experiments that the overall process is controlled by the electrode kinetics and not by the mass transport to the electrode surface. The decrease of the peak area with the flow rate then reflects the decrease of the residence time of the sample plug in the flow-through cell.

The peak heights in FIA were linear with the glucose concentration in the range from  $10^{-6}$  to  $10^{-3}$  mol  $l^{-1}$ . At higher concentrations the sensitivity decreased. Again, there is a striking agreement with the RDE experiments, where a 'saturation concentration' of 0.76 mmol  $l^{-1}$  of glucose was found. At higher concentrations the electrochemical regeneration of the catalyst becomes the limiting factor for the current.

The stability of electrode was tested in FIA experiments using a constant detection potential of +0.60 V. Within a period of 6 h, the relative standard deviation of the peak height for the repeated injection of a  $10^{-3}$  mol  $l^{-1}$  glucose solution was +1.8% ( $n=57$ ).

### 3.4. CoPC modified CCC

CoPC modified electrodes show effective oxidation of some small [60–62] and larger molecular com-

pounds [63–65], which normally exhibit a sluggish reaction at carbon electrodes. As shown in Fig. 7, in cyclic voltammetry CoPC exhibits electrocatalytic behaviour towards different compounds. Compared to pure CCC, the overpotentials for the oxidation of penicillamine and hydrazine in phosphate buffer (pH 7) were strongly reduced with CoPC-CCC electrodes, with anodic peak potentials of +0.34 and +0.28 V vs. Ag/AgCl, respectively. In previous work we have already shown that CoPC-CCC electrodes can be used for the detection of sulphhydryl compounds in flowing solutions [37]. The long-term stability of the CoPC-CCC electrode was shown to be much better than an analogous electrode with a carbon paste matrix.

In the literature a method has been described for the determination of bile acids by LC with pulsed amperometric detection [66]. Various bile acids, with molecular structures including one to three hydroxy groups, could be oxidized at a gold electrode. Since it has been shown before that electrode modification can replace the pulsed potential mode for detection, we have tested the use of CoPC-CCC electrodes with bile acids. In cyclic voltammetry, we found that CoPC catalyzed the oxidation of bile acids in 0.1 mol  $l^{-1}$  NaOH. For various bile acids (see Experimental section) anodic peak potentials between +0.54 and +0.59 V were observed. However, in two respects the behaviour of the electrode towards bile acids was different from that with, e.g., penicillamine. First, the anodic current in the backward scan was absent. Secondly, the anodic

response strongly decreased after the first scan with a freshly polished electrode (Fig. 7c). Attempts to detect bile acids in a flowing solution with CoPC–CCC electrodes, at a constant or pulsed potential, failed. A rapid decrease of the electrode activity was observed in all cases.

#### 4. Conclusions

CCC compares favourable to carbon paste in respect to available potential range and electrochemical reversibility for different oxidizable compounds. However, the main advantage of this matrix material for bulk-modification of electrodes over carbon paste is its mechanical stability. This makes the application of CCC electrodes in flow-through detection feasible. A highly reproducible sensitivity can be obtained. Compared to other solid matrix materials described in the literature, such as epoxy resins, CCC electrodes are easy to prepare and to renew.

As has been shown for the cuprous oxide electrodes, the results of CV and RDE batch experiments are easily translated to optimized conditions for detection in FIA, LC or capillary electrophoresis. For instance, the flow rate effect and the decrease of the sensitivity at high analyte concentrations as observed in FIA could be explained on the basis of kinetic data obtained with a RDE. From the limited set of examples with CoPC electrodes it appears that the observation of a catalytic effect in CV does not guarantee that a chemically modified electrode can be used in flow-through detection. An indication of the long-term stability in flow is given by the stability of CV signals in successive scans.

The use of modified CCC electrodes for detection in liquid chromatography and capillary electrophoresis is now further investigated in our laboratory.

#### References

- [1] P.T. Kissinger (Ed.), *Laboratory Techniques in Electroanalytical Chemistry*, Marcel Dekker, New York, 1984, pp. 289–319.
- [2] R.N. Adam, *Electrochemistry at Solid Electrodes*, Marcel Dekker, New York, 1969, pp. 26–27 and 280–283.
- [3] E. Pungor and E. Szepezvary, *Anal. Chim. Acta*, 43 (1968) 289.
- [4] H.S. Swofford, Jr. and R.L. Carman III, *Anal. Chem.*, 38 (1966) 966.
- [5] J.E. Anderson and D.E. Tallman, *Anal. Chem.*, 48 (1976) 209.
- [6] L.N. Klatt, D.R. Connell, R.E. Adams, I.L. Honigberg and J.C. Price, *Anal. Chem.*, 47 (1975) 2470.
- [7] N. Sleszynski, J. Osteryoung and M. Carter, *Anal. Chem.*, 56 (1984) 130.
- [8] J. Wang and B.A. Freiha, *J. Chromatogr.*, 298 (1984) 79.
- [9] M. Mascini, F. Pallozzi and A. Liberti, *Anal. Chim. Acta*, 43 (1973) 126.
- [10] J.M. Kauffmann, C.R. Linders, G.J. Patriarcho and M.R. Smith, *Talanta*, 35 (1988) 179.
- [11] J.E. Anderson, D.E. Tallman, D.J. Chesney and J.L. Anderson, *Anal. Chem.*, 50 (1978) 1051.
- [12] D.E. Weisshaar, D.E. Tallman and J.L. Anderson, *Anal. Chem.*, 53 (1981) 1809.
- [13] D.J. Chesney, J.L. Anderson, D.E. Weisshaar and D.E. Tallman, *Anal. Chim. Acta*, 124 (1981) 321.
- [14] D.E. Weisshaar and D.E. Tallman, *Anal. Chem.*, 55 (1983) 1146.
- [15] D.E. Tallman and D.E. Weisshaar, *J. Liquid Chromatogr.*, 6 (1983) 2157.
- [16] J.L. Anderson, K.K. Whiten, J.D. Brewster, T.Y. Ou and W.K. Nonidez, *Anal. Chem.*, 57 (1985) 1366.
- [17] S.L. Petersen, D.E. Weisshaar, D.E. Tallman, R.K. Schulze and J.F. Evans, *Anal. Chem.*, 60 (1988) 2385.
- [18] J.E. Anderson, D. Hopkins, J.W. Shadrick and Y. Ren, *Anal. Chem.*, 61 (1989) 2330.
- [19] T.Y. Ou and J.L. Anderson, *Anal. Chem.*, 63 (1991) 1651.
- [20] J.E. Anderson, J.B. Montgomery and R. Yee, *Anal. Chem.*, 63 (1991) 653.
- [21] B.R. Shaw and K.E. Creasy, *Anal. Chem.*, 60 (1988) 1241.
- [22] B.R. Shaw and K.E. Creasy, *J. Electroanal. Chem.*, 243 (1988) 209.
- [23] K.E. Creasy and B.R. Shaw, *Anal. Chem.*, 61 (1989) 1460.
- [24] J. Park and B.R. Shaw, *Anal. Chem.*, 61 (1989) 848.
- [25] C.L. Wang, K.E. Creasy and B.R. Shaw, *J. Electroanal. Chem.*, 300 (1991) 365.
- [26] G.N. Kamau, *Anal. Chim. Acta*, 207 (1988) 1.
- [27] C.P. Andrieux and J.M. Saveant, *J. Electroanal. Chem.*, 93 (1978) 163.
- [28] J. Ye, R.P. Baldwin and J.W. Schlager, *Electroanalysis*, 1 (1989) 133.
- [29] J.N. Barisci, G.G. Wallace, E.A. Wilke, M. Meaney and M.R. Smyth, *Electroanalysis*, 1 (1989) 245.
- [30] J.A. Cox and T.J. Gray, *Electroanalysis*, 2 (1990) 107.
- [31] R.P. Baldwin and K.N. Thomsen, *Talanta*, 38 (1991) 1.
- [32] M.K. Halbert and R.P. Baldwin, *Anal. Chem.*, 57 (1985) 591.
- [33] J. Wang and Z. Taha, *Anal. Chem.*, 62 (1990) 1413.
- [34] S.A. Wring, J.P. Hart and B.J. Birch, *Analyst*, 114 (1989) 1571.
- [35] D. Leech, J. Wang and M.R. Smyth, *Analyst*, 115 (1990) 1447.
- [36] J. Wang, T. Golden, K. Varughese and I.E. Rayes, *Anal. Chem.*, 61 (1989) 508.
- [37] X. Huang and W.Th. Kok, *Anal. Chim. Acta*, 273 (1992) 245.
- [38] R.S. Nicholson, *Anal. Chem.*, 37 (1965) 1351.



- [39] A.J. Bard and L.R. Faulkner, *Electrochemical Methods*, Wiley, New York, 1980, p. 230.
- [40] F. Beck and H. Schulz, *Electrochim. Acta*, 29 (1984) 1569.
- [41] T. Ikeda, C.R. Leidner and R.W. Murray, *J. Am. Chem. Soc.*, 103 (1981) 7422.
- [42] T. Ikeda, C.R. Leidner and R.W. Murray, *J. Electroanal. Chem.*, 138 (1982) 343.
- [43] N.K. Cenas, J.J. Kanāpieniene and J.J. Kulys, *J. Electroanal. Chem.*, 189 (1984) 163.
- [44] C.F. McFadden, L.L. Russell, P.R. Melaragno and J.A. Davis, *Anal. Chem.*, 64 (1992) 1521.
- [45] D.T. Fagan, I.F. Hu and T. Kuwana, *Anal. Chem.*, 57 (1985) 2759.
- [46] M. Gross and J. Jordan, *Pure Appl. Chem.*, 56 (1984) 1095.
- [47] M.E. Rice, Z. Galus and R.N. Adams, *J. Electroanal. Chem.*, 143 (1983) 89.
- [48] K.R. Kneten and R.L. McCreery, *Anal. Chem.*, 64 (1992) 2518.
- [49] J.N. Yang, Z.H. Yao and Z.P. Gao, *Anal. Chim. Acta*, 246 (1991) 341.
- [50] R.M. Wightman, E.C. Palk, S. Borman and M.A. Dayton, *Anal. Chem.*, 50 (1978) 1410.
- [51] J.A. Cox, R.K. Jaworski and P.J. Kulesza, *Electroanalysis*, 3 (1991) 869.
- [52] Y. Xie and C.O. Huber, *Anal. Chem.*, 63 (1991) 1714.
- [53] L.A. Larew and D.C. Johnson, *J. Electroanal. Chem.*, 262 (1989) 167.
- [54] J.E. Vitt, D.C. Johnson and D.E. Tallman, *Anal. Chem.*, 65 (1993) 231.
- [55] M. Fleischmann, K. Korinek and D. Pletcher, *J. Chem. Soc., Perkin Trans II*, 2 (1972) 1396.
- [56] S.V. Prabhu and R.P. Baldwin, *Anal. Chem.*, 61 (1989) 852.
- [57] S.V. Prabhu and R.P. Baldwin, *Anal. Chem.*, 61 (1989) 2258.
- [58] J.M. Zadel, J. Marioli and T. Kuwana, *Anal. Chem.*, 63 (1991) 649.
- [59] R.M. van Effen and D.H. Evans, *J. Electroanal. Chem.*, 103 (1979) 383.
- [60] J. Zegal, *J. Electroanal. Chem.*, 109 (1980) 389.
- [61] L.M. Santos and R.P. Baldwin, *Anal. Chem.*, 58 (1986) 848.
- [62] K.M. Korfhage, K. Ravichandran and R.P. Baldwin, *Anal. Chem.*, 56 (1984) 1514.
- [63] L.M. Santos and R.P. Baldwin, *Anal. Chem.*, 59 (1987) 1766.
- [64] L.M. Santos and R.P. Baldwin, *Anal. Chim. Acta*, 206 (1988) 85.
- [65] A.M. Tolbert, R.P. Baldwin and L.M. Santos, *Anal. Lett.*, 22 (1989) 683.
- [66] R. Dekker, R. van der Meer and C. Olieman, *Chromatographia*, 31 (1991) 549.

# Impedance analysis of the transport of counter ions at polypyrrole–Nafion composite electrodes

Chur-Min Chang, Hsuan-Jung Huang \*

*Department of Chemistry, National Sun Yat-sen University, Kaohsiung 80424, Taiwan*

Received 20 June 1994; revised manuscript received 1 August 1994

## Abstract

The ion transport accompanying the redox reactions of polypyrrole at a polypyrrole–Nafion composite electrode was investigated with systems containing specifically selected electrolytes. From the cyclic voltammetric and impedance data obtained, transport of cations was found to be responsible for the charge transfer process and parameters such as the charge transfer resistance,  $R_{ct}$ , the low frequency polymer resistance,  $R_p$ , the limiting capacitance,  $C_\ell$  and the diffusion coefficient,  $D_{ct}$  for the related cations were estimated. The electrochemical behaviour (i.e., electronic insulation and electronic conductance) of polypyrrole–Nafion composite electrodes was found to be the same as that of the polypyrrole electrodes, except that they appeared in regions of more negative potentials.

*Keywords:* Cyclic voltammetry; Impedance; Polypyrrole–Nafion composite electrodes

## 1. Introduction

Understanding the mechanism of redox reactions occurring at conductive polymer electrodes and extending the practical applications of these electrodes is of great importance. Therefore, study of the charge transport in conductive polymers has become an attractive and popular research topic in electrochemistry and electrochemical analysis [1–16]. Besides the studies on pure conductive polymer electrodes, the incorporation of conductive polymers like polypyrrole (PPy) and polyaniline into the electroinactive polymer networks of Nafion, poly(vinyl chloride), poly(vinyl alcohol) or polystyrene has been developed for improving the mechanical properties or for modifying the electrochemical characteristics of the conductive polymer electrodes and thus extending their applications [9–

19]. The combination of polypyrrole with Nafion is a typical example showing such characteristics. For the PPy-coated electrodes, the redox reactions are found to be accompanied with the doping–undoping mechanism of anions [1–5]. On PPy–Nafion composite electrodes the immobilized perfluorinated group of Nafion (which is a cation exchanger) serves as a charge compensator during the anodic polymerization of polypyrrole. Cations and solvent molecules, opposite to anions in plain polypyrrole electrodes, are the diffusing species accompanying the redox processes of the Nafion composited polypyrrole [13–16,20]. Although the characteristics of electrical conductivity and charge transfer in the PPy–Nafion composite film electrodes have been investigated, no systematic studies concerning the charge transport of counter ions on the electrochemical behaviour of the PPy–Nafion composite electrodes were reported. In this article, systems with various spe-

\* Corresponding author.

cifically selected electrolytes were adopted to identify the species responsible for the charge transport process accompanying the redox reactions of polypyrrole at the PPy–Nafion composite electrodes. Because cyclic voltammetry (CV) can provide valuable information on the reversibility of the reaction and criteria for discriminating the charge transfer process and the impedance method (a powerful technique for probing the charge and mass transport mechanism), the impedance method based on the conductive polymer film model was employed in combination with CV to elucidate the charge transport of counter ions during the redox reaction of polypyrrole at PPy–Nafion composite electrodes.

## 2. Experimental

### 2.1. Chemicals and solutions

Nafion (5 wt.% dissolved in a mixed solvent of lower aliphatic alcohols and water) was purchased from Aldrich. Sodium chloride, sodium butylsulfonate, ammonium chloride, methylammonium chloride, dimethylammonium chloride, trimethylammonium chloride and tetrabutylammonium bromide used for the preparation of solutions were purchased from Merck. All the chemicals used were of analytical reagent grade or better.

### 2.2. Preparation of PPy–Nafion composite electrodes

30  $\mu\text{l}$  of 1 wt.% Nafion solution (diluted with methanol–water, 9:1) was applied to the platinum electrode (with an area of 1.2  $\text{cm}^2$ ) and air dried to allow the solvent to evaporate.

The thickness of the Nafion film prepared was estimated to be 0.8  $\mu\text{m}$ . The PPy–Nafion composite electrodes were prepared by the further electrodeposition of pyrrole on the Nafion-coated Pt electrode. The anodic polymerization was performed in a deaerated aqueous solution containing 0.1 M pyrrole and 0.2 M NaCl in a conventional three-electrode chemical cell (with a Pt wire as the counter electrode and the Ag/AgCl in saturated KCl solution as the reference electrode) with the application of a constant current of 0.1  $\text{mA cm}^{-2}$ . The same electrochemical cell was used for the following electrochemical measurements.

### 2.3. Electrochemical measurements

Cyclic voltammetry was performed with a PARC 175 universal programmer associated with a PARC 173 potentiostat/galvanostat. Coulometric measurements were achieved with a PARC 179 coulometer. The ac impedance measurements were made with the PARC M378 electrochemical impedance system (including a PARC 276 interface and a 5280 lock-in amplifier). An ac voltage of 5 mV in amplitude (peak-to-peak) with a frequency range of 50 mHz to 0.1 MHz was superimposed on the dc potential and applied to the studied electrodes. The obtained current signal at the frequency range of 50 mHz to 10 Hz was analyzed with the FFT technique.

## 3. Results and discussion

The polymer films obtained by the electrodeposition of polypyrrole on the Nafion-coated Pt electrodes were brown-black in colour. The PPy film formed on the Nafion-coated electrode was smoother than that formed on the bare platinum electrode. This agrees with the literature report that PPy homogenizes well with Nafion to produce smoother composite layers [13–15]. The amount and the thickness of PPy film deposited on the Nafion-coated electrodes can be calculated from the charge consumed during electrodeposition, a PPy film of 0.5  $\mu\text{m}$  in thickness is supposed to be obtained from a consumed charge of 90  $\text{mC cm}^{-2}$  assuming that the amount of soluble oligomer formed is negligible [16].

To study the counter ion effect on the redox reactions of PPy, cyclic voltammetry of PPy–Nafion composite electrodes in solutions of 0.2 M NaCl, 0.2 M  $\text{CH}_3(\text{CH}_2)_3\text{SO}_3\text{Na}$ , 0.2 M  $(\text{CH}_3)_3\text{NHCl}$  and 0.2 M  $(\text{CH}_3\text{CH}_2\text{CH}_2\text{CH}_2)_4\text{NBr}$  were run respectively with a sweep rate of 10  $\text{mV/s}$  in the potential range of  $-1.20$  to 0.20 V. Fig. 1a shows the voltammograms obtained. From Fig. 1a, rather sharp and large cathodic peaks and broad anodic peaks are found for curves (1) and (2). The separation of peak potentials for curves (1) and (2) are about 40 and 60 mV, respectively. This implies that the reversibility of the redox reactions of PPy in the studied solution is very good. For curve (3), both the anodic and cathodic peaks become smaller and broader and the separation of peak potential also becomes larger (about 500 mV) compared with those

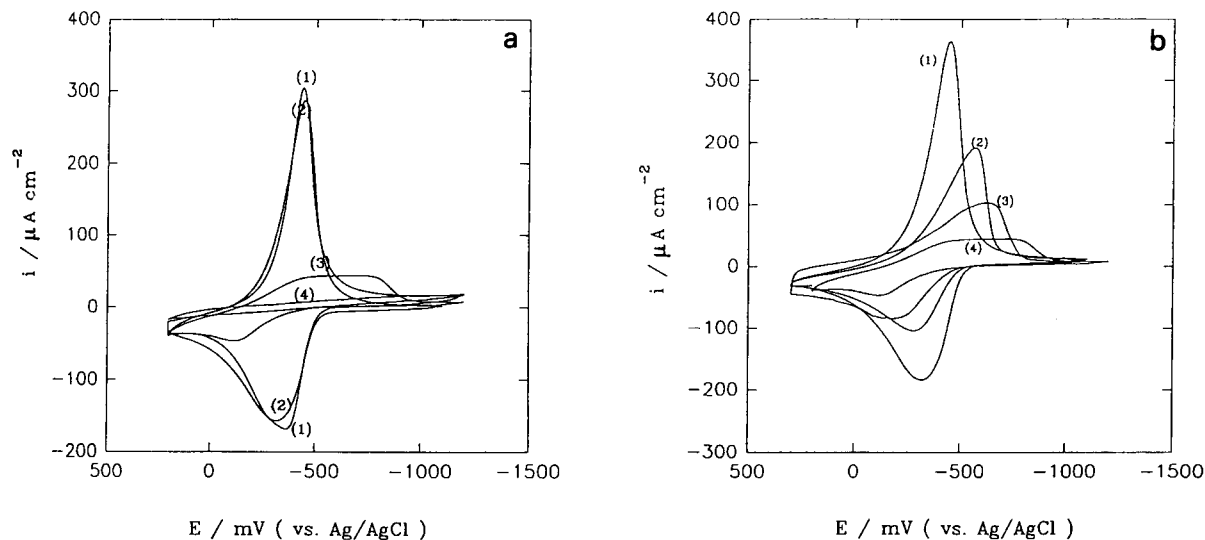


Fig. 1. Cyclic voltammograms for PPY-Nafion composite electrodes in 0.2 M solutions of (a) NaCl (curve 1),  $\text{CH}_3\text{CH}_2\text{CH}_2\text{CH}_2\text{SO}_3\text{Na}$  (curve 2),  $(\text{CH}_3)_3\text{NHCl}$  (curve 3) and  $(\text{CH}_3)_4\text{NBr}$  (curve 4) and (b)  $\text{NH}_4\text{Cl}$ ,  $\text{CH}_3\text{NH}_3\text{Cl}$ ,  $(\text{CH}_3)_2\text{NH}_2\text{Cl}$ ,  $(\text{CH}_3)_3\text{NHCl}$  (curves 1, 2, 3 and 4, respectively). Sweep rate is 10 mV/s.

of curves (1) and (2). For curve (4) neither the anodic nor the cathodic peak is found. Comparing the CVs in Fig. 1a with the electrolytes in the solutions, it is concluded that the redox reaction of PPY on the PPY-Nafion composite electrode is related to the characteristics of the cations in solution. The relatively large redox peaks and very good reversibility found for curves (1) and (2) can be attributed to the presence of highly mobilized hydrated  $\text{Na}^+$  ions in solution. For curve (3) (with rather large and bulky trimethylammonium ions, responsible for the charge transport process), the rate of the redox reactions of PPY decreases and this results therefore in small redox currents and deterioration of reversibility. For curve (4) the tetrabutylammonium ions are so large and bulky that they are not able to diffuse into the PPY-Nafion film to accomplish the charge transport process and therefore no redox currents are found. These observations are consistent with the report which states that when the PPY film is grown with large polymeric anions the cation and solvent molecules will be inserted and removed from the film to compensate the variation of charge in PPY film [20].

To further examine the cation effect on the PPY-Nafion composite electrodes, CVs for solutions containing the same anion but different ammonium ions were run. Fig. 1b shows the CVs obtained from 0.2 M solutions of  $\text{NH}_4\text{Cl}$ ,  $\text{CH}_3\text{NH}_3\text{Cl}$ ,  $(\text{CH}_3)_2\text{NH}_2\text{Cl}$  and

$(\text{CH}_3)_3\text{NHCl}$ . The CVs obtained show essentially the same features as those in Fig. 1a. The current of the redox peaks decreases and a better separation of peak potential is obtained because the radius of the ammonium ions in solutions increased. This further confirms that the redox reactions occurring at the PPY-Nafion film are accompanied and dominated by the transport of cations and the rate of the redox reactions is related to the size of the cations involved. Similar to the behaviour found for the PPY film the broader anodic peaks found for curves 1 and 2 in Fig. 1a and b should be attributed to the effect of expulsion of cations from the PPY-Nafion composite film during the oxidation process of PPY [5]. This expulsion effect is prominent for smaller ions.

Fig. 2a and b shows the impedance spectra obtained from PPY-Nafion composite electrodes in the same solutions used in Fig. 1. The direct current (dc) potential applied is kept at values corresponding to the cathodic half peak potentials. The applied dc potentials are listed in Table 1. The complex impedance plots obtained show the same characteristics as those for the thin redox and electronically conductive polymer films [21–23]. These plots can be interpreted using the modified Randles circuit as shown in Fig. 3 [23], where  $R_\Omega$  is the resistance of the electrolyte between the working and the reference electrode,  $R_{ct}$  is the charge transfer resistance of the redox reaction,  $C_{dl}$  is the double layer

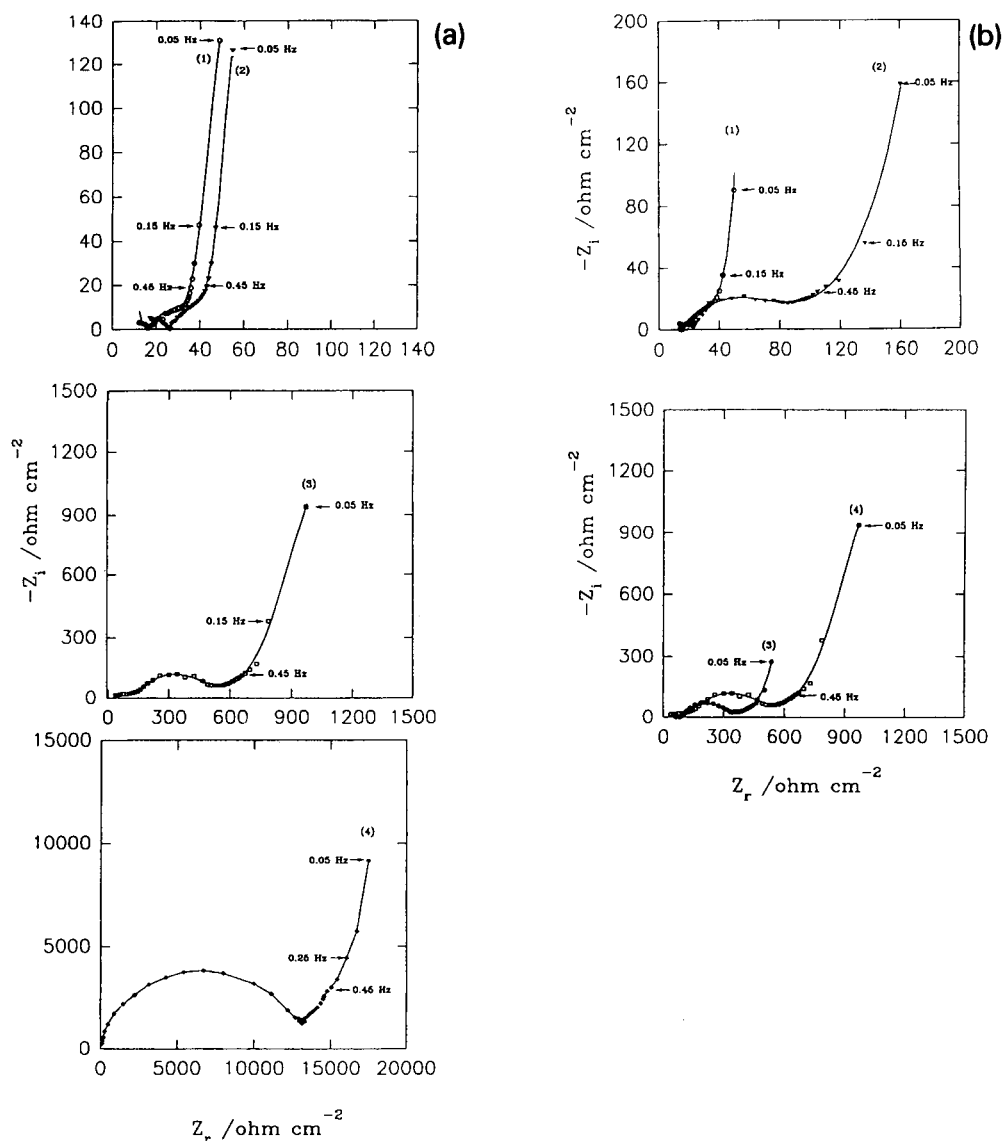


Fig. 2. Complex impedance plots (50 mHz–5.0 kHz) obtained for PPY–Nafion composite electrodes from the same solutions as those used in Fig. 1a and b, respectively.

capacitance of the composite polymer/electrolyte interface,  $Z_\omega$  is the Warburg impedance and  $C_\ell$  is the limiting capacitance in the non-Faradaic regimes. In the high frequency region of the plots, i.e., in the kHz range, the impedance response is associated with the electrode/electrolyte interface process. The related relaxation effect is displayed in the diagram as a semicircle. The value of  $R_{ct}$  may then be obtained from the intercept with the real axis. In the low-frequency region, i.e., in the Hz range, the impedance becomes

controlled by the diffusion of the counterions into the polymer electrode. The response assumes a linear behaviour with a frequency independent phase angle of  $\pi/4$  and is represented by the Warburg impedance element,  $Z_\omega$  in the equivalent circuit. When the frequency is reduced to very low values, e.g., in the mHz range, and if the thickness of the polymer film is sufficiently small, the diffusion process will be progressively limited in favour of a charge accumulation into the polymer film. Accordingly, the ac impedance

approaches a purely capacitive response with a phase angle of  $\pi/2$ . The associated capacitance  $C_\ell$  is the so-called limiting capacitance. In most of the plots shown in Fig. 2, the regions characteristic for the charge transfer, the diffusion of counterions and the restriction of diffusion behaviour by the film thickness are found.

From Fig. 2a, it can be seen that the impedance behaviour of the PPy–Nafion composite electrodes changes with the variation of size of the cations in solutions. The diameter of the semicircle which characterizes the charge transfer resistance  $R_{ct}$  of the redox reactions of PPy increases with the increment of the radius of the cations in solutions. Although the semi-circular arcs in Fig. 2 were a little deviated from that of the impedance plot of an idealized charge transfer process, the intercepts on the real axis were still estimated and used for the determination of  $R_{ct}$ . To evaluate these two intercept values, a least squares fit procedure was applied by fitting the impedance data with a circular function derived from the equivalent circuit in Fig. 3. The obtained  $R_{ct}$  values are listed in Table 1. According to Table 1 the  $R_{ct}$  values obtained from curve (4) are about three orders of magnitude larger than those obtained from curves (1) and (2). Due to the existence of such large  $R_{ct}$  values no redox current can be found for the PPy–Nafion composite electrode in the solution of tetrabutylammonium bromide. From Fig. 2b, the diameter of the semicircle increases from curve (1) to (4) as the radius of the ammonium ions in solutions increases. Accompanied by the increment of charge transfer resistance in solutions, the peak current decreases and the reversibility of the reaction becomes worse compared to what has been found from the CVs in Fig. 1.

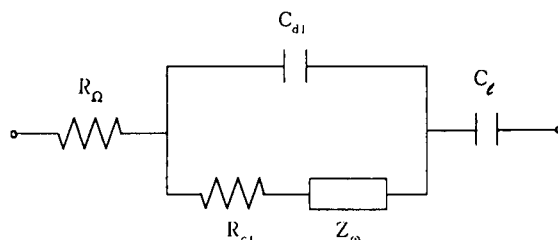


Fig. 3. Equivalent circuit used for the analysis of the impedance data. See text for explanation of variables.

From the impedance spectra, parameters related to the mass transfer of the studied electrolytes in the polymer film can be determined. From literature [21–23], in the diffusion controlled region, the impedance phase angle approaches  $\pi/4$ , and the magnitude of the impedance is given by

$$|Z| = (C_\ell)^{-1} \cdot \ell / (D_{ct}\omega)^{1/2} \quad (1)$$

where  $\omega$  is the angular frequency,  $\ell$  is the film thickness.  $C_\ell$  and  $D_{ct}$  are defined above. Values of  $C_\ell$  are related to  $Z_i$  and  $\omega$  by the following equation.

$$C_\ell^{-1} = d(-Z_i) / d(\omega^{-1}) \quad (2)$$

This equation applies to data in the very low frequency region where  $\omega \ll \ell^2 / D_{ct}$  and the phase angle approaches  $\pi/2$ . The reciprocal of  $C_\ell$  can be obtained from the slope of the linear plot of  $-Z_i$  vs.  $\omega^{-1}$ . Fig. 4 shows the example of such plots from data shown in Fig. 2a.

From the data in the diffusion control region (frequency ranged from 1 Hz to 200 Hz), plots of the total impedance  $Z$  versus  $\omega^{-1/2}$  were made (Fig. 5). From the slopes of these linear plots, in addition to the redox capacitances  $C_\ell$  obtained (from Eq. 2) and the known film thickness  $\ell$ , diffusion coefficient  $D_{ct}$  of the studied

Table 1  
Impedance parameters obtained from PPy–Nafion composite electrodes in various electrolytic solutions

Polymer coated electrode	Electrolyte (0.2 M)	Applied dc potential (V vs. Ag/AgCl)	$R_{ct}$ ( $\Omega/\text{cm}^2$ )	$R_\ell$ ( $\Omega/\text{cm}^2$ )	$C_\ell \times 10^3$ (Faraday)	$D_{ct} \times 10^{10}$ ( $\text{cm}^2/\text{s}$ )
PPy–Nafion	NaCl	–0.35	10	21	31.3	29.5
	$\text{CH}_3\text{CH}_2\text{CH}_2\text{CH}_2\text{SO}_3\text{Na}$	–0.32	14	20	29.8	27.6
	$(\text{CH}_3\text{CH}_2\text{CH}_2\text{CH}_2)_4\text{NBr}$	–0.60	13,000	1900	0.8	2.3
	$\text{NH}_4\text{Cl}$	–0.35	10	22	35.8	22.8
	$\text{CH}_3\text{NH}_3\text{Cl}$	–0.47	69	65	22.3	17.4
	$(\text{CH}_3)_2\text{NH}_2\text{Cl}$	–0.50	259	138	13.6	8.7
	$(\text{CH}_3)_3\text{NHCl}$	–0.50	480	190	10.2	6.7

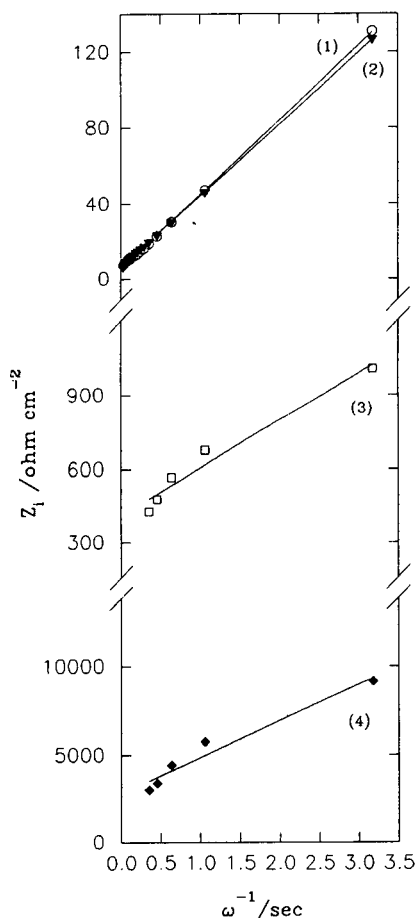


Fig. 4. Plots of imaginary part of impedance  $Z_i$  versus  $\omega^{-1}$  (50 mHz to 0.45 Hz or 2.35 Hz). Solutions used are the same as those in Fig. 1a.

counter ions in the PPY–Nafion films can be calculated. The low frequency polymer resistance,  $R_\ell$  was estimated by extrapolating the  $45^\circ$  straight line and the vertical line of the very low frequency limiting behaviour data to the  $Z_r$  axis [22]. The obtained parameters were summarized in Table 1.

From Table 1, it can be seen that values of  $R_{ct}$  and  $R_\ell$  increase and values of  $C_\ell$  and  $D_{ct}$  decrease with the increment of the radius of the cation in solution. The variation of impedance behaviour found for different ammonium ions shows this trend explicitly. For the PPY–Nafion electrodes, though the charge transfer phenomenon has been studied, no diffusion coefficient data of the cations studied in this experiment were reported. However, data of different cations incorporated into the Nafion film are available in the literature. The dif-

fusion coefficient of  $\text{Na}^+$  ions in Nafion film was reported to be  $9 \times 10^{-7} \text{ cm}^2 \text{ s}^{-1}$  by Yeager and Steck [24] while the diffusion coefficient of  $\text{Cp}_2\text{FeTMA}^+$ ,  $\text{Ru}(\text{bpy})_3^{2+}$  and  $\text{Os}(\text{bpy})_3^{2+}$  were reported by Fan and Bard [13] to be  $1.7 \times 10^{-10}$ ,  $4.0 \times 10^{-10}$  and  $0.7 \times 10^{-10} \text{ cm}^2 \text{ s}^{-1}$ , respectively. The  $D_{ct}$  values of the studied cations obtained in this experiment are about one order of magnitude larger than those of the organometallic species but about two orders of magnitude smaller than those of  $\text{Na}^+$  in a Nafion film.

Judged from the recent study of Vining and Meyer [25], incorporated species in the Nafion film are distributed between the different environments according to their charges and atomic/molecular structures. Hydrophilic ions remain in the aqueous regions and are

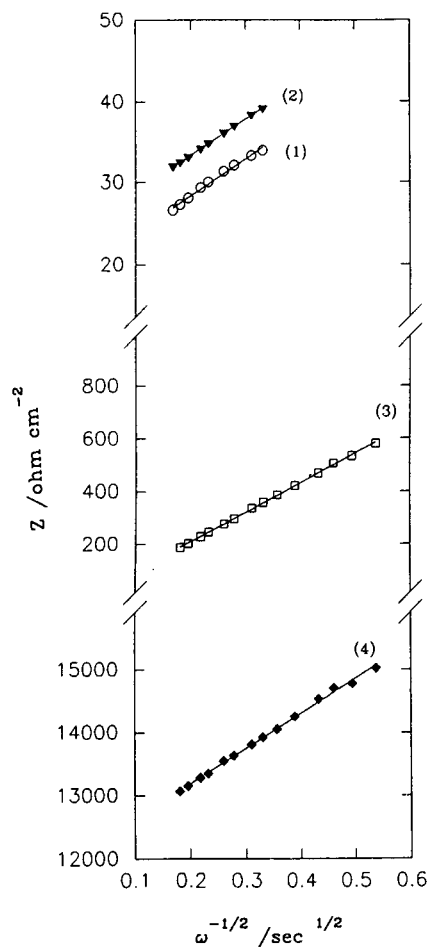


Fig. 5. Plots of impedance magnitude  $Z$  versus  $\omega^{-1/2}$  (1.65 Hz to 5.65 Hz or 0.55 Hz to 4.85 Hz) for data obtained from the same solutions as those in Fig. 1a.

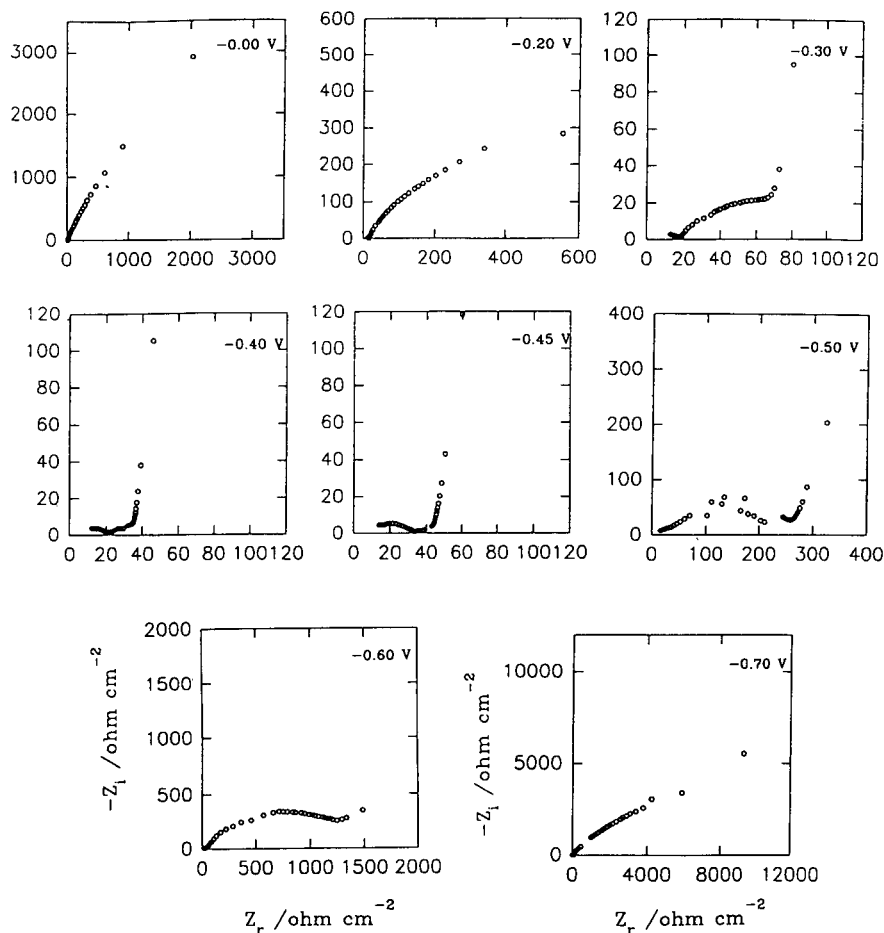


Fig. 6. Complex impedance plot (50 mHz–5.0 kHz) obtained for PPy–Nafion composite electrodes from 0.2 M solution of NaCl with various applied dc potentials.

able to diffuse through the polymer via the ion clusters and interconnecting channels at a rate which is not much below that for aqueous solutions. More hydrophobic ions accumulate mainly in the interfacial domains where the diffusion coefficients are low. In the system studied, where the polypyrrole was intercalated with the Nafion film, the region of ion clusters and interconnecting channels available for the diffusion of cations decreased. The diffusion coefficient for the studied ions should be smaller than those obtained from a pure Nafion film. On the other hand, the radii and the hydrophobicity of the studied ions are smaller than those of the organometallic species mentioned above, the diffusion coefficients of the studied ions should thus be larger than those of the organometallic species.  $D_{ct}$  values listed in Table 1 agree with the conclusion of Vining and Meyer [25].

The above results show the impedance behaviour of the PPy–Nafion composite film for electronically conductive states of the PPy film as the dc potential was held at the half peak potential. It is interesting to explore further the impedance behaviour of the PPy–Nafion composite electrode for cases not related to electronic conductance. Impedance spectra of the PPy–Nafion composite electrodes with a dc potential held at various values were therefore recorded in a solution of 0.2 M NaCl.

The impedance plots obtained from 0.00 to  $-0.70$  V in 0.2 M NaCl solution are shown in Fig. 6. A rather large charge transfer resistance,  $R_{ct}$  found for electrodes with an applied potential from 0.00 to  $-0.20$  V implies that no reduction or a very slow reduction reaction occurs at these potentials. The magnitude of  $R_{ct}$  decreases sharply as the applied potential becomes



Table 2  
Impedance parameters obtained from PPy–Nafion composite electrodes in 0.2 M NaCl solution with various applied dc potentials

Polymer coated electrode	Electrolyte (0.2 M)	Applied dc potential (V vs. Ag/AgCl)	$R_{ct}$ ( $\Omega/\text{cm}^2$ )	$R_\ell$ ( $\Omega/\text{cm}^2$ )	$C_\ell \times 10^3$ (Faraday)	$D_{ct} \times 10^{10}$ ( $\text{cm}^2/\text{s}$ )
PPy–Nafion	NaCl	–0.3	8	63	31	17.4
		–0.4	12	33	30	156.4
		–0.45	24	43	28	182.6
		–0.5	200	250	18	25.7

more negative than  $-0.30$  V. It reaches the minimum at  $-0.40$  V. After that the charge transfer resistance of the reduction reaction increases slowly as the applied potential becomes more negative. The rate of reduction becomes very slow when the applied potential is more negative than  $-0.70$  V. The phenomena of diffusion and restriction of diffusion behaviour can be clearly found in the potential range of  $-0.30$  to  $-0.60$  V. This impedance behaviour at different applied potentials agrees very well with the characteristics of the cyclic voltammogram of curve (1) shown in Fig. 1a.

The related impedance parameters  $R_{ct}$ ,  $R_\ell$ ,  $C_\ell$  and  $D_{ct}$  estimated from the impedance plots at various applied potentials are summarized in Table 2. The same variation of impedance parameters with applied potential is found in the studied potential range. A maximum  $D_{ct}$  value was found at  $-0.45$  V and indicates that the reduction current will be the largest at that potential. A cathodic peak potential of  $-0.45$  V was found from curve (1) in Fig. 1a and confirms this prediction.

From literature the electrochemical behaviour of PPy can be divided into three regimes according to the potential applied on the electrodes [5,26–30]. The first regime exists of a low potential region where the polymer behaves like an electronic insulator. In this regime, charge is injected into the bulk via a diffusion process [29,30]. The second regime occurs at a higher potential region where the polymer behaves like an electronic conductor. In this regime, charge transport occurs uniformly throughout the bulk of the polymer phase via a capacitive-like mechanism [5,26]. The third regime exists at the intermediate potential region. From the impedance behaviour studied above, the PPy–Nafion composite electrode shows the behaviour characterizing a state of very low electronic conductivity when the applied dc potential is more negative than  $-0.30$  V. The state of the electronic conductor can be

found when the applied potential is larger than  $-0.20$  V. The change of the electrochemical behaviour of the PPy–Nafion composite electrodes upon variation of the applied potential is consistent with that reported for PPy electrodes in the literature except that the same three states have shifted to a region of more negative potential.

#### 4. Conclusions

From the CVs and impedance spectra obtained and the impedance parameters estimated, it can be concluded that transport of cations is responsible for the charge transfer process accompanying the redox reactions occurring at the PPy–Nafion composite electrodes. The efficiency of the ion transport in the PPy–Nafion films decreases as the radius of the cation increases. The electrochemical behaviour characterized the regimes of electronic insulator and electronic conductor, and the states of intermediate regime for the PPy film are also found in the PPy–Nafion composite electrode but more negative potentials have to be applied to exhibit this behaviour. By referring to the fact that transport of anions dominates the charge transport process in the PPy films, it is believed that there should be some sort of composite film in which the transport of cations and anions can occur simultaneously and which can contribute to the charge transfer processes in the composite film. In this experiment, the weight ratio of PPy to Nafion in the composite film was estimated to be 1:7.3. It seems that the weight ratio of Nafion to PPy is excessively large. By increasing the weight ratio of PPy or decreasing the weight ratio of Nafion in the composite film, an environment favourable for the movement of both the anions and cations may be created and thus facilitate the simultaneous

transport of cations and anions in the PPy–Nafion composite film. The relationship between the charge transfer efficiency and the ratio of PPy to Nafion in the PPy–Nafion composite film and the possible applications of the specially designed composite electrode may deserve further investigation.

### Acknowledgements

The authors wish to express their gratitude to the National Science Council of Taiwan for the financial support of this work.

### References

- [1] T.A. Skotheim (Ed.), *Handbook of Conducting Polymer*, Vols. 1 and 2, Marcel Dekker, New York, 1986.
- [2] A.F. Diaz, J.I. Castillo, J.A. Logan and W.-Y. Lee, *J. Electroanal. Chem.*, 129 (1981) 115.
- [3] E.M. Genies, G. Bidan and A.F. Diaz, *J. Electroanal. Chem.*, 149 (1983) 101.
- [4] C.D. Paulse and P.G. Pickup, *J. Phys. Chem.*, 92 (1988) 7002.
- [5] D.J. Walton, C.E. Hall and A. Chyla, *Analyst*, 117 (1992) 1305.
- [6] P. Burgmayer and R.W. Murray, *J. Phys. Chem.*, 88 (1984) 2515.
- [7] T. Ikeda, C.R. Ledner and R.W. Murray, *J. Electroanal. Chem.*, 138 (1982) 343.
- [8] H. Mao and P.G. Pickup, *J. Am. Chem. Soc.*, 112 (1990) 1776.
- [9] A.F. Diaz and K.K. Kanazawa, *J. Chem. Soc., Chem. Commun.*, (1979) 635.
- [10] T.T. Wang, S. Tasaka, R.S. Hutton and P.Y. Lu, *J. Chem. Soc. Chem. Commun.*, (1985) 1343.
- [11] M.A. De Paoli, R.J. Waltman, A.F. Diaz and J. Bargon, *J. Chem. Soc. Chem. Commun.*, (1984) 1015.
- [12] O. Niwa and T. Tamamura, *J. Chem. Soc. Chem. Commun.*, (1984) 817.
- [13] F.-R.F. Fan and A.J. Bard, *J. Electrochem. Soc.*, 133 (1986) 301.
- [14] G. Nagasubramanian, S. Di Stefano and J. Moacanin, *J. Phys. Chem.*, 90 (1986) 4447.
- [15] R.M. Penner and C.R. Martin, *J. Electrochem. Soc.*, 133 (1986) 310.
- [16] T. Hirai, S. Kuwabata and H. Yoneyama, *J. Electrochem. Soc.*, 135 (1988) 1132.
- [17] Y. Ikariyama and W.R. Heineman, *Anal. Chem.*, 58 (1986) 1803.
- [18] T.Y. Sung and H.J. Huang, *Anal. Chim. Acta*, 246 (1991) 275.
- [19] B. Scrosati, *Prog. Solid State Chem.*, 18 (1988) 1.
- [20] K. Naoi, M. Lien and W.H. Smyrl, *J. Electrochem. Soc.*, 138 (1991) 440.
- [21] C. Ho, I.D. Raistrick and R.A. Huggins, *J. Electrochem. Soc.*, 127 (1980) 343.
- [22] T.B. Hunter, P.S. Tyler, W.H. Smyrl and H.S. White, *J. Electrochem. Soc.*, 134 (1987) 2198.
- [23] S. Panero, P. Prosperi, S. Passerini, B. Scrosati and D. Perlmutter, *J. Electrochem. Soc.*, 136 (1989) 3729.
- [24] H.L. Yeager and A. Steck, *J. Electrochem. Soc.*, 128 (1981) 1880.
- [25] W.J. Vining and T.J. Meyer, *J. Electroanal. Chem.*, 237 (1987) 191.
- [26] C.K. Chiang, M.A. Druy, S.C. Gau, A.J. Louis, A.G. MacDiarmid, Y.W. Park and H. Shirakawa, *J. Am. Chem. Soc.*, 100 (1978) 1013.
- [27] Z. Cai and C.R. Martin, *J. Electroanal. Chem.*, 300 (1991) 35.
- [28] M. Mao and P.G. Pickup, *J. Phys. Chem.*, 93 (1989) 6480.
- [29] R.M. Penner, L.S. Van Dyke and C.R. Martin, *J. Phys. Chem.*, 92 (1988) 5274.
- [30] R.M. Penner, and C.R. Martin, *J. Phys. Chem.*, 93 (1989) 984.



ELSEVIER

Analytica Chimica Acta 300 (1995) 25–31

ANALYTICA  
CHIMICA  
ACTA

# Application of enzyme-field effect transistor sensor arrays as detectors in a flow-injection analysis system for simultaneous monitoring of medium components. Part II. Monitoring of cultivation processes

T. Kullick<sup>a</sup>, U. Bock<sup>a</sup>, J. Schubert<sup>a</sup>, T. Scheper<sup>b</sup>, K. Schügerl<sup>a,\*</sup>

<sup>a</sup> Institute for Technical Chemistry, University of Hannover, Callinstrasse 3, D-30167 Hannover, Germany

<sup>b</sup> Institute of Biochemistry, Westfälische-Wilhelms University Münster, Wilhelm-Klemm Strasse 2, D-48149 Münster, Germany

Received 26 May 1994; revised manuscript received 5 August 1994

## Abstract

Glucose, maltose, sucrose, lactose, ethanol and urea concentrations were monitored simultaneously during the cultivation of *Escherichia coli* and *Saccharomyces cerevisiae* by means of enzyme field effect transistors (EnFETs) applying glucose dehydrogenase (GDH), maltase (MAL)/GDH, invertase (INV)/GDH,  $\beta$ -galactosidase ( $\beta$ -GAL)/galactose dehydrogenase (GALDH), alcohol dehydrogenase (ADH)/aldehyde dehydrogenase (ALDH), and urease. These enzymes were (co)immobilized on the pH sensitive gates of an eight-FET array. The FET array was integrated in a commercial FIA system.

**Keywords:** Flow injection; Sensors; Field effect transistor (FET); Glucose dehydrogenase; Maltase; Invertase;  $\beta$ -Galactosidase; Galactose dehydrogenase; Alcohol dehydrogenase; Aldehyde dehydrogenase; Urease

## 1. Introduction

In the foregoing paper [1] and in Ref. [2] the preparation, characterization and calibration of a glucose dehydrogenase (GDH) FET for glucose, a maltase (MAL)/GDH FET for maltose, an invertase (INV)/GDH FET for sucrose, a  $\beta$ -galactosidase ( $\beta$ -GAL)/galactose dehydrogenase (GALDH) FET for lactose and an alcohol dehydrogenase (ADH)/aldehyde dehydrogenase (ALDH) FET for ethanol were presented. The urease FET was characterized in Ref. [3]. These EnFETs were integrated in a commercial flow-injection (FI) system (EVA, Eppendorf-Netheler-Hinz, Ham-

burg) and used for the monitoring of several medium components simultaneously during the cultivation of *Escherichia coli* and *Saccharomyces cerevisiae* in synthetic media.

## 2. Experimental and results

### 2.1. On-line monitoring of glucose concentration during recombinant *Escherichia coli* cultivation on synthetic medium

Recombinant *Escherichia coli* K12 W 3110 carrying the plasmid pC<sub>HV1</sub> with the *Vibrio fischeri* lux gene was cultivated on a synthetic medium (Table 1) in a 2.0-l

\* Corresponding author.

Table 1  
Composition of synthetic medium used for the cultivation of *Escherichia coli* K12 W3110 (M9 minimal medium)

Component	Concentration or amount
Na <sub>2</sub> HPO <sub>4</sub> · 2H <sub>2</sub> O	2.63 g/l
KH <sub>2</sub> PO <sub>4</sub>	2.5 g/l
NaCl	0.5 g/l
(NH <sub>4</sub> ) <sub>2</sub> SO <sub>4</sub>	2.5
CaCl <sub>2</sub> solution	1 ml of 0.1 mol/l
MgCl <sub>2</sub> · 6H <sub>2</sub> O solution	1 ml of 1 mol/l
Tracer element solution	1 ml
Vitamin solution	200 ml
(thiamine + biotin)	each 5 mg/l)
Glucose	2.0 g/l
<i>Trace element solution</i>	
ZnSO <sub>4</sub> · 7H <sub>2</sub> O	1.38 g
FeCl <sub>3</sub> · 6H <sub>2</sub> O	5.40 g
MnSO <sub>4</sub>	1.60 g
CuCl <sub>2</sub>	0.17 g
CoSO <sub>4</sub> · 7H <sub>2</sub> O	0.56 g
H <sub>3</sub> BO <sub>3</sub>	0.06 g
Conc. HCl to 1 l H <sub>2</sub> O	10 ml

stirred tank reactor which was provided with standard instruments for measurement and control, pH, pO<sub>2</sub>, temperature, stirrer speed, an off-gas analyser as well as with a 0.2- $\mu$ m polypropylene microfiltration tubular on-line sampling module (ABC, Puchheim). The latter was connected to a flow-injection system (Eppendorf-Netheler-Hinz) (Fig. 1). Since the pH value was deci-

sive for the analysis, a pH regulator unit with a 300- $\mu$ m flow cell was applied to set and maintain the optimal pH for the analysis (Fig. 2).

The first channel was used for pH control and seven channels were provided with enzyme membranes.

During the batch cultivations of *E. coli* all seven FET gates were covered with the same enzyme: glucose dehydrogenase (GDH).

In Fig. 3 the course of the glucose concentration in the case of recombinant *Escherichia* cultivation is shown as measured with the on-line GDH-FET-FI system and with the off-line Yellow Spring Instruments (YSI) equipment. On account of the shift of the pH-electrode (Ingold) during the sterilization, the pH of the cultivation medium was not kept at the optimum 7.0, but at 6.4. Therefore the GDH-FET had to be recalibrated at pH 6.4.

The on-line signals of the particular channels exhibit rather large fluctuations, but their mean values agree with the off-line measurements fairly well.

## 2.2. Monitoring of glucose and ethanol concentrations during the cultivation of *saccharomyces cerevisiae* on synthetic medium

*Saccharomyces cerevisiae* DSM 2155 was batch cultivated on synthetic medium (Table 2) in a 10-l stirred tank bioreactor (Biostat ED, Braun Diessel). The reactor was provided with the standard instruments for measurement and control, pH, pO<sub>2</sub>, temperature, stirrer

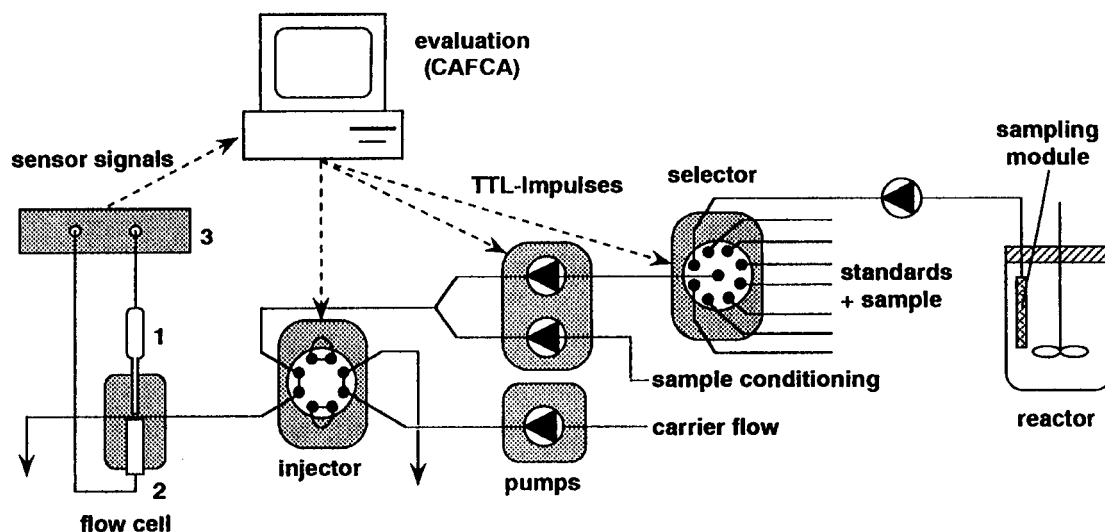


Fig. 1. Setup for the on-line monitoring with an EnFET-FIA system.

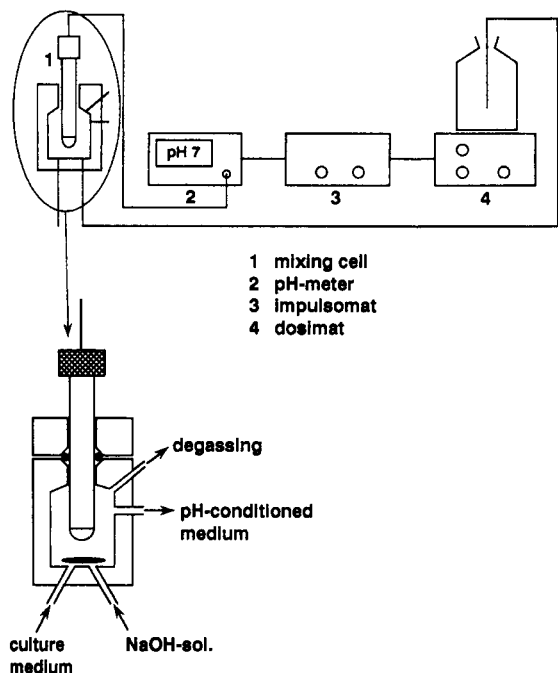


Fig. 2. pH regulator unit for setting and maintaining the optimal pH in the sample.

speed, an off-gas analyser as well as with the  $0.2 \mu\text{m}$  polypropylene microfiltration tubular on-line sampling module (ABC). Glucose and ethanol concentrations in *Saccharomyces cerevisiae* cultivation were monitored on-line as well as the concentration of urea which was given to the medium later. During the cultivation the pH value was maintained at 4.1. At this pH only the urease-FET has a satisfactory high signal, the GDH-FET signal ( $\text{pH}_{\text{opt}}$  8–9 with KP buffer) and ADH/

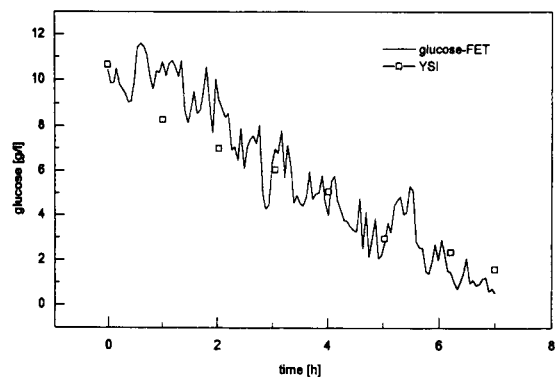


Fig. 3. On-line monitoring of glucose concentration with a GDH-FET-FIA system during the cultivation of *Escherichia coli* K12 W3110 on synthetic medium (Table 1). Off-line reference measurements were carried out with YSI equipment.

ALDH-FET signal ( $\text{pH}_{\text{opt}}$  7–8 and 8–9 with KP buffer) are negligible small.

On account of the fairly large amount of ammonium salts in the medium and because of their  $\text{p}K_{\text{a}}$  value of 9.21, at pH 9 a considerable part of these salts is present as ammonia, which inhibits the immobilized enzymes. Therefore, the pH optimum in the presence of ammonium salts is considerably lower (pH 7.0).

The first channel (No. 1) of the eight-channel FIA was kept free for pH monitoring, three channels (No. 2, 3, 4) were prepared with GDH for glucose measurement, three channels (No. 5, 6, 7) with ADH/ALDH for ethanol measurement and the last channel (No. 8) with urease for urea measurement, because the conversion of urea yields  $\text{CO}_2$  and  $\text{NH}_3$ , and the latter could impair the other EnFETs, if they were positioned downstream of the urease-FET.

In Figs. 4 and 5 the glucose and ethanol concentrations measured with the on-line GDH-FET and the ADH/ALDH-FET are plotted as a function of the cultivation time and the off-line concentrations measured with YSI equipment (glucose) and with a photometer (ethanol). The agreement is satisfactory.

To test the urease-FET at 17.5 h urea was added to the medium (Fig. 6). The urea concentration increased stepwise, but shortly after that, it reduced. Obviously urea was consumed by the yeast.

In another run, lactose was added to the medium at 15 h (Fig. 7). Lactose was also measured off-line using a test kit with a photometer. The lactose concentration

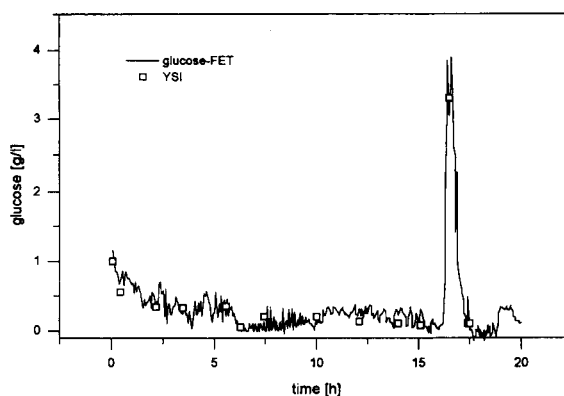


Fig. 4. On-line monitoring of glucose concentration with a GDH-FET-FIA system during the substrate limited cultivation of *Saccharomyces cerevisiae* DSM 2155 on synthetic medium (Table 2). At 16 h, addition of glucose to the medium to increase its concentration to 3.5 g/l. Off-line reference measurements were carried out with YSI equipment.

Table 2

Medium composition used for cultivation of *Saccharomyces cerevisiae*

Component	Concentration or amount
$(\text{NH}_4)_2\text{HPO}_4$	1.44 g/l
$\text{KH}_2\text{PO}_4$	2.5 g/l
KCl	0.9 g/l
$\text{CaCl}_2 \cdot 2\text{H}_2\text{O}$	0.42 g/l
$\text{MgSO}_4 \cdot 7\text{H}_2\text{O}$	0.34 g/l
Trace element solution per 30 g/l glucose	3 ml

*Trace element solution*

$(\text{NH}_4)_2\text{SO}_4$	150 mg/l
$(\text{NH}_4)_2\text{HPO}_4$	44 mg/l
KCl	18 mg/l
$\text{CaCl}_2$	14 mg/l
$\text{FeCl}_3 \cdot \text{H}_2\text{O}$	— <sup>a</sup>
$\text{ZnSO}_4 \cdot 7\text{H}_2\text{O}$	0.3 mg/l
$\text{MnSO}_4$	0.35 mg/l
$\text{CuSO}_4 \cdot 5\text{H}_2\text{O}$	0.08 mg/l

<sup>a</sup> Unknown.

remained constant. It was not consumed by the yeast. In this run channel No. 1 was connected to the pH sensor, No. 2 and 3 to the GDH-FET glucose sensors, No. 4 and 5 to the ADH/ALDH-FET ethanol sensors and No. 6, 7 and 8, to the  $\beta$ -GAL/GALDH-FET lactose sensors. The glucose concentration measured with a single channel showed strong fluctuation (Fig. 8). However, the mean values of the glucose channels agreed fairly well with the off-line YSI measurements.

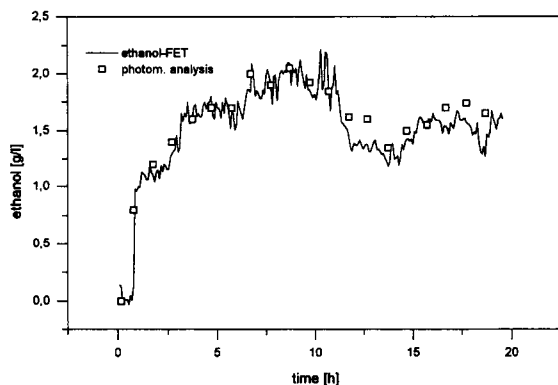


Fig. 5. On-line monitoring of the ethanol concentration with an ADH/ALDH-FET-FIA system during the substrate limited cultivation of *Saccharomyces cerevisiae* DSM 2155 on synthetic medium. At 16 h glucose was added to the medium. Off-line reference measurements were carried out with a spectrophotometer.

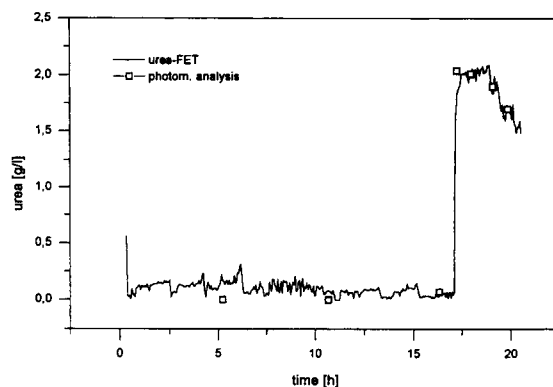


Fig. 6. On-line monitoring of urea concentration with an urease-FET-FIA system during the substrate limited cultivation of *Saccharomyces cerevisiae* DSM 2155 on synthetic medium. At 16 h urea was added to the medium. Spectrophotometric off-line measurements were carried out with the test kit of Merck.

The ethanol concentration was also measured off-line with a photometer (Fig. 9). The agreement between the on-line and off-line measurements was satisfactory.

During another run it was tested whether the crabtree effect caused by the high glucose concentration can be avoided, when disaccharides are used in the medium. For this purpose glucose, maltose and sucrose were added to the medium at different cultivation times and their concentrations were monitored on-line. Again No. 1 of the eight-channel FET system was kept free for pH measurements, No. 2 was prepared with GDH for glucose measurement, No. 3 and 4 with ADH/ALDH for ethanol measurement, No. 5 and 6 with INV/GDH for sucrose measurement and No. 7 and 8 with MAL/GDH for maltose measurement.

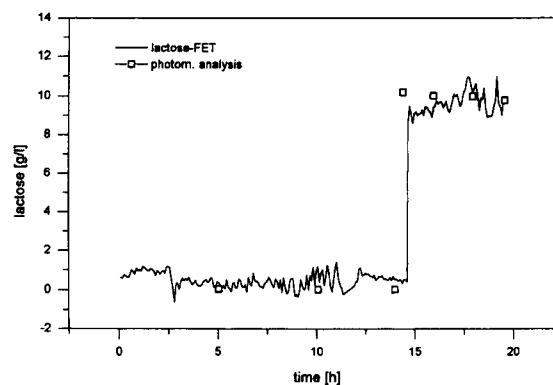


Fig. 7. On-line monitoring of lactose concentration with a  $\beta$ -GAL/GALDH-FET-FIA system during the cultivation of *Saccharomyces cerevisiae* DSM 2155 on a synthetic medium. At 15 h lactose was added to the medium. Spectrophotometric off-line measurements were carried out with the test kit of Boehringer.

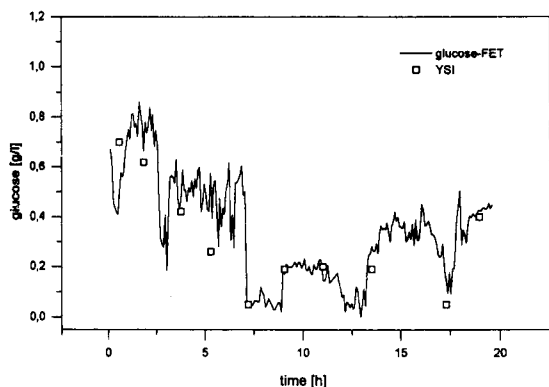


Fig. 8. On-line monitoring of glucose concentration with a GDH-FET-FIA system during the cultivation of *Saccharomyces cerevisiae* DSM 2155 on synthetic medium. Spectrophotometric off-line measurements were carried out with the test kit of Boehringer.

The glucose concentration was increased at 16 h from 0.3 to 3 g/l. On account of the high yeast concentration the added glucose was quickly consumed. The ethanol increased at the same time by about 1 g/l. Contrary to lactose, the disaccharides sucrose and maltose are consumed by the yeast [4]. In Figs. 10–13 the concentrations of glucose, ethanol, sucrose, and maltose, respectively, on-line monitored with the eight-channel EnFET array, are plotted as a function of the cultivation time at strong substrate limitation. One can see from the peak shapes, that glucose was consumed much quicker than sucrose and maltose. With disaccharides less ethanol was formed than with glucose. All of these on-line measured concentrations agree well with those measured off-line.

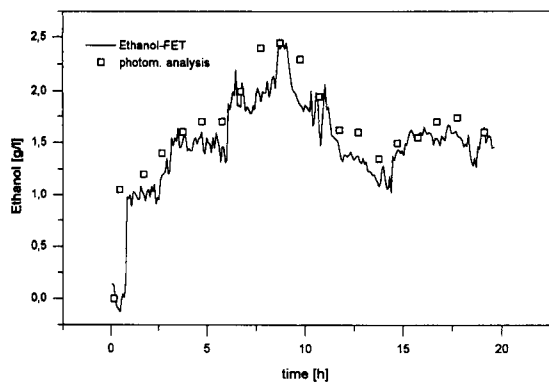


Fig. 9. On-line monitoring of the ethanol concentration with an ADH/ALDH-FET-FIA system during the cultivation of *Saccharomyces cerevisiae* DSM 2155 on synthetic medium. Spectrophotometric off-line measurements were carried out with test kit.

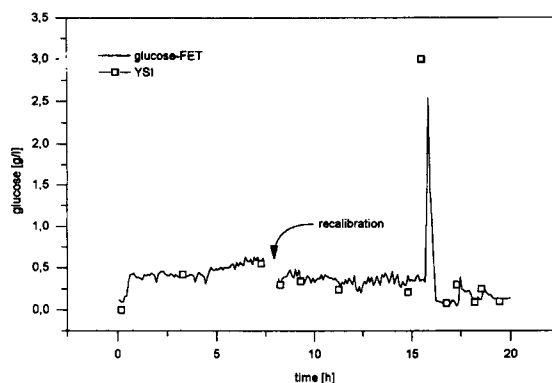


Fig. 10. On-line monitoring of glucose concentration with a GDH-FET-FIA system during the cultivation of *Saccharomyces cerevisiae* DSM 2155 on synthetic medium. At 16 h glucose was added to the medium. Off-line reference measurements were carried out with YSI equipment. The GDH-FET was recalibrated at 7.5 h.

If the buffer capacity of the culture medium changes during the cultivation a recalibration of the EnFETs is necessary.

During the run presented before, the buffer capacity changed during the cultivation. Therefore, besides an initial calibration, recalibrations were performed at intervals of 7.5 h.

In Fig. 14 the initial calibration curve for glucose is presented. This curve was described with the function:

$$f(x) = \frac{(p_1 \cdot x)}{(p_2 + x)} + p_3 \cdot x + p_4 \cdot x^2$$

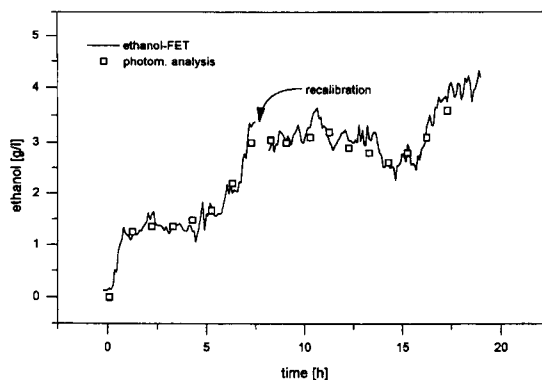


Fig. 11. On-line monitoring of ethanol concentration with an ADH/ALDH-FET-FIA system during the cultivation of *Saccharomyces cerevisiae* DSM 2155 on synthetic medium. At 15 h glucose was added to the medium. Spectrophotometric off-line reference measurements were carried out with a test kit. The ADH/ALDH-FET was recalibrated at 7.5 h.

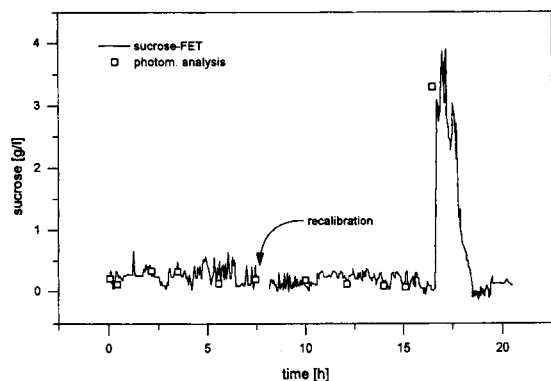


Fig. 12. On-line monitoring of sucrose concentration with an INV/GDH-FET-FIA system during the cultivation of *Saccharomyces cerevisiae* DSM 2155 on synthetic medium. At 17 h sucrose was added to the medium. Spectrophotometric off-line reference measurements were carried out with the test kit of Boehringer. The INV/GDH-FET was recalibrated at 7.5 h.

the curve fitting was carried out with a commercial program Origin<sup>®</sup> (MicroCal, 2.52):  $p_1 = 30.3$ ,  $p_2 = 7.1$ ,  $p_3 = 2.4$ ,  $p_4 = -0.2$ .

The recalibrations were performed with internal standards (Fig. 15). The glucose concentration was obtained from the intersection of the extrapolated calibration curve with the abscissa. In this run the differences between the original and recalibrated concentration values were only very small. This has to be checked and eliminated.

### 3. Discussion

The combination of different enzymes in an enzyme array can be impaired by the dissimilar pH optima of the enzymes. The selection of the proper enzymes and the optimum pH value of the carrier flow are critical for the high performance of the enzyme array detector.

When using a single channel, the signal fluctuation caused by the steep concentration gradient and the small area (0.25 mm<sup>2</sup>) of the particular enzyme membranes can be considerable. The use of at least two channels with the same enzyme is recommended.

On account of the close distance between the enzyme membranes and the potentiometric transducers (gates of the field effect transistors), the local and instantaneous variations of the pH value caused by the reaction in a particular enzyme membrane can influence the reaction rate in another membrane and its signal as well,

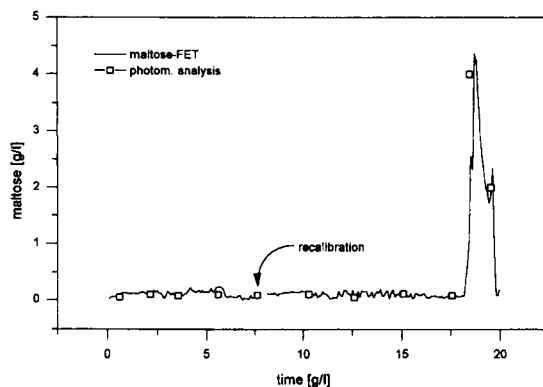


Fig. 13. On-line monitoring of maltose concentration with a MAL/GDH-FET-FIA system during the cultivation of *Saccharomyces cerevisiae* DSM 2155 on synthetic medium. At 18 h maltose was added to the medium. Spectrophotometric off-line reference measurements were carried out with a test kit of Boehringer. The MAL/GDH-FET was recalibrated at 7.5 h.

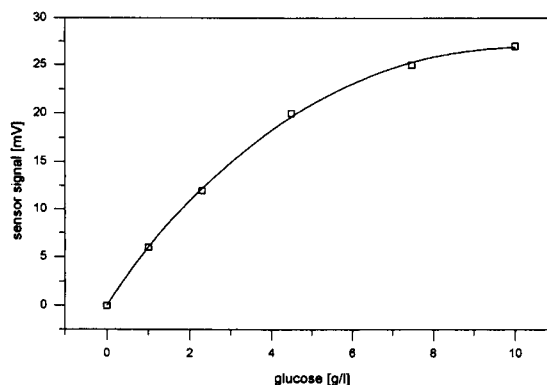


Fig. 14. Calibration graph of glucose in the concentration range between 1 and 10 g/l with GDH-FET-FIA system at the beginning of the cultivation.

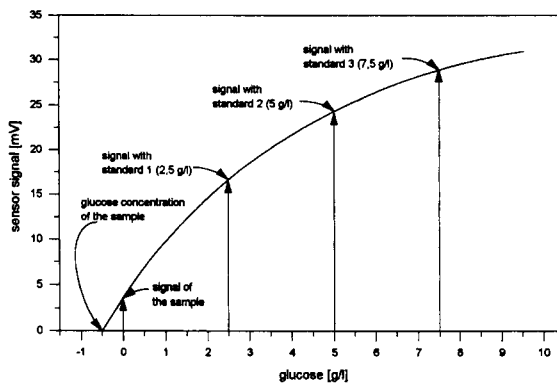


Fig. 15. Recalibration of the GDH-FET with internal standards in intervals of 7.5 h by adding glucose solution to the sample.



if the latter is positioned downstream from it. This cross-sensitivity has to be checked and eliminated by the use of a proper carrier flow and a proper sequence of the enzyme membranes. The validation of the signals with model media of known composition is absolutely necessary. On account of the short response time of the bioFET–FI systems, the sensor array signals are suitable for process control. When using four different membranes in a FI system for process monitoring, the price of the FI system per analyte is about US \$ 10,000, which is a reasonable price.

#### 4. Conclusion

The sensor array consisting of a single pH-FET and seven EnFET channels integrated into a single flow-injection system is well suitable for the on-line monitoring of the pH and several medium components simultaneously during the cultivation of microorganisms. Glucose, lactose, maltose, sucrose, ethanol and urea were monitored with the multichannel EnFET–FI

system using (co)immobilized GDH,  $\beta$ -GAL/GALDH, MAL/GDH, INV/GDH, ADH/ALDH and urease on the pH sensitive gate of eight FETs during the cultivation of *E. coli* and *S. cerevisiae*, respectively.

#### Acknowledgements

The authors gratefully acknowledge the financial support of the Ministry of Research and Technology of the Federal Republic of Germany, Bonn. Project No. 03164 OOA.

#### References

- [1] T. Kullick, M. Beyer, J. Henning, T. Lerch, C. Menzel, A. Zeitz, B. Hitzmann, T. Scheper and K. Schügerl, *Anal. Chim. Acta*, in press.
- [2] T. Kullick, Dissertation, University of Hannover, 1993.
- [3] F. Rütter, Dissertation, University of Hannover, 1991.
- [4] N.B. Trivedi, G.K. Jacobson and W. Tesch, *Bakers Yeast*, CRC Critical Reviews in Biotechnology, Vol. 4(1) 1993, pp. 75–109.



ELSEVIER

Analytica Chimica Acta 300 (1995) 33–43

ANALYTICA  
CHIMICA  
ACTA

# Role of axial ligation on potentiometric response of Co(III) tetraphenylporphyrin-doped polymeric membranes to nitrite ions

Elzbieta Malinowska<sup>1</sup>, Mark E. Meyerhoff\*

*Department of Chemistry, The University of Michigan, Ann Arbor, MI 48109, USA*

Received 8 June 1994

## Abstract

Two types of Co(III) tetraphenylporphyrins, Co(III)TPPX (I) and Co(III)(N)TPPX (II), where  $X = \text{Cl}^-$  or  $\text{NO}_2^-$  and  $\text{N} = \text{C}_5\text{H}_5\text{N}$  or  $\text{C}_6\text{H}_5\text{CH}_2\text{C}_5\text{H}_4\text{N}$ , are used as ionophores to prepare nitrite responsive polymeric membrane electrodes. The influence of the initial axial ligand ( $X^-$  and N) on the operative ionophore mechanism of these metalloporphyrins within the solvent polymeric membranes is examined. Results from potentiometric and electroanalysis experiments suggest that in the presence of nitrite in the test sample and internal solution, both types of Co(III) porphyrins studied (I and II) act as neutral carriers and that the addition of lipophilic cationic sites (e.g., tridodecylmethylammonium ions ( $\text{TDMA}^+$ )) to the organic membrane is essential to improve the selectivity and long term stability of sensors prepared with these species. Membranes formulated with (I) or (II) in the nitrite form along with TDMACl in plasticized PVC films exhibit the following selectivity sequence:  $\text{SCN}^- > \text{NO}_2^- \sim \text{ClO}_4^- > \text{Sal}^- > \text{NO}_3^- > \text{Br}^- > \text{Cl}^-$ . Membrane electrodes with added lipophilic cationic sites are shown to exhibit rapid, fully reversible and Nernstian response towards nitrite ions in the concentration range of  $10^{-1}$ – $10^{-5}$  M, with good long term stability.

**Keywords:** Ion-selective electrodes; Nitrite; Ionic sites; Selectivity; Metalloporphyrins

## 1. Introduction

It is now well established that the use of metalloporphyrins as ionophores in solvent/polymeric membrane electrodes can induce potentiometric anion selectivity patterns that differ significantly from the classical ‘‘Hofmeister’’ pattern observed for membranes doped with typical quaternary ammonium type anion exchangers. Such non-Hofmeister selectivity has been ascribed to the selective axial ligation between the metal centers in given porphyrins and certain anions

[1–9]. Among the porphyrins studied to date, two types of Co(III) porphyrins, one with [1,7,9] and one without [8] pyridine as a neutral second axial ligand have been suggested as ionophores for preparing sensors that exhibit potentially useful analytical selectivity towards thiocyanate and nitrite ions. In addition to Co(III) porphyrins, membrane electrodes prepared with analogous Co(III) cobyrinates [10–13] have also been shown to respond preferentially toward nitrite and thiocyanate ions, again presumably via selective axial coordination of these species with the central Co(III) ion. Interest in sensors with enhanced selectivity for nitrite has increased recently owing the discovery of the endogenous enzyme nitric oxide synthase (NOS) which catalyzes the oxidation of arginine to nitric oxide

\* Corresponding author.

<sup>1</sup> On leave from the Department of Analytical Chemistry, Warsaw Technical University, Poland.

and citrulline in a variety of human cells. The liberated NO reacts rapidly with water and oxygen to generate nitrite and nitrate ions [14,15]. Consequently, sensors, especially microelectrodes, that could detect nitrite or nitrate in the presence of large excess of chloride found in biological fluids could aid in understanding the multifaceted role of NO synthase in physiological processes.

Some of the previously reported membrane electrodes for nitrite formulated with Co(III) porphyrins have exhibited unusual response properties, including sigmoidal anion response functions and sub-Nernstian response slopes, even over a relatively narrow anion activity range [1,7]. Further, membranes prepared with Co(III) TPPSCN were reported to deteriorate significantly with respect to nitrite response function after soaking overnight in a nitrite solution [8]. This observation contradicts all current theories regarding the response of ion-selective electrodes toward primary ions. Only in the case of membranes doped with Co(III)(N)TPPBr (where N=pyridine) has a conventional log-linear nitrite response function been observed with a nearly theoretical slope and a selectivity for nitrite over chloride similar to that documented by Schulthess et al. [11] for the Co(III) cobyrinate-based sensors. However, significant EMF drift for freshly prepared membranes was observed and the long-term stability of such electrodes was not examined [9]. Thus, depending on the exact ligation form of the Co(III) porphyrins incorporated into polymeric membranes, varying nitrite response characteristics have been reported. It should be noted that the Co(III) porphyrins used in these previous studies were not initially in their nitrite form and the membranes did not contain lipophilic additives. It therefore appears that the precise chemistry leading to nitrite response of such membranes is not yet fully understood and further studies are warranted if analytical response characteristics of such sensors are to be improved (e.g., by changing the structure of the porphyrin, adding lipophilic ionic sites, etc.) to meet the growing need with respect to potentially monitoring NOS activity in biological systems.

It is known that the oxidation state of the metal center within the metalloporphyrin structure can dictate the possible mechanism for the interaction of anions with such ionophores at the sample/membrane interface [16]. When the metal center is in a +2 oxidation state, the overall charge on the metalloporphyrin in the

membrane is zero and thus the complex can act as a neutral carrier (i.e., interaction with anion forms negatively charged complex). On the other hand, if the metal center is in a +4 oxidation state only a charged carrier type mechanism can be responsible for potentiometric anion response (i.e., complex with analyte anion is neutral). When the stable oxidation state of the metal, however, is +3, either a charged or a neutral mechanism can be envisioned, depending on the preferred coordination number of the central metal ion and the nature of the coordinating ligands (neutral axial ligands, e.g., pyridine, water, other solvents and/or anions).

Knowledge of the operative mechanism of the metalloporphyrin based sensors is critical since optimization of membrane permselectivity is highly dependent on the incorporation of additional membrane components. Indeed, recently it has been demonstrated that the presence of lipophilic electrically charged additives improves the potentiometric behavior of certain anion-selective electrodes [7,17–19], including ones prepared with metalloporphyrins and cobyrinates. The type of additive required depends on the carrier mechanism involved. Electrode performance and selectivity is enhanced by the addition of tetraphenylborate derivatives when the anion ionophore serves as a charged carrier, while tetraalkylammonium species are required as additives to optimize the response characteristics of membranes doped with ionophores that function as anion selective neutral carriers.

Herein we report on the influence of the initial axial ligands of Co(III) tetraphenylporphyrin when used as an ionophore in plasticized PVC membranes to prepare nitrite responsive electrodes, and demonstrate that regardless of the initial ligand present, optimum response toward nitrite can only be achieved when tetraalkylammonium salts are added to the membrane formulation. This observation strongly suggests that all Co(III) porphyrins function as neutral carrier type ionophores within the organic membrane phase of such nitrite sensors.

## 2. Experimental

### 2.1. Reagents

Chloro(5,10,15,20-tetraphenylporphyrinato) cobalt(III) (Co(III)TPPCL), and its pyridine

(Co(III)(py)TPPCL) and benzylpyridine (Co(III)(bpy)TPPCL) derivatives were synthesized in accordance with previously published procedures [9,20,21]. The nitrite forms of the Co(III)TPP complexes were prepared by ion-exchange [9]. The final products were identified and characterized using TLC and CHN analyses. For polymer membrane preparation, *o*-nitrophenyloctylether (*o*-NPOE), dioctyl adipate (DOA), potassium tetrakis[bis(*m*-trifluoromethyl)phenyl]borate (KTFPB), tridodecylmethylammonium chloride (TDMACl), poly(vinyl chloride) (PVC, high mol.wt.), tetrahydrofuran (THF, distilled prior to use) were purchased from Fluka (Ronkonkoma, NY).

All aqueous solutions were prepared with salts and acids of the highest purity available. The sample solutions for all potentiometric measurements consisted of sodium salts of the given anions in 0.05 M 4-morpholinoethanesulfonic acid (MES), adjusted to the desired pH with NaOH.

## 2.2. ISE membranes and EMF measurements

Ion-selective electrode membranes containing 1 wt.% porphyrin and different amounts of ionic additives (KTFPB or TDMACl) in *o*-NPOE/PVC or DOA (2:1) were prepared as described previously [22]. Potentiometric measurements were performed with the following galvanic cell: Ag/AgCl/bridge electrolyte/sample/ion-selective membrane/inner filling solution/AgCl/Ag. The bridge electrolyte consisted of 0.1 M KNO<sub>3</sub>. The inner filling solution for the nitrite electrodes was a 0.01 M NaNO<sub>2</sub>/0.1 M NaCl solution, unless otherwise indicated. Prior to EMF measurements, the electrodes were conditioned overnight in a solution having the same composition as the inner filling solution.

All experiments were performed at ambient temperature (22 ± 2°C). Potentials were measured using a Macintosh IIcx computer with an NB-MIO-16X analog/digital input/output board (National Instruments, Austin, TX) and a custom built electrode interface module controlled by Lab-View 2 software (National Instruments) [23]. Potentiometric selectivity coefficients were determined according to the separate solution method [24] by using the experimental EMF values obtained for 0.1 M solutions of the test anions and a theoretical slope of -59.2 mV dec<sup>-1</sup> for the

primary anion. Activity coefficients were assumed to be constant for all analyte anions, and no correction was made for the slight changes in the liquid junction potential of the reference electrode.

## 2.3. Electrodialysis experiments

PVC membranes were prepared as described previously [22], using 1 wt.% Co(III)TPPCL or Co(III)TPPNO<sub>2</sub>, 66 wt.% *o*-NPOE and 33 wt.% PVC. For some experiments TDMACl was also added (100 mol-% relative to the ionophore). The cast membranes were approximately 150 μm thick. If needed (experiments with perchlorate and thiocyanate ions) membranes doped with Co(III)TPPCL were pre-treated for 12 h with a 1 M aqueous solutions of sodium perchlorate or thiocyanate, then rinsed with water and dried. Five Co(III)TPPX-doped (X = Cl<sup>-</sup>, ClO<sub>4</sub><sup>-</sup>, NO<sub>2</sub><sup>-</sup> or SCN<sup>-</sup>) polymer membranes were stacked against each other and mounted in a Plexiglas dialysis block. Approximately 5 ml of 0.1 M sodium salt of the appropriate anion, prepared in MES buffer, pH 5.5, was pipetted onto the cathode and anode sides of the membrane stack. A constant dc potential of 80 V was applied across the membrane stack for approximately 2 h. After electrodialysis, the membranes were separated, and a 0.5 cm<sup>2</sup> area was cut from the center of each membrane and weighed on an analytical balance. The membrane samples were then dissolved separately in 20 ml of fresh distilled THF and the absorbance of these solutions was measured at the λ<sub>max</sub> for the Soret band of the given Co(III)TPPX used. Absorption measurements were performed on a Perkin Elmer (Lambda 4B) UV/VIS spectrophotometer. The solution absorbance was then normalized to the cut membrane's weight. For each experiment, a sample of a non-electrodialyzed membrane, prepared in the exact same manner as the membranes subjected to electrodialysis, was analyzed to determine the initial porphyrin concentration in the membrane. Similar experiments were performed for membranes containing Co(III)TPPNO<sub>2</sub> and 100 mol-% (relative to the ionophore) of TDMACl. In this case, membranes were bathed in 1 M NaNO<sub>2</sub> solution on both sides followed by the same assay procedure described above.

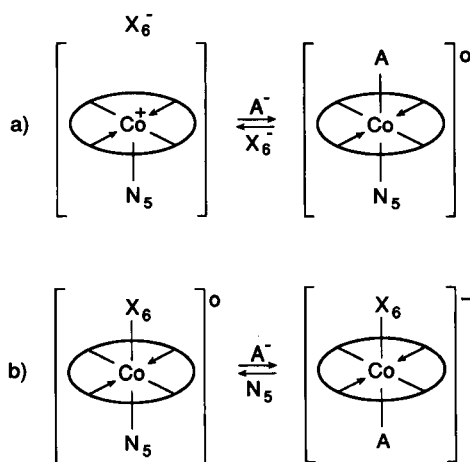


Fig. 1. Schematic representation of equilibria involved in possible charged (a) and neutral carrier (b) mechanisms for Co(III) porphyrins doped in polymeric membranes;  $N_5$ , a neutral axial ligand,  $X_6^-$ , an anionic axial ligand and  $A^-$ , an analyte anion.

#### 2.4. Ion-exchange experiments

To obtain direct spectral evidence of the ion-exchange ligation reactions that can occur with the various Co(III) porphyrins, the absorbance spectra of membranes prepared with Co(III) TPPCl, *o*-NPOE and PVC (wt.% as described above) were obtained after soaking for 12 h in 0.1 M solutions of perchlorate, chloride, nitrite or thiocyanate ions (sodium salts). Prior to recording the spectra, the membranes were

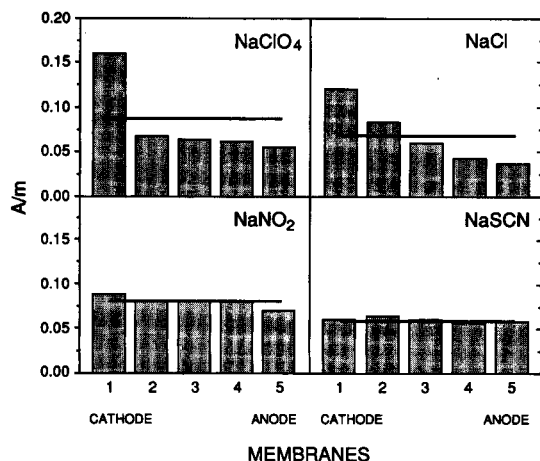


Fig. 2. Concentration profile of porphyrin in membranes after electro dialysis (at 80 V) of a stack of five Co(III) TPPX-doped membranes (*o*-NPOE/PVC = 2:1) in the presence of 0.1 M solutions of sodium salt (NaX) in 0.05 M MES buffer (pH 5.5) on each side of the stack;  $X^- = ClO_4^-, Cl^-, NO_2^-$  or  $SCN^-$ . The solid line indicates the initial distribution of Co(III) TPPX in membranes.

rinsed with water and dried. Then, 20 mg samples of each membrane were dissolved in 5 ml of fresh distilled THF and the absorbances were measured from 450 to 650 nm. For comparison purposes, membranes doped with Co(III) TPPNO<sub>2</sub> were treated in the same manner (i.e., soaked in salt solutions of perchlorate, chloride and thiocyanate ions), and the visible absorbance spectra of the dissolved films recorded.

### 3. Results and discussion

As stated previously, the oxidation state of the metal present in the porphyrin ring influences the carrier mechanism exhibited by membranes doped with metalloporphyrins. With Co(III) porphyrins, either a neutral or charged carrier mechanism is possible. The overall charge on Co(III) TPP complexes is +1, and thus the cobalt metal center, which generally has a coordination number of 6, is capable of binding two axial ligands. Schematic structures of the Co(III) porphyrin complex and the possible equilibria involving anions and neutral ligands are depicted in Fig. 1. From these equilibria it is readily apparent that a charged carrier mechanism ((a) in Fig. 1) is only possible when the Co(III) TPPX salt doped within the membrane can dissociate significantly. On the other hand, a neutral carrier mechanism would govern the response of membranes if an anion ( $X_6^-$ ) is tightly held by the metal center and the neutral ligand ( $N_5$ ) is exchangeable with the analyte anion, thereby forming a complex with two axially coordinated anionic ligands and an overall charge of -1 ((b) in Fig. 1). The specific nature of the axial ligands present in the Co(III) tetraphenylporphyrin structure may thus play an important role in determining which ionophore mechanism is operative in membranes doped with these species. For this reason, experiments described below included studies with Co(III) tetraphenylporphyrins that had both strong (e.g., pyridine derivatives) and weak neutral ligands (e.g., H<sub>2</sub>O or other solvents).

To assess, qualitatively, the operative mechanism of the Co(III) porphyrins in PVC membranes, electro dialysis experiments were conducted in the presence of various anions. Electro dialysis experiments are very useful in determining the specific charge of ion-ionophore complexes within polymer membrane phases [13,25,26]. As shown in Fig. 2, somewhat different

concentration profiles for the stack of five membranes is observed depending on which Co(III) TPPX species is present within the membranes and which anion is present in the solutions bathing both sides of the membranes. These results may be explained in terms of different degrees of anion coordination to the Co(III) center. As shown, in the presence of perchlorate, the Co(III) porphyrin accumulates at the cathodic side membrane and is depleted from the anodic side of the membrane stack. This suggests that under the influence of an electric field (80 V), the resulting current is carried primarily by a positively charged, uncomplexed porphyrin, Co(III) TPP<sup>+</sup>, in the polymer films. That is, Co(III) TPPClO<sub>4</sub> is dissociated significantly in the polymer membrane phase. The same result, albeit less dramatic, is observed for chloride ions. However, in the presence of nitrite and thiocyanate bathing anions, essentially flat concentration profiles of the Co(III) porphyrin in the stack of membranes is observed. This observation indicates that nitrite and thiocyanate anions coordinate directly and strongly to the cobalt ion in the tetraphenylporphyrin forming an essentially neutral complex in the membrane. From these electro dialysis data alone, one would conclude that the previously reported potentiometric response of Co(III) porphyrin-based membranes to nitrite and thiocyanate may be controlled by varying mechanisms depending on which counterion is present within the ionophore structure and/or membrane phase.

However, if in fact the Co(III) porphyrins function as charged carriers with respect to interactions with nitrite and thiocyanate, then in accordance with recent theory [17], the potentiometric selectivity and response properties of such membranes should improve significantly upon addition of lipophilic anionic sites to the membrane phase (e.g., tetraphenylborate derivatives). Indeed, it was found that freshly prepared membranes containing Co(III) TPPCl and anionic additives (KTFPB; 10–80 mol-%), when not conditioned in nitrite/thiocyanate solutions, and without nitrite (or thiocyanate) in the internal filling solution (i.e., only NaCl), do exhibit high potentiometric selectivity for nitrite and thiocyanate over most other anions tested, including perchlorate (see Fig. 3a). However, with such fresh membranes the slope of the calibration curves for both nitrite and thiocyanate are much greater than theoretical ( $> -100 \text{ mV dec}^{-1}$ ) and a stable potential upon addition of nitrite to the test solution is

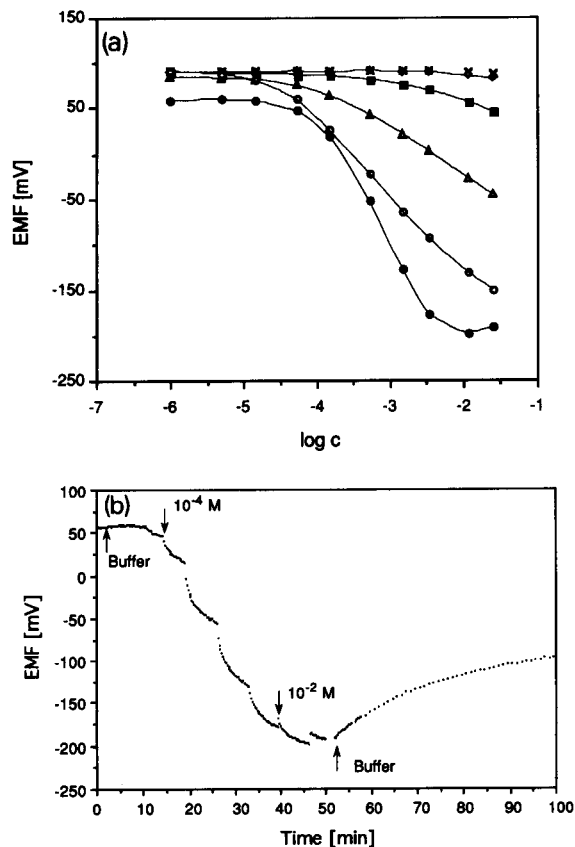


Fig. 3. (a) Potentiometric response of membrane electrode prepared with a membrane containing 1 wt.% Co(III) TPPCl, 30 mol-% (relative to the ionophore) KTFPB in DOA/PVC (2:1) to various anions in MES buffer, pH 5.5; (×) chloride, (◇) nitrate, (□) perchlorate, (△) salicylate, (○) thiocyanate, (●) nitrite (note: a 0.1 M NaCl solution was used as a internal electrolyte and as the conditioning solution); (b) dynamic response of electrode in (a) toward increasing nitrite concentrations and reversibility in buffer solution.

not achieved even after several minutes (Fig. 3b). Moreover the recovery time (response back to baseline) is very long (hours) and even repeated washings with buffer and sodium chloride does not return the membrane electrode to the initial baseline EMF value. Further, with repeated exposure to nitrite solutions, the electrode response deteriorates dramatically. The same unusual results are obtained for membranes prepared without lipophilic additives suggesting that the known endogeneous anionic site impurities present in the PVC membrane material [27,28] probably function in a manner analogous to the added lipophilic anionic sites.

The observed nitrite induced deterioration of the response characteristics of the membranes doped with

Co(III)TPPX species (with and without anionic membrane additives) suggests that some irreversible change of the ionophore takes place when the membranes are exposed to nitrite anions in the test solution. This change may also alter the mechanism by which the ionophore interacts with given anions. In fact, the addition of sodium nitrite into the internal electrolyte of the electrode and/or conditioning these membranes in a nitrite solutions causes the electrode to become cation responsive (data not shown). Spectrophotometric measurements can be used to establish that anion-exchange of the Co(III)TPP complexes definitely occurs within the membrane phase. The electronic absorption spectra of metalloporphyrins are useful for this purpose, since they are quite sensitive to the variations in central metal ion coordination [29]. Ligand exchange experiments were carried out on intact membranes of the same composition as those used to prepare electrodes in order to mimic more closely the conditions encountered during potentiometric measurements (see Experimental). The results showed that perchlorate ( $\lambda_{\max} = 542.6$  nm), chloride ( $\lambda_{\max} = 542.0$  nm) and thiocyanate ( $\lambda_{\max} = 541.5$  nm) of the Co(III)TPP complex can be readily displaced by nitrite ( $\lambda_{\max} = 539.1$  nm) in the membrane phase, while only thiocyanate is capable of displacing nitrite ions ( $\lambda_{\max} = 540.5$  nm) from the Co(III)TPP complex. Clearly, in the presence of nitrite, the Co(III)TPPX species is converted to the Co(III)TPPNO<sub>2</sub> form within the membrane phase, and this structure does not appear to interact with anions via a charged carrier mechanism. That is, the first nitrite ligand binds so tightly that it cannot enter into a reversible equilibrium with sample/internal solution nitrite ions. Based on these results it is concluded that membranes prepared with Co(III)TPPCL with or without KTFPB additives are not analytically useful for fabricating nitrite ion-selective electrodes.

The high affinity of the Co(III) porphyrin ionophore for nitrite ions is most likely explained by the ability of Co(III) to form  $\sigma$ - $\pi$  bonds with certain ligands. This phenomenon has been reported for Co(III) complexes in aqueous solutions [30,31] and should also be possible within the plasticized polymeric membrane phase of electrodes. The  $\sigma$  component of this double bond arises from the sharing of an electron pair originally present on the donor atom (ligand) while the  $\pi$  component originates from the "back-donation" of an

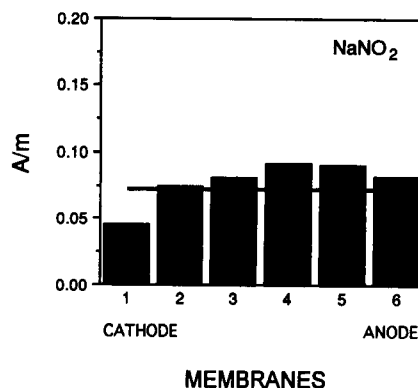


Fig. 4. Concentration profile of Co(III) porphyrin in membranes after electrodiagnosis of six membranes containing Co(III)TPPNO<sub>2</sub> and 100 mol-% of TDMACl relative to the ionophore (*o*-NPOE/PVC = 2:1). Both sides of the stack of membranes were bathed in a 0.1 M solution of NaNO<sub>2</sub> in 0.05 M MES buffer (pH 5.5).

electron pair from the central metal ion into the empty orbitals of a ligand which possesses suitable symmetry. In published reports, nitrite is quite distinct among various ligands in its ability to undergo  $\sigma$ - $\pi$  bonding [30].

Because nitrite coordinates so strongly with the cobalt(III) metal center through such  $\sigma$ - $\pi$  binding, it is likely that the only way to obtain theoretical and reversible nitrite or thiocyanate response for electrodes prepared with membranes containing Co(III) porphyrins is for nitrite (or thiocyanate) to also bind as a sixth ligand, thereby creating a negatively charged complex. Indeed, if Co(III)TPPNO<sub>2</sub> behaves as a neutral carrier (see Fig. 1b, where X and A are both nitrite), then only the presence lipophilic cationic additives should improve electrode performance. Indeed, preliminary studies [19] have already shown that membranes doped with Co(III)TPPCL along with TDMACl do exhibit reversible potentiometric response to nitrite with nearly theoretical response slopes in the 10<sup>-5</sup> to 10<sup>-1</sup> M range of nitrite concentration even after extensive conditioning in test solutions containing nitrite. For membranes containing 10–52 mol-% (relative to the ionophore) of TDMACl, the electrode function, detection limit, selectivities (data shown in [19]) and response time (a few seconds) are essentially the same. When the TDMACl levels go above 80 mol-%, the behavior of the electrode approaches that of a membrane formulated with TDMACl alone (i.e., Hofmeister selectivity). As shown in Fig. 4, electrodiagnosis experiments performed for the membranes containing Co(III)TPPNO<sub>2</sub> and 100 mol-% TDMACl in *o*-

NPOE/PVC reveal a gradual decrease in porphyrin content in the cathodic direction indicating that the presence of TDMA<sup>+</sup> ions in the membrane helps favor the formation of a negatively charged Co(III) porphyrin complex with nitrite. This provides further evidence that a neutral carrier mechanism is responsible for nitrite response when cationic sites are present in the membrane phase.

While cationic sites must be added to membranes formulated with Co(III) TPPX type structures to obtain significant and reproducible nitrite response, the situation is somewhat different when Co(III)(N) TPPX species are employed as ionophores (where N = pyridine or benzylpyridine). Indeed, it is well known that in non-aqueous solutions, many metalloporphyrins form pyridine complexes [20,32]. Unfortunately, there is no clear information about the affinity of pyridine (or benzylpyridine) to Co(III) porphyrins when nitrite is also present. Thus, when porphyrins with neutral pyridine and other organic bases are used as the initial ionophore within the polymer membranes, the mechanism of nitrite response could differ from the case without the aromatic base present. Indeed, membranes formulated with the pyridine and benzylpyridine derivatives alone (no additives) do exhibit significant potentiometric response to nitrite and this response deteriorates over a much longer period of time than membranes prepared with Co(III) TPPX species alone. For example, in the case of membrane electrodes prepared with pure CoTPPNO<sub>2</sub> and no additive, the observed slope toward nitrite is about  $-47 \text{ mV dec}^{-1}$  with freshly prepared membranes, but this response decreases dramatically to  $-23 \text{ mV dec}^{-1}$  for the second calibration run. In contrast, electrodes prepared with Co(III)(py) TPPNO<sub>2</sub> and Co(III)(bpy) TPPNO<sub>2</sub> doped membranes decrease in slope from  $-54$  to  $-30 \text{ mV dec}^{-1}$  and  $-56$  to  $-42 \text{ mV dec}^{-1}$  respectively, but only after a 2 week period of continuous use (see Fig. 5 for Co(III)(bpy) TPPX case). Further the response times, reversibility, and selectivity of such electrodes in their response to nitrite are more similar to electrodes prepared with membranes containing Co(III) TPPX plus TDMACl.

These observations are consistent with the results reported by Li and Harrison [9] who showed that membranes doped with Co(III)(py) TPPBr do exhibit reasonably good potentiometric response to nitrite, although the lifetime of such response was not exam-

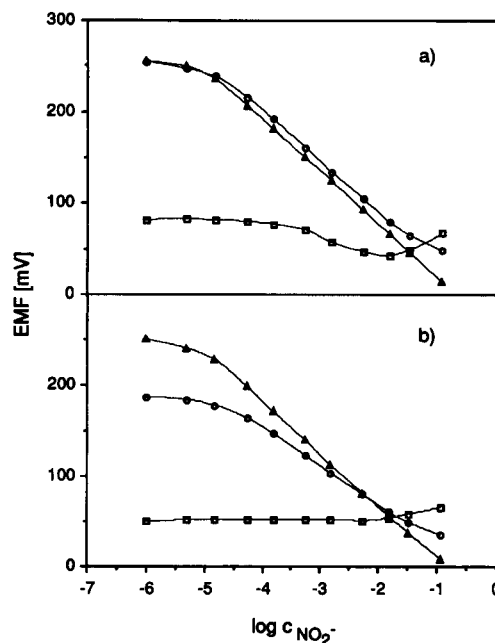


Fig. 5. Effect of age on potentiometric nitrite response of membrane electrode prepared with a membrane containing 1 wt.% Co(III)-(bpy)TPPCL in NPOE/PVC (2:1) in MES buffer, pH 5.3; (a) freshly prepared membrane electrode conditioned in a 0.01 M NaNO<sub>2</sub> solution for 24 h and (b) 2 week old membrane electrode: (O) without additives, (□) 8 mol-% (relative to the ionophore) of KTFPB, (Δ) 9 mol-% of TDMACl.

ined in detail. The origin of this response, however, now becomes clearer. Scheidt et al. [33] have suggested that nitrogen bases coordinated to Co(III)TPP can be easily dissociated when the second axial ligand is a nitrosyl ligand. They imply that the strength of the  $\sigma$ - $\pi$  bond between Co(III) and NO<sup>-</sup> is responsible for a decrease interaction of the nitrogen base. A similar process may take place within the membranes when the porphyrin pyridine derivatives are employed as ionophores. That is, the strong interaction of nitrite with Co(III)(N) TPP<sup>+</sup> structures can cause significant dissociation of the original base ligand. Considering that the pH of the aqueous test solutions used here is  $< 6$  and that the  $pK_a$  of pyridine is 5.25, a significant fraction of the initially bound pyridine could be protonated within the membrane phase and concomitantly begin to leach slowly into the sample solution as the membrane is conditioned in nitrite. Most importantly, however, the free protonated pyridine or benzylpyridine in the organic membrane phase can now serve as a counter cation site for the formation of negatively



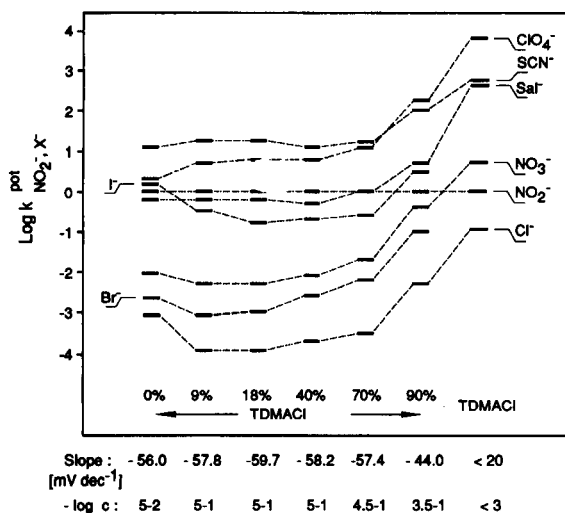


Fig. 6. Selectivity coefficients,  $\log k_{\text{NO}_2^-, X}$ , for electrodes prepared with polymeric membranes containing Co(III)(bpy)TPPNO<sub>2</sub> and different concentrations (mol-% relative to the ionophore) of TDMACl additive in *o*-NPOE/PVC (2:1). For comparison purposes, the results for membranes based on TDMACl alone in *o*-NPOE/PVC (2:1) are presented in the last column. Data for observed slopes and log concentration range of nitrite over which electrode yields linear EMF response are included.

charged Co(III)(TPP)(NO<sub>2</sub>)<sub>2</sub><sup>-</sup> complex. Thus, membranes formulated with Co(III)(N)TPPX type structures alone do appear to function as nitrite selective films only because protonated forms of the original base ligand provide the required sites for the porphyrins to serve as neutral carriers with respect to their interaction with nitrite. Unfortunately, the relative hydrophilicity of pyridinium and benzylpyridinium cations causes their gradual loss from the membrane phase, yielding sensors that cannot operate by the preferred neutral carrier mechanism over long periods of time. Fig. 6 illustrates how the potentiometric selectivity, response slope and linear response range of electrodes formulated with Co(III)(bpy)TPPX doped PVC membrane change as the amount of cationic additive salt (TDMACl) increases. These results exhibit the same trend as is observed for membranes containing Co(III)TPPX and TDMACl [19]. At the same time the long term stability with respect to potentiometric nitrite response is enhanced considerably (see Fig. 5). Non-anionic response to nitrite in the presence of KTFPB (Fig. 5) also indicates that neutral carrier mechanism occurs when the pyridine derivatives of Co(III)TPP are used as the ionophore in the membrane. Consequently, the preferred membrane for-

mulations for nitrite sensing should consist of a Co(III)TPPX or Co(III)(N)TPPX type structures in conjunction with added lipophilic cation species (e.g., TDMA<sup>+</sup>).

When using Co(III)TPPX or Co(III)(N)TPPX along with TDMACl to prepare nitrite sensitive membrane electrodes, where X is not nitrite, the pre-conditioning time in a nitrite solution is critical to obtain reproducible potentiometric response. Only after bathing in a nitrite solution for an extended period of time (to replace the initial X ligand), will a Nernstian response over a wide range of nitrite concentrations be observed. Li and Harrison [9], using a novel spatial imaging photometer (ISP), reported on the transport of NO<sub>2</sub><sup>-</sup> in polymer membranes containing Co(III)(py)TPPBr. They concluded that for a typical membrane thickness of 200 μm it would take about 0.5 h for the two diffusion fronts of penetrating NO<sub>2</sub><sup>-</sup>, coming from symmetric solutions on both sides of membranes, to meet in the middle of the membrane, and about 8 h to reach 99% of its equilibrium value at the membrane center. Observations made in this work indicate that nearly 12 h of conditioning in 0.01 M nitrite solution is required to achieve initial analytical performance comparable to membranes formulated initially with the nitrite form of the porphyrin structure.

To further prove that Co(III)TPPNO<sub>2</sub> can be successfully employed as a stable ionophore to prepare nitrite selective electrodes, and that previous problems with the electrochemical behavior of membranes doped with various Co(III) porphyrins was due, in large part,

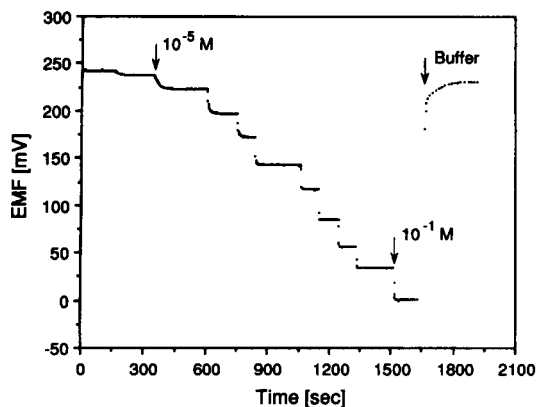


Fig. 7. Typical dynamic potentiometric response to nitrite and recovery time for a 1 month old electrode prepared with membrane containing Co(III)TPPNO<sub>2</sub> (1 wt.%) and TDMACl (10 mol-% relative to the ionophore) in *o*-NPOE/PVC (2:1).

Table 1

Potentiometric properties of  $\text{NO}_2^-$ -selective electrodes based on *o*-NPOE/PVC (2:1) membranes doped with Co(III)[TPP] $\text{NO}_2$  (1 wt.%) and TDMACl (10 mol-% relative to the ionophore) as cationic additive (data are means  $\pm$  S.D. for 3 electrodes)

	Slope <sup>a</sup> (mV dec <sup>-1</sup> )	$E^0$ (mV)	DL <sup>b</sup>	$\log k_{\text{NO}_2^-, Y}^{\text{pot}}$ for <sup>c</sup>					
				$\text{Cl}^-$	$\text{Br}^-$	$\text{NO}_3^-$	$\text{Sal}^-$	$\text{ClO}_4^-$	$\text{SCN}^-$
Fresh	$-58.4 \pm 0.2$	$-47.3 \pm 0.5$	$-5.1 \pm 0.1$	-4.0	-3.2	-2.6	-1.0	0.2	1.0
2 Months	$-57.2 \pm 0.3$	$-50.7 \pm 0.9$	$-4.8 \pm 0.1$	-3.7	-2.8	-2.2	-0.4	0.8	1.2

<sup>a</sup> With a constant background of 0.05 M MES buffer, pH 5.2.

<sup>b</sup> DL = detection limit,  $\log c_{\text{NO}_2^-}$ .

<sup>c</sup> SSM method, the selectivity coefficients calculated for 0.1 M solutions.

to a lack of knowledge regarding the exact anion carrier mechanism involved, membrane electrodes prepared with 1 wt.% Co(III)TPPNO<sub>2</sub>, 10 mol-% (relative to the ionophore) of TDMACl in *o*-NPOE/PVC (2:1) were studied for more than 2 months. Data, including the selectivity, detection limit, slope, etc., for three such electrodes tested over this 2 month period are presented in Table 1. As shown, the analytical performance of such electrodes remain relatively stable over the two month time period. Fig. 7 illustrates the dynamic response of such an electrode used repeatedly for almost 1 month. As can be seen, the response time and

reversibility remain excellent owing to the presence of lipophilic cation sites in the membrane.

Since it has been reported previously [4,34,35] that metalloporphyrin based anion selective membrane electrodes can exhibit significant pH response, the pH sensitivity of the optimized (with TDMACl) nitrite sensitive membranes was examined. From Fig. 8 it can be seen that the detection limit of the electrode depends on the sample pH. This can be explained by hydroxide ion interference, caused by a strong competing ligation reaction of OH<sup>-</sup> with NO<sub>2</sub><sup>-</sup> as a ligand on the central Co(III) ion of the porphyrin. Because HNO<sub>2</sub> is a weak acid ( $\text{p}K_a = 3.37$ ), reducing the pH to a value < 4 actually results in an increase in the EMF value of the electrode for a given sample total nitrite concentration, owing to the decrease concentration of nitrite under such conditions. Therefore, the combination of hydroxide interference and formation of HNO<sub>2</sub> at low pH, makes the useful pH range for these electrodes rather narrow (pH 4.0–5.5).

In comparison with Co(III) cobyrinates, which clearly have been shown to operate via a charged carrier mechanism [17], and exhibit optimum anion selectivity when 10–60 mol-% KTFPB is added to the membrane, polymer membranes doped with Co(III)TPPNO<sub>2</sub> and TDMACl exhibit a similar preference for nitrite and thiocyanate ions over all other anions tested except for highly lipophilic ClO<sub>4</sub><sup>-</sup> and I<sup>-</sup>. For these anions, the value of  $\log k_{\text{NO}_2^-, X^-}$  are higher by more than 2 units. Thus, at this point, the use of Co(III) cobyrinates operating via a charge carrier mechanism appear to yield somewhat more selective

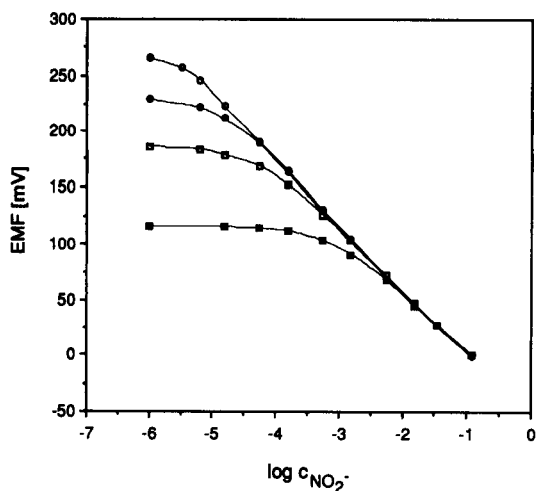


Fig. 8. The effect of sample pH on the potentiometric response to nitrite of electrodes prepared with membranes containing Co(III)TPPNO<sub>2</sub> (1 wt.%) and TDMACl (10 mol-% relative to the ionophore) in *o*-NPOE/PVC (2:1); (○) pH 4.5, (●) pH 5.5, (□) pH 6.8, (■) pH 7.4.

membranes than films doped with Co(III) porphyrins, which as shown above, clearly function as neutral carriers.

#### 4. Conclusions

Co(III) porphyrins behave as charged carriers in membrane electrodes only if a counterion (e.g.,  $\text{Cl}^-$ ) is distinctly dissociated from the cobalt center. These electrodes show good selectivity towards  $\text{NO}_2^-$  and  $\text{SCN}^-$  even in the presence of such lipophilic anions as  $\text{ClO}_4^-$ . However, the response of these electrodes is attributed to a non-equilibrium steady-state ion-exchange at the membrane/sample interface, whereby extraction of nitrite into the bulk of the membrane occurs. This extraction produces a different coordination state of the Co(III) metal center and as a consequence, a change in the operative response mechanism takes place. This hypothesis explains why membranes containing Co(III)TPPCL alone as the ionophore exhibit super-Nernstian responses to  $\text{NO}_2^-$  and  $\text{SCN}^-$  ions during the initial stages of use, and then rather quickly lose response toward these anions. Since the ligation of nitrite ions to the Co(III) center is very strong, Co(III)TPPNO<sub>2</sub> formed within the membrane exists as a neutral molecule. This species can then extract a second nitrite anion from the sample solution to form a negatively charged complex. However, this new complex can only be stabilized within the membrane phase if lipophilic counter cations are added to the membrane formulation. A similar situation is observed in the case of Co(III) porphyrins possessing a neutral base as an initial axial ligand (e.g., pyridine derivatives). However, as shown here, membranes formulated with such species can yield analytically useful short term response toward nitrite even in the absence of added cationic sites. This is now ascribed to the ability of dissociated base species to protonate in the membrane thus serving as the required cationic sites.

#### Acknowledgements

We gratefully acknowledge the National Institutes of Health (GM-28882) and the State Committee for Scientific Research (Project No. 2 0775 91) (Poland) for supporting this work.

#### References

- [1] D. Ammann, M. Huser, B. Kräutler, B. Rusterholz, P. Schulthess, B. Lindemann, E. Halder and W. Simon, *Helv. Chim. Acta*, 69 (1986) 849.
- [2] N.A. Chaniotakis, A.M. Chasser, M.E. Meyerhoff and J.T. Groves, *Anal. Chem.*, 60 (1988) 188.
- [3] A. Jyo and H. Egawa, *Anal. Sci.*, 8 (1992) 823.
- [4] N.A. Chaniotakis, S.B. Park and M.E. Meyerhoff, *Anal. Chem.*, 61 (1989) 566.
- [5] C.E. Kibbey, S.B. Park, G. Deadwyler and M.E. Meyerhoff, *J. Electroanal. Chem.*, 335 (1992) 135.
- [6] S.B. Park, W. Matuszewski, M.E. Meyerhoff, Y.H. Liu and K.M. Kadish, *Electroanalysis*, 3 (1991) 909.
- [7] M. Huser, W.E. Morf, K. Fluri, K. Seiler, P. Schulthess and W. Simon, *Helv. Chim. Acta*, 73 (1990) 1481.
- [8] A. Hodinár and A. Jyo, *Chem. Lett.*, (1988) 993.
- [9] X. Li and D.J. Harrison, *Anal. Chem.*, 63 (1991) 2168.
- [10] P. Schulthess, D. Ammann, W. Simon, C. Caderas, R. Stepánek and B. Kräutler, *Helv. Chim. Acta*, 67 (1984) 1026.
- [11] P. Schulthess, D. Ammann, B. Kräutler, C. Caderas, R. Stepánek and W. Simon, *Anal. Chem.*, 57 (1985) 1397.
- [12] R. Stepánek, B. Kräutler, P. Schulthess, B. Lindeman, D. Ammann and W. Simon, *Anal. Chim. Acta*, 182 (1986) 83.
- [13] M. Huser, W.E. Morf, K. Seiler, P. Schulthess and W. Simon, *Helv. Chim. Acta*, 73 (1990) 1481.
- [14] M.A. Marletta, A. Tayeh and J.M. Hevel, *BioFactors*, 2 (1990) 219.
- [15] S. Archer, *FASEB J.*, 7 (1993) 349.
- [16] H. Yim, C.E. Kibbey, S. Ma, D.M. Kliza, D. Lu, S.B. Park, C. Espadas-Torre and M.E. Meyerhoff, *Biosensors Bioelectron.*, 8 (1993) 1.
- [17] U. Schaller, E. Bakker, U.E. Spichiger and E. Pretsch, *Anal. Chem.*, 66 (1994) 391.
- [18] M. Rothmaier and W. Simon, *Anal. Chim. Acta*, 271 (1993) 135.
- [19] E. Bakker, E. Malinowska, R. Schiller and M.E. Meyerhoff, *Talanta*, (1994) in press.
- [20] H. Sugimoto, N. Ueda and M. Mori, *Bull. Chem. Soc. Jpn.*, 54 (1981) 3425.
- [21] T. Sakurai, K. Yamamoto, H. Naito and N. Nakamoto, *Bull. Chem. Soc. Jpn.*, 49 (1976) 3042.
- [22] P. Anker, E. Wieland, D. Ammann, R.E. Dohner, R. Asper and W. Simon, *Anal. Chem.*, 53 (1981) 1970.
- [23] M. Telting-Diaz, M.E. Collison and M.E. Meyerhoff, *Anal. Chem.*, 66 (1994) 576.
- [24] G.G. Guilbault, R.A. Durst, M.S. Frant, H. Freiser, E.H. Hansen, T.S. Light, E. Pungor, G. Rechnitz, N.M. Rice, T.J. Rohm, W. Simon and J.D.R. Thomas, *Pure Appl. Chem.*, 48 (1976) 127.
- [25] K. Fluri, J. Koudelka and W. Simon, *Helv. Chim. Acta*, 75 (1992) 1012.
- [26] T.M. Nahir and R.P. Buck, *Helv. Chim. Acta*, 76 (1993) 407.
- [27] E. Lindner, E. Graf, Z. Niegreis, K. Tóth, E. Pungor and R.P. Buck, *Anal. Chem.*, 60 (1988) 295.

- [28] A. van den Berg, P.D. van der Wal, M. Skowronska-Ptasinska, E.J.R. Sudhölter, D.N. Reinhoudt and P. Bergveld, *Anal. Chem.*, 59 (1987) 2827.
- [29] B.D. Berezin, *Coordination Compounds of Porphyrins and Phthalocyanines*, Wiley, New York, 1981.
- [30] M.M. Jones, *Elementary Coordination Chemistry*, Prentice-Hall, 1964.
- [31] J.E. Huheey, *Inorganic Chemistry*, Harper and Row, New York, 1978.
- [32] R.M. Izatt, J.S. Bradshaw, K. Pawlak, R.L. Bruening and B.J. Tarbet, *Chem. Rev.*, 92 (1992) 1261.
- [33] W.R. Scheidt and J.L. Hoard, *J. Am. Chem. Soc.*, 12 (1973) 8281.
- [34] D. Brown, N. Chaniotakis, I. Lee, S. Ma, S. Park and M. Meyerhoff, *Electroanalysis*, 1 (1989) 477.
- [35] A. Hodinar and A. Jyo, *Anal. Chem.*, 61 (1989) 1171.

# Ion-selective electrode measurements for the determination of formation constants of alkali and alkaline earth metals with low-molecular-weight ligands

Alessandro De Robertis \*, Patrizia Di Giacomo, Claudia Foti

*Dipartimento di Chimica Inorganica, Analitica e Struttura Molecolare, Università, Salita Sperone 31, I-98166 S. Agata di Messina, Italy*

Received 25 April 1994; revised manuscript received 26 August 1994

## Abstract

Formation constants of acetate, hydrogencarbonate, malonate, citrate and 1,2,3-propanetricarboxylate complexes with  $\text{Na}^+$ ,  $\text{K}^+$  and  $\text{Ca}^{2+}$  were determined potentiometrically using sodium, potassium and calcium selective electrodes, at 25°C and at different ionic strengths, in the range  $0 < I \leq 1$  M. Formation constants obtained by ion-selective electrode (ISE) measurements were compared with those obtained by different techniques. It has been found that the use of ISEs gives reliable results in the study of weak complexes, also under non-constant ionic strength conditions.

*Keywords:* Ion-selective electrodes; Alkali and alkaline earth metals

## 1. Introduction

In speciation studies of natural and biological fluids using thermodynamic models, the knowledge of formation constants of the complex species which may be formed between the various components present into the considered system, is of fundamental importance. Since alkali and alkaline earth cations are generally present in significant amounts in all natural and biological fluids, together with several inorganic and organic ligands, precise evaluation of the relative interactions is essential, and knowledge of the relative thermodynamic parameters (i.e., the formation constants of the complex species) makes this possible. With this premise in mind we have, over the last decade, systematically studied the formation and stability of weak complexes between alkali and alkaline earth metal ions

with low-molecular-weight carboxylic ligands [1–10], inorganic anions [11–13], and amino acids [14,15]. The technique was that of proton displacement, using a glass electrode as the indicator (pH-metric titrations) [16,17]. In order to confirm previous results, a different and possibly direct experimental technique could be helpful; moreover, in some cases, the proton displacement method is not suitable, and therefore other experimental techniques must be used anyhow.

Ion-selective electrodes (ISEs) have been widely used for several years for quantitative analysis, and several papers, compilations and books have been published [18–20]. The performances of ISEs have been carefully checked and, in general, quite good results have been obtained. Also, in the field of formation constant determinations, it has been shown that these electrodes can be used with good results, but, owing to a series of difficulties, their use has been limited to a few systems only.

\* Corresponding author.

Here we report a potentiometric study with sodium, potassium and calcium selective electrodes on the systems Na-(ac), Na-HCO<sub>3</sub>, Na-(mal), Na-(cit), Na-(tca), K-(cit), Ca-Cl, Ca-NO<sub>3</sub>, Ca-(ac), Ca-(mal), Ca-(tca) [(ac) = acetate, (mal) = malonate, (cit) = citrate, (tca) = tricarallylate, 1,2,3-propanetricarboxylate], in aqueous solution, at  $T = 25^{\circ}\text{C}$ , and  $I \leq 0.9$  M for Na complexes,  $I \leq 0.6$  M for K complexes and  $I \leq 1.0$  M for Ca complexes.

## 2. Experimental

### 2.1. Materials and potentiometric equipment

Solutions of NaCl, NaClO<sub>4</sub>, NaHCO<sub>3</sub>, NaNO<sub>3</sub>, Na(ac), Na<sub>3</sub>(cit) and KCl were prepared by weighing the corresponding salt (Carlo Erba, Fluka or Aldrich, purity > 99.6%), previously vacuum-dried; when necessary, concentrations were also checked using the Na-ISE electrode. Malonic and tricarallylic acids (Fluka, purity > 99.6%) were used without further purification. A Ca(NO<sub>3</sub>)<sub>2</sub> solution was prepared from the analytical reagent Fluka and standardized with EDTA [21]. (Me<sub>4</sub>N)Cl and (Me<sub>4</sub>N)NO<sub>3</sub> [(Me<sub>4</sub>N)<sup>+</sup> = tetramethylammonium cation] solutions were prepared from solid salts, previously recrystallized from a mixture of acetone-ethanol (90:10). A (Me<sub>4</sub>N)OH (Fluka) solution was standardized against potassium biphthalate (Fluka puriss grade). Standard solutions of tetramethylammonium salts of (ac)<sup>-</sup>, (mal)<sup>2-</sup>, (cit)<sup>3-</sup>, (tca)<sup>4-</sup> were prepared by total neutralization (glass electrode) of the corresponding acid (Fluka or Carlo Erba, analytical grade) with standard (Me<sub>4</sub>N)OH. All solutions were prepared by using doubly distilled water and grade A glassware, and were protected from atmospheric CO<sub>2</sub> by using soda lime traps.

To measure the free concentration of Na<sup>+</sup>, K<sup>+</sup> and Ca<sup>2+</sup>, two different potentiometers were used: an Amel Model 337 and a Metrohm model E654. The following ISEs, by Orion, were used: combination Ross type Model 86-11 for Na<sup>+</sup>; liquid membrane Models 93-19 and 93-20 for K<sup>+</sup> and Ca<sup>2+</sup>, respectively. As reference, an Ag/AgCl double junction Orion Model 90-02 was used. The instrumental resolution was 0.2 mV and the reproducibility  $\pm 2\%$  for all the systems. The titrant solutions were delivered by a Model 665 Metrohm

Table 1

Some experimental details for the calibration titrations of Na-, K- and Ca-ISEs in the various systems, at  $T = 25^{\circ}\text{C}$

System	Titant (M)	$\Delta I$ (M) <sup>a</sup>	$\Delta pM$ (M) <sup>b</sup>	No.
Na-(ac)	NaClO <sub>4</sub> 0.9934	0.02–0.29	0.54–1.66	4
	NaClO <sub>4</sub> 1.970	0.02–0.52	0.28–1.71	2
	NaCl <sup>c</sup> 2.005	0.27–0.37	0.86–1.74	5
Na-HCO <sub>3</sub>	NaClO <sub>4</sub> 1.970	0.008–0.52	0.28–2.09	6
	NaCl <sup>c</sup> 2.004	0.26–0.66	0.33–2.40	4
Na-(mal)	NaCl <sup>c</sup> 2.008	0.005–0.94	0.29–2.45	5
Na-(cit)	NaClO <sub>4</sub> 1.970	0.01–0.52	0.28–2.00	6
	NaCl <sup>c</sup> 2.008	0.02–0.68	0.30–2.74	8
Na-(tca)	NaCl <sup>c</sup> 2.004	0.26–0.63	0.36–2.40	6
K-(cit)	KCl <sup>c</sup> 1.519	0.15–0.51	0.39–2.38	4
Ca-Cl	Ca(NO <sub>3</sub> ) <sub>2</sub> <sup>d</sup> 0.3925	0.01–0.27	1.88–2.69	7
	Ca(NO <sub>3</sub> ) <sub>2</sub> <sup>d</sup> 0.3925	0.10–0.13	1.89–3.73	11
Ca-(mal)	Ca(NO <sub>3</sub> ) <sub>2</sub> <sup>e</sup> 0.3925	0.01–0.71	1.39–4.23	13
Ca-(tca)	Ca(NO <sub>3</sub> ) <sub>2</sub> <sup>e</sup> 0.3925	0.04–0.53	1.55–3.78	7

<sup>a</sup> Ionic strength intervals.

<sup>b</sup> Concentration intervals of M (M = Na<sup>+</sup>, K<sup>+</sup>, Ca<sup>2+</sup>).

<sup>c</sup> In the presence of (Me<sub>4</sub>N)Cl as ISA.

<sup>d</sup> In the presence of NaNO<sub>3</sub> as ISA.

<sup>e</sup> In the presence of (Me<sub>4</sub>N)NO<sub>3</sub> as ISA.

motorized burette having a minimum reading of 1  $\mu\text{l}$  and a reproducibility of  $\pm 2 \mu\text{l}$ .

### 2.2. Procedure

As reported in the enclosures, ISE measurements are highly dependent on the ionic strength ( $I$ ) of the solution. Since our measurements are carried out at different ionic strength values, and vary substantially during the experiments, it was first necessary to verify whether the equation for the dependence of activity coefficients on ionic strength, later described, fits all potentiometric experimental points. Therefore tests were performed by adding large amounts of standard solution of NaClO<sub>4</sub> (727 experimental points,  $\Delta I = 0.006$ – $0.54$ ,  $\Delta pNa = 0.27$ – $2.22$ ) or KCl (415 experimental points,  $\Delta I = 0.15$ – $0.51$ ,  $\Delta pK = 0.39$ – $2.38$ ) or Ca(NO<sub>3</sub>)<sub>2</sub> (552 experimental points,  $\Delta I = 0.020$ – $0.71$ ,  $\Delta pCa = 1.39$ – $4.23$ ) to distilled water (eventually with ionic strength adjustor, ISA) and by collecting the corresponding potentiometric (mV) values.

Table 2

Some experimental details for the measurement titrations of the various systems with Na-, K- and Ca-ISEs, at  $T = 25^\circ\text{C}$ 

System	Titrant (M)	Concentration (mM) in vessel	$\Delta I$ (M) <sup>a</sup>	$\Delta\text{pM}$ <sup>b</sup>	No. <sup>c</sup>
Na-(ac)	Na(ac) 0.6390	–	0.003–0.24	0.62–2.28	4
	Na(ac) 2.125	–	0.006–0.44	0.35–2.23	2
	NaCl 2.005	(Me <sub>4</sub> N)(ac) <sup>d</sup> 53.0–148.4	0.10–0.68	0.30–2.43	5
Na-HCO <sub>3</sub>	NaHCO <sub>3</sub> 0.1003	–	0.03–0.05	1.32–2.08	6
	NaCl 2.004	NaHCO <sub>3</sub> <sup>d</sup> 55.9–181.8	0.06–0.67	0.23–1.55	4
Na-(mal)	(Me <sub>4</sub> N) <sub>2</sub> (mal) 0.2383	NaCl <sup>d</sup> 76.4–568.9	0.08–0.94	0.30–1.35	5
Na-(cit)	Na <sub>3</sub> (cit) 0.5062	–	0.01–0.35	0.63–2.10	6
	(Me <sub>4</sub> N) <sub>3</sub> (cit) 0.2512	NaCl <sup>d</sup> 76.3	0.09–0.42	1.13–1.47	3
	NaCl 2.008	(Me <sub>4</sub> N) <sub>3</sub> (cit) <sup>d</sup> 52.6	0.47–0.70	0.34–2.57	5
Na-(tca)	NaCl 2.004	(Me <sub>4</sub> N) <sub>3</sub> (tca) <sup>d</sup> 26.8–56.0	0.37–0.71	0.32–2.51	6
K-(cit)	KCl 1.519	(Me <sub>4</sub> N) <sub>3</sub> (cit) <sup>d</sup> 28.5–44.6	0.17–0.56	0.42–2.50	4
Ca-Cl	(Me <sub>4</sub> N)Cl 1.794	Ca(NO <sub>3</sub> ) <sub>2</sub> 10.6–14.4	0.04–0.44	1.88–2.11	3
	NaCl 2.000	Ca(NO <sub>3</sub> ) <sub>2</sub> <sup>e</sup> 9.5–12.6	0.10–0.48	1.99–2.28	4
Ca-(ac)	Na(ac) 0.8147	Ca(NO <sub>3</sub> ) <sub>2</sub> <sup>e</sup> 5.2–16.5	0.10–0.41	1.91–2.88	11
Ca-(mal)	(Me <sub>4</sub> N) <sub>2</sub> (mal) 0.2471	Ca(NO <sub>3</sub> ) <sub>2</sub> <sup>f</sup> 3.9–51.0	0.02–0.71	1.39–3.17	13
Ca-(tca)	(Me <sub>4</sub> N) <sub>3</sub> (tca) 0.3040	Ca(NO <sub>3</sub> ) <sub>2</sub> <sup>f</sup> 6.4–38.2	0.07–1.14	1.57–3.09	7

<sup>a</sup> Ionic strength intervals.<sup>b</sup> Concentration intervals of M (M = Na<sup>+</sup>, K<sup>+</sup>, Ca<sup>2+</sup>).<sup>c</sup> Number of titrations.<sup>d</sup> In the presence of (Me<sub>4</sub>N)Cl as ISA.<sup>e</sup> In the presence of NaNO<sub>3</sub> as ISA.<sup>f</sup> In the presence of (Me<sub>4</sub>N)NO<sub>3</sub> as ISA.

Some experimental details for the calibration of ISEs and for measurement titrations, were reported in Tables 1 and 2, respectively. For the study of Na<sup>+</sup> complexes, solutions containing [(Me<sub>4</sub>N)<sub>n</sub>(X)]<sup>0</sup> [X<sup>n-</sup> = (ac)<sup>-</sup>, (mal)<sup>2-</sup>, (cit)<sup>3-</sup>, (tca)<sup>4-</sup>] were titrated with standard NaCl, or vice versa. As regards the K<sup>+</sup>-(cit) system, solutions containing [(Me<sub>4</sub>N)<sub>3</sub>(cit)]<sup>0</sup> were titrated with standard KCl. In the case of Ca<sup>2+</sup> complexes, the solutions under analysis were titrated with [(Me<sub>4</sub>N)<sub>n</sub>(X)]<sup>0</sup>. For each titration, separate calibrations were performed to calculate the formal potential,  $E^0$ , and the slope,  $s_E$ . (Me<sub>4</sub>N)NO<sub>3</sub> or (Me<sub>4</sub>N)Cl or NaNO<sub>3</sub> were used as ISA; minute quantities of (Me<sub>4</sub>N)OH were added to all solutions in order to reach the required pH values. In many cases, the same solutions were used first for the calibration and then for the titration (internal calibration).

### 2.3. Calculations

Calculations were performed by using the non-linear least squares computer program BSTAC [22]. This program is able to refine analytical concentrations, electrode constants ( $E^0$ ,  $s_E$ ), complex formation con-

stants and parameters for the dependence of formation constants on ionic strength. By using this program, calculations can be performed on potentiometric data arising from different types of electrodes (glass electrode, ISE for anions and cations) and the variations in ionic strength during the titration can be taken into consideration.

The dependence of formation constants on ionic strength was taken into account by using the Debye-Hückel type equation [23]

$$\log = \log T\beta - z^* \sqrt{I} / (2 + 3\sqrt{I}) + CI + DI^{3/2} \quad (1)$$

where  $\beta$  = overall formation constant at ionic strength  $I$ ,  $T\beta$  = formation constant at infinite dilution;  $C$  and  $D$  are empirical parameters to be determined for each system, and are independent of the chemical nature of the reactants, depending only on the stoichiometry of the reaction according to:

$$C = c_0 p^* + c_1 z^*; \quad D = dz^* \quad (2)$$

and

Table 3

Overall formation constants  $\beta^a$  for the formation of  $\text{Na}^+$ ,  $\text{K}^+$  and  $\text{Ca}^{2+}$  ligand complexes, and comparison with literature data, at  $T=25^\circ\text{C}$ 

Ligand	$p^a$	$\log \beta_p(\text{Na}^+)$				
		This paper	Literature	$I$ (M)	Ref.	Anal. Condit.
$\text{Cl}^-$	1	$-0.60 \pm 0.04^b$		0		
		-0.77		0.16		
		-0.73	-0.59	0.50	[13]	Lit. anal.
$\text{HCO}_3^-$	1	$0.12 \pm 0.02$	0.16	0	[25]	$\text{H}_2$ elec.
		-0.06		0.16		
$\text{ac}^-$	1	$-0.07 \pm 0.06$		0		
		-0.25		0.16		
		-0.24	-0.27	0.25	[4]	Glass
		-0.21	-0.27	0.49	[26]	Glass
$\text{mal}^{2-}$	1	$0.90 \pm 0.01$		0		
		0.54		0.16		
		0.53	0.57	0.25	[4]	Glass
$\text{cit}^{3-}$	1	$1.43 \pm 0.02$		0		
		0.93	1.03	0.1	[6]	Glass
		0.88		0.16		
		0.93	0.70	0.1	[27]	ISE
$\text{cit}^{3-}$	2	$2.31 \pm 0.02$		0		
		1.47	1.48	0.1	[6]	Glass
		1.39		0.16		
$\text{tca}^{3-}$	1	$1.30 \pm 0.02$		0		
		0.75		0.16		
$\text{tca}^{3-}$	2	0.74	0.82	0.25	[28]	Glass
		$2.00 \pm 0.02$		0		
		1.05		0.16		
		1.07	1.04	0.25	[28]	Glass

Ligand	$p^a$	$\log \beta_p(\text{K}^+)$				
		This paper	Literature	$I$ (M)	Ref.	Anal. Condit.
$\text{Cl}^-$	1	$-0.51 \pm 0.06^c$		0		
		-0.69		0.16		
		-0.68	-0.50	0.5	[13]	Lit. anal.
$\text{cit}^{3-}$	1	$1.42 \pm 0.05$		0		
		0.92	0.90	0.1	[6]	Glass
		0.87		0.16		
		0.92	0.59	0.1	[27]	ISE
$\text{cit}^{3-}$	2	$1.95 \pm 0.06$		0		
		1.11	1.03	0.1	[6]	Glass
		1.04		0.16		

$$p^* = \sum p_{\text{reactants}} - \sum p_{\text{products}}$$

$$z^* = \sum z_{\text{reactants}}^2 - \sum z_{\text{products}}^2$$

where  $p$  and  $z$  are the stoichiometric coefficients and charges, respectively. The values previously found [23] for empirical parameters are  $c_0=0.10$ ,  $c_1=0.23$  and  $d=-0.1$ . To take into consideration the depend-

ence of  $E^0$  on ionic strength [16] we have used an equation similar to Eq. 1, with identical values of empirical parameters:

$$E^{0'} = E^0 + s_E[-\sqrt{I} / (2 + 3\sqrt{I}) + CI + DI^{3/2}] \quad (3)$$

where  $E^{0'}$  = standard potential at ionic strength  $I$ .



Table 3 (continued)

Ligand	$p^a$	$\log \beta_p(\text{Ca}^{2+})$							
		This paper	Literature	$I$ (M)	Ref.	Anal. Condit.			
$\text{Cl}^-$	1	$0.43 \pm 0.08$	0.40	0	[13]	Lit. anal.			
		0.07		0.16					
$\text{NO}_3^-$	1	$0.70 \pm 0.05^d$	0.68	0	[24]	Solubility			
		$0.72 \pm 0.05^c$		0					
		0.34		0.16					
$\text{ac}^-$	1	$1.12 \pm 0.02$	0.93	0	[4]	Glass			
				1.12			0	[29]	Glass
				1.24			0	[30]	Glass
		0.76		0.48 <sup>f</sup>			0.16	[31]	ISE
$\text{mal}^{2-}$	1	$2.50 \pm 0.03$	2.39	0	[4]	Glass			
		1.83		1.51 <sup>g</sup>			0.1	[32]	Glass
		1.76					0.16		
$\text{tca}^{3-}$	1	$3.17 \pm 0.07$	2.12	0	[28]	Glass			
		2.05		0.16					
		2.03		0.25					
$\text{tca}^{3-}$	2	$4.5 \pm 0.2$	2.87	0	[28]	Glass			
		3.0		0.16					
		3.0		0.25					

<sup>a</sup> Formation constants refer to the reaction:  $p\text{M}^{n+} + \text{L}^{z-} = \text{M}_p\text{L}^{(np-z)}$  ( $\text{M}^{n+} = \text{Na}^+, \text{K}^+, \text{Ca}^{2+}$ );  $\beta_p = [\text{M}_p\text{L}^{(np-z)}] / [\text{M}^{n+}]^p [\text{L}^{z-}]$ .

<sup>b</sup> Errors are expressed as  $\pm 3$  times standard deviation.

<sup>c</sup> Obtained together in the study of the K–(cit).

<sup>d</sup> Obtained in the study of the Ca–(tca) system.

<sup>e</sup> Obtained in the study of the Ca–Cl system.

<sup>f</sup> 0.15 M NaCl medium.

<sup>g</sup>  $\text{NaClO}_4$  medium.

### 3. Results and discussion

The first results to take into consideration are those relative to the tests carried out (see Procedure) for the dependence of  $E^0$  on ionic strength. Assuming  $\text{NaClO}_4$  to be completely dissociated,  $\log {}^T\beta(\text{KCl}) = -0.29$  [13] and  $\log {}^T\beta(\text{CaNO}_3) = 0.68$  [24], we have calculated the experimental values of  $C$  (Eqs. 1–3):  $C_{\text{exp}} = 0.327 \pm 0.006, 0.325 \pm 0.009$  and  $1.012 \pm 0.008$  (errors expressed in terms of reproducibility) for Na-ISE, K-ISE and Ca-ISE, respectively. Predicted values are  $C = 0.32$  for  $\text{Na}^+$  and  $\text{K}^+$ , and 1.02 for  $\text{Ca}^{2+}$ , and this suggests that we can use the tested ISEs, and the Eqs. 1–3 in studies of complex formation constants with data deriving from ISE measurements, under variable ionic strength conditions. A typical experiment performed with ISE to calculate formation constants comprises the following steps. (a) Electrode calibration, obtained by addition of  $\text{M}^{n+}$  to pure water or to a solution containing a salt which does not interact with

the ligand under study (if the cation of the background salt interacts with the ligand, the relative formation constant must be taken into account). Formal potential  $E^0$  is obtained from the plot  $E$  vs.  $p\text{M}$  and its dependence on ionic strength is calculated by Eq. 3. (b) Addition step by step of ligand solution to  $\text{M}^{n+}$  solution changes drastically the shape of  $E = f(v)$ , and the difference  $\delta$  in Fig. 1 is a measure of the complexation of  $\text{M}^{n+}$  with the ligand (L). (c) For calculations of the formation of a simple 1:1 complex we have

$$E = E^0 + s_E \log [\text{M}^{n+}]_{\text{T}}$$

before ligand addition, and after

$$E_1 = E^0 + s_E \log [\text{M}^{n+}]$$

with

$$[\text{M}^{n+}] = [\text{M}^{n+}]_1 = 10^{(E_1 - E^0)/s_E}$$

$$[\text{M}^{n+}]_{\text{T}} = [\text{M}^{n+}] + K[\text{M}^{n+}][\text{L}]$$

$$= [\text{M}^{n+}] + K[\text{M}^{n+}][\text{L}]_{\text{T}} / (1 + K[\text{M}^{n+}])$$

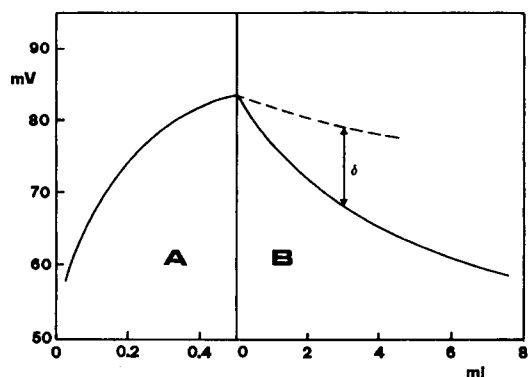


Fig. 1. Experimental values of  $E$  (mV) vs. ml of titrant (system  $\text{Ca}^{2+}$ – $\text{mal}^{2-}$ ). (A) ml of 0.3925 M  $\text{Ca}^{2+}$  added to pure water; (B) ml of 0.2479 M ( $\text{mal}^{2-}$ ) added to solution A. Dotted line represents the value of  $E$  if no complexation occurs.

where  $[M]_T$  and  $[L]_T$  are the total concentrations of the metal and ligand, respectively, from which the formation constant  $K$  can be calculated. In practice, the calculation of formation constants is obtained by suitable computer programs as reported in Experimental. The accuracy of the potentiometric systems ( $\leq 2\%$ ) indicates approximately the accuracy of formation constants, i.e.,  $\pm 0.01$  log units. In practice other experimental factors (errors in analytical concentrations, in particular) may render this error a higher value, but it represents the order of magnitude for the formation constant found.

Table 3 reports the equilibrium constant values found for  $\text{Na}^+$ ,  $\text{K}^+$  and  $\text{Ca}^{2+}$  complexes with different types of ligands at different ionic strength values, and a comparison between our own and literature data, the latter being obtained with various techniques or by literature analysis.

If we take the formation constant values of  $\text{Na}^+$ ,  $\text{K}^+$  and  $\text{Ca}^{2+}$  complexes into consideration, we come to the following considerations. (1) The estimated errors in stability constant values (expressed as  $\pm 3$  times the standard deviation) are generally very low [this error (see above discussion) is compatible with the accuracy of the experimental apparatus], with an average of  $\pm 0.04$ ; this indicates that the results, at least statistically, are correct. Only the stability constant of the  $[\text{Ca}_2(\text{tca})]^+$  complex has a significant error ( $\pm 0.2$ ) and this is because the degree of formation of the species, under our experimental conditions, is very low. (2) Concerning the stability constant of  $\text{Na}^+$ ,  $\text{K}^+$  and  $\text{Ca}^{2+}$  complexes, no significant differences were

observed between the data we derived from ISE measurements and literature data, generally obtained by pH-metric measurements (see Table 3). This behaviour shows the validity of pH-metric measurements in the determination of stability constant values by means of the proton displacement method. (3) The ISE measurements, if carried out in a suitable manner, allow us to determine the stability constants of very weak complexes, such as  $\text{NaCl}^0$  or  $\text{Na}(\text{ac})^0$  or  $\text{KCl}^0$ . (4) Eqs. 1–3, already utilized in many systems using pH-metric titrations, are also suitable for use in systems which employ macromolecules as the selective element, including those with bivalent cations.

We stress that the  $\log \beta(\text{NaCl})^0$  value is equal to that obtained from the refinement of potentiometric data deriving from titrations carried out with the Na-ISE [33], as is the  $\log \beta(\text{CaNO}_3)$  value, obtained from the refinement of data deriving from titrations designed for Ca–Cl and Ca–(tca) systems: practically there is no difference between them and the value found by Fedorov et al. [24]. Finally, the  $\log \beta(\text{KCl})^0$  value, obtained during the analysis of the K–(cit) system, is consistent with literature data [13], especially if we consider the previous data obtained from literature analysis. In any case, studies with the Cl-ISE are in progress.

## Acknowledgements

We thank CNR and MURST for financial support.

## References

- [1] P.G. Daniele, A. De Robertis, C. De Stefano, C. Rigano and S. Sammartano, *Ann. Chim. (Rome)*, 73 (1983) 619.
- [2] P.G. Daniele, A. De Robertis, C. Rigano and S. Sammartano, *Thermochim. Acta*, 72 (1984) 305.
- [3] A. De Robertis, C. De Stefano, C. Rigano and R. Scarcella, *Thermochim. Acta*, 80 (1984) 197.
- [4] P.G. Daniele, A. De Robertis, C. De Stefano, C. Rigano and S. Sammartano, *J. Chem. Soc., Dalton Trans.*, (1985) 2353.
- [5] A. Casale, A. De Robertis and S. Sammartano, *Thermochim. Acta*, 95 (1985) 15.
- [6] P.G. Daniele, A. De Robertis, C. De Stefano, A. Gianguzza and S. Sammartano, *J. Chem. Res.*, (S) 300 (M) 2316 (1990).
- [7] P.G. Daniele, A. De Robertis, C. De Stefano and S. Sammartano, *Ann. Chim. (Rome)*, 80 (1990) 117.
- [8] A. De Robertis and C. De Stefano, *Talanta*, 38 (1991) 439.

- [9] G. Cuffari, A. De Robertis, C. De Stefano and C. Foti, *J. Chem. Res.*, (S) 264 (M) 2501 (1991).
- [10] A. De Robertis, C. Foti and A. Gianguzza, *Ann. Chim. (Rome)*, 83 (1993) 485.
- [11] S. Capone, A. De Robertis, S. Sammartano and C. Rigano, *Thermochim. Acta*, 102 (1986) 1.
- [12] P.G. Daniele, A. De Robertis, C. De Stefano, A. Gianguzza and S. Sauartano, *J. Sol. Chem.*, 20 (1991) 495.
- [13] A. De Robertis, C. Rigano, S. Sammartano and O. Zerbinati, *Thermochim. Acta*, 115 (1987) 241.
- [14] A. Casale, A. De Robertis, C. De Stefano and A. Gianguzza, *Thermochim. Acta*, 140 (1989) 59.
- [15] A. De Robertis, C. De Stefano and A. Gianguzza, *Thermochim. Acta*, 117 (1991) 39.
- [16] S. Capone, A. De Robertis, C. De Stefano, S. Sammartano and R. Scarcella, *Talanta*, 34 (1987) 593.
- [17] A. De Robertis, C. De Stefano, S. Sammartano and C. Rigano, *Talanta*, 34 (1987) 933.
- [18] A. Lewenstam and A. Hulanicki, *Selective Electrode Rev.*, 12 (1990) 161.
- [19] H. Freiser (Ed.), *Ion-Selective Electrodes in Analytical Chemistry*, Vols. 1 and 2, Plenum Press, New York, 1980.
- [20] *Handbook of Ion-Selective Electrodes: Selectivity Coefficients*, CRC Press, Boca Raton, FL, 1990.
- [21] H.A. Flaschka, *EDTA Titration*, Pergamon, London, 1959.
- [22] C. De Stefano, P. Mineo, C. Rigano and S. Sammartano, *Ann. Chim. (Rome)*, 83 (1993) 243.
- [23] P.G. Daniele, A. De Robertis, C. De Stefano and S. Sammartano, in S. Alegret, J.J. Arias, D. Barceló, J. Casal and G. Rauret (Eds.), *Miscellany of Scientific Papers Offered to Enric Casassas*, Universitat Autònoma de Barcelona, Bellaterra, 1991.
- [24] V.A. Fedorov, A.M. Robov, I.I. Shmydko, N.A. Vorontsova and V.E. Mironov, *Zh. Neorg. Khim.*, 19 (1974) 1746.
- [25] F.S. Nakayama, *J. Inorg. Nucl. Chem.*, 33 (1971) 1287.
- [26] A. De Robertis, C. De Stefano, C. Rigano, S. Sammartano and R. Scarcella, *J. Chem. Res.*, (S) 42 (M) 629 (1985).
- [27] G.A. Rechnitz and S.B. Zamochnick, *Talanta*, 11 (1964) 1061.
- [28] C. De Stefano, C. Foti and A. Gianguzza, *Talanta*, in press.
- [29] D.W. Archer and C.B. Monk, *J. Chem. Soc.*, (1964) 3117.
- [30] G.H. Nancollas, *J. Chem. Soc.*, (1956) 744.
- [31] S. Glab, M. Maj-Zurawska, P. Lukomski and A. Hulanicki, *Anal. Chim. Acta*, 273 (1993) 493.
- [32] G. Ostacoli, A. Vanni and E. Roletto, *Ricerca Sci.*, 38 (1968) 318.
- [33] C. De Stefano, C. Foti, A. Gianguzza, C. Rigano and S. Sammartano, *Ann. Chim. (Rome)*, 84 (1994) 159.



ELSEVIER

Analytica Chimica Acta 300 (1995) 53–57

ANALYTICA  
CHIMICA  
ACTA

# Amperometric determination of oxidizable solutes in water with a solution exchange technique

Charles Gartske<sup>1</sup>, Calvin O. Huber\*

*Department of Chemistry, University of Wisconsin-Milwaukee, P.O. Box 413, Milwaukee, WI 53201, USA*

Received 9 May 1994; revised manuscript received 22 July 1994

## Abstract

Determination of oxidizable solutes in water is accomplished using amperometric detection in a solution exchange apparatus. The applied potential ( $E_a$ ) used is +0.5 V vs. SCE at a nickel working electrode. Electrode pretreatment is performed at -1.0 V vs. SCE. The background electrolyte is 0.1 M NaOH. Analyte solution drawn into the cell replaces background solution. No further convection occurs. Peak anodic current relative to the baseline is used as the analytical signal. The linear range extends down to 1  $\mu$ M for sucrose, diethylenetriamine, phenol, and ethanolamine. The determination time is 2 min per sample.

*Keywords:* Amperometry; Nickel oxide

## 1. Introduction

Amperometry commonly employs controlled convection. Often the reproducibility of the convection is one of the most demanding aspects of the method. The investigation described here included efforts to develop a measurement method which eliminates the need for stirring or continuous flow. Further advantages sought were small sample volume, simple operation, rapid response, and applicability to a wide array of oxidizable solutes.

The amperometric system selected for this purpose included an anodic nickel working electrode in basic solution. The analytical electrode process can be described as oxidative attack on analyte by higher

potential species on the electrode surface lattice [1–3]. Aliphatic as well as aromatic hydroxy and amine functionalities are oxidized. The rate determining step includes an alpha-hydrogen abstraction leaving a radical species. Typically, cyano and carboxylate products are produced from amine and hydroxy functionalities, respectively.

The goal for the project reported here was to design and examine the performance of a simple device for nickel oxide anodic amperometric measurements of typical organic solutes in water. Analytes were selected partly to reflect the oxidizable organic pollutants expected in waste water. The analytes chosen included sucrose (carbohydrates, cellulose, etc.), phenol (phenols), glycine, ethanolamine and diethylenetriamine (amino acids, peptides, proteins). Under the experimental conditions used, hydrocarbons can not be oxidized and so were not tested.

\* Corresponding author.

<sup>1</sup> Present address: S.C. Johnson Wax, 1525 Howe Street, Racine, WI 53403, USA.

## 2. Experimental

### 2.1. Apparatus

The diagram for the device is shown in Fig. 1. The main channel of the cell consists of 6 mm i.d. poly(vinyl chloride), Tygon(R)<sup>®</sup> tubing. The amperometric detector consisted of a three electrode system. The reference electrode was a saturated calomel electrode (Corning, Cat. No. 476350) which contacted the solution via a 1/2 inch poly(vinyl chloride) tee. The working and counter electrodes were 0.6 mm diameter nickel wires inserted through the flexible poly(vinyl chloride) Tygon(R)<sup>®</sup> tubing with a nominal working area of 0.01 cm<sup>2</sup>. The potentiostat and current follower circuits were based on operational amplifiers (device type 324) powered by two 6-V dry cell batteries. Analytical measurement readings were taken using an auto ranging ( $\pm 0.1$  mV) digital multimeter (Micronta Model 22-193) or a potentiometric strip chart recorder (Linear Model 1200). Applied potential was typically +0.5 V vs. SCE.

### 2.2. Procedure

Using the syringe (Fig. 1), background electrolyte was drawn into the cell to just above the reference electrode. Pretreatment consisted of applying  $-1.0$  V for 15 s followed by the applied analytical potential, typically +0.50 V, for 30 s. To perform the measure-

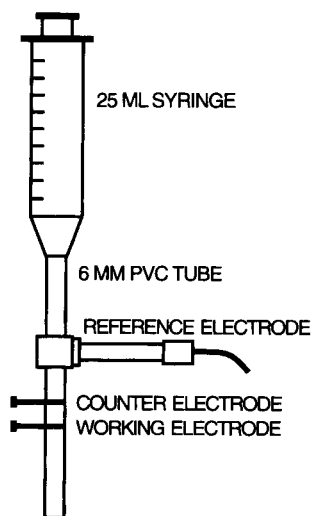


Fig. 1. Solution exchange apparatus.

ment step, 25 ml of analyte solution was drawn into the cell and the resulting current was measured. For storage between uses the cell was left dry and at open circuit.

### 2.3. Reagents

All chemicals were reagent grade. Calibration solutions were prepared using a background 0.1 M NaOH solution. Samples were adjusted to be 0.1 M in NaOH.

## 3. Results and discussion

Initial tubing diameters were chosen to be small, typically 1–2 mm i.d., in order to minimize sample volume. Very poor precision was encountered. Careful visual examination showed gas build-up at the working and counter electrode surfaces. At the working electrode (anode) the background current includes oxidation of water to produce oxygen gas. Correspondingly, hydrogen gas is produced at the counter electrode. In the case of smaller tubing diameters, the overall ratio of low polarity tubing surface area to solution volume is large. This encourages the build-up of oxygen and hydrogen bubbles at the electrode surfaces where bubble formation, with occasional dislodging, prevents good precision. With larger tubing diameters the ratio of tubing surface area to solution volume decreases, resulting in decreased bubble formation. 6 mm i.d. poly(vinyl chloride), Tygon(R)<sup>®</sup> tubing was found to be adequate to prevent bubble formation, while not requiring prohibitively large sample volumes.

### 3.1. Transient response signal shape

The analytical response current/time profiles are shown in Fig. 2. At the higher concentrations, a sharp maximum decays to a plateau value. At medium concentrations the peaks become less sharp, and at low concentration the analytical signal is a step response.

These anodic currents have been shown by Fleishmann et al. [1] to be principally controlled by surface reaction kinetics rather than by mass transport. Accordingly, in non-stirred solution horizontal current vs. time response would be expected and were observed for concentrations below a few tenths millimolar. At higher concentrations initial peaks were seen. These peaked responses were attributed either to mass transport influ-

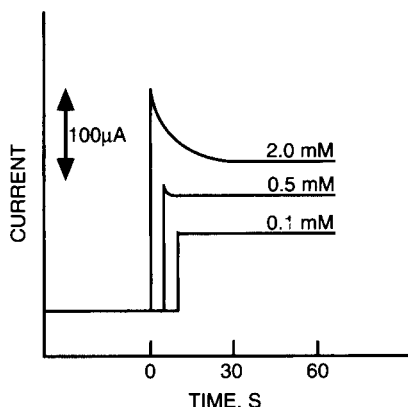


Fig. 2. Time-dependent response for sucrose solutions.

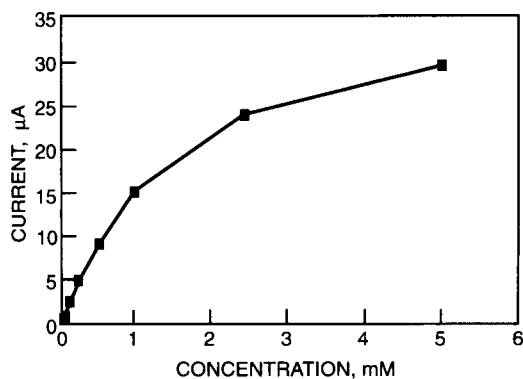


Fig. 3. Amperometric response for sucrose.

ences or to product desorption kinetics. The former were considered unlikely, because estimation of the apparent diffusivity using the profile shown in Fig. 2 for 2 mM concentration yielded a value of  $5 \times 10^{-6}$ , indicating a rate about an order of magnitude lower than diffusion control in the solution phase, yet well above the value for solid or semisolid diffusion in the electrode material. Thus, it was concluded that the peaked-shaped response was attributable to adsorption/desorption phenomena. Peak currents were used as analytical response rather than plateau currents because peak values provided a larger signal at higher concentrations.

The background current due to the oxidation of the 0.1 M NaOH solution was concluded to be kinetically controlled, because the magnitude of the current was small ( $1.5 \mu\text{A}$ ) for such high concentration species, and because when the solution was stirred, the background current was independent of stirring rate. Currents for analytes, in contrast, appear to be mass transport influenced based on the fact that flow rate changes affect current.

### 3.2. Current versus concentration profile

Fig. 3, depicting amperometric current versus sucrose concentration shows that up to about 0.5 mM sucrose the plot appears linear, whereas at the higher

Table 1

Amperometric response for sucrose with and without pretreatment for concentrations of 0.005 to 0.5 mM

	Slope ( $\mu\text{A}/\text{mM}$ )	Intercept ( $\mu\text{A}$ )	LOD <sup>a</sup> (mM)
Sucrose without pretreatment	39.6	0.13	0.06
Sucrose with pretreatment	225.6	-1.63	0.04

<sup>a</sup> LOD = Lower limit of detection =  $3 \times$  standard error of the estimate divided by slope.

Table 2

Amperometric responses for five analytes

	Slope ( $\mu\text{A}/\text{mM}$ )	Intercept ( $\mu\text{A}$ )	LOD <sup>a</sup> (mM)
Sucrose	226	-1.63	0.04
Glycine	165	1.43	0.02
Diethylenetriamine	340	2.64	0.10
Phenol	98	-0.42	0.03
Ethanolamine	114	4.34	0.10

<sup>a</sup> Lower limit of detection, three times the standard error of the estimate divided by the slope.

Table 3  
Anodic currents

Sample (in 0.1 M NaOH)	Convective amperometry	Solution exchange method
0.1 mM glycine	12 $\mu$ A	12 $\mu$ A
0.1 mM glycine + 0.1 mM calcium	6.7	21
0.1 mM glycine + 0.1 mM calcium + 0.1 mM oxalate	6–8	18

concentrations there is a distinct levelling effect. The levelling of the response curve may also be attributed to adsorption/desorption effects at the electrode surface. Reciprocal current versus reciprocal concentration plots were not linear, indicating non-adherence to a simple Langmuir adsorption model.

### 3.3. Electrode pretreatment

Analytical signals showed variations of as much as 10% due to the apparent oxidation state of the nickel oxide surface lattice. To obtain a more reproducible nickel oxide lattice a negative or reducing potential was applied to the electrode as a pretreatment before measurements. A pretreatment voltage range of  $-0.84$  to  $-1.09$  V vs. SCE was investigated. This range of pretreatment potentials was selected to be sufficiently cathodic to reduce all nickel oxides to nickel(O) while avoiding hydrogen evolution [4]. The pretreatment time was 30 s. Optimum precision occurred at  $-1.0$  V vs. SCE. Pretreatment times ranging from 5 to 60 s were examined. Precision was not improved for pretreatment times of 15 s or greater. A pretreatment time of 15 s was adopted for subsequent work. An added advantage from the pretreatment procedure was an approximately five-fold enhancement of sensitivity. The enhanced slope with pretreatment can be attributed to a higher activity surface generated by the freshly formed nickel oxide lattice following the pretreatment.

Table 2 summarizes measurements over the 0.005 to 0.50 mM linear concentration range for five analytes. Comparison of signal size for the five analytes agreed with earlier reports that amines are more reactive than hydroxyls and that oxidation current is enhanced by multiple reactive functional groups [2]. For these typical compounds the sensitivity per oxidative site seldom differs by more than a factor of three.

### 3.4. Calcium effects on amperometry

Previous studies with the nickel oxide electrode and anodic convective amperometry [5] showed that calcium strongly inhibited the amperometric currents. Typical data are shown in Table 3. The inhibition effect for the convective amperometry method was virtually independent of flow rate. The results shown in column three of Table 3 show an increase in anodic current due to calcium, i.e., opposite to results obtained using the convective amperometry method. Oxalate only partially masked the enhancement caused by calcium. Similar results were obtained with glucose, glutamate and ethanol as analytes.

To further examine the effects of solution movement, subsequent exchanges of sample solution were made. Samples without calcium give equal analytical peak currents, but when the calcium containing solution was injected a second time, an inhibited signal was obtained.

To interpret the remarkable difference in the calcium effect, positive interference for the solution exchange method presented here and negative interference for conventional flow stream amperometry, it must be noted that the only significant distinction is that of convection of the solution during the measurement step. In the method presented here, i.e., solution exchange, there is convection only during the exchange process with no imposed convection before or after. By contrast, in the convective amperometric technique there is constant convection. This observation suggests that mass transport phenomena, i.e., concentration gradient thickness, at the electrode/solution interface dictates the nature of the calcium effect.

Apparently, calcium species interact with the electrode surface oxide lattice. At the solution pH the predominant calcium species are  $\text{Ca}^{2+}$  and  $\text{CaOH}^+$ . The

Table 4  
Effect of hydroxide: interference on signal for 0.05 mM glycine by 0.1 mM calcium

Hydroxide concentration	Percent interference
0.03	+8
0.1	+9
0.3	+3
1.0	-15

relative amounts of  $\text{Ca}^{2+}$  and  $\text{CaOH}^+$  are roughly the same [6].

At the levels of calcium added (i.e., 0.1 mM), no calcium will exist as  $\text{Ca}(\text{OH})_2$ , because its solubility limit is 1.0 mM [6]. The equilibrium expression is:

$$\frac{[\text{Ca}^{2+}]}{[\text{Ca}(\text{OH})_2]_s[\text{H}^+]^2} = 10^{23}$$

For an electrode reaction controlled primarily by kinetics in a stirred solution, the surface pH can be expected to be near that of the bulk (i.e., pH 13). At this pH calcium oxide bridges with the metal oxide lattice can be speculated, e.g., calcium oxide bridging at the electrode surface would then compete with analyte for adjacent active nickel sites, resulting in a net decrease in analyte reaction. The solution exchange technique, in contrast, has minimal stirring so that a greater decrease in pH at the electrode surface occurs due to background and analytical anodic processes. At the lower interfacial pH the divalent calcium cation species would be the predominant form of calcium and it would be the only divalent cation. The enhancement of analytical current under these conditions may then be attributable to calcium cation occupation of exchangeable lattice cation sites, which would otherwise be occupied by protons that lower surface pH. Additionally, for anionic analytes, calcium ionic bridges might stabilize surface intermediates during alpha-carbon electron abstraction.

The rationale for the calcium effects outlined above infers that at a sufficiently high solution pH, the solution exchange method should show an inhibition, rather than an enhancement, due to the presence of calcium. Correspondingly, data were taken over a range of hydroxide concentrations. Applied potentials were selected at each hydroxide concentration in order to yield constant background currents. The data in Table 4 shows that as hydroxide concentration is increased from 0.03 to 1.0 M, the observed enhancement effect of calcium is replaced by an inhibition effect. These observations correspond with the proposed calcium effect surface chemistry.

### 3.5. Comparison with BOD testing

An application for an amperometric method for oxidizable solutes is the determination of oxidizable (i.e., oxygen demand) impurities in municipal wastewater. Historically, the biological oxygen demand (BOD) test has been used as the acceptable method [7]. Amperometric measurements by the present method were compared with BOD measurements. For amperometric measurements, samples were adjusted to 0.1 M NaOH with NaOH crystals. The results showed that while the present method showed a 25% decrease in oxidizable species during the wastewater treatment, the BOD method registered more than 90% decrease. This can be attributed to the fact that the amperometric method responds to true solutes, while in the BOD method reaction with suspended matter is included in the results. Thus, the present method offers a rapid assay of *soluble* oxidizable species.

### Acknowledgements

We thank Racine Sewage Treatment Plant (Racine, WI, USA) for their assistance.

### References

- [1] M. Fleischmann, K. Korinek and D. Pletcher, *J. Chem. Soc., Perkin Trans.*, 2 (1972).
- [2] N. Botros and C.O. Huber, *Anal. Chim. Acta*, 208 (1988) 247.
- [3] B.S. Hui and C.O. Huber, *Anal. Chim. Acta*, 134 (1982) 211.
- [4] *Atlas of Electrochemical Equilibria and Aqueous Solutions*, National Association of Corrosion Engineers, Houston, TX, 1974, p. 333.
- [5] B.S. Hui, *Examinations of Nickel Oxide Electrodes for Electroanalysis*, Ph.D. Thesis, University of Wisconsin-Milwaukee, August 1991, p. 111.
- [6] C.F. Baes, R.E. Mesmer, *The Hydrolysis of Cations*, Wiley, New York, 1976, p. 103.
- [7] *Standard Methods for the Determination of Water and Wastewater*, 16th edn., American Public Health Association, Washington, DC, 1985, pp. 418–419, 422–425 and 525–532.



# Amperometric glucose-sensing electrode based on carbon paste containing poly(ethylene glycol)-modified glucose oxidase and cobalt octaethoxyphthalocyanine

Fumio Mizutani \*, Soichi Yabuki, Seichiro Iijima

*National Institute of Bioscience and Human-Technology, 1-1 Higashi, Tsukuba, Ibaraki 305, Japan*

Received 1 March 1994; revised manuscript received 8 August 1994

## Abstract

An amperometric enzyme electrode for glucose was prepared by incorporating poly(ethylene glycol)-modified glucose oxidase and cobalt octaethoxyphthalocyanine [CoPc(OEt)<sub>8</sub>], a new mediator, into a carbon paste matrix. The polymer-modified enzyme exhibited a higher activity than the native enzyme in the hydrophobic carbon paste medium. CoPc(OEt)<sub>8</sub> could oxidize the enzyme at more negative potentials than unsubstituted cobalt phthalocyanine (CoPc). Further, the CoPc(OEt)<sub>8</sub>-mediated enzyme electrode showed a high stability: the electrode response to glucose did not decrease for at least 4 weeks (or for 700 assays), whereas the glucose response from a CoPc-mediated enzyme electrode fell to half of the initial value within 2 weeks (or after 300 assays). CoPc(OEt)<sub>8</sub>, a paraffin-oil soluble derivative of CoPc, incorporated in the bulk of carbon paste, diffused towards the electrode surface so as to renew continuously the electrode surface, which resulted in the high stability of the new mediator-based enzyme electrode.

*Keywords:* Amperometry; Glucose; Enzyme electrode; Octaethoxyphthalocyanine

## 1. Introduction

Analytical devices combining the specificity of enzymatic reactions with high sensitivity of amperometric transduction have attracted much interest in the last two decades [1,2]. Particular efforts in this field have been directed at devising a glucose-sensing electrode by using immobilized glucose oxidase (GOD) and immobilized electroactive molecules that mediate the electron transfer between the enzyme and the electrode [3,4]. Mediators for GOD described previously include ferrocene derivatives [5–21], benzoquinone [22,23] and others [24,25]. Recently, Rosen-Margalit

et al. [26] have reported that cobalt phthalocyanine (CoPc) was useful as a mediator.

Porous and electrically-conducting materials, such as conducting polymers [10–14], platinum black [27], and carbon paste (CP) [15–19,22,23], are very useful for the immobilization of the enzyme/mediator system. Such materials can enhance the sensor response by providing a large microscopic electrode area and a high electron conduction to a large amount of immobilized mediator [27–30]. The CP-based enzyme electrode is of particular interest. The most attractive feature of CP is its reservoir-like property: a stable electrochemical response can be achieved owing to the continuous renewal by the supply of the enzyme/mediator system from the reservoir in the CP bulk medium to the elec-

\* Corresponding author.

trode surface [19,31]. Although the activity of immobilized GOD in the CP matrix was rather low, this could be circumvented by the use of a poly(ethylene glycol) (PEG)-modified enzyme: the modification of GOD enhanced the affinity of the enzyme molecules for the hydrophobic CP matrix [18,32,33].

We have preliminarily tested a PEG-modified GOD/CoPc-incorporated CP electrode. The electrode showed good performance characteristics: the response to glucose was independent of oxygen partial pressure and the storage stability in test solutions was high, as has been noted previously for a CoPc-mediated glucose electrode [26]. However, the stability of the electrode towards repeated use was rather poor: when the determination of glucose (1 mM) was repeated 30 times a day for two weeks, the response gradually decreased and became ca. 50% of the initial value on the 14th day. This may be caused by the decomposition of CoPc molecules on the electrode surface during repeated use, and by insufficient renewal of the electrode surface. It is natural that CoPc hardly diffuses from the bulk of CP towards the electrode surface, because CoPc is virtually insoluble in paraffin oil that is a component of the CP. In order to circumvent the stability problem in repeated use, the incorporation of a paraffin oil-soluble derivative of CoPc is considered to be suitable. Such a CoPc-derivative can easily diffuse from the CP bulk towards the electrode surface so as to renew the surface, which would result in stable electrochemical responses against the repeated use.

In this paper the use of cobalt octaethoxyphthalocyanine [CoPc(OEt)<sub>8</sub>] (Fig. 1) as the mediator is described. The analogue of CoPc(OEt)<sub>8</sub>, zinc octaethoxyphthalocyanine, has been known to be soluble in various kinds of organic solvents, such as toluene and dichloromethane [34,35]. Further, CoPc(OEt)<sub>8</sub> is expected to be oxidized at more negative potentials than

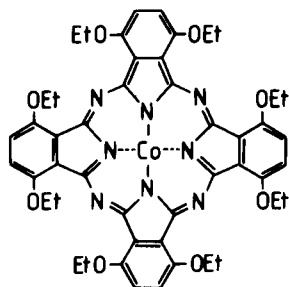


Fig. 1. Structural formula of CoPc(OEt)<sub>8</sub>.

CoPc owing to the electron donating property of the substituted ethoxy groups, which would provide an enzyme electrode that can be operated in a lower potential region.

## 2. Experimental

### 2.1. Materials

The enzymes used were GOD (EC 1.1.3.4, from *Aspergillus* sp., 100 U mg<sup>-1</sup>; Grade II, Toyobo, Osaka) and peroxidase (EC 1.11.1.7, from horseradish, 250 U mg<sup>-1</sup>; Grade III, Toyobo). Methoxy(polyethylene glycol)-succinimidyl succinate (activated PEG; average molecular weight, 5000), CoPc, paraffin oil and CP were obtained from Sigma (St. Louis, MO), Strem Chemical (Newburyport, MA), Merck (Darmstadt) and Bioanalytical Systems (West Lafayette, IN), respectively. CoPc was purified by reprecipitation: the CoPc as received was dissolved in 98% sulfuric acid, and the solution was diluted with water. The precipitate formed after dilution was carefully washed with water and acetone, and then dried in vacuo. Other reagents were of analytical-reagent grade and used without further purification. Deionized, doubly distilled water was used throughout.

The preparation of PEG-modified GOD through the reaction of the activated PEG and GOD was as described previously [32]. CoPc(OEt)<sub>8</sub> was prepared by the reaction of 3,6-diethoxyphthalonitrile with CoCl<sub>2</sub> in the presence of 1,8-diazabicyclo[5,4,0]-7-undecene and purified by column chromatography on alumina [34]. Found: C, 62.20; H, 5.49; N, 11.86%. Calculated for C<sub>48</sub>H<sub>48</sub>N<sub>8</sub>O<sub>8</sub>Co: C, 62.40; H, 5.23; N, 12.13%.

### 2.2. Enzyme electrodes

Two kinds of enzyme electrodes were prepared by using CoPc(OEt)<sub>8</sub> and CoPc, respectively. CoPc(OEt)<sub>8</sub> or CoPc, the PEG-modified GOD and CP, 5:10:85 by weight, were mixed in a mortar by a PTFE-coated spatula for 30 min, and a portion (ca. 20 mg) of the mixture was placed into a hole (2.3 mm diameter, 5 mm deep) in the electrode body shown in Fig. 2, which was remodelled from a microsyringe (Type 725LT; Hamilton, Reno, NV). By pushing the metal

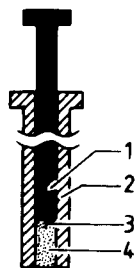


Fig. 2. Enzyme electrode. (1) Metal plunger; (2) glass tube; (3) platinum wire; and (4) CP.

plunger that also served as a leading wire to the CP mixture, the outer layer of CP projected over the glass cylinder, and the CP electrode surface could be renewed by removing the protruding layer.

The GOD activity in the CP electrodes was measured spectrophotometrically by using a peroxidase–phenol–4-aminoantipyrine chromogenic system [36].

The enzyme electrode thus prepared, an Ag/AgCl electrode and a platinum wire, served as the working, reference and auxiliary electrodes, respectively. All the potentials given in the present paper were measured against an Ag/AgCl electrode. The test solution used was an air-saturated 0.1 M potassium phosphate buffer (20 ml, pH 7,  $25.0 \pm 0.2^\circ\text{C}$ ), unless otherwise stated. The solution was stirred with a magnetic bar during measurement. The enzyme electrodes were stored in the phosphate buffer at  $4^\circ\text{C}$  when not in use.

### 3. Results and discussion

Fig. 3 shows the absorption spectra of paraffin oil solutions saturated with CoPc(OEt)<sub>8</sub> (a) and with

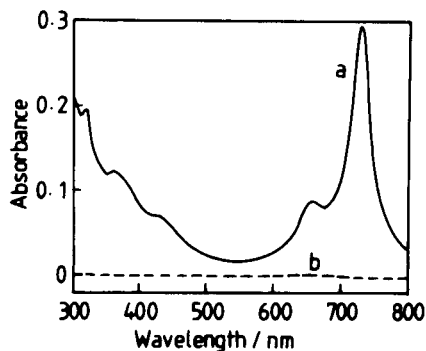


Fig. 3. Visible absorption spectra of paraffin oil solutions of (a) CoPc(OEt)<sub>8</sub> and (b) CoPc.

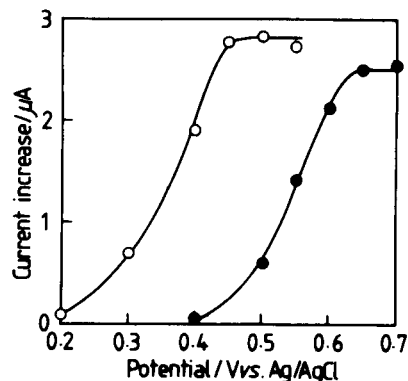
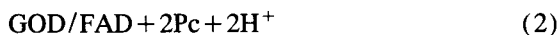


Fig. 4. Effect of potential on the current responses of the CoPc(OEt)<sub>8</sub>-based enzyme electrode (○) and the CoPc-based enzyme electrode (●) in the argon-saturated test solution.

CoPc (b). Each solution was prepared by adding an excess amount of the corresponding phthalocyanine into paraffin oil, stirring the oil–phthalocyanine mixture with a magnetic bar for 24 h at room temperature, and pipetting the supernatant after the centrifugation of the mixture. No discernible visible absorption peak was observed in curve (b), indicating that CoPc was virtually insoluble in paraffin oil. Hence in the CP matrix, which consists of graphite powder and paraffin oil, CoPc is in the solid state. On the contrary, CoPc(OEt)<sub>8</sub> was soluble in paraffin oil to give ca.  $5 \mu\text{M}$  solution (Curve b in Fig. 3). Thus, a portion of the CoPc(OEt)<sub>8</sub> incorporated into CP exists in a paraffin oil–solution state. The transport of the dissolved CoPc(OEt)<sub>8</sub> in CP from the bulk to the surface is expected to be much easier than for solid CoPc.

Fig. 4 shows the relationships between the steady-state current response for 1 mM glucose and the electrode potentials on the CoPc(OEt)<sub>8</sub>- and CoPc-based electrodes in the argon-saturated test solution. For each electrode–solution system, the current increased immediately after the addition of glucose and reached another steady state within 5 s. The close proximity of the enzymatic and transducing sites would result in a fast response to glucose. The introduction of air into the test solution did not bring about a discernible decrease in the current response on each electrode. This related to the large excess of accessible mediator and a high electron transfer rate between GOD and the phthalocyanines [26]. Hence subsequent experiments were performed in air-saturated test solutions.

The glucose response on each electrode increased with increasing electrode potential applied and reached a plateau in the positive potential region: the current increase started at 0.2 V and reached a plateau above 0.45 V on the CoPc(OEt)<sub>8</sub>-based enzyme electrode, whereas that starting at 0.4 V reached a plateau above 0.65 V on the CoPc-based electrode (Fig. 4). Owing to the electron donating effect of the substituted ethoxy groups, CoPc(OEt)<sub>8</sub> would be oxidized at potential more negative than unsubstituted CoPc. This brings about the negative shift of the potential of the electrocatalytic process for oxidizing glucose:



where GOD/FAD and GOD/FADH<sub>2</sub> denote the oxidized and reduced forms of flavin adenine dinucleotide within GOD, respectively, and Pc<sup>+</sup>/Pc, the mediator which is assumed to be a one-electron couple [26,37]. As the result, the CoPc(OEt)<sub>8</sub>-based enzyme electrode could be operated at a more negative potential than the CoPc-based system. Further, the magnitude of the glucose response on the CoPc(OEt)<sub>8</sub>-based enzyme electrode in the plateau region was larger than that the case of CoPc-based system (Fig. 4). This suggests that the paraffin oil-soluble phthalocyanine exhibits an enhanced electron transferability from the enzyme to CP by shuttling between them.

If the surface of each enzyme electrode was covered with a layer of CP containing the modified GOD (10%, w/v), whose thickness was 0.5 mm, the electrode response to glucose disappeared. While hydrogen peroxide is expected to be produced by the enzymatic reaction at the mediator-free electrode surface, the electrode potential applied (0.2–0.7 V) was not positive enough for oxidizing the product on CP. The glucose response from the CoPc-based electrode with the GOD/CP layer remained zero for more than 1 h. On the other hand, the response from the CoPc(OEt)<sub>8</sub>-based electrode with the GOD/CP layer increased gradually and was the same as that from the uncoated CoPc(OEt)<sub>8</sub>-based system (Fig. 4) within several minutes. These results demonstrate that CoPc(OEt)<sub>8</sub>

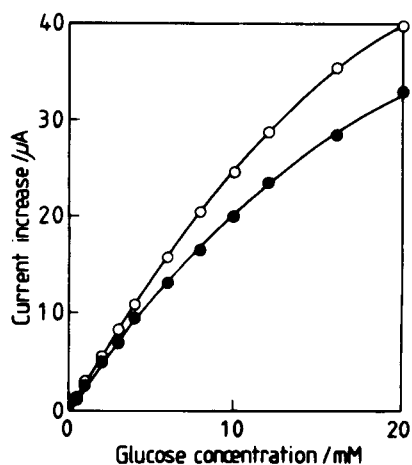


Fig. 5. Calibration graphs for glucose on the CoPc(OEt)<sub>8</sub>-based enzyme electrode (O) and the CoPc-based enzyme electrode (●).

diffuses from the bulk CP to the electrode surface much easier than CoPc.

The glucose response at each electrode was a few times larger than that on electrodes using the GOD as received, instead of the modified GOD (data not shown). The apparent GOD activity on the modified enzyme-doped electrode was ca. 30 mU cm<sup>-2</sup>, whereas that on the electrode using the same weight of the native GOD was ca. 10 mU cm<sup>-2</sup>. The higher activity of the modified GOD in the CP, owing to its enhanced affinity for the hydrophobic matrix, resulted in the increase in the glucose response [18].

The relative standard deviation for ten successive measurements of 1 mM glucose on each enzyme electrode was ca. 2%. Fig. 5 shows calibration graphs for the CoPc(OEt)<sub>8</sub>- and CoPc-based enzyme electrodes. The potentials applied were 0.45 V and 0.65 V for CoPc(OEt)<sub>8</sub>- and CoPc-based electrodes, respectively. Each electrode gave a linear current response up to 4 mM glucose, and a significant further increase in the response with an increase of the glucose concentration was observed in the range 4–20 mM. The detection limit was 3 μM (signal-to-noise ratio = 3) for each electrode.

The long-term stabilities of the CoPc(OEt)<sub>8</sub>- and CoPc-based enzyme electrodes were examined by determining 1 mM glucose 30 times each day by using each electrode. The average value of the response for the 30 measurements on the CoPc-based enzyme electrode gradually decreased and became ca. 50% of the

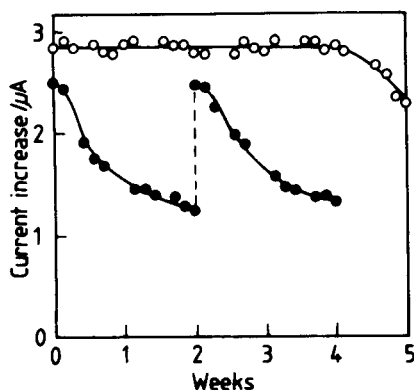


Fig. 6. Long-term stabilities of the CoPc(OEt)<sub>8</sub>-based enzyme electrode (○) and the CoPc-based enzyme electrode (●). On each electrode, the response for 1 mM glucose was measured 30 times a day. The average value of the 30 measurements is plotted against the number of days after the preparation of electrode. On the 14th day, the surface of the CoPc-based enzyme electrode was renewed by removing the outer layer of the CP.

initial value after two weeks, as shown in Fig. 6. On the 14th day, the metal plunger of the electrode body (Fig. 2) of the CoPc-based system was pushed in by 2 mm, and the outer CP layer projecting out of the glass tube of the electrode body was removed. After this renewal process, 30 measurements of 1 mM glucose were again carried out. The average value of the measurements just after the renewal was the same as the initial value, and the response/day-curve from the 14th to 28th day almost coincides with that in the first 14 days (Fig. 6). The poor stability of the CoPc-based enzyme electrode was thus circumvented by applying the surface-renewal process. However, the renewal process seems rather complicated. On the contrary, the average value of the response on the CoPc(OEt)<sub>8</sub>-based enzyme electrode did not decrease for 4 weeks, as shown in Fig. 6: the new mediator-based system exhibited far higher stability than the CoPc-based enzyme electrode. The PEG-modified GOD and CoPc(OEt)<sub>8</sub>, both of which were soluble in organic solvents, were supplied from the CP bulk medium so as to renew the electrode surface continuously. This resulted in the high stability of the CoPc(OEt)<sub>8</sub>-based enzyme electrode, as expected. Thus, not only the modification of enzyme [18,32,33] but also that of mediator with appropriate functional groups is effective for obtaining a CP enzyme electrode with good performance characteristics such as high stability and

fast electrode response independent of oxygen partial pressure.

## References

- [1] F. Mizutani and M. Asai, in D.L. Wise (Ed.), *Bioinstrumentation*, Butterworth, Boston, 1990, p. 317.
- [2] F. Scheller and F. Schubert, *Biosensors*, Elsevier, Amsterdam, 1992, p. 85.
- [3] R. Wilson and A.P.F. Turner, *Biosensors Bioelectron.*, 7 (1992) 165.
- [4] M.F. Cardosi and A.P.F. Turner, in A.P.F. Turner (Ed.), *Advances in Biosensors*, Vol. 1, JAI Press, London, 1991, p. 125.
- [5] A.E.G. Cass, G. Davis, G.D. Francis, H.A.O. Hill, W.J. Aston, I.J. Higgins, E.V. Protokin, L.D.L. Scott and A.P.F. Turner, *Anal. Chem.*, 56 (1984) 667.
- [6] M.A. Lange and J.Q. Chambers, *Anal. Chim. Acta*, 175 (1985) 89.
- [7] D.J. Claremont, C. Penton and J.C. Pickup, *J. Biomed. Eng.*, 8 (1986) 272.
- [8] E.J. D'costa, I.J. Higgins and A.P.F. Turner, *Biosensors*, 2 (1986) 71.
- [9] J.M. Dicks, S. Hattori, I. Karube, A.P.F. Turner and T. Yokozawa, *Ann. Biol. Clin.*, 47 (1989) 607.
- [10] C. Iwakura, Y. Kajiyama and H. Yoneyama, *J. Chem. Soc., Chem. Commun.*, (1988) 1019.
- [11] Y. Kajiyama, H. Sugai, C. Iwakura and H. Yoneyama, *Denki Kagaku*, 56 (1990) 1110.
- [12] Y. Kajiyama, H. Sugai, C. Iwakura and H. Yoneyama, *Anal. Chem.*, 63 (1991) 49.
- [13] N.C. Foulds and C.R. Lowe, *Anal. Chem.*, 60 (1988) 2473.
- [14] F. Mizutani and M. Asai, *Bull. Chem. Soc. Jpn.*, 61 (1988) 4458.
- [15] L. Gorton, H.I. Karan, P.D. Hale, T. Inagaki, Y. Okamoto and T.A. Skotheim, *Anal. Chim. Acta*, 228 (1990) 23.
- [16] J. Wang, L.-H. Wu, Z. Lu, R. Li and J. Sanchez, *Anal. Chim. Acta*, 228 (1990) 251.
- [17] A. Amine, J.-M. Kauffmann and G.J. Patriarche, *Talanta*, 38 (1991) 107.
- [18] F. Mizutani, S. Yabuki, A. Okuda and T. Katsura, *Bull. Chem. Soc. Jpn.*, 64 (1991) 2849.
- [19] A. Amine, J.M. Kauffmann, G.G. Guilbault and S. Bacha, *Anal. Lett.*, 26 (1993) 1281.
- [20] F. Mizutani and M. Asai, *Denki Kagaku*, 56 (1988) 1100.
- [21] S. Iijima, F. Mizutani, S. Yabuki, Y. Tanaka, M. Asai, T. Katsura, S. Hosaka and M. Ibonai, *Anal. Chim. Acta*, 281 (1993) 483.
- [22] T. Ikeda, H. Hamada, K. Miki and M. Senda, *Agric. Biol. Chem.*, 49 (1985) 541.
- [23] M. Senda, T. Ikeda and K. Miki, *Anal. Sci.*, 2 (1986) 501.
- [24] W.J. Albery, P.N. Bartlett and D.H. Carston, *J. Electroanal. Chem.*, 194 (1985) 223.
- [25] G. Jonsson and L. Gorton, *Biosensors*, 1 (1985) 355.
- [26] I. Rosen-Margalit, A. Bettelheim and J. Rishpon, *Anal. Chim. Acta*, 281 (1993) 327.

- [27] F. Mizutani and S. Yabuki, in S. Yamauchi (Ed.), *Chemical Sensor Technology*, Vol. 4, Kodansha, Tokyo, and Elsevier, Amsterdam, 1992, p. 167.
- [28] R.A. Bull, F.R. Fan and A.J. Bard, *J. Electrochem. Soc.*, 131 (1984) 687.
- [29] F. Mizutani, S. Iijima, Y. Tanabe and K. Tsuda, *J. Chem. Soc., Chem. Commun.*, (1985) 1729.
- [30] M. Umana and J. Waller, *Anal. Chem.*, 58 (1986) 2979.
- [31] R.W. Murray, *Electroanal. Chem.*, 13 (1984) 191.
- [32] S. Yabuki, F. Mizutani and T. Katsura, *Biosensors Bioelectron.*, 7 (1992) 695.
- [33] S. Yabuki, F. Mizutani and T. Katsura, *Sensors Actuators B*, 13–14 (1993) 166.
- [34] S. Iijima, F. Mizutani, Y. Tanaka and K. Ichimura, in G. Dryhurst and K. Niki (Eds.), *Redox Chemistry and Interfacial Behavior of Biological Molecules*, Plenum, New York, 1987, p. 515.
- [35] S. Iijima, F. Mizutani, M. Asai and K. Ichimura, *Denki Kagaku*, 57 (1989) 1215.
- [36] B.B. Bauminger, *J. Clin. Pathol.*, 27 (1974) 1015.
- [37] J. Rishpon, I. Rosen-Margalit, R. Harth, D. Ozer and A. Bettelheim, *J. Electroanal. Chem.*, 307 (1991) 293.



ELSEVIER

Analytica Chimica Acta 300 (1995) 65–70

ANALYTICA  
CHIMICA  
ACTA

# Amperometric glucose sensor using tetrathiafulvalene in Nafion gel as electron shuttle

Haiying Liu, Jiaqi Deng \*

*Department of Chemistry, Fudan University, Shanghai 200433, China*

Received 10 May 1994; revised manuscript received 1 August 1994

## Abstract

An amperometric mediated sensor for glucose has been contrived by using bovine serum albumin and glutaraldehyde to immobilize glucose oxidase on a Nafion–tetrathiafulvalene (TTF) modified electrode. It is further coated by Nafion. The inner Nafion membrane can prevent leaking of tetrathiafulvalene; the outer Nafion film serves as a barrier to electroactive anionic interferents such as ascorbate and urate and protects the biosensor from fouling agents. The experiment shows that  $TTF^+$  and  $TTF^{2+}$  can oxidize the reduced flavin adenine dinucleotide ( $FADH_2$ ) of glucose oxidase. The biosensor responds to glucose in less than 50 s and its calibration curve is linear from  $3.0 \times 10^{-4}$  to  $1.0 \times 10^{-2}$  M.

*Keywords:* Amperometry; Sensors; Glucose sensor; Tetrathiafulvalene; Nafion

## 1. Introduction

A second generation amperometric biosensor employing a non-physiological redox mediator instead of oxygen as an electron shuttle between enzyme and electrode has been developed to overcome the influence of oxygen variations and interference by electroactive species due to the high positive working potential in the first generation biosensors. However, there are some disadvantages: (1) the mediator can leak away from the enzyme electrode leading to deterioration problems when the sensor is used continuously or for multiple sample analysis; (2) several common electroactive constituents in biological samples, e.g., ascorbic acid and uric acid, become oxidized at the electrode either directly or catalytically by the mediator. With these in mind, some research groups have explored systems where the mediating species is chemically

bound in a way that allows communication between the redox centers of the enzyme and the mediator, but prevents the latter from leaching out of the electrode surface. For instance, one strategy involved the chemical attachment of electron relays (ruthenium pentamine or ferrocene derivatives) to the enzyme itself [1–5]. Cenas et al. [6,7] investigated systems where the mediating species (quinone) was chemically bound to a flexible polymer backbone. Later, these studies have been extended including systems where the mediating redox moieties are covalently attached to other polymers such as polypyrrole [8,9], poly(vinylpyridine) [10–12], polysiloxane [13–15] and poly(ethylene oxide) [16]. These systems allow electrons to shuttle between the enzyme's redox center and the electrode. To overcome such interference, several research groups used precast films such as dialysis, cellulose and polycarbonate film [17–19]. More recently, cast or electrodeposited ion-selective mem-

\* Corresponding author.

branes (e.g., Eastman AQ-29D or Nafion) have been utilized to discriminate against interfering species [20,21]. Though the Nafion coated glucose oxidase electrode showed to have a much improved stability in whole blood compared with an uncoated one, Nafion coating, formed by using Nafion solution diluted by the organic solvent, could cause denaturation of the enzyme. In this paper, a novel glucose sensor has been constructed to overcome these disadvantages by using two films of Nafion. The sensor is prepared by using glutaraldehyde and bovine serum albumin to immobilize glucose oxidase onto a Nafion-tetrathiafulvalene modified glassy carbon electrode and it is further coated by Nafion, which is a purely aqueous solution prepared from a 5 wt.% Nafion solution in a mixture of lower aliphatic alcohols and 10% water by distillation and which is not detrimental to the enzyme. The inner Nafion membrane immobilizes tetrathiafulvalene (TTF) on the electrode; the outer Nafion coating not only excludes electroactive anionic interferents such as ascorbate and urate from reaching the electrode but also keeps the sensor surface free from fouling agents. The TTF immobilized in Nafion works well to expedite exchange of electrons between the redox center of the enzyme and the electrode and the results show that the sensor has a good reproducibility and a lifetime of two months. It is demonstrated for the first time that the experiment demonstrates that both  $\text{TTF}^+$  and  $\text{TTF}^{2+}$  can oxidise the reduced flavin adenine dinucleotide ( $\text{FADH}_2$ ) of glucose oxidase.

## 2. Experimental

### 2.1. Reagents

Glucose oxidase (EC 1.1.3.4, 150,000 U  $\text{g}^{-1}$ , from *Aspergillus niger*) and tetrathiafulvalene (TTF) were obtained from Sigma. Glutaraldehyde was obtained from Merck. Nafion, 5 wt.% solution in a mixture of lower aliphatic alcohols and 10% water, was purchased from Aldrich. Bovine serum albumin (BSA) and D-glucose were purchased from Shanghai Chemical Reagent Co. Glucose solutions were stored overnight to allow to reach mutarotational equilibrium before use and purely aqueous Nafion solution was prepared according to the literature [22], having similar prop-

erties to that prepared from methanol solvent. All other chemicals used were of analytical reagent grade.

### 2.2. Apparatus

Cyclic voltammetry and stationary potential measurements were performed using a FDH 3204 cyclic voltamperograph (Scientific Equipment Co., Fudan University) and a type 3086  $x$ - $y$  recorder (Tokyo). The three-electrode system consisted of a glucose sensor as working electrode, a saturated calomel reference electrode (SCE) and a platinum wire as auxiliary electrode.

### 2.3. Nafion-TTF modified electrode construction

The glassy carbon electrode (4 mm in diameter) was polished with 0.3- $\mu\text{m}$  alumina paste, sonicated, rinsed with water, further cleaned in 1:1 nitric acid, acetone and doubly distilled water, successively. Next, the clean glassy carbon electrode was dried under an infrared lamp. Nafion-TTF was coated on the electrode by pipetting 4  $\mu\text{l}$  of acetone diluted Nafion (0.1%, w/v) containing 0.08 M TTF onto the electrode surface and letting it dry in air.

### 2.4. Construction of Nafion-TTF modified glucose sensor

20 mg glucose oxidase in 0.2 ml 0.1 M pH 7.0 phosphate buffer was thoroughly mixed with 15 mg BSA, after which 15  $\mu\text{l}$  of a 5% glutaraldehyde solution was added. Again the solution was completely mixed. Aliquots (7  $\mu\text{l}$ ) of the solution were pipetted onto the Nafion-TTF modified glassy carbon electrode. After being dried in air, the glucose sensor was dipped into a 0.5% (w/v) purely aqueous Nafion solution. After this dipping, the sensor was allowed to dry for 1 h at room temperature. When not in use, the sensor was kept in 0.1 M phosphate buffer (pH 7.0) at 4°C in a refrigerator.

### 2.5. Glucose sensor pretreatment

After fabrication and prior to experiments, the electrode response was stabilized by scanning between +0.45 and -0.2 V (vs. SCE) in phosphate buffer (pH 6.8) over a 15-min period of time. In this process,



TTF was oxidized to  $\text{TTF}^+$  when the potential was positive enough. Meanwhile, the  $\text{Na}^+$  ions in the sulphonate group of Nafion were substituted with  $\text{TTF}^+$  and entered the phosphate buffer. The electrochemical reaction of TTF in the Nafion film can be described as follows:



## 2.6. General procedure

Experiments were carried out in a conventional electrochemical cell holding pH 7.0 phosphate buffer (0.1 M) at  $25.0 \pm 0.5^\circ\text{C}$ . The cell, having a working volume of 5 ml, could be stirred during operation with a magnetic stirring bar. All solutions were thoroughly deoxygenated by bubbling  $\text{N}_2$  through the solution for at least 10 min. This was also done for glucose samples. In the constant potential experiments, a constant background current had to be obtained before samples of stock glucose solution were added to the buffer solution.

## 3. Results and discussion

### 3.1. Electrochemical characterization of the Nafion-TTF modified glucose sensor

The electrochemical behavior of tetrathiafulvalene has been studied [23–25]. Tetrathiafulvalene undergoes two one-electron oxidation processes in aqueous solution resulting in the formation of  $\text{TTF}^+$  and  $\text{TTF}^{2+}$ . The redox potentials of  $\text{TTF}^+$  and  $\text{TTF}^{2+}$  vary greatly with the method of immobilization and supporting electrolyte. Cyclic voltammetric waves at different scan rates of the Nafion-TTF modified glucose sensor are shown in Fig. 1 in 0.1 M phosphate buffer (pH 7.0). In the absence of glucose, the enzyme contributes no response and only the electrochemical behavior of TTF in Nafion polymer is observed. At a scan rate below 145 mV/s, the differences between the reduction and the oxidation peak potentials are less than 55 mV, indicating that there are fast charge transfers and counterion movements through the film, as well as charge transfer from the film to electrode. The sensor displays the characteristics of a kinetically fast redox couple attached to an electrode surface.

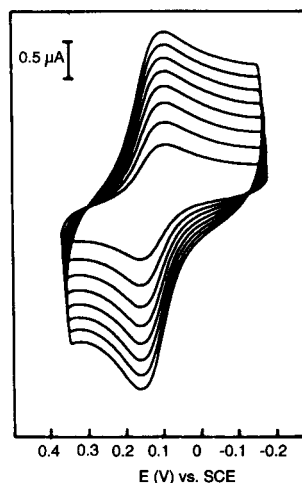


Fig. 1. Cyclic voltammograms of the Nafion-TTF modified glucose sensor reaching steady state at different scan rates (from inner to outer): 25, 45, 65, 85, 105, 125, 145, 165 mV/s in 0.1 M phosphate buffer (pH 7.0).

### 3.2. Catalytic oxidation of glucose with the Nafion-TTF modified glucose sensor

No catalytic oxidation current is found at the Nafion-TTF modified electrode when glucose is added to the phosphate buffer, but at the Nafion-TTF modified glucose sensor, two catalytic oxidation waves are observed with one reduction wave in the cathodic direction upon addition of glucose (Fig. 2), indicating that both  $\text{TTF}^+$

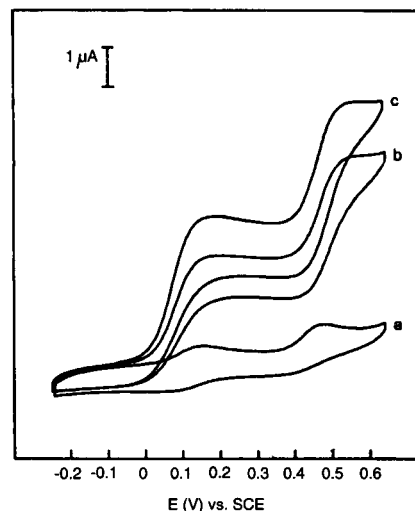


Fig. 2. Cyclic voltammograms of the Nafion-TTF modified glucose sensor with scan potential between  $-0.2$  and  $+0.65$  V (vs. SCE) at a scan rate of 25 mV/s in 0.1 M  $\text{N}_2$ -saturated phosphate buffer (pH 7.0). (a) No glucose; (b) 4 mM glucose; (c) 5 mM glucose.

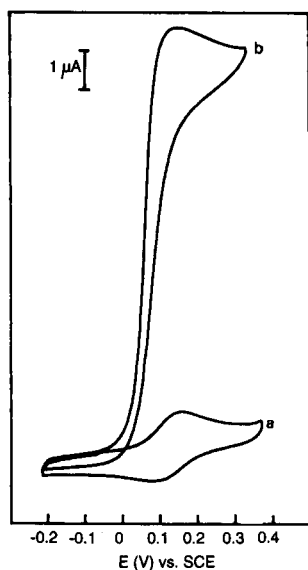


Fig. 3. Cyclic voltammograms of the Nafion-TTF modified glucose sensor with scan potential between  $-0.2$  and  $+0.38$  V at a scan rate of  $25$  mV/s in  $0.1$  M  $N_2$ -saturated phosphate buffer (pH 7.0) in absence of glucose (a) and presence of  $9.0$  mM glucose (b). Scan rate,  $25$  mV/s.

and  $TTF^{2+}$  can oxidize the  $FADH_2$  moiety of glucose oxidase. It is better, however, to control the working potential not to exceed  $+0.45$  V because electroactive species such as urate and ascorbate can be readily oxidized at the electrode causing interference. Fig. 3 shows typical cyclic voltammetric results for the sensor with a scanned potential between  $-0.20$  and  $+0.38$  V. Without glucose in solution, the voltammograms show TTF oxidation at approximately  $+0.15$  V with a scan rate of  $25$  mV/s. When glucose is added to the solution, the voltammetric behavior changes dramatically, with a sharp increase in the oxidation current and an almost complete disappearance of the reduction current, showing that a catalytic reaction occurs at the glucose sensor. The potential to recycle TTF in the Nafion film is more positive than that of the carbon paste-tetrathiafulvalene enzyme electrode for glucose [26]. Fig. 4 illustrates the mechanism of the Nafion-TTF modified glucose sensor.

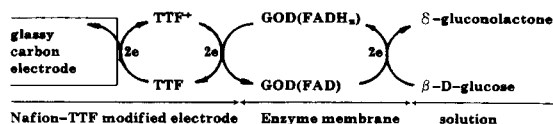


Fig. 4. Mechanism of Nafion-TTF modified glucose sensor.

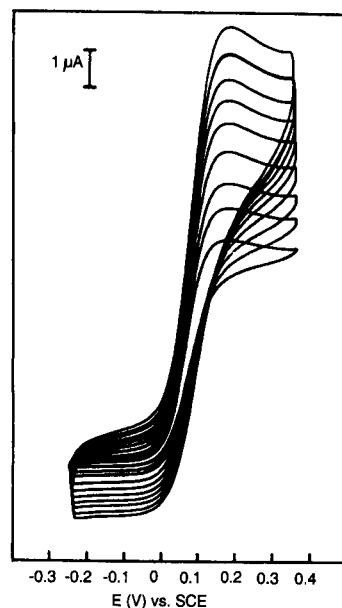
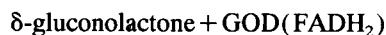
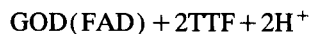
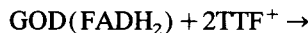


Fig. 5. Cyclic voltammograms of the Nafion-TTF modified glucose sensor at different speeds in  $0.1$  M  $N_2$ -saturated phosphate buffer containing  $5.0$  mM glucose, the scan rates (from inner to outer) are  $5, 15, 25, 45, 65, 85, 105, 125, 145$  mV/s, respectively.

$\beta$ -D-Glucose diffuses from solution to the enzyme layer through the membrane, where it is oxidized by the flavin adenine dinucleotide (FAD) of GOD, generating the reduced form  $GOD(FADH_2)$ :



$TTF^+$  oxidizes the  $GOD(\text{FADH}_2)$ , producing  $GOD(\text{FAD})$  again:



The reduced TTF form is oxidized at the electrode to regenerate the oxidized  $TTF^+$  ion, giving rise to the oxidation current.

Fig. 5 presents cyclic voltammograms for the Nafion-TTF modified glucose sensor in  $0.1$  M phosphate buffer containing glucose at various scan speeds. The catalytic current increases with increasing scan rate. The catalytic current is still apparent at higher scan rate. The absence of a reduction wave shows that, below  $145$  mV/s, the reproduction rate of TTF from  $TTF^+$  by reaction with  $GOD(\text{FADH}_2)$  is fast. At scan rates beyond  $200$  mV/s, a hysteresis appears and a

reduction wave is also observed. The appearance of the hysteresis and the reduction wave are dependent on scan rate, substrate concentration, film composition and thickness, temperature, and ionic strength.

### 3.3. Effect of pH and temperature on the Nafion-TTF modified glucose sensor

The pH dependence is demonstrated in Fig. 6, displaying an optimum response at pH 7.0. Extremes of pH result in irreversible denaturation of the enzyme. The effect of temperature on the sensor has been investigated between 10–50°C, at pH 7.0 phosphate buffer in the presence of 5.0 mM glucose. The experiment shows that the steady-state current response increases with temperature, reaching a maximum at about 50°C. Thereafter, the response declines rapidly presumably as a result of denaturation of the enzyme.

### 3.4. Calibration of the glucose sensor and its lifetime

Fig. 7 gives the calibration curve for the sensor. A linear relationship is observed between the current response and glucose concentration in the range from  $3.0 \times 10^{-4}$  to  $1.0 \times 10^{-2}$  M. Beyond that concentration, the calibration curve becomes non-linear, reaching a constant value at 20.0 mM. A steady-state catalytic current is reached at a potential between +0.15 and 0.20 V within 50 s. The reproducibility of the current response of the sensor is investigated at a glucose concentration of 6.0 mM and the relative standard deviation is 2.2% ( $n = 8$ ). The reproducibility of

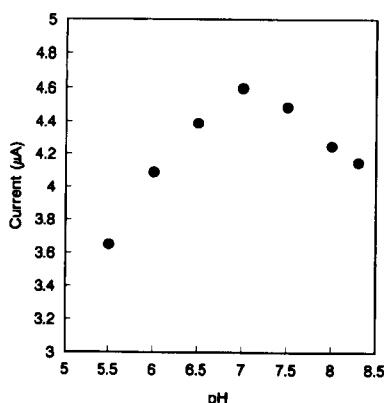


Fig. 6. Effect of pH on the Nafion-TTF modified glucose sensor, Steady-state current measured in the presence of 4.0 M glucose in 0.1 M  $N_2$ -saturated phosphate buffer (pH 7.0) at 25°C.

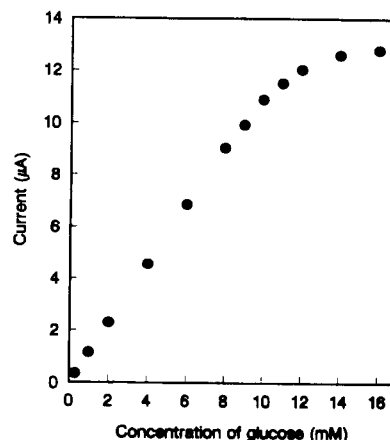


Fig. 7. Calibration plot for Nafion-TTF modified glucose sensor, Steady-state current was measured in 0.1 M  $N_2$ -saturated phosphate buffer (pH 7.0) at 25°C.

the construction of the sensor was examined by measuring the current response of six different electrodes in 6.0 mM glucose and the relative standard deviation was 4.2%. The life time study has been conducted for two months. The glucose sensor was stored in 0.1 M phosphate buffer (pH 7.0) at 4°C when not in use. The current response remains almost unchanged for a month, then tends to decrease gradually. After storage for two months, the decrease of the catalytic current was about 10%.

### 3.5. Studies of interference

Several substances have been examined as possible interferences for the glucose sensor. Analyses of phosphate buffers containing 8 mM glucose, to which the possible interferences are added, are executed. The reduction of glutathione (0.50 mM), L-glutamine (0.10 mM), lactate (0.5 mM), oxalate (0.5 mM), uric acid (0.2 mM), galactose (5.0 mM), ascorbate (0.15 mM), L-cystine (0.2 mM), L-lysine (0.2 mM), do not cause any observable interference to the determination of glucose. The lower operating potential (+0.15 V) with the use of TTF greatly minimizes interference from other electroactive species. Moreover, because of the Nafion coating, interference from anionic electroactive species such as uric acid and ascorbate is further reduced.

In mediated amperometric glucose sensors, oxygen, a natural mediator of glucose oxidase, can compete with the mediators in reoxidation of the reduced flavin

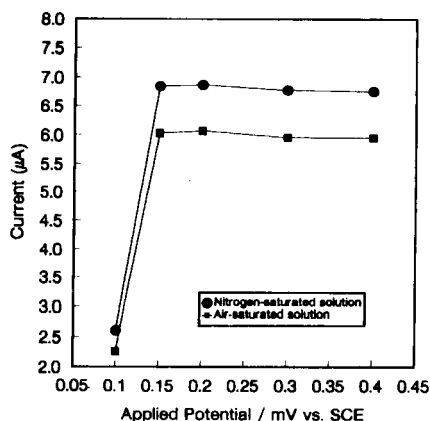


Fig. 8. Glucose (6 mM) response of Nafion–TTF modified glucose sensor in  $N_2$ -saturated and air-saturated solutions at several potentials.

adenine dinucleotide ( $FADH_2$ ) of glucose oxidase, causing a decrease in the measured current. With this in mind, we have examined the effects of oxygen interference by comparing the glucose response of the sensor in air-saturated solutions and with that measured in  $N_2$ -saturated solutions. Fig. 8 shows the results of this comparison. It is clear that  $O_2$  can compete with TTF in the reoxidation of  $FADH_2$  of glucose oxidase, leading to a decrease in the measured catalytic current. The decrease in catalytic current for the sensor in the air-saturated buffer is about 12% with a glucose concentration of 0.3–10 mM.

#### 4. Conclusions

The TTF immobilized in the Nafion membrane described in this work effectively facilitates a flow of electrons from redox centers of glucose oxidase to a glassy carbon electrode. Because of the domain structure, the hydrophilic domain of Nafion can retain the soluble  $TTF^+$  in the Nafion film, greatly improving the stability of the sensor. Enzyme activity is readily maintained by using Nafion as a protective membrane because the polymer is cast from a purely aqueous solution, not from a partially organic solvent one. The good stability of the sensor, and its ease of construction, hold great promise for practical applications in bioanalysis.

#### Acknowledgements

This work is supported by the National Science Foundation of China and the National Open Laboratory of Changchun Institute of Applied Chemistry, Chinese Academy of Sciences.

#### References

- [1] W. Schuhmann, T.J. Ohera, H.L. Schmidt and A. Heller, *J. Am. Chem. Soc.*, 113 (1991) 1394.
- [2] W. Schuhman, *Biosensors Bioelectron.*, 8 (1993) 191.
- [3] Y. Degani and A. Heller, *J. Phys. Chem.*, 91 (1987) 1285.
- [4] Y. Degani and A. Heller, *J. Am. Chem. Soc.*, 110 (1988) 2615.
- [5] Y. Kajiya and H. Yaneyama, *J. Electroanal. Chem.*, 328 (1992) 259.
- [6] N.K. Cenas, A.K. Pocius and J.J. Kulys, *Bioelectrochem. Bioenerg.*, 11 (1983) 61.
- [7] N.K. Cemas and J.J. Kulys, *Bioelectrochem. Bioenerg.*, 12 (1984) 583.
- [8] N.C. Foulds and C.R. Lowe, *Anal. Chem.*, 60 (1988) 2473.
- [9] J.M. Dicks, S. Hattori, I. Karube, A.P.F. Turner and T. Yokozawa, *Ann. Biol. Clin.*, 47 (1989) 607.
- [10] Y. Degani and A. Heller, *J. Am. Chem. Soc.*, 111 (1989) 2357.
- [11] A. Heller, *J. Phys. Chem.*, 96 (1992) 3579.
- [12] B.A. Gregg and A. Heller, *Anal. Chem.*, 62 (1990) 258.
- [13] P.D. Hale, H. Lee and Y. Okamoto, *Anal. Lett.*, 26 (1993) 1.
- [14] L. Gorton, H.I. Karan, P.D. Hale, T. Inagake, Y. Okamoto and T.A. Skotheim, *Anal. Chim. Acta*, 228 (1990) 23.
- [15] P.D. Hale, T. Inagaki, H.I. Karan, Y. Okamoto and T.A. Skotheim, *J. Am. Chem. Soc.*, 111 (1989) 3482.
- [16] P.D. Hale, H.L. Lan, L.I. Boguslavsky, H.I. Karan, Y. Okamoto and T.A. Skotheim, *Anal. Chim. Acta*, 251 (1991) 121.
- [17] A.E.G. Cass, G. Davis, G.D. Francis, H.A.O. Hill, W.J. Aston, I.J. Higgins, E.V. Plotkin, L.D.L. Scott and A.P.F. Turner, *Anal. Chem.*, 56 (1984) 667.
- [18] H. Gunasingham and C.H. Tan, *Electroanalysis*, 1 (1989) 423.
- [19] H. Lerner, J. Giner, J.S. Soeldner and C.K. Colton, *Ann. NY Acad. Sci.*, 428 (1984) 263.
- [20] L. Gorton, H.I. Karan, P.D. Hale, T. Inagaki, Y. Okamoto and T.A. Skotheim, *Anal. Chim. Acta*, 228 (1990) 23.
- [21] P.D. Hale and T.A. Skotheim, *Synth. Mat.*, 28 (1989) 853.
- [22] J. Weber, L. Kavan and M. Sticha, *J. Electroanal. Chem.*, 307 (1991) 293.
- [23] K.N. Kuo, P.R. Moses, J.R. Lenhard, D.C. Green and R.W. Murray, *Anal. Chem.*, 51 (1979) 745.
- [24] M. Kamche, H. Menet and A. Moradpour, *J. Am. Chem. Soc.*, 104 (1982) 4520.
- [25] J.D. Norton, W.E. Benson, H.S. White, B.D. Pendley and H.D. Abruna, *Anal. Chem.*, 63 (1991) 1909.
- [26] H. Gunasingham and C.H. Tan, *Analyst*, 115 (1990) 35.

# Competitive amperometric morphine sensor based on an agarose immobilised molecularly imprinted polymer

Dario Kriz, Klaus Mosbach \*

*Department of Pure and Applied Biochemistry, Chemical Center, University of Lund, P.O. Box 124, S-221 00 Lund, Sweden*

Received 21 March 1994; revised manuscript received 28 July 1994

## Abstract

A morphine-sensitive device was constructed based on a molecularly imprinted polymer. The imprinted polymer exhibited recognition properties previously. A method of detection based on competitive binding was used to measure morphine in the concentration range 0.1–10  $\mu\text{g}/\text{ml}$ . A morphine concentration of 0.5  $\mu\text{g}/\text{ml}$  gave a peak current (by oxidation) of 4 nA. The method of morphine detection involves two steps. In the first step, morphine binds selectively to the molecularly imprinted polymer in the sensor. In the second step, an electroinactive competitor (codeine) is added in excess, whence some of the bound morphine is released. The released morphine is detected by an amperometric method. The advantages of this type of sensor compared to biosensors based on antibodies, enzymes or cells are discussed. This sensor, based on an artificial recognition system, demonstrates autoclave compatibility, long-time stability and resistance to harsh chemical environments.

*Keywords:* Biosensors; Morphine sensor; Pseudo biosensor; Molecular imprinting

## 1. Introduction

The increased interest in medical, environmental and industrial analysis during the last decade has created a need for simple devices for the detection of various substances in aqueous and non-aqueous environments. In this context, biosensors have attracted much attention. Unfortunately, problems often arise with biosensors, due to their containing a biological component. Particular problems concern long-time stability, irreversible deactivation at high temperatures and in harsh chemical environments, and operation in organic phases [1,2].

Synthetic polymers with predetermined molecular recognition properties can be prepared using a molecular imprinting methodology [3–6]. One approach

involves an initial prearrangement of functional monomers in the presence of a print molecule prior to polymerisation. The resulting macroporous polymer contains recognition sites which due to their shape and arrangement of functional groups have affinity for the print molecules (Fig. 1). Various types of print molecules have been utilised; for example amino acid derivatives [7], sugars [8], sugar derivatives [9],  $\beta$ -blockers [10], bronchodilators and tranquilisers [11]. The binding properties of some of these molecularly imprinted polymers (MIPs) have been compared to those of some antibodies, giving comparable results [11].

Combining the molecular imprinting methodology with biosensor technology was expected to result in an interesting new sensing technique. The traditional way of constructing a biosensor, by combining an enzyme,

\* Corresponding author.

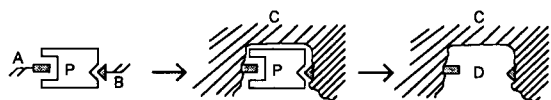


Fig. 1. Principle of the molecular imprinting methodology. The print molecule (P) and the monomers (A and B) are allowed to prearrange before the polymerisation is initiated. A macroporous polymer (C) is formed containing sites complementary to the print molecule. Removal of the print molecule by washing leaves sites (D) specific for print molecules and free for binding.

antibody or a living organism and a transducer to obtain a measurable signal, was modified by replacing the biological component with an artificial component (MIP against morphine). Thus, a pseudobiosensor was created. Morphine detection was chosen as a model system. Earlier sensors have been reported involving capacitance measurements on MIPs in organic phases [12]. Our sensor, based on an amperometric approach in an aqueous phase, was not expected to suffer from the disadvantages of biosensors described above. Improved characteristics were expected with respect to long-time stability and tolerance of high temperatures, harsh chemical environments and exposure to organic phases. The ability to autoclave the sensor is of particular relevance in order to avoid microorganism contamination of the sample.

## 2. Materials and methods

### 2.1. Preparation of the sensors

The molecularly imprinted polymers were prepared by procedures similar to those described in earlier papers [13]. A platinum wire (0.6 mm diam.) was

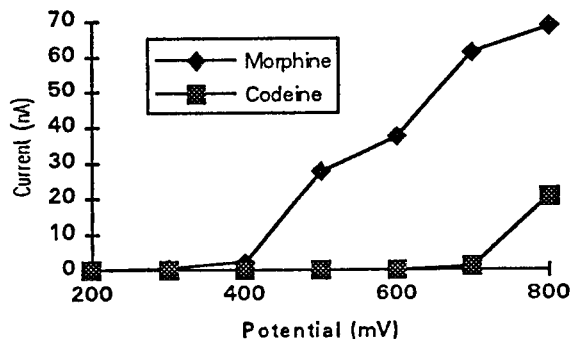


Fig. 2. Current obtained for the electrochemical oxidation of 1 µg/ml morphine or codeine in 20 mM citrate buffer, pH 6.0, containing 10% ethanol at various working electrode potentials.

melted into a glass tube. Thereafter, the outer part (15 mm) of the wire was dipped into a warm suspension (60°C) containing 0.15 g suspended MIP particles (1–25 µm diam.) in 0.8 g 4% aqueous agarose solution. Finally, the agarose was crosslinked by treatment with a suspension containing 100 µl epichlorhydrine and 5 mg NaBH<sub>4</sub> in 1.0 ml of 1.0 M NaOH at 60°C for 2 h [14]. The agarose layer thickness was examined by microscopy and estimated to be approximately 0.5 mm. Three types of sensors were prepared, based on MIPs against morphine (M-MIP) or L-phenylalanine anilide (O-MIP) or only an agarose layer without an MIP (Pt-Ag.). The L-phenylalanine anilide imprinted polymer was assumed to have a similar macroporous structure to the morphine imprinted polymer, and was used as a reference polymer. One sensor with M-MIP but without crosslinking was made in order to determine the effect of the crosslinking treatment on the sensor response.

### 2.2. Amperometric measurements

The morphine and reference sensors were used as working electrodes in a three-electrode system. The working electrode (4.2 mm<sup>2</sup>) was kept at a constant potential versus an Ag/AgCl reference electrode. A platinum auxiliary electrode (950 mm<sup>2</sup>) was used. All measurements were performed in 40 ml of 20 mM citrate buffer at pH 6.0 containing 10% ethanol. This buffer was chosen because the binding properties of the morphine imprinted polymer were found to be optimal under these conditions [15]. The ethanol was used to increase the wettability of the MIP particles. Initially, the sensors were equilibrated at the desired potential in the buffer until a constant background current was achieved (24 h, approximately 10 nA), whence morphine was added. When the current reached equilibrium (*i<sub>m</sub>*), after 2 h, 200 µl of a solution containing 10 mg/ml codeine in citrate buffer was added. The resulting current peak (*i<sub>c</sub>*) after approximately 20 min was recorded. The sensor was washed and the process repeated using different amounts of morphine.

## 3. Results and discussion

### 3.1. Optimisation of the working electrode potential

In order to achieve optimal electrochemical oxidation conditions for morphine versus codeine, we exam-

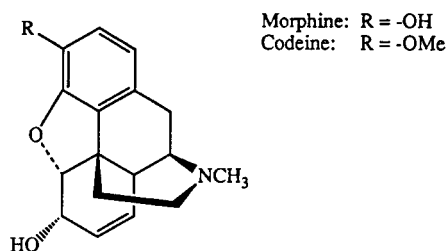


Fig. 3. Structures of morphine and codeine. The methyl group which replaces the hydrogen at the 3-hydroxy group position in morphine decreases the susceptibility to electrochemical oxidation.

ined the current response at various working electrode potentials (Fig. 2). In the subsequent measurements we chose the potential +500 mV because the current caused by the oxidation of codeine was negligible at this potential.

The difference in chemical structure between morphine and codeine is given in Fig. 3. The electrochemical oxidation of morphine has been proposed to have a complicated mechanism involving an electron oxidation at the 3-hydroxy group, prior to its ionisation, followed by dimerisation of the free radical to pseudomorphine [16].

### 3.2. Comments on the sensor response

The current recorded for a sensor during the measuring procedure is illustrated in Fig. 4. The definition of the currents  $i_m$  (equilibrium current after the morphine addition) and  $i_c$  (the peak current after the codeine addition) are also given. The current is caused by the electrochemical oxidation of unbound morphine.

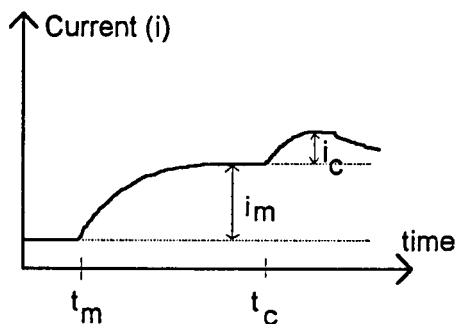


Fig. 4. Change in the current at the working electrode versus time. At time  $t_m$  morphine is added, causing the current to increase. After 2 h the current is constant and the value  $i_m$  is recorded. Codeine, which is added at time  $t_c$ , displaces some of the bound morphine. The released morphine is detected at the working electrode and causes a current peak  $i_c$ .

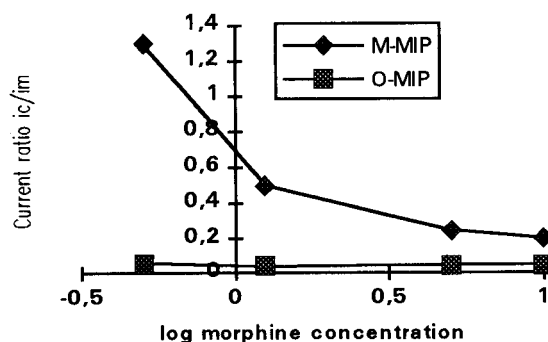


Fig. 5. Current ratio  $i_c/i_m$  as a function of the log(morphine concentration) (in  $\mu\text{g/ml}$ ) for the morphine and reference sensors.

The equilibrium current  $i_m$  is achieved when the local concentration of morphine at the working electrode surface has reached a constant level. This process is time-consuming due to diffusion limitations and the slow binding of morphine to the MIP. The principle of the sensor is that codeine acts as an electroinactive competitor which causes a release of bound morphine from the MIP. A portion of the released morphine diffuses to the metal surface of the working electrode and undergoes electrochemical oxidation. This causes an increase in the current. A similar approach employing antibodies instead of MIPs has been reported [17].

The morphine binding properties of the M-MIP and the O-MIP based sensors at various morphine concentrations, expressed as a current ratio  $i_c/i_m$ , are illustrated in Fig. 5. Evidently, the difference between the current ratio  $i_c/i_m$  in the two sensor types, and hence the amount of bound morphine displaced by the addition of codeine, is much more apparent at lower morphine concentrations. This may be explained if both polymers bind morphine weakly and non-specifically but in addition the morphine imprinted polymer contains a small population of binding sites with a very high affinity for morphine which the reference polymer lacks. A parallel investigation in this laboratory using radioligand assays has given actual values of the dissociation constants for the morphine imprinted polymer [15].

### 3.3. Influence of harsh treatment on sensor response

The application of biological recognition systems in sensor devices is often limited by their short life-time as mentioned in the introduction. The stability of our synthetic recognition system was demonstrated by exposing the sensors to various types of harsh treat-

ments (Table 1). It should be emphasized that the autoclave compatibility of the MIP-based sensors observed has great significance to sensor technology. Thus, contamination of the sensor by living organisms is easily avoided. Exposure of the MIP based sensors to strongly acidic or basic environments or to heavy metals does not have any significant effect on the molecular recognition properties. The MIP based sensors may even be exposed to organic media without loss of activity. Most of the MIPs produced in this laboratory have been designed to work in organic solvents. The resistance of the MIP based sensors to all of the described harsh treatment procedures suggests they may be especially suitable for industrial use. Furthermore, it was observed that storage of the morphine sensors in water for up to 4 weeks did not alter the response.

### 3.4. Sensor response

When the morphine sensors (containing M-MIP) were exposed to an increasing concentration of morphine (0–10 mg/ml), we observed a clear increase in the current peak  $i_c$  caused by addition of codeine (Fig. 6). As expected, this effect was much less evident when using reference sensors (containing O-MIP). When an agarose covered-platinum electrode was used, no change in the current was observed. In addition three morphine sensors (containing M-MIP) were prepared

Table 1

Sensor response (for 1  $\mu\text{g}/\text{ml}$  morphine) obtained for various morphine sensors that have been treated with heat, acid, base, organic solvents or heavy metals

Sensor treatment	Sensor response (%)
Heat (120°C for 20 min)	98
Acid (1 M HCl for 2 h)	102
Base (1 M NaOH for 2 h)	100
Organic solvent (acetone for 2 h)	96
Heavy metals (1% $\text{Ag}^+$ and 1% $\text{Hg}^{2+}$ for 2 h)	94

The response is calculated as the codeine-induced peak current ( $i_c$ ) ratio for the treated and the non-treated sensor. The reference sensors were not affected by similar treatments. The sensors are necessarily base-stable, because the cross-linking procedure involves exposure to 1.0 M NaOH for 2 h. Thus, a sensor containing agarose (and M-MIP) that was not crosslinked was treated with 1.0 M NaOH for 2 h. There was no difference in sensor response between crosslinked and non-crosslinked sensors. This indicates that the crosslinking procedure did not affect the response of the sensors.

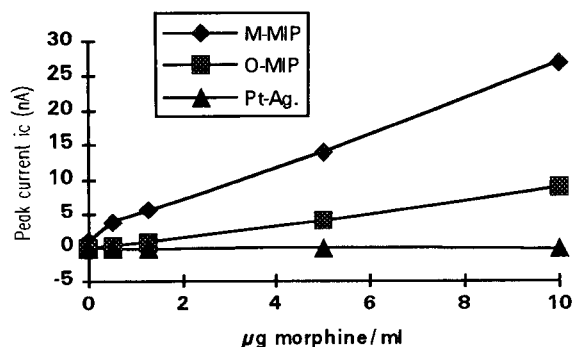


Fig. 6. Codeine induced peak current  $i_c$  as a function of the morphine concentration (0–10  $\mu\text{g}/\text{ml}$ ) present in the solution. Three sensor types were examined, the morphine sensor (M-MIP), reference sensor (O-MIP) and agarose-covered platinum electrode (Pt-Ag).

under identical conditions. The values of the responses (for 1  $\mu\text{g}/\text{ml}$  morphine) for the different sensors were reproducible to within 10%. A 0.5  $\mu\text{g}/\text{ml}$  morphine solution gave a peak current of 4 nA. The detection limit ( $S/N = 2$ ) is ca. 0.05  $\mu\text{g}/\text{ml}$  morphine.

In principle, the sensor configuration described allows the determination of morphine. The advantage of the present system, involving competition with a structurally related yet not electrochemically active compound (i.e., codeine), lies in the fact that the bound morphine can be determined in the presence of other species. Other electrochemically active compounds present in the sample will contribute to the equilibrium current  $i_m$  but only morphine will be effected by the addition of codeine. A prior isolation step specific for morphine followed by its release and determination would be an obvious alternative but with the drawback of being time consuming and complicated.

The present investigation may be considered as a first step in devising sensors based on molecular imprints with the ultimate goal of giving rise to an immediate signal on binding into the cavity. This would give rise to sensors with excellent mechanical and chemical stability; in addition recognition elements (imprints) can be prepared for which there is no corresponding biological alternative. Future investigations will focus on decreasing the response time and the detection limit of the presented morphine sensor. We also intend to apply it to real biological samples.

### Acknowledgements

Financial support from the Swedish Research Council for Engineering Sciences and technical support from



the Chemel Research Institute, Malmö, Sweden, is gratefully acknowledged. Furthermore the authors thank Dr. Richard Ansell for linguistic advice.

## References

- [1] D. Griffiths and G. Hall, *TIBTECH*, 11 (1993) 122.
- [2] F. Scheller and F. Schubert, *Biosensors*, Elsevier, Amsterdam, 1992
- [3] B. Sellergren, B. Ekberg and K. Mosbach, *J. Chromatogr.*, 347 (1985) 1.
- [4] R. Arshady and K. Mosbach, *Makromol. Chem.*, 182 (1981) 687.
- [5] G. Wulff, *Am. Chem. Soc. Symp. Ser.*, 308 (1986) 186.
- [6] K. Mosbach, *Trends Biochem. Sci.*, 19 (1994) 9.
- [7] L.I. Andersson, D.J. O'Shannessey and K. Mosbach, *J. Chromatogr.*, 513 (1990) 167.
- [8] G. Wulff, and J. Haarer, *Makromol. Chem.*, 192 (1991) 1329.
- [9] G. Wulff and M. Minarik, *J. Liq. Chromatogr.*, 13 (1990) 2987.
- [10] L. Fischer, R. Müller, B. Ekberg and K. Mosbach, *J. Am. Chem. Soc.*, 113 (1991) 9358.
- [11] G. Vlatakis, L.I. Andersson, R. Müller and K. Mosbach, *Nature*, 361 (1993) 645.
- [12] E. Hedborg, F. Winqvist, I. Lundström, L.I. Andersson and K. Mosbach, *Sensors Actuators A*, 37–38 (1993) 796.
- [13] D.J. O'Shannessey, B. Ekberg and K. Mosbach, *Anal. Biochem.*, 177 (1989) 144.
- [14] J. Porath, J.-C. Janson and T. Låås, *J. Chromatogr.*, 60 (1971) 167.
- [15] L.I. Andersson, R. Müller, G. Vlatakis and K. Mosbach, (1994) submitted for publication.
- [16] T. D. Wilson, *J. Chromatogr.*, 301 (1984) 39.
- [17] K. Nakumara, M. Aizawa and O. Miyawaki, in *Electroenzymology Coenzyme Regeneration*, Springer Verlag, Berlin, 1988, p. 48.



ELSEVIER

Analytica Chimica Acta 300 (1995) 77–83

ANALYTICA  
CHIMICA  
ACTA

# Diamond like carbon coated films for enzyme electrodes; characterization of biocompatibility and substrate diffusion limiting properties

Séamus P.J. Higson <sup>\*,1</sup>, Pankaj M. Vadgama

*Department of Medicine (Section of Clinical Biochemistry), University of Manchester, Hope Hospital, Eccles Old Rd., Salford M6 8HD, UK*

Received 4 January 1994; revised manuscript received 8 July 1994

## Abstract

The biocompatibility and substrate diffusion limiting properties for a range of diamond like carbon (DLC) coated microporous polycarbonate and DLC coated dialysis (haemodialysis) membranes have been studied. This characterisation builds upon previous findings where DLC coated membranes imparted enhanced enzyme electrode performance. In this study electrode linear ranges have been extended from 10 mM glucose for a 0.01  $\mu\text{m}$  pore size membrane to 160 mM. These findings correlated with the duration of DLC deposition and associated reductions in permeability for glucose. Permeability coefficient ratios for both microporous and dialysis membranes were also found to be important with low glucose/ $\text{O}_2$  permeability ratios imparting extensions in glucose linear response range. DLC coated membranes employed within enzyme electrodes have also been shown to exhibit enhanced haemocompatibility as determined by both sensitivity change and surface deposition of blood components examined by scanning electron microscopy. Correlations are made between the reduced losses in sensor response to biofouling/working electrode passivation processes, and extended linear ranges that DLC coated membranes may impart to enzyme electrode performance. Particular reference is made to the determination of glucose levels within whole blood.

*Keywords:* Biosensors; Diamond like carbon coated films; Enzyme electrodes

## 1. Introduction

Optimization of enzyme electrodes for simplified reagentless analysis regimens [1] has been achieved through the exploitation of membrane technology [2], mediator chemistry [3] as well as for example optical techniques [4,5] and the use of chemically modified electrodes [6,7].

Generally it has proved necessary to protect devices with surface coatings and materials of enhanced bio-

compatibility [8] to reduce the rate of deposition of an outer biofouling layer. Hitherto, the biocompatibility of diamond like carbon (DLC) has been demonstrated both in vitro and in vivo [9,10]. It has the advantage of lending itself to deposition on a wide range of substrates [11–14] and constitutes strong yet flexible surface layers [15,16]. Furthermore DLC may be deposited on thermally sensitive media, since deposition from the neutral saddle field source may be performed at room temperatures [14].

We recently reported coating microporous polycarbonate membranes with DLC where the membrane was a covering outer layer of an  $\text{H}_2\text{O}_2$  based amperometric

\* Corresponding author.

<sup>1</sup> Present address: Department of Chemistry, The Manchester Metropolitan University, Chester St., Manchester M1 5GD, UK.

glucose enzyme laminate electrode [17]. This study indicated that enzyme electrode stability increased, provided covering membranes had both low porosity (<0.2%) and were coated with DLC.

The present work reports the efforts of a systematic variation in DLC deposition time on high porosity membranes and consequences for observed surface biofouling in whole blood.

As with the previous study, effects on the permeability coefficient,  $P$ , ratios for glucose/ $O_2$  at polycarbonate membranes have been determined by an independent diffusion chamber method. Comparisons are also made with regard to response times, linearity and the enhanced biocompatibility that DLC coated membranes may impart to enzyme electrodes.

## 2. Experimental

### 2.1. Chemicals

Glucose oxidase from *Aspergillus niger* (75% protein, 150,000 units/g solid) and bovine serum albumin (fraction V) were purchased from Sigma (Poole). D-Glucose disodium hydrogenphosphate, sodium dihydrogenphosphate, sodium benzoate, sodium chloride and glutaraldehyde (AnalaR grade) were purchased from BDH (Poole). All chemicals were used without further purification. A buffer (pH 7.4) comprising  $5.28 \times 10^{-2}$  M  $Na_2HPO_4$ ,  $1.3 \times 10^{-2}$  M  $NaH_2PO_4$ ,  $5.1 \times 10^{-3}$  M NaCl and  $6.24 \times 10^{-3}$  M sodium benzoate was prepared in distilled water. This buffer was used for all enzyme preparations, electrochemical studies and diffusional determinations.

### 2.2. DLC coating of polycarbonate and dialysis membranes

Polycarbonate membranes were purchased from Poretics (Livermore), and dialysis (haemodialysis) membranes were obtained from Gambro (Lund). The DLC coating procedure was performed by Atom Tech (Middlesex), and has been previously described. The method involves a fast atom bombardment (FAB) cleaning process for 5 min in a neutral saddle field argon source followed by the coating of DLC in the same argon source with a hydrocarbon introduced to the beam [10]. Polycarbonate membranes of a nominal

pore size of  $0.01 \mu\text{m}$  and dialysis membranes were coated with a range of deposition durations. Control membranes without DLC coating were similarly cleaned by subjection to 5 minutes FAB. All times are specified in terms of total deposition time (here, 50% of the coating was applied to each side with the specified deposition rate being  $0.45 \mu\text{m}$  thickness per hour).

### 2.3. Apparatus

An oxygen electrode assembly, Rank Brothers (Bot-tisham) as previously described [2], was utilized for glucose oxidase enzyme electrodes. The working electrode (anode) was polarized at +650 mV (vs. Ag/AgCl) for the oxidation of  $H_2O_2$ . The cell comprised a central 2 mm diameter platinum disc with a surrounding pre-anodised 12 mm outer diameter, 1 mm wide silver ring (Ag/AgCl), acting as a combined reference and counter electrode. The purpose built voltage polarization source and potentiostat were constructed by the Chemistry workshops (University of Newcastle), and an  $x-t$  chart recorder (Lloyd, Fareham) was used to record amperometric responses of the electrode assembly from the potentiostat current follower. A blood gas analyser (Instrumentation Laboratory Model IL1802) was employed for the analysis of  $pO_2$  levels within buffer aliquots.

Blood samples used for biocompatibility evaluation were stored in fluoride/oxalate tubes, as used for routine blood glucose analyses.

### 2.4. Fabrication of enzyme electrodes

A composite solution of glucose oxidase (GOD) (2560 units/ml) and bovine serum albumin (BSA) (0.1 g/ml) was prepared in buffer solution.  $6 \mu\text{l}$  of GOD-BSA solution and  $3 \mu\text{l}$  of glutaraldehyde (5% w/v) were mixed rapidly and placed on a  $1 \text{ cm}^2$  portion of  $0.05 \mu\text{m}$  pore size polycarbonate membranes. A  $1 \text{ cm}^2$  portion of the DLC coated polycarbonate or dialysis membrane was then placed on top, and glass slides used to compress the enzyme and membrane laminate under finger pressure for approximately 5 min. The resulting cross-linked electrode assembly was mounted over the working electrode prior to final electrode cell assembly and fixation, by means of a rubber "O-ring".

### 2.5. Determination of permeability coefficients

Solute mass transfer measurements were carried out at  $22 \pm 1^\circ\text{C}$  using a classical diffusion chamber apparatus comprising two membrane separated chambers [17], as previously described. Each chamber was of 170 ml volume; these were clamped together to retain two stainless steel discs and two sealing rubber O-rings which held the membrane of interest. The cross-sectional area available for mass transport was  $7.07\text{ cm}^2$ . The solute of interest (100 mM glucose or  $\text{O}_2$  gas purging) was introduced into one chamber to create a concentration gradient and mass transfer was determined by assaying solute concentrations in both chambers at periodic intervals. Oxygen samples were obtained from a closed system and were extracted by a glass syringe and sealed within 1 ml glass vials to prevent mixing with the atmosphere, prior to  $p\text{O}_2$  analysis. Oxygen within one chamber was consumed by placing cross-linked GOD–BSA films in excess, to maintain oxygen concentrations across the membrane of interest.  $p\text{O}_2$  levels were determined by the Model IL1802 blood gas analyser. Aliquots analyzed for  $p\text{O}_2$  levels from chambers containing BSA–GOD films confirmed that all oxygen was consumed. Permeability coefficients were calculated as previously reported [18].

### 2.6. Electron microscopy

Electron micrographs were taken using a Cambridge Instruments scanning 360 electron microscope. All samples were coated with gold using an Emscope SC500 sputter coater machine. Membranes that had not been exposed to blood were coated directly. Membranes for study that had been exposed to whole blood were first washed in buffer and then immersed in a standard electron microscopy fixative 4% (w/v) containing glutaraldehyde buffer [19]; the preparation was then allowed to dry in air slowly and sputter coated with gold as before.

## 3. Results and discussion

DLC coated membranes with very low pore sizes ( $0.01\ \mu\text{m}$ ) and pore densities of  $6 \times 10^8$  pores  $\text{cm}^{-2}$  were previously found to show enhanced biocompati-

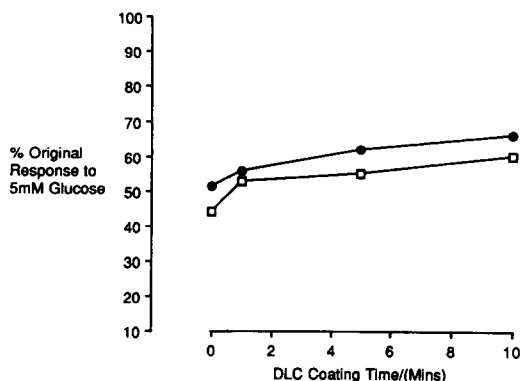


Fig. 1. Relationship between percentage original response to 5 mM glucose following 30 min exposure to whole blood. Inner  $0.05\ \mu\text{m}$  pore size polycarbonate membrane, double sided DLC coated covering membrane: (□)  $1\ \mu\text{m}$  pore size polycarbonate membrane. (●) Dialysis membrane.

bility [17]. Enzyme electrodes with larger  $1\ \mu\text{m}$  pore size polycarbonate DLC coated and non-coated covering membranes respectively were therefore constructed to determine the influence of DLC coating on biocompatibility. In a similar fashion, coated and non-coated dialysis membranes were examined. All sensors possessed  $0.05\ \mu\text{m}$  pore size inner polycarbonate membranes and the working electrode was polarised at  $+650\text{ mV}$  vs.  $\text{Ag}/\text{AgCl}$ .

Responses to 5 mM glucose solutions were recorded before and after 30 min exposure to whole blood (Fig. 1). Percentage losses of response following exposure to whole blood appeared to be greater for a sensor employing a  $1\ \mu\text{m}$  pore size polycarbonate membrane than sensors with smaller pore size membranes [17]; however the degree of loss is diminished as DLC is first applied to a membrane (in comparison to the uncoated membrane, 0 min coating) with a further improvement as the coating duration is increased. Electrode performances with DLC coated dialysis membranes also follow a similar trend with increased DLC coating durations. Surface architecture almost certainly influences the deposition of formed elements in blood and so biofouling [20]. In addition, it has been shown low molecular weight solutes within blood may traverse the sensor and subsequently passivate the working electrode [21]. It follows that DLC coatings in addition to reducing surface biofouling may potentially afford greater protection against working electrode passivation processes which contribute to the loss of sensor responses on exposure to whole blood.

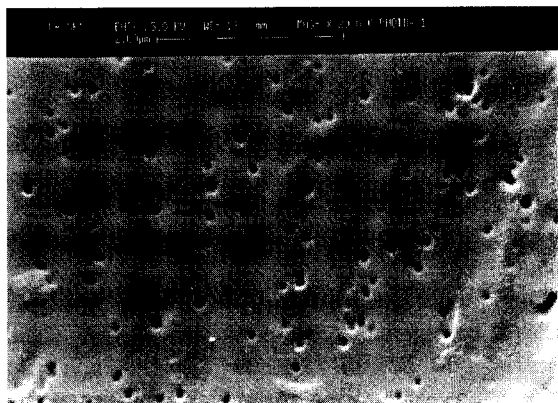


Fig. 2. Electron micrograph of a microporous 0.05  $\mu\text{m}$  pore size polycarbonate membrane.

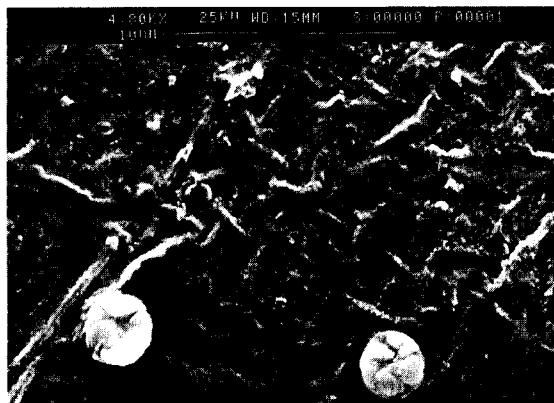


Fig. 5. Electron micrograph of a microporous 0.05  $\mu\text{m}$  pore size polycarbonate membrane with 10 min DLC coating following 30 min exposure to whole blood.

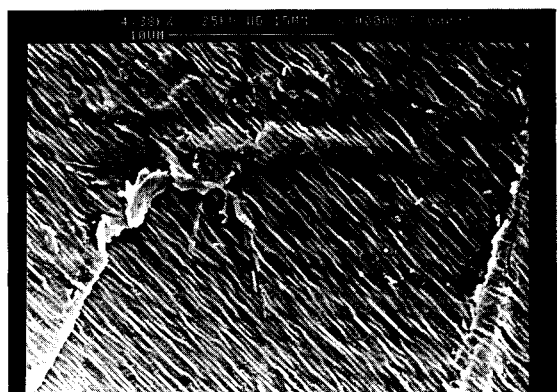


Fig. 3. Electron micrograph of a microporous 0.05  $\mu\text{m}$  pore size polycarbonate membrane with 10 min DLC coating.

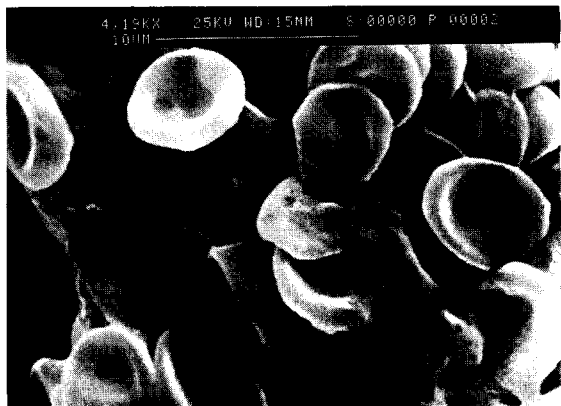


Fig. 4. Electron micrograph of a microporous 0.05  $\mu\text{m}$  pore size polycarbonate membrane following 30 min exposure to whole blood.

Fig. 2 shows a typical SEM of a 0.05  $\mu\text{m}$  pore size polycarbonate membrane illustrating both random distribution of pores and a degree of variation in the commercially available product. After a 10 min coating duration of DLC (Fig. 3), the pores are not discernible and the carbon surface shows a “striated” appearance, probably due to the specific orientation and rotation of the sample with respect to the saddle field source during the coating process. Figs. 4 and 5 show the same membranes following 30 min exposure to unstirred whole blood, with the uncoated polycarbonate showing red cell and possibly other components from blood adherent to the membrane surface. In contrast after DLC coating there is a much reduced surface adherence of red cells, though some deposition of amorphous material has clearly occurred.

Fundamentally the  $\text{sp}^3$  orbitals of DLC [14] will provide a highly stable and chemically non-reactive

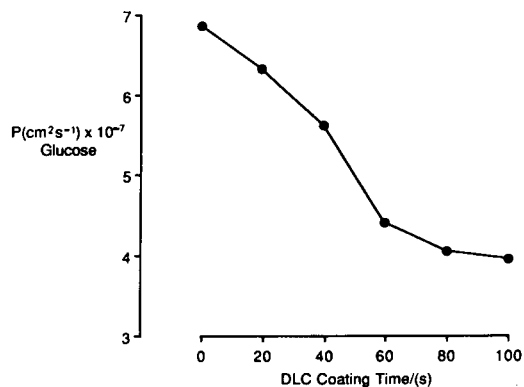


Fig. 6. between permeability coefficient,  $P$ , for glucose across double-sided DLC coated 0.01  $\mu\text{m}$  pore size polycarbonate membranes.

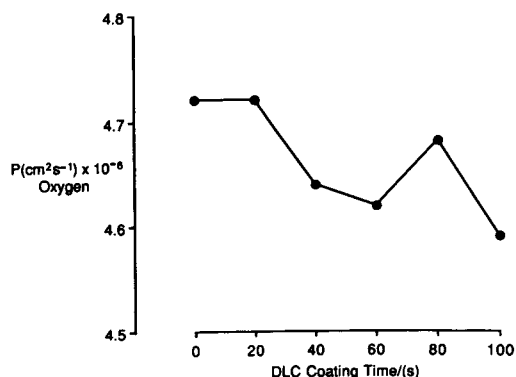


Fig. 7. Relationship between permeability coefficient,  $P$ , for oxygen across double sided DLC coated  $0.01 \mu\text{m}$  pore size polycarbonate membranes.

surface and this may have relevance to the extent of the surface interaction with blood.

The  $P$  values for glucose and  $\text{O}_2$  determined across  $0.01 \mu\text{m}$  pore size membranes (Figs. 6 and 7), respectively, for membranes coated with; 0, 20, 40, 60 and 100 s durations of DLC show a clear downward trend. As the DLC coating is increased the permeability coefficient for glucose (Fig. 6) is progressively lowered. Though a similar trend was observed for  $\text{O}_2$  (Fig. 7)  $\text{O}_2$  transport is maintained relative to glucose and the glucose/ $\text{O}_2$   $P$  ratio, therefore decreases markedly with increasing DLC deposition (Fig. 8). It is probable that glucose permeability is progressively lowered by a physical encroachment of pores by the surface build up of DLC. The differential effect on glucose/ $\text{O}_2$  suggests that either  $\text{O}_2$  is able to diffuse across a thin DLC layer, or that coverage of the membrane surface by DLC is incomplete due to variable deposition at a topologically non-uniform surface.

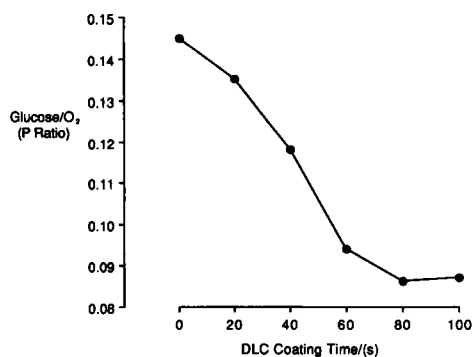


Fig. 8. Relationship between glucose/ $\text{O}_2$  permeability coefficient,  $P$ , ratios across double sided DLC coated  $0.01 \mu\text{m}$  pore size polycarbonate membranes.

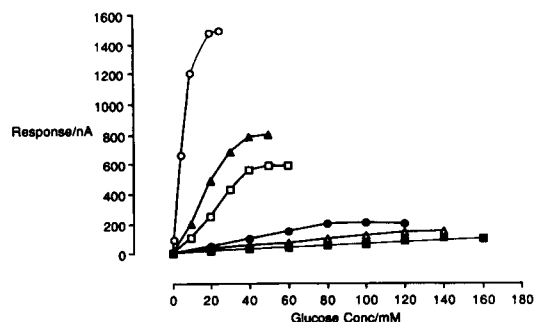


Fig. 9. Glucose electrode calibration graphs;  $0.05 \mu\text{m}$  pore size inner membranes. Double sided DLC coated covering  $0.01 \mu\text{m}$  pore size polycarbonate membranes. Differing DLC duration depositions: (○) uncoated, (▲) 20 s, (□) 40 s, (●) 60 s, (△) 80 s, (■) 100 s.

Calibration curves for enzyme electrodes with outer polycarbonate membranes of  $0.01 \mu\text{m}$  pore size with 20–100 s duration of DLC deposition (Fig. 9) show a progressive extension of linear range associated with lowering of response. Though responses appear rather small for a 100 s deposition on the scale used, current resolution to within  $0.5 \text{ nA}$  readily enabled determination down to  $5 \text{ mM}$  glucose.

DLC appears to allow a tailoring of membrane permeability with a degree of fine control that is not readily possible with solution deposition of coating layers [2]. DLC coatings would appear also to be suitable for other enzyme electrodes, and may offer a way of scale-up production of coated membranes with reproducible permeabilities. It is thought that low-molecular-weight solutes may traverse the enzyme laminate and passivate the working electrode [21]. Previous studies by us demonstrated that sensors employing DLC coated covering membranes suffered reduced losses of sensor performance on exposure to whole blood [17]. Control of low-molecular-weight solute diffusion across the covering DLC membrane may have therefore aided the enhanced electrode performance reported earlier by reducing the flux of passivating solute across the sensor [17]. It therefore appears that the effects of DLC coatings at membrane surfaces are inter-related, so as to enhance surface biocompatibility, linearise sensor responses and reduce working electrode passivation. It is therefore probable that these mechanisms collectively may act in a complementary manner to enhance sensor performance.

Of equal interest is the finding that glucose and  $\text{O}_2$  transport across DLC coated dialysis membranes can

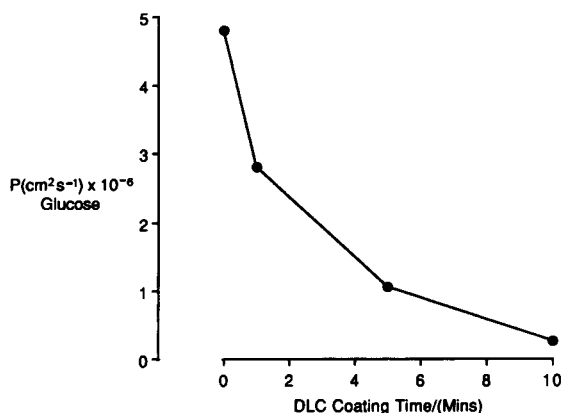


Fig. 10. Relationship between permeability coefficients,  $P$ , for glucose across double sided DLC coated dialysis membranes.

also be manipulated (Figs. 10 and 11). Extended DLC deposition times are needed, no doubt because of the initial high intrinsic permeability of dialysis membranes. However it should be noted that the reducing effect on  $\text{O}_2$  permeability parallels the effect on glucose more closely than with microporous polycarbonate, and there is a lesser impact on the glucose/ $\text{O}_2$  permeability (Fig. 12). Subsequent glucose electrode calibrations for sensors employing DLC coated dialysis membranes again show extended linearity ranges (Fig. 13). Both in the case of polycarbonate and dialysis membranes the lowest permeability towards glucose is associated with the greatest extensions of linearity (Fig. 9), rather than the lowest glucose/ $\text{O}_2$   $P$  ratios (Fig. 12).

The kinetic dependence of GOD activity on  $\text{O}_2$  tension is complex, but an approximate sevenfold increase in activity is reported with a twenty fold increase (5–

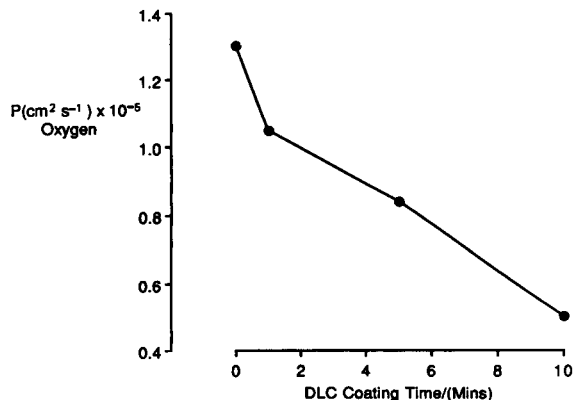


Fig. 11. Relationship between permeability coefficients,  $P$ , for oxygen across double sided DLC coated dialysis membranes.

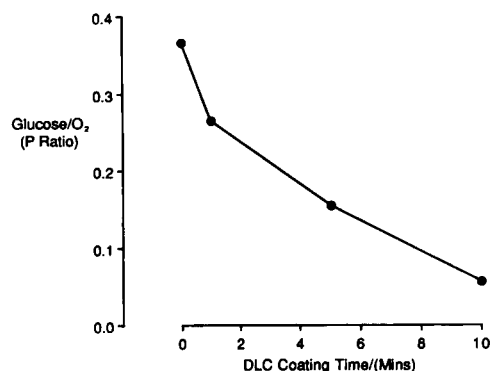


Fig. 12. Relationship between glucose/ $\text{O}_2$  permeability coefficient,  $P$ , ratios across double sided DLC coated dialysis membranes.

100%) in oxygen tension [22], and so a stoichiometric deficit is likely to occur at higher glucose levels. The membrane technology approach here, helps to counter the  $\text{O}_2$  deficit problem while at the same time lowering the effective local concentration of glucose within the enzyme layer.

Though an extension of linearity to ca. 140 mM glucose with a  $0.01\ \mu\text{m}$  pore size was achieved, it is likely that with further fine-tuning of deposition, greater extensions of linear range will be possible.

#### 4. Conclusions

High permeability polycarbonate and dialysis membranes when coated with DLC were found to exhibit enhanced biocompatibilities, when exposed to whole blood. Accordingly glucose sensors employing DLC

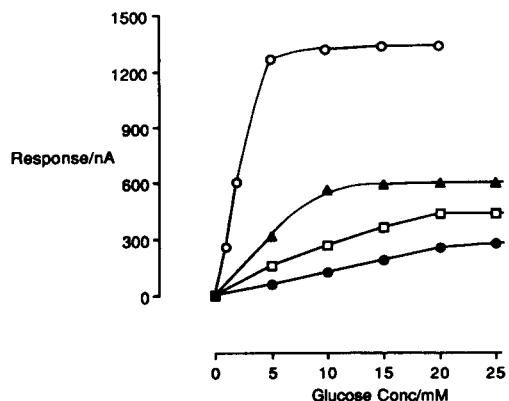


Fig. 13. Glucose electrode calibrations,  $0.05\ \mu\text{m}$  pore size inner dialysis membranes. Covering dialysis membranes with differing DLC deposition times: (○) uncoated, (▲) 1 min DLC deposition, (□) 5 min DLC deposition, (●) 10 min DLC deposition.

coated outer covering membranes were found to have suffered smaller losses of response following exposure to whole blood. SEMs of such membranes showed that DLC coated surfaces reduce protein and red blood cell adherence to the membrane surface.

Permeability coefficient ( $P$ ) ratios for glucose/ $O_2$  across DLC coated low porosity polycarbonate and dialysis membranes have been correlated with subsequent enzyme electrode performance when used as covering membranes. Membranes with lower glucose/ $O_2$   $P$  ratios were found to impart extended linearities, but membranes with the lowest  $P$  values towards glucose were found to affect the greater extensions in sensor linearity irrespective of other factors.

DLC coatings at membrane surfaces have been shown to reduce cell adherence/biofouling and be capable of tailoring low-molecular-weight solute flux and it is proposed that such processes enhance sensor performance in a complementary fashion.

### Acknowledgements

The authors would like to thank the SERC and DTI for financial support for this work.

### References

- [1] P. Vadgama, *J. Membr. Sci.*, 50 (1990) 141.
- [2] W.H. Mullen, S.J. Churchouse, F.H. Keedy and P. Vadgama, *Anal. Chim. Acta*, 183 (1986) 59.
- [3] A.E.G. Cass, G. Davis, G.D. Francis, H.A.O. Hill, W.J. Aston, I.J. Higgins, E.V. Plotkin, L.D.L. Scott and A.P.F. Turner, *Anal. Chem.*, 56 (1984) 667.
- [4] N. Takai, I. Sakuma, A. Kaneko, T. Fujie, K. Taguchi and S. Nagaoka, *Artif. Organs*, 15 (1991) 86.
- [5] C. Schelp, T.H. Scheper, F. Buckmann and K.F. Readon, *Anal. Chim. Acta*, 255 (1991) 223.
- [6] P.D. Hale and T.A. Skotheim, *Synth. Met*, 28 (1989) C853.
- [7] W.J. Albery, A.E.G. Cass and Z.X. Shu, *Biosensors Bioelectron.*, 5 (1990) 379.
- [8] A.P.F. Turner, I. Karube and G.S. Wilson, *Biosensors – Fundamentals and Applications*, Oxford University Press, Oxford, 1987.
- [9] L.A. Thomson, F.C. Law, J. Franks and N. Rushton, *Biomaterials*, 12 (1991) 37.
- [10] A.C. Evans, J. Franks and P.J. Revell, *Medical Device Technology*, May (1991) 26.
- [11] C. Wild, P. Koidl and J. Wagner, *E.M.R.S Symposia Proc.*, 17 (1987) 1374.
- [12] T. Taguchi, M. Morikawa, Y. Hiratsuk and K. Toyoda, *E.M.R.S Symposia Proc.*, 17 (1987) 123.
- [13] M.J. Mirtich, *E.M.R.S Symposia Proc.*, 17 (1987) 377.
- [14] J. Franks, *J. Vac. Sci.*, A71 (1989) 2307.
- [15] J.C. Angus, *E.M.R.S. Symposia Proc.*, 17 (1987) 179.
- [16] D.G. Thompson, *Proc 30th Ann. Tech. Conf., SVC*, (1987) 135.
- [17] S.P.J. Higson and P.M. Vadgama, *Anal. Chim. Acta*, 271 (1993) 125.
- [18] Y. Sun, S. Furusaki, A. Yamauchi and K. Ichimura, *Biotechnol. Bioeng.*, 34 (1989) 55.
- [19] D.C. Pease, in *Histology Techniques for Electron Microscopy*, Academic Press, 2nd edn., New York, p. 34.
- [20] C. Hougie and R.F. Bough, in R. Biggs and C.R. Rizza (Eds.), *Human Blood Coagulation, Haecostasis and Thrombosis*, Blackwell, Oxford, 1984.
- [21] S.P.J. Higson, M.A. Desai, S. Ghosh and P. Vadgama, *J. Chem. Soc., Faraday Trans.*, 89 (1993) 2847.
- [22] P.D. Boyer, H. Lardy and K. Myback, in *The Enzymes*, Academic Press, New York, 1963.



# Diamond like carbon films for enzyme electrodes; characterisation of novel overlying permselective barriers

Séamus P.J. Higson <sup>\*,1</sup>, Pankaj M. Vadgama

*Department of Medicine (Section of Clinical Biochemistry), University of Manchester, Hope Hospital, Eccles Old Road, Salford M6 8HD, UK*

Received 23 December 1993; revised manuscript received 8 July 1994

## Abstract

Diamond like carbon (DLC) coated microporous polycarbonate membranes have been studied for use as novel composite permselective barriers membranes for a glucose enzyme electrode. Permeability coefficients,  $P$ , for key electrochemically active interferents across uncoated and DLC coated polycarbonate membranes has been compared. Interferent responses have then been assessed for sensors incorporating such membranes, and their relationship to differing DLC depositions assessed. Membranes with smaller pore sizes (0.03 and 0.01  $\mu\text{m}$ ) and extended DLC depositions (up to 7 min coating), while imparting some enhanced selectivity towards glucose, failed to show major discrimination for glucose over interferents as shown by  $P$  values: maximum glucose-to-interferent  $P$  ratios being 1.36 and 1.25 for ascorbate and urate, respectively. The implications of these findings are discussed.

*Keywords:* Biosensors; Diamond like carbon coated films; Enzyme electrodes

## 1. Introduction

The optimisation of oxidase based amperometric enzyme electrodes has been achieved through a variety of routes [1]. The most notable of these include the use of solute diffusion controlling and other protective membranes [2], exploitation of artificial (non-oxygen) mediators [3], and the use of conducting polymers [4] as alternatives to noble metals or carbon as working electrode materials.

An important general problem to measurement in biological samples is the presence of electrochemically active interferents. These lead to errors in measurement irrespective of whether a high polarising voltage regime

is used as for  $\text{H}_2\text{O}_2$  detection, or alternatively a mediator facilitated low polarising voltage is achieved [5,6].

The most prevalent of the reports on mediators have been those dealing with the organometallic mediators such as ferrocene [3] where anodic polarisation potentials of +240 mV vs. Ag/AgCl have been realised, but where nevertheless some interferent contribution to the response is not wholly avoided (e.g., as to ascorbate) [3].

A further approach has been the interposing of a barrier membrane between the enzyme layer and the working electrode [1,7], selective for the detectible entity. Membranes such as cellulose acetate [8] or Nafion [9] have been reported with the mechanism for selectivity based on a complex combination of molecular weight exclusion, charge and intramembrane partitioning.

\* Corresponding author.

<sup>1</sup> Present address: Department of Chemistry, the Manchester Metropolitan University, Chester St., Manchester M1 5GD, UK.

We have previously reported the use of covering microporous polycarbonate membranes coated with diamond like carbon (DLC) for the construction of a glucose oxidase enzyme electrode capable of glucose concentration determinations within whole undiluted blood [10]. These membranes were developed for the differential and absolute control of  $O_2$  and substrate permeability, extending the apparent enzyme  $K_M$  and therefore, the linear dynamic range of the electrode. Furthermore, DLC is chemically inert, exhibiting an apparently high degree of biocompatibility [11], and can be formed as strongly adherent but flexible coatings which may be applied to thermally unstable materials [12]. Operationally, it was observed that despite the lack of internal permselective membranes of the cellulose acetate type, electrodes could be fabricated that nevertheless allowed reliable determination of glucose concentrations within whole (undiluted) blood samples [10]. This was an unexpected observation, given the anticipated lack of molecular selectivity of membrane materials of 0.01–0.1  $\mu\text{m}$  pore size.

This study is aimed at quantitating the permeability of such membranes in order to determine possible mechanisms for selectivity, and as a route to the design of future selective barrier materials.

## 2. Experimental

### 2.1. Chemicals

Glucose oxidase from *Aspergillus niger* (75% protein 150,000 units/g solid), and bovine serum albumin (BSA), fraction V were purchased from the Sigma (Poole). D-Glucose, disodium hydrogenphosphate, sodium dihydrogenphosphate, sodium benzoate and sodium chloride (AnalaR grade) were purchased from BDH (Poole). All chemicals were used without further purification.

A buffer (pH 7.4) comprising  $5.28 \times 10^{-2}$  M  $\text{Na}_2\text{HPO}_4$ ,  $1.3 \times 10^{-2}$  M  $\text{NaH}_2\text{PO}_4$ ,  $5.1 \times 10^{-3}$  M  $\text{NaCl}$  and  $6.24 \times 10^{-3}$  M sodium benzoate was prepared in distilled water. This buffer was used for all enzyme preparations, electrochemical studies and diffusional determinations unless otherwise stated. A further buffer of pH 8.5 was prepared by adjusting the concentration of  $\text{Na}_2\text{HPO}_4$ , within the original buffer.

### 2.2. DLC coating of polycarbonate

Polycarbonate membranes were purchased from Poretics (Livermore). DLC coated membranes were prepared commercially by Atom Tech; the process has previously been described in detail [12–16]. The method involves a fast atom bombardment (FAB) cleaning process for 5 min in a neutral saddle field argon source, followed by the coating of DLC in the same argon source with a hydrocarbon introduced to the beam [14]. Polycarbonate membranes of pore size 0.01  $\mu\text{m}$  and dialysis membranes were coated for a range of deposition times. Control membranes without DLC coating were similarly cleaned for 5 min FAB.

DLC coating times quoted define total deposition times; therefore, membranes have 50% of the coating deposited on each surface; the deposition rate of DLC being 0.45  $\mu\text{m}$  thickness per hour.

### 2.3. Apparatus

An oxygen electrode assembly (Rank, Bottisham) as previously described [2], was utilised for preparation of the glucose oxidase based enzyme electrodes.

The working electrode (anode) was polarised at +650 mV (vs. Ag/AgCl) for the oxidation of  $\text{H}_2\text{O}_2$ . The cell comprised a central 2 mm diameter platinum disc as a working electrode with an outer pre-anodised 12 mm outer diameter, 1 mm wide silver ring (Ag/AgCl) acting as a combined reference and counter electrode. The purpose built voltage polarisation source and potentiostat were constructed by the Chemistry workshops, (University of Newcastle) and a  $x-t$  chart recorder, (Lloyd, Fareham) was used to record amperometric responses of the electrode assembly from the potentiostat current follower. A blood gas analyser (Instrumentation Laboratory, IL1802) was used in the clinical biochemistry laboratories (Hope Hospital) for the determination of  $pO_2$  levels within buffer sampled aliquots.

### 2.4. Fabrication of enzyme electrodes

A composite solution of glucose oxidase (GOD, 2560 units/ml) and bovine serum albumin (BSA, 0.1 g/ml) was prepared in buffer. 6  $\mu\text{l}$  of the GOD/BSA mixture and 3  $\mu\text{l}$  of glutaraldehyde (5%, w/v) were mixed rapidly and placed onto a 1  $\text{cm}^2$  of polycarbonate

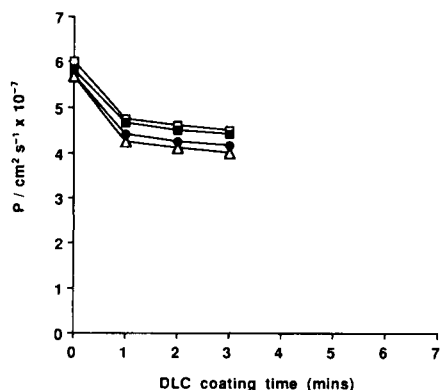


Fig. 1. Permeability coefficients ( $P$ ) for glucose (□), paracetamol (■), ascorbate (●), and urate (△) across  $0.01 \mu\text{m}$  pore size DLC coated polycarbonate membranes.

membrane of the required pore size. A  $1 \text{ cm}^2$  portion of the DLC coated polycarbonate or dialysis membrane was then placed on top, and glass slides used to compress the enzyme and membrane laminate under finger pressure for approximately 5 min. The resulting cross-linked enzyme/membrane laminate was thoroughly rinsed in buffer and was placed over the working electrode prior to final electrode assembly.

### 2.5. Determination of permeability coefficients

Solute mass transfer measurements across dialysis and polycarbonate membranes to assess their permeability were performed at  $22 \pm 1^\circ\text{C}$  in a classical two compartment diffusion chamber apparatus as previously described [10,17].

Both compartments were of 170 ml volume and were separated by two stainless steel discs and two sealing rubber "O" rings clamped together to retain the required membrane, giving a defined cross-sectional area available for mass transport of  $7.07 \text{ cm}^2$ . The solute of interest was rapidly injected into one chamber and mass transport determined by measuring concentrations in both chambers at periodic intervals. Permeability coefficients were calculated as previously described [17].

## 3. Results and discussion

A sensor has recently been described by us that has permitted glucose determinations within whole undi-

luted blood with good correlations with standard clinical biochemistry analyses; this sensor achieved the required selectivity without an underlying permselective membrane, although a DLC coated covering polycarbonate membrane was employed [10].

Accordingly, the permeability coefficients ( $P$ ) for paracetamol, ascorbate, urate and glucose have been determined (Figs. 1–4) across DLC coated and uncoated polycarbonate membranes of 0.01, 0.03, 0.05 and  $0.1 \mu\text{m}$  pore size, respectively. The permeability coefficients for all species increase as the membrane pore size is increased, but with DLC coating, a reduction in permeability is observed with increasing deposition time. These findings are consistent with a membrane offering a mean reduced pore "aperture".

Figs. 1–4, however, also show two possible relevant features regarding selectivity for microsolute. Firstly, even for small ( $0.01 \mu\text{m}$ ) pore size DLC coated membranes, although such coated membranes do not show strong selectivity as measured by the permeability coefficient, there is a consistently greater reduction of permeability for the anions studied (urate, ascorbate) with respect to the neutral species. Secondly, the permeability of membranes as used in the previously reported enzyme electrode [10] is lowered to ca. 10% of the original percentage which probably represents "fine tuning" to the lowest possible degree before absolute blockage of the membrane occurs; such tailoring of permeability has not previously been possible with deposition techniques [17]. In the light of this data, enzyme electrodes employing DLC coated membranes

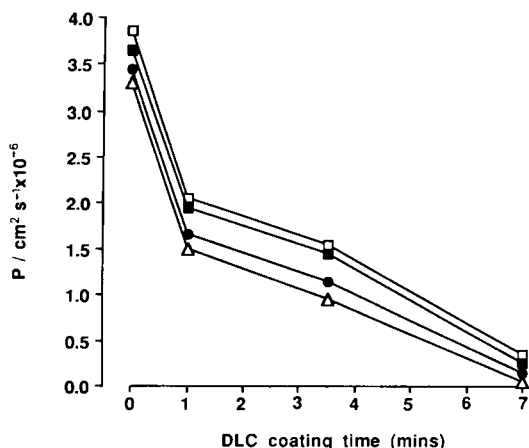


Fig. 2. Permeability coefficients ( $P$ ) for glucose (□), paracetamol (■), ascorbate (●), and urate (△) across  $0.03 \mu\text{m}$  pore size DLC coated polycarbonate membranes.

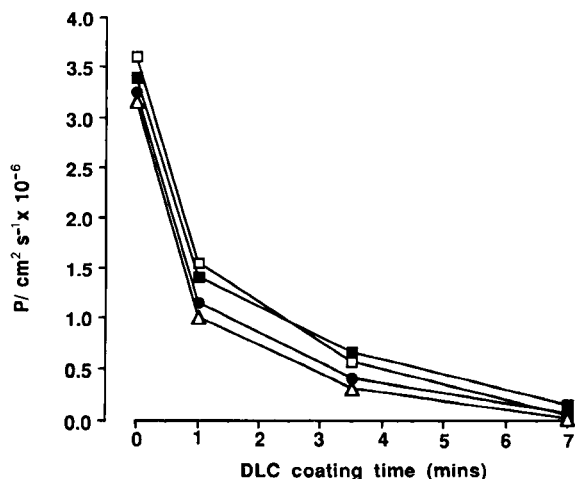


Fig. 3. Permeability coefficients ( $P$ ) for glucose (□), paracetamol (■), ascorbate (●), and urate (△) across  $0.05 \mu\text{m}$  pore size DLC coated polycarbonate membranes.

appear to show higher levels of selectivity against interferent species [10] than would be expected. One possible explanation for this is an “amplification” of the flux of signal generating species to the working electrode due to the potentiating effects of: (i) the slightly higher flux of glucose through the outer membrane compared with the interferents, and (ii) degradation of glucose and intra-membrane production of  $\text{H}_2\text{O}_2$ ; here the shorter diffusional distance could lead to steeper intra membrane concentration gradients to the working electrode.

A possible explanation for the greater membrane resistance to the anions may involve the increasing wall effects within the membrane pores, equivalent to the exclusion of anionic interferents previously reported for polymeric permselective membranes (e.g., cellulose acetate [8] and polyether sulphone) [7]. Although neither uncoated or DLC coated polycarbonate membranes have formal charge groups, there is likely to be a finite interfacial charge developing in the electrolyte solution. Calibration profiles for enzyme electrodes in the presence and absence of interferents, (Fig. 5), may however implicate a further mechanism. At the pH of the glucose measurement, the net anionic charge of albumin,  $pI$  (4.7–4.9) [18], might be expected to further hinder the transport of the anionic interferents. An explanation in part accounted for by charge repulsion effects becomes more attractive when one considers the concentration dependence of selectivity (Fig. 5). It appears that interferent contributions

(due to a fixed concentration) only become significant when the enzyme layer experiences a higher glucose flux. This is observed by the separation of the background (glucose only) and glucose/interferent response curves. Thus for the non-coated (and most permeable) polycarbonate at high glucose values ( $> 10 \text{ mM}$ ), the interference due to ascorbate, urate and paracetamol becomes apparent. Here, it is probable that despite ambient solution buffering, the enzyme mediated production of gluconolactone (and therefore gluconic acid) will lower the local enzyme layer pH, and the protective barrier action of enzyme layer will be diminished. In order to investigate this possible effect further, glucose calibration curves with and without interferents were determined using buffered solutions at pH 8.5 (Fig. 6). As anticipated all enzyme electrode responses were slightly lower than those observed at pH 7.4 due to a further deviation from the optimal pH for the enzyme (glucose oxidase optimal pH 5.6–6.0 [19]). However, it can be observed that the interferent contribution to amperometric responses remain suppressed in comparison to the calibration profiles of Fig. 5 at pH 7.4 for sensors employing non-coated membranes. Indeed, at 20 mM glucose and pH 7.4 there is a ca. 105 nA deviation observed between the glucose response in the presence or absence of interferents; contrastingly, at pH 8.5 and at the same glucose concentration there is a deviation of only ca. 50 nA between the differing calibration profiles.

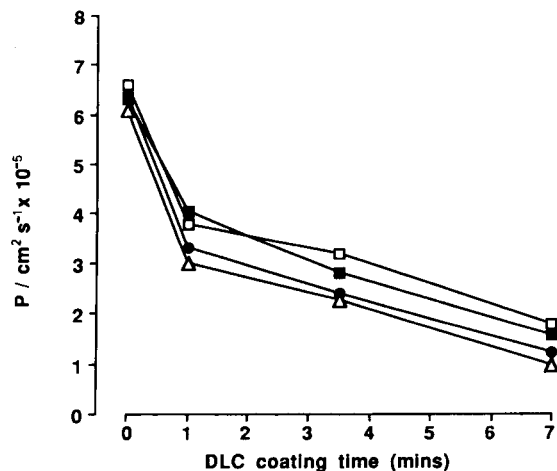


Fig. 4. Permeability coefficients ( $P$ ) for glucose (□), paracetamol (■), ascorbate (●), and urate (△) across  $0.1 \mu\text{m}$  pore size DLC coated polycarbonate membranes.

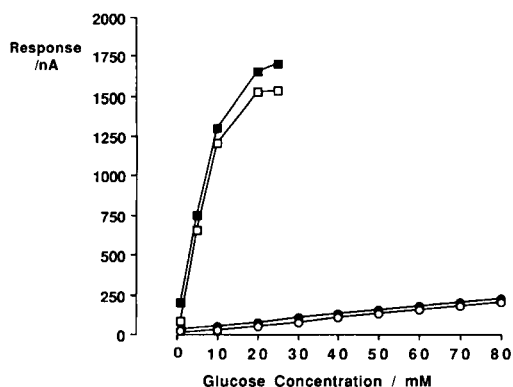


Fig. 5. (□) Glucose response, 0.01  $\mu\text{m}$  pore size polycarbonate covering membrane. (■) Glucose + 1 mM paracetamol, urate and ascorbate response, 0.01  $\mu\text{m}$  pore size polycarbonate covering membrane. (○) Glucose response, 0.01  $\mu\text{m}$  pore size polycarbonate covering membrane with 1 min DLC coating. (●) Glucose + 1 mM paracetamol, urate and ascorbate response, 0.01  $\mu\text{m}$  pore size polycarbonate covering membrane with 1 min DLC duration coating. All electrodes employ 0.05  $\mu\text{m}$  pore size inner membrane, pH 7.4

The scheme proposed here is depicted in Fig. 7. We have previously observed enzyme layer inhibition at an amperometric glucose electrode due to a probable accumulation of gluconic acid [20]. Moreover it has been shown that even in high buffer capacity solutions, there is evidence for local enzyme layer pH change with  $\text{H}^+$  generating/consuming reactions [21], which may lend further support to the theory presented here.

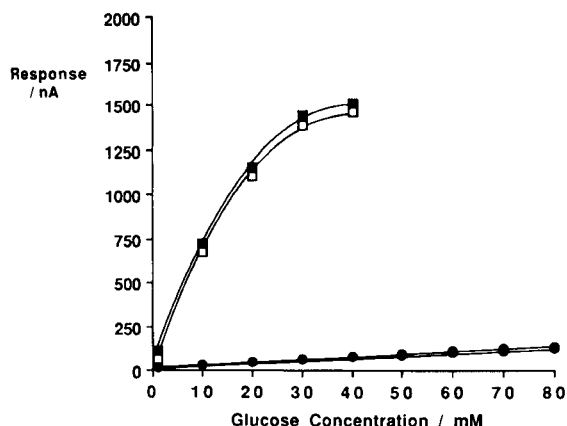


Fig. 6. (□) Glucose response, 0.01  $\mu\text{m}$  pore size polycarbonate covering membrane. (■) Glucose + 1 mM paracetamol, urate and ascorbate response, 0.01  $\mu\text{m}$  pore size polycarbonate covering membrane. (○) Glucose response, 0.01  $\mu\text{m}$  pore size polycarbonate covering membrane with 1 min DLC coating. (●) Glucose + 1 mM paracetamol, urate and ascorbate response, 0.01  $\mu\text{m}$  pore size polycarbonate covering membrane with 1 min DLC duration coating. All electrodes employ 0.05  $\mu\text{m}$  pore size inner membrane, pH 8.5

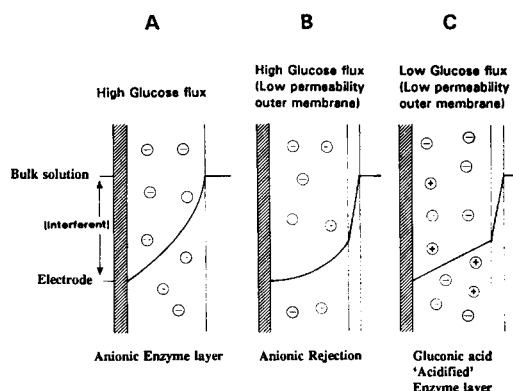


Fig. 7. (A) A high permeability outer membrane permits interferent flux to the enzyme layer, but experiences charge repulsion by the anionic enzyme layer, so reducing flux to the working electrode. (B) A low permeability membrane reduces interferent flux to the enzyme layer, where it is further restricted by the anionic matrix. (C) At conditions of high glucose flux, the acidified enzyme matrix offers less hindrance to the passage of anionic interferents to the working electrode.

A glucose concentration gradient will always be established between the bulk solution and the working electrode (Fig. 7). It is therefore possible that by the model suggested here, the glucose concentration profile across the enzyme layer may lead to a polarisation in  $\text{H}^+$  concentration from gluconic acid production, with the lowest  $\text{H}^+$  concentration adjacent to the working electrode. However higher concentrations of interferent anions closer to the working electrode will still affect a greater solute flux to the working electrode and will so facilitate interferent mass transport.

#### 4. Conclusions

Enzyme electrodes employing very low permeability DLC coated microporous membranes were found to exhibit unexpected independence from the effects of electroactive interferents.

These effects were only partly explained by differing permeability coefficients achieved with coated membranes. The fact that selectivity here is primarily against anionic interferents suggests a charge rejection mechanism due in part possibly to a membrane surface charge, but in particular to the negative charge on the enzyme/albumin layer proteins. With a much attenuated access to an enzymic or other affinity membrane material, it may thus be possible to achieve solute flux

discrimination to an extent not possible with “open access” materials.

### Acknowledgements

The authors would like to thank the SERC and DTI for financial support for this work.

### References

- [1] P. Vadgama, *J. Membr. Sci.*, 50 (1990) 141.
- [2] W.H. Mullen, F.H. Keedy, S.J. Churhouse and P. Vadgama, *Anal. Chim. Acta*, 183 (1986) 59.
- [3] A.E.G. Cass, G. Davis, G.D. Francis, H.A.O. Hill, W.J. Aston, I.J. Higgins, E.V. Plotkin, L.D.L. Scott and A.P.F. Turner, *Anal. Chem.*, 56 (1984) 667.
- [4] P.N. Bartlett, *J. Electroanal. Chem.*, 300 (1991) 75.
- [5] P. Vadgama and P.W. Crump, *Analyst*, 117 (1992) 1657.
- [6] A.P.F. Turner, I. Karube and G.S. Wilson, *Biosensors – Fundamentals and Applications*, Oxford University Press, Oxford, 1987.
- [7] S. Churhouse, C. Battersby, W. Mullen and P. Vadgama, *Biosensors*, 2 (1986) 325.
- [8] Z. Koochaki, I. Christie and P. Vadgama, *J. Membr. Sci.*, 57 (1991) 83.
- [9] L. Gorton, H.I. Karan, P.D. Hale, T. Inagaki, Y. Okamoto and T.A. Skotheim, *Anal. Chim. Acta*, 228 (1990) 23.
- [10] S.P.J. Higson and P.M. Vadgama, *Anal. Chim. Acta*, 271 (1993) 125.
- [11] L.A. Thompson, F.C. Law, J. Franks and N. Ruston, *Biomaterials*, 2 (1991) 37.
- [12] A.C. Evans, J. Franks and P.J. Revell, *Medical Device Technology*, May (1991) 26.
- [13] C. Wild, P. Koidl and J. Wagner, *E.M.R.S. Symposia Proc.*, 17 (1987) 1374.
- [14] J. Franks, *J. Vac. Sci.*, A71 (1989) 2307
- [15] J.C. Angus, *E.M.R.S. Symposia Proc.*, 17 (1987) 179.
- [16] D.G. Thompson, *Proc 30th Ann. Tech. Conf. SVC*, (1987) 135.
- [17] Y. Sun, S. Furusaki, A. Yamauchi and K. Ichamura, *Biotechnol. Bioeng.*, 34 (1989) 55.
- [18] E.G. Young, Occurrence, in M. Florin and E.H. Stotz (Eds.), *Classification, Preparation and Analysis of Proteins (Comprehensive Biochemistry, Vol 7, Proteins (part I))*, Elsevier, Amsterdam, 1963.
- [19] *Merk Index*, 10th edn., 1983, Merck and Co Inc., Rahway, NJ, Ref. 4320, p. 4323.
- [20] P. Vadgama, A.K. Covington and K.G.M.M. Alberti, *Anal. Chim. Acta*, 136 (1982) 403.
- [21] P. Vadgama, *Analyst*, 111 (1986) 875.

# Thin-film biosensor for the measurement of glucose concentration in human serum and urine

Pengguang Yu \*, Ding Zhou

*Department of Environmental Chemical Engineering, Harbin Institute of Technology, Harbin 150001, China*

Received 20 April 1994; revised manuscript received 1 August 1994

---

## Abstract

Solid-state technology and pulse electroplating were used to fabricate a glucose biosensor based on hydrogen peroxide detection. This glucose biosensor was composed of thin-film electrodes, and enzyme-immobilized and deactivated enzyme-immobilized membranes. The electrodes were fabricated by metallic film deposition. Cr and Ni adhesive layers were applied successively by vapour deposition on the thermally oxidized SiO<sub>2</sub> isolating layer on a silicon substrate, and then the two metallic layers were patterned by the photolithographic method. Subsequently, a 1 μm thick Au layer was applied by means of pulse electroplating, forming two anodes and one common cathode in each sensor chip. On one anode, glucose oxidase (GOD) was immobilized by cross-linking with bovin serum albumin and glutaraldehyde. A deactivated GOD-immobilized membrane was formed on the other anode, which worked as a reference working electrode. A novel differential measurement system was used to treat the output signals of the two anodes by adjusting the initial position of the response curves, compensating amplifications of the individual *I*-*V* converters and treating the output signals with a subtraction circuit in order to decrease measurement error. The test results showed that the signal of ascorbic acid up to 4.5 mmol l<sup>-1</sup> or uric acid up to 1.2 mmol l<sup>-1</sup> was successfully cancelled. Glucose concentrations in the range 0.02–4.0 mmol/l could be detected and an excellent linear response was obtained in the low concentration range. The correlation coefficient between the result of the enzyme electrode and the clinically enzymatic method for glucose measurement in human serum was 0.9912. Correlated results between the biosensor method and the routine clinical method for the measurement of glucose concentration in urine were obtained. The lifetime of the enzyme electrode was over 2 months.

**Keywords:** Biosensors; Glucose; Serum; Urine; Thin-film biosensors

---

## 1. Introduction

The blood glucose value indicates hyper- and hypoglycaemia, both of which can result from a

variety of endocrine disorders. The rapid and reliable determination of glucose levels in critically ill patients is of great importance. It is essential that the measurement can be carried out in untreated blood and urine samples in order to avoid a time-consuming sample treatment. Even though glucose electrodes have been successfully used in some laboratories, the question still remained of how to reduce measurement errors in human serum and urine. Some

---

\* Corresponding author. Present address: Laboratory of Electro-analytical Chemistry, Changchun Institute of Applied Chemistry, Chinese Academy of Sciences, Changchun 130022, China.

alternative approaches that overcome this problem are to use electronic mediators [1–4], cellulose membranes [5], Nafion barriers [6] and electropolymerized films [7]. However, the mediator molecules diffuse away with time from the electrode surface into the aqueous solution, thus preventing long-term stability and high precision. The toxicity of mediators limits continuous and *in vivo* application.

Thin-film technology offers the possibility of the mass production of potentiometric and amperometric devices. However, devices based on ion-sensitive field-effect transistors suffer from instability. Thin-film electrodes can be introduced to overcome some of the drawbacks and have proved capable of producing high-quality sensors [8,9]. For instance, thin-film electrodes with Au as the working electrode material have shown good responses to neurotransmitter concentrations in physiological solutions [10]. Such devices seem to be well suited for use in the construction of electrochemical enzyme biosensors.

Some thin-film glucose biosensors utilizing glucose oxidase (GOD) are applicable for clinical inspection of diabetics [9,11]. The main fabrication process consisted of metallic film deposition and photolithographic techniques widely used in solid-state circuit fabrication technology. The output signal was the electrical current change caused by the GOD enzymatic reaction. However, many reducing substances in blood and urine samples, such as ascorbic acid and uric acid, are also oxidized on the surface of the anodes and interfere with the measurement of the hydrogen peroxide. For suppressing the signals from interferences, a hydrogen peroxide permselective membrane between the sample solution and the surface of the electrode was needed [12], and differential techniques between the working electrode and reference working electrode were used in the measurement system. Owing to the different properties of the two working electrodes, the signals measured on the electrodes caused by interferences are not equivalent. Therefore, a simple differential circuit cannot suppress the interference completely.

In this paper, we describe the construction of a planar thin-film glucose biosensor and a novel differential output measurement system, and present the results of the measurement of the glucose concentration in clinical applications.

## 2. Experimental

### 2.1. Fabrication of thin-film electrodes for the measurement of hydrogen peroxide

Thin-film  $\text{H}_2\text{O}_2$  electrodes were constructed by using integrated circuit (IC) technology and pulse electroplating. Fig. 1 shows the electrode pattern on the sensor chip. A silicon wafer with a thermal oxide  $\text{SiO}_2$  (500 Å thickness) as passivating layer was used as the substrate. There are three electrodes on the sensor chip; each structure consisted of a Cr adhesion layer (500 Å thick), an Ni transition layer (1000 Å thick) and an Au protection layer (1 μm thick). After standard cleaning procedures, the Cr and Ni layers were applied by vapour deposition. The electrode geometries were patterned by utilizing photolithographic technology. An Au layer was introduced to cover all sides of the metallic electrodes by using pulse electroplating to act as the electrochemical electrodes. A polysiloxane rubber was used to encapsulate the sensor, leaving only the active area in which each electrode dimensions are 0.4 mm × 6 mm. The use of pulse electroplating gave the possibility of forming Au electrodes in specific areas and decreased the consumption of gold compared with the procedure of evaporating or sputtering deposition of an Au layer, hence lowering the cost of the sensor fabrication. The central electrode was a common

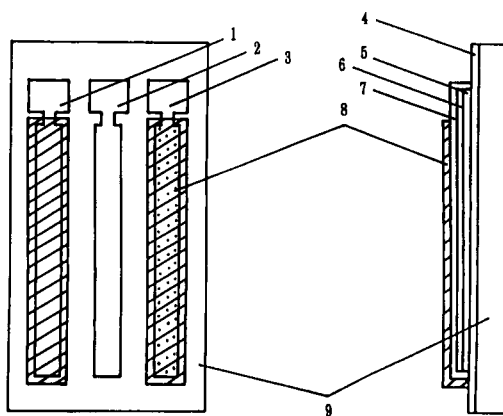


Fig. 1. Configuration of the thin-film glucose biosensor. 1 = Reference working electrode; 2 = common cathode; 3 = enzymatic working electrode; 4 =  $\text{SiO}_2$  insulating layer; 5 = Cr layer; 6 = Ni layer; 7 = Au layer; 8 = enzyme membrane; 9 = silicon substrate.



cathode and the other two were anodes. One of the anodes functioned as an enzymatic working electrode by immobilizing active enzyme on its surface, and the other as a reference working electrode with a deactivated immobilized enzyme membrane.

## 2.2. Chemicals

Glucose oxidase (GOD) (EC 1.1.3.4, type II, 72 U mg<sup>-1</sup>) was obtained from Sigma and bovine serum albumin (BSA) and glutaraldehyde from Beijing Branch, Chinese Medical. All other chemicals were of analytical-reagent grade. A 0.1 mol l<sup>-1</sup> stock buffer solution (pH 7.0) was prepared by dissolving Na<sub>2</sub>HPO<sub>4</sub> and KH<sub>2</sub>PO<sub>4</sub> in deionized water, and all aqueous solution were made with this buffer solution. The concentration of the standard glucose solution, which was prepared freshly every 2 weeks, was 5.55 mmol l<sup>-1</sup>.

## 2.3. Immobilization of enzymes

In order to prepare robust immobilized enzyme membranes, the electrodes were rinsed several times after immersion in 2.5 wt.% glutaraldehyde solution for 1 h. A 5-mg amount of GOD and 3 mg of BSA were dissolved in 10 μl of phosphate buffer solution, then 4 μl of 2.5 wt.% glutaraldehyde solution were added and mixed as soon as possible. A 3 μl volume of the mixed solution was coated on the surface of one anode on the biosensor chip. In the same manner, a deactivated GOD membrane was selectively deposited on the surface of the other anode. The pattern and construction of the integrated biosensor chip containing working electrode, reference working electrode and common cathode are shown in Fig. 1.

## 2.4. Procedures

The biosensor chip was immersed in 7 ml of phosphate buffer solution (pH 7.0) stirred magnetically at room temperature. After the anode currents had become steady, the reaction was started by adding a certain amount of serum or urine sample. In the sample solution, glucose molecules diffused into the immobilized enzyme membrane, and consequently the hydrogen peroxide liberated by the en-

zyme reaction was monitored by the measuring circuit from which the two anode currents and their differential value were output. At 0.65 V, the change in the anode current was proportional to the glucose concentration in the sample solution. After each operation, the measurement cell was washed thoroughly for the next determination.

Changes in the output currents on the two anodes were also caused by some interfering substances in the measured sample. For suppressing errors caused by interfering substances, a differential measurement circuit can be adopted. However, some differential measurement systems reported in the literature [11,13,14] were only composed of subtraction circuits, which were used to treat current outputs of two working electrodes. Because several differences existed between the working enzyme electrode and reference working electrode, such as the effective active electrode areas, the thickness and components of immobilized membrane and surface properties, different responses of the two electrodes to interfering substances occurred. Therefore, measurement errors within the differential output resulted, and the error changed with the concentrations of interferents in sample solutions. In this work, a novel differential measurement system was used to treat the output signals of the two anodes by adjusting the initial position of the response curves, compensating amplification for the output signals of the two anodes, respectively, and final treatment of the above treated signals with a subtraction circuit. The diagram of the

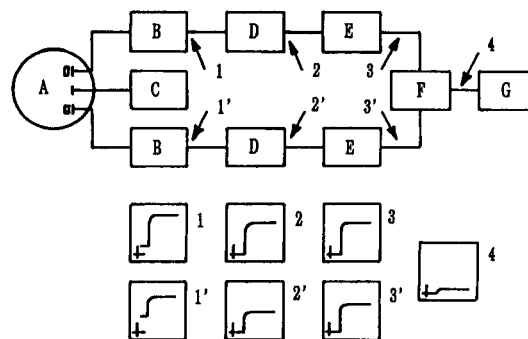


Fig. 2. Schematic diagrams of the novel differential circuit and waveforms at series output points. A = Measurement cell; B = I-V converters; C = potentiostats; D = initial adjusters; E = compensators of amplification; F = differential circuit; G = recorder.

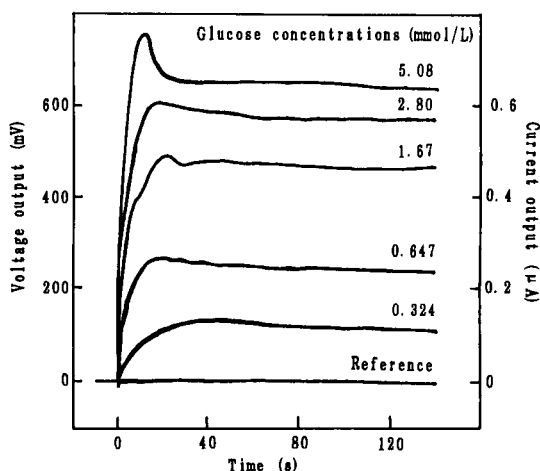


Fig. 3. Time–response curves of the enzyme and reference electrodes to glucose sample solutions of different concentrations.

principle of the novel differential circuit is shown in Fig. 2. The two current–voltage converters were used to convert the two anode currents into potentiometric signals separately, the initial adjusters were applied to adjust the baselines of the response curves of the two anodes to the same level, the amplification compensators made the two anodes have equivalent sensitivity to interferents, the treated output signals of the two anodes were subtracted by the differential circuit and the final signals, which were proportional only to the concentration of glucose in the sample solution, were recorded.

### 3. Results and discussion

#### 3.1. Time–response and calibration

The time–response curves for the detection of glucose at different concentrations are shown in Fig. 3. The measurements were carried out by recording the current changes of the enzyme and reference working electrodes after the injection of glucose solution. The time when the output of the enzyme working electrode reached 95% of the maximum value was less than 20 s on average. Fig. 4 shows the calibration graph for glucose detection. The range of glucose concentration that could be detected was 0.02–4.0 mmol l<sup>-1</sup>, and an excellent linear response was obtained in the range of low concentrations. The

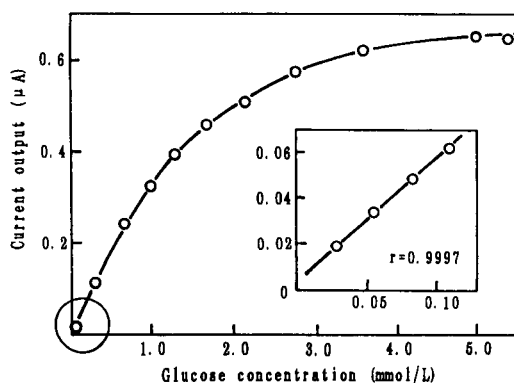


Fig. 4. Calibration graph for the thin-film glucose biosensor.

output saturation above 4 mmol l<sup>-1</sup> is caused by oxygen consumption in the microenvironment on the surface of the biosensor. Therefore, it is suggested that detection is carried out at low concentrations by diluting the sample solution.

#### 3.2. Responses to interfering substances

Ascorbic acid and uric acid in human blood and urine are the main interfering substances that cause errors in the measurement of glucose concentration. The response of the biosensor to ascorbic acid at a certain concentration was measured in the same way as for the measurement of glucose. Fig. 5 shows the response curves of the outputs of the enzyme working electrode, reference working electrode and differ-

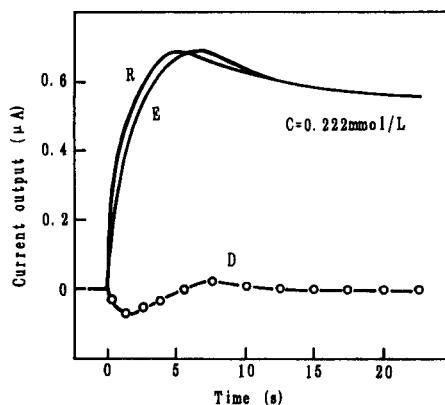


Fig. 5. Time responses of ascorbic acid from enzyme working electrode (E), reference working electrode (R) and differential output (D).

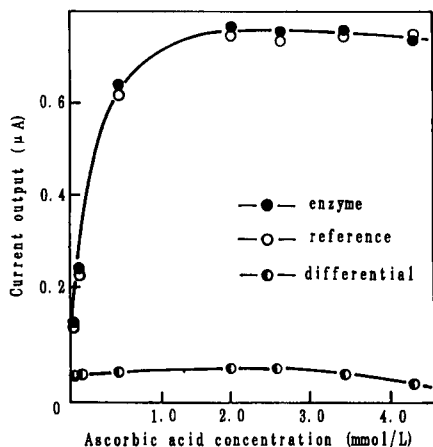


Fig. 6. Current outputs of (●) enzyme and (○) reference working electrodes due to ascorbic acid and (●) their differential output.

ential circuit. It was found that the response curves of the two working electrodes were almost identical. If the reference working electrode was bare or coated with pure BSA, the response was faster or slower, respectively, than that of the enzyme working electrode. Figs. 6 and 7 show graphs of the suppression of the interfering signals by the novel differential system from ascorbic acid and uric acid, respectively. Ascorbic acid signals with concentrations up to 4.5 mmol l<sup>-1</sup>, which is 50 times higher than the normal level in human body fluids, are almost completely cancelled. It was also found from both results that the differential system could decrease the interfering signals to a level below 5%.

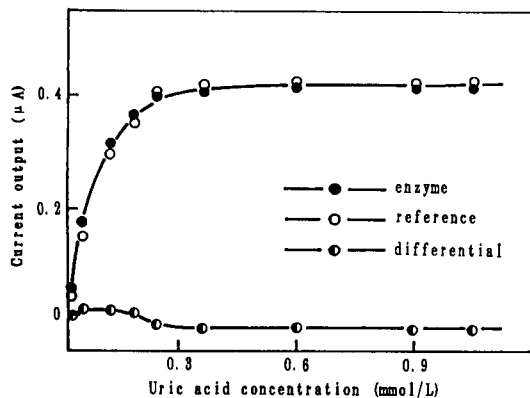


Fig. 7. Current outputs of (●) enzyme and (○) reference working electrodes due to uric acid and (●) their differential output.

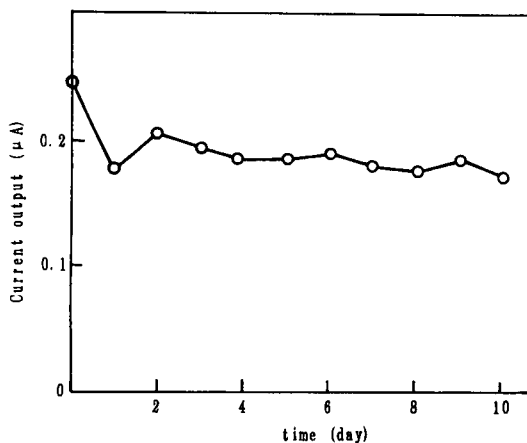


Fig. 8. Daily tests of the glucose biosensor.

### 3.3. Reproducibility

Fig. 8 shows the reproducibility of the measurements tested by repeated detection of glucose. It was shown that the output decreased by about 16% after 10 days of repeated use. The relative standard deviation was about 0.1%. Therefore, it is necessary to calibrate the response of the biosensor before each new measurement. After daily use, the biosensor was washed thoroughly and stored in 0.1 mol l<sup>-1</sup> phosphate buffer solution at 4°C, and the lifetime of the biosensor was more than 2 months.

### 3.4. Measurement of glucose in human serum

Prior to the measurement of glucose concentration in human serum, the biosensor was immersed into a vessel containing 7 ml of phosphate buffer solution which was stirred magnetically. When the output currents of the two anodes had become steady, after about 40 s in most instances, 30 μl of standard glucose solution of concentration 5.55 mmol l<sup>-1</sup> were injected, and a steady output value from the differential measurement system, denoted  $E_1$ , was obtained after about 30 s. Subsequently, 30 μl of analyte sample were injected into the vessel, and the output value, denoted  $E_2$  was measured. The glucose concentration of the measured sample could then be calculated with the simplified equation

$$C_x = \frac{E_2 - E_1}{E_1} \times 5.55 \text{ (mmol l}^{-1}\text{)}$$

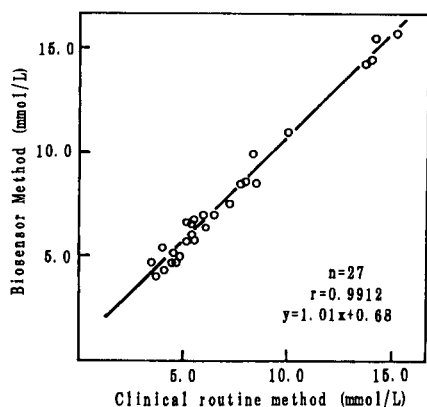


Fig. 9. Comparison of the biosensor method with a standard clinical analysis for serum glucose measurement.

The glucose concentration in human serum was determined with the biosensor using the proposed method, and the results were compared with those obtained by a spectrophotometric method on a standard clinical laboratory analyser. The biosensor measured glucose in serum directly, whereas the spectrophotometric method measured serum glucose with the use of GOD and a chromogenic system. It was obvious that the method with the biosensor was simple and rapid compared with the routine clinical method. The linear regression equation  $y = 1.01x + 0.68$  were obtained for steady-state measurements from the results with the biosensor system ( $y$ , mmol

$l^{-1}$ ) and the clinical spectrophotometric method ( $x$ ,  $mmol l^{-1}$ ), the correlation coefficient obtained for the analysis of 27 patients' samples being 0.9912, as shown in Fig. 9.

### 3.5. Determination of glucose in human urine

Following the procedure proposed above, a series of fourteen urine samples were assayed in order to compare this method with the method of  $CuSO_4$  reduction by heating, which is the qualitative analysis routinely used in clinical laboratories. The correlation between the results of these two methods is shown in Fig. 10. It is clear that the biosensor method has advantages such as rapidity, cleanliness and the possibility of obtaining quantitative results.

## 4. Conclusions

The measurement of glucose in blood and urine sample involves many considerations, which determine the practical application of any biosensor in routine laboratory use. First, the manufacturing techniques of the biosensor should be suitable for mass production, so as to reduce the costs. Second, the chemical and physical properties of the enzyme used should be well stabilized. Third, the operating costs, including materials and labour, should be acceptable. Finally, the simplicity of operation has to be considered, and the instrument should be easily maintainable. The results in this paper clearly show the advantages of the proposed method, as follows.

The techniques used for manufacturing the basic hydrogen peroxide electrode on a silicon substrate are appropriate to current IC processes, and the biosensor chip holds the promise of cost reduction.

Immobilized GOD was proved to be stable, and maintained the activity for at least 2 months.

The entire assay can be done within 3 min. No additional reagents or further coupling steps are needed. Particularly for urine samples the biosensor assay does not need boiling of the sample, which is a routine treatment used in a clinical examination.

The measurement system does not need special maintenance and the cost of the small-dimensional instrument is over 50 times lower than those of some clinical analysers.

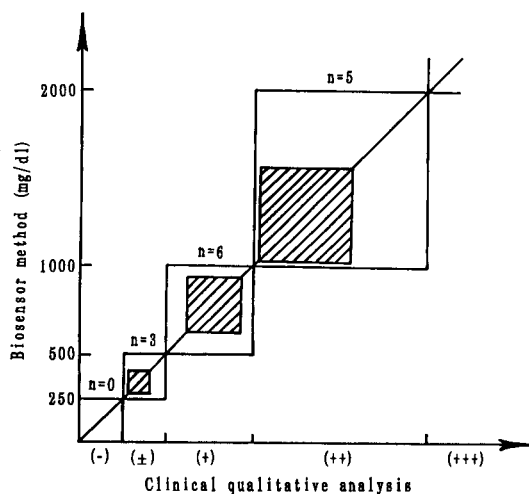


Fig. 10. Comparison of the biosensor method with a standard clinical analysis for urine glucose measurement.

Because of the above advantages, thin-film biosensors appear to be promising for use in routine analyses for glucose in the fields of medical inspection, fermentation, chemical engineering, the food industry, etc.

### Acknowledgement

The authors gratefully acknowledge financial assistance from the Chinese National Natural Science Foundation.

### References

- [1] P.W. Stoecker and A.M. Yacynych, *Sel. Electrode Rev.*, 12 (1990) 137.
- [2] A.E.G. Cass, C. Davis, G.D.L. Scott and A.P.F. Turner, *Anal. Chem.*, 56 (1984) 667.
- [3] D. Belanger, E. Brassard and G. Fortier, *Anal. Chim. Acta*, 228 (1990) 311.
- [4] A. Amine, J.-M. Kauffmann and G.J. Patriarche, *Anal. Lett.*, 24 (1991) 1293.
- [5] J. Wang, T. Golden, Y. Lin and L. Angnes, *J. Electroanal. Chem.*, 333 (1992) 65.
- [6] G. Fortier, M. Vaillancourt and D. Belanger, *Electroanalysis*, 4 (1992) 275.
- [7] R.J. Geise, J.M. Adams, N.J. Barone and A.M. Yacynych, *Biosensors Bioelectron.*, 6 (1991) 151.
- [8] M. Koudelka, S. Gernet and N. Dekaoji, *Sensors Actuators*, 18 (1989) 157.
- [9] E. Tamiya and I. Karube, *Sensors Actuators*, 15 (1988) 199.
- [10] C. Pifl, A. Jachimowicz, G. Urban, F. Koghl, P. Goiser, J. Theiner and G. Nauer, *Sensors Actuators B*, 1 (1990) 468.
- [11] T. Schalkhammer, E. Mann-Buxbaum, F. Pittner and G. Urban, *Sensors Actuators B*, 4 (1991) 273.
- [12] T. Tsuchida and K. Yoda, *Enzyme Microb. Technol.*, 3 (1981) 326.
- [13] J. Kimura, N. Ito, T. Kuriyama, M. Kikuchi, T. Arai, N. Negeshi and Y. Tomita, *J. Electrochem. Soc.*, 136 (1989) 1744.
- [14] I. Takatsu and T. Moriizumi, *Sensors Actuators*, 11 (1987) 309.



ELSEVIER

Analytica Chimica Acta 300 (1995) 99–105

ANALYTICA  
CHIMICA  
ACTA

# Latex piezoelectric immunoassay: effect of interfacial properties

Hedayat O. Ghourchian, Naoki Kamo \*

*Laboratory of Biophysical Chemistry, Faculty of Pharmaceutical Sciences, Hokkaido University, Sapporo 060, Japan*

Received 14 February 1994; revised manuscript received 1 August 1994

## Abstract

Latex piezoelectric immunoassay is a technique for detecting agglutination of antibody- or antigen-bearing latex by an immunoreaction using a piezoelectric quartz crystal; the agglutination decreases the oscillation frequency of the crystal. This is advantageous in that immobilization of antibody or antigen on the crystal surface is unnecessary. In this report, different kinds of chemical functional groups were immobilized on the electrode surface, allowing us to consider the effect of interfacial structure on the frequency change. Electrode modifications such as self-assembly of alkanethiol and aminoalkoxysilane monolayers, and polyethylenimine-glutaraldehyde coating as well as plasma treatment were examined. The sensitivity of the system was found to imitate the interfacial properties so that modification of the electrode surface could improve the response. Among the methods examined for this electrode surface modification, the polyethylenimine-glutaraldehyde modification had the advantages of high reproducibility, fast operation and simplicity. It was also suggested that the frequency change originated primarily from the immunoreaction at the interface.

**Keywords:** Biosensors; Immunoassay; Piezoelectric immunoassay; Antibody-bearing latex; Rheumatoid factor; Alkanethiol monolayers; Aminoalkoxysilane monolayers; Polyethylenimine; Quartz crystal microbalance

## 1. Introduction

The piezoelectric quartz crystal is a very sensitive micro-gravimetric device, and its application as a mass sensor dates back to 1959 [1]. The oscillating frequency of the mass sensor is changed by adsorption of substances on the crystal surface. One of the most interesting uses is for immunoassay. The general way of utilizing the device as an immunosensor involves coating of the crystal with a certain film to which either antigen or antibody is fixed by chemical treatment. An immunoreaction increases the mass on the surface of the quartz crystal, which is recognized by the decrease in oscillating frequency. The drawback of such a pie-

zoelectric immunosensor is its lack of reversibility [2,3].

Latex piezoelectric immunoassay (LPEIA) is a relatively new immunosensing method [4–6]. LPEIA is based on the fact that agglutination of antibody- or antigen-bearing latexes by immunoreaction in the solution causes a frequency change of the quartz crystal dipped into the solution. In contrast to the usual method, this technique does not require the immobilization of the antibody or antigen on the surface of the crystal. We [6] previously modified the original method of LPEIA [4], and found a method with good reproducibility.

Factors which cause a frequency change of a piezoelectric quartz crystal in a liquid have been described [7,8], but the exact mechanism governing the frequency change of LPEIA is not yet clear. In the present

\* Corresponding author.

paper, we show that the magnitude of the frequency change in LPEIA depends mostly on properties of the electrode surface, and consider the mechanism based on these results.

## 2. Experimental

### 2.1. Apparatus and materials

A 9 MHz AT-cut quartz crystal (8×8 mm) with gold or silver electrodes, diameter 5 mm, on both sides was used in all experiments, and was obtained from Yakumo Tsushin Kogyo (Tokyo). In order to expose only one side of the crystal to assay solutions, a previously-designed detection cell [6] with a total volume of 150  $\mu\text{l}$  was used. The equipment for measuring frequency changes was the same as described previously [6].

Antibody-bearing latex (2.5 g/l) covered with polyclonal antibodies against rheumatoid factor (RF) and RF serum (76 I.U./ml) were obtained from Hitachi Chem. Co. Bovine serum albumin (BSA) and polyethylenimine (PEI, as a 50% w/v aqueous solution) were purchased from Sigma (St. Louis, MO).  $\gamma$ -N-(2-Aminoethyl)-3-aminopropyltrimethoxysilane (AATSi) was obtained from Tokyo Kasei (Tokyo). Immunoglobulin G (IgG, 96%) was obtained from Cosmo (Tokyo). Octadecyl mercaptan was purchased from Aldrich (Milwaukee, WI). 1-Decanethiol, 1-decanol, 1-decanal, *n*-decylamine, decanoic acid, glutaraldehyde (20% aqueous solution), molecular sieves 3 Å (1/16 inch) and other chemicals were obtained from Wako (Osaka). Water of 18.3 M $\Omega$  cm was prepared with a Millipore Milli-Q apparatus (Tokyo).

### 2.2. Coating procedures

After the crystal was washed with water, followed by ethanol, coating was carried out at room temperature as follows:

#### *Thin polyethylenimine-glutaraldehyde film*

PEI is frequently used to immobilize proteins [9–11]. A mixture of methanol and pure water was used as solvent whose weight ratio of water to methanol was 15:85. A 2  $\mu\text{l}$  portion of 3% PEI in the mixed solvent was applied to the crystal surface. The dried film was

washed with water to remove the excess PEI. Three to five drops of 0.2% glutaraldehyde (pH 6.5) were placed on the PEI-coated surface for 30 min. It was then rinsed with water.

#### *Alkanethiol monolayers*

A hydrophobic monolayer was formed on the electrode when the crystal was dipped in  $1 \times 10^{-3}$  M 1-dodecanethiol in degassed ethanol for 10 min [12,13]. To obtain a hydrophilic surface thereafter it was coated with a long-chain alkane terminated by a hydrophilic group: The crystal was immersed in  $1 \times 10^{-3}$  M of ethanolic solution of 1-decanol, *n*-decylamine, 1-dodecanol or dodecanoic acid for 60 min, then rinsed with ethanol.

#### *Aminoalkoxysilane monolayers*

The crystal was coated with silicon dioxide (using a high frequency sputtering technique, Ulvac SMH-2106 RE, Tokyo), and immersed in a solution of 0.15% AATSi in dehydrated benzene for 3 h. The crystal was kept in an aqueous 0.2% glutaraldehyde solution (pH 6.5) for 10 min. After air-drying, it was washed with water.

#### *Physical treatment*

The electrode surface was cleaned either by plasma treatment under argon (150 millitorr) for 5 min (Plasma Cleaner PDX-3XG, Harrick, New York) or a surface heat-regeneration process [6].

### 2.3. Protein immobilization

The PEI-coated crystal, prepared as described above, was fixed horizontally on a base and 40  $\mu\text{l}$  of protein (50 mg/ml human IgG in 20 mM phosphate buffer pH 7.3 or 75 mg/ml BSA in 20 mM acetate buffer, pH 5) was deposited on the crystal and dried. The crystal was then dipped in water for 10 min. Unreacted aldehyde groups on the crystal were blocked with 0.1 M glycine solution.

### 2.4. Measuring procedure

A phosphate buffered saline (PBS) solution containing 20 mM sodium–potassium phosphate and 0.17 M sodium chloride at pH 7.4 was used. A 9 MHz quartz crystal was fastened to the detection cell, into which

100  $\mu\text{l}$  of the PBS was poured. The solution was gently agitated with a small stirring bar ( $2 \times 2$  mm, about 120 rpm). When the frequency no longer changed, 40  $\mu\text{l}$  of the antibody-coated latex solution (2.5 g/l) was added. After stabilization of the frequency, 10  $\mu\text{l}$  of the standard serum containing RF (76 I.U./ml) was added. The frequency then decreased and the rate of this frequency change gradually lessened. After 60 min the total shift caused by the addition of RF was recorded.

When responses were studied using crystals whose electrode surfaces were modified by various methods to the change in viscosity ( $\eta$ ) and density ( $\rho$ ) of the surrounding medium, PBS–sucrose solutions of varying concentrations of sucrose were used. The values of  $\rho$  and  $\eta$  of the solution were taken from Ref. [20]. When the frequency change of the crystal in PBS solution stabilized, the solution was replaced with a sucrose–PBS solution. This solution was replaced by the more concentrated sucrose solution after the stabilization of the frequency change.

### 2.5. Thickness measurement

The film thickness on the electrodes was estimated using the quartz crystal microbalance method at controlled temperature and humidity.

## 3. Results and discussion

### 3.1. Effect of interfacial properties on sensitivity

The electrode surface was treated or modified by various methods to allow consideration of the relation between the sensitivity of LPEIA and electrode surface properties.

#### Cleaning of the surface

Fig. 1 shows LPEIA responses of a bare crystal and crystals after three kinds of treatment. A frequency change of about 180 Hz was observed when the quartz crystal (gold electrode) was washed with pure water, followed by ethanol. Similar or somewhat larger responses were obtained using the argon-plasma treatment or the heat-regeneration process. On the other hand, an acidic treatment (washing the gold electrode with concentrated sulfuric acid or a mixture of sulfuric acid and hydrogen peroxide at room temperature)

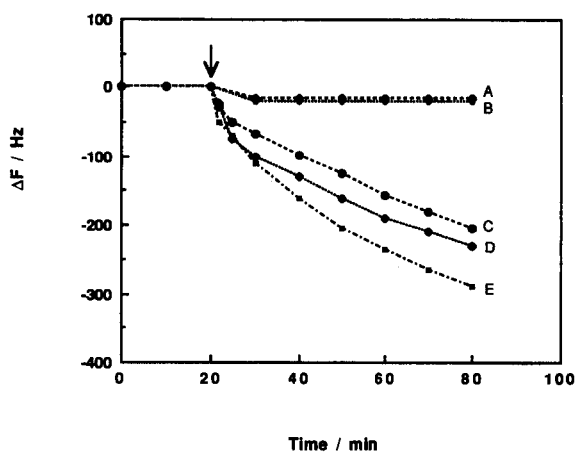


Fig. 1. Comparison of the LPEIA frequency changes when five kinds of treatments were made to the gold-electrode crystals. Lines A and B show the LPEIA frequency change (denoted as  $\Delta F$ ) after washing with sulfuric acid and a mixture of sulfuric acid plus hydrogen peroxide (970:30, w/w), respectively. The data were taken as mean values of two measurements. Line C (mean value of three measurements) shows the  $\Delta F$  for a bare crystal which was washed with water, followed by ethanol. Lines D and E show  $\Delta F$  after the plasma treatment under argon (150 millitorr) and the heating regeneration process, respectively. The arrow shows the time RF was added to the solution. The final concentrations of latex and RF were 0.66 mg/ml and 5.06 I.U./ml, respectively. The temperature was 27°C. The other conditions were the same as mentioned in the measuring procedure.

greatly reduced the sensitivity of LPEIA. This acidic treatment did not destroy the piezoelectric response, because the treated crystal could respond to viscosity changes in solutions as shown later.

#### Alkanethiol monolayers

The hydrophobic surface was prepared by self-assembly of dodecanethiol on gold or silver electrodes. Consistent with earlier findings [14], formation of alkanethiol monolayers on the electrode reached about 80–90% of maximum within a few minutes, and thereafter proceeded slowly. The monolayer formation was estimated by the procedure for thickness measurement described in the Experimental section. Results showed that the maximum sensitivity was obtained at the stage of 80–90% accomplishment of the monolayer formation, and that the response was larger than that of the ethanol-washed crystal by about 20 Hz (data not shown). With increase in incubation time using the alkanethiol solution, the response of LPEIA decreased gradually, and after 16 h was almost equal to that of an untreated crystal. It seems probable that in a short self-



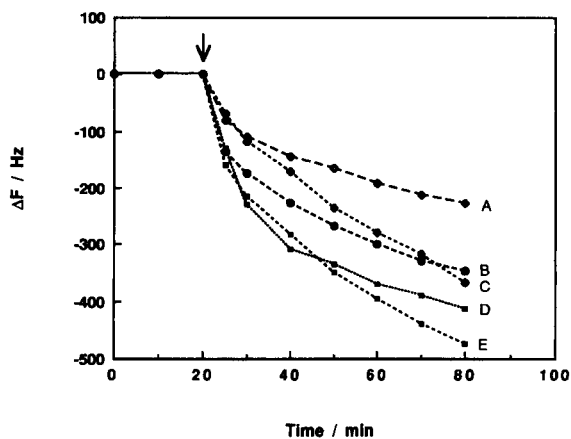


Fig. 2. Variation of LPEIA sensitivity by various modifications of the electrode surface. (A)  $\Delta F$  of the silver electrode whose surface had been modified with an ethanolic solution of dodecane thiol ( $1 \times 10^{-3}$  M) for 10 min. Curves B, C, D and E are  $\Delta F$  when the hydrophobic surface formed by dodecane thiol was converted to a hydrophilic one using the following reagents:  $1 \times 10^{-3}$  M ethanolic solutions of *n*-decylamine (B), dodecanoic acid (C), 1-decanol (D) and 1-dodecanol (E). Experimental conditions were the same as in Fig. 1. Curves A, B, C, D and E were, respectively, the mean value of 3, 4, 2, 2 and 3 independent measurements.

assembling time the monolayer on the electrode is not sufficiently well-packed so that the outer part of the monolayer would have liquid-like properties with some mobility. This may facilitate interfacial interactions and produce higher sensitivity, although the magnitude of the increase was not great.

#### Hydrophilic surface on alkanethiol monolayers

The sensitivity was examined when the solid-liquid interface properties were changed to hydrophilic: the hydrophobic dodecanethiol monolayer was overlaid with a layer of long-chain alkane terminated by a hydrophilic group. Fig. 2 shows the time course of frequency changes when *n*-decylamine (B), dodecanoic acid (C), 1-decanol (D) or 1-dodecanol (E) was employed as a surface modifier. Curve A was the control. The formation of a bi- or multi-layer having hydrophilic groups at the interface greatly improved the response.

#### Aminoalkoxysilane monolayers

Using a sputtering technique a silicon dioxide layer with a thickness of about 260 Å (mean value of 10 independent measurements with a standard deviation of 17) was deposited on the electrode surface. The response of the silicon dioxide sputtered crystal (Fig.

3A) was comparable with that of the original crystal (see Fig. 1C) or the heat-regenerated crystal (Fig. 1E). When free  $\text{NH}_2$  groups were fixed on the oxide-containing surface by reaction with AATSi, the crystal showed a larger response (Fig. 3B). On the other hand, the frequency change decreased a little when the AATSi surface was coated with glutaraldehyde (Fig. 3C).

Despite the hydrophilicity of the silicon dioxide surface, the frequency change did not improve much, but the fixation of a free amine or aldehyde group improved the sensitivity remarkably. This indicated that the hydrophilicity of the surface alone was not enough for to bring about a response improvement, but the presence of an amine or aldehyde group on the surface was effective in improving sensitivity.

#### Thin polyethylenimine-glutaraldehyde film

A thin layer of PEI was formed on the gold surface of the crystal. The film thickness, estimated using a quartz crystal microbalance, was about 50 Å (average of 5 independent measurements). Crosslinking of the polymer with a relatively low concentration of glutaraldehyde solution (0.2%) yielded a thin and stable film. The film thickness after the cross-linking increased to about 85 Å. LPEIA with this PEI-aldehyde-modified crystal gave much larger frequency changes, as shown in Fig. 4B.

Curve A in Fig. 4 shows the frequency change observed with the PEI-treated crystal: a small decrease

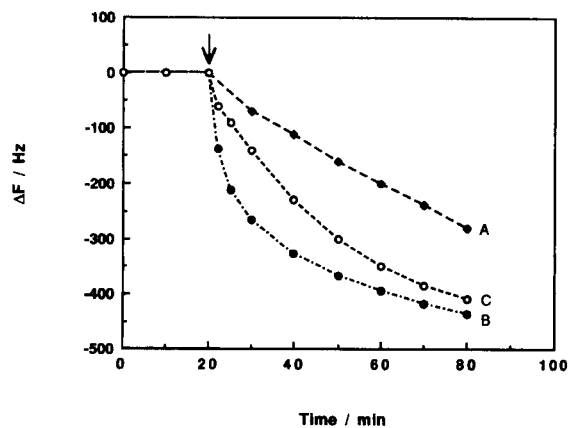


Fig. 3. Variation of the LPEIA sensitivity with various layers coated on the gold electrode. (A) Silicon dioxide coated crystal. (B) Crystal on which AATSi was reacted with silicon dioxide as a basal film. (C) After B was treated with glutaraldehyde. Experimental conditions were the same as in Fig. 1.

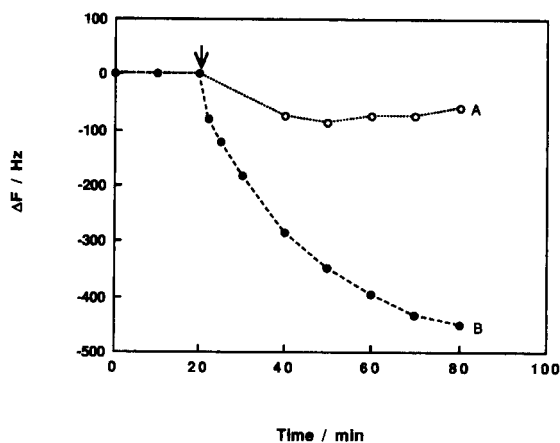


Fig. 4. Variation of the LPEIA sensitivity with various layers coated on the gold electrode. (A) The electrode was coated with PEI (mean value of 2 measurements). (B) The crystal was treated with PEI and covered with glutaraldehyde (mean value of 3 measurements). Experimental conditions were the same as in Fig. 1.

in the frequency was initially observed, and a tendency for a reverse in the response was noticed. The reason of this behavior is not known at present.

### 3.2. Mechanistic consideration

There are two possible factors which may cause the frequency change in the piezoelectric quartz crystal in the liquid phase. The first is the change in  $(\rho\eta)^{1/2}$  (where  $\rho$  and  $\eta$  stand for the density and viscosity of the solution, respectively) [7,8]. Formation of agglutinated latexes by immunoreaction may increase  $\eta$ .

The second factor inducing the frequency change is the binding of substances to the electrode surface. A crystal with immobilized human IgG was set in the detection cell and 150  $\mu\text{l}$  of PBS was poured into the cell. After frequency stabilization, 12  $\mu\text{l}$  of RF serum was added to the solution, and about 1 h later a frequency change of about 350 Hz was observed. The solution inside the cell was then replaced with 150  $\mu\text{l}$  of fresh PBS solution after three washings with PBS, and there was a frequency shift of about 20 Hz. This could be related to the factor of  $(\rho\eta)^{1/2}$  whose change was caused by the addition of RF macromolecules to the solution. The main part of the response, 330 Hz, could have been caused by the mass increase on the surface due to the immunocomplex formation. As a control experiment, we used a BSA-immobilized crystal instead of the human IgG-immobilized one, and there was essentially no response (data not shown).

In the present paper, we have shown that various modifications on the electrode surface greatly changed the magnitude of the response. Previous authors showed that the crystal was able to monitor the  $\rho\eta$  change in solution, but the magnitude was influenced by certain interfacial factors such as surface roughness [15,16], surface stress [17], interfacial slip [18] and hydrophilicity or hydrophobicity [19]. Hence, it occurred to us that the surface modification might alter the sensitivity to  $\rho\eta$  change, which would, in turn, alter the sensitivity in LPEIA. Fig. 5 represents plots of the frequency change vs.  $(\rho\eta)^{1/2}$  using crystals to which various surface treatments or modifications were applied. It reveals that these treatments did not change the sensitivity to the  $\rho\eta$  change. It is concluded, therefore, that the  $\rho\eta$  change may not be a main factor in LPEIA, but that the binding or adsorption of latexes or agglutinated latexes onto the electrode surface may be of greatest importance.

It has been shown, therefore, that the antigen-bearing latexes were able to bind to the electrode surface. The crystal whose silver electrode was coated with PEI-

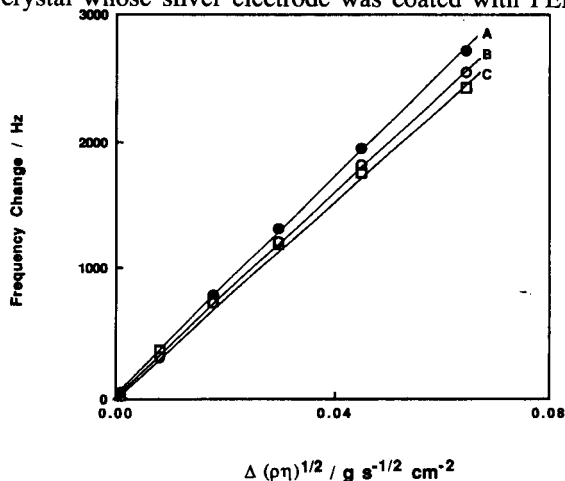


Fig. 5. Invariance of frequency changes to  $\rho\eta$  change by the surface modification. In the abscissa,  $\Delta$  stands for the difference of the values of  $(\rho\eta)^{1/2}$  from that of water. (A) Frequency change of a bare gold electrode. (B) Frequency change of a crystal having a gold electrode whose surface was treated with a mixture of sulfuric acid and hydrogen peroxide. Curve C indicates the frequency change of a gold electrode whose surface had been modified with an ethanolic solution of octadecyl mercaptan ( $1 \times 10^{-3}$  M) for 20 min. Each point is the mean value of three measurements and the standard deviations were in the ranges between 6.50–34.06, 5.29–22.81 and 8.96–65.65 for lines A, B and C, respectively. The temperature was kept constant at 20°C. The regression coefficients of lines A, B and C are, respectively, 1.000, 0.999 and 1.000.

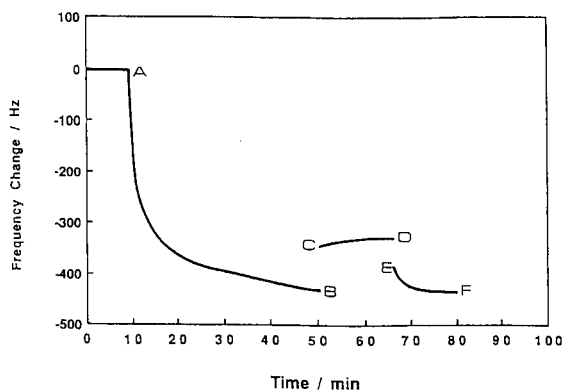


Fig. 6. Antibody-bearing latexes bound strongly to the electrode surface. A crystal with a PEI-coated silver electrode was set in the detection cell and a 20  $\mu\text{l}$  aliquot of antibody-bearing latex was added to 150  $\mu\text{l}$  of PBS (curve A–B). After 50 min, the latex suspension was replaced with 150  $\mu\text{l}$  of fresh PBS solution (curve C–D). After stabilization of the frequency, 20  $\mu\text{l}$  of antibody-bearing latex was again added and the frequency was restored to its previous value (curve E–F).

aldehyde was set in the detection cell and latexes were added. As shown by curve A–B in Fig. 6, a change of 432 Hz was observed with the addition of 20  $\mu\text{l}$  of stock latex solution. The latex suspension was then removed gently with an aspirator. After washing the crystal three times with PBS solution, the bathing solution was replaced with 150  $\mu\text{l}$  of fresh PBS solution. About 15 min later, the frequency shift of about 106 Hz was stabilized (Fig. 6C–D). With the addition of 20  $\mu\text{l}$  of the stock antibody-bearing latex, the frequency was restored to its previous value (Fig. 6E–F). These findings indicate that the antibody-bearing latexes can bind to the electrode surface, and that the binding is so strong that washing detaches only a small part of adsorbed latexes ( $106/432 = 24.5\%$ ).

If these adsorbed antibody-bearing latexes have an important role in the LPEIA response, there should be a good correlation between the amount of latex adsorbed and the response. Fig. 7 shows the binding isotherm of the antibody-bearing latex, using a crystal whose electrode surfaces were modified by PEI-aldehyde coating (A), a bare crystal (B) and one subjected to sulfuric acid treatment (C). Comparison of the isotherm with the magnitude of the LPEIA response (Figs. 4B, 1C and 1A) implied that the order of response magnitude with various treatments was the same as that of latex-binding, but that the proportionality between them was not quantitative; for example, sulfuric acid

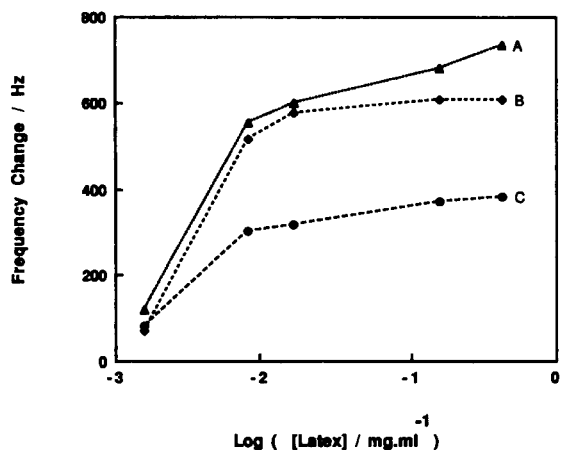


Fig. 7. Antibody-bearing latex binding isotherm. The surfaces of crystals with gold electrodes were modified by the following typical methods: PEI coating (A), washing with water followed by ethanol (B), and sulfuric acid treatment (C). The antibody-bearing latexes were added successively into 150  $\mu\text{l}$  of PBS solution in the compartment of the detection cell.

treatment produced a small LPEIA response while the frequency change of its latex binding was about one half of the PEI-aldehyde treated crystal. This suggests the importance of the chemical environment on the electrode surface which facilitates the immunoreaction.

Analysis of the time courses of the responses shown in Figs. 1, 2, 3 and 4 showed that the initial rate of frequency change was not always proportional to the final change, when data obtained with various treated or modified crystals were compared (data not shown). However, if the same treated crystal was used, the results were proportional at least in the low-concentration region. A typical example is the comparison shown by the open and closed circles in Fig. 3; one set of data was obtained with a crystal whose surface was covered with free amine, the other set was that obtained with glutaraldehyde. The ultimate results did not differ greatly, but the initial rates were obviously different.

Although analysis of the time-course of the response as well as the exact mechanism of LPEIA await further considerations, it is clear from findings described here that the binding or adsorption of the latexes plays an important part in LPEIA.

#### 4. Conclusions

From the results obtained with crystals whose surface were subjected to various treatments or modifica-

tions, it is concluded that the binding or adsorption of the antibody-bearing latexes plays an essential part in LPEIA. From the standpoint of clinical applications, the PEI-aldehyde modification proved to have advantages of better reproducibility, fast operation and simplicity.

### Acknowledgements

The authors wish to thank Dr. Kazuhiko Takahashi of the Hygienic Chemistry Lab. of this Faculty for his useful advice, Dr. Katsuaki Shimazu of the Division of Material Science, Hokkaido University for the plasma treatment, and Dr. Kazuhisa Sueoka and Prof. Koichi Mukasa of the Solid State Electronics Lab., Hokkaido University, for use of the sputtering technique. This work was partly supported by a grant from the Ministry of Education, Science and Culture (Japan), from the Hokkaido Government and from the Suzuken Memorial Foundation.

### References

- [1] G.Z. Sauerbrey, *Z. Phys.*, 155 (1959) 206.
- [2] G.G. Guilbault, J.H.T. Luong and E. Prusak-Sochaczewski, *Bio/Technology*, 7 (1989) 349.
- [3] J. Janata, *Anal. Chem.*, 64 (1992) 197R.
- [4] S. Kurosawa, E. Tawara, N. Kamo, F. Ohta and T. Hosokawa, *Chem. Pharm. Bull.*, 38 (1990) 1117.
- [5] M. Muratsugu, S. Kurosawa and N. Kamo, *Anal. Chem.*, 64 (1992) 2483.
- [6] H.O. Ghourchian, N. Kamo, T. Hosokawa and T. Akitaya, *Talanta*, 41 (1994) 401.
- [7] S. Bruckenstein and M. Shay, *Electrochim. Acta*, 30 (1985) 1295.
- [8] K.K. Kanazawa and J.G. Gordon II, *Anal. Chim. Acta*, 175 (1985) 99.
- [9] S.F. D'Souza, J.S. Melo, A. Deshpande and G.B. Nadkarni, *Biotechnol. Lett.*, 8 (1986) 643.
- [10] D. Guoqiang, R. Kaul and B. Mattiasson, *Appl. Microbiol. Biotechnol.*, 37 (1992) 305.
- [11] J.H.T. Luong, E. Prusak-Sochaczewski and G.G. Guilbault, *Ann. NY Acad. Sci.*, 613 (1990) 439.
- [12] C.D. Bain, E.B. Troughton, Y.T. Tao, J. Evall, G.M. Whitesides and R.G. Nuzzo, *J. Am. Chem. Soc.*, 111 (1989) 321.
- [13] C.D. Bain and G.M. Whitesides, *J. Am. Chem. Soc.*, 111 (1988) 3556.
- [14] A. Ulman, *Introduction to Ultrathin Organic Films*, Academic Press, New York, 1991, pp. 279–286.
- [15] R. Schumacher, G. Borges and K.K. Kanazawa, *Surf. Sci.*, 163 (1985) L621.
- [16] R. Schumacher, *Angew. Chem., Int. Ed. Engl.*, 29 (1990) 329.
- [17] K.E. Heusler, A. Grzegorzewski, L. Jaeckel and J. Pietrucha, *Ber. Bunsenges. Phys. Chem.*, 92 (1988) 1218.
- [18] W.C. Duncan-Hewitt and M. Thompson, *Anal. Chem.*, 64 (1992) 94.
- [19] M. Thompson, C.L. Arthur and G.K. Dhaliwal, *Anal. Chem.*, 58 (1986) 1206.
- [20] R.C. Weast and D.R. Lide (Eds.), *CRC Handbook of Chemistry and Physics*, CRC Press, Boca Raton, FL, 1989–1990, D-222.

# Catalytic method for the determination of traces of tungsten by linear scan voltammetry

Zhi-Liang Jiang <sup>\*</sup>, Lin-Xiu Liao, Min-Deng Liu

*Computer and Analysis Testing Center, Guangxi Normal University, Guilin, China*

Received 1 February 1994

## Abstract

A novel, sensitive and selective catalytic method for the determination of tungsten is described, based on the W(VI)-catalysed redox reaction between methyl red and Ti(III) in a hydrochloric acid medium; methyl red exhibits a sensitive oscillopolarographic wave at  $-0.68$  V vs. SCE in NaOH solution. A calibration graph from  $3.2$  to  $72$  ng ml<sup>-1</sup> W (detection limit  $1.1$  ng ml<sup>-1</sup>) is obtained by the fixed-reaction time procedure. The influence of 29 foreign ions on the catalytic determination of W was examined; none interfered at  $< 100$ -fold excess. The method is used to determine W in steel and ore samples, with satisfactory results.

*Keywords:* Catalytic methods; Voltammetry; Tungsten

## 1. Introduction

Methyl red (MR) is a commonly used indicator in acid–base titrations. Because its coordination effect is very weak, its complexes do not seem to have been reported to give polarographic adsorption waves [1,2]. Catalytic methods with linear scan voltammetry at a dropping mercury electrode (DME) (that is, oscillopolarography) provides a link between organic reagents and inorganic oscillopolarographic analysis [3–8]. Recently MR has been used to determine ultratrace amounts of Ru<sup>9</sup>, Mn<sup>10</sup>, Os<sup>11</sup> and NO<sub>2</sub><sup>-</sup> [12] by catalytic methods with oscillopolarographic detection. Catalytic methods for tungsten are rare [13–18]. To develop such a method, some known catalytic systems for tungsten were tested. The results indicate that some of the W(VI)–Ti(III) azo-compound sys-

tems can be utilized for the determination of traces of tungsten with oscillopolarographic detection. In the present work, the W(VI)–Ti(III)–MR catalytic system is studied in detail. A sensitive and selective method was developed, with a detection limit of  $1.1$  ng ml<sup>-1</sup> W and a calibration range of  $3.2$ – $72$  ng ml<sup>-1</sup> based on the fixed-time procedure. Compared with other reported catalytic methods for W [13–18], the new method is one of the most sensitive, and has very high selectivity.

## 2. Experimental

### 2.1. Apparatus

A Model JP-2 single-sweep oscillopolarograph (Chendu Instrumental Factory) was used for the oscillopolarographic measurements. The settings were: dropping mercury period 7 s; scan rate  $250$  mV s<sup>-1</sup>;

<sup>\*</sup> Corresponding author.

scanning potential range 500 mV in the negative direction; initial scanning potential  $-400$  mV;  $I_p''$  (second derivative wave); and a three-electrode system, DME, SCE and platinum electrode. A Model JY-501B thermostated water bath was used.

## 2.2. Reagents

A standard solution of  $1 \text{ mg ml}^{-1}$  W(VI) was prepared according to the following procedure: weigh out  $0.1794 \text{ g}$  of  $\text{Na}_2\text{WO}_4 \cdot 2\text{H}_2\text{O}$  and place in a  $100\text{-ml}$  beaker. Add doubly distilled water to dissolve, transfer to a  $100\text{-ml}$  standard flask and dilute to the mark with water. Prepare working solutions by dilution shortly before use.

A  $1.00 \times 10^{-5} \text{ M}$  aqueous methyl red solution,  $0.92 \text{ M TiCl}_3$ ,  $0.10 \text{ M HCl}$  and  $1.0 \text{ M NaOH}$  solutions were used.

## 2.3. Procedure

The thermostated water bath temperature was controlled at  $20^\circ\text{C}$  and all reactions were carried out at this temperature.

Into a  $25\text{-ml}$  graduated test-tube fitted with a glass stopper,  $1.0 \text{ ml}$  of  $1.00 \times 10^{-5} \text{ M}$  methyl red and  $1.0 \text{ ml}$  of  $0.10 \text{ M HCl}$  were added, the solution was diluted accurately to the  $10\text{-ml}$  mark with water,  $2.5 \text{ ml}$  of  $1.0 \text{ M NaOH}$  and  $30 \mu\text{l}$  of  $0.92 \text{ M TiCl}_3$  were added and mixed well. A portion of the solution was transferred into the polarographic cell and the second derivative peak current  $(I_p'')_i$  was recorded. This represents the current at reaction time zero. Into a  $25\text{-ml}$  graduated test-tube fitted with a glass stopper a solution containing  $40\text{--}900 \text{ ng}$  of W(VI) were transferred,  $1.0 \text{ ml}$  of  $1.00 \times 10^{-5} \text{ M MR}$  and  $1.0 \text{ ml}$  of  $0.10 \text{ M HCl}$ , the solution was diluted accurately to  $10 \text{ ml}$  with water, and mixed well. A  $30 \mu\text{l}$  portion of  $0.92 \text{ M TiCl}_3$  was injected to start the reaction. After  $6 \text{ min}$  the reaction was quenched by addition of  $2.5 \text{ ml}$  of  $1.0 \text{ M NaOH}$ . The second derivative peak current  $(I_p'')_{\text{cat}}$  was measured. The  $\log((I_p'')_i / (I_p'')_{\text{cat}})$  value was obtained. The  $(I_p'')_{\text{uncat}}$  value for the uncatalysed (blank) reaction was measured in a similar manner. The  $\log((I_p'')_{\text{uncat}} / (I_p'')_{\text{cat}})$  values were plotted as a function of tungsten concentration to prepare a calibration graph.

## 3. Results and discussion

### 3.1. Oscillopolarographic behaviour of methyl red

In aqueous hydrochloric acid media MR has no oscillopolarographic wave, but it gives a sensitive wave at  $0.68 \text{ V}$  vs. SCE in  $0.18 \text{ M NaOH}$  (Fig. 1) [10,11]. The second derivative peak is most sensitive, and was chosen for use.  $I_p''$  is proportional to MR concentration in the range of  $6 \times 10^{-8}\text{--}5 \times 10^{-6} \text{ M}$ . The influence of Ti(IV), Ti(III) and ascorbic acid on the measurement of methyl red in  $0.18 \text{ M NaOH}$  was examined. No effect was observed.

### 3.2. W(VI)–Ti(III)–methyl red catalytic reaction system

In dilute hydrochloric acid, traces of W(VI) have a strong catalytic effect on the slow reaction between methyl red and Ti(III), but MR does not give an oscillopolarographic wave. In NaOH solution, the indicator reaction does not occur, although MR exhibits a sensitive single-sweep oscillopolarographic wave. Hydrochloric acid was chosen as the reaction medium and supporting electrolyte. Excess NaOH was added when a fixed time had elapsed to enable the oscillopolarographic detection to be used. The catalytic reaction could also be used for spectrophotometric determination of tungsten, but the measurement range of the absorbance is narrow. The measurement range for  $I_p''$ , however, is very wide, and is more sensitive than the spectrophotometric measurement. Thus, single-sweep oscillopolarography was

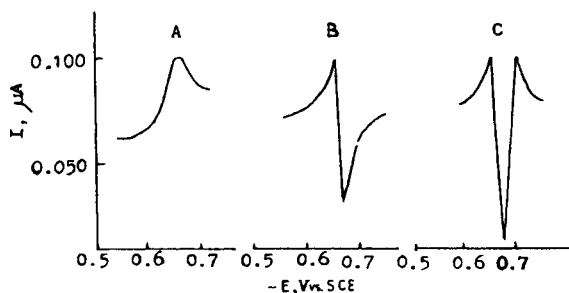


Fig. 1. Single-sweep oscillopolarographic wave of  $8.00 \times 10^{-7} \text{ M MR}$ – $0.18 \text{ M NaOH}$ . (A) Normal wave; (B) first derivative; (C) second derivative.

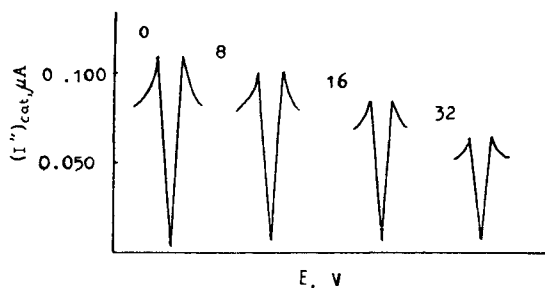


Fig. 2. Relationship between  $I_p''$  and W(VI) concentration ( $\text{ng ml}^{-1}$  W). For other conditions see text.

selected as the detection technique for the indicator reaction.

Under the chosen conditions, the reaction rate increases with W(VI) concentration (Fig. 2).

### 3.3. Effects of variables

The effects of the concentrations of hydrochloric acid, MR and Ti(III), reaction temperature and time on  $\log((I_p'')_i/(I_p'')_{\text{cat}})$  and  $\log((I_p'')_i/(I_p'')_{\text{uncat}})$  were investigated.

The results show that  $\log((I_p'')_i/(I_p'')_{\text{cat}})$  is highest and the blank value is lowest when the concentrations of hydrochloric acid and Ti(III) are in the range 0.0056–0.010 M and 0.0015–0.0030 M, respectively, so 0.0080 M hydrochloric acid and 0.0022 M Ti(III) were chosen for use. Fig. 3 indicates that  $\log((I_p'')_i/(I_p'')_{\text{uncat}})$  increases when the MR concentration decreases below  $8 \times 10^{-7}$  M. So  $8 \times 10^{-7}$  M which gives high sensitivity and a low blank value, was selected for use.

Under the chosen conditions, reaction temperatures of 14, 16, 20, 25 and 30°C were tested. A

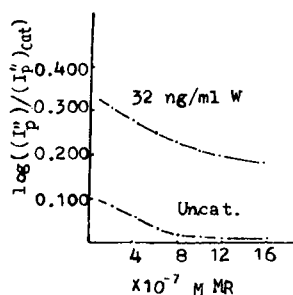


Fig. 3. Effect of methyl red concentration. For other conditions see the procedure.

reaction temperature of 16–20°C gave the best difference between the catalysed and uncatalysed reactions, so 20°C was chosen. At this temperature the  $\log((I_p'')_i/(I_p'')_{\text{cat}})$  value increases with reaction time for 10 min, and the blank value is very low. A fixed-reaction time of 6 min was selected for use, giving a good compromise between high sensitivity and short analysis time.

### 3.4. Calibration graph

Under these chosen conditions, the calibration graph was rectilinear over the range 3.2–72  $\text{ng ml}^{-1}$  W(VI), the highest concentration giving a  $\log((I_p'')_i/(I_p'')_{\text{cat}})$  value of 0.74. The  $2\sigma$  detection limit was 1.1  $\text{ng ml}^{-1}$  W. The relative standard deviations for ten determinations of 16, 32 and 64  $\text{ng ml}^{-1}$  W were 5.1, 3.5 and 2.8%.

### 3.5. Effect of foreign ions

The influence of 29 foreign ions on the catalytic determination of 32  $\text{ng ml}^{-1}$  W was examined. The results are listed in Table 1. The tolerance limit is that giving not more than  $\pm 5\%$  error. Table 1 shows that the catalytic method with oscillopolarographic detection for W has very good selectivity.

### 3.6. Analysis of samples

Analysis of steel samples: Weigh out 10 mg of steel, and place in a 50-ml beaker. Add 3 ml of 4 M sulphuric acid, heat to dissolve the sample, add 0.3

Table 1  
Influence of foreign ions on determination of 32  $\text{ng ml}^{-1}$  W

Tolerance limit (ion)/(W)	Ion added
$1 \times 10^5$	$\text{NH}_4^+$ , $\text{ClO}_4^-$ , $\text{CO}_3^{2-}$ , $\text{PO}_4^{3-}$
$4 \times 10^4$	$\text{NO}_3^-$ , $\text{ClO}_3^-$
$5 \times 10^3$	Mg(II), Ca(II), Al(III)
$1 \times 10^3$	Zn(II), Cu(II), Mn(II), $\text{I}^-$
$8 \times 10^2$	Mo(VI), Hg(II)
$5 \times 10^2$	V(V), Pb(II)
$4 \times 10^2$	Cd(II), Ba(II), Co(II), Ni(II)
$3 \times 10^2$	Ag(I), Cr(VI), Fe(III)
$2 \times 10^2$	As(III), Sb(III), Ce(III)
$1 \times 10^2$	Te(IV), Se(IV)

Table 2  
Analysis results and recovery for steel samples

Standard steel	W added (ng)	W found (ng)	Recovery (%)	Content (%)	
				This method	Standard value
C steel	0	304	–	0.152 <sup>a</sup>	0.155
	100	400	96		
	200	500	98		
CrMoWV steel	0	423	–	0.423 <sup>a</sup>	0.430
	200	625	101		
	300	720	99		
Middle-low alloy steel	0	343	–	0.323 <sup>a</sup>	0.340
	200	518	97.5		
	400	724	100		

<sup>a</sup> Mean value of three determinations.

ml of 7 M nitric acid to oxidise W, and evaporate to near dryness. After cooling, add about 10 ml of water, adjust to pH 5–6 with 1.2 M NaOH, and add 5 ml more of 1.2 M NaOH. Filter into a 100-ml beaker, adjust to pH 5 with dilute HCl. Transfer into a 100-ml standard flask, and dilute to the mark with water. Pipette a portion of the sample solution into a 25-ml graduated test tube and follow the measurement procedure (above).

The satisfactory results of analyses of steel and ore samples are shown in Tables 2 and 3, respectively.

### 3.7. Analysis of ore samples

Weigh out 0.3000 g of ore sample and place in an iron crucible; add 3 g of Na<sub>2</sub>O<sub>2</sub>. Fuse at 700°C for about 10 min, cool, and transfer into a 100-ml beaker with about 30 ml of hot water. Boil for about 10 min. After cooling, filter into a beaker, adjust to pH 5 with dilute HCl. Transfer to a 100-ml standard flask, and dilute to the mark with water. Pipet a

portion of the sample solution into a 25-ml graduated test tube and follow the measurement procedure given above. The results are shown in Table 3.

## References

- [1] Q. Li, *Yejin Fenxi*, 11 (1991) 27.
- [2] Z. Zhang, *Huaxue Shiji*, 13 (1991) 291.
- [3] Z. Jiang, *Xiyou Jinshu*, 12 (1988) 310.
- [4] Z. Jiang, *Xiyou Jinshu*, 16 (1992) 353.
- [5] L. Wang and Z. Jiang, *Chem. Res. Chin. Univ.*, 9 (1993) 85.
- [6] Z. Jiang, *Anal. Chim. Acta*, 278 (1993) 53.
- [7] Z. Jiang, *Fenxi Cheshi Xuebao*, 12 (1993) 11.
- [8] Z. Jiang and C. Qin, *Electroanalysis*, 5 (1993) 535.
- [9] Z. Jiang, *Talanta*, 38 (1991) 621.
- [10] Z. Jiang, *Yejin Fenxi*, 12 (1992) 22.
- [11] L. Wang and Z. Jiang, *Guangxi Kexuebao*, in press.
- [12] Z. Jiang, A. Liang and G. Dai, *Chem. J. Chin. Univ.*, 13 (1992) 749.
- [13] H. Goto and S. Ikeda, *J. Chem. Soc. Jpn., Pure Chem. Sect.*, 73 (1952) 654.
- [14] S.U. Kreingold and A.N. Vasnev, *Zavod. Lab.*, 44 (1978) 265.
- [15] C.G. Papadopoulos and G.S. Vasilikiotis, *Mikrochim. Acta*, III (1985) 31.
- [16] E.S. Omarova, E.F. Speranskaya and M.T. Kozlovskii, *Zh. Anal. Khim.*, 23 (1968) 1826.
- [17] R.N. Voevutskaya, V.K. Pavlova and A.T. Pilipenko, *Zh. Anal. Khim.*, 34 (1978) 1299.
- [18] H. Liu and X. Dong, *Fenxi Huaxue*, 18 (1990) 30.
- [19] B. Xu, *Fenxi Huaxue*, 12 (1984) 331.

Table 3  
Determination of tungsten in ore samples

Sample	Single determinations (%)	Mean value (%)	Oscillopolarography [19] (%)
Ore I	0.00250, 0.00254, 0.00255	0.00253	0.00245
Ore II	0.00340, 0.00343, 0.00345	0.00343	0.00342



# Screen-printed amperometric biosensors for glucose and alcohols based on ruthenium-dispersed carbon inks

Joseph Wang <sup>a,\*</sup>, Qiang Chen <sup>a</sup>, María Pedrero <sup>1,a</sup>, José M. Pingarrón <sup>b</sup>

<sup>a</sup> Department of Chemistry and Biochemistry, New Mexico State University, Las Cruces, NM 88003, USA

<sup>b</sup> Department of Analytical Chemistry, Complutense University, 28040 Madrid, Spain

Received 15 April 1994; revised manuscript received 25 July 1994

---

## Abstract

A ruthenium-dispersed carbon ink is used for the fabrication of screen-printed enzyme electrodes. The dispersed ruthenium particles offer an efficient electrocatalytic action towards the detection of enzymatically-liberated peroxide and dihydronicotinamide adenine dinucleotide (NADH). Highly selective biosensing of glucose is accomplished at a potential region (0.0 to +0.2 V) where interfering reactions are minimized. Similarly, the metallized strip surface (with co-immobilized alcohol dehydrogenase and  $\text{NAD}^+$ ) facilitates the low-potential biosensing of ethanol without the assistance of redox mediators.

**Keywords:** Amperometry; Biosensors; Disposable electrodes; Ruthenium; Glucose; Ethanol; Screen-printing technology

---

## 1. Introduction

Amperometric biosensors, which couple the inherent biospecificity of redox enzymes with the sensitivity of amperometric transduction, are of considerable interest for decentralized medical diagnostic [1–3]. Particularly attractive for such clinical applications are disposable strips mass produced by the thick film (screen-printing) technology [4,5]. For example, the two commercial sensors for decentralized monitoring of blood glucose levels are based on single-use printed carbon working electrodes, in connection with glucose oxidase and ferrocene or ferricyanide mediators [6,7]. While commercial graphite inks are commonly used for printing the transducing electrode, tailor-made inks should greatly improve the performance of future screen-printed strips.

The goal of this paper is to combine the efficient electrocatalytic activity of ruthenium microparticles with the attractive features of screen-printed enzyme electrodes. Recent work in our laboratory has demonstrated that ruthenium-dispersed carbon surfaces offer a strong and preferential catalytic action towards the oxidation of the enzymatically-liberated hydrogen peroxide or dihydronicotinamide adenine dinucleotide (NADH) [8,9]. Such catalytic activity has been exploited for developing effective carbon-paste based biosensors for glucose and alcohols based on mixing of ruthenium-dispersed graphite with mineral oil and glucose oxidase (GOx) or alcohol dehydrogenase (ADH). Similar advantages are reported in the following sections for the preparation of disposable probes for glucose and alcohol, utilizing a ruthenium-dispersed carbon ink. In particular, we wish to report on the remarkable selectivity of the glucose strip which allows cathodic detection of glucose at 0.0 V, with

---

\* Corresponding author.

<sup>1</sup> On leave from Complutense University, Madrid, Spain.

negligible contributions from easily oxidizable compounds, and without the need for a redox mediator.

## 2. Experimental

### 2.1. Apparatus

Amperometric and chronoamperometric experiments were performed with the Bioanalytical Systems (BAS) Model CV-27 voltammetric analyzer, in connection with a BAS X-Y-t recorder. Experiments were carried out in a 10 ml electrochemical cell (BAS, Model VC-2). The enzyme strip working electrode, reference electrode (Ag/AgCl; BAS Model RE-1) and platinum wire auxiliary electrode joined the cell through holes in its PTFE cover.

### 2.2. Screen-printing fabrication

A semi-automatic screen printer (Model TF-100, MPM Inc., Franklin, MA) was used for fabricating the enzyme strips. The ruthenium-containing carbon ink was prepared by first mixing 3.3 g cellulose acetate (Aldrich), 7 ml acetone (Sigma) and 15 ml cyclohexanone (Sigma). Subsequently, a 3.5 g portion of this suspension was mixed with a mixture of 0.34 g ruthenium-on-carbon (Aldrich) and 1.34 g carbon powder (Johnson Matthey number 14736, 1  $\mu\text{m}$ ). Ordinary (non-metallized) carbon inks were prepared in a similar fashion by using the Johnson-Matthey carbon powder. The ink was printed on a rectangular (4  $\times$  34 mm) alumina ceramics substrate through a patterned stencil to yield a 1.5  $\times$  30 mm structure. Its drying proceeded for 30 min at 150°C. An insulating layer was subsequently printed over most of the printed carbon area, leaving a 1.5  $\times$  5 mm working electrode area and a similar area (on the opposite side) to serve for electrical contact. The insulator (Protective coating Type 240-5B, ESL Inc.) was cured for 4 h at 200°C.

### 2.3. Reagents

All solutions were prepared with deionized water. Glucose oxidase (from *Aspergillus niger*, EC 1.1.3.4., 181,000 units/g) and alcohol dehydrogenase (ADH, from baker's yeast, EC 1.1.1.1., 30,000 units/g) were received from Sigma (catalog numbers G-7141 and A-

7011, respectively). Hydrogen peroxide was purchased from Aldrich. Glucose,  $\beta$ -nicotinamide adenine dinucleotide ( $\beta$ -NAD<sup>+</sup>), its reduced form ( $\beta$ -NADH), ascorbic acid, uric acid, phenol and acetaminophen were also received from Sigma, and used without further purification. Ethanol was purchased from Quantum Chemical Co. The poly(ester-sulfonic acid) polymer (Eastman AQ 29D, 30% dispersion) was received from Eastman Chemical Products; prior to mixing with the ADH enzyme and its NAD<sup>+</sup> cofactor, it was diluted 20-fold with deionized water. The supporting electrolyte was 0.05 M phosphate buffer solution (pH 7.4).

### 2.4. Electrode modification

Glucose oxidase/polyphenol films were grown electrochemically on the screen-printed electrodes from a 1 ml solution containing  $5 \times 10^{-3}$  M phenol and 1810 units (10 mg) of glucose oxidase in 0.05 M phosphate buffer. Electropolymerization was initiated by applying a potential of +0.80 V (vs. Ag/AgCl) and stirring the solution for 15 min. The resulting enzyme strip was then thoroughly rinsed with deionized water, and was kept in phosphate buffer (at 4°C) before and between tests. The ADH enzyme electrodes were obtained by covering the screen-printed electrodes with 5  $\mu\text{l}$  of a 200  $\mu\text{l}$  solution containing 600 units (20 mg) ADH, 20 mg NAD<sup>+</sup> and 160  $\mu\text{l}$  1.5% Eastman AQ 29D, and drying (for 15 min) at 45°C with a heat gun.

## 3. Results and discussion

Biosensors based on the two major groups of redox enzymes, hydrogen peroxide producing oxidases and NAD<sup>+</sup>-dependent dehydrogenases, usually require high operating potentials where unwanted reactions (of coexisting electroactive constituents) take place. Screen-printed strips based on ruthenium-dispersed inks offer a preferential catalytic action towards the peroxide and NADH products, and hence greatly enhance the selectivity of the corresponding substrate measurements. The sensing advantages, associated with the use of the new ink formulation, are achieved without compromising the adherence to the surface, interparticle binding and overall mechanical stability of the strip.

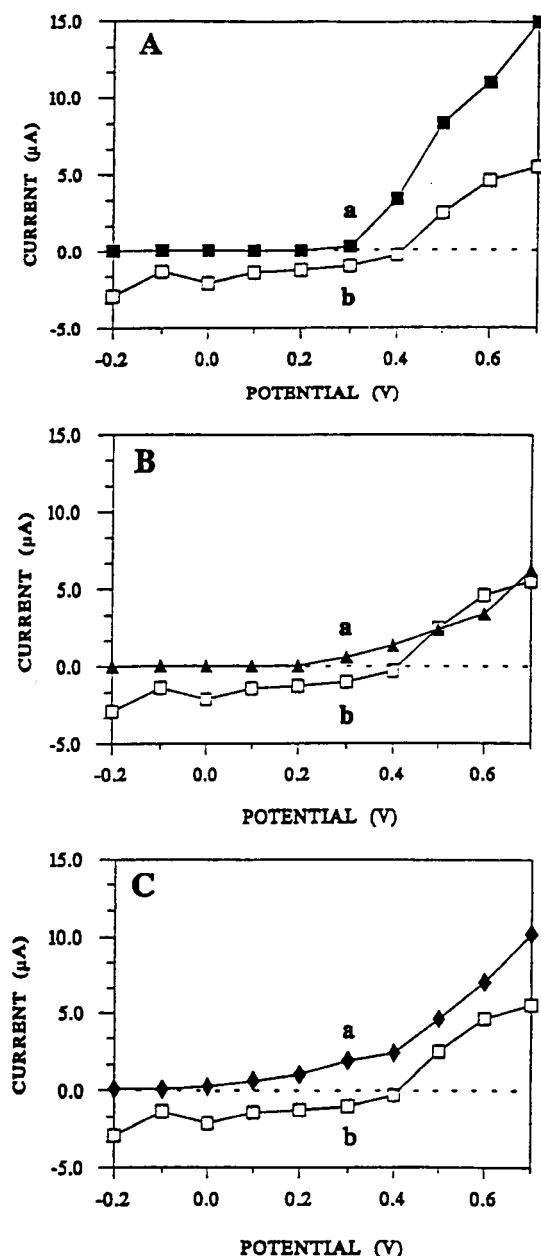


Fig. 1. Hydrodynamic voltammograms for  $1.5 \times 10^{-3}$  M acetaminophen (A(a)), uric acid (B(a)), ascorbic acid (C(a)), and hydrogen peroxide (A(b), B(b), and C(b)), at the ruthenium-dispersed carbon strips. Solution stirring, 300 rpm; electrolyte, 0.05 M phosphate buffer (pH 7.4).

### 3.1. Glucose biosensing

Fig. 1 shows hydrodynamic voltammograms at the ruthenium-dispersed strip for three easily oxidizable

components, acetaminophen (A(a)), uric acid (B(a)) and ascorbic acid (C(a)), along with that of hydrogen peroxide (b). The anodic detection of hydrogen peroxide starts at +0.40 V, with a cathodic response at more negative potentials. Indeed, hydrogen peroxide can be detected over the entire (-0.2 to +0.7 V) potential range examined. A similar potential profile was observed recently at ruthenium-dispersed carbon paste electrodes [8], indicating that the carbon matrix is not influencing the reactivity of the ruthenium particles towards the peroxide species. The common electroactive interferences, in contrast, can be detected only above +0.3 V (acetaminophen), +0.2 V (uric acid) and 0.0 V (ascorbic acid). The data of Fig. 1 thus indicate a preferential catalytic action of the ruthenium-dispersed strip towards hydrogen peroxide. A judicious turning of the operating potential to the optimal region (where coexisting electroactive species are not detected) should thus offer highly selective monitoring of substrates of various peroxide-generating oxidase enzymes. Recently described metallized screen-printed electrodes, based on palladium [10] or platinum [11] containing inks, require significantly higher potentials (of 0.3–0.5 V vs. Ag/AgCl) for the detection of the liberated peroxide. High selectivity, approaching that of the ruthenium-based strip, was obtained recently for the codeposition of rhodium particles and glucose oxidase onto a sensor strip [12]. On-going mechanistic studies should elucidate why metals, such as ruthenium or rhodium, are so reactive toward hydrogen peroxide. Since dispersed catalytic sites provide a better catalytic efficiency compared to bulk metal electrodes, attention is given also to the spatial distribution and size of the metal centers.

Fig. 2 demonstrates the selectivity of the oxidase-based glucose strip at different operating potentials (using relevant clinical concentrations). As expected from the voltammetric data (of Fig. 1), the glucose response over the 0.0 to +0.2 V potential range is not influenced by the presence of uric acid or acetaminophen; ascorbic acid also has a negligible effect upon the response. The selectivity is compromised at higher anodic potentials, where all three oxidizable compounds display a significant response. Note also (from C) the well-defined glucose response at a 0.0 V operating potential. Overall, the data of Fig. 2 indicate that while the polyphenol film (used for entrapping the enzyme) cannot eliminate (exclude) potential inter-

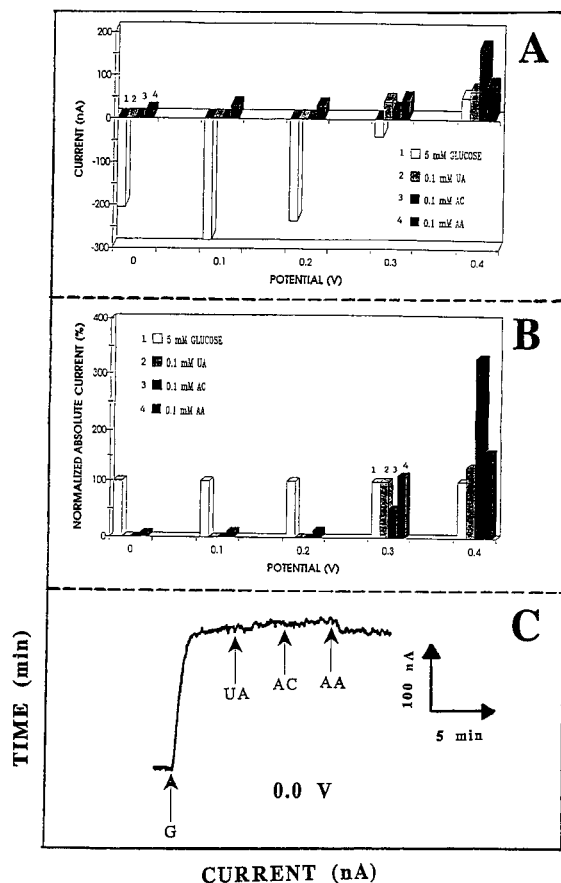


Fig. 2. Response of the ruthenium-dispersed enzyme carbon strip electrode to  $5.0 \times 10^{-3}$  M glucose (G),  $1.0 \times 10^{-4}$  M uric acid (UA),  $1.0 \times 10^{-4}$  M acetaminophen (AC) and  $1.0 \times 10^{-4}$  M ascorbic acid (AA) at different operating potentials ranging from 0.0 V to +0.4 V. (A) Actual response; (B) normalized response; (C) current-time tracing at 0.0 V. Other conditions, as in Fig. 1.

ferences, such unwanted reactions can be addressed by the preferential catalytic action of the ruthenium sites.

The favorable signal-to-noise characteristics, associated with the low-potential operation, facilitate the biosensing of low substrate concentrations. Fig. 3 compares the amperometric response (at +0.2 V) of the ruthenium-dispersed (a) and ordinary (b) carbon strip electrodes to successive ( $5 \times 10^{-4}$  M) increments in the glucose concentration. While the ordinary strip is not responsive at this potential to the additions of glucose, the metallized strip responds rapidly to these changes (producing steady-state with ca. 30 s), and yielding a detection limit of about  $2 \times 10^{-4}$  M (based on  $S/N=3$ ). The limited linearity, with curvature above  $1.5 \times 10^{-3}$  M, is indicative of kinetic limitation.

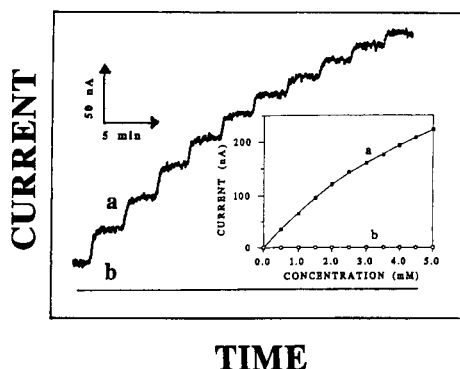


Fig. 3. Amperometric response to successive additions of  $5.0 \times 10^{-4}$  M glucose at the ruthenium-dispersed (a) and the ordinary (b) enzyme carbon strip electrode. Operating potential +0.2 V. Other conditions, as in Fig. 1.

A prolonged series of 25 repetitive chronoamperometric measurements of  $3 \times 10^{-3}$  M glucose was used to evaluate the reproducibility (potential step to +0.2 V; not shown). Such an experiment yielded a mean current of 219 nA, a range of 215–222 nA, and a relative standard deviation of 0.9%.

### 3.2. Alcohol biosensing

Over 200 dehydrogenase enzymes depend on the  $\text{NAD}^+/\text{NADH}$  couple, and thus the anodic detection of the liberated NADH is often used for the biosensing of numerous substrates. Such detection, however, requires a considerable overvoltage [13,14]. The ruthenium sites of the present strip offer a marked lowering of the overvoltage for the oxidation of NADH. Fig. 4 compares hydrodynamic voltammograms for NADH at the ruthenium-dispersed (A) and plain (B) carbon strips. As expected, no response is observed at

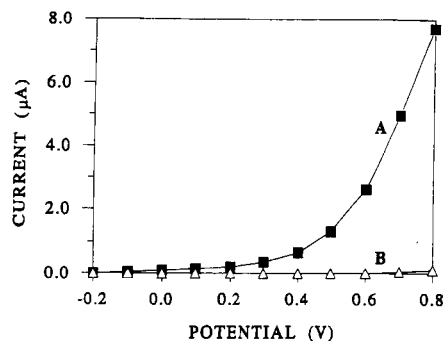


Fig. 4. Hydrodynamic voltammograms for  $1.0 \times 10^{-3}$  M NADH at the ruthenium-dispersed (A) and the ordinary (B) carbon strip electrodes. Conditions as in Fig. 1.

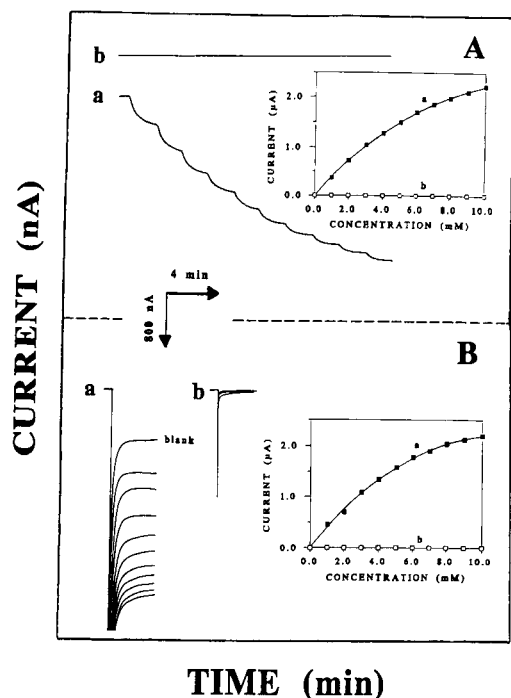


Fig. 5. Amperometric (A) and chronoamperometric (B) responses to successive additions of  $1.0 \times 10^{-3}$  M ethanol at the ruthenium-dispersed (a) and the ordinary (b) ADH/NAD<sup>+</sup> enzyme carbon strip electrodes. Operating potential +0.6 V. Other conditions, as in Fig. 1.

the ordinary strip at potentials lower than +0.7 V. In contrast, with the metallized strip, the response to NADH starts at +0.3 V, and rises sharply at higher potentials. A similar profile was reported [9] for a ruthenium-dispersed carbon paste.

Disposable biosensors based on different NAD<sup>+</sup>-dependent dehydrogenases can greatly benefit from the electrocatalytic action of the metal-dispersed strip. For example, the coimmobilization of ADH and NAD<sup>+</sup> onto the strip offers effective biosensing of various alcohols. Fig. 5 displays amperometric (A) and chronoamperometric (B) calibration data at +0.6 V for ethanol at the ruthenium (a) and carbon (b) ADH/NAD<sup>+</sup>/Eastman AQ coated strips. The metallized biosensor responds favorably to the  $1 \times 10^{-3}$  M increments in the ethanol level. In contrast (and in accordance with the voltammetric data of Fig. 4), the ordinary strip is not responding to these additions. As expected for biocatalytic reactions, the resulting calibration plots at the ruthenium dispersed strip display non-linearity, with a curvature starting above  $2 \times 10^{-3}$

M and levelling off above  $8 \times 10^{-3}$  M (see insets). Such low-potential of measurements of NADH, without the assistance of a surface-bound redox mediator, could be expanded to sensors based on other NAD<sup>+</sup>-dependent dehydrogenases (e.g., lactate dehydrogenase). Unlike the highly selective detection of the liberated peroxide species, the catalytic detection of NADH is accomplished at potentials where interfering reactions are not fully eliminated. Alcohol sensor strips with higher selectivity may thus be fabricated by coupling the metallized carbon ink with the activity of alcohol oxidase.

In conclusion, in this study we demonstrated how a judicious tailoring of the ink formulation can be used to facilitate the biosensing of glucose and ethanol. In particular, the strong and preferential catalytic action of the ruthenium particles towards the oxidation of hydrogen peroxide offers a highly selective biomonitoring of glucose. Such "built-in" electrocatalytic function eliminates the need for artificial electron acceptors. (It should be pointed out that mediated glucose strips, e.g., those based on ferrocene derivatives are also influenced by the presence of ascorbic acid.) Compared to mediated strips, the new metallized surfaces do not address the oxygen dependence, as they still rely on the use of oxygen as the cofactor. A membrane coverage may be required to extend the limited linear range of both sensors. Additional improvements may be achieved by using mixed-metals inks and by optimizing the fabrication process. We are currently exploring the influence of the ink composition and printing conditions upon the electrocatalytic behavior and sensor performance. We also wish to understand the mechanism of the catalytic action of ruthenium particles and to probe their microenvironment and spatial distribution within the printed surface. We hope that such knowledge and understanding will lead to optimal dispersion of the metal centers (for maximum catalytic activity) and will thus facilitate the mass production of metallized screen printed biosensors.

#### Acknowledgements

M. P. acknowledges a fellowship from the Universidad Complutense of Madrid (Conv. 1993).

**References**

- [1] A. Turner, I. Karube and G. Wilson (Eds.), *Biosensors*, Oxford Science Publication, Oxford, 1987.
- [2] A. Cass (Ed.), *Biosensors: A Practical Approach*, Oxford University Press, Oxford, 1990.
- [3] J. Wang, *Anal. Chem.*, 65 (1993) 450R.
- [4] M. Alvarez-Icarza and U. Bilitewski, *Anal. Chem.*, 65 (1993) 525A.
- [5] D. Craston, C. Jones, D. Williams and N. El Murr, *Talanta*, 38 (1991) 17.
- [6] M. Green and P. Hilditch, *Anal. Proc.*, 28 (1991) 374.
- [7] B.D. Davis, *Clin. Chem.*, 38 (1992) 2093.
- [8] J. Wang, L. Fang, D. Lopez and H. Tobias, *Anal. Lett.*, 26 (1993) 1819.
- [9] J. Wang, E. G. Romero and A.J. Reviejo, *J. Electroanal. Chem.*, 353 (1993) 113.
- [10] J. Wang and Q. Chen, *Analyst*, (1994) in press.
- [11] M. F. Cardosi and S. W. Birch, *Anal. Chim. Acta*, 276 (1993) 69.
- [12] J. Wang and Q. Chen, *Anal. Chem.*, 66 (1994) 1007.
- [13] W. Blaedel and R. Jenkins, *Anal. Chem.*, 47 (1975) 1337.
- [14] J. Wang and E. G. Romero, *Electroanalysis*, 5 (1993) 427.

# Characterisation of inhibitors of acetylcholinesterase by an automated amperometric flow-injection system

Alexander Günther \*, Ursula Bilitewski

*Department of Enzyme Technology, Project Group Biosensors, Mascheroder Weg 1, 38124 Braunschweig, FRG*

Received 19 April 1994; revised manuscript received 8 July 1994

## Abstract

Acetylcholinesterase was immobilised on magnetic particles and integrated in a flow-injection system via a magnetic reactor. Enzyme activity was determined amperometrically using acetylthiocholine chloride as enzyme substrate. This system was applied to enzyme inhibition tests. Inhibition constants and lower detection limits were determined for carbofuran, paraoxon, malaoxon and paraoxon-methyl. The resulting data were compared to those obtained with a photometric test, i.e. the determination of thiocholine via its reaction with the Ellman's reagent 5,5'-dithio-bis-2-nitrobenzoic acid using the same flow system. As they correlated well to those reported for the native enzyme the flow-injection analysis device can be applied to automated determination and characterisation of enzyme inhibitors.

*Keywords:* Amperometry; Flow injection; Acetylcholinesterase; Inhibition test

## 1. Introduction

The specific reaction of the native acetylcholinesterase is the catalytic saponification of the neurotransmitter acetylcholine involved in signal transmissions in nervous tissue. In a first step the enzyme substrate is bound to the active site of the enzyme leading to the formation of an acetylic enzyme, which is quickly hydrolysed in a second step. Esters such as organophosphorous compounds or derivatives of the carbamic acid are converted in an identical way, whereas phosphorylated or carbamylated acetylcholinesterase hydrolyses only very slowly. Thus, the decrease of the enzyme activity allows the application of these compounds in agriculture (insecticides) or even military (nerve gases) [1–3].

Due to the biological importance of these reactions various methods were developed for the determination of the activity of acetylcholinesterases and, as a consequence, for the determination of enzyme inhibitors [4–9]. To date, at least two systems are commercially available using the formats of an enzymatic testkit [10] and of an enzyme electrode, respectively [11].

To improve sample throughput in analytical laboratories or allow on-line monitoring of processes or waterways automation of the inhibition test is required. This can be achieved by usage of a flow-injection analysis (FIA) system [12,13] and either regeneration of the enzyme after each inhibition test [14,15] or automated replacement of the inhibited enzyme [16]. Thus, a FIA device was already described with cholinesterases being immobilised on magnetic particles and kept in the flowing system via a magnetic reactor comprising a permanent magnet together with an electromagnet.

\* Corresponding author.

By switching on the electromagnet, the magnetic field of the permanent magnet was compensated and the magnetic particles were released from the system. The determination of acetylcholinesterase activity was based on the reaction of thiocholine with 5,5'-dithio-bis-2-nitrobenzoic acid [17].

The aim of the work presented here was a further improvement of the system by replacing the photometric determination of thiocholine by its electrochemical oxidation at Pt electrodes, thus eliminating the need for an additional reagent. The Pt electrodes were produced by screen-printing technology which has proven to be a suitable technology for low-cost fabrication of electrodes [18,19]. Both systems were compared with respect to determination of inhibition constants, standard deviations of the test, achievable lower detection limits and influence of sample matrices.

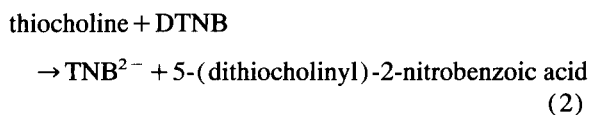
## 2. Principles

### 2.1. Determination of enzyme activity

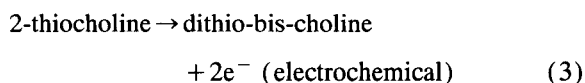
The activity of acetylcholinesterases (AChE) was determined either photometrically or amperometrically. Both detection principles are based on the enzymatic saponification of the thioester acetylthiocholine to thiocholine and acetic acid (Eq. 1):



The amount of thiocholine was determined with Ellman's reagent, 5,5'-dithio-bis-2-nitrobenzoic acid (DTNB), which is converted by thiocholine quantitatively to the yellow dianion 5-thio-2-nitrobenzoic acid ( $\text{TNB}^{2-}$ ) (Eq. 2) [17].



The amperometric determination of cholinesterase activity was based on electrochemical oxidation of thiocholine at Pt electrodes (Eq. 3). The potential had to be optimised with respect to an optimal ratio of the currents due to thiocholine oxidation and oxidation of the counter ion of the enzyme substrate, i.e.  $\text{Cl}^-$  or  $\text{I}^-$ .



In both FIA systems the peak heights were proportional to enzyme activity. Therefore, enzyme inhibition was monitored by decrease of peak heights and the remaining enzyme activity ( $A\%$ ) could be calculated according to Eq. 4:

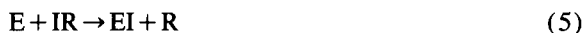
$$A\% = \frac{a_r - a_{bl}}{a_0 - a_{bl}} * 100 \quad (4)$$

with  $a_r$  being the original peak height,  $a_{bl}$  the blank signal (only enzyme substrate without enzyme) and  $a_0$  the final peak height.

### 2.2. Calculation of the kinetic data

The dependence of the remaining enzyme activity on the inhibitor concentrations was used to calculate the inhibition constants ( $k_i$ ) of the insecticides with linear regression. Three assumptions were made to obtain the fundamental equations: (i) the concentration of the enzyme-substrate complex was very low; (ii) the formation of the enzyme-substrate complex was faster than its decomposition; and (iii) the reaction was irreversible.

This led to the following one-step mechanism of enzyme inhibition reaction:



where E = enzyme, IR = inhibitor, EI = inhibitor bound to enzyme and R = leaving residue of the inhibitor. This could be expressed mathematically via [4]:

$$\frac{dA}{dt} = k_i * c(\text{IR}) * A \quad (6)$$

where  $A$  = enzyme activity and  $k_i$  = inhibition constant. The integration of Eq. 6 leads to Eq. 7 and allows the calculation of the inhibition constant  $k_i$  from the slope of the graph  $\log A\%$  versus  $c(\text{IR})$  (Eq. 8).

$$\ln \frac{a_t}{a_0} = k_i * c(\text{IR}) * t_i \quad (7)$$

$$\log A\% = \log 100 + k_i * c(\text{IR}) * t_i * \ln 10^{-1} \quad (8)$$

where  $t_i$  = inhibition time. The obtained inhibition constants  $k_i$  could be used to calculate a theoretical detection limit for each inhibitor ( $c_{\min}(\text{IR})$ ) with  $A\%_{\max}$  being dependent on the standard deviation of the tests.

$$c_{\min}(\text{IR}) = \frac{\ln(A_{\max}/100)}{-k_i * t_i} \quad (9)$$



### 3. Experimental

#### 3.1. Reagents and materials

Distilled, deionised water was used for the preparation of all solutions unless stated otherwise. Acetylcholinesterase (AChE, EC 3.1.1.7) from bovine erythrocytes was obtained from Boehringer (Mannheim). Acetylthiocholinechloride and -iodide, 5,5'-dithio-bis-2-nitrobenzoic acid (DTNB, Ellman's Reagent) and tris-(hydroxy-methyl)-methylamine (Trizma Base) were purchased from Sigma (Deisenhofen). The substrate solutions (6 mM) were prepared in distilled water to reduce hydrolysis. The photometric test was done in 0.01 M buffer (pH 8,5) mixing Trizma Base with 0.1 M HCl from Riedel-de Haën (Seelze). Sodium chloride and sodium hydroxide for the immobilization [17], and potassium iodide for the determination of the electroactivity of the iodide ions were also obtained from Riedel-de Haën. Potassium phosphates ( $K_2HPO_4$  and  $KH_2PO_4$ ) for the preparation of 0.01 M buffer (pH 8.0) for the amperometric test and glycine (for the immobilization) were bought from Merck (Darmstadt). All insecticides were purchased from Riedel-de Haën with a purity of 99%. The examined inhibitors were: paraoxon (*O,O*-diethyl-*O*-4-nitrophenylphosphate), paraoxon-methyl (*O,O*-dimethyl-*O*-4-nitrophenylphosphate), malaoxon (*S*-[1,2-bis-(ethoxycarbonyl)ethyl]-*O,O*-dimethylthiophosphate) and carbofuran (2,3-dihydro-2,2-dimethylbenzofuran-7-yl-methylcarbamate). Stock solutions (10

mg/l) of insecticides were prepared in methanol (J.T. Baker, Gross-Gerau) and were diluted with carrier buffer directly before use in the inhibition test to keep their hydrolysis low.

#### 3.2. Enzyme immobilization

The immobilization of the AChE on aminoterminated magnetic particles (Biomag 4100, Paesel and Lorei, Frankfurt) was carried out as described earlier [16] using the glutaraldehyde method. Glutaraldehyde (25% solution in water) was obtained from Merck-Schuchardt (Hohenbrunn). In this work 5 mg AChE in 10 ml potassium phosphate buffer was used for the immobilization. Before application in the FIA the suspension was diluted 1:100 with carrier buffer.

#### 3.3. FIA manifold

The flow-injection manifold is shown schematically in Fig. 1. It comprised 4 peristaltic pumps (Jungkeit, Nörten Hardenberg), 1 injection valve (V100 Perstorp Analytic, Rodgau), 5 2/3-way valves (Lee, Westbrook, CT) the detection unit and the magnetic reactor [16]. The tubing was made of PTFE (Omnifit, Cambridge) with a diameter of 0.8 mm and the carrier buffer was pumped through the system at 1.0 ml/min. The volume of the injection loop was 22  $\mu$ l. The FIA was controlled using a home made software.

A homogeneous suspension of the magnetic particles with the immobilized enzyme was obtained by stirring

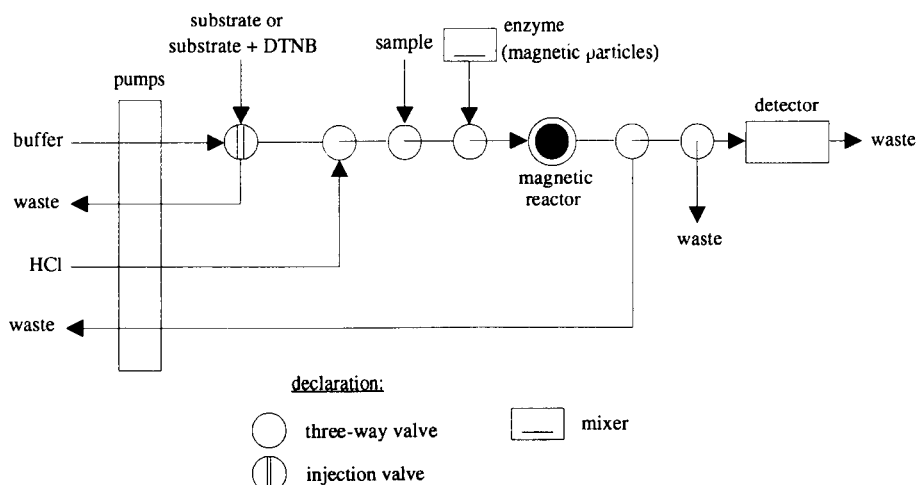


Fig. 1. FIA manifold for the detection of enzyme inhibitors.

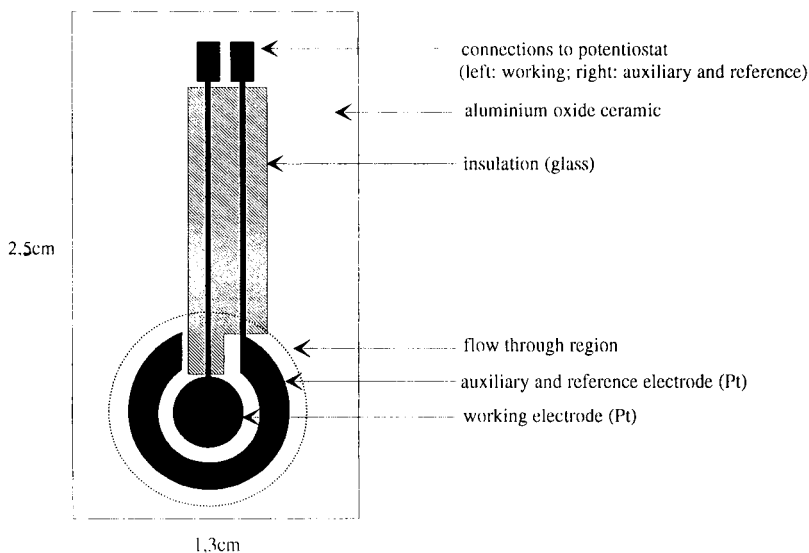


Fig. 2. Pt thick-film electrode for amperometric detection in FIA systems.

and was sucked into the magnetic reactor using the pump, which was also used for sucking the sample or standard solutions. 2/3-way valves were used to allow removal of the enzyme after a test by HCl washing and preventing the sample and the magnetic particles from passing the flow-through cell of the detector.

#### 3.4. Detection principles

Photometric detection of the  $\text{TNB}^{2-}$  was done at 412 nm with a photometer equipped with a suitable flow-through cell (Knauer, Berlin).

The amperometric detection took place at a Pt thick-film electrode which was developed and produced by screen-printing technology at the GBF (Fig. 2)

[18,19]. This electrode was integrated in the FIA system using a home-made flow through cell (Fig. 3). Thiocholine was oxidised at various oxidation potentials (+150 to +600 mV) at the working electrode (inner part of the screen-printed electrode, see Fig. 2). For the electrochemical measurements two different enzyme substrates (acetylthiocholineiodide and -chloride) were tested due to the blanc current of their counterions. The connection of the auxiliary and the reference electrode led to the outer ring of the screen-printed thick-film electrode (see Fig. 2). The potential of this electrode was determined versus a Ag/AgCl reference electrode (Ingold Argenthal, Ingold Meßtechnik, Steinbach) at 25°C in a 0.01 M  $\text{KP}_i$  buffer (pH 8.0) with a Schott CG 822 in an additional experiment (Schott Geräte, Hofheim) to be +200 mV.

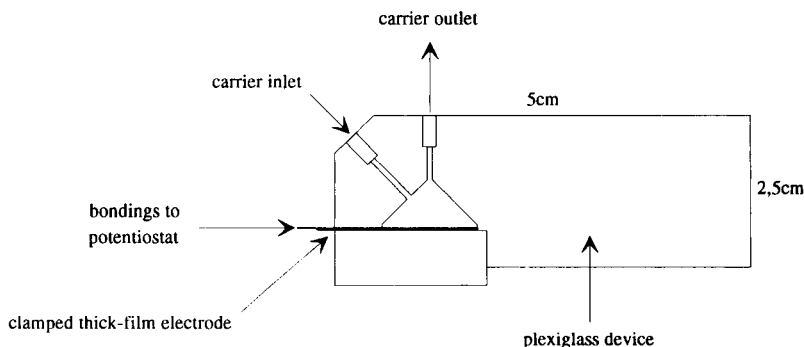


Fig. 3. Laboratory-made flow through cell for Pt thick-film electrodes.

### 3.5. Inhibition tests

For both detection systems ten inhibition tests with carbofuran were carried out for the calculation of a standard deviation of the enzyme inhibition test principle. Additionally the low decreasing enzyme activity in pure carrier buffer was taken in consideration whether an inhibition was a specific or nonspecific one.

One cycle for an inhibition test included the following steps: (i) determination of a blank signal for thiocholine ( $a_{bl}$ ). (ii) Filling the magnetic reactor with magnetic particles which were kept in the flowing system by magnetic forces of the permanent magnet inside the magnetic device. (iii) Determination of the initial activity of the enzyme in the reactor ( $a_0$ ) three times by three injections of the substrate. (iv) Incubation with an inhibitor for 10 min (1 min flow, 9 min stopped flow). (v) Determination of the remaining enzyme activity ( $a_r$ ) using the above mentioned procedure for the initial enzyme activity. (vi) Compensation of the magnetic field by switching on the electromagnet allowing an automatic release of the inhibited enzyme out of the flow system by washing with 0.1 M HCl. (vii) Confirmation of the complete removal of the inhibited enzyme by a second blank peak ( $a_{bl}$ ). After that a new inhibition test could be started.

Each activity test with ( $a_0$  and  $a_r$ ) or without ( $a_{bl}$ ) enzyme included a stopped flow for 30 s, when the injected substrate was in the magnetic reactor. This increased the amount of converted substrate. The enzyme in the magnetic reactor in each test was estimated to be 66 mU allowing kinetic controlled reaction. The whole test required 25 min when using photometric determination of enzyme inhibition and 40 min in the amperometric test, the difference being caused by the different geometries of the flow through cells. Remaining enzyme activities were calculated from Eq. 4 by using the mean values of  $a_r$ ,  $a_0$  and  $a_{bl}$ .

## 4. Results and discussion

### 4.1. Amperometric determination of cholinesterase activity

The photometric cholinesterase inhibition assay is based on the hydrolysis of acetylthiocholine iodide (ATCI) and determination of thiocholine through its

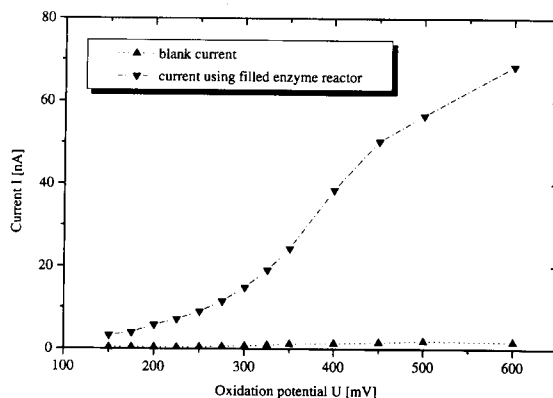


Fig. 4. Oxidation current at the screen printed thick-film electrode injecting 6 mM acetylthiocholine chloride in the FIA system with and without enzyme in the magnetic reactor.

reaction with DTNB. As thiocholine can also be electrochemically oxidised [20], the influence of the potential applied to screen-printed Pt electrodes was investigated. At potentials exceeding 200 mV a strong increase of the blank signal, i.e. signal without enzymatic hydrolysis of ATCI, was observed, probably due to electrochemical oxidation of the iodide counterion. The determination of a 6 mM KI solution in carrier buffer using the same procedure in the FIA system showed the same current increase. At 300 mV the blank signal was in the same order of magnitude as the signal after enzymatic hydrolysis. Thus, the applicability of acetylthiocholine chloride (ATCCI) was tested. In Fig. 4 the potential dependence is shown: the blank signal could be neglected in the whole potential range, whereas increasing currents due to oxidation of thiocholine were observed from 300 mV leading to a half-wave potential of approximately 400 mV. Therefore, in the following ATCCI was used as enzyme substrate in the amperometric assay, and ATCI was used in the photometric assay.

Electrochemical oxidation of thiocholine may lead to dimerised products [21,22] causing fouling effects of the working electrode. Due to low prevailing current densities, this was observed at low potentials (150 mV) already within 3 successive determinations of enzyme activity, whereas at 600 mV the current decreased significantly only within several hours of operation. The electrodes could be used for at least one week of continuous operation.

Neither acetic acid, the leaving group of acetylthiocholine, nor methanol (1% solution), the solvent

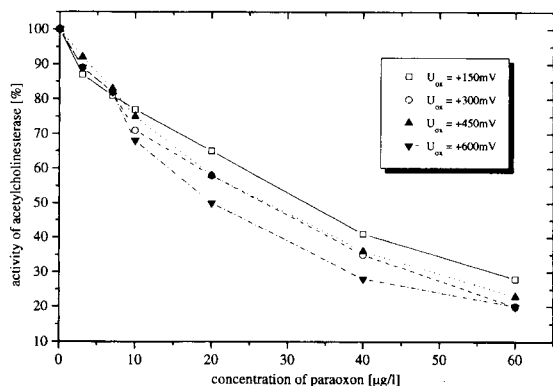


Fig. 5. Influence of paraoxon on the enzyme activity of acetylcholinesterase using various oxidation potentials for thiocholine for the determination of enzyme activity.

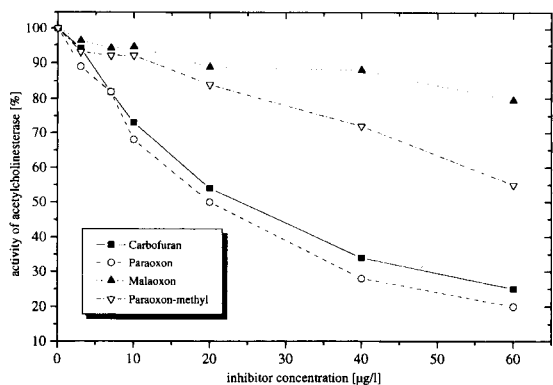


Fig. 6. Remaining enzyme activity after inhibition of acetylcholinesterase using various insecticides and the amperometric detection principle at an oxidation potential of +600 mV.

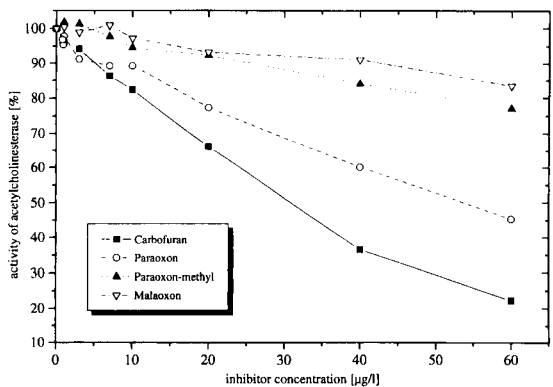


Fig. 7. Remaining enzyme activity after inhibition of acetylcholinesterase using various insecticides and the photometric detection principle.

used for preparation of stock solutions of enzyme inhibitors, had any influence on the amperometric assay.

#### 4.2. Inhibition tests using amperometric detection

In Fig. 4 it was shown that the sensitivity of the electrochemical thiocholine determination increased with increasing potential. Thus, the influence of the potential was also tested for the inhibition tests. In Fig. 5 data obtained for paraoxon-ethyl are shown demonstrating that no influence was observed. This is due to the fact that the enzyme activity was determined before and after the incubation with the inhibitor eliminating the low sensitivity at low potentials. Due to the improved longterm applicability of the electrode at higher potentials, a potential of 600 mV was used in the following investigations.

Inhibition tests were carried out with different compounds covering the concentration range from 1 µg/l to 60 µg/l. Results are summarized in Fig. 6. They demonstrate the strong inhibitory potential of carbofuran and paraoxon-ethyl for acetylcholinesterase from bovine erythrocytes compared to the inhibitory effects of malaoxon and paraoxon-methyl. This was confirmed by the inhibitory constants being calculated according to Eq. 8. They were in the same order of magnitude as those obtained for the soluble enzyme [23] (Table 1).

According to Eq. 9 the inhibition constants can also be used to calculate the lower detection limits achievable for the different compounds. Considering the standard deviation of the activity assay a remaining enzyme activity of less than 95% was taken as inhibition of the enzyme due to the presence of an inhibitor. Thus, lower detection limits for the four inhibitors could be calculated and compared to those achieved by the FIA device. Data are summarized in Table 1 and a good correlation was found. Thus, this FIA method could be used for the determination of inhibition constants of compounds and, vice versa, the inhibition constants could be used for estimation of the achievable lower detection limits.

#### 4.3. Inhibition tests with photometric determination

Both ATCI and DTNB showed increasing spontaneous hydrolysis when increasing the pH of phosphate (pH 6.5–8.0) and Tris buffer (pH 8.0–9.0), thus low pH was required for storage. However, the activity of

Table 1  
Practical (column 2) and theoretical data (column 3) of inhibition tests with amperometric detection using immobilized AcChE

Inhibitor	Lower detection limits achieved with the FIA device ( $\mu\text{g/l}$ )	Lower detection limits calculated from Eq. 9 ( $\mu\text{g/l}$ )	$k_i \times 10^5$ ( $1 \text{ mol}^{-1} \text{ min}^{-1}$ )	$k_i \times 10^5$ ( $1 \text{ mol}^{-1} \text{ min}^{-1}$ ) [23]
Carbofuran	3	2.6	4.6	9.0
Paraoxon-ethyl	3	2.1	6.7	6.0
Paraoxon-methyl	7	8.5	1.8	2.2
Malaoxon	7	7.0	1.4	2.6

The inhibition constants (column 4) are mean values of the four investigated oxidation potentials and are compared with literature data of the native enzyme (column 5, [23]).

acetylcholinesterase and its sensitivity to inhibitors increased also with increasing pH. That is why the photometric test described in literature is performed at pH 7.2 [10,23]. Using the FIA device this problem could be solved by using Tris buffer, pH 8.5, as carrier solution, and solving ATCI and DTNB in distilled water.

In Fig. 7 remaining activities of the enzyme after incubation with malaoxon, carbofuran, paraoxon-methyl and paraoxon-ethyl in the concentration range from 0.8 to 60  $\mu\text{g/l}$  are summarised and inhibition constants were calculated (Eq. 8) (Table 2). They were again used for the calculation of lower detection limits taking remaining activities of less than 95% as significant for the inhibition of the enzyme due to the presence of inhibitors (Table 2).

#### 4.4. Application to real samples

In environmental analysis biochemical systems are developed as screening tests allowing a rapid decision on the contamination of samples. Thus, the FIA systems described above were applied to samples of drinking

water and water from a small brook in Braunschweig, to which carbofuran and paraoxon-ethyl were added in a concentration range from 1–20  $\mu\text{g/l}$ , focusing on the correct decision for contaminated samples. The results are given in Table 3. All samples with a remaining activity of less than 95% were indicated as positive. Considering the achievable lower detection limits of 3  $\mu\text{g/l}$  for both compounds (Tables 1 and 2) no false-negative samples were indicated. Quantitative analysis showed even sufficient recovery rates, only for high paraoxon-ethyl concentrations the inhibitory effect observed with the amperometric system in standard solutions was significantly higher than in water samples.

## 5. Conclusion

Inhibition tests of acetylcholinesterase were automated using a FIA device comprising a magnetic enzyme reactor. Determination of enzyme activity was changed from the photometric Ellman's test to amperometric oxidation of thiocholine using various oxida-

Table 2  
Lower detection limits (practical and calculated from Eq. 9) and inhibition constants obtained with the FIA device and photometric detection of enzyme activity

Inhibitor	Lower detection limits achieved with the FIA device ( $\mu\text{g/l}$ )	Lower detection limits calculated from Eq. 9 ( $\mu\text{g/l}$ )	$k_i \times 10^5$ ( $1 \text{ mol}^{-1} \text{ min}^{-1}$ )	$k_i \times 10^5$ ( $1 \text{ mol}^{-1} \text{ min}^{-1}$ ) [23]
Carbofuran	3	2.0	5.7	9.0
Paraoxon-ethyl	3	4.0	3.5	6.0
Paraoxon-methyl	10	12.7	1.0	2.2
Malaoxon	20	17.9	0.9	2.6

For comparison, inhibition constants obtained from the literature for the native enzyme are also given [23].

Table 3

Application of the inhibition test with acetylcholinesterase using drinking and brook water for sample preparation (see text for further details)

Sample	Inhibitor	Amperometric detection		Photometric detection	
		Remaining activity (%)	Indication	Remaining activity (%)	Indication
Drinking water	0 mg/l	97	–	100	–
	0 mg/l	94	+	101	–
	1 µg/l carbofuran	91	+	99	–
	5 µg/l	76	+	90	+
	10 µg/l	72	+	77	+
	20 µg/l	53	+	59	+
	1 µg/l paraoxone	94	+	94	+
	5 µg/l	89	+	90	+
	10 µg/l	83	+	85	+
	20 µg/l	71	+	81	+
Brook water	0 µg/l	99	–	103	–
	0 µg/l	103	–	99	–
	1 µg/l carbofuran	100	–	98	–
	5 µg/l	90	+	87	+
	10 µg/l	77	+	73	+
	20 µg/l	59	+	57	+
	1 µg/l paraoxone	105	–	89	+
	5 µg/l	95	±	93	+
	10 µg/l	87	+	88	+
	20 µg/l	74	+	76	+

tion potentials and requiring no additional reagent, such as DTNB.

The system was applied to the determination of inhibition constants of paraoxon-ethyl and -methyl, carbofuran and malaoxon and to analysis of real samples. The inhibition constants were independent of the detection principle and correlate well with those known for the soluble enzyme. For carbofuran and paraoxon-ethyl, the strongest inhibitors of acetylcholinesterase from bovine erythrocytes, lower detection limits of 3 µg/l were obtained.

### Acknowledgements

We would like to thank Wiebke Drewes and Gabriele C. Chemnitius who were responsible for the development of the thick film electrodes, Matthias Stiene for the excellent driving software for the flow-injection system and Henning Schillig and Detlef Hanisch who were involved in the design of the flow through cell.

### References

- [1] D.M. Quinn, *Chem. Rev.*, 87 (1987) 955.
- [2] W.N. Aldridge and E. Reiner, *Enzyme Inhibitors as Substrates, Interactions of Esterases with Esters of Organophosphorous and Carbamic Esters*, Elsevier, New York, 1975.
- [3] H.C. Froede and I.B. Wilson, in P.D. Boyer (Ed.), *The Enzymes*, Vol. 5, Academic Press, New York, 1971.
- [4] P. Skladal and M. Mascini, *Biosensors Bioelectron.*, 7 (1992) 335.
- [5] A.M. Nyamsi Hendji, N. Jaffrezic-Renault, C. Martelet, P. Clechet, A.A. Shul'ga, V.I. Strikha, L.I. Netchiporuk, A.P. Soldatkin and W.B. Wlodarski, *Anal. Chim. Acta*, 281 (1993) 3.
- [6] K. Stein and G. Schwedt, *Anal. Chim. Acta*, 272 (1993) 73.
- [7] J.-L. Marty, N. Mionetto, T. Noguer, F. Ortega and C. Roux, *Biosensors Bioelectron.*, 8 (1993) 273.
- [8] J.C. Fernando, K.R. Rogers, N.A. Anis, J.J. Valdes, R.G. Thompson, A.T. Eldefrawi and M.E. Eldefrawi, *J. Agric. Food Chem.*, 41 (1993) 511.
- [9] W. Trettnak, F. Reininger, E. Zinterl and O.S. Wolfbeis, *Sensors Actuators B*, 11 (1993) 87.
- [10] *Cholinesterase-Hemmtest, Screening Test zur Bestimmung von Cholinesterase hemmenden Organophosphat- und Carbamat-Pestiziden in Wasser*, Boehringer Mannheim GmbH, Mannheim.

- [11] Biosensor-Test LCW 570, Acetylcholinesterase Pestizid Screening, Dr. B. Lange GmbH, Düsseldorf.
- [12] R.D. Schmid and W. Künnecke, *J. Biotechnol.*, 14 (1990) 3.
- [13] *Journal of Biotechnology*, Vol. 3, 1993, Special Issue: Biosensors and Flow Injection Analysis.
- [14] I.A. Takruni, A.M. Almuaid and A. Townshend, *Anal. Chim. Acta*, 282 (1993) 307.
- [15] C. Tran-Minh, *Anal. Proc.*, 30 (1993) 73.
- [16] R. Kindervater, W. Künnecke and R.D. Schmid, *Anal. Chim. Acta*, 234 (1990) 113.
- [17] G.L. Ellman, K.D. Courtney, V. Andres, Jr. and R.M. Featherstone, *Biochem. Pharmacol.*, 7 (1961) 88.
- [18] M. Alvarez-Icaza and U. Bilitewski, *Anal. Chem.*, 65 (1993) 525A.
- [19] U. Bilitewski, in G. Costa and S. Miertus (Eds.), *Proc. Conference on Trends in Electrochemical Biosensors*, World Scientific, Singapore, 1992, p. 59.
- [20] R. Gruss, F. Scheller, M.J. Shao and C.C. Lui, *Anal. Lett.*, 22 (1989) 1159.
- [21] L.H. Goodson and W.B. Jacobs, *Methods Enzymol.*, 44 (1976) 647.
- [22] L.A. Allison and R.E. Shoup, *Anal. Chem.*, 55 (1983) 8.
- [23] P. Hertzprung, L. Weil and K.E. Quentin, *Z. Wasser-Abwasser-Forsch.*, 22 (1989) 67.

# Gradient flow-injection amperometry based on induced retention by the detector coating

Joseph Wang \*, Liang Chen, Hui Wu

*Department of Chemistry and Biochemistry, New Mexico State University, Las Cruces, NM 88003, USA*

Received 12 May 1994; revised manuscript received 25 July 1994

---

## Abstract

A novel approach for enhancing the selectivity of amperometric flow-injection systems is described. This strategy relies on the use of coated electrodes to induce longer residence times for the target analyte (within the detector) compared to the interfering species. Selective measurements of the analyte are thus performed on the tailing edge of its peak, after passage of the interfering species from the detector. Surface coatings with different permeability properties, including charge-exclusion Nafion or hydrophobic lipid and alkanethiol films are thus used to retain and selectively detect counterionic or nonpolar analytes, after the elution of co-ionic and polar interferences, respectively, from the detector.

*Keywords:* Amperometry; Flow injection; Selectivity

---

## 1. Introduction

The coupling of amperometric detection and flow-injection analysis (FIA) has been proven to be extremely useful for numerous analytical applications [1–3]. Such interest is attributed to the inherent sensitivity of amperometric detectors, their selectivity towards electroactive species, and their attractive dynamic properties. Such operation, however, may lack the desired selectivity when complex mixtures of electroactive species are concerned. Chemical and physical separations (dialysis, solvent extraction, low resolution chromatography, etc.) in the flow manifold, are usually used to impart a higher degree of selectivity. Alternately, added selectivity can be achieved through the detector and its operation. These include the use of multielectrode [4,5] or potential scanning [6,7] detection schemes, or tailoring of the surface with an appro-

prate chemical modifier or biological entity [8,9]. Yet, new dimensions of information are highly desired to enhance the selectivity of electrochemical detectors.

The present paper reports on a novel approach to impart high selectivity to amperometric FIA systems, based on the use of detector coatings to achieve different stretchings of solute zones. By judiciously selecting the surface coating one can thus induce a prolonged retention of the target analyte, while allowing rapid elution of non-partitioning interfering species from the detector compartment. Various electrode coatings have been shown useful for the uptake of different classes of electroactive species [10]. Such a partition process is shown below to induce longer residence times under flow injection conditions. The surface coating can thus be viewed as a stationary phase (supported on the detector). Such a “built-in” separation step (within the detector) is coupled with measurement of different regions of the dispersed peak (and not of the traditional

---

\* Corresponding author.



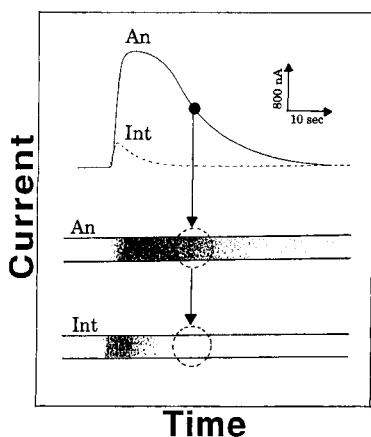


Fig. 1. Dispersion of the analyte (AN) and interference (INT) zones and the corresponding amperometric FIA outputs. The stretching of the analyte zone accrues from its preferential permeability into the detector coating.

peak height). In particular, a greatly enhanced selectivity is achieved through measurements on the decaying portion of the peak, i.e., after passage of the interfering species (Fig. 1). Such an amperometric FIA operation represents a useful extension of gradient FIA techniques [11,2], which exploit different segments of the sample zone for obtaining the analytical information. The characteristics and advantages of this time-resolved operation are illustrated in the following sections in connection with the detection of biologically important compounds at Nafion-, lipid-, or alkanethiol-coated thin-layer amperometric detectors.

## 2. Experimental

### 2.1. Apparatus.

The flow-injection system consisted of the carrier reservoir, Rainin Model 5041 sample injection valve (20  $\mu\text{l}$  volume), interconnecting PTFE tubing, and the amperometric detector. Most experiments employed a platinum thin-layer detector (Model TL-10A, BAS). Experiments involving *n*-alkanethiol coatings employed a large-volume wall-jet detector [12], with a gold disk working electrode (Model MF-2014, BAS). A thin layer detector (Model TL-4, BAS) was used in connection with the carbon paste experiments. A gravity feed of the carrier was used. All experiments were controlled by a CV27 voltammetric analyzer (BAS), in connection with a BAS X-Y-t recorder.

### 2.2. Surface modification

Prior to their coating the platinum and gold electrodes were polished with 0.05  $\mu\text{m}$   $\alpha$ -alumina particles and rinsed thoroughly with double distilled water. The Nafion-coated electrode was prepared by placing 5  $\mu\text{l}$  of the Nafion solution (Aldrich, diluted to 2% in ethanol) to cover the active disk and allowing to air dry. The lipid-coated detector was prepared by adding 12 mg of cholesterol (CH) to 1 ml of a chloroform solution containing 10 mg of phosphatidylcholine (PC). 5  $\mu\text{l}$  of the resulting PC/CH mixture were placed twice on the platinum surface, allowing the solvent to evaporate (each time). The film of *n*-alkanethiol was prepared by immersing the gold electrode in a quiescent solution of  $5 \times 10^{-3}$  M octadecyl mercaptan (in ethanol). After a 1 min equilibration, the electrode was removed from the solution, rinsed with double distilled water, and allowed to dry.

### 2.3. Reagents and procedure

All solutions were prepared with doubly distilled water. Dopamine, epinephrine, norepinephrine, acetaminophen, chlorpromazine, 3,4-dihydroxyphenylacetic acid (dopac), promethazine, uric acid, hydrogen peroxide (Sigma), Ascorbic acid, octadecyl mercaptan (Aldrich) and ethanol (Quantum chemical) were used without further purification. The supporting electrolyte carrier solution was a 0.05 M phosphate buffer (pH 7.4).

Flow-injection measurements were made by applying the desired working potential and allowing the transient current to decay. Different delay times (from the point of injection) were used for sampling the current. All experiments were performed at room temperature.

## 3. Results and discussion

Various solute permeation processes, at different detector surface coatings, were examined for manipulating the retention and enhancing the selectivity of amperometric flow-injection systems. The utility of thin-layer detectors based on Nafion and lipid coatings, as well as a wall-jet cell with an alkanethiol-modified gold electrode will be illustrated below.

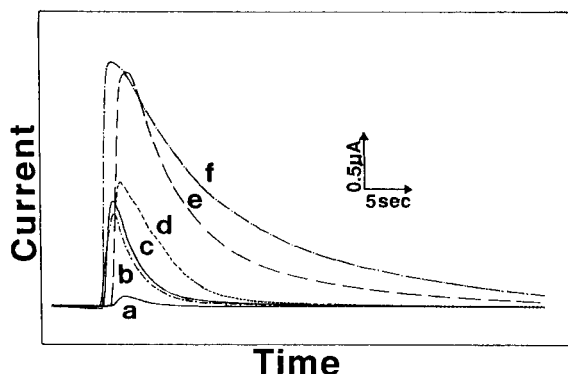


Fig. 2. Flow-injection amperometric peaks for  $1 \times 10^{-3}$  M uric acid (a), dopac (b), ascorbic acid (c), acetaminophen (d), epinephrine (e) and dopamine (f) at the Nafion-coated platinum thin-layer detector. Flow rate, 0.6 ml/min; applied potential, +0.70 V; electrolyte and carrier, 0.05 M phosphate buffer (pH 7.4).

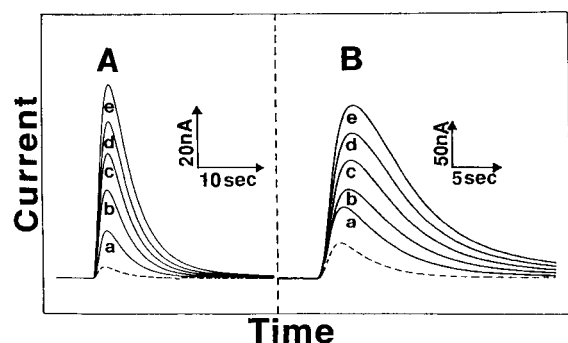


Fig. 3. (A) Flow-injection peaks for  $1 \times 10^{-4}$  M uric acid solutions containing increasing levels of norepinephrine,  $(1-5) \times 10^{-5}$  M (a–e). (B) Flow-injection peaks for  $1 \times 10^{-4}$  M acetaminophen solutions containing increasing levels of epinephrine,  $(1-5) \times 10^{-5}$  M (a–e). Flow rate, 1.0 ml/min. Other conditions, as in Fig. 2. Dotted lines represent the response for the uric acid (A) and acetaminophen (B) solutions ( $1 \times 10^{-4}$  M).

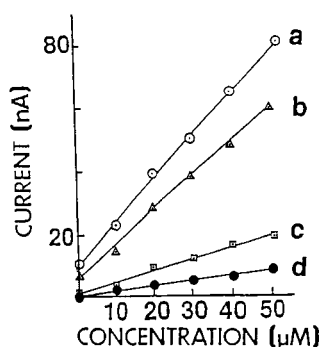


Fig. 4. Calibration plots for norepinephrine in the presence of  $1 \times 10^{-4}$  M acetaminophen obtained by measuring the current at different times following the injection: 2.5 (a), 5.0 (b), 10.0 (c) and 15.0 (d) sec. Other conditions, as in Fig. 3A.

### 3.1. Nafion-coated thin-layer detector

Nafion perfluorinated films have been widely used in electroanalysis due to their tremendous ion-exchange affinity for organic cations [10,13–15]. Such ion-exchange properties are extremely useful for the new gradient flow-injection approach. Fig. 2 displays flow-injection peaks for six biologically significant compounds (present at the same concentration). As expected, significantly larger peak heights are observed for the cationic catecholamines (e, f) in comparison to the anionic dopac and ascorbic or uric acids (a–c). Yet, traditional peak height measurements do not offer the desired selectivity due to incomplete rejection of anionic interferences. For example, the epinephrine peak height is only 2.24-, 2.54- and 20.6-times larger than those of the ascorbic acid, dopac, and uric acid, respectively. It is possible, however, to selectively measure the primary neurotransmitters by using a gradient technique, associated with their greatly prolonged retention in the detector compartment. While all the six compounds display a rapid rise in the current, the descending parts of their peak are largely different. The dispersion of the solute zone follows the order: dopamine > epinephrine > acetaminophen > ascorbic acid > dopac > uric acid.

Such induced stretching of the zone for counter-ionic solutes, and the rapid elution of co-ionic ones, can be exploited for time-resolved gradient measurements. By judiciously selecting an appropriate time (on the tailing edge), one can thus perform selective measurements of the catecholamines, in the presence of otherwise interfering species. The nature of the partition process ensures that the response at different delay times is linear. For example, Fig. 3 shows flow-injection peaks for uric acid (A) and acetaminophen (B) solutions containing increasing levels of norepinephrine and epinephrine, respectively,  $(1-5) \times 10^{-5}$  M (a–e). Also shown (as dotted lines) are the corresponding peaks without the neurotransmitter. The additive response at short times following the injection does not permit selective measurement of the neurotransmitters. In contrast, the increased dispersion of the neurotransmitter zones, associated with their permeation into the Nafion coating, allows selective measurements at longer times. This is clearly indicated from the resulting calibration plot for norepinephrine (Fig. 4), obtained at 2.5 (a), 5 (b), 10 (c) and 15 (d) s following the injection. The

Table 1  
Influence of procedure parameters on the width of the FIA peak

pH	Flow-rate (ml min <sup>-1</sup> )	W <sub>0.6</sub> (s)					
		Volume of Nafion solution (μl)					
		Dopamine		Ascorbic acid		Acetaminophen	
		5	10	5	10	5	10
7.4	0.5	19.5	24.7	6.1	3.2	4.4	4.5
	1.0	15.5	24.2	5.7	3.2	3.8	4.3
	1.5	12.8	20.0	5.1	2.8	3.6	4.1
5.5	0.5	18.7	19.5	4.2	3.2	4.0	4.2
	1.0	14.0	17.0	3.3	3.0	3.5	3.8
	1.5	12.5	15.0	2.8	2.6	2.8	3.3

Other conditions, as in Fig. 2.

large current intercepts, observed at short times, diminish at longer times (reflecting the elution of the acetaminophen interference from the detector compartment). Note also the linear dependence upon the neurotransmitter concentration, obtained at the different delay times (with decreasing slopes at longer times). Similar improvements were observed in measurements of dopamine ( $(1-5) \times 10^{-5}$  M) in the presence of large excess ( $1 \times 10^{-3}$  M) of ascorbic acid (not shown). The data of Figs. 3 and 4 indicate that the time immediately after passage of the interferent zone should be selected for achieving the desired selectivity while minimizing the loss in sensitivity. Normalized plots of (current/peak current) vs. time should offer an even more dramatic visualization of the differences in half-peak width.

Various experimental parameters influencing the stretching of solute zones within the detector compartment (and hence the resulting selectivity) were explored (Table 1). For example, the width of the dopamine peak (at 60% height),  $W_{0.6}$ , decreased, e.g., from 24.2 to 17.0 s upon lowering the pH from 7.4 to 5.5. Such behavior reflects the influence of the pH upon the ion-exchange partitioning of dopamine. In contrast, the peak widths for ascorbic acid and acetaminophen decreased only from 6.1 to 5.1 s, and from 4.4 to 3.6 s, respectively. Increasing the carrier flow rate, from 0.5 to 1.5 ml/min resulted in a significant decrease of the dopamine  $W_{0.6}$ , from 19.5 to 12.8 s. The flow rate effect was less pronounced for the non-interacting solutes

(ascorbic acid and acetaminophen). By increasing the film thickness (through casting of a 10 μL Nafion solution instead of 5 μl), the dopamine  $W_{0.6}$  (at 1.0 ml/min) increased from 15.5 to 24.2 s, while that of ascorbic acid decreased from 5.7 to 3.2 s. According to the data of Table 1, one must thus adjust the current-sampling delay time (of the new gradient FIA operation) to suit the procedure parameters of each particular case.

### 3.2. Hydrophobic coatings

The new amperometric gradient scheme is not limited to charge-exclusion ion-exchange coatings. Similar advantages can be achieved by exploiting the partition of nonpolar analytes into lipid [16,17] or long-chain alkanethiol [18] surface layers. Fig. 5 displays the flow-injection amperometric response for several biologically relevant compounds at alkanethiol (A) and phospholipid/cholesterol (B) coated detectors. Both films induce long residence times (30–75 s) of the hydrophobic drugs chlorpromazine (c) and promethazine (d). In contrast, polar species such as ascorbic acid, dopamine or hydrogen peroxide rapidly elute

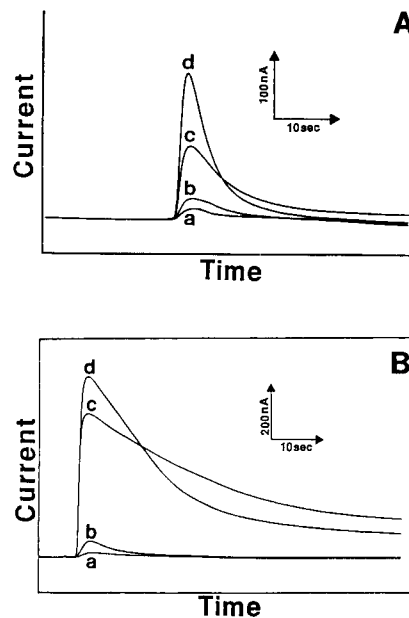


Fig. 5. Flow-injection amperometric peaks at alkanethiol (A) and lipid (B) coated electrodes for ascorbic acid (A(a), B(b)), hydrogen peroxide (A(b)), dopamine (B(a)), chlorpromazine (A, B(c)) and promethazine (A, B(d)). Solute concentration:  $2 \times 10^{-4}$  M (A);  $5 \times 10^{-5}$  M (B). Flow rate, 1.0 ml/min. Other conditions, as in Fig. 1.

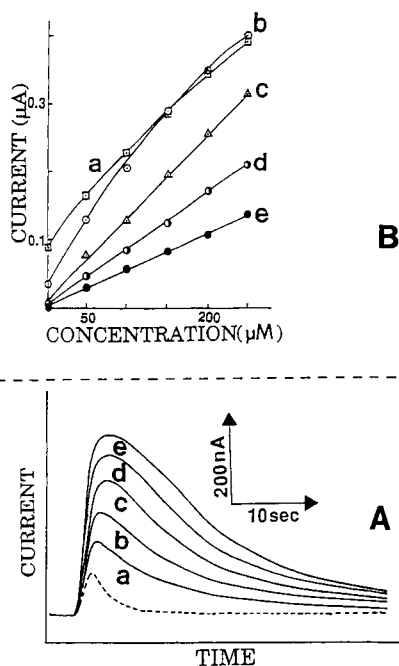


Fig. 6. Flow injection peaks for  $5 \times 10^{-4}$  M ascorbic acid solutions containing increasing levels of promethazine,  $(5-25) \times 10^{-5}$  M (A(a-e)) s. Also shown (B), are the resulting calibration plots at different times following the injection: 2.5 (a), 5 (b), 10 (c), 15 (d) and 20 (e) s. The dotted line represents the response for the  $5 \times 10^{-4}$  M ascorbic acid solution. Other conditions, as in Fig. 5(B).

from the detector compartment (peak widths of 5–10 s; a, b). The inherent stability of thiolate-derivatized detectors under hydrodynamic conditions has been documented [18].

The practical analytical utility of this hydrophobic “stretching” is illustrated in Fig. 6, for selective measurements of promethazine in the presence of ascorbic acid. While the lipid-coated electrode attenuates the ascorbic acid signal, common peak height measurements still suffer from a severe additive response. In contrast, the gradient FIA operation permits convenient measurement of the drug (after passage of the ascorbic acid). Calibration plots thus obtained on the decaying portion of the peak (at 10, 15 and 20 s from the point injection) exhibit the desired linearity and a negligible intercept (B(c-e)). In contrast, the ascorbic acid interference at shorter times results in curved plots and a large current intercept (B(a,b)).

### 3.3. Bare electrodes

The new FIA gradient operation is not limited only to coated electrodes. Bare (unmodified) electrodes can

also be exploited for this task, provided that they induce an appropriate interaction with the target analyte. Carbon paste electrodes represent one such example, as they preferentially extract hydrophobic solutes into their mineral oil binder [19]. Fig. 7A displays flow-injection peaks for dopamine (a), dopac (b), promethazine (c) and ascorbic acid (d). The dispersion of the solute zone, which reflects the trend in the hydrophobicity, follows the order: promethazine > dopamine > dopac > ascorbic acid. Such profiles can serve as a basis for the selective determination of dopamine in the presence of ascorbic acid, which is a well-known bioanalytical problem. Fig. 7B shows the FIA response to  $1 \times 10^{-5}$  M ascorbic acid solutions containing increasing levels of dopamine  $(1-5) \times 10^{-5}$  M. Delay times longer than 9 s offer elution of the interfering ascorbic acid and can be used for convenient quantification of the neurotransmitter.

## 4. Conclusions

In summary, the ability of surface coatings to retain “interacting” solutes has been exploited for developing a new time-resolved FIA gradient procedure. Such on-detector separation can simplify the FIA flow man-

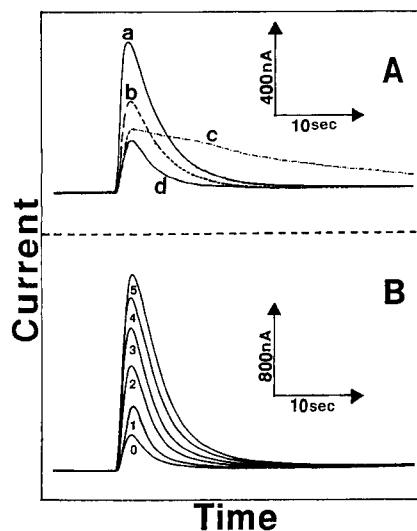


Fig. 7. Gradient FIA amperometry at a bare carbon paste detector. (A) peaks for  $5 \times 10^{-5}$  M dopamine (a), dopac (b), promethazine (c) and ascorbic acid (d). (B) Peaks for  $1 \times 10^{-5}$  M ascorbic acid solutions containing increasing levels of dopamine,  $(1-5) \times 10^{-5}$  M (1–5), along with the response for the  $1 \times 10^{-4}$  M ascorbic acid solution (0). Flow rate, 1.0 ml/min. Other conditions, as in Fig. 2.

ifold and facilitate the miniaturization of FIA systems. This operation represents a unique case in FIA, where the dispersion within the detector compartment – and not in the flow manifold – is deliberately manipulated. The diversity and versatility of surface coatings can be exploited for obtaining the desired separation. While the new gradient approach has been demonstrated within the context of amperometric measurements, it can be readily expanded to other (non-electrochemical) detection schemes.

## References

- [1] M.D. Luque de Castro, *Electroanalysis*, 4 (1992) 601.
- [2] J. Ruzicka and E.H. Hansen, *Flow Injection Analysis*, 2nd edn., Wiley, New York, 1989.
- [3] D. MacKoul, D.C. Johnson and K.G. Schick, *J. Anal. Chem.*, 56 (1984) 436.
- [4] D.A. Roston, R. Shoup and P.T. Kissinger, *Anal. Chem.*, 54 (1982) 417A.
- [5] J. Hoogvliet, J. Reijn and W.P. van Bennekom, *Anal. Chem.*, 63 (1991) 2418.
- [6] J. Wang, E. Ouziel, C. Yarnitzky and M. Ariel, *Anal. Chim. Acta*, 102 (1978) 99.
- [7] R. Taits, P. Bury, B. Finnin, B. Reed and A.M. Bond *Anal. Chem.*, 65 (1993) 3252.
- [8] J. Wang, *Anal. Chim. Acta*, 234 (1990) 41.
- [9] E. Wang, H. Ji and W. Hou, *Electroanalysis*, 3 (1991) 1.
- [10] J. Wang, *Electroanalysis*, 3 (1991) 255.
- [11] J. Ruzicka and E.H. Hansen, *Anal. Chim. Acta*, 145 (1983) 1.
- [12] J. Wang and B. Freiha, *Anal. Chem.*, 57 (1985) 1776.
- [13] M.N. Szentirmay and C.R. Martin, *Anal. Chem.*, 56 (1984) 1898.
- [14] J. Wang, P. Tuzhi and T. Golden, *Anal. Chim. Acta*, 194 (1987) 129.
- [15] G. Gerhardt, A. Oke, G. Nagy, B. Moghaddam and R.N. Adams, *Brain Res.*, 290 (1984) 390.
- [16] O. Garcia, P. Quintela and A. Kaifer, *Anal. Chem.*, 61 (1989) 979.
- [17] J. Wang and Z. Lu, *Anal. Chem.*, 62 (1990) 826.
- [18] J. Wang, H. Wu and L. Angnes, *Anal. Chem.*, 65 (1993) 1893.
- [19] J. Wang and B.A. Freiha, *Anal. Chem.*, 56 (1984) 849.



ELSEVIER

Analytica Chimica Acta 300 (1995) 133–141

ANALYTICA  
CHIMICA  
ACTA

# Chalcogenide based all-solid-state thin electroplated ion-selective membrane for Hg(II) flow-injection determinations<sup>1</sup>

M. Neshkova \*, E. Pancheva

*Institute of General and Inorganic Chemistry, Bulgarian Academy of Sciences, bl. 11, Sofia 1113, Bulgaria*

Received 10 May 1994; revised manuscript received 1 August 1994

## Abstract

The response to Hg(II) of a thin all-solid-state Te-doped silver chalcogenide membrane, described by the general formula  $\text{Ag}_{2+\delta}\text{Se}_{1-x}\text{Te}_x$ , which has been electrochemically prepared following a previously proposed approach, has been investigated. The kinetics of formation of the membrane's secondary dynamic response to Hg(II) has been successfully combined with the precise timing and transient signal, typical for flow-injection (FI) measurements, in developing a sensitive and reliable mercury FI detector. Under optimized stream conditions it exhibits a linear Nernstian response, with a double slope of the calibration graph of  $59 \text{ mV dec}^{-1}$ , over the mercury(II) concentration range  $10^{-6}$ – $10^{-3}$  M, the typical sample throughput amounting to about 70 samples per hour. The observed chemical amplification of the signal is due to the specificity of the processes dominating the initial step in formation of the steady-state signal of the membrane to mercury. The analytical performance of the Hg(II) FI detector, as regards sensitivity, reproducibility, selectivity and long-term stability has been thoroughly investigated. The exact procedure for membrane electrodeposition is given and the potential of the proposed approach as a cost-effective way for preparing chalcogenides of unique structure and properties has been outlined in the above context.

*Keywords:* Flow injection; Ion-selective electrodes; Mercury(II) FI detector;  $\text{Ag}_{2+\delta}\text{Se}_{1-x}\text{Te}_x$

## 1. Introduction

The introduction of flow-injection (FI) marked an important breakthrough in automated continuous flow systems [1–3]. The modulation principle underlying the flow-injection analysis (FIA) yields a system with numerous practical properties, which provides a great variety of approaches to monitoring [2,4]. Since the early 1980s, wide application of this technique for on-line process control has been a growing trend [5].

The ever increasing tendency to miniaturization and integration of FI detectors, along with the demand for

low-cost disposable sensors for environmental and industrial monitoring, have stimulated lately the search for alternative approaches to the preparation of ion-selective electrodes (ISEs) that would suit better the specific requirements of flow dynamics. The design of classical ISEs has been systematically changed, tubular and “sandwich” type constructions being given preference due to some proven advantages [6–11]. The introduction of photocured polymer membrane ISEs for FI multi-ion detectors is a remarkable achievement in this direction [12,13]. Another important development trend is aimed at finding new sensor materials (most often semiconductors with non-stoichiometric composition) of appropriate chemical and electrical properties which have proved to contribute signifi-

\* Corresponding author.

<sup>1</sup> This paper was presented at Anatech'94.

cantly to the quality of the transient output signal in FIA [9,14,15].

The development of a good sensor for Hg(II) has long been a subject of concern to analytical chemists. The efforts in this direction have been reviewed by Radic [16] recently. Up to now, however, there are no commercially available Hg(II) ion-selective electrodes, AgI/Ag<sub>2</sub>S pressed pellet ones being used most often for indirect determination of Hg(II) in potentiometric titration [17]. Neither homogeneous pressed-pellet or other type Hg–chalcogenide membranes [18,19] nor their admixture with Ag<sub>2</sub>S [20] have proved reliable materials for Hg(II) ISEs.

Through cathodic electrodeposition of thin (1–3 μm) metal chalcogenide membranes onto inert electroconductive substrates, all-solid-state ISEs for Cu(II), Ag(I), cyanide and Pb(II), have been developed in this laboratory [15,21–23]. These electrodes represent a competitive alternative to their pressed-pellet commercial counterparts in several respects. Their major advantage, from an analytical point of view, is that they are better suited for FI detection in terms of sensitivity, stability and selectivity [15]. From technological point of view, electrodeposition offers a cost-effective *in situ* technique for obtaining membranes with optimum composition and structure, respectively, improved surface properties and conductivity. A further advantage of this approach is its compatibility with microelectronic processing.

FIA does not only stimulate the search for new sensors with adequate dynamic characteristics, but also offers a reliable tool for sensor testing and development [24]. The present paper reports of such a FIA-aided detector based on the kinetics of the secondary response to Hg(II) of a thin electroplated non-stoichiometric tellurium-doped silver selenide membrane of a composition given by the general formula: Ag<sub>2+δ</sub>Se<sub>1-x</sub>Te<sub>x</sub>. Tested as a primary ISE for Ag(I) [25], this membrane has shown a remarkable selectivity in the presence of Hg(II) which is known to exert a strong interference with the electrode function of the conventional pressed-pellet Ag<sub>2</sub>S membrane [26,27]. This striking difference, along with the complete lack of a poisonous effect on the Ag electrode function after prolonged exposure of the electroplated Ag<sub>2+δ</sub>Se<sub>1-x</sub>Te<sub>x</sub> membrane to Hg(II) solutions, have provoked thorough investigations of the response of this membrane to Hg(II).

## 2. Experimental

### 2.1. Membrane preparation and characterization

The underlying principle of cathodic electrodeposition of metal chalcogenides, and the selection of optimum conditions for electrochemical preparation of Te-doped silver selenide membranes, in particular, have been discussed in detail elsewhere [15,23].

Throughout the present study, Te-doped silver selenide membranes were electrodeposited using two compositions of the electrolytic bath of a constant molar Ag:Se ratio equal to 1:25, and the Te:Se molar ratio varied from 1:7.5 to 1:15. Such a formulation comprises typically:  $2 \times 10^{-3}$  M silver nitrate,  $5 \times 10^{-2}$  M sodium selenite, 0.5 M sulphuric acid, and  $3.3 \times 10^{-3}$  (or  $6.7 \times 10^{-3}$ ) M potassium tellurite. The electrodeposition was carried out under potentiostatic control (Elpan EP-21 high-output potentiostat, Poland) in a two-compartment electrolytic cell at a constant stirring rate. A Pt cathode was used in all experiments as an inert conductive substrate onto which silver chalcogenide was deposited at potentials ranging from +20 to –30 mV vs. SCE. The substrate was pre-shaped and sized, depending on the application, either as a cylindrical Pt electrode (for batch measurements), or embedded in the Perspex cylinder screw of the “sandwich” type flow-cell [15] to give a flat surface of 0.5–1 cm<sup>2</sup>. The thickness of the deposited silver chalcogenide membrane varied from 1.1 to 1.5 μm, corresponding to 1300–1700 mC cm<sup>-2</sup> quantity of electricity consumed. The resulting membranes were greyish-blue in colour, bright and perfectly adhesive. Energy dispersive x-ray fluorescence microanalysis (EDAX) data suggest the following formula for non-stoichiometric Te-doped silver selenide membranes: Ag<sub>2.40</sub>Se<sub>0.85</sub>Te<sub>0.15</sub>.

Cathodically deposited thin chalcogenide membranes have to be treated as all-solid-state ISEs in the thermodynamic sense defined by Buck and Shepard [28] and differ substantially in standard potential,  $E^0$ , from the second-kind Me/MeX (X = Se, S, Te) electrodes obtained most often by chemical coating or anodic dissolution of the corresponding metal in the presence of X<sup>2-</sup> ions [28,29]. The standard potential of the Ag<sub>2+δ</sub>Se<sub>1-x</sub>Te<sub>x</sub>-membrane,  $E^0$  ( $a_{\text{Ag}} = 1$ ), determined experimentally, was found to be 1.07 V vs. SHE, which agrees well with the theoretically estimated

value for the carbon contacted all-solid-state silver selenide electrodes [30].

## 2.2. Flow-injection experimental set-up

### Flow cell

The “sandwich” type cell described in [15] was used. Such a construction ensures that a very thin (0.15 mm) controllable stream of solution passes tangentially to the detector surface. The volume of the cell varied within the range 8–11  $\mu\text{l}$ .

### Flow manifold

The single-line flow manifold scheme presented in [15] was employed. The Rheodyne Model 5020 injection valve had a 100  $\mu\text{l}$  loop. Connections of PTFE tubing (0.5 mm i.d.) were used. The flow rate was varied from 2 to 6  $\text{ml min}^{-1}$ , 5  $\text{ml min}^{-1}$  being considered as the optimum rate for the present experiments. The dispersion coil was 70 cm long (0.5 mm i.d.). The transient signal was recorded by an Endim 621.02  $Y-t$  laboratory strip chart recorder connected to the detector cell through a pH meter (OP-208, Radelkis, Hungary).

The carrier stream in most of the experiments contained:  $1 \times 10^{-2}$  M potassium nitrate and  $1 \times 10^{-2}$  M nitric acid to which silver nitrate was added to give the final concentration of  $3 \times 10^{-7}$  or  $2 \times 10^{-6}$  M. Incidentally, silver(I) in the carrier was replaced by  $3 \times 10^{-7}$  M  $\text{Hg}(\text{NO}_3)_2$ .

## 2.3. Procedures

### Hg(II) standards

The electrode response to Hg(II) was evaluated in batch experiments either using mercury standards of fixed ionic strength and pH ( $1 \times 10^{-2}$  M nitric acid and  $1 \times 10^{-2}$  M potassium nitrate), prepared by serial dilution of 0.05 M stock mercury(II) nitrate solution (Merck) to cover the concentration range  $10^{-6}$ – $10^{-4}$  M, or by a consecutive spiking of stock mercury solution microvolumes into a stirred 500 ml ionic strength adjusting buffer of pH 2 (nitric acid). Mercury(II)–glycine ion buffers were prepared by keeping the ligand concentration (in a great excess with respect to mercury) and pH constant, and varying the total mercury concentration in order to cover the concentration range of free mercury from  $2 \times 10^{-7}$  to  $8 \times 10^{-9}$  M. The typical composition of the Hg(II)–glycine buffers was:

$2 \times 10^{-2}$  M glycine + 0.05 M potassium nitrate +  $10^{-2}$  M acetate buffer (pH 4) and total mercury concentration varied from  $2 \times 10^{-3}$  M to  $10^{-4}$  M. The following values for the stability constants were used in calculating the free mercury(II) concentration:  $\log \beta_1 = 10.5$  and  $\log \beta_2 = 19.5$  [31].

## 3. Results and discussion

### 3.1. $\text{Ag}_{2+\delta}\text{Se}_{1-x}\text{Te}_x$ membrane response to Hg(II) under different operation modes

The steady-state investigation of Hg(II) interference with the primary silver(I) response of  $\text{Ag}_{2+\delta}\text{Se}_{1-x}\text{Te}_x$  thin electroplated membranes points out to a rather unusual behaviour of this hyper-stoichiometric (with respect to silver) membrane, which could be summarized as follows.

(i) The membrane response to silver(I) never gets blocked or poisoned, even after the membrane is in contact with mercury(II) solution for a long period of time. A  $\text{Ag}_{2+\delta}\text{Se}_{1-x}\text{Te}_x$  membrane, soaked overnight in  $1 \times 10^{-2}$  M mercury(II) solution, restores almost immediately the previously recorded potential values when re-calibrated against silver(I) without any special pretreatment of the membrane but simple distilled water rinsing, thus exhibiting a remarkable reproducibility of its standard potential ( $E^0(a_{\text{Ag}} = 1) = 1070 \pm 2$  mV vs. SHE). This experiment, if repeated many times, does not cause any visible damage to the membrane (which is only 1.5  $\mu\text{m}$  thick) as regards its structural uniformity and adhesion. It is only its colour that changes reversibly from greyish-blue (in silver solutions) to dark grey (in mercury solutions).

(ii) The non-stoichiometric membrane is responsive to Hg(II) following two different Nernstian patterns for the concentration ranges above and below  $1 \times 10^{-4}$  M mercury(II). The calibration in the concentration range above  $1 \times 10^{-4}$  M yields a calibration curve which follows a function close to the two-electron Nernstian. Special attention, however, deserves its response to mercury(II) in the concentration range  $10^{-7}$ – $10^{-4}$  M. Following always the semi-log function, the initial calibrations result in a graph approaching a double-Nernstian slope, i.e., 59 mV  $\text{dec}^{-1}$ . On further day-to-day calibration, the initially observed slope is gradually transformed into a normal



Nernstian one. The rate of this slope decay depends on time of contact of the membrane with mercury(II) solution as well as on its concentration. The potential is poorly reproducible (within several mV) and strongly dependent on the hydrodynamic conditions (stirring), which makes the analytical applicability of the steady-state response problematic.

(iii) The lack of irreversible poisoning effect of mercury(II) on the  $\text{Ag}_{2+\delta}\text{Se}_{1-x}\text{Te}_x$  membrane justifies calculating the selectivity coefficient,  $K_{\text{Ag,Hg}}$ .  $\log K_{\text{Ag,Hg}} = -2.4$ , if calculated by the mixed interference method (mercury(II) interferent being fixed at  $1 \times 10^{-4}$  or  $1 \times 10^{-5}$  M in the silver standards). A value close to the above one is obtained,  $\log K_{\text{Ag,Hg}} = -2.6$ , by the separate solution method (for  $C_{\text{Hg}} > 1 \times 10^{-4}$  M).

(iv) The response to mercury(II) seems to be accompanied by its inclusion into the membrane (as evidenced by EDAX). The included mercury could be reversibly eliminated by treating the membrane with silver standards. EDAX gives the following elemental mean composition for the untreated membrane: 74.23 wt.% Ag, 19.46 wt.% Se and 6.32 wt.% Te. A membrane, repeatedly calibrated against mercury(II) in the concentration interval  $10^{-7}$ – $10^{-4}$  M, while obeying a double-Nernstian response, shows an inclusion of only 5.6 wt.% resp. 2.8 at.% of mercury at the expense of the initial silver content as evidenced by EDAX. The Se and Te content is not changed measurably in that case.

The inclusion of mercury into a membrane soaked overnight in  $10^{-2}$  M Hg(II) solution amounts to 35.4 wt.% again at the expense of the initial silver. For the membrane regenerated in silver(I) solution, the mercury inclusion does not surpass 4–5 wt.%. EDAX data imply that it is the extent of mercury inclusion that causes the observed gradual decay of the initial double-Nernstian slope, the maximum admissible quantity of mercury inclusion being 6–7 wt.%.

All the above findings suggest that in its response to Hg(II) the non-stoichiometric Te-doped silver selenide membrane follows a mechanism different from the generally accepted metathesis replacement interference one [32–35]. Although elucidation of the mechanism is beyond the scope of the present investigation, the above fact should not come as a surprise bearing in mind the solid–liquid structure duality that has been reported for several silver chalcogenides which are

close in composition to the electroplated membrane [36–38].

Whatever the theoretical explanation of these phenomena may be, the experiments under steady-state mode give evidence that the membrane is reversibly responding to both Ag(I) as primary ion and Hg(II) as secondary ion. The experimentally proved time-dependent slope of the electrode function for mercury(II), in the concentration range  $10^{-7}$ – $10^{-4}$  M, along with the slow kinetics of its transformation controlled by the extent of mercury inclusion, and the preserved (under all circumstances) membrane response to silver(I) suggest that such a behaviour of the Te-doped silver selenide non-stoichiometric membrane could favourably be exploited, in combination with precise timing and the perfectly reproducible hydrodynamics of FIA, to develop a mercury(II)-sensitive detector for flow-injection potentiometry (FIP).

A practical dynamic response of the  $\text{Ag}_{2.40}\text{Se}_{0.85}\text{Te}_{0.15}$  membrane to different Hg(II) concentrations was registered by injecting comparatively big volumes of standards (2 ml) into a carrier solution containing  $3 \times 10^{-7}$  M  $\text{Hg}(\text{NO}_3)_2$ ,  $2 \times 10^{-2}$  M  $\text{KNO}_3$ , pH 2 ( $\text{HNO}_3$ ), and flow rate  $5 \text{ ml min}^{-1}$ , thus approaching closer the FI experimental conditions (Fig. 1A). It can be seen from the figure that 80% of the steady-state response is reached after less than 3 s, following a very steep  $dE/dt$  profile throughout the whole concentration range and giving a double-Nernstian electrode function. Such a dynamic response, when combined with a precise timing of the FI experiment, yields a very sensitive and stable signal trace which is highly reproducible irrespective of the direction of concentration change, the same slope of the electrode function of  $59 \text{ mV dec}^{-1}$  being preserved (Fig. 1B). This remarkable improvement in quality of the transient signal becomes obvious when compared to the steady-state one, obtained in the continuous calibration mode (Fig. 1C).

### 3.2. FI system optimization

Fig. 2 shows the dependences of peak height ( $H$ ) and peak width at  $1/2H$  and  $1/4H$  ( $W_{1/2}$  and  $W_{1/4}$ , respectively) on stream rate and carrier solution composition. The observed peak height independence of the flow dynamics, throughout the examined range of flow rates, points to the dominant role of membrane

properties in determining the quality and shape of the transient signal. On the other hand, the steadiness in signal peak height favours the choice of stream parameters that would ensure an as-short-as-possible membrane contact with mercury in order to keep the inclusion of mercury into the membrane below the critical wt.% (evidenced under steady-state conditions) and still preserving adequate sensitivity. In the above context, 100  $\mu\text{l}$  injection volume and 5  $\text{ml min}^{-1}$  flow rate seem an acceptable compromise ensuring a theoretical time of about 1.4 s for the sample to pass through the detector cell.

The beneficial role of the measured ion, even when added in very low concentrations to the carrier, for achieving better membrane conditioning and improved carry-over has been well recognized [6]. For reasons already discussed, a permanent contact of the membrane with mercury, even at concentrations as low as  $3 \times 10^{-7}$  M, results in a day-to-day decay in the initially observed double-Nernstian slope of the calibration graph (of about 1–2 mV per day). For most analytical applications such results are still pretty acceptable as the FI detector performs perfectly reproducibly within a day. To stabilize the slope of the Nernstian electrode function at  $59 \text{ mV dec}^{-1}$  seems quite challenging, however, in order to improve the accuracy of FI determination. Bearing in mind the factors that have been experimentally proved to control the slope under steady-state conditions, a parallel investigation

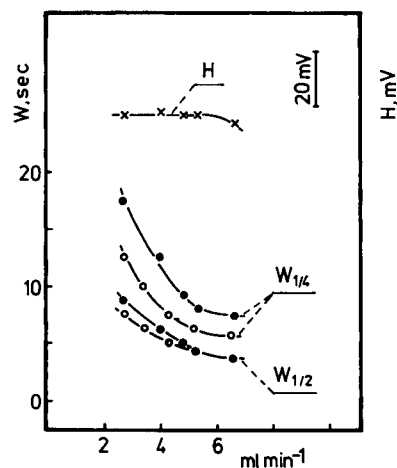


Fig. 2. Peak height ( $H$ ) and peak width at 1/2 and 1/4 $H$  ( $W_{1/2}$  and  $W_{1/4}$ , resp.) as a function of flow rate and carrier composition for 100  $\mu\text{l}$  injected  $1 \times 10^{-4}$  M Hg(II) sample. ( $\bullet$ )  $3 \times 10^{-7}$  M Ag(I) in the carrier, ( $\circ$ )  $1 \times 10^{-6}$  M Ag(I) in the carrier.

of the membrane transient response to Ag(I) and Hg(II) was undertaken. A separate FI calibration with respect to each of the above ions under fixed flow conditions was found to yield two parallel calibration curves, identical in slope, and shifted only 5 mV from each other in the potential scale. This indicates a considerable change in apparent dynamic selectivity of the membrane in favour of mercury. In practice this experiment shows that the membrane cannot differentiate between equal concentrations of the two ionic species under FI mode. This fact was made use of in replacing

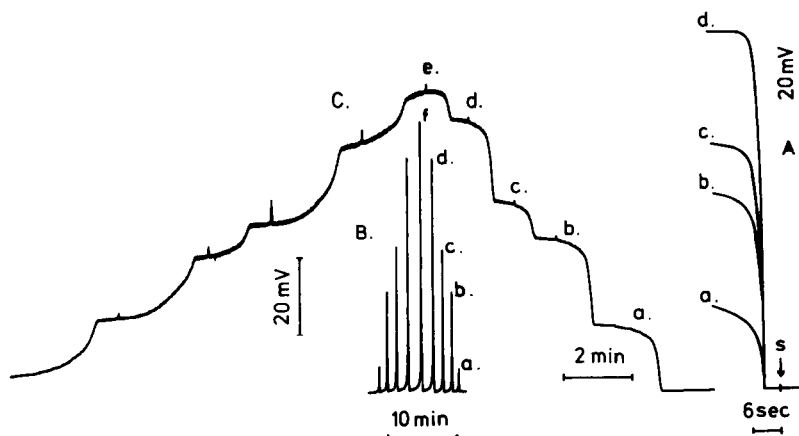


Fig. 1. Response of the  $\text{Ag}_{2+6}\text{Se}_{1-x}\text{Te}_x$  membrane to different Hg(II) concentrations: (a)  $1 \times 10^{-6}$  M, (b)  $5 \times 10^{-6}$  M, (c)  $1 \times 10^{-5}$  M, (d)  $5 \times 10^{-5}$  M, and (e)  $1 \times 10^{-4}$  M, under FI (A and B) and continuous (C) mode at  $5 \text{ ml min}^{-1}$  flow rate and a carrier composition of  $1 \times 10^{-2}$  M  $\text{KNO}_3 + 1 \times 10^{-2}$  M  $\text{HNO}_3 + 3 \times 10^{-7}$  M  $\text{Hg}(\text{NO}_3)_2$ . (A) Practical response time obtained for 2 ml injected standards, (B) FI trace: 100  $\mu\text{l}$  injected standards, 70 cm dispersion coil length, (C) Continuous response record: Hg(II) standards propelled consecutively through the detector cell.

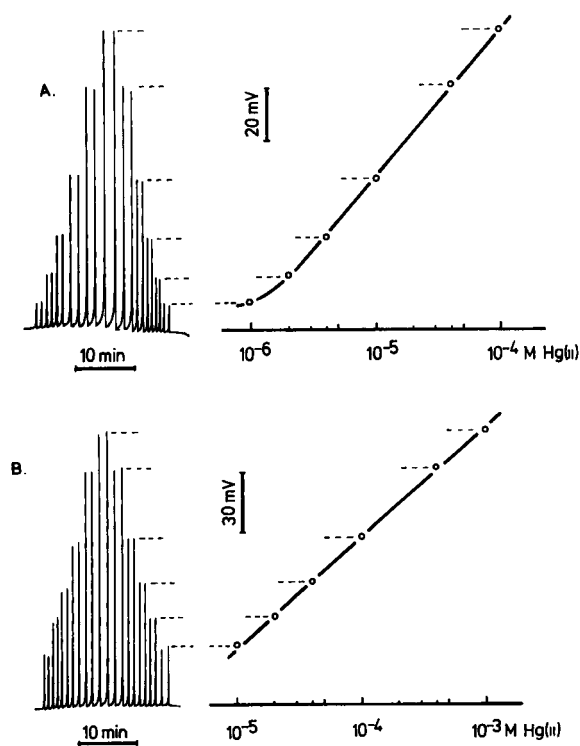


Fig. 3. Hg(II) calibration runs with increasing and decreasing concentrations at  $5 \text{ ml min}^{-1}$  flow-rate and  $104 \mu\text{l}$  injected sample volume. (A)  $3 \times 10^{-7} \text{ M Ag(I)}$  in the carrier solution ( $1 \times 10^{-2} \text{ M KNO}_3 + 1 \times 10^{-2} \text{ M HNO}_3$ ), (B)  $2 \times 10^{-6} \text{ M Ag(I)}$  in the carrier.

mercury in the carrier stream with silver (Fig. 2). Important benefits obtained as a result of this change included perfect conditioning of the membrane throughout the FI detection, improved carry-over, and stable and reproducible day-to-day performance, a double-Nernstian response being always preserved.

Under pre-set conditions: flow rate,  $5 \text{ ml min}^{-1}$ ; sample injection volume,  $100 \mu\text{l}$ ; dispersion coil length,  $70 \text{ cm}$ ; and  $3 \times 10^{-7} \text{ M}$  silver nitrate in the carrier solution, a typical sample throughput of 65–70 samples per hour was found.

### 3.3. Analytical performance of the Hg(II) FI detector

#### Linearity range reproducibility and long-term stability

The linearity exhibited by the FI detector extends over the Hg(II) concentration range of  $10^{-6}$ – $10^{-3} \text{ M}$ , giving a double-Nernstian ( $59 \text{ mV dec}^{-1}$ ) slope of the calibration graph (Fig. 3A and B). The observed “chemical amplification” of the FI output signal [39]

is due to the specificity of the potential generating processes that occur at the membrane/stream interface and govern the transient response. Bearing in mind that the initial membrane composition does not contain mercury, a very fast and reversible formation of a “surface complex” might be supposed to be the first step of the potential generation processes taking place at the membrane surface and governing the steady-state response to mercury. During this first step, silver is drained out of the membrane, thus forming a secondary response to mercury, which is responsible for the observed double-Nernstian slope. Though detailed elucidation of the mechanism of dynamic response formation is beyond the scope of the present paper, it should be mentioned here that the above conjecture is also supported by EDAX data. Only 3 at.% of Hg have been found in a membrane used as a FI detector of Hg(II) for three weeks, accompanied by an equivalent decrease in Ag content (initially estimated at 70 at.%).

In view of the membrane secondary response to mercury(II), a long-term performance evaluation of the FI detector presents a crucial test for assessing its practical usage. A fortnight-long day-to-day calibration of the detector, including a minimum of 4 calibration runs in both concentration directions and triplicate injections at each concentration, was performed. A statistical evaluation of the results obtained are summarized in Table 1. The data show a remarkable stability and reproducibility of the baseline and peak potentials, which rule out the occurrence of any metathesis reactions on the membrane surface. This was also supported by EDAX data. The relative standard deviation

Table 1  
Hg(II) flow-injection signal stability with time

$C_{\text{Hg(II)}} \text{ (M)}$	$E_{\text{peak}} \text{ (mV vs. Ag/AgCl), } n = 10, P = 0.95$	$H_{\text{peak}} \text{ (mV), } n = 10, P = 0.95$
$1 \times 10^{-6}$	$+434.7 \pm 2.8$	$12.5 \pm 1.9$
$2 \times 10^{-6}$	$+448.2 \pm 2.9$	$26.0 \pm 2.5$
$5 \times 10^{-6}$	$+470.5 \pm 2.8$	$48.4 \pm 2.8$
$1 \times 10^{-5}$	$+487.9 \pm 2.1$	$65.7 \pm 2.0$
$5 \times 10^{-5}$	$+529.5 \pm 2.0$	$106.2 \pm 2.0$
$1 \times 10^{-4}$	$+547.5 \pm 2.1$	$124.9 \pm 1.6$
Carrier ( $3 \times 10^{-7} \text{ M Ag}^+$ )	$+421.8 \pm 2.4$	–

Linearity range,  $1 \times 10^{-6}$ – $1 \times 10^{-4} \text{ M}$ . Slope,  $57.1 \pm 1.0 \text{ mV dec}^{-1}$ . Linear correlation coefficient,  $R = 0.9994$ .  $n = 10$ .

(R.S.D.) guarantees high precision and accuracy in Hg(II) FI determination.

It should be specially emphasized that the electrochemical approach to sensor preparation allows for in situ stripping and re-deposition of the membrane every time it gets damaged and loses performance, which makes the FI detector a reliable, low-cost and efficiently renewable sensor appropriate for process monitoring.

### Selectivity

The selective performance is another important detector characteristic which was investigated next. The obtained results are summarized in Table 2.

The interferent ions were introduced as components of the injected Hg(II) standards in concentrations given in the table. A high selectivity to Hg(II) was observed with most of the investigated metal cations, without any limitation in linearity and slope of the calibration curves. The parameter  $E^{0'}$  given in Table 2, is the extrapolated peak potential (for  $a_{\text{Hg}} = 1$ ) and is calculated by the computer programme used. It indicates that irrespective of the type of interfering ion, the calibration provides a family of curves, very close to each other. Chloride ions exert a strong interference with sensor performance which is closely related to the secondary response mechanism suggested earlier. The membrane is tolerable to high concentrations of sulphate, nitrate and perchlorate ions. From an analytical point of view it is important to note that mild oxidants, such as Fe(III), do not interfere with the membrane response to Hg(II). Strong oxidants as potassium permanganate, however, cause severe corrosion of the membrane, and hence the signal is blocked.

Table 2  
Flow-injection response to Hg(II) in the presence of interfering ions

Interfering ion	$C_{\text{interf.}}$ (M)	Hg(II) linearity range	Linear correlation coefficient	$S$ (mV dec <sup>-1</sup> )	$E^{0'}$ ( $a_{\text{Hg}} = 1$ ) (mV vs. Ag/AgCl)
Cu(II)	$1 \times 10^{-3}$	$2 \times 10^{-6}$ – $8 \times 10^{-5}$	0.9999	61.5	808
	$1 \times 10^{-2}$	$2 \times 10^{-6}$ – $8 \times 10^{-5}$	0.9999	64.2	820
Ni(II)	$1.2 \times 10^{-2}$	$2 \times 10^{-6}$ – $8 \times 10^{-5}$	1	62.1	811
Co(II)	$1 \times 10^{-2}$	$2 \times 10^{-6}$ – $8 \times 10^{-5}$	0.9994	59.5	799
Zn(II)	$1 \times 10^{-2}$	$2 \times 10^{-6}$ – $8 \times 10^{-5}$	0.9999	63.3	814
Cd(II)	$1 \times 10^{-2}$	$2 \times 10^{-6}$ – $8 \times 10^{-5}$	0.9999	64.4	819
Pb(II)	$1 \times 10^{-2}$	$2 \times 10^{-6}$ – $8 \times 10^{-5}$	0.9990	63.3	814
Fe(III)	$1 \times 10^{-3}$	$2 \times 10^{-6}$ – $1 \times 10^{-4}$	0.9999	63	805
	$1 \times 10^{-2}$	$2 \times 10^{-6}$ – $1 \times 10^{-4}$	0.9999	59.6	797

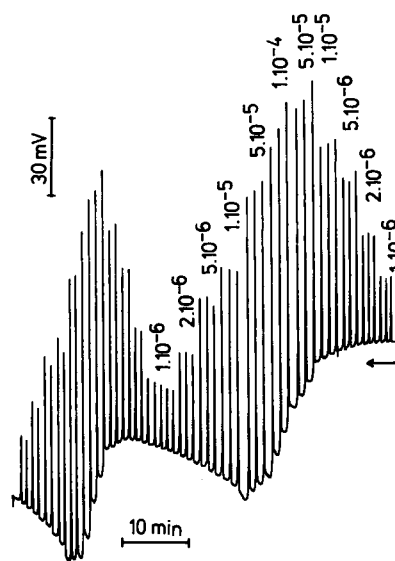


Fig. 4. Typical baseline profile of the detector FI response to Hg(I).

The membrane transient response to Hg(I) was also examined. A typical mercury(I) signal trace is presented in Fig. 4. Even a very short time of contact of the membrane with mercury(I) causes a systematic change in standard potential manifested by a characteristic profile of the baseline, as evident from the figure. The reason for the observed behaviour is still not well understood.

### 3.4. Effect of pH and complex formation on Hg(II) FI response

Fig. 5 presents the calibration graphs for Hg(II), obtained when the carrier and injected samples contain  $10^{-2}$  M nitric acid or acetate buffer (pH 4 and 5.5).

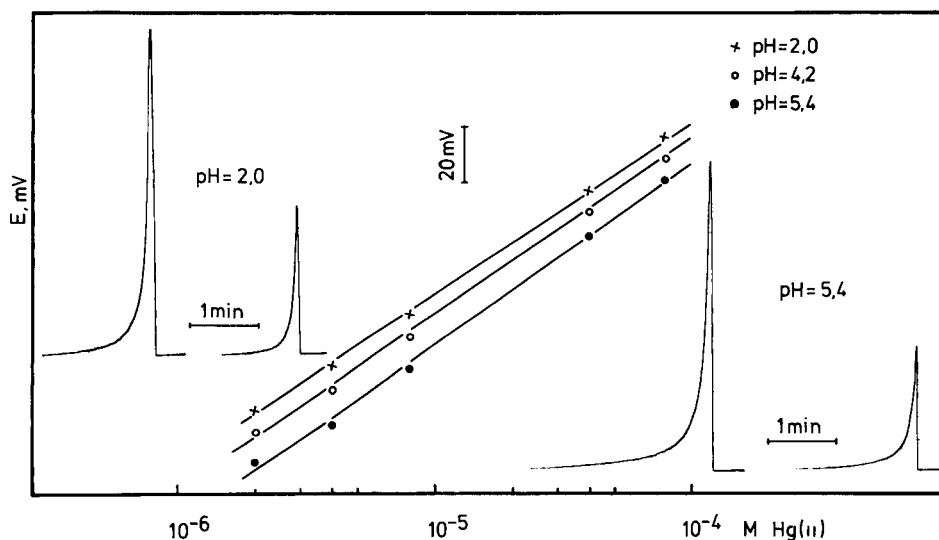


Fig. 5. Effect of pH on the FI response to Hg(II). Calibration graphs for pH 2 ( $1 \times 10^{-2}$  M  $\text{HNO}_3$ ), and pH 4.2 or 5.4 (acetate buffer).

Although the linearity range and the slope of the calibration curves are preserved in acetate buffer, the base-to-base line width of the signal is significantly increased and the reproducibility is poorer. On the other hand, the observed shift of the graphs in acetate buffer to more negative potentials is too small to reflect mercury(II) participation in complexation side reactions with acetate, thus indicating that the total rather than the free Hg(II) concentration is sensed. The calculated side reaction coefficient ( $\log \alpha_{\text{Hg}}(\text{CH}_3\text{COO}^-) = 6$  [40]) for the above reaction at pH 4 and total acetate concentration  $10^{-2}$  M implies a negative shift of about 360 mV (vs. 5 mV observed) of the calibration graph at pH 4 with respect to that at pH 2 (nitric acid).

The response of the FI detector to Hg(II) concentrations below  $10^{-6}$  M was tested using Hg–glycine ion buffers (pH 4 always fixed) to cover a free Hg(II) concentration range from  $10^{-8}$ – $10^{-6}$  M in the injected samples. (Instead of Ag(I), the same ion-buffer was added to the carrier solution, in this case, which kept the free Hg(II) concentration at  $n \times 10^{-9}$  M). The transient record with injected ion buffers preserves the same profile and baseline stability as observed with Hg(II) standards. However, a comparison of the peak potential values actually recorded for the injected Hg–glycine ion buffer samples with those recorded with injected Hg(II) standards (of concentration equal to the total concentration of the Hg(II) in the ion buffers) points out clearly that in both cases the FI detector is

measuring the total mercury concentration. The explanation of this fact must obviously be sought in the mechanism of formation of the secondary membrane response to Hg(II). The important, from an analytical point of view, conclusion which can be drawn at present is that the FI detector is not appropriate for Hg speciation measurements.

#### 4. Conclusions

On grounds of the obtained results it may be concluded that the kinetics of the secondary response of electroplated  $\text{Ag}_{2.40}\text{Se}_{1-x}\text{Te}_x$  membranes to mercury(II) could favourably combine with the precise timing and transient response of FI technique to develop a reliable FI detector for mercury(II). The unique membrane composition and properties have proved to be crucial for the observed response to mercury, although the exact mechanism of response formation is not known yet. In this context, the potential of the electrochemical approach for preparing metal chalcogenide films of sophisticated compositions and unique properties deserves to be specially emphasized.

The high sensitivity, selectivity and long-term stability as well as the observed “chemically amplified” double-Nernstian slope of the electrode function stand on the positive side of the performance assessment of the newly developed Hg(II) FI detector. A further

increase of the lower detection limit could be easily obtained through flow-preconcentration. The detector response to total rather than free Hg(II) content in complex media limits its applicability to solving speciation problems though. The low cost of such detector along with the possibility for in situ re-deposition of the sensing chalcogenide membrane every time it loses performance, and its compatibility with microelectronic signal processing, makes it attractive for process control applications.

The capacity of the approach used in this investigation to yield a chemically amplified Nernstian FI response seems very promising for improving the accuracy of direct FI potentiometry using ISEs. Further extension of the application range of this approach requires better knowledge on how the dynamic response depends on membrane composition, surface structure and conductivity, and this is still the least examined aspect of ISE for the time being, both on an experimental and theoretical level.

## Acknowledgements

Financial support from the National Scientific Research Fund (Grant X-309) is gratefully acknowledged.

## References

- [1] C.B. Ranger, in D.P. Manka (Ed.), *Automated Stream Analysis for Process Control*, Vol. 1, Academic Press, New York, 1982, p. 39.
- [2] J. Ruzicka, *Anal. Chim. Acta*, 190 (1986) 155.
- [3] M. Gisin and C. Thommen, *Trends Anal. Chem.*, 8 (1989) 62.
- [4] K.R. Beebe, W.W. Blasek, R.A. Bredewig, J.P. Chauvel, Jr., R.S. Harner, M. LaPack, A. Leugers, D.P. Martin, L.G. Wright and E. Deniz Yalvac, *Anal. Chem.*, 65 (1993) 199R.
- [5] M. Gisin and C. Thommen, *Anal. Chim. Acta*, 190 (1986) 165.
- [6] W.E. van der Linden and R. Oostervink, *Anal. Chim. Acta*, 101 (1978) 419.
- [7] J.F. van Staden, *Anal. Chim. Acta*, 179 (1986) 407.
- [8] S.D. Kolev and E. Pungor, *Anal. Chem.*, 60 (1988) 1700.
- [9] J.F. van Staden, *Analyst*, 115 (1990) 581.
- [10] S. Alegret, J. Alonso, J. Bartroli, A.A.S.C. Machado, J.F.F.C. Lima and J.M. Paulis, *Quim. Anal.*, 6 (1987) 278.
- [11] K. Toth, E. Lindner, E. Pungor and S.D. Kolev, *Anal. Chim. Acta*, 234 (1990) 57.
- [12] R.W. Cattrall, P.J. Iles and I.C. Hamilton, *Anal. Chim. Acta*, 169 (1985) 403.
- [13] T.J. Cardwell, R.W. Cattrall, P.C. Hauser and I.C. Hamilton, *Anal. Chim. Acta*, 214 (1988) 359.
- [14] K. Toth, J. Fucsko, E. Lindner, Zs. Feher and E. Pungor, *Anal. Chim. Acta*, 179 (1986) 359.
- [15] M. Neshkova, *Anal. Chim. Acta*, 273 (1993) 255.
- [16] N. Radic, *Sel. Electrode Rev.*, 11 (1989) 177.
- [17] W.E. Morf, *The Principles of Ion-Selective Electrodes and of Membrane Transport*, Akademiai Kiado, Budapest and Elsevier, Amsterdam, 1981, pp. 183.
- [18] G. Kahr, *Dissertation*, ETH, Zurich, N=4927 (1972).
- [19] M. Neshkova and H. Sheytanov, in E. Pungor and I. Buzas (Eds.), *Proceedings of the Conference on Ion-Selective Electrodes*, Budapest, 1977, Akademiai Kiado, Budapest, 1978, p. 503.
- [20] W.E. van der Linden and R. Oostervink, *Anal. Chim. Acta*, 108 (1979) 169.
- [21] M. Neshkova and H. Sheytanov, *J. Electroanal. Chem.*, 102 (1979) 189.
- [22] M. Neshkova and E. Pancheva, *Ion-Selective Membrane for Cyanide, Iodide and Silver and the Method of its Preparation*, Bulg. Patent G 01 N 27/30 N=48307 (1989).
- [23] M. Neshkova and E. Pancheva, *Anal. Chim. Acta*, 242 (1991) 73.
- [24] J. Ruzicka, *Fresenius' Z. Anal. Chem.*, 329 (1988) 653.
- [25] M. Neshkova and E. Pancheva, in preparation.
- [26] P.L. Bailey, *Analysis with Ion-Selective Electrodes*, Heyden, London, 1980, p. 115.
- [27] R. De Marco, R.W. Cattrall, J. Liesegang, G.L. Nyberg and I.C. Hamilton, *Anal. Chem.*, 62 (1990) 2339.
- [28] R.P. Buck and V.R. Shepard, *Anal. Chem.*, 46 (1974) 2097.
- [29] M. Koebel, *Anal. Chem.*, 46 (1974) 1559.
- [30] B.K. Nestic and M.S. Jovanovic, *J. Serb. Chem. Soc.*, 55 (1990) 613.
- [31] A. Ringbom, *Complexation in Analytical Chemistry*, Interscience, New York, 1963, pp. 331 and 334.
- [32] M. Gratzl, E. Lindner and E. Pungor, *Anal. Chem.*, 57 (1985) 1506.
- [33] W.E. Morf, *Anal. Chem.*, 55 (1983) 1165.
- [34] A. Lewenstam, A. Hulanicki and T. Sokalski, *Anal. Chem.*, 59 (1987) 1539.
- [35] S. Imai, T. Ohachi and I. Taniguchi, *Solid State Ionics*, 35 (1989) 343.
- [36] R. Miida and M. Tanaka, *Solid State Ionics*, 40/41 (1990) 362.
- [37] M. Kobayashi, *Solid State Ionics*, 39 (1990) 121.
- [38] T.R. Berube, R.P. Buck, E. Lindner, M. Gratzl and E. Pungor, *Anal. Chem.*, 61 (1989) 453.
- [39] M. Neshkova, E. Pancheva, J. Fucsko, G. Nagy and E. Pungor, *Anal. Chim. Acta*, 259 (1992) 149.
- [40] A.E. Martell and R.M. Smith, *Critical Stability Constants*, Vol. 3, Plenum Press, New York, p. 3

## Continuous flow-injection–atomic absorption spectrometric method for the determination of Ondansetron

L. Lahuerta Zamora<sup>a</sup>, J. Martínez Calatayud<sup>b,\*</sup>

<sup>a</sup> *Departamento de Química, Colegio Universitario CEU, Moncada (València), Spain*

<sup>b</sup> *Departament de Química Analítica, Universitat de València, València, Spain*

Received 4 August 1993; revised manuscript received 28 March 1994

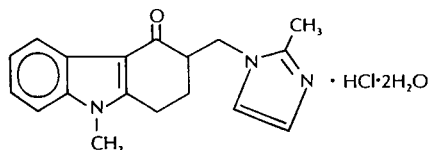
### Abstract

A flow-injection procedure for the indirect determination of the new drug Ondansetron is proposed. The method is based on the reaction of the drug in an oxidative solid-phase reactor included in the flow assembly. The reactor was made by lead dioxide physically entrapped by polymerization; the released lead(II) was monitored by atomic absorption spectrometry at 217.0 nm. The procedure gave a linear calibration graph up to 20  $\mu\text{g ml}^{-1}$  of Ondansetron with a sample throughput of 338 samples  $\text{h}^{-1}$ .

*Keywords:* Atomic absorption spectrometry; Flow injection; Ondansetron; Solid-phase reactors; Pharmaceutical analysis

### 1. Introduction

Ondansetron is a recently commercialized drug, acting as a potent and selective antagonist of 5-HT<sub>3</sub>, which has been approved for the treatment of chemotherapy-induced emesis. It is a white powder, soluble in water, formulated in intravenous injections and orally administered tablets [1–3].



The main metabolic routes result in *N*-demethylation and hydroxylation of the indole nucleus, and then conjugation of the hydroxylated metabolites with gluconic acid and sulphate. Ondansetron and its metabolites are

excreted in urine with about 10% of the unaltered drug [4,5].

Only a few analytical procedures for the determination of Ondansetron have been published and no analytical procedure is recommended in Pharmacopoeias. A liquid chromatographic (LC) method with spectrophotometric detection has been described for Ondansetron in pharmaceutical formulations [6,7]. The procedure has also been applied to plasma samples with prior solid-phase extraction. An extractive-spectrophotometric procedure has recently been developed for the determination of Ondansetron in human urine samples [8]; the method is based on the reaction of Ondansetron with Bromocresol Green forming an ion-association compound which is extracted into a chloroform layer, the absorbance at 420.8 nm being measured.

This paper reports the flow-injection (FI) oxidimetric determination of Ondansetron as a quick and simple procedure for control of pharmaceutical formulations. The flow assembly contains a solid-phase reactor,

\* Corresponding author.

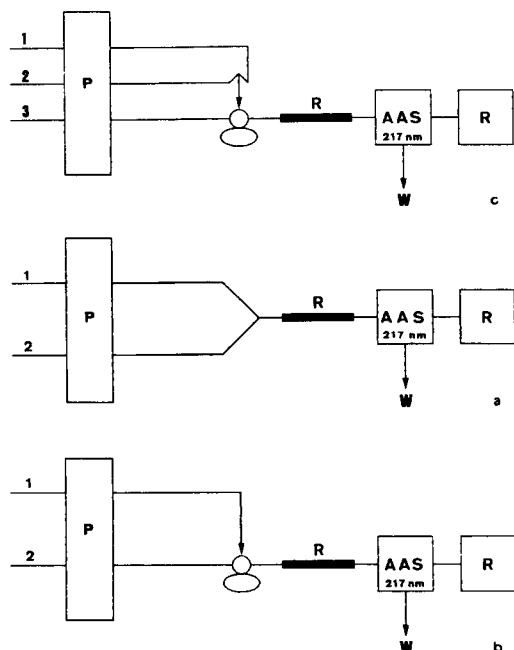


Fig. 1. Flow-injection manifolds. (a) Flow manifold used in the study of the reactivity of Ondansetron. Solid phase reactor in different media. (b) FIA configuration used for testing the influence of sulphuric acid (in sample and carrier solutions) at different concentrations on the oxidation of Ondansetron. (c) FIA configuration selected for the determination of Ondansetron in pharmaceutical formulations.

obtained by the entrapment of lead dioxide by the polymerization of unsaturated esters. The use of solid-phase reactors in FIA has recently been reviewed [9] and also its application to pharmaceutical analysis [10,11]. The use of such reactors is a consolidated trend in FIA, and other continuous-flow methodolo-

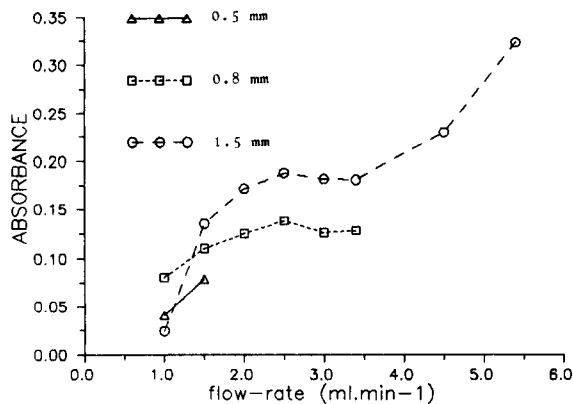


Fig. 2. Optimization study of the solid-phase reactor. Influence of flow-rate with different i.d. of the solid-phase reactor.

gies, mainly owing to the advantages offered over homogeneous systems. A preliminary screening study on the analytical behaviour of Ondansetron in aqueous solutions is also presented in this article. The study was necessary owing to the small number of reported data in the literature on the chemical characteristics of the drug.

## 2. Experimental

### 2.1. Reagents and apparatus

Aqueous solutions of Ondansetron (Glaxo, pure grade), sodium chloride (Panreac, a.r.), starch (Probus), glucose (Panreac, a.r.), lactose (UCB, a.r.), citric acid and sodium citrate (Probus, a.r.), sucrose (Probus, a.r.) and diphenhydramine (Benadryl, pure) were prepared with distilled water. All other solutions were also prepared with distilled water. The solid-phase reactor was prepared with  $\text{PbO}_2$  (UCB, a.r.) and polyester resin solution Al-100 (from Reposa) containing low-molecular-weight polyester chains and a cobalt compound as activating agent for the reaction, and methyl ethyl ketone (from Akco) as a catalyst. Other reagents, such as mineral acids, acetic acid, ammonia and alkali metal hydroxides, were of analytical-reagent grade.

### 2.2. Continuous-flow assembly

Fig. 1c shows the continuous-flow manifold; the sample injector was a Rheodyne Model 5041 and the peristaltic pump a Minipuls 2 from Gilson. The determination of lead was carried out by means of a Varian Model SpectraAA-10 atomic absorption spectrometer equipped with a Pb lamp (from Photron) at a wavelength of 217.0 nm. The internal diameters of the PTFE tubing were 0.8 and 1.5 mm for the manifold and the solid-phase reactor, respectively.

### 2.3. Procedures

The preparation of the solid-phase reactor was carried out according to the previously published procedure [11] in which 7.013 g of lead dioxide were added to 10.021 g of the polyester resin solutions followed by 0.2 g of methyl ethyl ketone. The dried solid was broken with a hammer and powdered with a coffee grinder.



The reactor was prepared by introducing the selected-sized particles with the aid of a mini-funnel into a PTFE tube of 1.5 mm i.d.

### 3. Results and discussion

Preliminary qualitative experiments with the aim of testing the reactivity of Ondansetron with different reagents were carried out by batch procedures and visual observation. Studies were carried out by placing in a test-tube 1 ml of the aqueous acidic or alkaline medium, adding 1 ml of the reagent and then 1 ml of the Ondansetron solution; aqueous insoluble reagents were also tested by adding pure solid powder. The media tested, all  $1 \text{ mol l}^{-1}$ , were HCl,  $\text{HClO}_4$ ,  $\text{HNO}_3$ , citrate buffer (pH 4), ammonia and sodium hydroxide. The sensitivity (visual limit of detection) of the positive reactions was also tested.

Changes were observed with the following reagents; pD {defined as  $-\log[\text{Ondansetron (g)}/\text{volume (ml)}]}$  values are also reported:  $\text{IO}_4^-$ , 5.44 in  $1.0 \text{ mol l}^{-1}$  HCl;  $\text{S}_2\text{O}_8^{2-}/\text{Ag(I)}$ , 4.74 in  $1.0 \text{ mol l}^{-1}$  HCl;  $\text{PbO}_2$ , 5.14 and 4.74 in HCl and  $\text{HNO}_3$ , respectively;  $\text{BiO}_3^-$ , 4.44 and 4.74 in HCl and  $\text{HNO}_3$ ;  $\text{MnO}_4^-$ , 5.14 in  $\text{HNO}_3$ . Precipitation was observed with  $\text{I}_3^-$  (pD 5.44) in different media as a result of the formation of an ion-association compound.

Lead dioxide and  $\text{NaBiO}_3$  were preselected to be entrapped and to test the oxidative determination of Ondansetron in a continuous-flow system (depicted in Fig. 1a) provided with a spectrophotometric detector and a flow cell of 1 cm pathlength. Ondansetron solutions ( $500 \mu\text{g ml}^{-1}$ ) were continuously flowing for up to 1 h; media tested were HCl and  $\text{HNO}_3$ . The results showed lead dioxide to be a suitable reagent for the oxidative determination of Ondansetron. The experiment was then repeated with  $25 \mu\text{g ml}^{-1}$  of Ondansetron and HCl,  $\text{HNO}_3$  and  $\text{HClO}_4$  for 30 min. The outputs were constant during the period studied.

Having selected entrapped lead dioxide for preparing the solid-phase reactor, a study of the influence of different acids was carried out by means of the flow manifold depicted in the Fig. 1a, in which the absorbances were continuously read for 20 min; column length, 12.5 cm; i.d., 1.5 mm; reagent "concentration", 1.75 g lead dioxide/g resin. The absorbances obtained calculated as the difference from distilled water were  $\text{H}_2\text{SO}_4$ ,

0.186;  $\text{HNO}_3$ , 0.145; HCl, 0.310 decreasing to 0.124 in 20 min,  $\text{HClO}_4$ , 0.217 decreasing in media such as HCl to 0.103,  $\text{H}_3\text{PO}_4$ , 0.052 and acetic acid, 0.0. All the acid media tested, except HCl and  $\text{HClO}_4$ , produced constant outputs during 20 min.

Further studies were carried out with the acidic media producing the highest outputs, i.e., sulphuric, nitric and hydrochloric acid. The study of the HCl influence was carried out in the same flow assembly with a  $1.0 \text{ mol l}^{-1}$  HCl stream at  $75^\circ\text{C}$  to avoid the formation of  $\text{PbCl}_2$  on the lead dioxide particles. The outputs, with Ondansetron or pure distilled water, were constant during 20 min; the average absorbances were 1.184 ( $30 \mu\text{g ml}^{-1}$  Ondansetron) and 0.976, respectively.

A final test was made with HCl using the FIA assembly depicted in Fig. 1b; the Ondansetron content in stream 1 was  $30 \mu\text{g ml}^{-1}$ , with  $2.0 \text{ mol l}^{-1}$  HCl in channel 2. The baseline with  $1.0 \text{ mol l}^{-1}$  HCl was higher than the sample injections (negative peaks), average 1.090. However the background noise was clearly diminished when the carrier was distilled water (0.059) and the peak heights were 0.476 and 0.661 for injections of distilled water and Ondansetron, respectively.

The influence of  $\text{HNO}_3$  and  $\text{H}_2\text{SO}_4$  were tested by merging the acidic solution of different concentrations, from  $2.0$  to  $10^{-4} \text{ mol l}^{-1}$ , with the aqueous solution containing  $25 \mu\text{g ml}^{-1}$  of Ondansetron (assembly depicted in Fig. 1a). The absorbances obtained, calculated as the difference between the blank solution (distilled water) and the ondansetron solution, showed sulphuric acid to be the best acidic medium. The test carried out with sulphuric acid produced absorbances from 0.043 at  $5 \times 10^{-2} \text{ mol l}^{-1}$  acid to 0.414 at  $2.0 \text{ mol l}^{-1}$ ; the nitric acid series resulted in absorbances from 0 at  $0.1 \text{ mol l}^{-1}$  to 0.321 at  $2.0 \text{ mol l}^{-1}$ ; in addition background noise with nitric acid media was about twice that with sulphuric acid. Sulphuric acid was selected for further work.

The influence of sulphuric acid concentration was studied by injecting a sample aliquot of  $400 \mu\text{l}$  of freshly prepared  $15 \mu\text{g ml}^{-1}$  Ondansetron solution (assembly in Fig. 1b). The sample solutions were prepared and injected into the sample/carrier streams: (a) sulphuric acid/sulphuric acid, both at the same concentration; (b) sulphuric acid/distilled water; and (c) distilled water/sulphuric acid. Table 1 depicts the results obtained in the three series.

Table 1  
Influence of the concentration of sulphuric acid on the FIA outputs

Conc. acid (mol l <sup>-1</sup> )	a	b	c
0.1	0.118	0.129	0.058
0.5	0.255	–	0.142
1.0	0.292	0.303	0.173
2.0	0.330	0.343	0.203
4.0	0.275	–	0.132

All solutions were 15 µg ml<sup>-1</sup> in Ondansetron, sample volume 400 µl.

(a) Samples of Ondansetron in sulphuric acid solution were injected into a carrier stream of sulphuric acid at the same concentration as the sample solution.

(b) Sample solution in sulphuric acid and carrier of distilled water.

(c) Sample solution in water and carrier of sulphuric acid.

The configuration of the continuous – flow manifold could be important in influencing the degree of reactivity and the dispersion produced. The efficiency of the flow manifold in which the solid-phase reactor was placed between the injector and detector (depicted in Fig. 1b) was tested and the results were compared with those obtained with the bed reactor in the sample loop. Aqueous solutions of Ondansetron after merging with the sulphuric acid solution were injected into a carrier stream of distilled water. Bearing in mind the importance on the degree of reactivity due to the length of the sample solution–solid reagent contact period, tests were carried out at different flow-rates (reactor in the injector-detector path) or for different time periods of the stopped solution (by controlling the time during which the sample is inside the sample loop) of the injection valve; column length, 12.5 cm; i.d., 1.5 mm; particle size, 200–300 µm; and “concentration” of lead dioxide in the polymeric material, 1.75 g/g. The results obtained in the first set of experiments were flow-rate (arbitrary units)–absorbance (difference with blank injection) = 100–0.093, 300–0.207, 700–0.456 and 900–0.451. A second set with the reactor bed in the sample loop, produced the following outputs (difference from blank injections), contact period (stopped-flow of the sample inside the valve, in seconds)–absorbance: 0–0.233, 1–0.331 and 15–0.306, 30–0.340. The manifold with the bed reactor in the injector–detector path with a carrier flow-rate corresponding to 700 was selected for further work.

Connectors for the merging points could be important with respect to the peak height and reproducibility.

Tests were carried out to select the confluence of Ondansetron–sulphuric acid solutions, and the type called “arrow tip” was adopted. Absorbance (average of ten replicates) was 0.254 for a 0.5 mm vs. 0.219 for a 0.8 mm i.d. of the connector.

Further studies were carried out to optimize the characteristics of the solid-phase reactor, namely internal diameter, particle size and ratio of reagent to amount of resin. Then the optimization of the FIA parameters was studied; the parameters tested were carrier flow-rate, sample volume, column length and the flow-rate of nebulization. The studies were carried out by a sequential procedure based on the univariate method (parameters were tested in the reported order) and a further re-optimization of some parameters (carrier flow-rate, sample volume and column length) with the aid of the values previously selected as optimum. Finally, the influence of temperature was also studied.

The influence of the internal diameter of the reactor was tested with three PTFE tubes of 1.5, 0.8 and 0.5 mm i.d., and different flow-rates over the range 1.0–5.4 ml min<sup>-1</sup> (column length, 12.5 cm; particle size, 200–300 µm and ratio of g of lead dioxide to g of resin, 1.75). It was observed that an increase in flow-rate resulted in increased outputs, which were higher with larger internal diameter (see Fig. 2); 1.5 mm and 5.4 ml min<sup>-1</sup> were selected for further work.

The influence of the particle size was studied over the range 90–120 to 250–300 µm (with FIA parameters

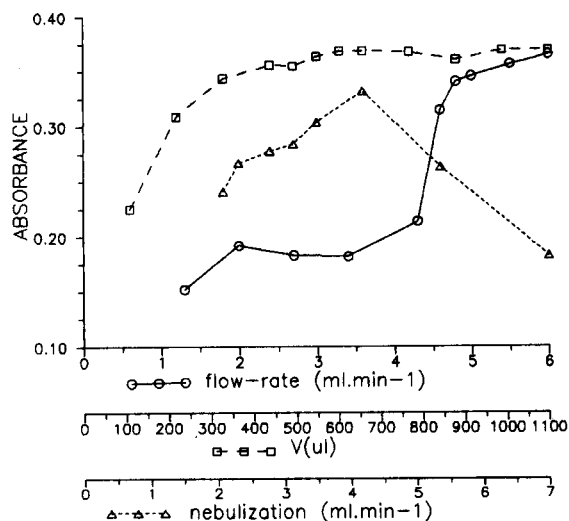


Fig. 3. Optimization of manifold and detector parameters, flow-rate, sample volume and nebulization flow-rate.

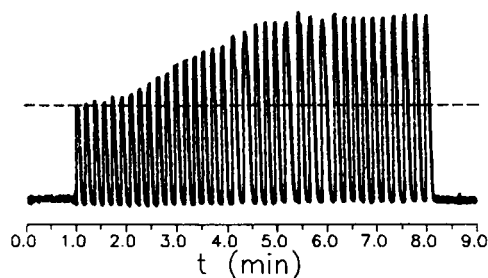


Fig. 4. in vitro availability of Ondansetron in tablets.

as specified above). The outputs increased with increase in particle size up to 200–250  $\mu\text{m}$ , then decreased. A particle size of 200–250  $\mu\text{m}$  was selected for further work.

The ratio of the amount of reagent to the amount of resin was studied from 0.1 to 4.9. The results obtained were (ratio, max. absorbance): 0.1, 0.121; 0.4, 0.219; 0.7, 0.213; 1.3, 0.156; 1.9, 0.115; 2.5, 0.118; 3.1, 0.135; 3.7, 0.111; 4.3, 0.131 and 4.9, 0.110. Transient signals increased up to 0.7, then decreased; a ratio of 0.7 was selected as the optimum.

Other parameters tested (i.e., flow-rate and sample volume) are also depicted in Fig. 3, the selected values being 5.4  $\text{ml min}^{-1}$  and 405  $\mu\text{l}$ , respectively. The column length was studied from 5 to 26 cm and resulted in the selection of 15 cm. The aspiration flow-rate (nebulization) of the atomic absorption spectrometer was tested from 2.0 to 6.5  $\text{ml min}^{-1}$  with the aid of a Perkin-Elmer Z5000 spectrometer which allows the study of higher values. The influence of this parameter is also depicted in Fig. 3 and 3.9  $\text{ml min}^{-1}$  was selected as the aspiration flow-rate.

#### 4. Analytical figures of merit

The calibration graph was studied at two different temperatures: (a) at room temperature, when the calibration graph was linear over the range 0.5–20  $\mu\text{g ml}^{-1}$  Ondansetron and could be described by the equation  $A = 0.020 + 0.023c$ , with a correlation coefficient of 0.9990; (b) with the column inside a water-bath at 80°C, when the calibration graph was linear over the range 4–16  $\mu\text{g ml}^{-1}$  and the corresponding equation was  $A = 0.0121 + 0.036c$ ; with a correlation coefficient of 0.9980.  $A$  is the absorbance at 217.0 nm and  $c$  the concentration of Ondansetron in  $\mu\text{g ml}^{-1}$ .

The reproducibility of the determination and the sample throughput were tested at room temperature and carrier flow-rate 6.0  $\text{ml min}^{-1}$  and at 80°C and carrier flow rate 5.5  $\text{ml min}^{-1}$ . The concentration of Ondansetron in the injected sample solution aliquots was 10  $\mu\text{g ml}^{-1}$ . The results obtained, R.S.D. in % and sample throughput in samples  $\text{h}^{-1}$ , were: (a) at room temperature, 29 replicates, 2.0% and 279 (mean absorbance 0.228); (b) at 80°C, 35 replicates, 1.8% and 338 (mean absorbance 0.312). The day-to-day reproducibility was determined from four independent calibration graphs on different days, preparing new columns and solutions for each experiment. The calculated equations (and correlation coefficients) were:  $A = 0.015 + 0.024c$  (0.997);  $A = 0.020 + 0.023c$  (0.999);  $A = 0.000 + 0.024c$  (0.998); and  $A = 0.008 + 0.024c$  (0.990); mean slope, 0.024 with R.S.D. = 2.1%.

The tolerance of the method to foreign compounds which can be found in formulations containing Ondansetron was investigated using solutions containing 10  $\mu\text{g ml}^{-1}$  of Ondansetron and adding various concentrations of the interfering compounds up to 12550  $\mu\text{g ml}^{-1}$  or when the relative error (with respect to pure Ondansetron solutions) was up to about 3%. The results obtained are shown in Table 2.

The study of the lifetime of the solid-phase reactor was carried out by means of a sequential series of experiments in which the Ondansetron solution (100  $\mu\text{g ml}^{-1}$ ) was continuously flowing through the reactor for 15 min, and then a series of injections of the solution containing 10  $\mu\text{g ml}^{-1}$  of Ondansetron were performed. After the series of injections the reactor was washed with 0.1  $\text{mol l}^{-1}$   $\text{Na}_2\text{EDTA}$  (pH 13) solution for 15 min and then washed again by a continuous flow of distilled water for 5 min. This sequence was repeated

Table 2  
Influence of foreign compounds on the determination of Ondansetron

Compound	Concentration ( $\mu\text{g ml}^{-1}$ )	Relative error (%)
NaCl	500	2.8
Starch	500	2.8
Lactose	500	1.9
Citric acid	1230	1.9
Glucose	12550	1.8
Sucrose	500	0.3
Diphenhydramine	125	0.5

Table 3  
Column lifetime

	Replicates/ times	Conc. drug ( $\mu\text{g ml}^{-1}$ )	A	R.S.D. (%)
Injections	27	10	0.277	2.0
Continuous flow	15 min	100		
Injections	15	10	0.021	2.6
Washing	15 min			
Na <sub>2</sub> EDTA				
Washing H <sub>2</sub> O	5 min			
Injections	19	10	0.196	1.9

Continuous flow through the solid-phase reactor of aqueous Ondansetron solution of  $100 \mu\text{g ml}^{-1}$  for 15 min is equivalent to 1300 injections of a  $40\text{-}\mu\text{l}$  volume containing  $10 \mu\text{g ml}^{-1}$  of the drug.

several times. The results are given in Table 3. The reactivity decreases with use, and after washing with Na<sub>2</sub>EDTA the reactor shows good reproducibility.

The analytical application to commercially available samples was studied by testing the in vitro availability of the Ondansetron in tablets. A flow assembly was prepared in which the tablet was placed in a platinum basket in the tip of the mechanic stirrer rod and introduced into the water-bath; the rotation speed of the sample was ca. 3 rpm. Aliquots of the resulting solution

were injected into the FIA assembly. The medium tested was 0.1 M HCl and a water-bath at room temperature ( $20^\circ\text{C}$ ) was used. The results obtained for absorbance vs. time (min) are depicted in Fig. 4.

## References

- [1] Glaxo, Ondansetron, Manual de Información Técnica, ZFR-4602, Madrid.
- [2] D.B. Beleslin, *Gastroenterohepatoloski Arhiv.*, 10 (1991) 133.
- [3] A.J. Freeman, K.T. Cunningham and M.B. Tyers, *Anti-Cancer Drugs*, 3 (1992) 79.
- [4] P.K. Burnette and J. Perkins, *Pharmacotherapy*, 12 (1992) 120.
- [5] A. Butler, J.M. Hill, S.J. Ireland, C.C. Jordan and M.B. Tyers, *Br. J. Pharmacol.*, 94 (1988) 397.
- [6] P.V. Colthup and J.L. Palmer, *Eur. J. Cancer Clin Oncol.*, 25 (1989) 71.
- [7] R.E. Leak and J.D. Woodford, *Eur. J. Cancer Clin. Oncol.*, 25 (1989) S63.
- [8] L. Lahuerta Zamora and J. Martínez Calatayud, *Anal. Chim. Acta*, in press
- [9] J.V. Garcia Mateo and J. Martínez Calatayud, *Chem. Anal. (Warsaw)*, 38 (1993) 1.
- [10] J.V. Garcia Mateo and J. Martínez Calatayud, *Pharm. Tech. Int.*, 4 (1992) 17 and 30.
- [11] L. Lahuerta and J. Martínez Calatayud, *Talanta*, 40 (1993) 1067.



ELSEVIER

Analytica Chimica Acta 300 (1995) 149–153

ANALYTICA  
CHIMICA  
ACTA

## Turbidimetric determination of sulphate in waters employing flow injection and lead sulphate formation

Ricardo Erthal Santelli <sup>a,\*</sup>, Paulo Roberto Salgado Lopes <sup>a</sup>,  
Regina Célia Leme Santelli <sup>a</sup>, Angela De Luca Rebello Wagener <sup>1,b</sup>

<sup>a</sup> Geochemistry Department, Federal Fluminense University, Niterói, RJ-24020-007, Brazil

<sup>b</sup> Chemistry Department, Pontifícia Universidade Católica do Rio de Janeiro, Rio de Janeiro 22453-900, Brazil

Received 31 May 1994; revised manuscript received 1 August 1994

### Abstract

An analytical flow-injection procedure based on  $\text{PbSO}_4$  colloidal formation is proposed as a turbidimetric determination of sulphate in natural waters. Ethanol–water was used as a medium in order to improve the sensibility of the method. Both chemical and flow variables as well as interfering species were studied. A detection limit of  $0.3 \mu\text{g SO}_4^{2-} \text{ ml}^{-1}$  was found, and the analytical range (according to Beer's law) was  $2\text{--}20 \mu\text{g SO}_4^{2-} \text{ ml}^{-1}$ . The precision was better than 3% R.S.D. and the sample throughput was ca.  $35 \text{ h}^{-1}$ . The method, when compared with a standard methodology, gave good results when applied to water analysis.

**Keywords:** Flow injection; Turbidimetry; Sulphate; Waters

### 1. Introduction

The determination of sulphate in waters is very important for geochemical and environmental studies. In natural waters, sulphur is transported as dissolved sulphate from terrestrial to marine or lacustrine environments by rivers [1].

The gravimetric  $\text{BaSO}_4$  method is a well known procedure to perform the determination of sulphate accurately [2]. However, due to the analytical characteristics of the gravimetric analysis, this procedure is very time consuming and is not convenient to be applied to environmental studies, in which usually large numbers of samples are involved. Flow injection

has often been used as a technique to solve environmental analytical problems since its introduction by Ruzicka and Hansen in 1975 [3]. Several flow procedures for the determination of sulphur have been described in the literature. Krug et al. [4] were the first authors who proposed a flow-injection turbidimetric determination using  $\text{BaSO}_4$ . An analytical range of 10 to  $200 \mu\text{g ml}^{-1}$  with very good reproducibility (R.S.D. < 0.85%) and high sample throughput ( $180 \text{ h}^{-1}$ ) was obtained. Poly(vinyl alcohol) was used as a protector to stabilize the  $\text{BaSO}_4$  suspension. This method was improved by several authors [5–8] in order to obtain better detection limits and system performance. In a comparison with the methyl thymol blue spectrophotometric method made by Marsden and Tyson [9], the turbidimetric method was considered the best to be used for saline water analysis with an

\* Corresponding author.

<sup>1</sup> Present Address: IAEA-MEL, Marine Environment Studies Laboratory, MC-98000, Monaco.

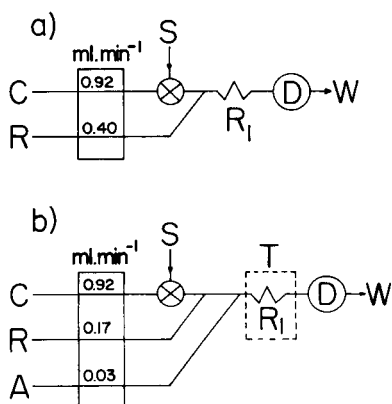


Fig. 1. Flow-injection manifold diagrams. (a) Flow system used to test variables. (b) Flow system utilized for sulphate determination. C = Carrier,  $1 \times 10^{-3}$  M HNO<sub>3</sub>; R = reagent, 1.9% Pb(NO<sub>3</sub>)<sub>2</sub> + 1% PVA; A = auxiliary sulphate line,  $100 \mu\text{g SO}_4^{2-} \text{ ml}^{-1}$ ; S = sample,  $1300 \mu\text{l}$ ; R<sub>1</sub> = precipitation reactor coil,  $100 \text{ cm} \times 0.5 \text{ mm}$  i.d.; T = thermostatic bath,  $61^\circ\text{C}$ ; D = spectrophotometer,  $410 \text{ nm}$ ; W = waste. All solutions in ethanol–water (1:1).

analytical range of  $1\text{--}100 \mu\text{g ml}^{-1}$  and a detection limit of  $0.45 \mu\text{g ml}^{-1}$ . Several flow procedures to achieve this determination can be found in the literature [10–13].

A turbidimetric method using PbSO<sub>4</sub> in ethanol–water medium was proposed as a tool for the determination of sulphate [14]. It has been found that the stability of the PbSO<sub>4</sub> suspension and the detection limit are better than those obtained with the BaSO<sub>4</sub> method.

## 2. Experimental

### 2.1. Solutions

Distilled and deionized water was used to prepare all solutions and reagents. 95% ethanol of analytical grade was used throughout.

A standard stock sulphate solution of  $1000 \mu\text{g ml}^{-1}$  was prepared by dissolving 1.4792 g of dry Na<sub>2</sub>SO<sub>4</sub> in water and making the volume up to 1000 ml. Working solutions were prepared daily by dilution in ethanol–water (1:1).

A reagent solution of 1.9% w/v Pb(NO<sub>3</sub>)<sub>2</sub> and 1% w/v poly(vinyl alcohol) (PVA) in ethanol–water (1:1) was prepared by dissolution of 1 g of PVA in 50 ml of warm water under stirring. After cooling, 1.9 g of Pb(NO<sub>3</sub>)<sub>2</sub> was added and dissolved. 50 ml of 95%

ethanol was added and the volume completed up to 100 ml with water. This solution was prepared immediately before use and filtered when necessary.

The carrier solution was  $1 \times 10^{-3}$  M HNO<sub>3</sub> in ethanol–water (1:1); the sulphate solution was  $100 \mu\text{g ml}^{-1}$ , also in ethanol–water (1:1).

### 2.2. Flow-injection manifold

A flow-injection manifold was built up using an Ismatec IPN-12 peristaltic pump furnished with Tygon tubes. A home-made commutator constructed with Perspex was used for sample introduction. PTFE tubes of 0.5 mm i.d. were also utilized. A Micronal B-380 spectrophotometer equipped with a 178.010 QS flow cell was used. Peak heights were recorded with a Philips x–y recorder. A schematic diagram of the flow system is shown in Fig. 1a. In this system, a sample volume of  $1000 \mu\text{l}$  was inserted into the carrier which immediately merged with the reagent. The sample plug, after reaction into the precipitation coil, was monitored at  $410 \text{ nm}$ .

## 3. Results and discussion

### 3.1. Flow-injection system optimization

In order to improve the performance of the flow system, both the chemical and flow variables were studied using the flow system depicted in Fig. 1a.

Table 1  
Effect of concomitant species in the sulphate determination using the flow system of Fig. 1b (sulphate concentration of  $25 \mu\text{g SO}_4^{2-} \text{ ml}^{-1}$ )

Species	Concentration ( $\mu\text{g ml}^{-1}$ )	Ratio interferent/analyte	Relative signal
Na <sup>+</sup>	500	20	0.99
K <sup>+</sup>	500	20	1.01
Ca <sup>2+</sup>	500	20	1.02
Mg <sup>2+</sup>	500	20	0.98
Br <sup>-</sup>	500	20	0.97
I <sup>-</sup>	500	20	1.70
	200	8	1.02
Cl <sup>-</sup>	1500	60	1.40
CO <sub>3</sub> <sup>2-</sup>	25	1	1.00

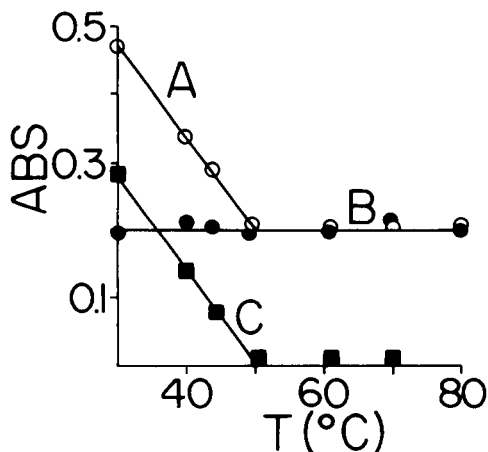


Fig. 2. Temperature effect on the sulphate and chloride signals in the flow system of Fig. 1b. (A)  $2 \mu\text{g SO}_4^{2-} \text{ ml}^{-1} + 1450 \mu\text{g Cl}^{-} \text{ ml}^{-1}$ ; (B)  $20 \mu\text{g SO}_4^{2-} \text{ ml}^{-1}$ ; (C)  $1450 \mu\text{g Cl}^{-} \text{ ml}^{-1}$ .

### 3.2. Chemical variables

Acidity is an important factor in colloidal formation. This variable was studied in the range of  $1 \times 10^{-5}$  M to 1 M  $\text{HNO}_3$  both in the carrier stream and sample. The highest signals were obtained between  $1 \times 10^{-2}$  and  $1 \times 10^{-4}$  M  $\text{HNO}_3$  (pH range of 2–4). For a pH higher than 4 and lower than 2, the signals decreased slowly, and therefore a working pH of 3 was chosen (carrier  $1 \times 10^{-3}$  M  $\text{HNO}_3$  and samples with pH adjusted to 3 with  $\text{HNO}_3$ ).

The solvent composition was studied in the range of 30–60% (v/v) ethanol. The results obtained show that for ethanol concentrations between 50–60% higher signals were found. Concentration above 60% ethanol could not be tested, owing to the insolubility of the reagent, while below 50% ethanol, the signals decreased.

The  $\text{Pb}(\text{NO}_3)_2$  concentration in the reagent was tested in a range of 0.9–5.6% (w/v). A small decrease in the signal with increasing concentration was observed. For PVA, tests were carried out in the range of 0.2–2.6% (w/v) and best results were obtained above 1%. The reagent composition for this work was chosen to be 1.9%  $\text{Pb}(\text{NO}_3)_2$  and 1% PVA in ethanol–water (1:1).

The results obtained with the flow system depicted in Fig. 1a were not linear at low concentrations. An auxiliary line pumping a  $100 \mu\text{g ml}^{-1}$  sulphate solution was introduced in order to increase the linearity. This

Table 2  
Precision studies using real samples (data in  $\mu\text{g SO}_4^{2-} \text{ ml}^{-1}$ )

Sample	Results	R.S.D. (%)	n
Sea water 1 (1:200) <sup>a</sup>	$2812 \pm 200$	7.1	5
Sea water 2 (1:200)	$3012 \pm 180$	6.0	7
Sea water 2 (1:400)	$3068 \pm 165$	5.4	4
Sea water 2 (1:500)	$3048 \pm 152$	5.0	3
River water 3 (1:10)	$53 \pm 2$	3.8	4
Potable water 4	$6.4 \pm 0.3$	4.7	5

<sup>a</sup> Dilutions before sample preparation.

modified system is shown in Fig. 1b. With this system, a sample volume of  $1300 \mu\text{l}$  was introduced by the commutator into the carrier stream and merged successively with the reagent and the auxiliary sulphate streams. The absorbance of the sample plug, after reaction, was measured at 410 nm.

### 3.3. Flow variables

The effect of the carrier flow rate was studied between  $0.52$  and  $1.84 \text{ ml min}^{-1}$ . When the flow rates increase, the signals decrease slowly probably due to the lowering of the residence times. In order to maintain sufficient sensitivity without loss in the sample throughput, we worked with  $0.92 \text{ ml min}^{-1}$ . Similar results were found with the reagent and auxiliary sulphate line flow rates. Flow rates of  $0.17 \text{ ml min}^{-1}$  and  $0.03 \text{ ml min}^{-1}$  were chosen for this work. The precipitation reactor coil length was tested between 20–200

Table 3  
Results obtained for sulphate determination with proposed methodology and with standard method (data in  $\mu\text{g SO}_4^{2-} \text{ ml}^{-1}$ )

Sample	This method <sup>a</sup>	APHA Standard Method <sup>b</sup>
Sea water 1 (1:200) <sup>c</sup>	$2812 \pm 200$	2900
Saline lagoon (1:200)	$3503 \pm 167$	3455
River water 1	$9.6 \pm 0.4$	11.6
River water 2 (1:10)	$71 \pm 4$	79
Potable water 1	$7.2 \pm 0.4$	8.0
Potable water 2 (1:10)	$27 \pm 1$	28
Potable water 3 (1:5)	$12.0 \pm 0.5$	11
Well water 1 (1:10)	$34 \pm 1$	36

<sup>a</sup> Mean of three independent determinations.

<sup>b</sup> Ref. 2.

<sup>c</sup> = Dilutions before sample preparation.

cm (40–400  $\mu\text{l}$ ). Best results were found with a length of 100 cm. Reactor coil lengths lower and higher than 100 cm provoked irregularities in the signals due to the shortening of the residence time and to the increased dispersion, respectively. Sample volumes were varied in the range of 130–1300  $\mu\text{l}$ . The signals obtained with 1300  $\mu\text{l}$  were of the same order of magnitude as the infinite volume situation. All subsequent investigations were carried out with a sample volume of 1300  $\mu\text{l}$ .

The effect of the precipitation reactor coil temperature was studied in the range of 30–80°C. This variable did not change the absorbance signals. Sonication was tested with no significant changes in the signals.

### 3.4. Interference study

Some cationic and anionic species normally found in water samples were studied as potential interferents. Anionic species as  $\text{Cl}^-$ ,  $\text{Br}^-$ ,  $\text{I}^-$  and  $\text{CO}_3^{2-}$  and cationic species as  $\text{Na}^+$ ,  $\text{K}^+$ ,  $\text{Ca}^{2+}$  and  $\text{Mg}^{2+}$  were assayed and the results are shown in Table 1. From those results, it can be concluded that  $\text{Cl}^-$  is the most relevant interfering species. The  $\text{PbCl}_2$  solubility depends on the temperature, and therefore tests were done to overcome this interference by thermostating the precipitation reactor coil. It can be seen in Fig. 2 that above 55°C the signal in the presence of 1450  $\mu\text{g Cl}^- \text{ ml}^{-1}$  was similar to the one obtained with  $\text{SO}_4^{2-}$  solution. Also, analytical curves were performed with solutions containing 4–20  $\mu\text{g SO}_4^{2-} \text{ ml}^{-1}$ , prepared in synthetic sea water [15] diluted from 1:200 to 1:800. These curves show similar slopes (0.00935 and 0.00930) corroborating that neither interference nor ionic strength effects occurred. Saline waters could be analyzed with this procedure maintaining the precipitation reactor coil at 61°C.

### 3.5. Analytical features

With the flow system depicted in Fig. 1b, analytical curves with good linearity were obtained in the range of 2–20  $\mu\text{g ml}^{-1}$  (correlation coefficient better than 0.998) and typical equations like  $A = -0.001 + 0.00935[\text{SO}_4^{2-} (\mu\text{g ml}^{-1})]$ . The detection limit, estimated according IUPAC recommendations, was found to be 0.3  $\mu\text{g ml}^{-1}$ . The R.S.D. was assessed by eleven injections of 2  $\mu\text{g SO}_4^{2-} \text{ ml}^{-1}$  solution and was better than 3%. Precision studies were also carried out

with several real samples. The results are reported in Table 2. For three separate determinations of the same sample, standard deviations were in the range of 3.8 to 7.1%, reflecting the poorer colloidal stability. These results contradict the results reported by Elenkova et al. [14] who found much better colloidal formation and stability with  $\text{PbSO}_4$  than with  $\text{BaSO}_4$ . For this reason, the achieved precision was not so good as the one which was obtained for the  $\text{BaSO}_4$  method [4]. Also, washing the system with a complexing agent (as it was done in the  $\text{BaSO}_4$  method, [5–8]) was not required due to the fact that  $\text{PbSO}_4$  did not adhere on the tube walls. Flow system washing is only necessary when solutions containing high concentrations of sulphate are unintentionally introduced into the system. The analytical throughput was about 35  $\text{h}^{-1}$ .

### 3.6. Application

The system stability described was good enough to perform water analysis. Several water samples (fresh and saline) were analyzed by using the flow-injection system shown in Fig. 1b. The same samples were analyzed by a standard method [2]. Prior to the analysis of fresh water samples, the pH was adjusted to 3 with  $\text{HNO}_3$  and 95% ethanol was added to prepare the ethanol–water (1:1, v/v) solution. For the saline water, a dilution was needed before pH correction and ethanol addition. The ethanol–water mixture cannot be made directly in the flow system because of the viscosity difference, which gives rise to Schlieren noise. However, for the analysis of several saline samples, a small dilution chamber could be placed before the sample loop, and automatic dilution could be performed. Table 3 shows the results obtained for sulphate determination in several samples.

In conclusion, the developed method can be applied to natural water analysis as an inexpensive and rapid technique that yields results with good precision and accuracy.

### Acknowledgements

The authors are indebted to CNPq for the grants and scholarships and to H. Bergamin F<sup>o</sup> for the critical comments.



**References**

- [1] M.V. Ivanov and J.R. Freney (Eds.), *The Global Biogeochemical Sulphur Cycle*, SCOPE, 1983.
- [2] APHA, *Standard Methods for the Examination of Water and Wastewater*, 15th edn., American Public Health Association, 1981.
- [3] J. Ruzicka and E.H. Hansen, *Anal. Chim. Acta*, 78 (1975) 145.
- [4] F.J. Krug, H. Bergamin F<sup>o</sup>, E.A.G. Zagatto and S.S. Jorgensen, *Analyst*, 102 (1977) 503.
- [5] S. Baban, D. Beethestone, D. Betteridge and P. Sweet, *Anal. Chim. Acta*, 114 (1980) 319.
- [6] J.F. van Staden, *Fresenius' Z. Anal. Chem.*, 310 (1982) 239.
- [7] J.F. van Staden, *Fresenius' Z. Anal. Chem.*, 312 (1982) 438.
- [8] F.J. Krug, E.A.G. Zagatto, B.F. Reis, O. Bahia F<sup>o</sup>, A.O. Jacintho and S.S. Jorgensen, *Anal. Chim. Acta*, 145 (1983) 179.
- [9] A.B. Marsden and J.F. Tyson, *Anal. Proc.*, 26 (1989) 157.
- [10] F. Lazaro, M.D. Luque de Castro and M. Valcárcel, *Analisis*, 13 (1985) 147.
- [11] L.D. Mee, *Sci. Total Environ.*, 49 (1986) 27.
- [12] J. Möller and B. Winter, *Fresenius' Z. Anal. Chem.*, 320 (1985) 451.
- [13] J. Atienza, M.A. Herrero, A. Maquieira and R. Puchades, *Crit. Rev. Anal. Chem.*, 22 (1991) 331.
- [14] N.G. Elenkova, R.A. Tsoneva and T.K. Nedelcheva, *Talanta*, 37 (1980) 67.
- [15] K. Grasshoff, M. Ehrhardt and K. Kremling, (Eds.), *Methods of Seawater Analysis*, 2nd edn., Verlag Chemie, Weinheim, 1983.

# Determination of mono-*ortho* substituted chlorobiphenyls by multidimensional gas chromatography and their contribution to TCDD equivalents

Jacob de Boer <sup>a,\*</sup>, Quy T. Dao <sup>a</sup>, Peter G. Wester <sup>a</sup>, Søren Bøwadt <sup>b</sup>,  
Udo A.Th. Brinkman <sup>c</sup>

<sup>a</sup> DLO-Netherlands Institute for Fisheries Research, P.O. Box 68, 1970 AB IJmuiden, Netherlands

<sup>b</sup> CEC Joint Research Centre, Environmental Institute, I-21020 Ispra (VA), Italy

<sup>c</sup> Free University, Department of Analytical Chemistry, De Boelelaan 1083, 1081 HV Amsterdam, Netherlands

Received 4 May 1994; revised manuscript received 7 August 1994

---

## Abstract

The mono-*ortho* chlorobiphenyls (CBs) 60, 74, 114, 123, 157, 167 and 189 were determined in Aroclor mixtures and aquatic organisms by multidimensional gas chromatography with electron capture detection (MDGC/ECD), using a combination of an Ultra 2 and an FFAP column. MDGC/ECD is recommended as the most suitable technique for direct determination of these CBs, without a liquid chromatographic (LC) pre-separation of mono-*ortho* CBs from the other CBs. Dependent, to some extent, on the stationary phase used, single-column determinations of these CBs easily yield too high results due to the presence of interferences. The contribution of the mono-*ortho* CBs studied to the total 2,3,7,8-tetrachlorodibenzo-*p*-dioxin (TCDD) equivalents (TEQs) from CBs in fish is highly dependent on the toxic equivalency factors (TEFs) used and varies between 0.02 and 22%. This contribution is mainly due to CBs 74, 114, 157 and 167 which may easily be determined by taking three heart-cuts and combining them into one MDGC/ECD run. The analytical error is negligible compared with the huge uncertainty of the TEFs. A need for more precise TEFs is emphasized.

**Keywords:** Gas chromatography; Chlorobiphenyls; Mono-*ortho* chlorobiphenyls; TCDD equivalents (TEQs)

---

## 1. Introduction

Over the last two decades polychlorinated biphenyls (PCBs) have been determined extensively in various matrices. The introduction of capillary gas chromatographic (GC) columns enabled the determination of individual chlorobiphenyl congeners (CBs) [1–3]. Information from toxicological research identified non-*ortho* and mono-*ortho* substituted CBs as the major

contributors to the total toxic effect (expressed as TCDD equivalents or TEQs) of PCBs in organisms, despite their extremely low concentrations [4,5]. Due to these low concentrations, the non-*ortho* substituted CBs cannot be determined simultaneously with the other CBs by single-column GC with electron capture detection (ECD), or even multidimensional GC (MDGC/ECD), because it is impossible to determine CBs that differ more than 1000-fold in concentration in one run [6]. Despite its wider linear range, also with mass spectrometric (MS) detection difficulties may

---

\* Corresponding author.

rise when co-eluting peaks must be determined which have such a large difference in concentration. Consequently, pre-separation techniques had to be developed in which the non-*ortho* CBs are separated from the other CBs prior to GC [7,8]. Concentrations of the major mono-*ortho* CBs in biological samples vary widely. For example, in Dutch eel CB 118 (2,4,5,3',4'-penta CB) concentrations are in the order of 100 µg/kg wet weight, while CBs 105 (2,3,4,3',4'-penta CB) and 156 (2,3,4,5,3',4'-hexa CB) are normally present in 10-fold lower concentrations. These three CBs can be determined by single-column GC with ECD or MS detection, provided appropriate column dimensions and a suitable stationary phase are selected [2,3].

It is currently supposed that the non-*ortho* CBs 77 (3,4,3',4'-tetra CB), 126 (3,4,5,3',4'-penta CB) and 169 (3,4,5,3',4',5'-hexa CB) together with the mono-*ortho* CBs 105, 118 and 156 are the major CB contributors to the TEQs in most biological samples [4,5,8]. However, information on the concentration of a number of other mono-*ortho* CBs, viz. CBs 60 (2,3,4,4'-tetra CB), 74 (2,4,5,4'-tetra CB), 114 (2,3,4,5,4'-penta CB), 123 (3,4,5,2',4'-penta CB), 157 (2,3,4,3',4',5'-hexa CB), 167 (2,4,5,3',4',5'-hexa CB) and 189 (2,3,4,5,3',4',5'-hepta CB), which generally occur in low concentrations (approximately 0.5–5% of CB 118 [10–14]), is too scarce to be reliable. Consequently, it is not yet completely clear, to which extent these CBs contribute to the TEQs and which of them are the more important ones.

Two procedures have been described to determine these mono-*ortho* CBs: (1) similarly to non-*ortho* CBs by GC/ECD or GC/MS after a pre-separation on carbon columns or with LC [10,12–14], or (2) directly by GC/ECD, GC/MS or MDGC, without pre-separation [15–19]. Although the concentrations of the additional mono-*ortho* CBs are higher than those of the non-*ortho* CBs, they are still extremely low compared to those of the major CBs and direct determination in complex environmental samples has been shown to be very difficult. Recent intercomparison exercises [20,21] indicate that coefficients of variation for CBs 105 and 156 in single-column GC analysis are consequently distinctly higher (30–60%) than those of the major CBs 101 (2,4,5,2',5'-penta CB), 153 (2,4,5,2',4',5'-hexa CB), 180 (2,3,4,5,2',4',5'-hepta CB), etc. (10–20%), and do not decrease significantly even when using smaller internal column diameters.

The most likely cause are interfering compounds, that are either present in the sample or have entered the extract as a contaminant. As a consequence single-column GC/ECD of the mono-*ortho* CBs discussed in the present study is not being recommended. Apart from some exceptions [13,14] literature data on the determination of mono-*ortho* CBs are generally not supported by information on detection limits, recovery or repeatability. In the present study we have evaluated an MDGC/ECD determination of the mono-*ortho* CBs, with due attention to analytical validation. Besides, the contribution of the CBs to the TEQs in fish has been calculated.

## 2. Experimental

### 2.1. Chemicals and samples

CB crystals obtained from Promochem (Wesel, Germany) were used as calibrants in this study. The internal standard 1,2,3,4-tetrachloronaphthalene (TCN) and isooctane, the solvent for the final extracts and for the Aroclor solutions were also obtained from Promochem.

GC separation of mono-*ortho* CBs was optimised using technical PCB mixtures Aroclor 1242, 1248, 1254 and 1260 (Monsanto, St. Louis, MO), extracts obtained from eels from three different locations in the Netherlands (river Roer, river Lek and Ketelmeer) and an extract of blubber from a juvenile seal from the Wadden Sea, a gift of Dr. P. Reijnders of the DLO-Institute for Forestry and Nature Management (Texel, Netherlands). Samples were taken in 1992, except for the Ketelmeer eel, that were sampled in 1991. The latter sample was saponified, cleaned and fractionated according to a procedure for the determination of non-*ortho* CBs [8], while the other samples were Soxhlet-extracted, cleaned and fractionated according to the method of de Boer [22].

In order to calculate the contribution of the mono-*ortho* CBs to the TEQs in fish, the analytes were determined in two eel samples from the rivers Rhine and Meuse, a pike-perch sample from the river Rhine and a cod liver sample from the southern North Sea (Dutch coast). The non-*ortho* CBs and CBs 105, 118 and 156 in these samples had already been determined before [23].

Table 1  
GC/ECD and MDGC/ECD conditions, used in the present study

Parameters	Single-column GC		MDGC	
	CP-Sil 8	CP-Sil 19	HP-Ultra 2	HP-FFAP
Column length (m)	50	50	25	25
Column i.d. (mm)	0.15	0.15	0.20	0.20
Film thickness ( $\mu\text{m}$ )	0.30	0.30	0.30	0.30
GC type	CE Vega	PE 8500	Sichromat	Sichromat
Carrier gas (pressure, kPa)	H <sub>2</sub> (265)	H <sub>2</sub> (357)	N <sub>2</sub> (200)	N <sub>2</sub> (110)
Linear carrier gas velocity ( $\text{cm s}^{-1}$ )	33	46	14	10
Injection volume ( $\mu\text{l}$ )	0.5	1	1	–
Autoinjector type	A 2005	AS-200B	manual	–
Splitless time (min)	2	2	0.6	–
Injector temperature ( $^{\circ}\text{C}$ )	270	270	270	–
Septum purge ( $\text{ml min}^{-1}$ )	2	2	2	–
Detection	<sup>63</sup> Ni ECD	<sup>63</sup> Ni ECD	<sup>63</sup> Ni ECD	<sup>63</sup> Ni ECD
Detector temperature ( $^{\circ}\text{C}$ )	310	360	320	320
Make-up gas (flow, $\text{ml min}^{-1}$ )	N <sub>2</sub> (60)	N <sub>2</sub> (60)	N <sub>2</sub> (35)	N <sub>2</sub> (35)
Initial oven temperature ( $^{\circ}\text{C}$ )	90	90	90	220
Initial isothermal period (min)	3	3	1	–
Initial programming rate ( $^{\circ}\text{C min}^{-1}$ )	30	30	30	–
Second isothermal temperature ( $^{\circ}\text{C}$ )	215	215	215	–
Second isothermal period (min)	40	40	30	–
Second programming rate ( $^{\circ}\text{C min}^{-1}$ )	5	5	5	–
Final isothermal temperature ( $^{\circ}\text{C}$ )	270	270	270	–
Final isothermal period (min)	30	35	44–74	80

## 2.2. Gas chromatographic techniques

Fused silica wall-coated open tubular columns were used for all GC analyses. Their dimensions and the conditions under which they were used are given in Table 1. For MDGC a Sichromat 2-8 GC with two independently controlled ovens was used (Siemens AG, Karlsruhe) [24]. Heart-cuts from the first column are transferred to the second column by the use of a valveless switching technique, in which instead of the gas flow, the pressure drop along the coupling piece – a glass capillary, i.d. 0.17 mm (“live-T-piece”) – is used for column switching. Through special auxiliary flow arrangements, the cut transfer to the second column and the connection of the first (“monitor”) detector can be carried out with negligible deterioration of the peak shape. The pressure drop type of adjustment of the flow is made easy by digital reading. The adjustments are stable over a long period of time and are reproducible with repeated applications using the same pair of columns. The number of heart-cuts made during

a run is in principle not limited. Although the system also functions when helium is used, nitrogen is preferred because a better precision (0.01 min) for the heart-cuts is obtained.

The temperature programme of the first oven was designed to obtain an optimal separation of CBs at the first column. For the second column a higher temperature would have been preferred, but due to more bleeding from the FFAP column observed at temperatures above 220 $^{\circ}\text{C}$ , this was not possible without a deterioration of the quality of the chromatogram.

Aroclor mixtures and biological samples were analysed twice with single-column GC/ECD: once on a CP-Sil 8 (5% phenyl 95% methyl polysiloxane) column and once on a CP-Sil 19 (85% methyl 7% phenyl 7% cyanopropyl 1% vinyl polysiloxane) column. For MDGC an HP-Ultra 2 (5% phenyl 95% methylpolysiloxane) column and an HP-FFAP (polyethylene glycol terephthalic acid ester) column were chosen. These columns were selected on basis of the relatively long retention times of mono-*ortho* CBs on

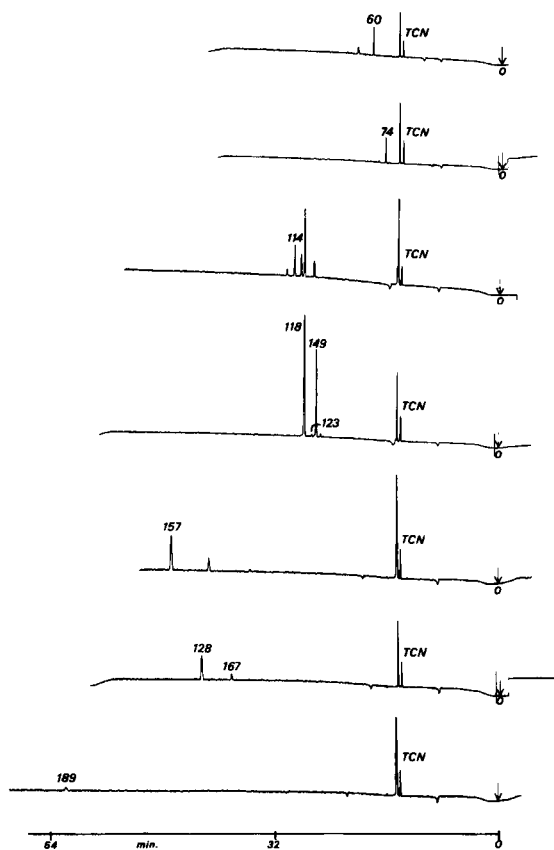


Fig. 1. Separate heart-cuts of CBs 60, 74, 114, 123, 157, 167 and 189 from Aroclor 1254. For conditions, see Table 1; TCN = tetrachloronaphthalene (internal standard).

the FFAP column, which should enhance resolution in combination with a SE-54-type stationary phase [3]. Fig. 1 shows chromatograms of the heart-cuts of the

seven mono-*ortho* CBs of interest present in Aroclor, and the internal standard TCN. It was not possible to include the heart-cuts of all seven peaks in one GC run. Peaks of other CBs, separated from the target CBs in a single heart-cut would then co-elute again with peaks of compounds present in other heart-cuts. For example, the peaks present in the heart-cut of CB 123 would interfere with those in the heart-cut of CB 114. Consequently, heart-cuts were combined in the following way: (1) TCN: 20.20–20.75 min, CB 60: 26.39–27.15 min, CB 114: 38.56–39.12 min, CB 167: 44.93–45.40 min, CB 157: 47.18–47.59 min and CB 189: 52.04–53.75; (2) TCN: 20.20–20.75 min, CB 74: 23.60–24.00 min and CB 123: 36.58–37.80 min.

### 3. Results and discussion

All seven mono-*ortho* CBs were determined in four Aroclor mixtures and in four biological samples. Because co-elution with other CBs or interfering compounds, which will invariably result in too high concentrations, is the main, and essential only, cause of interference to be expected, the experimental data, i.e. the CB concentrations found, were selected as the most important criteria to evaluate the methods used – the lower concentrations obviously being the more reliable ones. Illustrative examples of the experimental results obtained are given in Tables 2 and 3.

To confirm the determined concentrations of the mono-*ortho* CBs in the Aroclors, the same batches of Aroclor were also analysed by GC/ECD at the CEC Joint Research Centre (Ispra, Italy). Here, serial-cou-

Table 2

Concentrations (% w/w) of mono-*ortho* CBs in Aroclor mixtures, determined by single-column GC/ECD and MDGC/ECD

CB <sup>a</sup>	Structure	GC/ECD		MDGC/ECD	
		Aroclor	CP-Sil 8	CP-Sil 19	Ultra 2/FFAP
60	2,3,4,4'-tetra	1248	–	2.1	4.2
74	2,4,5,4'-tetra	1254	1.3	1.5	1.3
114	2,3,4,5,4'-penta	1260	0.07	0.03	0.03
123	3,4,5,2',4'-penta	1242	–	0.28	<0.02
157	2,3,4,3',4',5'-hexa	1260	3.4	–	0.08
167	2,4,5,3',4',5'-hexa	1260	–	–	0.18
189	2,3,4,5,3',4',5'-hepta	1260	0.55	0.15	0.14

–: no value because of obvious co-elution.

<sup>a</sup> According to Ballschmiter and Zell [9].

Table 3  
Concentrations ( $\mu\text{g kg}^{-1}$  wet weight) of mono-*ortho* CBs in aquatic organisms, determined by single-column GC/ECD and MDGC/ECD

CB	Structure	Samples	GC/ECD		MDGC/ECD
			CP-Sil	8CP-Sil 19	Ultra 2/FFAP
60	2,3,4,4'-tetra	Eel river Lek	–	<1	<1
74	2,4,5,4'-tetra	Eel river Lek	25	25	25
114	2,3,4,5,4'-penta	Eel river Roer	na	16	5.7
123	3,4,5,2',4'-penta	Eel river Lek	–	4.4	<2
157	2,3,4,3',4',5'-hexa	Eel Ketelmeer	1.7	–	1.2
167	2,4,5,3',4',5'-hexa	Seal blubber	–	–	<0.8
189	2,3,4,5,3',4',5'-hepta	Eel river Lek	2.1	4.9	<2

na: not analysed; –: no values because of obvious co-elution.

pled CP-Sil 8 and HT-5 columns were used with a DB-17 column as confirmation column [25]. The data obtained in this way replace earlier data on mono-*ortho* CBs in Aroclor mixtures reported by that group [18] in which a too high value for CB 114 (2,3,4,5,4'-penta CB) and too low values for CBs 157 (2,3,4,3',4',5'-hexa CB) and 167 (2,4,5,3',4',5'-hexa CB) were presented. This vividly demonstrates the difficulty of reliably measuring these small peaks in single-column or serial-coupled-column GC: the presence of interferences, and/or small shifts in retention times easily lead to inaccurate results, even at a highly qualified laboratory.

### 3.1. Comparison of MDGC and single-column GC

The results of Tables 2 and 3 show that for CBs 114 (2,3,4,5,4'-penta CB), 123 (3,4,5,2',4'-penta CB), 157 (2,3,4,3',4',5'-hexa CB), 167 (2,4,5,3',4',5'-hexa CB) and 189 (2,3,4,5,3',4',5'-hexa CB) in Aroclor mixtures and in biological samples the lowest concentrations are obtained by MDGC. The higher results obtained by single-column GC should all be explained by co-elution with other CBs or with interferences. In some cases – CBs 60 (2,3,4,4'-tetra CB), 123 and 167 on CP-Sil 8 and CBs 157 and 167 on CP-Sil 19 – co-elution was obvious, hence concentrations of the mono-*ortho* CBs concerned have not been calculated.

The high CB 114 concentration in river Roer eel (Table 3) is most probably due to co-elution with CB 146 (2,4,5,2',3',5'-hexa CB) [18]. CB 123 co-elutes with CB 149 (2,3,6,2',4',5'-hexa CB), one of the major CBs, on a CP-Sil 8 column [2,18] and with CB 107 (2,3,5,2',4'-penta CB) on a CP-Sil 19 column [2].

CB 157 co-elutes with CBs 173 (2,3,4,5,6,2',3'-hepta CB) and 200 (2,3,4,6,2',3',5',6'-octa CB) on a CP-Sil 8 column and with CB 180 (2,3,4,5,2',4',5'-hepta CB) on a CP-Sil 19 column [3]. CB 167 co-elutes with CB 128 (2,3,4,2',3',4'-hexa CB) on a CP-Sil 8 column and with CB 202 (2,3,5,6',2',3',5',5'-octa CB) on a CP-Sil 19 column.

CB 60 co-elutes with CB 56 (2,3,3',4'-tetra CB) on the Ultra 2 column and with the same CB on the FFAP column. Consequently, CB 60 cannot be determined by MDGC using the Ultra 2/FFAP column combination. With a combination of DB 5 and SB-Smectic columns an unambiguous determination of CB 60 should be possible [3,26]. A drawback of the liquid crystalline CB-Smectic column is, however, its strong bleeding.

The high concentrations of CBs 114 and 189 in Aroclor 1260 on a CP-Sil 8 column (Table 2) and of CB 189 in river Lek eel on a CP-Sil 19 column (Table 3) cannot be explained on the basis of literature data on co-elution with other CBs. Probably, therefore, these high results are caused by interferences that easily occur at this ultra-trace level [20,21]. Interferences may be present in the sample extract, due to insufficient clean-up, or may be eluted from a contaminated injector liner. Also phthalate esters from autosampler vial septa may contaminate the sample solution, once it has been in contact with these septa [27] as we, and others, have demonstrated by means of GC/MS analysis.

Actually, concentrations in Aroclor mixtures and biological samples determined by MDGC and single-column GC were essentially the same only for CB 74 (2,4,5,4'-tetra CB) which is present in relatively large concentrations.

Admittedly, based on literature data it is presumably possible to find a column for each CB at which no co-elution with other CBs will occur. For example, separation from other CBs is reported for CBs 157 and 167 on a CP-Sil 88 column [2,3,19]. However, due to the frequent presence of interferences at this ultra-trace level, it will be extremely difficult to produce reproducible data for all mono-*ortho* CBs by single-column GC. Indeed, repeatability data of single-column GC determinations of mono-*ortho* CBs are very scarce. In a recent intercomparison exercise, single-column determinations of mono-*ortho* CBs 105 (2,3,4,3',4'-penta CB), 118 (2,4,5,3',4'-penta CB) and 156 (2,3,4,5,3',4'-hexa CB) in fish, which are present in at least 10-fold higher concentrations than the mono-*ortho* CBs discussed in the present study, resulted in coefficients of variation of around 100%, despite the extensive advice on column selection that was given during previous exercises [28].

The use of MS as a detection technique may offer some advantage in single-column GC. However, this advantage is restricted to co-eluting CBs with different chlorine content. Indeed, some of the co-eluting pairs above, such as CB 114 and 146, 123 and 149, 157 and 173 and 167 and 202 may also be resolved and determined by single column GC/negative chemical ionization (NCI)-MS, although some care is needed in case of strong concentration differences. In such cases lower mass fragments of higher CBs may interfere with higher mass fragments of lower CBs, which may lead to biased results. High resolution MS may solve also this problem. GC/NCI-MS has a more than 10-fold higher sensitivity for CBs with more than four chlorine atoms [29]. Combining MDGC and NCI-MS or high-resolution MS, i.e. combining in that way a high separation efficiency and a highly sensitive and selective detection, obviously is a rather interesting option for the determination of mono-*ortho* CBs. The application of low resolution MS with electron impact (EI) for the determination of mono-*ortho* CBs is very limited because its sensitivity is about 10-fold lower than that of GC/ECD [29]. The low concentrations of the mono-*ortho* CBs will in general not enable a proper determination by GC/EI-MS. Only for the mono-*ortho* CBs 105, 118 and 156 GC/EI-MS may be applicable.

Table 4 compares the results of the determination of mono-*ortho* CBs in Aroclor mixtures carried out in our laboratory and at Ispra. CB 60 (2,3,4,4'-tetra CB) is

Table 4  
Results of an intercomparison on the determination of mono-*ortho* CB concentrations in Aroclor mixtures (% w/w).

CB	A 1242	A 1248	A 1254	A 1260	Laboratory
74	2.3	4.1	1.3	0.09	a
	2.1	4.0	1.1	0.02	b
114	0.04	0.13	0.19	0.03	a
	0.04	0.14	0.25	<0.01	b
123	<0.02	0.09	0.14	<0.03	a
	0.04	0.09	0.22	<0.01	b
157	<0.01	<0.01	0.24	0.08	a
	<0.01	0.02	0.30	0.15	b
167	<0.03	0.03	0.45	0.18	a
	<0.01	0.03	0.39	0.13	b
189	0.0001	0.0003	0.04	0.14	a
	<0.01	<0.01	0.04	0.10	b

a = Data produced by MDGC/ECD at the Netherlands Institute for Fisheries Research; b = data produced by GC/ECD with serial coupled CP-Sil 8 and HT 5 columns at the CEC Joint Research Centre.

not included because no methods providing reliable CB 60 data were available in either laboratory when the interlaboratory study was performed. In view of the very low concentrations of the mono-*ortho* CBs in Aroclor mixtures, especially of the higher CBs in the lower chlorinated Aroclors and of the lower CBs in the higher chlorinated Aroclors, fully acceptable results were obtained with a mean difference of 20%. A difference of more than 50% was observed in only three cases. The results from our laboratory were not consistently higher or lower than those from the other. This adds to the conclusion that both MDGC and the alternative of serial-coupled-column GC may be considered reliable methods.

The present results cannot be compared with literature data on mono-*ortho* CB concentrations in Aroclor mixtures [16], because different supplies of Aroclors were used.

### 3.2. Contribution of mono-*ortho* CBs to TCDD equivalents

Concentrations of CBs can be expressed as TCDD equivalents (TEQs) by multiplying them with a toxic equivalency factor (TEF). TEFs determined by different authors are given in Table 5.

TEQs of mono-*ortho* CBs in three eel samples and a pike-perch from Dutch freshwater locations and in cod liver from the southern North Sea determined by

Table 5  
Overview of non-, mono- and di-ortho substituted CBs for which TEFs have been reported

CB	Structure	TEFs	TEFs				
			Kannan, 1988 [33]	Dutch WG, 1991 [30]	Safe, 1992 [31]	Safe, 1993 [32]	WHO, 1994 [34]
<i>Non-ortho</i>							
77	3,4,3',4'	-tetra	0.0027	0.01	0.01	0.01	0.0005
126	3,4,5,3',4'	-penta	0.4	0.1	0.1	0.1	0.1
169	3,4,5,3',4',5'	-hexa	0.0016	0.005	0.05	0.05	0.01
<i>Mono-ortho</i>							
60	2,3,4,4'	-tetra	–	0.00001	0.001	–	–
74	2,4,5,4'	-tetra	–	0.00001	0.001	–	–
105	2,3,4,3',4'	-penta	0.0011	0.0001	0.001	0.001	0.0001
114	2,3,4,5,4'	-penta	0.000095	0.0005	0.001	0.0002	0.0005
118	2,4,5,3',4'	-penta	0.000008	0.00005	0.001	0.0001	0.0001
123	3,4,5,2',4'	-penta	0.000095	0.00005	0.001	0.0002	0.0001
156	2,3,4,5,3',4',5'	-hexa	0.000046	0.0005	0.001	0.0004	0.0005
157	2,3,4,3',4',5'	-hexa	0.00013	0.0005	0.001	0.0003	0.0005
167	2,4,5,3',4',5'	-hexa	0.000007	0.00001	0.001	–	0.00001
189	2,3,4,5,3',4',5'	-hepta	0.000008	<0.00001	0.001	–	0.0001
<i>Di-ortho</i>							
170	2,3,4,5,2',3',4'	-hepta	–	–	–	–	0.0001
180	2,3,4,5,2',4',5'	-hepta	–	–	–	–	0.00001

using the TEFs of the Dutch Working Group on TEFs [30] are given in Table 6. TEQs of the mono-ortho CBs discussed in this study were compared with TEQs of the CBs 77 (3,4,3',4'-tetra CB), 126 (3,4,5,3',4'-penta CB), 169 (3,4,5,3',4',5'-penta CB) and 105 (2,3,4,3',4'-penta CB), 118 (2,4,5,3',4'-penta CB) and 156 (2,3,4,5,3',4'-hexa CB) in the same samples, which had been determined before [23]. The contribution of TEQs of CBs 60, 74, 114, 123, 157, 167 and 189 to the total TEQs from CBs (CB-TEQ) ranges from 0.5 to 6% in all samples, with CBs 74, 114, 157

and 167 as the only significant contributors (Table 6). The higher contribution in eel is probably caused by metabolic degradation of the non-ortho CBs 77 and 126 in this fish species [23], which makes the contribution of the non-ortho CBs in eel relatively less important.

#### Influence of different TEFs

TEQs of the mono-ortho CBs studied and their contribution to CB-TEQ in the samples of Table 6 have also been calculated by using other available sets of

Table 6  
Contribution of mono-ortho CBs to CB-TEQ, based on TEFs of the Dutch WG on TEFs [30]

Sample	TEQ (ng kg <sup>-1</sup> ) of CB:							Sum (ng kg <sup>-1</sup> )	Percent of total CB-TEQ
	60 <sup>a</sup>	74	114	123	157	167	189		
Eel Meuse	0.03	0.10	<0.1	<0.02	1.3	0.07	<0.03	1.5	4
Eel Ketelmeer	<0.003	0.08	0.16	<0.03	0.6	0.05	<0.01	0.9	3
Eel Rhine	0.06	0.23	<0.4	<0.04	1.3	0.09	<0.03	1.7	6
Pike-perch Rhine	nm	0.02	<0.05	<0.005	<0.05	0.003	<0.001	<0.1	<3
Cod liver North Sea	0.05	0.21	<0.5	<0.05	0.75	0.1	<0.02	1.1	0.5

<sup>a</sup> CP-Sil 19/ECD data, possible co-elution with CB 99; nm = not measured.



Table 7  
TEQ values (ng kg<sup>-1</sup>) of CBs 60, 74, 114, 123, 157, 167 and 189 in fish calculated using different TEFs

Sample	Kannan, 1988		Dutch WG, 1991		Safe, 1992		Safe, 1993		WHO, 1994	
	TEQ <sup>a</sup>	% of total <sup>b</sup>	TEQ <sup>a</sup>	% of total <sup>b</sup>	TEQ <sup>a</sup>	% of total <sup>b</sup>	TEQ <sup>a</sup>	% of total <sup>b</sup>	TEQ <sup>c</sup>	% of total <sup>d</sup>
Eel Meuse	0.07	0.2	1.5	4	23	6	0.78	1	1.7	3
Eel Ketelmeer	0.07	0.07	0.9	3	15	10	0.42	0.7	0.9	2
Eel Rhine	0.08	0.1	1.7	6	44	22	0.78	1.5	1.7	4
Pike-perch Rhine	0.04	0.05	<0.1	<3	2.0	15	0.06	<1	<0.1	<0.1
Cod liver North Sea	0.1	0.02	1.1	0.5	40	9	0.45	<0.1	1.0	0.5

<sup>a</sup> TEQ of CBs 60, 74, 114, 123, 157, 167 and 189.

<sup>b</sup> Total CB-TEQ of CBs 77, 126, 169, 105, 118, 156, 60, 74, 114, 123, 157, 167 and 189.

<sup>c</sup> TEQ of CBs 114, 123, 157, 167 and 189.

<sup>d</sup> Total CB-TEQ of CBs 77, 126, 169, 105, 118, 156, 114, 123, 157, 167, 189, 170 and 180.

TEF values (Table 7) [30–34]. The broad range of TEF values (Table 5) presently in use makes the TEQ values of these mono-*ortho* CBs cover an about 1000-fold wide range for all samples analysed (0.04–44 ng kg<sup>-1</sup>); the total CB-TEQ also varies dramatically (from 4 to 500 ng kg<sup>-1</sup>; data not shown). Obviously, compared with this huge uncertainty in TEQ values, the analytical error of 8–23% is negligible. Even when the MDGC method would be applied by several laboratories, which could lead to R.S.D. values of around 100%, as has been shown for other CBs [28], this error would still be much smaller than the uncertainty in the TEFs. Although the recent introduction of interim TEFs by the World Health Organisation (WHO) [34] may result in a more uniform calculation of TEQs, this does not mean that those TEFs will be more accurate, given the broad range of TEF values from which the WHO-TEFs have been distilled. For a sound interpretation of analytical data on CBs a stronger toxicological basis is obviously required.

Compared with the results obtained using TEFs of the Dutch WG (Table 6), the contribution of the present set of mono-*ortho* CBs to CB-TEQ calculated using the TEFs of Safe [32] and Kannan et al. [33] are lower (<0.1–1.5%), and much lower (0.04–0.1%), respectively, whereas TEFs of Safe [31] result in a much higher contribution of the same mono-*ortho* CBs to CB-TEQ: 6–22%. Use of the WHO-TEFs leads to a contribution of the present mono-*ortho* CBs to CB-TEQ of <0.1–4%, which is comparable with the results obtained using Dutch WG TEFs.

Based on WHO-TEFs, 85–90% of CB-TEQ in fish samples is caused by CBs 126 (3,4,5,3',4'-penta CB),

118 (2,4,5,3',4'-penta CB), 156 (2,3,4,5,3',4'-hexa CB) and 170 (2,3,4,5,2',3',4'-hepta CB). From among the mono-*ortho* CBs studied CB 157 (2,3,4,3',4',5'-hexa CB) is the only significant contributor (0.3–2.6%).

#### Analytical consequences of contribution to TEQ

The data in Tables 6 and 7 clearly show that the contribution of CBs 60 (2,3,4,4'-tetra CB), 123 (3,4,5,2',4'-penta CB) and 189 (2,3,4,5,3',4',5'-hepta CB) to CB-TEQ is negligible, irrespective of the set of TEF values used. Consequently, it is sufficient to determine CBs 74 (2,4,5,4'-tetra CB), 114 (2,3,4,5,4'-penta CB), 157 (2,3,4,3',4',5'-hexa CB) and 167 (2,4,5,3',4',5'-hexa CB) in order to assess the contribution of the mono-*ortho* CBs studied to CB-TEQ. Heart-cuts of these CBs can easily be determined in one MDGC run. Combining these four heart-cuts in one MDGC run results in an analysis time of 130 min (Fig. 2).

#### 3.3. Quality control aspects

Because of the relatively low concentrations of the mono-*ortho* CBs studied in environmental samples, quality control aspects such as repeatability, analyte recovery and detectability should be duly considered. In the literature, data on quality control aspects of these mono-*ortho* CB determinations are very scarce.

The repeatability of the method was tested for CBs 74 (2,4,5,4'-tetra CB), 114 (2,3,4,5,4'-penta CB), 157 (2,3,4,3',4',5'-hexa CB) and 167 (2,4,5,3',4',5'-hexa CB) in five independent replicate analyses of an eel

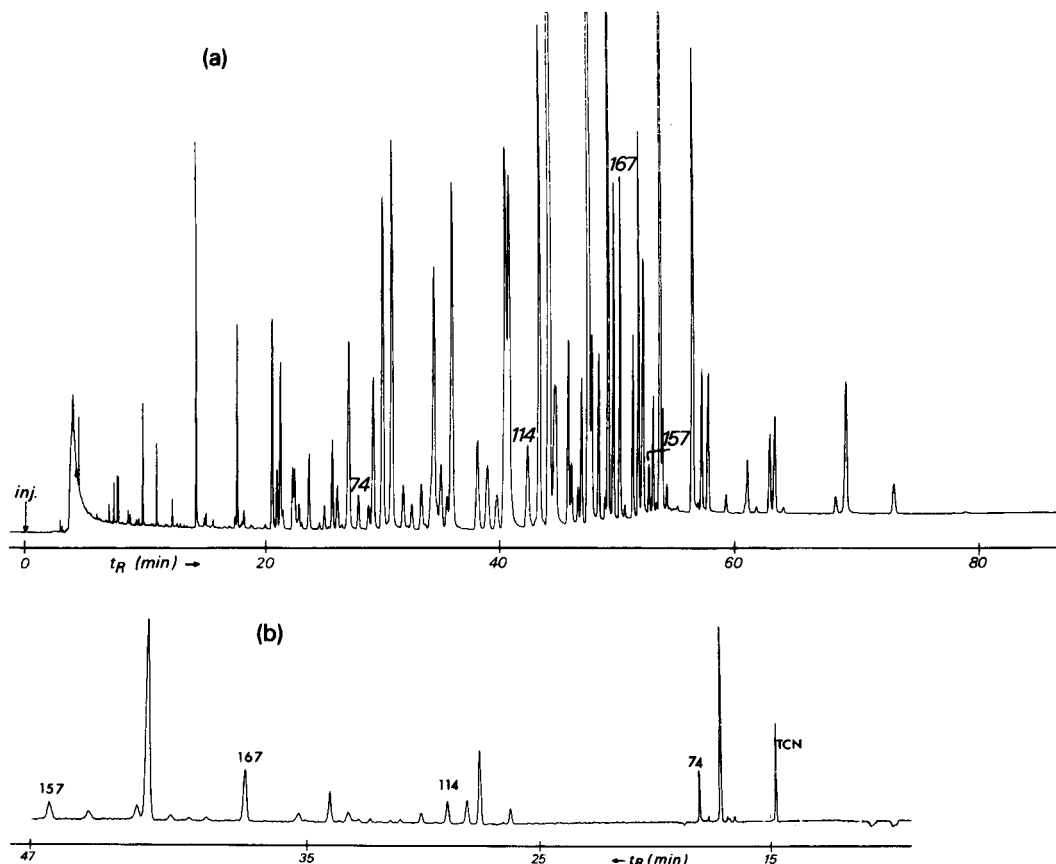


Fig. 2. (a) GC/ECD chromatogram of an eel sample on an HP-Ultra-2 column. For conditions, see Table 1; (b) combined heart-cuts of CBs 74, 114, 157 and 167 from the chromatogram of Fig. 2a analysed on an FFAP column. For conditions, see Table 1; TCN = tetrachloronaphthalene (internal standard).

sample from the Rhine estuary. The R.S.D. values varied between 8% (CB 74) and 23% (CB 114) ( $n=5$ ) (Table 8). The concentrations of the CBs varied between  $2 \mu\text{g kg}^{-1}$  wet weight (ww) (CB 114) and  $25 \mu\text{g kg}^{-1}$  ww (CB 74). As is to be expected, lower

R.S.D. values were found at the higher concentrations.

Two recovery experiments were carried out by spiking an eel sample with the CBs of interest at concentrations similar to their original level and at a 10-fold higher level. In both experiments the CB recoveries

Table 8  
Repeatability, recoveries and detection limits of CBs 74, 114, 157 and 167 in eel (MDGC/ECD)

CB	Concentration ( $\mu\text{g kg}^{-1}$ )	R.S.D. <sup>a</sup> (%)	Recovery <sup>b</sup> (%)	Recovery <sup>c</sup> (%)	Detection limit (pg)
74	25	8	110	83	5
114	2	23	89	94	10
157	4	19	98	89	10
167	24	15	120	98	10

<sup>a</sup>  $n=5$ .

<sup>b,c</sup> Spike of an eel sample at <sup>b</sup> level of original CB concentrations in that sample, and <sup>c</sup> 10-fold higher level.

were over 80%, and in most instances over 90%. These values are comparable to recoveries for non- and mono-*ortho* CBs reported in the literature [13,14].

Absolute detection limits of the MDGC/ECD system were between 5 and 10 pg for all seven mono-*ortho* CBs studied. For most biological tissues this means that detection limits will be between 0.5 and 4  $\mu\text{g kg}^{-1}$ . A higher sample intake will cause a further decrease of the detection limits (down to 0.05–0.4  $\mu\text{g kg}^{-1}$ ) and facilitate analyses at very low CB levels. This was actually achieved when analysing the Ketelmeer eel and the seal (Table 3).

A detection limit of 0.5  $\mu\text{g kg}^{-1}$  for the individual CBs can be converted into detection limits expressed as  $\text{ng kg}^{-1}$  TEQ. To quote an example, when the Dutch WG TEFs are used, the results are as follows: CB 60: 0.005, CB 74: 0.005, CB 114: 0.2, CB 123: 0.02, CB 157: 0.2, CB 167: 0.02 and CB 189: 0.02. With these detection limits the contribution of each mono-*ortho* CB to CB-TEQ in eel can be detected down to 0.02–0.6%.

#### 4. Conclusions

MDGC/ECD is recommended for the determination of the mono-*ortho* substituted CBs 60 (2,3,4,4'-tetra CB), 74 (2,4,5,4'-tetra CB), 114 (2,3,4,5,4'-penta CB), 123 (3,4,5,2',4'-penta CB), 157 (2,3,4,3',4',5'-hexa CB), 167 (2,4,5,3',4',5'-hexa CB) and 189 (2,3,4,5,3',4',5'-hepta CB) in biological samples. The combination of an HP-Ultra 2 and an FFAP column can be used to determine all these CBs except CB 60. For the latter compound MDGC using a DB5 and an SB-Smectic column is recommended. Analytical validation of the method yields satisfactory results, and the detection limits for individual CBs of around 0.5  $\mu\text{g kg}^{-1}$  enable the determination of the contribution to CB-TEQ of below 0.1%. As regards the significance of the analytical data presented in this study to the calculation of TEQs, two remarks should be made.

(i) Dependent on the set of TEF values used, the contribution of the present CBs to CB-TEQ varies between 0.02 and 22%. Irrespective of the TEFs used, the contribution of CBs 60, 123 and 189 is negligible. Consequently, it is sufficient to determine CBs 74, 114, 157 and 167. Such an analysis can easily be carried out in one MDGC/ECD run.

(ii) Although the introduction of interim WHO-TEFs may lead to a more uniform approach of TEQ calculations, this TEF set is not necessarily more accurate than other sets. Obviously, compared with the enormously wide range of TEF values – which, in a way, reflects a distinct uncertainty about the true values – the analytical error of the mono-*ortho* CB determinations is negligible. Since utilizing the presently available TEFs, and the TEQs therewith calculated, for health risk assessment [35] may have far-reaching consequences if the inherent uncertainties are not properly considered, it is of utmost importance to establish a sounder toxicological basis which will enable the use of much more accurate and precise TEF values.

#### References

- [1] J. de Boer and Q.T. Dao, *J. High Resolut. Chromatogr.*, 12 (1989) 755.
- [2] B. Larsen, S. Bøwadt and R. Tilio, *Int. J. Environ. Anal. Chem.*, 47 (1992) 47.
- [3] J. de Boer, Q.T. Dao and R. van Dortmond, *J. High Resolut. Chromatogr.*, 15 (1992) 249.
- [4] S. Tanabe, N. Kannan, A. Subramanian, S. Watanabe and R. Tatsukawa, *Environ. Pollut.*, 47 (1987) 147.
- [5] S. Safe, *Crit. Rev. Toxicol.*, 21 (1990) 51.
- [6] N. Kannan, G. Petrick, D.E. Schulz, J.C. Duinker, J.P. Boon, E. van Arnhem and S. Jansen, *Chemosphere*, 23 (1991) 1055.
- [7] P. Haglund, L. Asplund, U. Järnberg and B. Jansson, *Chemosphere*, 20 (1990) 887.
- [8] J. de Boer, C.J.N. Stronck, F. van der Valk, P.G. Wester and M.J.M. Daudt, *Chemosphere*, 25 (1992) 1277.
- [9] K. Ballschmiter, R. Bacher, A. Mennel, R. Fisher, U. Riehle and M. Swerev, *J. High. Resolut. Chromatogr.*, 15 (1992) 260.
- [10] C.S. Hong, B. Bush and J. Xiao, *Ecotoxicol. Environ. Safety*, 23 (1992) 118.
- [11] J. Falandysz, N. Yamashita, S. Tanabe and R. Tatsukawa, *Z. Lebensm. Unters. Forsch.*, 194 (1992) 120.
- [12] E. Storr-Hansen, *Chemosphere*, 24 (1992) 1181.
- [13] L.L. Williams, J.P. Giesy, N. DeGalan, D.A. Verbrugge, D.E. Tillitt, G.T. Ankley and R.L. Welch, *Environ. Sci. Technol.*, 26 (1992) 1151.
- [14] K.M. Wilson-Yang, J.P. Power, E.A. Chisholm and D.J. Hallett, *Chemosphere*, 23 (1991) 1139.
- [15] J.C. Duinker, D.E. Schulz and G. Petrick, *Anal. Chem.*, 60 (1988) 478.
- [16] D. Schulz, G. Petrick and J. Duinker, *Environ. Sci. Technol.*, 23 (1989) 852.
- [17] E. Storr-Hansen, *J. Chromatogr.*, 558 (1991) 375.
- [18] B. Larsen, S. Bøwadt and S. Facchetti, *Int. J. Environ. Anal. Chem.*, 47 (1992) 147.
- [19] B. Larsen, S. Bøwadt, R. Tilio and S. Facchetti, *Chemosphere*, 25 (1992) 1343.

- [20] J. de Boer and J. van der Meer, Report on step 3b of the ICES/IOC/OSPARCOM intercomparison exercise on the analysis of chlorobiphenyl congeners in marine media (1993), Cooperative Research Report, Int. Council for Exploration of the Sea, Copenhagen, in press.
- [21] A. Aminot, J. de Boer, W.P. Cofino, D. Kirkwood, B. Petersen and D. Wells, Report on the intercomparison exercises in 1994 – Nutrients in seawater, trace metals in sediments, chlorobiphenyls in fish oil (1993), Measurements and Testing Programme (BCR) of the European Community, Brussels.
- [22] J. de Boer, *Chemosphere*, 17 (1988) 1811.
- [23] J. de Boer, C.J.N. Stronck, W.A. Traag and J. van der Meer, *Chemosphere*, 26 (1993) 1823.
- [24] J. de Boer and Q.T. Dao, *J. High Resolut. Chromatogr.*, 14 (1991) 593.
- [25] S. Bøwadt, H. Skejøl-Andresen, L. Montanarella and B. Larsen. *Int. J. Environ. Anal. Chem.*, (1994) in press.
- [26] F.R. Guenther, S.N. Chesler and R.E. Rebbert, *J. High Resolut. Chromatogr.*, 12 (1989), 821.
- [27] S.C. Leung and B.Y. Giang, *Bull. Environ. Contam. Toxicol.*, 50 (1993) 528.
- [28] J. de Boer and J. van der Meer, Report on step 4 of the ICES/IOC/OSPARCOM intercomparison exercise on the analysis of chlorobiphenyl congeners in marine media (1994), Cooperative Research Report, Int. Council for Exploration of the Sea, Copenhagen, in press.
- [29] P.G. Wester and J. de Boer, in H. Fiedler, H. Frank, O. Hutzinger, W. Parzefall, A. Riss and S. Safe (Eds.), *Proc. 13th Int. Symp. Dioxin'93*, Vienna, Organohalogen Compounds, Vol. 14, 1993, p. 121.
- [30] A.K.D. Liem, R.M.C. Theelen, W. Slob and J.H. van Wijnen. Report 730501.034 (1991), National Institute of Public Health and Environmental Protection, Bilthoven, Netherlands.
- [31] S. Safe, *Chemosphere*, 25 (1992) 61.
- [32] S. Safe, in H. Fiedler, H. Frank, O. Hutzinger, W. Parzefall, A. Riss and S. Safe (Eds.), *Proc. 13th Int. Symp. Dioxin'93*, Vienna, Organohalogen Compounds, Vol. 14, 1993, p. 53.
- [33] N. Kannan, S. Tanabe and R. Tatsukawa, *Bull. Environ. Contam. Toxicol.*, 41 (1988) 267.
- [34] U.G. Ahlborg, G.C. Becking, L.S. Birnbaum, A. Brouwer, H.J.G.M. Derks, M. Feeley, G. Golor, A. Hanberg, J.C. Larsen, A.K.D. Liem, S.H. Safe, C. Schlatter, F. Waern, M. Younes and E. Yrjänheikki, *Chemosphere*, 28 (1994) 1049.
- [35] L.M.G.Th. Tuinstra, C. Koopman-Esseboom, P.J.J. Suir, M. Huisman, E.R. Boersman, in H. Fiedler, H. Frank, O. Hutzinger, W. Parzefall, A. Riss and S. Safe (Eds.), *Proc. 13th Int. Symp. Dioxin'93*, Vienna, Organohalogen Compounds, Vol. 13, 1993, p. 59.



ELSEVIER

Analytica Chimica Acta 300 (1995) 167–171

ANALYTICA  
CHIMICA  
ACTA

# Size exclusion chromatography of aluminium species in natural waters<sup>1</sup>

Lillian Zernichow, Walter Lund\*

*Department of Chemistry, University of Oslo, Box 1033, N-0315 Oslo, Norway*

Received 6 May 1994; revised manuscript received 1 August 1994

## Abstract

Size exclusion chromatography was used in order to characterize organically bound aluminium in natural water samples. A Superose column was used, with 0.1 M acetate buffer (pH 4.6) as mobile phase. Three detection systems were used; graphite furnace atomic absorption spectrometry, post-column reaction with pyrocatechol violet and UV spectrometry at 254 nm. A single peak was obtained for organic aluminium in natural waters. The results indicated that aluminium binds with a broad size range of humic substances, and that the inorganic aluminium was present in polymeric form.

*Keywords:* Atomic absorption spectrometry; Size exclusion chromatography; Aluminium species; Natural waters; Pyrocatechol violet

## 1. Introduction

The environmental effect of aluminium depends on the form in which it occurs [1–4]. The species  $\text{Al}^{3+}$  and  $\text{AlOH}^{2+}$  are probably more toxic than polymeric forms and organically bound aluminium. In natural waters above pH 4.5, the predominating aluminium species are usually complexes with hydroxide, fluoride and organic ligands [5]. The organic ligands may be mainly humic substances, since these constitute a major part of the dissolved organic material in natural water [6]. The most frequently used method for fractionation of aluminium in natural waters is probably the method developed by Driscoll [7], which employs a cation-exchange resin to separate non-labile (mainly organic) aluminium species from labile cationic aluminium spe-

cies. However, various other methods have been employed for the determination of operationally defined fractions of aluminium, based on ion exchange, reaction with colorimetric and fluorimetric reagents, dialysis, ultrafiltration, and the use of a fluoride ion selective electrode [8–10].

The present work was undertaken in an attempt to characterize organically bound aluminium in freshwaters. Since a major part of the species will be complexes with humic substances, size exclusion chromatography (SEC) was chosen. A mobile phase with pH 4.6 was used, because this was close to the pH of the water samples. Detection by post-column reaction with pyrocatechol violet (PCV) was investigated, since this could eventually be used in a field laboratory. In addition, aluminium was detected off-line by graphite furnace atomic absorption spectrometry (GFAAS). Kerven et al. [11] have used SEC to separate an aluminium–fulvic acid complex from inorganic aluminium species, while Gardiner et al. [12] studied the

\* Corresponding author.

<sup>1</sup> Part of this paper was presented at the 12th International Symposium on Microchemical Techniques, Cordoba, Spain, 7–12 September, 1992.

distribution of organic and inorganic aluminium species in soil solution by SEC. SEC has also been used for the study of inorganic aluminium complexes [13–17].

## 2. Experimental

### 2.1. Apparatus

A Shimadzu chromatographic system was used, which consisted of a LC-6A pump, a SPD-6AV UV–visible spectrophotometric detector and a C-R3A integrator. A Rheodyne 7125 injector with a loop volume of 200  $\mu\text{l}$  was used. The size exclusion column was a Superose 12 HR 10/30 column (Pharmacia), with 10 mm i.d. and 300 mm length. For the atomic absorption measurements, a laboratory-made fraction collector was placed after the UV–visible detector. The atomic absorption equipment consisted of a Perkin Elmer Model 5000 spectrometer with Zeeman background correction, a HGA-400 graphite furnace, a 3600 data system, and an Anadex DP-9501B printer. The aluminium hollow cathode lamp was operated at 25 mA; the 309.3 nm line was used. The graphite tubes used were pyrolytically coated. For the post-column reaction, a Gilson Minipuls 3 peristaltic pump with 4 channels and PTFE tubing with 0.5 mm inner diameter were used. The reaction coil consisted of 6 m knitted tubing.

### 2.2. Reagents and samples

The reagents used were of analytical grade. Standard aluminium solutions were prepared by dilution of a 1000 mg/l Al stock solution (Spectrosol, BDH) with deionized water. The solutions were acidified to pH 2 with nitric acid. Blue dextran 2000 (50 mg/l, Pharmacia) was used to determine the total exclusion limit of the column. For calibration of the column, the following substances were used: Globular proteins (Pharmacia): 500 mg/l ribonuclease A, 150 mg/l chymotrypsinogen A, 350 mg/l ovalbumin, 350 mg/l albumin, with molecular weights of 13,700, 25,000, 43,000 and 67,000 dalton, respectively. The column was also calibrated with sodium polystyrene-4-sulphonates (Pressure Chemicals), molecular weights 1600, 4000, 6500 and 16,000 dalton, respectively. The concentration of each standard was 1.0 g/l. The stan-

dards were injected one at a time, and detected at 254 nm.

Freshwater samples were collected from streams and lysimeter experiments in the Birkenes catchment in southern Norway. The area is spruce forested, with granitic bedrock. The samples had a pH of 4.4–4.6. For all samples, the total organic carbon was 5–8 mg/l C, non-labile aluminium was 200–350  $\mu\text{g/l}$  Al and labile aluminium was 150–500  $\mu\text{g/l}$  Al, as determined by the Driscoll method [7]. All samples were stored in polyethylene bottles at 4°C.

### 2.3. Procedures

**SEC.** An acetate buffer was added to the samples before injection, so that the sample matrix matched exactly the mobile phase with respect to the ionic strength and pH. The samples were filtered during injection, by using a syringe equipped with a 0.45  $\mu\text{m}$ , 13 mm Millex HV (Millipore) filter. The sample loop volume was 200  $\mu\text{l}$ . The 0.1 M acetate buffer used as mobile phase consisted of 0.05 M sodium acetate and 0.05 M acetic acid, pH 4.6. The flow-rate was 0.4 ml/min. The organic material was detected at 254 nm.

**GFAAS.** The eluate from the column was separated into 0.6 ml fractions; about 40 fractions were collected. All fractions were acidified to pH 2 with nitric acid (65%). Three aliquots per fraction were analyzed. The sample volume was 10  $\mu\text{l}$ , and the temperature programme was as follows: Drying 100°C, ramp time 10 s, hold time 15 s; ashing 1300°C, ramp time 20 s, hold time 10 s; atomization 2400°C, hold time 3 s. The gas flow (Ar) was 300 ml/min during drying and ashing; gas stop was used during atomization. The optimal conditions were established by recording the appropriate ashing and atomization curves. Peak areas were used throughout. The detection limit was found to be 6  $\mu\text{g/l}$  Al.

**Post-column reaction.** The manifold is shown in Fig. 1. The flow-rates (in ml/min) are given in the figure. The carrier was 0.1 M acetate buffer, pH 4.6. The iron-masking reagent consisted of 10 mM 1,10-phenanthroline and 0.5 M hydroxylammonium chloride [18]. The concentration of pyrocatechol violet (Sigma) was 1 mM. The pH in the final flow was adjusted to 6.2 with a buffer consisting of 3.0 M hexamethylenetetramine to which hydrochloric acid had been added (0.2 M final concentration) [19]. With a 6 m coil, the reaction time

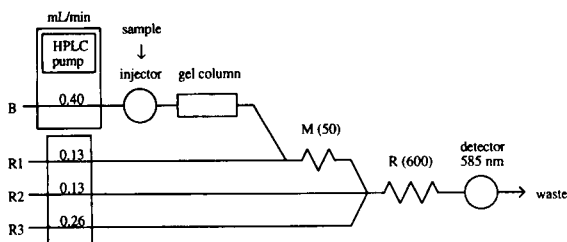


Fig. 1. Manifold for the determination of aluminium by post-column reaction with pyrocatechol violet. B, 0.1 M acetate buffer, pH 4.6; R1, iron-masking reagent; R2, 1 mM pyrocatechol violet; R3, pH 6.2 buffer; M/R, mixing/reaction coil (length in cm).

was 2.4 min. The aluminium–PCV complex was detected at 585 nm.

### 3. Results and discussion

The total exclusion volume of the column was 7.0 ml (blue dextran) and the total permeation volume was 22.5 ml (manufacturers value). From Fig. 2A it can be seen that a single peak with a retention volume of 16 ml is obtained for the organic material detected at 254 nm. The different freshwater samples gave very similar chromatographic peaks. The shape and retention volume of the chromatographic peak was found to be independent of the total concentration of organic material in the sample. If the sample was not matrix-matched with the mobile phase, some fine structure (or negative response if detection is done at 225 nm) was observed at the tail of the peak.

When the ionic strength of the mobile phase was increased from 0.05 to 0.4 M (0.05, 0.1, 0.2 and 0.4 M acetate buffers; pH 4.6), the retention volume increased from 14.8 to 16.9 ml. Similar results have been reported by De Haan et al. [20] for Sephadex type G gels, and by Becher et al. [21] and Berdén and Berggren [22] for TSK type SW gels. The result is in accordance with the theory [23], which predicts that the humic molecule will decrease in overall size as a result of coiling, when the ionic strength increases. However, an alternative interpretation is possible, since the increased retention volumes at higher ionic strength may be a function of adsorptive interaction between the humic substances and the stationary phase [24,25]. When deionized water was used as mobile phase, total exclusion of the organic material was observed. A similar effect has been reported by other workers [20,21,24].

The total exclusion may be a result of the large hydrodynamic volume of the humic substances in pure water, but the negative charges on the humic substances can also contribute to the exclusion.

When the pH of the mobile phase was changed from 5.4 to 4.6, and further to 3.8, the corresponding retention volumes changed from 16.2 to 15.9, and then to 15.3 ml. This result indicates that the size of the humic substances increases with decreasing pH. Ritchie and Posner [26] observed a similar effect, but other authors [27–29] have observed the opposite effect. The peak area decreased slightly with decreasing pH. Interpretation of the effect of pH on humic substances is difficult when metal ions are present [26].

For lack of suitable standards for humic substances, both globular proteins and polystyrene sulphonates were used for calibrating the column [21,22,30]. Berdén and Berggren [22] preferred polystyrene sulphonates for calibration, since they have an open structure and are polyelectrolytes. Cameron et al. [31] found that globular proteins are more compact than humic substances. A linear relationship between the retention volume and the logarithm of the molecular weight was obtained for the globular proteins (except for chymotrypsinogen A), and also for the polystyrene sulphonates (except for the 1600 dalton molecule). The retention volume of the organic material in the water samples (16 ml) was outside the range of the standards available for calibration (11.3–14.3 ml). When the molecular weight of the organic material was calculated on the basis of the extrapolated curve for the globular

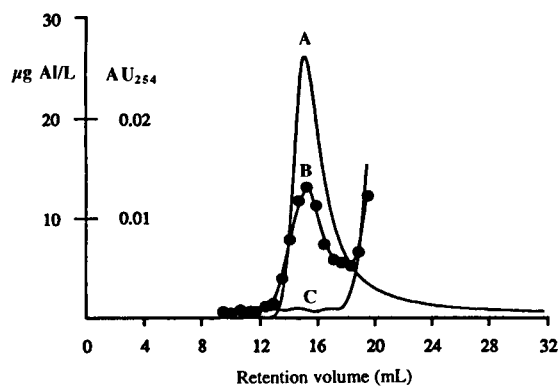


Fig. 2. Size exclusion chromatograms of a freshwater sample and a standard solution of aluminium; mobile phase 0.1 M acetate buffer, pH 4.6. (A) Freshwater, UV detection at 254 nm; (B) freshwater GFAAS detection of Al; (C) 2 mg/l Al standard solution, GFAAS detection.

proteins (omitting chymotrypsinogen A), a value of about 8000 dalton was obtained. Based on the curve for the polystyrene sulphonates (omitting the value at 1600 dalton), a molecular weight of 800 dalton was obtained. Since neither of the substances used for calibration were acceptable models for humic substances, and they also had low retention volumes, it was not possible to draw conclusions regarding the molecular weight of the humic substances from these experiments.

### 3.1. Detection of aluminium species

A typical chromatogram, obtained when aluminium was detected by GFAAS, is shown in Fig. 2B. From the figure it can be seen that aluminium is eluted as a single peak at a retention volume of 16 ml. The peak coincides with the UV peak, indicating that aluminium is associated with the organic material in the water sample. Both the retention time and peak width are the same for the UV and aluminium peaks, indicating that aluminium binds with a broad size range of humic substances. The increase in the aluminium signal at retention volumes above 18 ml is probably due to the elution of inorganic aluminium, since this part of the curve coincides with the chromatogram of an aluminium standard solution (curve C). The concentration of aluminium in the fractions collected above 20 ml are not shown in the figure, because the results were irreproducible. The aluminium which was eluted after 20 ml was probably present as inorganic polymeric (colloidal) species which might have been formed in the column, since the results for aluminium after 20 ml were irreproducible, even for a standard solution of aluminium. Gardiner et al. [12], using a Superose column, pH 3.8 acetate buffer as mobile phase and GFAAS for detection, did not observe effects similar to those described above for the detection of inorganic aluminium.

When the sample was not matrix matched with the mobile phase, an extra aluminium peak was obtained in the chromatogram for both the natural water sample and the inorganic aluminium standard solution, as can be seen from Fig. 3. This illustrates the importance of matching the sample matrix with the mobile phase, which has not always been done [12].

The aluminium species were also detected by post-column reaction with pyrocatechol violet. The PCV

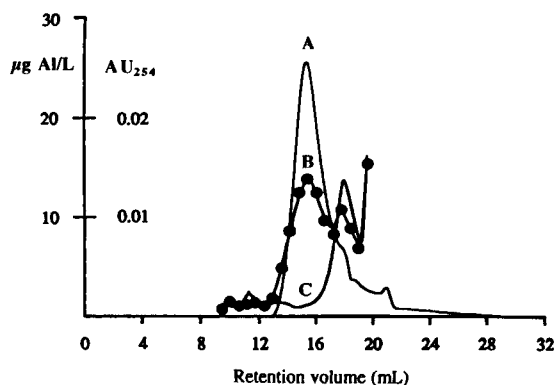


Fig. 3. Size exclusion chromatograms of a freshwater sample and a standard solution of aluminium; mobile phase 0.1 M acetate buffer, pH 4.6. (A) Freshwater, UV detection at 254 nm; (B) freshwater, GFAAS detection of Al; (C) 2 mg/l Al standard solution, GFAAS detection. The solutions were not matrix matched with the mobile phase prior to injection.

method is well established for the determination of aluminium [18,19,32,33], and the post-column procedure used was similar to that described by Røyset for flow-injection analysis [34]. With this detection system, only a single peak at a retention volume of 16 ml was obtained. The peak coincided with the UV peak, indicating that PCV reacted with organically bound aluminium. No aluminium signal was obtained at retention volumes above 18 ml; thus the aluminium species which eluted in this region did not react with PCV. When the time for reaction between aluminium and PCV was increased from 2 to 6 min, by increasing the length of the reaction coil, this had no effect on the chromatogram. Owing to the dilution (about 30 times) of the sample in the chromatographic system, the concentration of eluted aluminium was close to the detection limit of the PCV method.

## 4. Conclusions

When SEC was used for the speciation of aluminium in natural waters, a single broad peak was observed for the organic material detected at 254 nm, and also for aluminium detected by GFAAS or PCV. The retention time and peak width were the same for the UV and aluminium peaks, indicating that aluminium binds with a broad size range of humic substances. Apart from this fact, SEC does not provide much information regarding the organic aluminium species. Only organic alumin-



ium could be detected reliably. Inorganic aluminium was detected irreproducibly by GFAAS, and not at all by PCV, which may indicate the presence of polymeric (colloidal) forms of aluminium.

### Acknowledgements

The authors wish to thank Kent Easthouse for performing the initial experiments, Kjetil Kopperud for providing water samples and Prof. Hans Martin Seip for cooperation throughout the study. We also acknowledge the financial support from the Norwegian Research Council, project no. 434.88-93/005-013.

### References

- [1] H. Sigel and A. Sigel (Eds.), *Metal Ions in Biological Systems, Aluminium and Its Role in Biology*, Vol. 24, Marcel Dekker, New York, 1988.
- [2] T.E. Lewis (Ed.), *Environmental Chemistry and Toxicology of Aluminium*, Lewis Publishers, Michigan, 1989.
- [3] G. Sposito (Ed.), *The Environmental Chemistry of Aluminium*, CRC Press, Boca Raton, FL, 1989.
- [4] Workshop of Aluminium and Health, *Environ. Geochem. Health*, 12(1–2) (1990).
- [5] C.T. Driscoll and W.D. Schecher, in H. Sigel and A. Sigel (Eds.), *Metal Ions in Biological Systems, Aluminium and Its Role in Biology*, Vol. 24, Marcel Dekker, New York, 1988, p. 59.
- [6] E.M. Thurman and R.L. Malcolm, in R.F. Christman and E.T. Gjessing (Eds.), *Aquatic and Terrestrial Humic Materials*, Ann Arbor Science, Ann Arbor, MI, 1983, p. 1.
- [7] C.T. Driscoll, *Int. J. Environ. Anal. Chem.*, 16 (1984) 267.
- [8] P.R. Bloom and M.S. Erich, in G. Sposito (Ed.), *The Environmental Chemistry of Aluminium*, CRC Press, Boca Raton, FL, 1989, p. 1.
- [9] P.M. Bertsch, in S.A. Norton, S.E. Lindberg and A.L. Page (Eds.), *Acidic Precipitation*, Vol. 4, Springer, New York, 1990, p. 63.
- [10] N. Clarke, L.-G. Danielsson and A. Sparén, *Int. J. Environ. Anal. Chem.*, 48 (1992) 77.
- [11] G.L. Kerven, D.G. Edwards, C.J. Asher, P.S. Hallman and S. Kokot, *Aust. J. Soil Res.*, 27 (1989) 79.
- [12] P.E. Gardiner, R. Schierl and K. Kreutzer, *Plant Soil*, 103 (1987) 151.
- [13] S. Von Schönherr and H.-P. Frey, *Z. Anorg. Allg. Chem.*, 452 (1979) 167.
- [14] J.W. Akitt and A. Farthing, *J. Chem. Soc., Dalton Trans.*, (1981) 1606.
- [15] C. Changui, W.E.E. Stone and L. Vielvoye, *Analyst*, 115 (1990) 1177.
- [16] T. Yokoyama, C. Yamanaka and T. Tarutani, *J. Chromatogr.*, 403 (1987) 151.
- [17] A.K. Alva and M.E. Sumner, *Water Air Soil Pollut.*, 57–58 (1991) 121.
- [18] A.D. Wilson and G.A. Sergeant, *Analyst*, 88 (1962) 109.
- [19] W.K. Dougan and A.C. Wilson, *Analyst*, 99 (1974) 413.
- [20] H. De Haan, R.I. Jones and K. Salonen, *Freshwater Biol.*, 17 (1987) 453.
- [21] G. Becher, G.E. Carlberg, E.T. Gjessing, J.K. Hongslo and S. Monarca, *Environ. Sci. Technol.*, 19 (1985) 422.
- [22] M. Berdén and D. Berggren, *J. Soil Sci.*, 41 (1990) 61.
- [23] K. Ghosh and M. Schnitzer, *Soil Sci.*, 129 (1980) 266.
- [24] A.M. Posner, *Nature*, 198 (1963) 1161.
- [25] R.M. Town and H.K.J. Powell, *Anal. Chim. Acta*, 256 (1992) 81.
- [26] G.S.P. Ritchie and A.M. Posner, *J. Soil Sci.*, 33 (1982) 233.
- [27] E.T. Gjessing, *Physical and Chemical Characteristics of Aquatic Humus*, Ann Arbor Science, Ann Arbor, MI, 1976, p. 52.
- [28] B. Kriebek, J. Kaigl and V. Ornzinsky, *Chem. Geol.*, 19 (1977) 73.
- [29] J. John, B. Salbu, E.T. Gjessing and H.E. Bjørnstad, *Water Res.*, 22 (1988) 1381.
- [30] H.E. Evans, R.D. Evans and S.M. Lingard, *Sci. Total Environ.*, 81/82 (1989) 297.
- [31] R.S. Cameron, R.S. Swift, B.K. Thornton and A.M. Posner, *J. Soil Sci.*, 23 (1972) 342.
- [32] H.M. Seip, L. Müller and A. Naas, *Water, Air, Soil Pollut.*, 23 (1984) 81.
- [33] T.J. Sullivan, H.M. Seip and I.P. Muniz, *Int. J. Environ. Anal. Chem.*, 26 (1986) 61.
- [34] O. Røyset, *Anal. Chim. Acta*, 185 (1986) 75.

# Assessing chromatographic peak purity using condition index and singular value evolving profiles

Gregory A. Bakken, John H. Kalivas \*

*Department of Chemistry, Idaho State University, Pocatello, ID 83209, USA*

Received 3 August 1994

---

## Abstract

A new method for determining chromatographic peak purity is presented. The method uses condition index evolving profiles (CIEPs) and singular value evolving profiles (SVEPs). To produce a CIEP or a SVEP, singular value decompositions are performed on data matrices containing the analyte's pure-component spectrum and sample spectra as they evolve over a chromatographic time profile. Visual inspection of condition indices and singular values as they evolve over time enables detection of less than 0.5% of a spectrally similar impurity with no chromatographic resolution ( $R_s = 0$ ). Additionally, the CIEPs and SVEPs allow estimation of chromatographic pure regions. This method represents an extension of CIEPs which have been used in successful library searches of multicomponent mixtures based on gas chromatography–Fourier transform infrared spectra and liquid chromatography–UV–visible spectra.

*Keywords:* Chromatography; Peak purity; Condition index evolving profiles; Singular value evolving profiles

---

## 1. Introduction

Determining the purity of chromatographic peaks denotes a difficult problem, especially in pharmaceutical research. In a worst case scenario, trace amounts of a spectrally similar impurity, e.g., an isomer, at low chromatographic resolution must be detectable. One commonly used technique for impurity detection is liquid chromatography coupled to an UV–visible diode-array detector. This technique generates a spectrochromatogram, i.e., a matrix with columns representing spectra and rows representing chromatograms. Once a spectrochromatogram has been obtained, various mathematical procedures are available to assess chromatographic peak purity [1–14]. The graphical procedure described in this paper accom-

plishes impurity detection with  $R_s = 0$  as demonstrated using simulated situations. An impurity whose presence has been established can then be identified by computer-oriented methods or through laboratory work.

The method described in this paper makes use of the graphical library searching algorithm developed in our laboratory based on condition index evolving profiles (CIEPs) [15,16]. In the next section, the CIEP process is briefly described as it pertains to impurity detection. The next section also defines a new graphical approach to chromatographic purity determination based on singular value evolving profiles (SVEPs). Following these discussions, the paper describes results of CIEPs and SVEPs for impurity detection using spectrochromatograms composed of simulated chromatographic situations and real UV spectra. For the first phase of

---

\* Corresponding author.

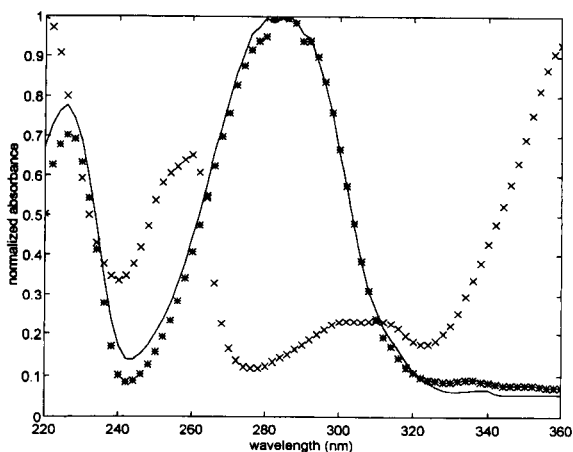


Fig. 1. Spectra of (★) 4-hydroxyacetophenone, (—) 4-hydroxybutyrophenone and (×) 3-carbomethoxy-7-methyl-4-pyrido[1,2-a]pyrimidinone.

evaluation reported here, simulated data is used in order to carefully control the degree of chromatographic resolution. Spectrally similar isomers 4-hydroxyacetophenone and 4-hydroxybutyrophenone and a spectrally dissimilar compound are used in the simulations (see Fig. 1).

When co-eluting components are present in the sample, the CIEP and SVEPs obtained depend on the degrees of chromatographic resolutions, concentration levels of co-eluting components, and spectral similarities [15,16]. This study is only concerned with detection of impurities where the resolution is poor or non-existent and sample chromatograms appear pure. The authors deem this as worst case scenario. Trends described are general and applicable to other more obvious circumstances.

## 2. CIEP and SVEP

In order for a CIEP or a SVEP to operate, a  $p \times t$  data matrix  $\mathbf{D}$  must be available where  $p$  denotes the number of wavelengths and  $t$  represents time. This type of data matrix is typically termed a spectrochromatogram because  $\mathbf{D}$  contains both spectroscopic and chromatographic data. That is, columns are spectra measured at respective time increments (time slice) and rows are chromatograms measured at respective wavelengths (wavelength slice).

The first step in evaluating  $\mathbf{D}$  for impurities is to normalize each spectrum in  $\mathbf{D}$  to a vector length of one.

A series of singular value decompositions (SVDs) are then performed on respective  $p \times 2$  data matrices  $\mathbf{L}$  composed of the analyte's pure-component spectrum in column 1 (also normalized to a vector length of one) and successive spectra from  $\mathbf{D}$  in column 2. The analyte is the major component forming the chromatographic peak. Executing an SVD on an  $\mathbf{L}$  results in  $\mathbf{L} = \mathbf{U}\mathbf{S}\mathbf{V}'$  where  $\mathbf{U}$  symbolizes the  $p \times 2$  matrix of eigenvectors for  $\mathbf{L}\mathbf{L}'$ ,  $\mathbf{V}$  denotes the  $2 \times 2$  matrix of eigenvectors for  $\mathbf{L}'\mathbf{L}$ , and  $\mathbf{S}$  signifies the  $2 \times 2$  diagonal matrix with non-negative diagonal singular values  $\sigma_1$  and  $\sigma_2$  ( $\sigma_1 \geq \sigma_2$ ). Two condition indices,  $\eta_1$  and  $\eta_2$ , can be generated where  $\eta_i = \sigma_{\max} / \sigma_i$ ,  $i = 1, 2$ . The largest condition index  $\eta_2$  corresponds to the condition number of  $\mathbf{L}$ .

A CIEP is produced by plotting time versus all  $\eta_2$  values computed for each  $\mathbf{L}$  formed sequentially by replacing the second column of  $\mathbf{L}$  with spectra from  $\mathbf{D}$ . If no impurities are present, the CIEP should approximately trace out where the pure-component elutes and have a distinct shape. This forms the basis of spectral library searching with a CIEP [15,16]. When other co-eluting components are present in the sample, a CIEP is still able to identify the analyte as present. The CIEP obtained depends on the degrees of chromatographic resolutions, concentration levels of co-eluting components, and spectral similarities. This paper addresses the situation where co-eluting components may only be present at trace levels. It will be shown that significant deviations from a pure-component CIEP indicate that the spectrochromatogram is not pure. The Results and discussion section describes the deviations.

Two SVEPs can be formed for each CIEP, one for the first singular value (SVEP1) and another for the second singular value (SVEP2). The SVEP for the first singular value is a plot of time versus each  $\sigma_1$  obtained during the SVDs performed on  $\mathbf{L}$ . Similarly, the SVEP for the second singular value is a plot of time versus  $\sigma_2$ . If the spectrochromatogram consists of a pure-component, SVEP1 will approximately trace out the chromatographic profile for that component while SVEP2 traces the inverse. As with a CIEP, respective SVEPs depend on the degrees of chromatographic resolutions, concentration levels of co-eluting impurities, and spectral similarities. Significant deviations from pure-component SVEPs indicate that the spectrochromatogram is not pure. The Results and discussion section describes the deviations.

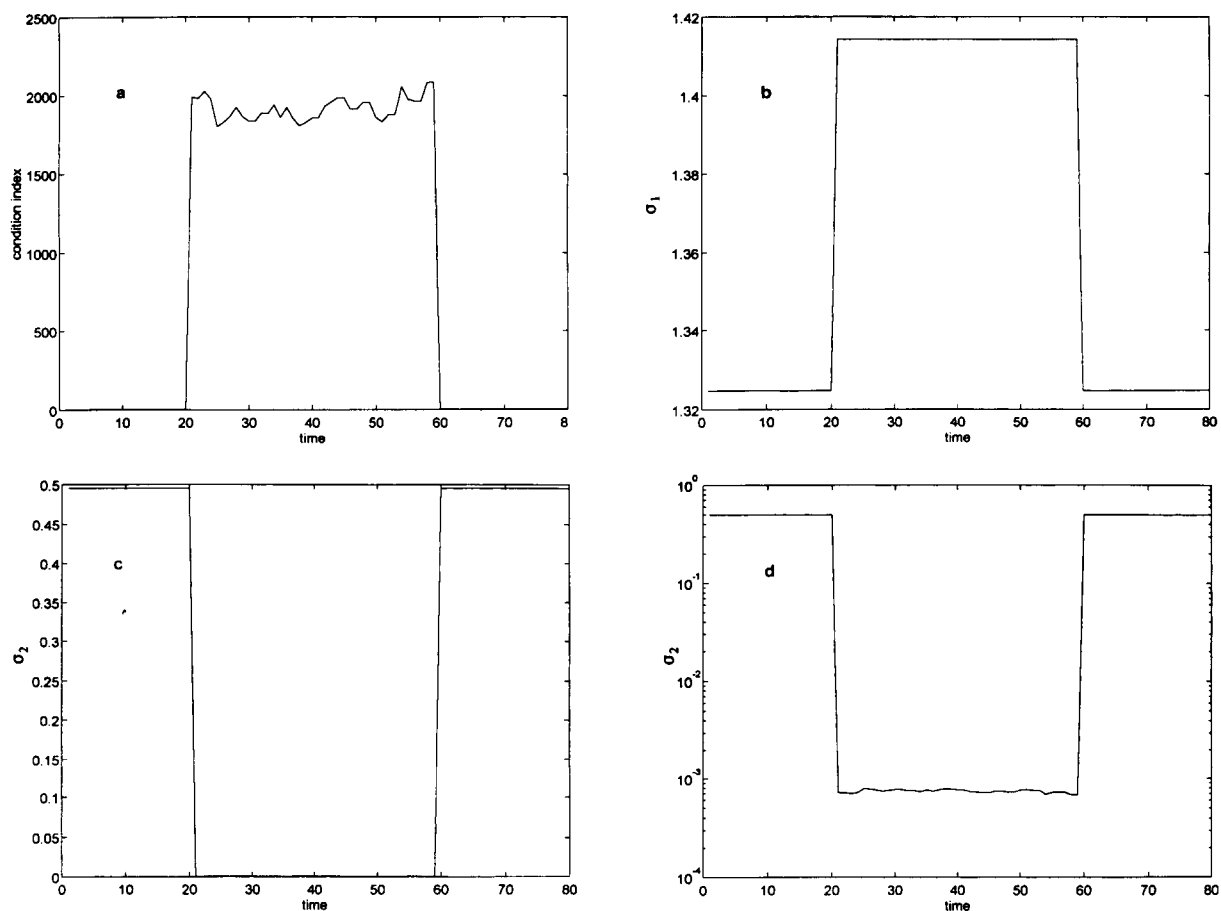


Fig. 2. (a) CIEP for a pure-component sample containing 4-hydroxyacetophenone using 0.1% noise. (b) SVEP for the largest singular value  $\sigma_1$ . (c) SVEP for the smallest singular value  $\sigma_2$ . (d) Logarithmic plot of  $\sigma_2$ .

Both a CIEP and SVEPs can be visually inspected to determine the presence of impurities. While a CIEP is a good indicator, it will be demonstrated that SVEP2 enhances the technique by providing more clarity. This paper presents limits of detection found by visual inspection of CIEPs and SVEPs for various situations.

### 3. Experimental

Chromatographic peaks were simulated using Gaussian curves. Two components with similar spectra were used and their spectra are shown in Fig. 1. The analyte was 4-hydroxyacetophenone while the impurity was the isomer 4-hydroxybutyrophenone. In other situations, the spectrally dissimilar component 3-carbethoxy-7-methyl-4-pyrido[1,2-*a*]pyrimidinone acted as

an impurity. Eighty time units were used. The chromatogram of the analyte was always centered at  $t = 40$  with a standard deviation equal to 4 time units producing a peak width of 16 time units. Peak widths and centers of impurity chromatograms were varied in order to observe the influence of chromatographic resolution on impurity detection. Impurity peak width and center values are noted in the Results and discussion section. Resolution was defined as  $R_s = 2\Delta t / (W_a + W_b)$  where  $\Delta t$  represents the distance between chromatographic maxima and  $W_a$  and  $W_b$  signify respective peak widths. All spectrochromatograms were set to a baseline of  $1 \times 10^{-5}$  if values were less than this.

A noise-free matrix  $\mathbf{D}^*$  representing a noise-free simulated spectrochromatogram is created using  $\mathbf{D}^* = \mathbf{RC}$  where  $\mathbf{R}$  denotes the  $p \times n$  matrix containing pure-component spectra of the analyte and  $n - 1$  impu-

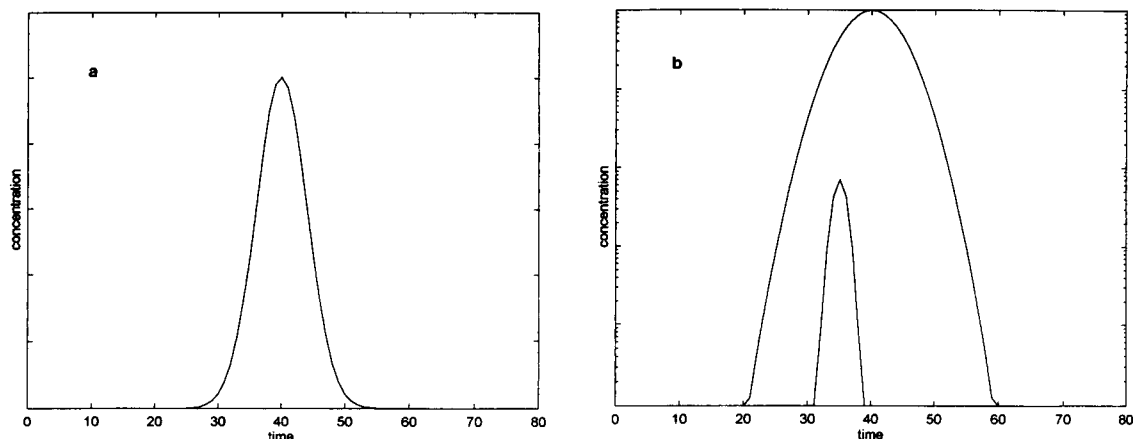


Fig. 3. (a) Sample chromatogram of a two-component sample with 0.7% impurity,  $R_s = 0.5$ , and 0.1% noise. 4-hydroxyacetophenone is the analyte ( $t = 40$ ) and 4-hydroxybutyrophenone is the impurity ( $t = 35$ ). (b) Logarithmic plots of pure-component chromatograms composing the sample chromatogram.

rities normalized to unit concentration and  $\mathbf{C}$  represents the  $n \times t$  matrix containing chromatograms of the analyte and impurities. Noise proportional to each signal in the noise-free spectrochromatogram was added to each respective signal to form a spectrochromatogram,  $\mathbf{D}$ , containing noise. Spectra from  $\mathbf{D}$  were sequentially placed in column 2 of matrix  $\mathbf{L}$  while the pure-component spectrum of the analyte was always placed in column 1. All spectra in  $\mathbf{L}$  are normalized to a vector length of one. Singular value decompositions are performed on these  $\mathbf{L}$  matrices producing respective condition indices and singular values. Percent impurity and resolution were varied to find limits of detection at predetermined noise levels. All simulations and data analyses were performed on IBM/AT compatible computers using built-in functions of MATLAB 4.0 (The MathWorks, Natick, MA).

#### 4. Results and discussion

If no impurities co-elute with the analyte, the CIEP, SVEP1, and SVEP2 for a pure-component spectrochromatogram should approximately trace out where the pure-component elutes (see Fig. 2). Condition indices prior to and after a pure-component elutes are relatively small. In these regions,  $\mathbf{L}$  contains the pure-component spectrum in column 1 and baseline noise in column 2 and two appropriately sized non-zero singular values are computed (see Figs. 2b and 2c). Thus,  $\mathbf{L}$  is essentially well-conditioned and has rank 2,

i.e., the chemical rank is 1 but the mathematical rank is 2. The condition index dramatically increases when the pure-component begins to elute. This stems from the fact that the collinearity between the two columns of  $\mathbf{L}$  causes one singular value to be large and the other singular value to be small. Random noise present in the two collinear spectra keep  $\mathbf{L}$  from being singular and rank 1. The noise appearing in the CIEP illustrated in Fig. 2a primarily stems from the small random variation in  $\sigma_2$ . Fig. 2d shows SVEP2 using a logarithmic plot and exhibits the random nature of  $\sigma_2$  due to noise in the spectrochromatogram. Thus, when the ratios  $\sigma_1/\sigma_2$  are computed, the small random variations appear in the CIEP shown in Fig. 2a.

Displayed in Fig. 3 are the sample chromatogram and logarithmic plots of the analyte and impurity chromatograms using a peak center of  $t = 35$  for the impurity. The peak width for the impurity is 4 time units resulting in a resolution value of 0.5. The investigated situation used 4-hydroxyacetophenone as the analyte and isomer 4-hydroxybutyrophenone as the impurity present at a 0.7% level relative to the analyte. A 0.1% noise level was added to the simulated spectrochromatogram. Comparing the CIEPs and SVEPs shown in Fig. 4 to those in Fig. 2 for a pure-component, significant deviations become apparent in the CIEP and SVEP2. The SVEP1 in Fig. 4b appears to show no significant deviations and hence, is unable to serve as an indicator for detection of impurities at trace levels. Consequently, this paper only concentrates on the CIEP and SVEP2 for impurity detection. Visual inspection

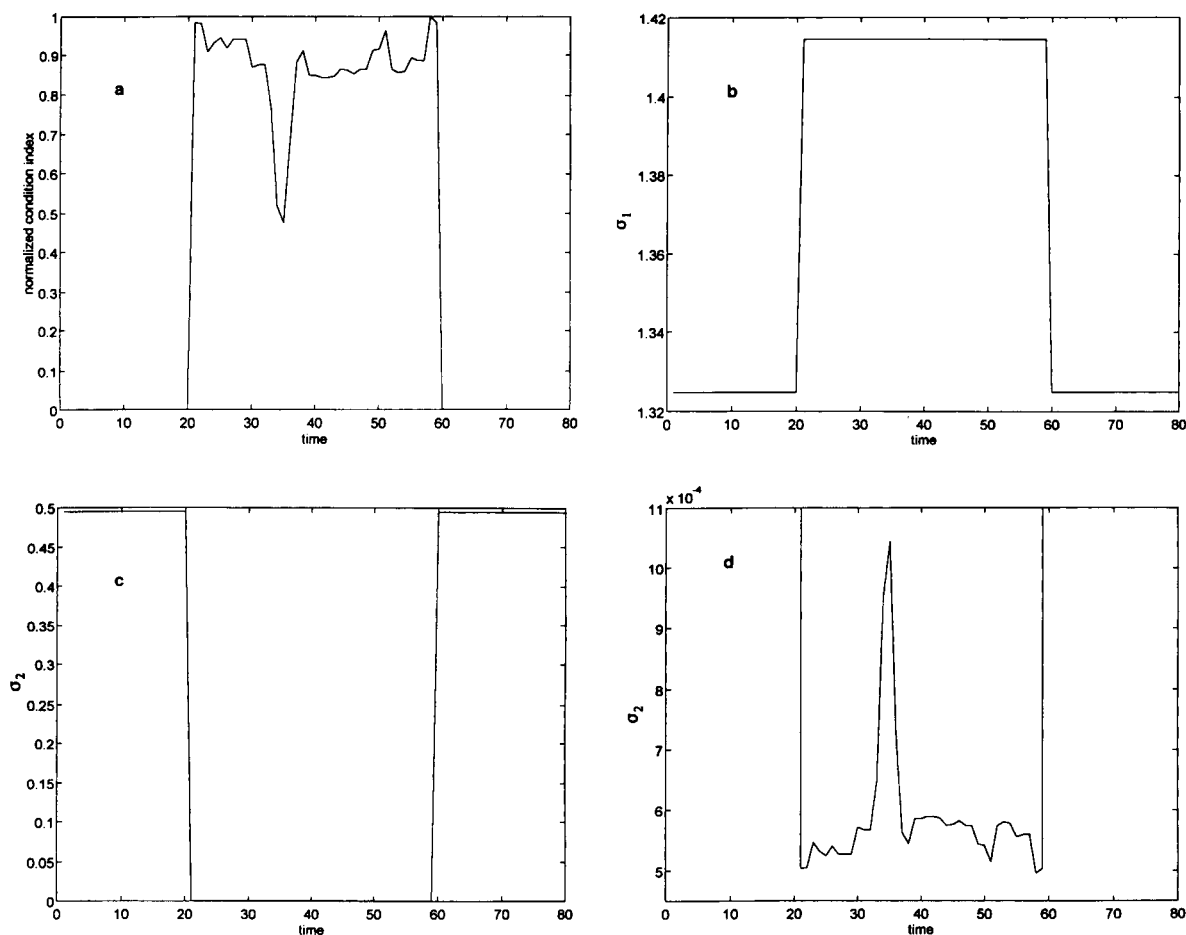


Fig. 4. (a) CIEP for the situation pictured in Fig. 3 (analyte 4-hydroxyacetophenone, impurity 4-hydroxybutyrophenone 0.7%, and  $R_s = 0.5$ ). (b) SVEP for the largest singular value  $\sigma_1$ . (c) SVEP for the smallest singular value  $\sigma_2$ . (d) Expanded y-axis of the SVEP2 from Fig. 4c.

of the CIEP and SVEP2 will be used to determine whether or not an impurity is present.

The large downward spike at  $t = 35$  in the CIEP plot in Fig. 4a indicates a sudden change in the ratio of singular values and the presence of an impurity. Confirmation can be obtained by inspecting the corresponding SVEP2 plot. The SVEP2 plot displayed in Fig. 4c does not indicate the presence of an impurity. However, expanding the y-axis (see Fig. 4d) reveals a sharp increase in the second singular value at  $t = 35$  implying that an impurity does indeed exist in the sample. The other small peaks in this plot result from random noise. It is interesting to note that the smallest singular values  $\sigma_2$  trace out the chromatographic profile of the impurity. Provided the impurity is completely contained

within the analyte chromatogram, this observation occurs consistently regardless of the resolution. The second singular value increases when the impurity begins to elute because  $\mathbf{L}$  now contains two components. The increase in  $\sigma_2$  indicates that  $\mathbf{L}$  is further away from being a rank 1 matrix. That is, the size of the smallest singular value for a matrix, in this case  $\sigma_2$ , quantitates the distance the matrix is from being full rank minus 1 [17]. As the impurity decreases in concentration, the second singular value decreases as well implying that  $\mathbf{L}$  is becoming closer to a rank 1 matrix again.

Limits of detection were obtained for several situations using visual inspection of the CIEPs and SVEP2s and are shown in Fig. 5. These limits were obtained

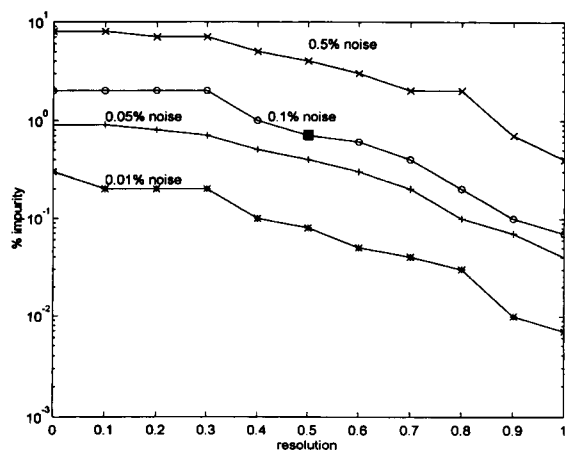


Fig. 5. Limits of detection obtained with 4-hydroxyacetophenone as analyte and 4-hydroxybutyrophenone as the impurity. ■ Indicates the situation shown in Fig. 3.

using 4-hydroxyacetophenone as the analyte and 4-hydroxybutyrophenone as the impurity with a chromatographic peak width of 4 time units. Each line defines a different noise level with impurity detection being above a line. From Fig. 5, it can be concluded that the greater the degree of chromatographic resolution, the lower the concentration level which can be detected for a specific noise level. For the situation previously described in Fig. 3, a solid square box has been placed on Fig. 5 to indicate the position of the simulation. As can be seen, the solid square box is in the detection region above the 0.1% noise line and the impurity is detectable.

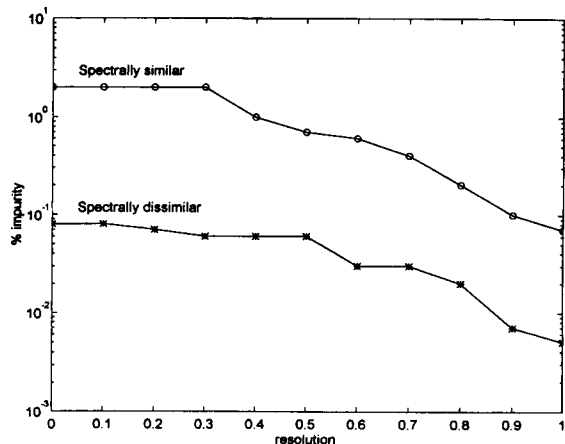


Fig. 6. Limits of detection using 0.1% noise with 4-hydroxyacetophenone as analyte and (O) 4-hydroxybutyrophenone as impurity, and (★) 3-carbethoxy-7-methyl-4-pyrido[1,2-*a*]pyrimidinone as the impurity.

Spectrally dissimilar impurities can also be detected using the described procedure. Fig. 6 shows detection limits obtained using 4-hydroxyacetophenone as the analyte and 4-hydroxybutyrophenone as the impurity and limits obtained using 4-hydroxyacetophenone as the analyte and 3-carbethoxy-7-methyl-4-pyrido[1,2-*a*]pyrimidinone as the impurity. Both situations involve a 0.1% noise level and impurity chromatographic peak widths of 4 time units. As expected, the limits of detection for spectrally dissimilar components are lower than those for spectrally similar components at the same noise level. The lowest amount of a spectrally dissimilar impurity detectable at specific  $R_s$  values depends on the degree of spectral dissimilarity. The greater the dissimilarity between the analyte and impurity, the lower the detection limit for the impurity.

Another situation studied used 4-hydroxyacetophenone as the analyte and the isomer 4-hydroxybutyrophenone as a 2.0% impurity with a peak width of 15.5 time units and  $R_s = 0$ . This study was performed to investigate what happens when  $R_s = 0$  and the impurity chromatographic peak width approaches that of the analyte. Fig. 7a shows logarithmic plots for the analyte and impurity chromatograms with chromatographic centers of  $t = 40$  for both the analyte and impurity. The sample chromatogram appears as a pure sample similar to that shown in Fig. 3a. A 0.1% noise level was added to the spectrochromatogram. As shown in Figs. 7b and 7c, detection under these conditions is difficult. However, even under these circumstances, the CIEP still contains a broad downward peak at  $t = 39$ . Likewise, the SVEP2 contains the indicative upward broad peak at  $t = 39$ . Using visual inspection of CIEPs and SVEP2s for several situations, Fig. 8 displays limits of detection obtainable as a function of the impurity chromatographic peak width. Noise was added at the 0.1% level. As expected, lower detection limits exist for an impurity spectrally dissimilar to the analyte. The detection limits start to significantly decrease once the impurity begins to maintain a peak width greater than the analyte peak width (16 time units in this case). This results from the fact that the impurity is no longer embedded in the analyte chromatographic peak and a chromatographic pure region for the impurity now exists. The influence of chromatographic pure regions for an impurity on CIEPs and SVEP2s is described next.

Pictured in Fig. 9a are the logarithmic plots for the analyte and impurity chromatograms when the predic-

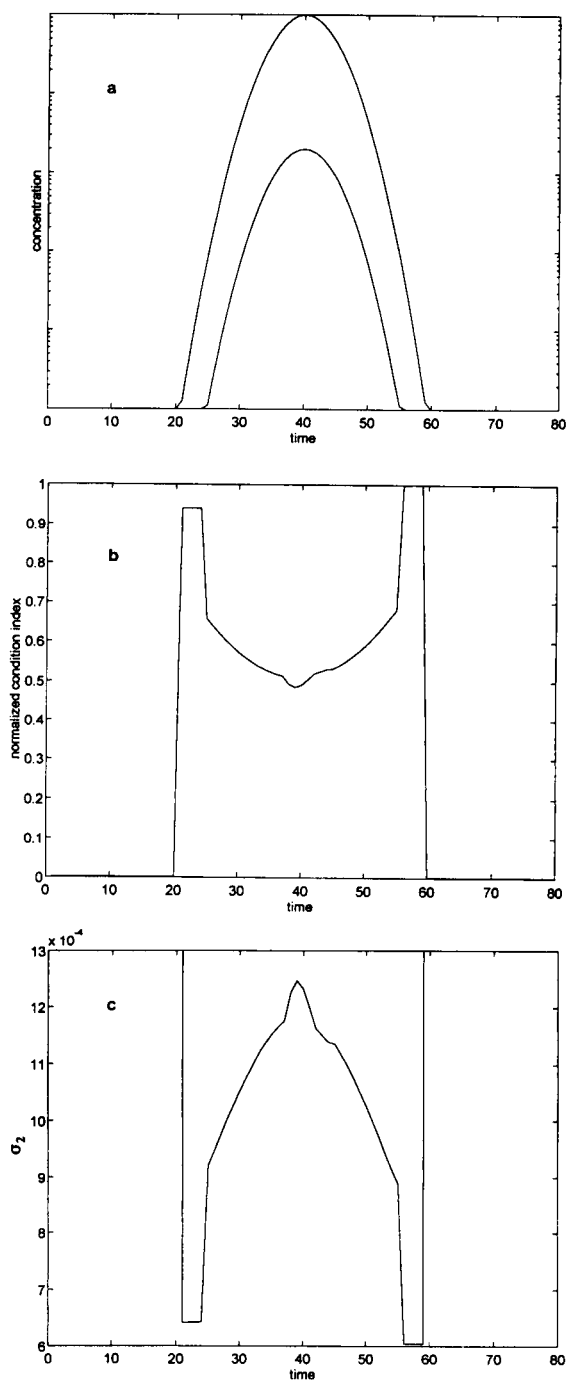


Fig. 7. (a) Logarithmic plots of pure-component chromatograms composing the sample chromatogram with 2% impurity,  $R_s = 0$ , and 0.1% noise. 4-Hydroxyacetophenone is the analyte and 4-hydroxybutyrophenone is the impurity. (b) CIEP. (c) SVEP2 with an expanded y-axis.

ament consists of an impurity chromatographic peak not embedded in the analyte peak, but rather only partially overlapped by the analyte peak. The sample chromatogram appears as a pure sample similar to that shown in Fig. 3a. Component 4-hydroxyacetophenone represents the analyte and the spectrally similar isomer 4-hydroxybutyrophenone denotes the impurity present at a 0.1% level with a chromatographic center of  $t = 24$ . The impurity chromatographic peak width is 8 time units producing a  $R_s = 1.33$ . A 0.1% noise level was added to the spectrochromatogram. The CIEP and SVEP2 shown in Figs. 9b and 9c show different trends than when the impurity chromatographic peak is embedded in the analyte peak. When compared to the CIEP and SVEP2 patterns for a pure-component shown in Fig. 2, a significant difference can be observed. In particular, the SVEP2 plot shows a level region and then a drop-off confirming that indeed, an impurity exists in the sample.

The CIEP and SVEP2 techniques are also able to detect multiple impurities. Fig. 10a contains logarithmic plots of analyte and impurity chromatograms for a situation with two impurities present. As before, the sample chromatogram appears as a pure sample similar to that shown in Fig. 3a. The analyte is 4-hydroxyacetophenone while the component 4-hydroxybutyrophenone is present as a 0.05% impurity in addition to 3-carbethoxy-7-methyl-4-pyrido[1,2-*a*]pyrimidinone

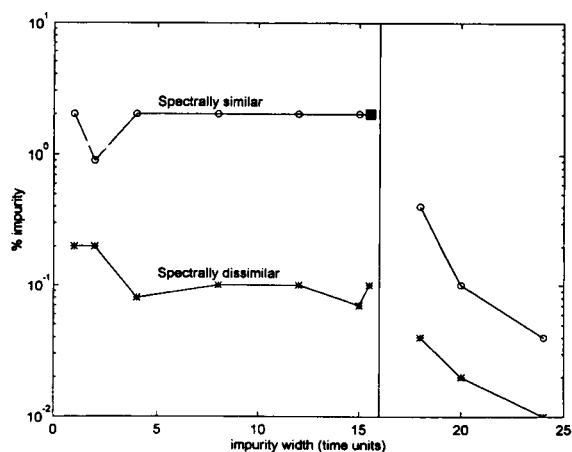


Fig. 8. Limits of detection using 0.1% noise,  $R_s = 0$ , with 4-hydroxyacetophenone as analyte with a chromatographic peak bandwidth of 16 time units, and varying impurity peak widths. (○) 4-Hydroxybutyrophenone as impurity, and (★) 3-carbethoxy-7-methyl-4-pyrido[1,2-*a*]pyrimidinone as the impurity. ■ Indicates the situation in Fig. 7.



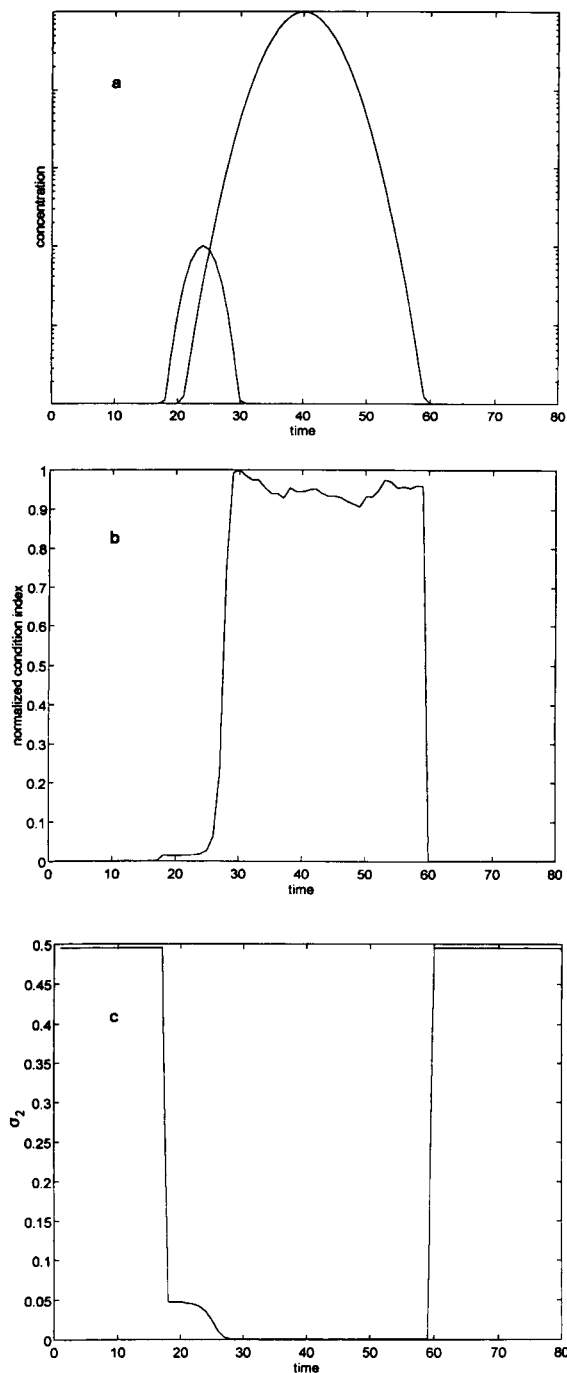


Fig. 9. (a) Logarithmic plots of pure-component chromatograms composing the sample chromatogram with 0.1% impurity,  $R_s = 1.33$ , and 0.1% noise. 4-Hydroxyacetophenone is the analyte and 4-hydroxybutyphenone is the impurity. (b) CIEP. (c) SVEP2.

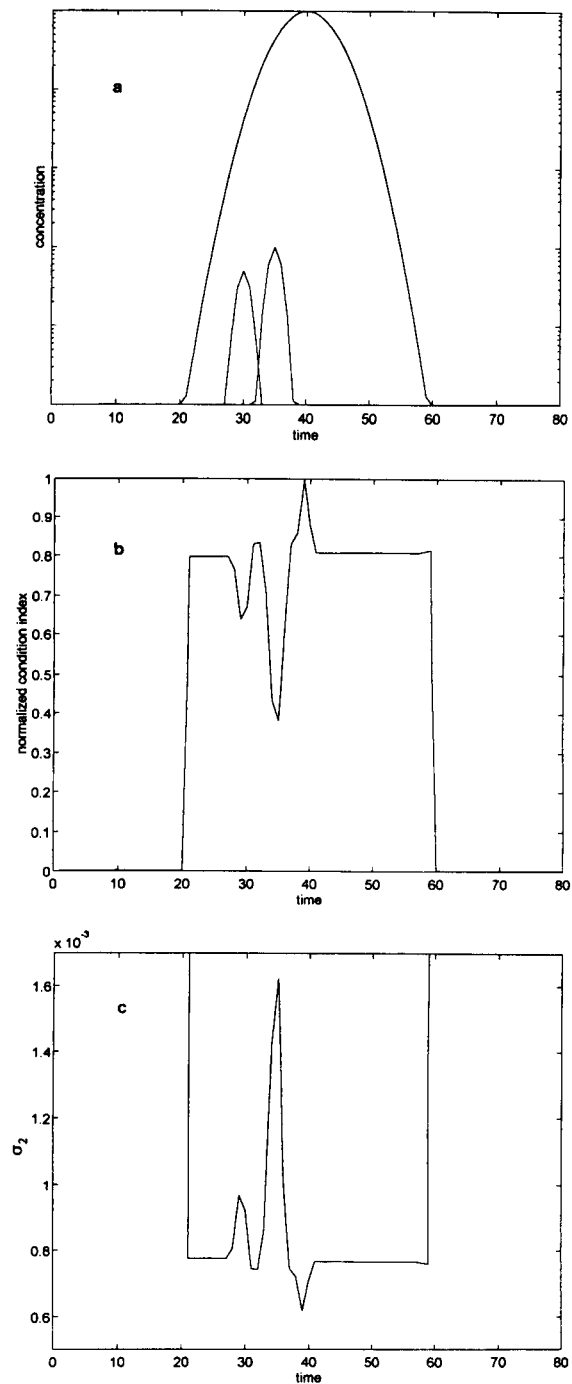


Fig. 10. (a) Logarithmic plots of pure-component chromatograms composing the sample chromatogram with 4-hydroxyacetophenone as the analyte in conjunction with 0.05% impurity 4-hydroxybutyphenone (chromatographic center  $t = 30$ ) and 0.1% impurity 3-carbethoxy-7-methyl-4-pyrido[1,2-*a*]pyrimidinone (chromatographic center  $t = 35$ ) with 0.1% noise. See text for description of  $R_s$  values. (b) CIEP. (c) SVEP2 with an expanded y-axis.

as a 0.1% impurity. Chromatographic peak centers in Fig. 10a for the impurities correspond to  $t=30$  and  $t=35$  respectively. Each impurity has a peak width of 4 time units and the spectrochromatographic noise level was 0.1%. Resolution between the analyte and 4-hydroxybutyrophenone was  $R_s=1$ , while  $R_s=0.5$  for the analyte and 3-carbethoxy-7-methyl-4-pyrido[1,2-*a*]pyrimidinone. Resolution can also be calculated between the two impurities, giving a value of 1.25 for this situation. Figs. 10b and 10c show the corresponding CIEP and SVEP2. Although the situation described is not an extreme case, it clearly demonstrates that multiple impurities can be detected. Two well-defined peaks manifest at  $t=29$  and  $t=35$  in the CIEP and SVEP2 plots. Each peak indicates the presence of an impurity and traces the elution profiles used to generate the sample spectrochromatogram.

If two or more impurities are present and they all elute with  $R_s=0$  relative to the analyte, the total concentration level detectable would depend on the degrees of spectral dissimilarity between impurities and between the impurities and analyte.

In summary, the performance of CIEPs and SVEPs demonstrated in this paper supports the concept that they can be used as methods for testing chromatographic peak purity provided the analyte's pure-component spectrum is known. The method was tested on simulated liquid chromatography, but it represents a general approach and should be applicable to other chromatographic methods such as gas and ion chromatography. Additionally, the results of this simulated study indicate that CIEPs and SVEPs can be used to provide information on chromatographic pure regions. The process of impurity detection and determination of chromatographic pure regions are currently under further investigation using actual situations previously described [4].

## Acknowledgements

The work described was supported by NSF-Idaho EPSCoR Program and by National Science Foundation grant number OSR-9350539.

## References

- [1] A.F. Fell, H.P. Scott, R. Gill and A.C. Moffat, *J. Chromatogr.*, 282 (1983) 123.
- [2] J.G.D. Marr, G.G.R. Seaton, B.J. Clark and A.F. Fell, *J. Chromatogr.*, 506 (1990) 289.
- [3] H.R. Keller and D.L. Massart, *Anal. Chim. Acta*, 263 (1992) 21.
- [4] H.R. Keller, D.L. Massart and J.O. De Beer, *Anal. Chem.*, 65 (1993) 471.
- [5] H.R. Keller and D.L. Massart, *Anal. Chim. Acta*, 246 (1991) 379.
- [6] H.R. Keller, D.L. Massart, Y.Z. Liang and O.M. Kvalheim, *Anal. Chim. Acta*, 263 (1992) 29.
- [7] Y.Z. Liang and O.M. Kvalheim, *Anal. Chim. Acta*, 276 (1993) 425.
- [8] S.J. Vanslyke and P.D. Wentzell, *Anal. Chem.*, 63 (1991) 2512.
- [9] S.J. Vanslyke and P.D. Wentzell, *Chemom. Intell. Lab. Syst.*, 20 (1993) 183.
- [10] P.J. Gemperline and J.C. Hamilton, *Anal. Chem.*, 61 (1989) 2240.
- [11] S. Ebel and W. Mueck, *Chromatographia*, 25 (1988) 1075.
- [12] T.P. Bridge, M.H. Williams and A.F. Fell, *J. Chromatogr.*, 465 (1989) 59.
- [13] R.E. Synovec, E.L. Johnson, T.J. Bahowick and A.W. Sulya, *Anal. Chem.*, 62 (1990) 1597.
- [14] T.J. Bahowick and R.E. Synovec, *Anal. Chem.*, 64 (1992) 489.
- [15] T.D. Jarvis and J.H. Kalivas, *Anal. Chim. Acta*, 266 (1992) 13.
- [16] T.D. Jarvis and J.H. Kalivas, *Anal. Chim. Acta*, 272 (1993) 53.
- [17] J.H. Kalivas and P.M. Lang, *Mathematical Analysis of Spectral Orthogonality*, Marcel Dekker, New York, 1994.



ELSEVIER

Analytica Chimica Acta 300 (1995) 183–191

ANALYTICA  
CHIMICA  
ACTA

# Indirect conductimetric detection of amino acids after liquid chromatographic separation

Oi-Wah Lau \*, Chuen-Shing Mok

*Department of Chemistry, The Chinese University of Hong Kong, Shatin, Hong Kong*

Received 12 January 1994; revised manuscript received 21 June 1994

## Abstract

A liquid chromatographic method using indirect conductimetric detection is proposed for the determination of low levels of organic compounds, which does not require any special functional characteristics of the analyte. The signal detected is proportional to the molar concentration of the analyte and independent of its nature. The detector response is linearly dependent on analyte concentrations over at least three orders of magnitude. The basis of the detection is to create a conducting background, which will decrease on elution of the organic compounds. The theory of the method is discussed, with special reference to the quantitative displacement of the conducting species of the mobile phase from the column by the analyte on sample injection. The proposed method has been applied to study the chromatographic behaviour of twenty-one amino acids, where a 5- $\mu\text{m}$  Econosil CN column was used as the stationary phase with a mixture of water–acetonitrile–tetrahydrofuran (70:20:3) containing 1 mM perchloric acid or trichloroacetic acid as the mobile phase. The proposed method allows as little as 10 ng of each amino acid to be determined.

*Keywords:* Liquid chromatography; Conductimetry; Amino acids

## 1. Introduction

Amino acids exist in the dipolar ion form both in aqueous solution and in solid crystals [1]. They can form cations or anions with the change in pH and this enables them to be separated by either cation or anion exchange columns.

The traditional method for the separation and determination of amino acids employs an automatic amino acid analyser involving ion-exchange liquid chromatography with post-column derivatization using either ninhydrin [2], fluorescamine [3] or *o*-phthalaldehyde [4]. They have also been determined by thin-layer chromatography [5], however, the method is not precise.

Gas chromatography (GC) has also been employed for the determination of amino acids [6], but all the GC methods require derivatization of amino acids before measurements and are technically tedious. Liquid chromatography (LC) is currently the commonest method of analysis. However, most LC procedures for amino acids also require pre-column [8–10] or post-column [11–13] derivatization to enable detection at low levels by spectrophotometry or spectrofluorimetry.

The derivatization methods, though sensitive, suffer from the drawback that the procedures are tedious and that the analyte measured needs to react in a quantitative manner with the reagents concerned. Further, some amino acids, e.g. proline and hydroxyproline, which are secondary amines, do not react with the fluorescent agents fluorescamine and *o*-phthalaldehyde, and it is necessary to oxidize them prior to detection [14].

\* Corresponding author.

Though the refractive index detectors can detect amino acids directly without derivatization, they are less sensitive compared with UV or fluorescence detection after derivatization.

Conductimetric detection in LC was developed since the introduction of ion chromatography by Small et al [15]. This mode of detection has been used for the detection of ionizable species. The method has been applied to the detection of organic compounds after the formation of ionic derivatives [16–18].

Our recent investigation shows that indirect conductimetric detection is a sensitive method for the determination of amino acids after LC separation. The present work describes the application of this technique to determine amino acids after LC separation, where no derivatization of the amino acids is required. The theory and factors affecting detector response of this method of detection will be discussed.

## 2. Experimental

### 2.1. Apparatus

The LC system consisted of a Beckman 110B solvent delivery pump with an Alltech Free-Flow pulse dampener, a Wescan Model 21511001 conductivity detector with a Model 24020001 temperature controller and Model 26650051 column compartment, a Rheodyne injection valve with a 20- $\mu$ l sample loop, and a Beckman 427 signal integrator. An analytical column from Alltech, 5- $\mu$ m Econosil CN (250 mm  $\times$  4.6 mm i.d.) cartridge, was used. Instrumental settings were: mobile phase flow rate, 1 ml/min; column temperature, 30°C; detector zero suppression (coarse), 2; detector range, 1 or 10; and chart speed, 0.5 cm/min.

Peaks were detected as negative changes in conductance, and the detector–integrator connections were reversed in polarity to give a positive display of peaks on the integrator.

### 2.2. Reagents

HPLC grade solvents were used to prepare the mobile phase. Mobile phases were degassed by shaking in an ultrasonic bath for 30 min before use. All other chemicals were of analytical reagent grade. Water used

was distilled, and deionized by passing through a Millipore Milli-Q 50 ultra pure water system.

### 2.3. Standard solutions

Amino acids (from Pierce, amino acids standard kit) were used as received. Standard solutions were prepared fresh daily by dissolving the amino acids in and diluting them with the mobile phase to the required concentrations, unless otherwise specified.

### 2.4. Procedure

The standard solutions were injected directly into the chromatograph. The following mobile phases were used to study the chromatographic behaviour of the amino acids. (A) Water–acetonitrile–tetrahydrofuran (77:20:3, v/v) containing 0.5, 1.0, 1.5 or 2.0 mM HClO<sub>4</sub>; and (B) water–acetonitrile–tetrahydrofuran (77:20:3, v/v) containing 0.5, 1.0, 1.5 or 2.0 mM CCl<sub>3</sub>COOH. (*Warning*: perchloric acid should be diluted with water before mixing with the organic solvents. All dilutions should be carried out in a perchloric acid fumehood.)

The chromatographic system was found to stabilise in about 2 h, which was typical of LC systems.

The signal integrator was activated immediately after each injection.

## 3. Results and discussion

### 3.1. The proposed method

The proposed method is very simple, where a 5- $\mu$ m Econosil CN (250 mm  $\times$  4.6 mm i.d.) column was employed for the separation of the amino acids, and a water–acetonitrile–tetrahydrofuran (77:20:3) mixture with 1 mM perchloric acid or trichloroacetic acid used as the mobile phase with conductimetric detection. The purpose of adding millimolar amounts of acid to the mobile phase is to create a background conductance in the system. As the conductance of amino acids is much smaller, the elution of amino acids in the proposed system causes a decrease in conductance, which enables indirect conductimetric detection of the amino acids. The purpose of adding a small amount of tetrahydrofuran to the mobile phase is to improve the column

efficiency and to facilitate the degassing of the mobile phase.

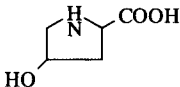
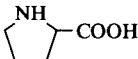
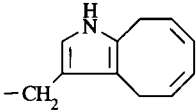
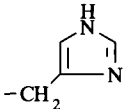
All the amino acids under study were found to be eluted in the proposed system and exhibited well-defined peaks.

### 3.2. Separation of amino acids

The retention times ( $t_R$ ) and capacity factors ( $k'$ ) of twenty one common amino acids eluted using the proposed mobile phases are shown in Table 1. The proposed system could not give clear separation of

amino acids with very close retention times, e.g. the pairs of amino acids: Glu–Thr, Phe–Leu, Iso–Leu and Asp–Ser. Nevertheless the proposed system could give baseline resolution of at least fourteen amino acids in about 80 min and a typical chromatogram of a mixture of these amino acids is shown in Fig. 1. The resolution obtained is comparable to many commonly used chromatographic separations of amino acids after derivatization. Thus the proposed system was considered to be satisfactory bearing in mind that the cyano column used is a general purpose column, which is not designed for the separation of amino acids.

Table 1  
Separation of amino acids with the general formula of  $RCH(NH_3^+)COO^-$

Amino acid	R	Abbreviation	$pK_{b1}^b$	Retention time, $t_R$ (min)	Capacity factor, $k'$
L-Hydroxyproline <sup>a</sup>		Hypro	12.08	5.44	1.38
L-Aspartic acid	-CH <sub>2</sub> COOH	Asp	11.93	6.35	1.77
L-Cysteine–HCl monohydrate	-CH <sub>2</sub> SH	CySH	–	6.63	1.90
L-Proline <sup>a</sup>		Pro	12.0	6.94	2.03
L-Asparagine	-CH <sub>2</sub> CONH <sub>2</sub>	Asp(NH <sub>2</sub> )	–	7.21	2.15
L-Serine	-CH <sub>2</sub> OH	Ser	11.79 <sup>c</sup>	7.29	2.18
L-Glutamine	-CH <sub>2</sub> CH <sub>2</sub> CONH <sub>2</sub>	Glu(NH <sub>2</sub> )	–	7.53	2.29
L-Threonine	-CH(OH)CH <sub>3</sub>	Thr	–	7.58	2.31
L-Glutamic acid	-CH <sub>2</sub> CH <sub>2</sub> COOH	Glu	11.90	8.08	2.53
Glycine	-H	Gly	11.647	8.92	2.90
L-Alanine	-CH <sub>3</sub>	Ala	11.649	9.75	3.26
L-Methionine	-CH <sub>2</sub> CH <sub>2</sub> SCH <sub>3</sub>	Met	11.72	10.77	3.70
L-Valine	-CH(CH <sub>3</sub> ) <sub>2</sub>	Val	11.71 <sup>c</sup>	11.28	3.93
L-Tyrosine	-CH <sub>2</sub> C <sub>6</sub> H <sub>4</sub> OH	Tyr	11.80	11.75	4.13
L-Phenylalanine	-CH <sub>2</sub> C <sub>6</sub> H <sub>5</sub>	Phe	11.42 <sup>c</sup>	14.10	5.16
L-Leucine	-CH <sub>2</sub> CH(CH <sub>3</sub> ) <sub>2</sub>	Leu	11.669	14.17	5.19
L-Isoleucine	-CH(CH <sub>3</sub> )C <sub>2</sub> H <sub>5</sub>	Ileu	11.679	14.19	5.20
L-Tryptophan		Try	11.62	22.24	8.71
L-Histidine		His	7.90	44.62	18.48
L-Lysine	-(CH <sub>2</sub> ) <sub>4</sub> NH <sub>2</sub>	Lys	5.05	77.99	33.06
L-Arginine	-(CH <sub>2</sub> ) <sub>2</sub> CH <sub>2</sub> NHC(NH)(NH <sub>2</sub> )	Arg	4.96	85.72	36.43

<sup>a</sup> The entire formula.

<sup>b</sup> Ionization constants in water at 25°C taken from Ref. [25].

<sup>c</sup> Values for the DL forms.

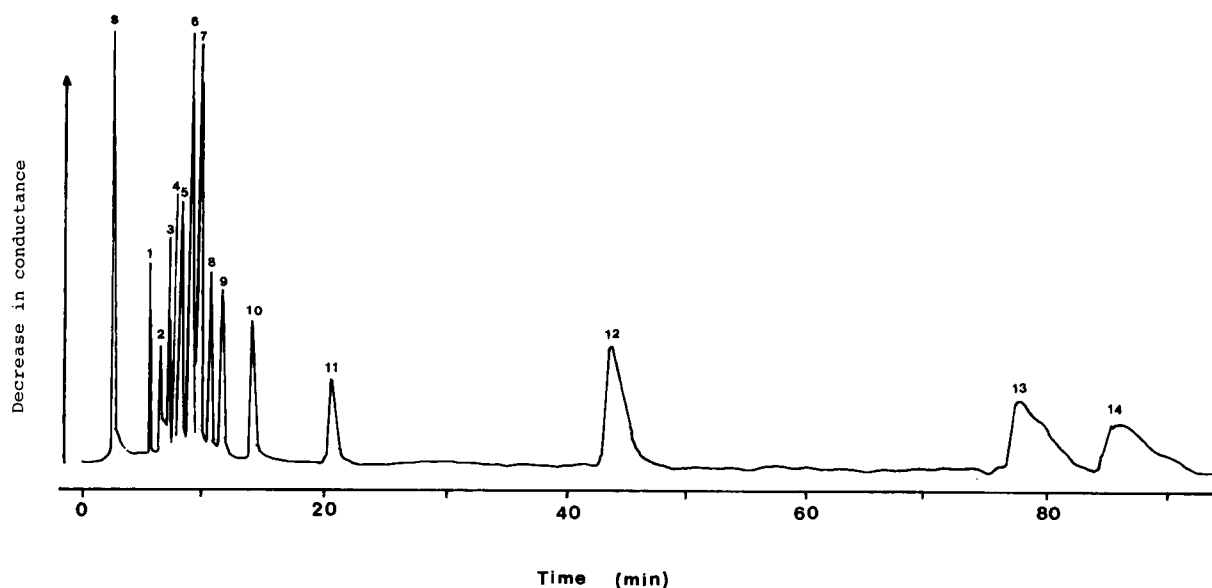


Fig. 1. Indirect conductimetric detection of amino acids after separation using a 5- $\mu\text{m}$  Econosil cartridge. Peaks ( $t$ , in min): 1 = Hypo (5.44); 2 = Asp (6.35); 3 = Pro (6.94); 4 = Glu( $\text{NH}_2$ ) (7.53); 5 = Glu (8.08); 6 = Gly (8.92); 7 = Ala (9.75); 8 = Met (10.77); 9 = Tyr (11.75); 10 = Phe (14.1); 11 = Try (22.24); 12 = His (44.62); 13 = Lys (77.99) and 14 = Arg (85.7). Amino acid quantities: ca. 0.8  $\mu\text{g}$  each.

The elution order of the amino acids in the present system as shown in Table 1 is as follows: Hyp, Asp, Pro, Ser, Thr, Glu, Gly, Ala, Met, Val, Tyr, Phe, Leu, Ile, Try, His, Lys, Arg. This is very broadly similar to that of amino acids separated by a cation exchange column [19] (Asp, Hyp, Thr, Ser, Glu, Pro, Gly, Ala, Val, Met, Ile, Leu, Tyr, Phe, Try, Lys, His, Arg).

Ion-exchange and hydrophobic interaction are two main factors [7] governing the elution order of amino acids on ion exchange columns, where hydrophobic interaction affects the elution order to a larger extent. Similarly, in the present system with a cyano column for the separation of amino acids, the elution behaviour of these acids can be explained in terms of (1) the ion exchange and hydrophobic interaction of the amino acids with the column, and (2) the polar interaction of the  $-\text{COOH}$ ,  $-\text{OH}$ ,  $-\text{SH}$  and  $-\text{CONH}_2$  functional groups of the amino acids with the mobile phase. It can be seen from Table 1 that the retention times of the amino acids were found to increase, in general, with increase in the value of  $\text{p}K_{\text{b}1}$ , suggesting that the ion exchange interaction of the amino acids with the stationary phase was an important operating mechanism. When the  $\text{p}K_{\text{b}1}$  values are similar, other factors become important. The amino acids that were eluted first (from L-hydroxyproline to L-glutamic acid) all carry polar

groups such as  $-\text{COOH}$  and  $-\text{OH}$ , which will increase their solubilities in the mobile phase. On the other hand, the elution order of these acids are also affected by their hydrophobicity, e.g. aspartic acid has one carbon atom less than glutamic acid and was observed to be eluted earlier. For glycine, alanine, valine and leucine, having no polar group on the side chain but instead having 0, 1, 3 and 4 carbon atoms on the side chain, respectively, the elution order was found to follow the number of carbon atoms, i.e. the increasing order of hydrophobicity.

### 3.3. Linear range

The calibration graphs of the integrator peak area counts against the quantities of each amino acid were found to be linear over the concentration range studied, i.e. 0.5 to 500  $\mu\text{g}/\text{ml}$  for an injection volume of 20  $\mu\text{l}$ , for all the amino acids listed in Table 2. The correlation coefficient for all calibration graphs were between 0.999 and 1. The calibration graphs using peak height counts were less linear, especially at concentrations of amino acids above 100  $\mu\text{g}/\text{ml}$ , as larger quantities of amino acids were found to result in broader peaks, where the peak height cannot give an accurate estimation of the amount of amino acids.

Table 2  
Effect of the mass ( $M$ ) and capacity factor ( $k'$ ) of amino acids on their detector responses <sup>a</sup>

Amino acid <sup>b</sup>	$A \times M^c / 10^7$	$B = A/k'$	$B \times M / 10^7$
Hypro (131.13)	1.66	91,533	1.20
Asp (133.10)	1.53	64,737	0.86
Pro (115.13)	2.18	93,140	1.07
Asp(NH <sub>2</sub> ) (132.12)	2.03	71,423	0.94
Thr (119.12)	3.44	125,145	1.49
Glu (147.13)	3.44	92,472	1.36
Ser (105.09)	3.32	145,003	1.52
Glu(NH <sub>2</sub> ) (146.15)	3.48	103,836	1.52
Gly (75.07)	4.20	192,780	1.45
Ala (89.09)	4.97	171,021	1.52
Met (149.21)	3.85	69,768	1.04
Val (117.15)	4.91	106,529	1.25
Tyr (181.19)	4.14	55,297	1.00
Phe (165.19)	4.09	48,033	0.79
Leu (131.17)	5.37	78,866	1.03
Ileu (131.17)	5.10	74,710	0.98
Try (204.22)	5.71	32,076	0.66
His (155.16)	14.0	48,962	0.76
	Average = 4 (R.S.D. = 67.5%)		Average = 1.14 (R.S.D. = 26.4%)

<sup>a</sup> The mobile phase used was that containing 1 mM HClO<sub>4</sub> as described in *Procedure*.

<sup>b</sup> Molecular mass ( $M$ ) of the amino acids in parentheses.

<sup>c</sup>  $A \times M = (\text{Area count in } \mu\text{g}) \times M$ .

The smallest quantity of amino acid that can be measured with an accuracy of within 20% of the actual value at 95% confidence level by the integrator was about 0.5  $\mu\text{g}/\text{ml}$  for a sample size of 20  $\mu\text{l}$ , i.e. 10 ng or about 0.1 nanomole of amino acid for all the amino acids under study. The proposed method is less sensitive than that using *o*-phthalaldehyde (OPA)–mercaptoethanol, or 9-fluorenylmethyl chloroformate (FMOC-Cl) derivative fluorescence detection by 1–2 orders of magnitude, and the phenylisothiocyanate (PITC) derivative with UV detection by about two orders of magnitude [20,21]. Nevertheless, the proposed method is less subject to contamination and interferences from the reagents, on-column degradation of the derivatives, and problems associated with derivatization such as completeness of the derivatization reaction.

### 3.4. Detection theory

The linear relationship between the change in conductance and the concentration of amino acid observed can be deduced by considering the change in conductance of the eluent when the amino acids are eluted

from the column. When the mobile phase containing perchloric acid was used, the partition of the perchlorate ion and the hydronium ion between the stationary phase and the mobile phase will be constant at system equilibrium.

Amino acids are amphiprotic, and the cationic form or the anionic form may predominate depending on the pH of the solution. When the amino acid is loaded onto the column, it displaces hydronium and perchlorate ions adsorbed on the surface of the stationary phase, resulting in an instantaneous increase in concentration of the ionic species in the mobile phase, as evidenced by the sharp negative solvent peak shown in Fig. 2, which indicates an increase in conductance. In the absence of such displacement, the baseline will remain constant.

When the chromatographic system is at equilibrium, the background conductance of the eluent,  $G_B$ , as indicated by the conductivity detector of the system can be deduced according to Gjerde and Fritz [22] to be:

$$G_B = \frac{(\lambda_{\text{o,E}}^+ + \lambda_{\text{o,E}}^-) C_E I_E}{10^{-3} K} \quad (1)$$

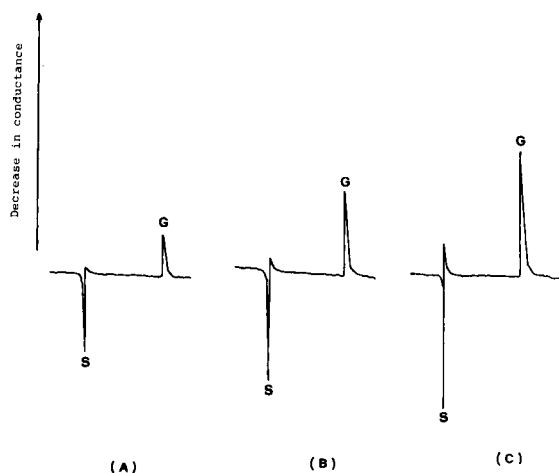


Fig. 2. Relationship between solvent peak height and glutamic acid concentration. Solvent peak (S) at 2.5 min. Glutamic acid (G) at 8.3 min. Glutamic acid concentration: (A) 51  $\mu\text{g/ml}$ , (B) 101  $\mu\text{g/ml}$ , (C) 152  $\mu\text{g/ml}$ .

where  $\lambda_{\text{o,E}}^+$  and  $\lambda_{\text{o,E}}^-$  denote the ionic conductance at infinite dilution of the cation and anion of the eluent conducting species, respectively,  $C_{\text{E}}$  and  $I_{\text{E}}$  are respectively the concentration of the eluent conducting species and the fraction of the species that is ionised, and  $K$  is the cell constant of the detector cell. As the conducting species creating the background conductance are in the millimolar concentration range, there will be little loss in accuracy to assume that the ionic conductance is at infinite dilution. It is further assumed that elution of an amino acid from the stationary phase involves a 1 for 1 exchange with the eluent conducting species to preserve electroneutrality [22].

As amino acid can exist in the cationic form, the anionic form or dipolar form in the mobile phase, the conductance measured at the detector during amino acid elution can be considered as that due to the cationic form,  $G_{\text{C}}$ , and the anionic form,  $G_{\text{A}}$ , as shown respectively in Eq. 2 and Eq. 3 below:

$$G_{\text{C}} = \frac{\lambda_{\text{o,E}}^+(C_{\text{E}}I_{\text{E}} - C_{\text{s}}I_{\text{s}})}{10^{-3}K} + \frac{\lambda_{\text{o,E}}^-C_{\text{E}}I_{\text{E}}}{10^{-3}K} + \frac{\lambda_{\text{o,s}}^+C_{\text{s}}I_{\text{s}}}{10^{-3}K} \quad (2)$$

$$G_{\text{A}} = \frac{\lambda_{\text{o,E}}^-(C_{\text{E}}I_{\text{E}} - C_{\text{s}}I_{\text{s}}')}{10^{-3}K} + \frac{\lambda_{\text{o,E}}^+C_{\text{E}}I_{\text{E}}}{10^{-3}K} + \frac{\lambda_{\text{o,s}}^-C_{\text{s}}I_{\text{s}}'}{10^{-3}K} \quad (3)$$

where  $\lambda_{\text{o,s}}^+$ ,  $\lambda_{\text{o,s}}^-$ ,  $C_{\text{s}}$  are defined for the sample and have the same meaning as the analogous terms for the eluent

conducting species defined above, and  $I_{\text{s}}$  and  $I_{\text{s}}'$  are respectively the fractions of the amino acid that form cations and anions. Note that for simplicity the dipolar form of the amino acid is assumed to contribute to the conductance both as the cationic form and the anionic form. The change in conductance at sample elution is therefore given by

$$\begin{aligned} \Delta G &= (G_{\text{C}} - G_{\text{B}}) + (G_{\text{A}} - G_{\text{B}}) \\ &= \frac{C_{\text{s}}I_{\text{s}}(\lambda_{\text{o,s}}^+ - \lambda_{\text{o,E}}^+)}{10^{-3}K} + \frac{C_{\text{s}}I_{\text{s}}'(\lambda_{\text{o,s}}^- - \lambda_{\text{o,E}}^-)}{10^{-3}K} \\ &= -C_{\text{s}} \frac{I_{\text{s}}(\lambda_{\text{o,E}}^+ - \lambda_{\text{o,s}}^+) + I_{\text{s}}'(\lambda_{\text{o,E}}^- - \lambda_{\text{o,s}}^-)}{10^{-3}K} \quad (4) \end{aligned}$$

It follows from Eq. 4 that the change in conductance at sample elution is directly proportional to the concentration of the amino acid. Further, the signal will be a decrease in conductance so far as the sum of the bracket terms is positive, which is true in the present solvent system due to the high ionic conductance of the hydronium ion. Moreover, for amino acids with very high molecular mass, the effect of the term  $\lambda_{\text{o,s}}^+$  and  $\lambda_{\text{o,s}}^-$  would be reduced, and hence the change in conductance is essentially directly proportional to the concentration and independent of the nature of the amino acids.

Furthermore,  $I_{\text{s}}'$  decreases with increase in acidity of the mobile phase, and in the extreme case,  $I_{\text{s}}' = 0$  and  $I_{\text{s}} = 1$ , which is the case where the amino acid is present exclusively in the cationic form, and only displacement of the cationic species from the column will take place (i.e. hydronium ion in the present system). The reverse is true for the case of decrease in acidity of the mobile phase.

### 3.5. Detector response

#### Effect of the analyte

As the detector response is due to the displacement by the amino acid of the ionic species adsorbed on the stationary phase, hence in the absence of other mobile phase–amino acid interactions, the detector response could be deduced from Eq. 4 to be similar for all the amino acids, assuming that  $\lambda_{\text{o,s}}^+ \ll \lambda_{\text{o,E}}^+$  and  $\lambda_{\text{o,s}}^- \ll \lambda_{\text{o,E}}^-$  and that all  $I_{\text{s}}$  values for the amino acids are similar, and all  $I_{\text{s}}'$  values for the amino acids are also similar at the pH of the mobile phase.

The above prediction was studied by assessing the effect of the nature of 18 amino acids on the detector



Table 3

Detector response of amino acids with the mobile phase water–acetonitrile–tetrahydrofuran (77:20:3) and perchloric acid with concentrations as shown below

Amino acid	Area count per $\mu\text{g}/10^5$				Area ratio
	Perchloric acid (mM)				
	0.5	1.0	1.5	2.0	
Hyp	0.72	1.44	1.83	2.37	1:2:2.5:3.3
Pro	1.09	2.06	2.71	3.50	1:1.9:2.5:3.2
Glu	1.14	2.34	3.24	3.91	1:2.1:2.8:3.4
Met	1.51	2.74	3.46	4.42	1:1.8:2.3:2.9
Tyr	1.38	2.56	3.03	3.32	1:1.9:2.2:2.4
Phe	1.47	2.80	3.20	3.85	1:1.9:2.2:2.6

response. The response, indicated by the peak area count per  $\mu\text{g}$  of amino acid ( $A$ ), was recorded for each amino acid after 20  $\mu\text{l}$  of the respective standard solution was injected into the chromatograph. This was converted to molar concentrations by multiplying  $A$  by the relative molecular mass ( $M$ ) of each amino acid, where the change in mass due to protonation is assumed to be negligible, as follows:  $A \times M = (\text{area count}/\mu\text{g}) \times M = \text{area count}/(\mu\text{g}/M) \propto \text{area count}/\text{No. of molecules per } \mu\text{g}$ .

As shown in Table 2, it can be seen that the average value for  $A \times M$  was found to be 4 (R.S.D. = 67.5%). The majority of the  $A \times M$  values is close to 4.

Further, the area of the peak in a chromatographic system was found to be related to the speed of travel of the analyte through the detector [23], so that it may be necessary to account for this effect, which can be done by dividing the peak area count per  $\mu\text{g}$  of amino acid by the capacity factor,  $k'$ , denoted as  $B$ , which is calculated for each amino acid and also included in Table 2. It can be seen that the average value of  $B \times M$  (column 4 of Table 2) was 1.1 with a much smaller R.S.D. of 26.4%. It can thus be concluded that the detector response is related to number of molecules and not so much dependent on the nature of the molecules. This confirms experimentally the conclusion drawn from Eq. 4 above.

#### *Effect of acid in the mobile phase*

The detector responses of six amino acids using different concentrations of perchloric acid and trichloroacetic acid are shown in Tables 3 and 4, respectively.

The detector response of each amino acid was found to increase with the concentrations of both acids, and the response was found to be only a few percent higher with perchloric acid than that with equivalent concentration of trichloroacetic acid in the mobile phase.

As can be seen from Eq. 4, the difference in signal response of the two acids is due to the difference in ionic conductance of the perchlorate ion and that of the trichloroacetate ion, and the difference is small when compared with the total conductance, where the highly conducting hydronium ion is the common cation for both acids.

The increase in the detector response with the increase in acid concentration can be ascribed to the increase in  $I_s$  in Eq. 4, i.e. the increase in the fraction of the cationic form of the amino acids, which then caused an increase in the amount of hydronium ion displaced. The slight decrease in retention time with an increase in acid concentration is expected to cause a slight change in signal responses, as described above; however, the effect on detector response is also expected to be small.

#### *3.6. Relationship between amino acid concentration and solvent peak height*

The chromatograms of amino acids were found to give a negative solvent peak at about 2.5 min. The chromatograms of L-glutamic acid shown in Fig. 2 are used to illustrate the change in height of the solvent peak with analyte concentration. The correlation coefficients for the plot of the concentrations of three amino

Table 4

Detector response of amino acid with the mobile phase water–acetonitrile–tetrahydrofuran (77:20:3) and trichloroacetic acid with concentrations as shown below

Amino acid	Area count per $\mu\text{g}/10^5$				Area ratio
	Trichloroacetic acid (mM)				
	0.5	1.0	1.5	2.0	
Hyp	0.65	1.19	1.75	2.23	1:1.8:2.7:3.4
Pro	0.98	1.93	2.48	3.29	1:2.0:2.5:3.4
Glu	0.87	2.05	3.22	3.98	1:2.4:3.7:4.6
Met	1.38	2.40	3.27	4.10	1:1.7:2.4:3.0
Tyr	1.26	2.22	2.91	3.44	1:1.8:2.3:2.7
Phe	1.32	2.36	3.05	3.78	1:1.8:2.3:2.9

Table 5  
Effect of perchloric acid on the retention time

Amino acid	Retention time (min)			
	Perchloric acid (mM)			
	0.5	1.0	1.5	2.0
L-Hydroxyproline	5.6	5.4	5.3	5.3
L-Proline	7.2	7.0	6.7	6.6
L-Glutamic acid	8.7	8.1	7.5	7.3
Glycine	9.9	8.9	8.1	7.8
L-Methionine	11.8	10.7	9.8	9.5
L-Tyrosine	13.1	11.7	10.6	10.2
L-Phenylalanine	15.6	14.1	12.8	12.3
L-Tryptophan	26.1	22.3	19.4	18.3

acids, namely, L-alanine, L-glutamic acid and L-tryptophan with solvent peak height were found to be  $> 0.975$  for both peak height and peak area, indicating that the negative solvent peak height is directly proportional to the analyte concentration. This proves the quantitative displacement of the ionic species from the column by the analyte species as explained above.

Note that water had been used initially to prepare the amino acids mixture for Fig. 1, with subsequent dilution by the mobile phase, and hence the final solution had a lower perchloric acid concentration than the mobile phase. This explains why in the chromatogram shown in Fig. 1 a large positive peak appeared at 2.45 min, which was due to the lower acid concentration in the sample compared with that in the mobile phase.

### 3.7. Effect of acid concentration on retention time

From Tables 5 and 6, it can be seen that there was a decrease in the retention times for all the amino acids with an increase in acid strength, possibly due to an increase in ionic strength [24]. This observation is similar to the reduction in retention with increasing ionic strength for an ion-exchange separation.

## 4. Conclusion

The proposed method is simple and sensitive for detection of amino acids after LC separation. Unlike many of the detection methods which require derivatization, this method does not depend on the presence

Table 6  
Effect of trichloroacetic acid on the retention time

Amino acid	Retention time (min)			
	Trichloroacetic acid (mM)			
	0.5	1.0	1.5	2.0
L-Hydroxyproline	5.7	5.6	5.5	5.4
L-Proline	7.4	7.2	6.9	6.8
L-Glutamic acid	9.0	8.4	7.9	7.5
Glycine	10.2	9.4	8.6	8.1
L-Methionine	12.5	11.4	10.3	9.8
L-Tyrosine	14.0	12.7	11.2	10.5
L-Phenylalanine	17.0	15.4	13.4	12.8
L-Tryptophan	29.3	25.0	20.6	19.1

of particular functional groups on the compound, and all amino acids can be detected, including the secondary amines proline and hydroxyproline. The method can detect down to nanogram quantities of amino acids and is equally sensitive for all the amino acids.

The proposed method can be carried out in any laboratory equipped with a liquid chromatograph and a conductivity detector, and can be handled easily. It is anticipated that the method will be of wide application to amino acid determinations. Further work on the applications of the proposed method is underway, and the findings will be reported as they become available.

## References

- [1] H.F. Walton and R.D. Rocklin, *Ion Exchange in Analytical Chemistry*, CRC Press, Boca Raton, Florida, 1990, pp. 151, 159 and 156.
- [2] P.B. Hamilton, *Anal. Chem.*, 35 (1963) 2055.
- [3] S. Udenfriend, S. Stein, P. Boehlen, W. Dairman, W. Leimgruber, and M. Weigele, *Science*, 178 (1972) 871.
- [4] D.W. Hill, F.H. Walters, T.D. Wilson and J.D. Stuart, *Anal. Chem.*, 51 (1979) 1338.
- [5] Z. Deyl and J. Rosmus, *J. Chromatogr.*, 20 (1965) 514.
- [6] P. Husek and K. Macek, *Chromatogr. Rev.*, 19 (1975) 139.
- [7] R. Macrae (Ed.), *HPLC in Food Analysis*, Academic Press, Orlando FL, 1988, pp. 463 and 448.
- [8] C. de Jong, G.J. Hughes, E. van Wieringen and K.J. Wilson, *J. Chromatogr.*, 241, (1982) 345.
- [9] T. Kawasaki, M. Maeda and A. Tsuji, *J. Chromatogr.*, 328 (1985) 121.
- [10] C.R. Krishnamurti, A.M. Heindze and G. Galzy, *J. Chromatogr.*, 315 (1984) 321.
- [11] M.K. Radjai and R.T. Hatch, *J. Chromatogr.*, 196 (1980) 319.

- [12] N. Seiler and B. Knodgen, *J. Chromatogr.*, 341 (1985) 11.
- [13] N. Kiba and M. Kaneko, *J. Chromatogr.*, 303 (1984) 396.
- [14] A.M. Felix and G. Terkelsen, *Anal. Biochem.*, 56 (1973) 610.
- [15] H. Small, T.S. Stevens and W.C. Bauman, *Anal. Chem.*, 47 (1975) 1801.
- [16] J.M. Lorrain, C.R. Fortune and B. Dellinger, *Anal. Chem.*, 53 (1981) 1302.
- [17] D.L. DuVal, M. Rogers and J.S. Fritz, *Anal. Chem.*, 57 (1985) 1583.
- [18] T. Okada and T. Kuwamoto, *Anal. Chem.*, 58 (1986) 1375.
- [19] A.G. Georgiadis and J.W. Coffey, *Anal. Biochem.*, 56 (1973) 121.
- [20] L.A. Currie (Ed.), *Detection in Analytical Chemistry*, ACS Symposium Series 361, American Chemical Society, Washington, DC, 1988, pp. 275–285.
- [21] R.B. Holman, A.J. Cross and M.H. Joseph (Eds.), *High Performance Liquid Chromatography in Neuroscience Research*, Wiley, Chichester, 1993 pp. 103–109.
- [22] D.T. Gjerde and J.S. Fritz, *Anal. Chem.*, 53 (1981) 2324.
- [23] S.R. Bakalyar and R.A. Henry, *J. Chromatogr.*, 126 (1976) 327.
- [24] J.Å. Jönsson (Ed.), *Chromatographic Theory and Basic Principles*, Marcel Dekker, New York, 1987., p. 325; and references cited therein.
- [25] R.C. Weast (Ed.), *CRC Handbook of Chemistry and Physics*, 61st edn., CRC Press, Boca Raton, FL, 1980, C-712.



ELSEVIER

Analytica Chimica Acta 300 (1995) 193–200

**ANALYTICA  
CHIMICA  
ACTA**

# Study of the responses of a gas chromatography–reduction gas detector system to gaseous hydrocarbons under different conditions

Xu-Liang Cao \*, C. Nicholas Hewitt, K.S. Waterhouse

*Institute of Environmental and Biological Sciences, Lancaster University, Lancaster LA1 4YQ, UK*

Received 9 June 1994

---

## Abstract

The response of a reduction gas detector (RGD) to  $C_2$ – $C_6$  alkenes,  $C_2$ – $C_6$  alkanes, isoprene and benzene has been investigated using gas chromatography (GC) with a packed column. The RGD is considerably more sensitive to alkenes than is the flame ionization detector. The detection limit of this present GC/RGD system for alkenes is about 0.01 ng. It has much greater sensitivity to alkenes than to alkanes. Its sensitivity increases with increasing HgO bed temperature, but its selectivity towards alkenes decreases at the same time. The selectivity of the RGD may not be significant for much heavier molecules. The sensitivity of the RGD is inversely proportional to the carrier gas flow rate through the HgO bed. The baseline of the system increases significantly with increasing oven temperature.

*Keywords:* Gas chromatography; Reduction gas detector

---

## 1. Introduction

Since the more reactive hydrocarbons (e.g., alkenes) have a greater reactivity for OH radicals than the non-reactive hydrocarbons (e.g., alkanes), that is to say, the former compounds will have much higher potentials for ozone formation than the latter [1], the priority in atmospheric monitoring programmes which focus on photochemical ozone production is therefore the quantitation of the reactive volatile organic compounds (VOCs), rather than of the nonreactive species. Under some circumstances it would therefore be advantageous to utilize a detection system that has enhanced sensitivity towards alkenes but is relatively insensitive to alkanes and other less reactive VOC species.

The reduction gas detector (RGD), which was originally developed for detecting the reducing gases CO and  $H_2$  [2], has been used for the detection of reactive volatile organic compounds [3,4] due to its high sensitivity and selectivity. Although it was engineered for use with packed gas chromatography (GC) columns, a capillary GC/RGD system has also been developed recently, and been used for environmental analysis [5,6]. In order to operate this system at optimum conditions for the analysis of hydrocarbons, it is necessary to investigate the effect of different conditions on the responses of the RGD to different hydrocarbons. In this work, the responses of the RGD to both  $C_2$ – $C_6$  alkenes and alkanes have been studied in detail as functions of the HgO bed temperatures and carrier gas flow rates. The linearity of the detector response has also been

---

\* Corresponding author.

studied, and its performance compared with that of the flame ionisation detector (FID).

## 2. Principles of the reduction gas detector

When a certain gaseous species passes through a heated bed of solid mercury(II) oxide (HgO), the following general reaction will take place:

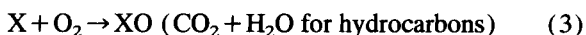


where X represents any appropriate reducing gas. The resultant mercury vapour concentration is directly proportional to the inlet gas concentration and is quantitatively detected by means of an ultraviolet photometer located immediately downstream of the reaction bed.

In fact, mercury vapour is always present above the heated bed of mercury oxide in the detector due to the following reaction,



and the mercury vapour evolved in this reaction will determine the baseline response of the detector. Because of the O<sub>2</sub> generated in reaction (2), the following reaction will occur for any combustible gas passing through the heated bed of mercury oxide,



thus the pressure of O<sub>2</sub> will decrease, and reaction (2) will proceed further. This will lead to an increase in mercury vapour concentration. Therefore, any combustible gases, whether they are reducing gases or not, can, in theory, be detected by the reduction gas detector. Of course, for reducing gases (e.g. alkenes), reactions (1) and (3) will both take place, while for the non-reducing gases (e.g., alkanes), only reaction (3) takes place.

The sensitivity of detection with this system for a given gaseous species is a function of the stoichiometric relationship of reactants and products. Such relationships are determined by both equilibrium constants and reaction rates, which are specific to the gas species being detected. For example, carbon monoxide reacts with nearly 100% conversion efficiency [7], while hydrogen undergoes incomplete reaction with approximately 10% conversion to mercury vapour [7]. As a result, the detection limit for hydrogen is approximately 10 times greater than for carbon monoxide.

## 3. Experimental

Gas chromatographic measurements were made using a Hewlett-Packard 5890 Series II gas chromatograph fitted with an RGD. The carrier gas used was helium. A catalytic combustion filter was used in con-

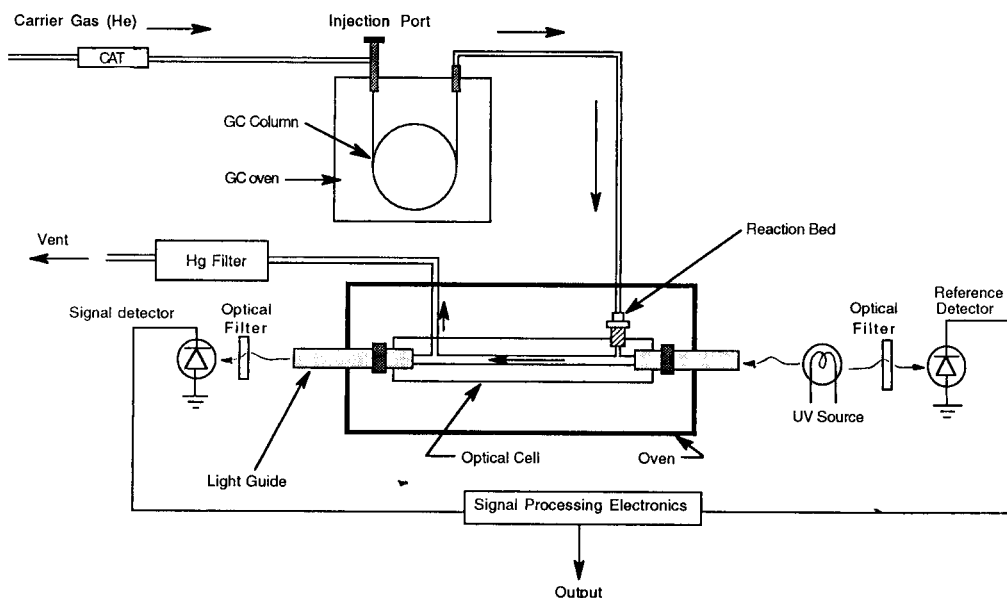


Fig. 1. Schematic diagram for the GC/RGD system. CAT = catalytic combustion filter.

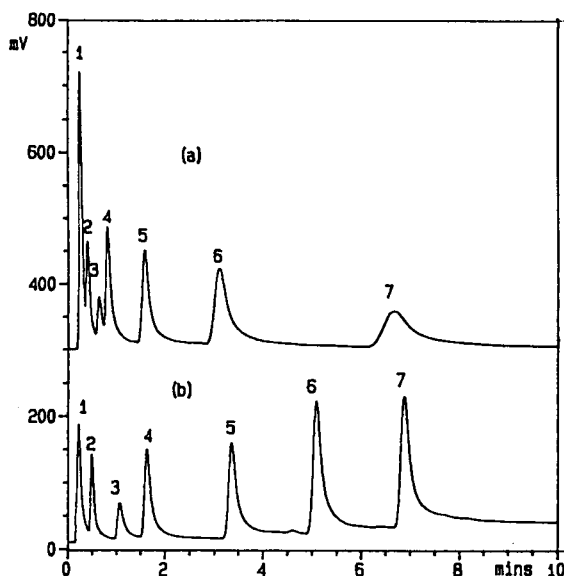


Fig. 2. Chromatograms of alkenes using an RGD. Sample: 1 ml of 0.15 ppm alkenes. GC conditions: (a) 80°C isothermal, splitless; (b) 50°C (1 min) to 110°C at 10°C/min, splitless. Flow rate of He through HgO bed: (a) 31.6 ml/min; (b) 37.5 ml/min. Peak No. 1=air peak (containing CO and H<sub>2</sub>); 2=ethene; 3=acetylene; 4=propene; 5=1-butene; 6=1-pentene; 7=1-hexene.

junction with an organic/water vapour trap (molecular sieve) for carrier gas purification. The reduction gas detector employed in this work was an RGD-2 (Trace Analytical, Menlo Park, CA). A schematic diagram of the GC/RGD system is shown in Fig. 1. The GC column was a stainless steel tube (121.92 cm × 2.2 mm i.d.) packed with Unibeads 3S with mesh size 80/100 (Alltech), which was connected to the RGD by a stainless steel tube (60 cm × 2.2 mm i.d.). Sample vapours were introduced into the GC column for analysis by direct injection using a gas tight syringe.

A 15 ppmv Scotty<sup>®</sup> standard calibration mixture of C<sub>2</sub>–C<sub>6</sub> alkenes which also contains acetylene and a

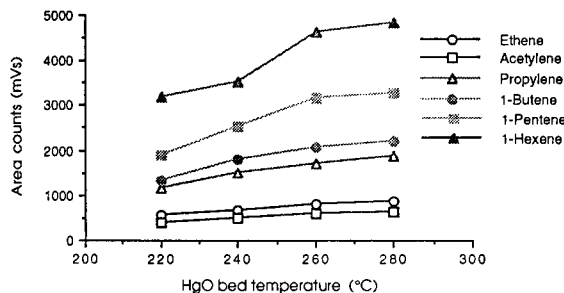


Fig. 3. Variation of RGD response for alkenes with HgO bed temperatures.

1000 ppmv Scotty standard calibration mixture of C<sub>2</sub>–C<sub>6</sub> alkenes were used for this work. Dilutions of these standards were made by injecting known volumes of vapours into a 1-l glass flask. Mixtures of isoprene and benzene vapours were prepared by injecting a known amount of liquid compound into a 1-l flask.

## 4. Results and discussions

### 4.1. The effect of HgO bed temperature on the responses of alkenes

As mentioned above, the sensitivity of the reduction gas detector depends on the equilibrium constant and the reaction rate for each gas and these will vary with different HgO bed temperatures. For the reactive hydrocarbons, both reactions (1) and (3) will take place, but reaction (1) will contribute the majority of the Hg vapour generated. In order to investigate the responses to alkenes at different HgO bed temperatures, a known amount of alkenes (C<sub>2</sub>–C<sub>6</sub>) was injected into the column at bed temperatures of 220 to 280°C. A typical chromatogram is shown in Fig. 2a, and the results are summarized in Fig. 3.

It can be seen from Fig. 2a that even at an HgO bed temperature of 280°C, peak tailing is still a problem. This will be much worse at low bed temperatures, and is almost certainly due to incomplete reactions on the HgO bed, the large dead volume of the whole GC/RGD system, adsorption of mercury vapour and cooling of the analytes during transfer from the GC column to the detector. Raising the HgO bed temperature will increase the efficiency of the reaction but the dead volume can only be minimized by designing a micro-RGD system with a heated transfer line.

Fig. 3 shows that the HgO bed temperature has a significant effect on the response to alkenes, especially for the heavier molecules. For all hydrocarbons, the response increases with increasing HgO bed temperature. This is due to the fact that the equilibrium constants and reaction rates of reactions, (1), (2) and (3), increase with increasing temperature. Thus, in order to make optimum use of the RGD, the HgO bed temperature should be as high as possible.

The RGD response factors (area counts per ng of hydrocarbon) were calculated for alkenes at different HgO bed temperatures, and the results are shown in

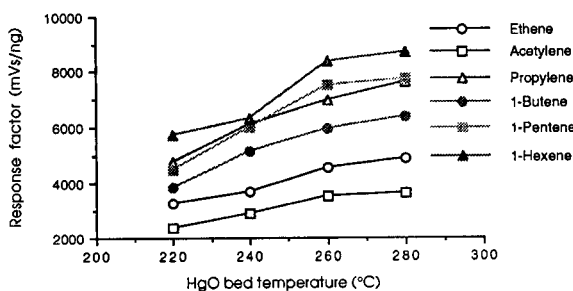


Fig. 4. Variation of RGD response factors for alkenes with HgO bed temperatures.

Fig. 4. For all alkenes, the response factors increase with increasing HgO bed temperatures. At a given HgO bed temperature, the response factor generally increases with the carbon number, except for propylene which has a very high response factor. This may be due to the incomplete nature of reaction (1) for these alkenes, while the conversion efficiency of reaction (1) for propylene may be much greater than for 1-butene or even 1-pentene.

#### 4.2. The effect of HgO bed temperature on the responses of alkanes

It can be seen from reactions (2) and (3) that the RGD can also detect non-reducing gases or vapours so long as they are combustible. In order to investigate the RGD response towards alkanes, known amounts of alkanes were injected into the GC column at different HgO bed temperatures (220–280°C). The results are summarized in Fig. 5. It can be seen that the alkanes give very low responses at low temperatures, but their responses increase rapidly with increasing HgO bed temperature. At higher HgO bed temperatures reaction (2) will proceed faster and will release more O<sub>2</sub> for reaction (3), thus more alkanes will be oxidized.

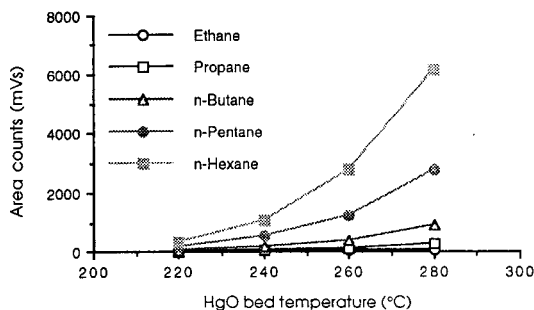


Fig. 5. Variation of RGD response for alkanes with HgO bed temperatures.

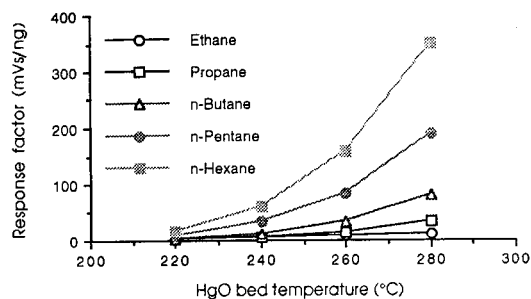


Fig. 6. Variation of RGD response factors for alkanes with HgO bed temperatures.

The RGD response factors ( $\text{mV s ng}^{-1}$ ) at different HgO bed temperatures were also calculated for alkanes, and the results are shown in Fig. 6. The response factors increase sharply with increasing HgO bed temperatures for the heavier molecules, while there is a slight increase for the lighter molecules. This may be due to the fact that even at low temperatures (220°C), the O<sub>2</sub> released from reaction (2) will be sufficient for combustion of the lighter molecules, thus their response ratios will not be increased significantly by addition of more O<sub>2</sub> released from reaction (2) at higher temperatures. For the heavier molecules, only a small fraction will be combusted by the O<sub>2</sub> released from reaction (2) at low temperatures (220°C). With increasing HgO bed temperatures, more O<sub>2</sub> will be released, and thus more alkanes will be oxidized.

#### 4.3. The effect of HgO bed temperature on the selectivity of the RGD

One of the characteristics of the reduction gas detector is its selectivity. Reducing gases or vapours give much higher responses than those from non-reducing gases or vapours. This gives the potential of using the RGD to detect trace levels of reducing gases or vapours present in high concentrations of non-reducing gases or vapours. In order to investigate the selectivity of the RGD towards alkenes, relative to alkanes, the ratios of alkene and alkane response factors for the detector at different HgO bed temperatures have been calculated, and the results are shown in Figs. 7 and 8. It can be seen that the ratios of alkene to alkane response factors generally decrease significantly with increasing HgO bed temperatures, especially for the lighter hydrocarbons. At a given HgO bed temperature (e.g., 220°C), the ratios of alkene to alkane response factors decrease

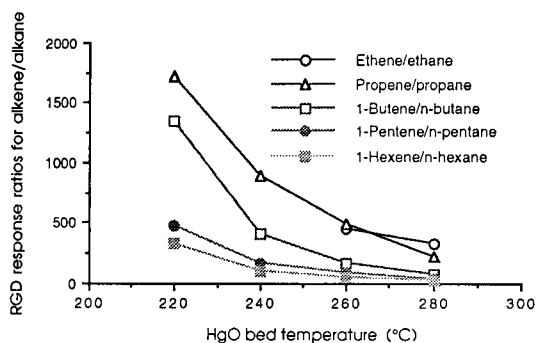


Fig. 7. Variation of RGD alkene/alkane response ratios with bed temperatures.

significantly with increasing carbon number. Their range varies between 1719 (for propylene/propane at 220°C) and 25 (for 1-hexene-*n*-hexane at 280°C). Although the RGD sensitivity towards alkenes will be greater at higher HgO bed temperatures, the sensitivity towards alkanes will also be increased at the same time. That is to say, the RGD selectivity will be decreased at higher HgO bed temperatures. Thus, in some cases the sensitivity of the detector may have to be sacrificed to some extent in order to make full use of its selectivity.

The RGD response factors for two other reactive hydrocarbons, isoprene and benzene, were also determined at an HgO bed temperature of 280°C, and they are 5940 and 4268 mV s ng<sup>-1</sup>, respectively. The ratios of isoprene to *n*-pentane, and benzene to *n*-hexane RGD response factors at 280°C are 31.6 and 12.2, respectively. They are both much greater than 1, which indicates that reaction (1) is the main reaction involved in isoprene and benzene detection at this bed temperature. However, their ratios are both much lower than those of 1-pentene-*n*-pentane (41) and 1-hexene-*n*-hexane (25), which indicates that they are not as reactive as

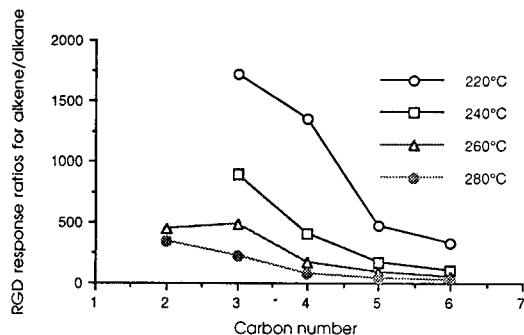


Fig. 8. Variation of RGD alkene/alkane response ratios with carbon number at different HgO bed temperatures.

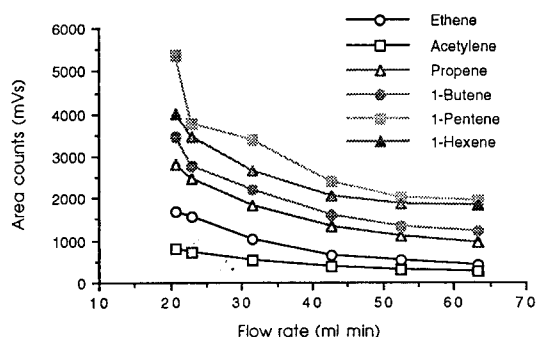


Fig. 9. Variation of RGD responses for alkenes with carrier gas (He) flow rate.

1-pentene and 1-hexene, and that their conversion efficiencies for reaction (1) are lower than those of 1-pentene and 1-hexene, respectively.

It should be noted that the exposure of the HgO bed to aromatic compounds may irreversibly impair its reactivity and may necessitate bed replacement [7]. This may be due to their incomplete oxidation by reaction (3), leading to the formation of black carbon. Chlorinated compounds, leading to the formation of a HgCl<sub>2</sub> precipitate, may also damage the bed and efforts should be taken to avoid exposure of the HgO bed to these compounds.

#### 4.4. The effect of flow rate on the responses to alkenes

Because the carrier gas flow rate through the reaction bed has an effect on the mercury vapour concentration, the reduction gas detector is very sensitive to the carrier gas flow rate, especially when using a packed GC column. At a given reaction bed temperature, the changes in flow rate will have an inverse effect on mercury vapour concentration, i.e., doubling the flow rate will halve the concentration. In order to investigate the effect of carrier gas flow rate on the responses to alkenes, a known amount of alkene mixture was injected onto the GC column at different carrier gas flow rates. The results are shown in Fig. 9. It can be seen that the response to the alkenes decreases significantly with increasing flow rate, especially for the heavier molecules. Thus, the carrier gas flow rate through the reaction bed should be as low as possible (about 20 ml/min) in order to optimize the RGD sensitivity.

It should be noted that the detector noise and drift are directly related to the production of mercury vapour



Table 1  
Ratios of RGD and FID response factors for hydrocarbons

	Propylene	1-Butene	1-Pentene	1-Hexene	Isoprene	Benzene
Ratio of RGD/FID response factors <sup>a</sup>	380	318	385	433	297	213

<sup>a</sup> RGD at 280°C, FID factor assumed to be 20 mV s ng<sup>-1</sup>.

from the thermal dissociation of HgO. The residence time of a gas sample within the reaction bed is also inversely proportional to the flow rate, and is an important consideration when optimizing sensitivity to gas species which react incompletely.

#### 4.5. Comparison between the responses of the RGD and FID to hydrocarbons

In order to investigate the sensitivity of the RGD towards hydrocarbons relative to the conventional FID, the ratios of the RGD and FID response factors (mV s ng<sup>-1</sup>) for each compound were calculated by using the RGD response factors at 280°C and the average FID response factor (20 mV s ng<sup>-1</sup>) for hydrocarbons, and the results are shown in Table 1. It can be seen that the RGD is at least 200 times more sensitive than the FID for the detection of alkenes.

The minimum detectable amounts of alkenes using the present GC/RGD system, based on a signal to noise ratio of 2, are shown in Table 2. It can be seen that generally they are very close to the typical detection limits currently obtainable with a high resolution capillary GC/FID (about 0.01 ng) even though a packed column was used with the RGD in this work. It will be

Table 2  
Detection limits of the present GC/RGD systems for hydrocarbons

Compound	Detection limit (ng) <sup>a</sup>
Ethene	0.008
Acetylene	0.017
Propene	0.010
1-Butene	0.014
1-Pentene	0.017
1-Hexene	0.022
Isoprene	0.023
Benzene	0.044

<sup>a</sup> Signal-to noise ratio = 2.

possible to lower them substantially by improving the chromatography and hence peak shapes of the compounds.

#### 4.6. Linearity of responses to hydrocarbons

The linearity of response is very important for the quantitation of substances by GC. In order to investigate the linearity of the RGD responses to hydrocarbons, different amounts (from 0.03 ng for ethene to 2.77 ng for 1-hexene) of alkenes, isoprene and benzene vapours were injected onto the GC column, and their responses in area counts plotted against the mass of hydrocarbons injected. The results are shown in Fig. 10. The parameters for the linear response to hydrocarbons are listed in Table 3. It can be seen that the responses of all hydrocarbons increase linearly with increasing mass of hydrocarbons, and the correlation coefficients for all hydrocarbons were greater than 0.99.

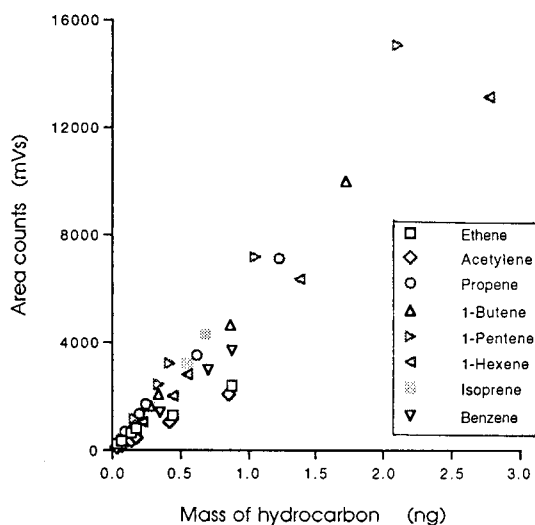


Fig. 10. Linearity of RGD response to C<sub>2</sub>–C<sub>6</sub> hydrocarbons.

Table 3  
Parameters for the linearity of RGD responses

Compound	Equation <sup>a</sup>	Correlation coefficient ( <i>r</i> ) <sup>b</sup>
Ethene	$y = 2465x + 287$	0.995
Acetylene	$y = 2428x + 64.1$	1.000
Propene	$y = 5581x + 219$	0.999
1-Butene	$y = 5719x + 34.2$	0.999
1-Pentene	$y = 7104x - 11.6$	0.999
1-Hexene	$y = 4718x + 10.4$	0.999
Isoprene	$y = 6359x - 97.4$	0.999
Benzene	$y = 4417x - 125$	1.000

<sup>a</sup>  $y$  = Response in area counts (mV s),  $x$  = amount of hydrocarbon (ng).

<sup>b</sup>  $n = 6$ .

The RGD-2 has a linearity potentiometer which is used for the adjustment of linearity of larger outputs, and the range of linearity will be much greater. However, because the RGD is a very sensitive detector and is most suitable for the determination of very low concentrations of hydrocarbons (ppbv or pptv level), it is normally not necessary to use this linearity potentiometer, and it was not used in the above experiments.

The linearity of response of the RGD will be affected by changes in the carrier gas flow rate, which may be ignored if the changes in flow rate are small (< 10%). The aging of the HgO bed will also cause gradual changes in response. Thus, the linearity of the system should be checked frequently for optimum quantitation. Since the response varies from compound to compound, it is necessary to calibrate the RGD with individual hydrocarbon compounds.

#### 4.7. The effect of GC oven temperature on the baseline

It can be seen from Fig. 2a that under isothermal conditions, the peaks of the lighter molecules cannot be separated very well, and the peaks of heavier molecules are very broad. Thus, temperature programming should be used when analysing real samples which may contain compounds with wide range boiling points.

Fig. 2b shows a chromatogram of C<sub>2</sub>–C<sub>6</sub> alkenes analysed under temperature programming conditions (50°C (1 min) to 110°C at 10°C/min) in an attempt to overcome these limitations. It can be seen that all the peaks are separated adequately, and the peak shapes are improved. However, the baseline increased signif-

icantly with increasing oven temperature. This may be due to the fact that as the oven temperature increases, the carrier gas flow rate will decrease, which will increase the Hg vapour concentration, as mentioned above. This problem may be eased by using a capillary column [6], since the carrier gas flow rate through the capillary column is very small compared to the flow rate of make-up gas, thus the total carrier gas flow rate will be almost constant, even when the GC oven temperature changes.

## 5. Conclusions

The reduction gas detector (RGD) is very sensitive and selective towards alkenes (compared to alkanes), and it is considerable more sensitive than the FID for these compounds. The detection limit of the present GC/RGD system for alkenes is about 0.01 ng, which will be improved by improving the chromatographic peak shapes of the compounds.

The RGD has greater sensitivity to alkenes than to alkanes. The sensitivity increases with increasing HgO bed temperature, but its selectivity towards alkenes will decrease at the same time. At a given HgO bed temperature, the ratio of the alkene and alkane response factors decreases with increasing carbon number. That is to say, the selectivity of the RGD may not be significant for much heavier molecules. Thus, in some applications, the sensitivity of the RGD may have to be sacrificed to some extent in order to make full use of its selectivity.

The RGD is very sensitive to the carrier gas flow rate, especially when using a packed GC column. At a given reaction bed temperature, the changes in flow rate will have an inverse effect on mercury vapour concentration. Thus, the carrier gas flow rate through the reaction bed should be as low as possible (about 20 ml/min) in order to optimize the detector sensitivity.

## Acknowledgements

We would like to thank the Government of the People's Republic of China, the British Council, and the Natural Environment Research Council for funding.

**References**

- [1] R.G. Derwent and M.E. Jenkin, *Atmos. Environ.*, 25A (1991) 1661.
- [2] W.M. Doizaki and M.D. Levitt, *J. Chromatogr.*, 285 (1984) 210.
- [3] D. Ohara and H.B. Singh, *Atmos. Environ.*, 22 (1988) 2613.
- [4] J.P., Greenberg, P.R. Zimmerman, B.E. Taylor, G.M. Silver and R. Fall, *Atmos. Environ.*, 27A (1993) 2689.
- [5] X.-L. Cao and C.N. Hewitt, *J. Chromatogr.*, 648 (1993) 191.
- [6] X.-L. Cao, C.N. Hewitt and K.S. Waterhouse, *J. Chromatogr.*, 697 (1994) 115.
- [7] Reduction gas detector (RGD2) operating manual, Trace Analytical, Menlo Park, CA, 1989.

# Studies on the behaviour of $\alpha$ -, $\beta$ - and $\gamma$ -cyclodextrins and some derivatives under reversed-phase liquid chromatographic conditions

A. Bielejewska, M. Koźbiał, R. Nowakowski, K. Duszczyk, D. Sybilska \*

*Institute of Physical Chemistry, Polish Academy of Sciences, Kasprzaka 44/52, 01-224 Warsaw, Poland*

Received 1 March 1994; revised manuscript received 16 August 1994

## Abstract

The separation processes of  $\alpha$ -,  $\beta$ - and  $\gamma$ -cyclodextrins and their various methyl derivatives have been investigated with Knauer polarimetric (Chiralyser) and refractive index (RI) detectors. RP18 and RP8 hydrocarbon packings and an  $\text{NH}_2$  bonded phase were applied as stationary phases. Aqueous methanolic or ethanolic solutions were used as mobile phases. It has been found that the Chiralyser detector response is approximately linear at low concentrations of solutes and that its detection capabilities are about 40 times better than those of the RI detector. Differences in the order of elution of  $\alpha$ -,  $\beta$ - and  $\gamma$ -cyclodextrins have been observed for various stationary phases as well as for various mobile phase compositions. The optimal conditions for analytical determinations of cyclodextrins and their derivatives have been discussed.

**Keywords:** Liquid chromatography; Inclusion compounds; Cyclodextrins

## 1. Introduction

Remarkable progress in the chemistry of cyclodextrins, as well as in their practical applications, has been achieved in the last decade. The new  $\alpha$ -,  $\beta$ - and  $\gamma$ -cyclodextrin derivatives, largely varying in their properties, are successively offered to the market. They find applications in industry and in various branches of science including analytical chemistry. The growing significance of cyclodextrins as chiral discriminating agents, for recognition of enantiomers of numerous compounds of acidic, basic and neutral nature, seems to be also worth mentioning.

As a consequence the analysis of the purity of cyclodextrins themselves is a problem of great impor-

tance. For this purpose liquid chromatography can be considered as the method of choice. Many classical chromatographic methods have been used for the separation of cyclodextrins: partition chromatography on cellulose [1], adsorption chromatography on charcoal [2], gel chromatography on Sephadex G-15 [3] and on polyacrylamide [4]. More recently the use of hydrocarbon packings [5] and an  $\text{NH}_2$  bonded phase have been reported as cation exchange resins [5,6]. Some applications of reversed-phase liquid chromatography (RPLC) to the separation of oligosaccharides have been also described [7].

The main difficulties during the analysis of saccharides are caused by limitations of the detection systems. Refractive index detection may be considered as universal but this technique suffers from relatively low sensitivity and cannot be used in combination with a

\* Corresponding author.

gradient elution method. Spectrophotometric detection at wavelengths below 200 nm is only a little more sensitive but may be easily disturbed. Some indirect techniques have been reported [8,9] together with a post-column derivatization procedure [10] and the use of high temperature gas chromatography for the analysis of alkylated cyclodextrins [11].

In this paper a chiral (polarimetric) detector for the reversed-phase liquid chromatographic separation of  $\alpha$ -,  $\beta$ - and  $\gamma$ -cyclodextrins and some derivatives is described.

The compounds under investigation were  $\alpha$ -,  $\beta$ - and  $\gamma$ -cyclodextrin ( $\alpha$ -CD,  $\beta$ -CD,  $\gamma$ -CD), their methyl derivatives (2,3,6-tri-*O*-methyl)- $\alpha$ -,  $\beta$ - and  $\gamma$ -cyclodextrin (TM- $\alpha$ -CD, TM- $\beta$ -CD, TM- $\gamma$ -CD), (2,6-di-*O*-methyl)- $\beta$ -cyclodextrin (DM- $\beta$ -CD), and hydroxypropyl- $\beta$ -cyclodextrin (HP- $\beta$ -CD).

## 2. Experimental

### 2.1. Reagents

All cyclodextrins (CDs) were the obtained from Chinoin (Budapest); one sample of HP- $\beta$ -CD has been

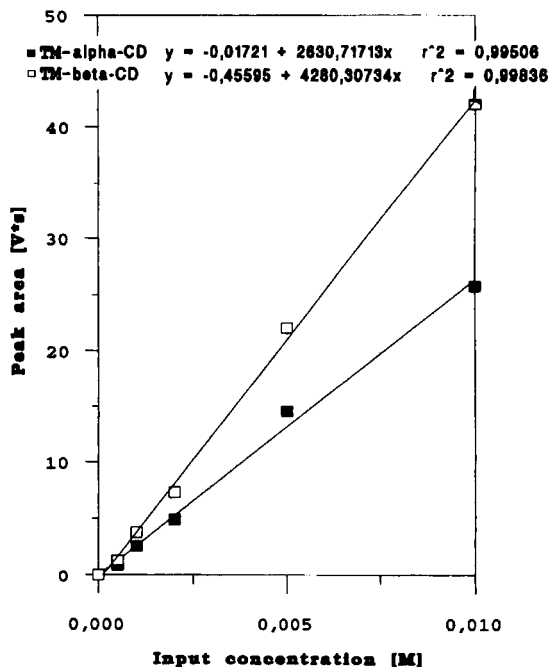


Fig. 1. Calibration graphs of TM- $\alpha$ -CD and TM- $\beta$ -CD for polarimetric detection. Column: 250  $\times$  4 mm i.d., packed with LiChrosorb RP18. Mobile phase: ethanol–water (60:40, v/v). Flow rate: 0.95 ml/min. Injection volume: 5  $\mu$ l.

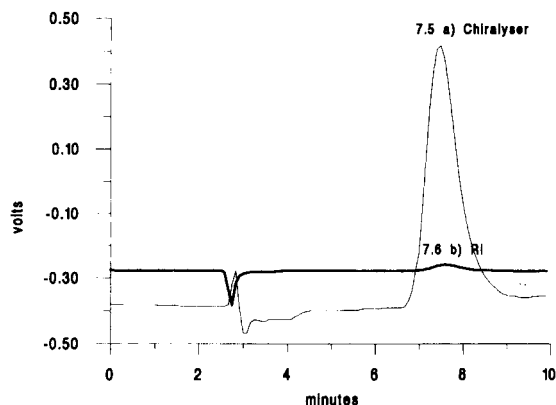


Fig. 2. Chromatograms of the same concentration of TM- $\beta$ -CD (a) performed with the RI detector and (b) the polarimetric detector. Column and mobile phase as in Fig. 1. The injection volume for the RI detector is 20  $\mu$ l and for the polarimetric detector 5  $\mu$ l.

donated by Roquette (France, 62136 Lestrem). 10- $\mu$ m LiChrosorb RP8, 10- $\mu$ m LiChrosorb RP18 and 10- $\mu$ m LiChrosorb NH<sub>2</sub> were obtained from Merck (Darmstadt). Other reagents and solvents were of analytical reagent grade and were used without further purification.

### 2.2. Apparatus and procedures

Chromatographic experiments were performed using a Waters (Vienna) Model 590 chromatograph, a Rheodyne type 7125 injector equipped with 5- $\mu$ l or 20- $\mu$ l loops and two types of detectors (a Knauer (Berlin) Type 198 refractive index detector and a Knauer “Chiralyser 1.4” detector).

For analytical purposes three columns were used: a 250  $\times$  4 mm i.d. column packed with 10- $\mu$ m LiChrosorb RP18 (I), and two columns (II, III) of 100  $\times$  4 mm i.d. packed with 10- $\mu$ m LiChrosorb RP8 and 10- $\mu$ m LiChrosorb NH<sub>2</sub>, respectively.

The mobile phases were aqueous methanolic or ethanolic solutions. All measurements have been performed at ambient temperature.

## 3. Results

### 3.1. Preliminary tests of detection system (with respect to cyclodextrins)

Preliminary tests of the polarimetric detection system preceded the more exact studies on separation and

Table 1  
Capacity factors ( $k'$ ) of various CDs on various columns depending of the eluent composition at ambient temperature

	NH <sub>2</sub>		RP8		RP18	
	MeOH	90% EtOH	5% MeOH	10% MeOH	5% EtOH	10% MeOH
$\alpha$ -CD	1.2	3.7	6.1	2.2	0.8	1.8
$\beta$ -CD	1.7	4.6	15.3	6.3	4.3	6.5
$\gamma$ -CD	2.4	8.3	7.9	3.2	1.4	1.5

Columns used: 100  $\times$  4 mm i.d. filled with LiChrosorb RP8, flow rate 0.5 ml/min; 250  $\times$  4 mm i.d. filled with LiChrosorb RP18, flow rate 0.95 ml/min; 100  $\times$  4 mm i.d. filled with LiChrosorb NH<sub>2</sub>, flow rate 0.5 ml/min.

determination of cyclodextrins. Its goal was to obtain a crude estimation of the linearity of the detection system and an approximation of the detectabilities.

All cyclodextrins offered to the market are produced from starch, and are optically active (right-handed). The specific rotations determined at 25°C using the D line of sodium are +150.5, +162 and +177.4 for  $\alpha$ -CD,  $\beta$ -CD and  $\gamma$ -CD, respectively [12,13]. This has been taken as the basis for the design of the detection system. In order to compare the properties of the refractive index and chiral detector being applied, the measurements were first carried out on the refractive index detector and then on the chiral detector.

It has been found that the relationship between peak area and concentration of cyclodextrins in the injected sample (of the same volume) can be considered as linear for dilute solutions, and this is in agreement with earlier observations that a plot of rotation versus cyclodextrin concentration is linear within the 0– $1.5 \times 10^{-2}$  M range [13]. Peak area versus TM- $\beta$ -CD

Table 2  
Capacity factors ( $k'$ ) of various CD derivatives on different columns depending of the eluent composition at ambient temperature

	RP8	RP18	
	70% MeOH	60% EtOH	90% MeOH
DM- $\beta$ -CD	1.6	0.5	–
TM- $\beta$ -CD	4.7	1.3	1.1
TM- $\alpha$ -CD	–	1.8	2.0
TM- $\gamma$ -CD	–	0.7	0.6

Columns and flow rates as in Table 1.

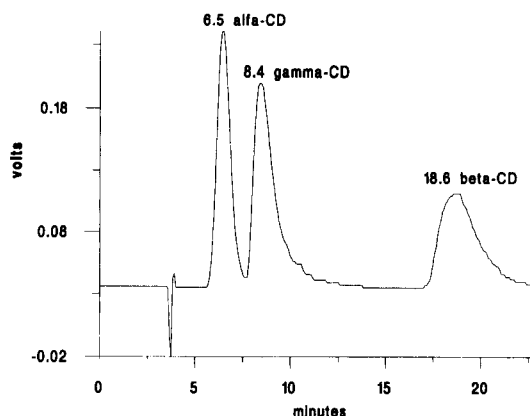


Fig. 3. Chromatogram of a mixture of  $\alpha$ -,  $\beta$ - and  $\gamma$ -CD. Column: 250  $\times$  4 mm i.d., packed with LiChrosorb RP18. Mobile phase: ethanol–water (5:95, v/v). Flow rate: 0.95 ml/min. A polarimetric detector was used.

and TM- $\alpha$ -CD concentration plots showing the chiral detector behaviour are presented in Fig. 1.

Fig. 2 presents chromatograms of TM- $\beta$ -CD samples of the same concentration registered with the RI and with the chiral detector. It is seen that the detection limit achieved by the Chiralyser under experimental conditions is much lower than that of the RI detector. Our evaluations indicate that it is ca. 40 times lower (2  $\mu$ g and 80  $\mu$ g, respectively).

### 3.2. Separations

Aqueous ethanol and methanol solutions were found to be very suitable as mobile phases for the separation of CDs using columns filled with NH<sub>2</sub> bonded and hydrocarbon phases.

#### $\alpha$ -, $\beta$ - and $\gamma$ -cyclodextrins

In Table 1 the capacity factors ( $k'$ ) of various CDs determined on the LiChrosorb NH<sub>2</sub>, LiChrosorb RP8 and LiChrosorb RP18 columns depending on the eluent composition are presented.

Fig. 3 shows the chromatogram of a mixture of  $\alpha$ -,  $\beta$ - and  $\gamma$ -CDs performed on the LiChrosorb RP18 column with aqueous ethanol as eluent and demonstrates the utility of the method for analytical purposes.

#### Permethyated derivatives

The methyl derivatives of  $\beta$ -CD are much more strongly adsorbed on hydrophobic stationary phases than free  $\beta$ -CD itself. Their elution requires higher

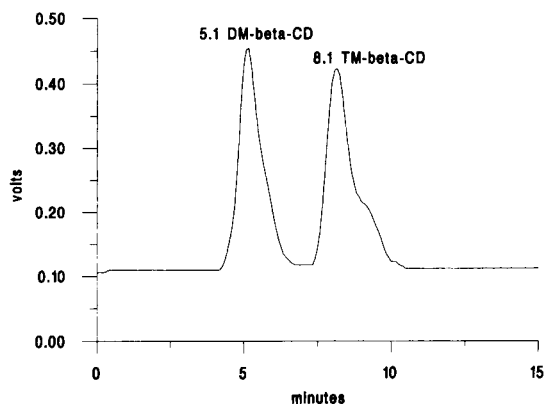


Fig. 4. Chromatogram of the DM- $\beta$ -CD and TM- $\beta$ -CD mixture. Column, mobile phase and detector as in Fig. 1.

concentrations of organic additive (ethanol or methanol) in the aqueous mobile phase solutions. Fig. 4 presents a chromatogram of a DM- $\beta$ -CD and TM- $\beta$ -CD mixture on LiChrosorb RP18 with aqueous ethanol as eluent.

Similarly to the behaviour of methyl derivatives of  $\beta$ -CD the strong adsorption on RP18 of methylated  $\alpha$ -CD and  $\gamma$ -CD was also observed. The capacity factors for methylated derivatives of cyclodextrins determined on the RP18 column are presented in Table 2.

Figs. 5 and 6 demonstrate the separation of TM- $\alpha$ -CD, TM- $\beta$ -CD and TM- $\gamma$ -CD achieved with ethanolic and methanolic eluents.

The retention times of parent  $\alpha$ -CD,  $\beta$ -CD and  $\gamma$ -CD, as well as DM- $\beta$ -CD, TM- $\beta$ -CD, TM- $\alpha$ -CD and TM- $\gamma$ -CD differ significantly from each other. All these compounds can therefore be effectively separated under appropriate conditions. As may be deduced the

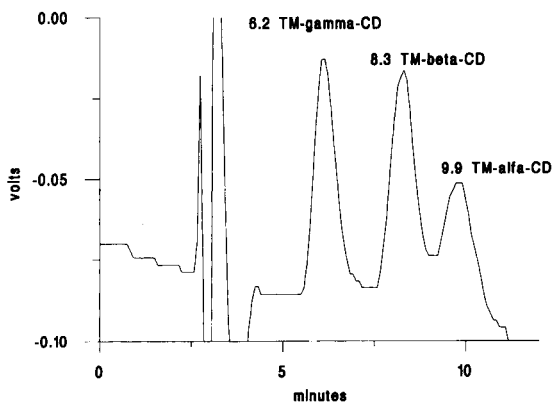


Fig. 5. Chromatogram of TM- $\alpha$ -CD, TM- $\beta$ -CD and TM- $\gamma$ -CD. Column, mobile phase and detector as in Fig. 1.

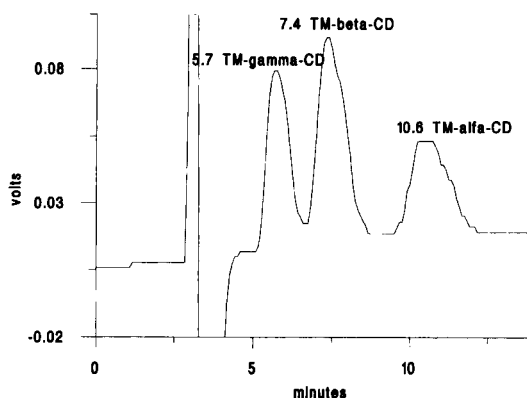


Fig. 6. Chromatogram of TM- $\alpha$ -CD, TM- $\beta$ -CD and TM- $\gamma$ -CD. Mobile phase methanol–water (90:10, v/v), column and detector as in Fig. 1.

selectivity can be increased or reduced by changing the water–alcohol composition of the eluent.

Comparing the detectors it is important to mention that only the Chiralysler makes it possible to work in the gradient mode. Fig. 7 shows an example of the separation of  $\beta$ -CD, DM- $\beta$ -CD and TM- $\beta$ -CD using gradient elution with methanolic solution.

Fig. 8 presents the comparison of chromatograms of various HP- $\beta$ -CD samples derived from different sources. It appears to be that the mixtures are very complex.

## 4. Discussion

### 4.1. Sequence of elution

For LiChrosorb NH<sub>2</sub> the order of elution is  $\alpha$ -> $\beta$ -> $\gamma$ -CD, and this is in accordance with their molecular

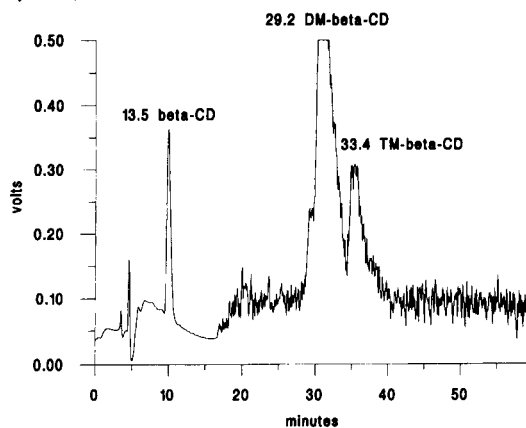


Fig. 7. Chromatogram of  $\beta$ -CD, DM- $\beta$ -CD and TM- $\beta$ -CD obtained using gradient elution with methanolic solutions. Column and detector as in Fig. 1.

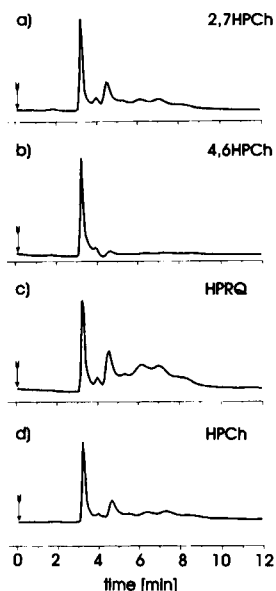


Fig. 8. Chromatograms of commercial HP- $\beta$ -CD from different firms. Mobile phase: ethanol–water (10:90, v/v). Flow rate, 0.95 ml/min. Column as in Fig. 1. (a) 2,7HP- $\beta$ -CD from Chinoïn, (b) 4,6HP- $\beta$ -CD from Chinoïn, (c) HP- $\beta$ -CD from Roquette without specification, (d) HP- $\beta$ -CD from Chinoïn without specification.

weights. On hydrocarbon phases, CDs behave differently.

For both RP phases the adsorption of  $\beta$ -CD is much stronger than the adsorption of  $\alpha$ -CD or  $\gamma$ -CD. This unexpected elution order may be explained within the framework of the solvophobic theory [14]. The  $\alpha$ - and  $\gamma$ -CD retention behaviour is almost the same. For example, for LiChrosorb RP18 and ethanolic eluent (5% ethanol) a separation factor ( $\alpha$ ) for  $\gamma/\alpha$ -CD is 1.75 while for  $\beta/\gamma$ -CD it is 3.07 and for  $\beta/\alpha$ -CD it is 5.38.

#### 4.2. Composition of the mobile phase solutions

It also seems to be of interest that CDs exhibit different sequences of elution for different alcoholic additives. From LiChrosorb RP18,  $\alpha$ -CD is eluted before  $\gamma$ -CD using the ethanolic eluent, while for methanolic solution  $\gamma$ -CD precedes  $\alpha$ -CD. Assuming that the degree of CD complexation of alcohol should enhance the elution power of the mobile phase solution the observed differences may be partly explained by various affinities of CDs towards methanol and ethanol. Big differences between the stability constants of ethanol and methanol complexes with CDs have been

already observed [15]: changes from 5.6 to 0.93 for  $\alpha$ -CD and from 0.93 to 0.32 for  $\beta$ -CD.

It is seen that for methanolic solutions better resolution between TM- $\beta$ -CD and TM- $\alpha$ -CD is achieved than between TM- $\gamma$ -CD and TM- $\beta$ -CD. In contrast, for ethanolic eluent a better separation between TM- $\gamma$ -CD and TM- $\beta$ -CD was achieved than between TM- $\beta$ -CD and TM- $\alpha$ -CD.

#### 4.3. Chiralyser

Chiroptical detectors are used for the chromatographic separation of enantiomers. The advantages and limitations of these detectors have been recently discussed in detail [16]. In the current paper we developed another branch of polarimetric detector applications, i.e., its use to monitor the separation and to quantitate the complex mixtures of the compounds differing a little in composition but belonging to the same class. Such mixtures are frequently derived from natural sources like oligosaccharides, amino acids and peptides.

#### Acknowledgements

This work was supported by grant 202429101 from the State Committee for Scientific Research.

#### References

- [1] J.N.J.J. Lammers, *Starke*, 19 (1967) 70.
- [2] J.N.J.J. Lammers, *J. Chromatogr.*, 41 (1969) 462.
- [3] J.H. Carter and E.Y. Lee, *Anal Biochem.*, 39 (1971) 521.
- [4] K. Kainume, A. Nogami and C. Mercier, *J. Chromatogr.*, 121 (1976) 361.
- [5] B. Zsádon, K.H. Otta, F. Tudos and J. Szejtli, *J. Chromatogr.*, 172 (1979) 490.
- [6] H. Hokse, *J. Chromatogr.*, 189 (1980) 98.
- [7] N.W.H. Cheetham and G. Teng, *J. Chromatogr.*, 336 (1984) 161.
- [8] T. Takeuchi, M. Murayama and D. Ishri, *J. High Resolut. Chromatogr.*, 13 (1990) 69.
- [9] T. Takeuchi, T. Miwa, A. Hemmi and T. Maeda, *J. High Resolut. Chromatogr.*, 16 (1993) 419.
- [10] M. Kramer and H. Engelhardt, *J. High Resolut. Chromatogr.*, 15 (1992) 24.
- [11] G. Schomburg, A. Deege, H. Hiurichs, E. Hubinger and H. Husonann, *J. High Resolut. Chromatogr.*, 15 (1992) 579.



- [12] J. Szejtli, *Cyclodextrins and their Inclusion Complexes*, Akademiai Kiado, Budapest, 1982.
- [13] A. Burari and L. Barcza, *J. Incl. Phenom.*, 7 (1989) 379.
- [14] R. Nowakowski, Ph.J.P. Cardot, A.W. Coleman, E. Villand and G. Guiochon, in preparation.
- [15] Y. Matsui and K. Mochida, *Bull. Chem. Soc. Jpn.*, 52 (1979) 2808.
- [16] J. Zukowski, Y. Tang, A. Berthod and D. Armstrong, *Anal. Chim. Acta*, 258 (1992) 83.



ELSEVIER

Analytica Chimica Acta 300 (1995) 207–214

**ANALYTICA  
CHIMICA  
ACTA**

# Ion chromatographic determination of traces of some oxoanions with direct spectrophotometric detection

Y.S. Fung \*, K.L. Dao

*Department of Chemistry, University of Hong Kong, Hong Kong*

Received 3 December 1993

## Abstract

Investigation of the use of a single analytical procedure using the non-suppressed ion chromatographic method with direct spectrophotometric detection capable of determining eight oxoanions simultaneously is presented in this paper. Potassium phosphate was found to be the most suitable eluent for UV absorbance detection at 205 nm. Oxoanions  $\text{AsO}_3^{3-}$ ,  $\text{SeO}_3^{2-}$ ,  $\text{AsO}_4^{3-}$ ,  $\text{VO}_3^-$ ,  $\text{SeO}_4^{2-}$ ,  $\text{WO}_4^{2-}$ ,  $\text{MoO}_4^{2-}$  and  $\text{CrO}_4^{2-}$  were detected at  $\text{ng ml}^{-1}$  levels with well separated peaks at retention time  $< 25$  min. The working range is in the range  $\text{ng ml}^{-1}$  to  $50 \mu\text{g ml}^{-1}$ . The method is sufficiently sensitive to determine As(V), V(V), Mo(VI) and Cr(VI) anions (and  $\text{NO}_3^-$ ) directly in a river water sample. The accuracy of these results was established by comparison with conventional atomic absorption methods.

*Keywords:* Chromatography; Oxoanions; Metal speciation; Waters

## 1. Introduction

Analysis for trace amounts of elements such as chromium, vanadium, tungsten, molybdenum, selenium and arsenic is often needed in environmental monitoring, as all these elements have been recognized as dangerous or potentially dangerous pollutants [1,2]. The inorganic form of these elements exists mainly as oxoanions in natural waters and their major oxidation states are Cr(VI), V(V), W(VI), Mo(VI), Se(VI), and As(V). For selenium and arsenic, chemical speciation is particularly important as each form has a completely different ecological fate with a great difference in their impact on the environment. Thus, analytical methods capable of differentiating the various oxidation states are needed. The method must be very

sensitive, as the concentration of concern in the environment is very low, at the sub- $\mu\text{g ml}^{-1}$  level.

The most common methods for the analysis of these anions use atomic absorption spectrometry (AAS) [3–7]. As many of these elements are refractory and their concentrations are extremely low in the environment, nitrous oxide has to be used as the flame oxidant to enhance the atomisation. Hydride generation methods are often used to increase the sensitivity for some of these anions.

As result of different analytical demands for different metals, separate sets of experimental conditions are often needed for the analysis of each of the metals. Other sensitive methods for the analysis of individual oxoanion such as UV-visible spectrophotometry [8–10], graphite furnace AAS [11], inductively coupled plasma atomic emission spectrometry [12,13] and x-ray fluorescence spectrometry [14] all require pre-con-

\* Corresponding author.

centration with specific and time consuming sample preparation steps. Thus, a simple analytical procedure is needed capable of multi-element analysis for these oxoanions, as it would decrease greatly the time required for a given analysis.

The advance of ion chromatography (IC) since the 1970s provides a sensitive tool for multi-element analysis of anions and methods had been developed using suppressed IC for the determination of selenium, arsenic, molybdenum and chromium as their oxoanions under alkaline conditions using carbonate as the eluent [15,16]. However, the need to use a dedicated and expensive IC system restricts the general application of the technique.

The recent advance of single column ion chromatography (SCIC) which makes use of conventional liquid chromatography equipment provides an opportunity for developing a more general technique for multi-element analysis for these anions. However, the techniques developed were restricted to the analysis of one or two anions [17,18]. Thus, a procedure for multi-oxoanion analysis needs to be developed by use of non-suppressed IC.

As most of the oxoanions are strong UV absorbers in the range 195–220 nm, a procedure for direct spectrophotometric determination would be suitable for analyses for oxoanions in environmental samples with complicated matrices as the absorption wavelength could be carefully selected to achieve the required selectivity and sensitivity.

This paper presents the work done to select a suitable absorption wavelength and eluent for the direct spectrophotometric determination of oxoanions after ion chromatographic separation, the optimisation of the analytical parameters and the evaluation of the application of the procedure to river water analysis.

## 2. Experimental

### 2.1. Reagents and standard solutions

All chemicals used in the present studies were analytical grade reagents unless otherwise stated. Water was distilled and deionised before use. The stock solutions of  $1000 \mu\text{g ml}^{-1}$  of the various anions standards were prepared by dissolving the corresponding salts in deionised water. Working standard solutions were

obtained by diluting the stock solutions as required; sodium salts were used in all cases except for chromate which was prepared from the potassium salt. Mixed standard solutions were prepared from individual standard solutions. The selenium and arsenic standard solutions were freshly made from standard stock solutions on a daily basis.

### 2.2. Equipment and apparatus

The ion chromatograph consisted of a Perkin-Elmer Series 3 pump, a Rheodyne Model 7125 high pressure injection valve with a  $100 \mu\text{L}$  sampling loop, a Hamilton PRP-X100 column ( $150 \text{ mm L.} \times 4.6 \text{ mm i.d.}$ ) with a guard column packed with PRP-1 resin, a Milton Roy (SpectroMonitor 3100) variable wavelength absorbance detector, and a Hitachi strip chart recorder.

For AAS measurements, a Varian AA-575 atomic absorption spectrometer was used. An air-acetylene flame was used for atomisation of Cr, acetylene-nitrous oxide for Mo, W and V, and hydride generation was used as a sample introduction technique for Se and As prior to atomisation in an air-hydrogen flame.

### 2.3. Ion chromatographic procedure

The eluents were prepared by dissolving dipotassium hydrogenphosphate, sodium citrate or sodium tartrate in 1 l of deionised water. The pH of the eluents was adjusted according to the cation of the salt used either by KOH or NaOH solution. The eluents were filtered through a  $0.45 \mu\text{m}$  nylon 66 membrane filter and degassed under vacuum prior to use. A glass tube packed with Carbosorb AS (6–12 mesh, BDH) was inserted over the eluent reservoir to decrease the ingress of atmospheric  $\text{CO}_2$  so as to maintain a constant pH for the eluent. The eluent flowrate was normally set at  $1.5 \text{ ml min}^{-1}$  or as otherwise stated and the operating temperature was maintained at  $25^\circ\text{C}$ . All samples were passed through a  $0.45 \mu\text{m}$  filter immediately before injection into the ion chromatograph.

## 3. Results and discussion

### 3.1. Selection of wavelength

Many common inorganic anions such as fluoride, chloride, sulfate, phosphate and perchlorate do not

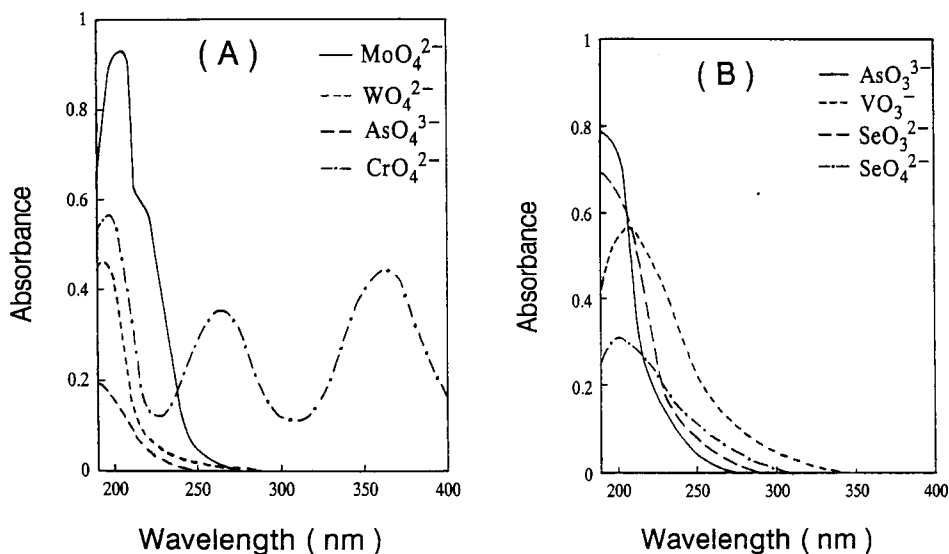


Fig. 1. UV absorption spectra for metal oxoanions. (A) Molybdate, tungstate, arsenate and chromate; (B) arsenite, vanadate, selenite and selenate.

absorb in the range 195 to 220 nm [19–21], but nitrate, nitrite, bromide and many metal oxoanions show appreciable absorption in this wavelength range [22]. Thus, some degree of selectivity for detection is possible, which can be used to differentiate the UV-absorbing anions in samples containing high levels of UV-transparent ions, such as chloride and sulfate [23,24]. As all oxoanions absorb strongly in the UV region, their UV absorption spectra were measured (Fig. 1). The spectra for SeO<sub>4</sub><sup>2-</sup>, MoO<sub>4</sub><sup>2-</sup>, VO<sub>3</sub><sup>-</sup>, WO<sub>4</sub><sup>2-</sup> and CrO<sub>4</sub><sup>2-</sup> show maxima around 200 to 205 nm while AsO<sub>3</sub><sup>3-</sup> and AsO<sub>4</sub><sup>3-</sup> have their maximum absorption at ca. 190 nm. For wavelengths below 200 nm, many other inorganic anions start to absorb and thus 205 nm was chosen as the wavelength for general detection of oxoanions, as it has the least interference and allows good sensitivity for most of the oxoanions.

### 3.2. Choice of eluent composition

Phthalate is the most common eluent used in SCIC procedures for indirect spectrophotometric determination of inorganic anions [25–28]. However, its application for trace oxoanion analysis leads to many problems such as long retention time, low sensitivity and frequent occurrence of inverted peaks in the chromatogram. The long retention time is caused by the strong affinity of the oxoanions for the column. The

occurrence of an inverted peak is due to the strong UV absorbing properties of some of the oxoanions at the monitored wavelength. Thus, a search was performed to find suitable alternative eluents.

One important consideration for eluent selection is that all components must be essentially non-absorbing in the desired wavelength range. For this reason, eluents such as phosphate, citrate and tartrate [29–34] are used as the mobile phase. Amongst these eluents, potassium phosphate showed the least absorption at 205 nm while citrate and tartrate exhibited higher absorption at this wavelength. During the tests for these eluents, they were adjusted to pH > 8.0 because many oxoanions are unstable in acidic solutions. For example, arsenite has a pK<sub>a</sub> value of 9.18 [35] and behaves as a weak acid at lower pH. Similarly, tungsten exists mainly as tungstate at pH ≥ 8.5 whereas hexatungstic acid predominates at lower pH.

Results for the use of 5 mM sodium tartrate as the eluent are shown in Fig. 2A using a standard mixture of common anions and oxoanions (Cl<sup>-</sup>, NO<sub>3</sub><sup>-</sup>, SO<sub>4</sub><sup>2-</sup>, AsO<sub>4</sub><sup>3-</sup>, VO<sub>3</sub><sup>-</sup>, WO<sub>4</sub><sup>2-</sup>, MoO<sub>4</sub><sup>2-</sup> and CrO<sub>4</sub><sup>2-</sup>). The Cl<sup>-</sup>, SO<sub>4</sub><sup>2-</sup> and AsO<sub>4</sub><sup>3-</sup> peaks show up as inverted peaks and the WO<sub>4</sub><sup>2-</sup> peak is absent. The occurrence of an inverted peak is due to the weaker absorption of the anions compared to tartrate; the absence of a WO<sub>4</sub><sup>2-</sup> peak is due to the strong complexation of tartrate with tungstate giving a product which strongly interacts with the ion

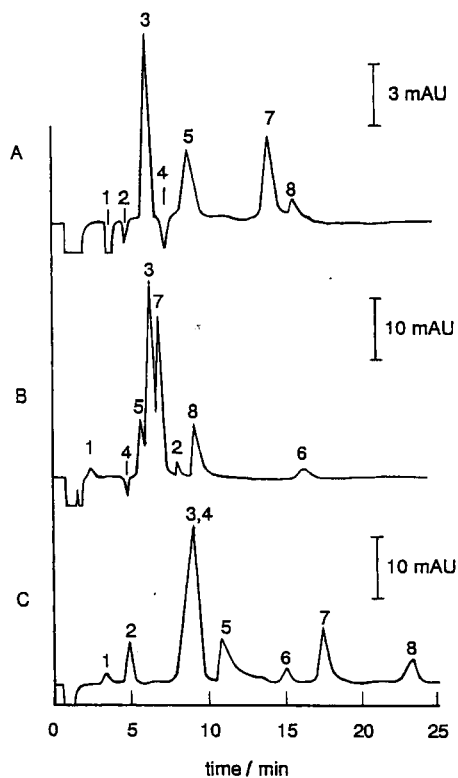


Fig. 2. The effect of the eluent for direct spectrophotometric detection of oxoanions. Flow rate = 1.0 ml/min; wavelength = 205 nm; sample volume = 100  $\mu$ l. Peaks: (1) 50 mg/l  $\text{Cl}^-$ ; (2) 10 mg/l  $\text{AsO}_4^{3-}$ ; (3) 5 mg/l  $\text{NO}_3^-$ ; (4) 50 mg/l  $\text{SO}_4^{2-}$ ; (5) 2 mg/l  $\text{VO}_5^-$ ; (6) 10 mg/l  $\text{WO}_4^{2-}$ ; (7) 2 mg/l  $\text{MoO}_4^{2-}$ ; (8) 10 mg/l  $\text{CrO}_4^{2-}$ . (A) 5 mM sodium tartrate, pH 8.7; (B) 5 mM sodium citrate, pH 8.6; (C) 5 mM potassium phosphate, pH 8.5. mAU = Absorbance  $\times 10^3$ .

exchange column. Both of the above effects are undesirable.

The use of 5 mM sodium citrate led to fewer inverted peaks but an undesirable compression of the peaks within the shorter elution time. Thus, the nitrate, vanadate and molybdate peaks overlap (Fig. 2B) at a retention time around 7 min. The best ion chromatogram was obtained by using 5 mM potassium phosphate as the eluent (Fig. 2C) under alkaline conditions as it gives no inverted peaks and all the peaks eluted are symmetrical and clearly resolved. Thus, phosphate was selected as the eluent for optimisation of the analytical procedure.

### 3.3. Optimisation of chromatographic conditions

The effect of the eluent concentration on the selectivity and sensitivity of the IC method is shown in Figs.

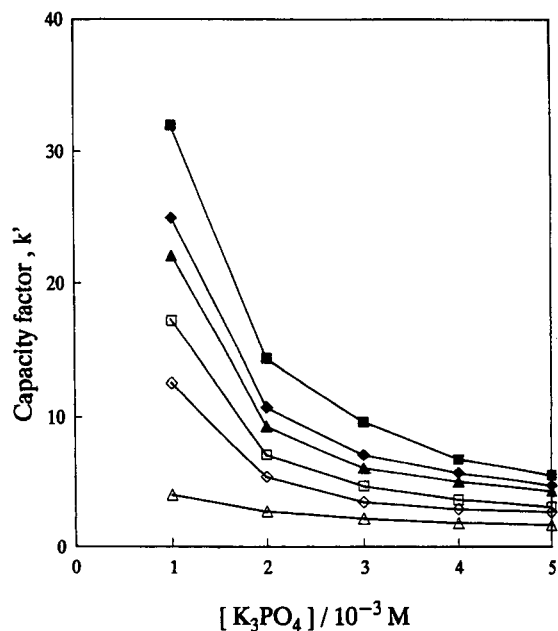


Fig. 3. The effect of eluent on the capacity factor ( $k'$ ) for metal oxoanions.  $[\text{K}_3\text{PO}_4] = 1-4$  mM, pH = 10.0; wavelength = 205 nm; flow rate = 1.5 ml/min; sample volume = 100  $\mu$ l.  $\Delta$ ,  $\text{AsO}_4^{3-}$ ;  $\diamond$ ,  $\text{VO}_5^-$ ;  $\square$ ,  $\text{SeO}_4^{2-}$ ;  $\blacktriangle$ ,  $\text{WO}_4^{2-}$ ;  $\blacklozenge$ ,  $\text{MoO}_4^{2-}$ ;  $\blacksquare$ ,  $\text{CrO}_4^{2-}$ .

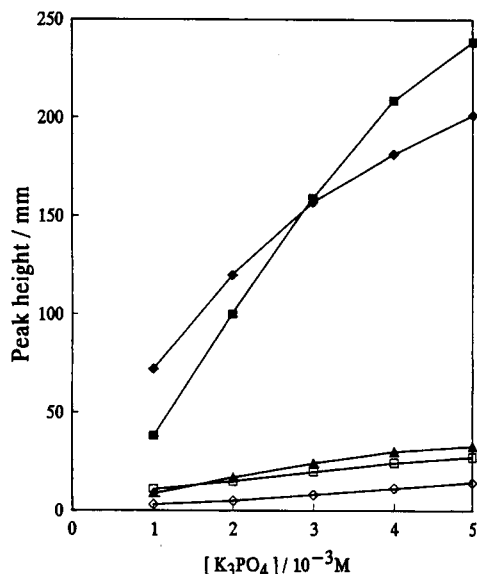


Fig. 4. The effect of eluent concentration on the peak height for metal oxoanions. Conditions as for Fig. 3.  $\diamond$ , 20 mg/l each of  $\text{SeO}_4^{2-}$ ,  $\text{AsO}_4^{3-}$ ;  $\square$ , 5 mg/l  $\text{WO}_4^{2-}$ ;  $\blacktriangle$ , 5 mg/l  $\text{CrO}_4^{2-}$ ;  $\blacklozenge$ , 5 mg/l  $\text{VO}_5^-$ ;  $\blacksquare$ , 5 mg/l  $\text{MoO}_4^{2-}$ .

3 and 4, respectively. The retention of all anions in general becomes shorter with increasing eluent concentration. However, the differences in the retention times for different oxoanions are smaller at lower phosphate concentration (Fig. 3). Thus, a compromise in selectivity and time of analysis needs to be made. A higher phosphate concentration also leads to larger peak heights (Fig. 4).

The ionic strength of the eluent increases with the eluent concentration and this will decrease the interaction of anions with the ion-exchange sites in the column. The retention of strongly held anions is more strongly affected than the loosely held ions. This is shown clearly by the fact that by increasing  $K_3PO_4$  concentration from 1.0 to 4.0 mM, the capacity factor  $k'$  value of  $CrO_4^{2-}$  decreases from 33.2 to 7.5 (a 78% decrease), and that of  $AsO_4^{3-}$  from 4.2 to 2.3 (a 45% decrease).

For eluent concentrations higher than 3 mM, separation of these oxoanions becomes more difficult due to the overlapping of the early eluted oxoanions with the injection peak. For eluent concentrations < 2 mM, the retention of these oxoanions become greater and consequently peak broadening of the late eluting oxoanions is observed. Based on a consideration of the above factors, 3 mM  $K_3PO_4$  was chosen as the eluent concentration.

The pH of the eluent was found to have a strong effect on the retention and shape of the analyte peaks in the ion chromatogram (Fig. 5). This is due to the fact that pH could affect the ionic charge on the multicharged phosphate anion ( $pK_2 = 7.2$  and  $pK_3 = 12.4$ ) with the ionic charge and eluent strength being greater at higher pH of the mobile phase, thus leading to shorter elution time (Fig. 5). However, an inverted system peak was found to appear near  $VO_3^-$  when the eluent pH was higher than 9.3. The retention time of this system peak is independent of the eluent concentration when the eluent pH is kept constant. However, it shifts to a shorter retention time with increasing height when the eluent pH is > pH 10. The system peak becomes negligible for an eluent of  $pH \leq 9.0$ . In addition, poor separation amongst oxoanions is observed as the pH increases above 10.0. In order to avoid system peak interference, 3 mM  $K_2HPO_4$  at pH 9.0 was selected as the eluent.

Under the optimised conditions, the ion chromatograms for the separation of different oxoanions are

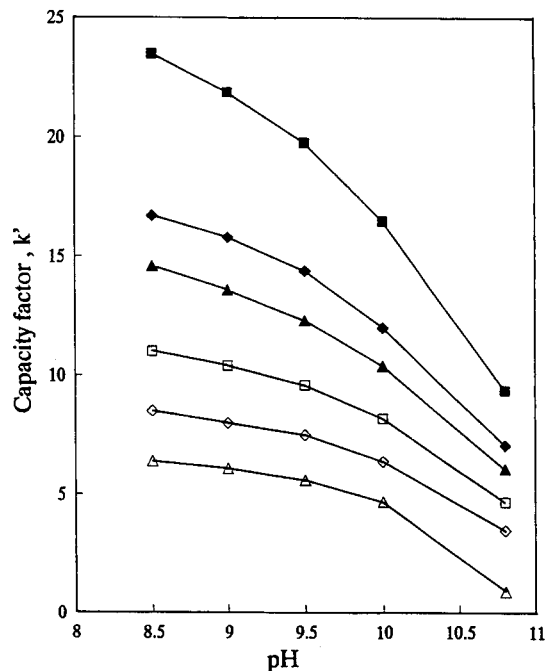


Fig. 5. The effect of pH on the capacity factor ( $k'$ ) for metal oxoanions. [ $K_3PO_4$ ] = 3 mM; wavelength = 205 nm; flow rate = 1.5 ml/min; sample volume = 100  $\mu$ l.  $\Delta$ ,  $AsO_4^{3-}$ ;  $\diamond$ ,  $VO_3^-$ ;  $\square$ ,  $SeO_4^{2-}$ ;  $\blacktriangle$ ,  $WO_4^{2-}$ ;  $\blacklozenge$ ,  $MoO_4^{2-}$ ;  $\blacksquare$ ,  $CrO_4^{2-}$ .

shown in Figs. 6 and 7. The separation of different oxidation forms of As and Se are shown in Fig. 6. The  $AsO_3^{3-}$  peak is fairly close to the water dip and its retention time could be adjusted by decreasing the pH (20% increase from pH 9.0 to 8.0) and eluent concentration (15% increase from  $K_2HPO_4$  concentration of 3 mM to 2 mM). However, the change of pH and eluent concentration could also affect other oxoanions and the conditions used are the results of a compromise for the separation of commonly occurring oxoanions, which are all well separated with symmetrical peaks as shown by the chromatogram (Fig. 7). The total time for a sample run was  $\leq 20$  min. If the determination of  $AsO_3^{3-}$  is affected by the water dip, 2.5 mM  $K_2HPO_4$  at pH 8.5 can be used as the eluent to improve their separation. However, the sensitivity for other oxoanions will be decreased by about 10% under these conditions.

The working range and detection limits for the various oxoanions are shown in Table 1. Most of the anions could be detected at  $ng\ ml^{-1}$  levels with a working range up to about  $50\ \mu g\ ml^{-1}$ .

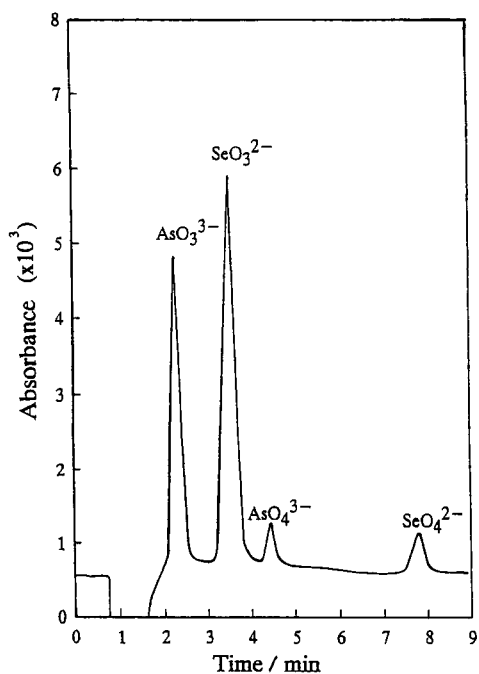


Fig. 6. Chromatogram for the separation of arsenite, selenite, arsenate and selenate, each 1 mg/l. Conditions: eluent = 3 mM  $\text{K}_2\text{HPO}_4$ , pH 9.0; wavelength = 205 nm; flow rate = 1.5 ml/min; sample volume = 100  $\mu\text{l}$ .

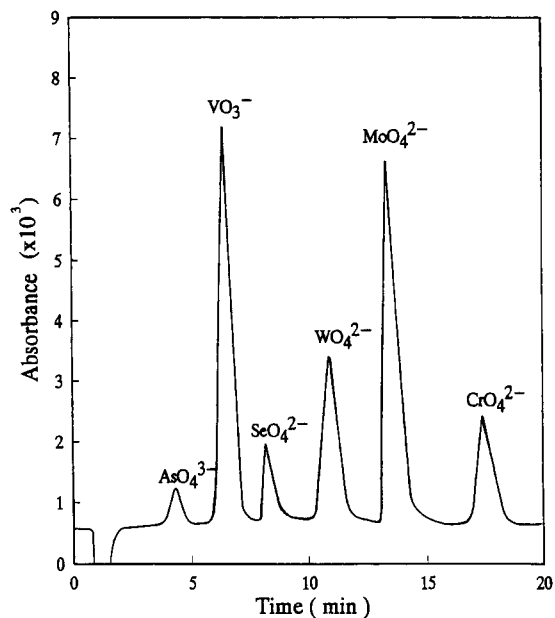


Fig. 7. Chromatogram for the separation of other oxoanions. Arsenate, 1 mg/l; vanadate, 0.2 mg/l; selenate, 2 mg/l; tungstate, 0.2 mg/l; molybdate, 0.2 mg/l; chromate, 0.2 mg/l. Conditions as for Fig. 6.

Table 1

The working range and retention time for ion chromatographic determination of metal oxoanions (conditions as in Fig. 6)

Metal oxoanion	Retention time (min)	Working range <sup>a</sup> ( $\mu\text{g ml}^{-1}$ )
$\text{AsO}_3^{3-}$	2.5	0.002–50
$\text{SeO}_3^{2-}$	3.9	0.001–50
$\text{AsO}_4^{3-}$	4.6	0.02–50
$\text{VO}_3^-$	6.8	0.002–30
$\text{SeO}_4^{2-}$	8.4	0.03–50
$\text{WO}_4^{2-}$	11.4	0.005–15
$\text{MoO}_4^{2-}$	13.6	0.001–50
$\text{CrO}_4^{2-}$	18.0	0.005–50

<sup>a</sup> The lowest concentration is the detection limit, signal-to-noise = 2.

### 3.4. Applicability studies

Results for the application of the technique developed for river water analysis are shown in Fig. 8 and Table 2. For the eight oxoanions under study, four of them were found in the river water sample with detectable concentrations. The concentrations of these oxoanions were also determined by AAS. All anions were

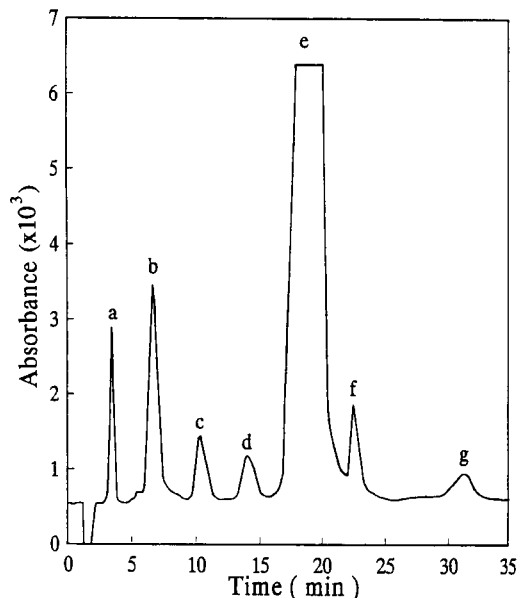


Fig. 8. Chromatogram of a sample of river water spiked with a mixture of arsenic and selenium oxoanions. Peaks: (a) arsenite, (b) arsenate, (c) selenite, (d) selenate, (e) nitrate, (f) molybdate and (g) chromate; arsenite and selenite = 0.1 mg/l, arsenate and selenate = 1 mg/l. Eluent = 2.5 mM  $\text{K}_2\text{HPO}_4$ , pH 8.5; other conditions as in Fig. 6.

Table 2  
Recovery of various elements as oxoanions in river water

Element	Present ( $\mu\text{g ml}^{-1}$ )	Added ( $\mu\text{g ml}^{-1}$ )	Found <sup>a</sup> ( $\mu\text{g ml}^{-1}$ )	Recovery (%)
As(III)	ND	0.081	0.077	95
As(V)	0.015	0.540	0.535	96
Se(IV)	ND	0.062	0.061	98
Se(VI)	ND	1.10	1.04	95
V(V)	0.013	0.258	0.264	97
W(VI)	ND	0.370	0.358	97
Mo(VI)	0.026	0.302	0.324	99
Cr(VI)	0.015	0.224	0.230	96

<sup>a</sup> Replicate analyses of five samples. ND = not detected.

added at known concentrations to the river water sample for recovery tests. Recoveries of >95% were obtained from the eight oxoanions studied.

The results obtained using the AAS and the IC procedures are compared and given in Table 3. Using the matched pair *t*-test method [36], the 5% *t* value calculated based on the difference in the results obtained by the IC and AAS methods is 0.777. The computed *t* value is within the statistical *t* value of 3.182 for 4 degrees of freedom. Thus, no statistically significant difference was obtained using the two methods for the determination of these oxoanions at the 95% confidence level.

The chromatogram obtained for the river water sample, however, also gives a large peak for nitrate, which could interfere with the determination of the other oxoanions, as nitrate is normally present at the  $\mu\text{g ml}^{-1}$  level in river water. A preconcentration and cleanup procedure has been developed to solve the problem for environmental water samples with high nitrate content; the results will be reported in another paper.

Table 3  
Comparison of trace element determinations in river water by IC and AAS methods

Element	Found by IC <sup>a</sup> ( $\text{ng ml}^{-1}$ )	Found by AAS <sup>a</sup> ( $\text{ng ml}^{-1}$ )
As	15.3 ± 0.9	14.2 ± 1.0
V	13.0 ± 0.7	13.6 ± 0.9
Mo	26.4 ± 1.3	27.5 ± 1.7
Cr	14.9 ± 0.9	15.8 ± 0.8

<sup>a</sup> Replicate analyses of five samples.

## 4. Conclusions

The analytical procedure developed is shown capable of multi-oxoanion determination using non-suppressed ion chromatography. Under the optimised conditions, the oxoanions could be determined at  $\text{ng ml}^{-1}$  levels and the procedure can be applied directly for river water analysis, with results verified using conventional AAS.

## Acknowledgements

We would like to acknowledge the support of the Hong Kong University Research Grants Committee for the above work.

## References

- [1] S.E. Manahan, *Environmental Chemistry*, 4th edn., Brook and Cole Publ., California, 1984, p. 150.
- [2] L. Fishbein, *Int. J. Environ. Anal. Chem.*, 17 (1984) 113.
- [3] S.M. Workman and P.N. Soltanpour, *Soil Sci. Soc. Am. J.*, 44 (1980) 1331.
- [4] R.C. Chu, G.P. Barron and P.A.W. Baumgarner, *Anal. Chem.*, 44 (1972) 1476.
- [5] B.B. Mesman and T.S. Thomas, *Anal. Lett.*, 8 (1975) 449.
- [6] F.D. Pierce and H.R. Brown, *Anal. Chem.*, 49 (1977) 1417.
- [7] P.D. Goulden and P. Brookabunk, *Anal. Chem.*, 46 (1974) 1413.
- [8] W. Qian-Feng and L. Peng-Fel, *Talanta*, 30 (1983) 275.
- [9] C.A. Snyder and D.A. Isola, *Anal. Chem.*, 51 (1979) 1478.
- [10] J.P. Riley and D. Taylor, *Anal. Chim. Acta*, 41 (1968) 175.
- [11] S.X. Quan, J.L. Zhu and N.Z. Ming, *At. Spectrosc.*, 3 (1982) 41.
- [12] V. Dupont, Y. Auger, C. Jeandel and M. Wartel, *Anal. Chem.*, 63 (1991) 520.
- [13] B. Pahlavanpour, M. Thompson and L. Thorne, *Analyst (London)*, 105 (1980) 756.
- [14] J.G. Bergmann, C.H. Ehrhardt, L. Granatelli and J.L. Janik, *Anal. Chem.*, 39 (1967) 1259.
- [15] Yu.A. Zolotov, O.A. Shpigun and L.A. Bubchikova, *Fresenius' Z. Anal. Chem.*, 316 (1983) 8.
- [16] S.S. Goyal, A. Hafez and D.W. Rains, *J. Chromatogr.*, 537 (1991) 269.
- [17] R.W. Siergiej and N.D. Danielson, *J. Chromatogr. Sci.*, 21 (1983) 362.
- [18] R.G. Gerritse and J.A. Adeney, *J. Chromatogr.*, 347 (1985) 419.
- [19] P.R. Haddad and A.L. Heckenberg, *J. Chromatogr.*, 300 (1984) 357.



- [20] R.N. Reeve, *J. Chromatogr.*, 177 (1980) 393.
- [21] T. Kamiura, Y. Mori and M. Tanaka, *Anal. Chim. Acta*, 154 (1983) 319.
- [22] R.P. Buck, S. Singhadeja and L.B. Rogers, *Anal. Chem.*, 26 (1954) 1240.
- [23] H.J. Cortes, *J. Chromatogr.*, 234 (1982) 517.
- [24] U. Leuenberger, R. Gauch, K. Rieder and E. Baumgartner, *J. Chromatogr.*, 202 (1980) 461.
- [25] F.G.P. Mullins, *Analyst*, 112 (1987) 665.
- [26] H.J. Cortes and T.S. Stevens, *J. Chromatogr.*, 295 (1984) 269.
- [27] H. Small and T.E. Miller, *Anal. Chem.*, 54 (1982) 462.
- [28] N. Chauret and J. Hubert, *J. Chromatogr.*, 469 (1989) 329.
- [29] S.H. Kok, K.A. Buckle and M. Wooton, *J. Chromatogr.*, 260 (1983) 189.
- [30] N.E. Skelley, *Anal. Chem.*, 54 (1982) 712.
- [31] S. Rokushika, Y.Q. Zong, L.S. Zhuo and H. Hiroyuki, *J. Chromatogr.*, 280 (1983) 69.
- [32] B.B. Wheals, *J. Chromatogr.*, 262 (1983) 61.
- [33] R.G. Gerritse, *J. Chromatogr.*, 171 (1979) 527.
- [34] P.E. Jackson, P.R. Haddad and S. Dilli, *J. Chromatogr.*, 295 (1984) 471.
- [35] N. Hirayama and T. Kuwamoto, *J. Chromatogr.*, 447 (1988) 323.
- [36] E.L. Bauer, *A Statistical Manual for Chemists*, 2nd edn., 1971, Academic Press, New York, p. 65.

# Peroxidatic activity of metalloporphyrin binding to serum albumin: enhancement effect of serum albumin on metalloporphyrin catalyzed luminol chemiluminescence reaction

Jian-Ke Tie<sup>1</sup>, Wen-Bao Chang, Yun-Xiang Ci<sup>\*</sup>

*Department of Chemistry, Peking University, Beijing 100871, China*

Received 9 April 1994; revised manuscript received 20 June 1994

## Abstract

The metalloporphyrin (M-P) catalyzed luminol–H<sub>2</sub>O<sub>2</sub> chemiluminescence (CL) system can be significantly enhanced in the presence of serum albumins. The enhancement may be explained in terms of the formation of a molecular complex between M-P and serum albumin. The hydrophobic and coordination interactions between M-P and serum albumin were confirmed by comparing the degree of enhancement by the protein on different types of M-P catalyzed CL reactions and by comparing the catalytic activity of M-P/bovine serum albumin (BSA) and M-P/BSA/anti-BSA complexes. Only the non-ionic M-P catalyzed CL reaction was significantly enhanced, and the enhanced CL reaction was inhibited by an immunoreaction. The optimum conditions of the M-P/albumin complex catalyzed CL reaction were evaluated by using a flow-injection system, which was very similar to that using hemoglobin as the catalyst. A brief prospective on the general applicability of the enhanced CL reaction for the determination of serum albumin (2.5–500 μg/ml) is given.

*Keywords:* Chemiluminescence; Catalytic methods; Metalloporphyrins; Serum albumin

## 1. Introduction

Because of their importance in biological and photochemical processes, porphyrins and metalloporphyrins (M-P) have attracted much interest. M-P have been intensively investigated as biomimetic model systems for catalase, peroxidase and cytochrome P-450 in recent years [1–5]. As ideal chemical models for these enzymes, a fifth ligand for M-P (such as the phenolic hydroxyl group of tyrosine for catalase, the imidazole group of histidine (His) for peroxidase and the sulfhydryl group of cystine for cytochrome P-450) that char-

acterizes these enzymes is often necessary. Its position is *trans* to the reactive side of the porphyrin plane such that the substrate can locate on the opposite face of the M-P. A previous report shows that a small amount of lipophilic carboxylic acid and a heterocyclic nitrogen base (serving as the axial ligand) strongly accelerates the hydrogen peroxide oxygenation of alkanes catalyzed by Mn-tetraarylporphyrin [6]. Baldwin et al [7] have investigated microperoxidase-8 as a peroxidase model with 18-His as the fifth ligand for M-P. We have reported that the peroxidatic activity of M-Pr is greatly inhibited when two axial coordination sites are occupied by pyridine or an amino acid [8,9]. All of these reports suggest that the axial ligands were critical for the catalytic activity of M-P. From the point of view of

<sup>\*</sup> Corresponding author.

<sup>1</sup> Present address: Life Science Center, College of Life Science, Peking University, Beijing 100871, China.

analytical chemistry, M-P have been widely used as peroxidase substitutes in calorimetric [10–12], fluorometric [13,14] and chemiluminescence (CL) [15–17] analysis.

Most peroxidases and apparently all myoglobins are monomeric hemoproteins with the same prosthetic group and proximal His ligand, yet  $\text{H}_2\text{O}_2$  reacts far more rapidly with the former than with the latter. This provides a classic example among metalloproteins of the ability of the protein to control functions. Therefore, metal complexes bound to protein have been of interest in connection with a metalloenzyme model [18,19]. There are only a few reports concerning M-P included in and/or bound to proteins [20–22], and catalytic peroxidase model reactions catalyzed by these M-P/protein complexes (non-covalent binding) have never been reported. In the present paper, the enhancement effect of albumin on the M-P catalyzed luminol CL reaction was investigated by using a flow-injection system. Hydrophobic and coordination interactions between albumin and M-P were evaluated by using an immunoreaction and by comparing the degrees of enhancement by serum albumin in different kinds of M-P catalyzed CL reactions. The optimum conditions for use of the M-P/albumin complex as the peroxidase model in the luminol CL reaction have been investigated. The feasibility of utilizing the phenomenon as a means of determination of serum albumin was conducted.

## 2. Experimental

### 2.1. Reagents

Human serum albumin (HSA), bovine serum albumin (BSA), hemoglobin (bovine blood), and luminol were purchased from Sigma. Hydrogen peroxide (30%) was purchased from Oriental Chemical Works (Tianjin, China). Tetrakis(4-aminophenyl)porphyrin [TPPA<sub>4</sub>] was purchased from Er-Mei Mountain Chemical Co. Other reagents were analytical-reagent grade and purchased from Beijing Chemical Works. All aqueous solutions were prepared in doubly distilled water.

The following reagents were used as received: rabbit serum albumin (RSA), ovalbumin (OVA) and anti-BSA from Dr. Nian-Qing Lu which were prepared by

the method of Kabat [23], monoclonal anti-fetoprotein (AFP) (purified on DEAE Sephadex A-50) from the Chinese Medical Science Academy Cancer Institute.

Metal porphyrin complexes of Mn-tetrakis(sulphophenyl)porphyrin (Mn-TPPS<sub>4</sub>), Mn-tetrakis(*N*-methylpyridiniumyl)porphyrin (Mn-TMPyP) and Mn-TPPA<sub>4</sub> were prepared as described earlier [9] except that Mn-TPPA<sub>4</sub> was prepared by refluxing the  $\text{Mn}(\text{CH}_3\text{COO})_2$  and TPPA<sub>4</sub> in ethanol-water (1:1). Working solution of Mn-TPPA<sub>4</sub> was prepared by diluting  $1 \times 10^{-5}$  M ethanol stock solution with 0.01 M phosphate buffered saline (PBS) (pH 7.5).

### 2.2. Apparatus

The flow system used for flow-injection analysis was identical with the system used previously [9]. Luminol and  $\text{H}_2\text{O}_2$  reagent solutions were pumped (4.0 ml/min for each solution) and mixed through a mixture loop (150 × 1 mm i.d.) by one peristaltic pump of the Intelligent Flow Injection Sampler (Xi'an Spring Institute) and delivered directly to the flow cell. The catalyst solution was pumped by another pump and a certain amount of the solution (150  $\mu\text{l}$ ) was injected automatically into the luminol/ $\text{H}_2\text{O}_2$  stream by the solenoid valve. The peak height of the CL signal was monitored by a GD-1 luminometer (Northwest Research Institute of Geology) and recorded by a Pen Type 3056 recorder.

### 2.3. Procedures

Interactions between M-P and proteins were performed in 0.01 M PBS (pH 7.5).  $2 \times 10^{-7}$  M Mn-TPPA<sub>4</sub> and 50  $\mu\text{g}/\text{ml}$  HSA final concentrations were reacted at pH 7.5. The mixture was used as the catalyst solution to optimize the CL reaction conditions. The optimum pH was obtained by varying the pH of luminol/ $\text{H}_2\text{O}_2$  stream with 0.1 M glycine-NaOH buffer.

## 3. Results and discussion

### 3.1. Optimization of the CL reaction conditions

The optimum conditions for the M-P/albumin complex catalyzed CL reaction were tested by using the flow-injection system. It was designed to give a continuous flow of  $\text{H}_2\text{O}_2$  and luminol which resulted

Table 1  
Effect of base denaturation of serum albumin on enhanced CL reaction

Protein	Enhancement factor before denaturation (fold)	Enhancement factor after denaturation (fold)
HSA	25	5.4
BSA	7.6	3.0
RSA	3.4	1.6

Luminol,  $2.5 \times 10^{-4}$  M;  $H_2O_2$ ,  $1 \times 10^{-2}$  M; M-P,  $2 \times 10^{-7}$  M; albumin, 10  $\mu$ g/ml. Base denaturation was performed by dissolving the protein (2.5 mg/ml) in 0.05 M NaOH. CL measurements were carried out as described in the text. The results are the average of three measurements.

in the determination of a constant CL background signal. As often is the case in other CL systems, the pH is a major factor influencing the CL intensity. The optimum pH for the M-P catalyzed luminol CL reaction is close to 12 [9], but it is not suitable for the albumin-enhanced CL system for two reasons. First, the optimum pH of serum albumin interaction with M-P is close to 7. At high pH even the heme of natural hemoprotein (such as hemoglobin, myoglobin and catalase) is dissociated from these proteins [24]. Second, at high pH protein will be denatured and the enhancement effect is decreased. This was further confirmed by comparing the enhancement effect of proteins before and after base denaturation (Table 1). Therefore, 0.1 M glycine–NaOH was used as a buffer for pH optimization. The relative CL intensity in the absence and presence of serum albumin as the function of pH are shown in Fig. 1. It indicates that at lower pH (pH < 9.1) M-P alone shows little catalytic activity. The injection of M-P (in the absence of protein) causes a negative CL signal because there is a constant CL background signal, and there is a dilution effect of the sample on the luminol/ $H_2O_2$  stream. In the presence of HSA or BSA, however, the catalytic activity of M-P is enhanced and a positive CL signal is produced by the injection of the samples into the luminol/ $H_2O_2$  stream, as Fig. 1 shows. As the pH increases the intensity of the M-P catalyzed CL reaction increased more rapidly than that of M-P/albumin complex as the catalyst. When the pH is increased further, the addition of serum albumin will inhibit the M-P catalyzed CL reaction (pH > 9.9 for HSA and pH > 9.7 for BSA) as shown in Fig. 1. This is because at high pH the protein is denatured and the two axial coordination sites of M-

P are occupied by amino acids from the denatured protein so that the catalytic decomposition of  $H_2O_2$  by M-P was inhibited (Table 1) [9]. Therefore, pH 9.1 was chosen as the optimum pH for the albumin enhanced M-P/luminol/ $H_2O_2$  CL system because of the low background signal and the high signal/background ratio. It is close to that of hemoglobin as the catalyst [24].

During the research, it was found that when glycine–NaOH buffer was used, there is a high background signal (*B*) from the luminol/ $H_2O_2$  stream. Even though 0.1 M sodium barbital–HCl buffer can reduce *B*, it still has a high value. However, when the two buffers were mixed together, *B* is greatly reduced, the extent depending on their ratio. The optimum buffer ratio was examined by using 50  $\mu$ g/ml HSA and  $2 \times 10^{-7}$  M Mn-TPPA<sub>4</sub> as the final concentrations as described above. The relative CL intensity of the HSA enhanced CL reaction (*S*) and *S/B* as a function of the ratio of glycine and sodium barbital buffer is shown in Fig. 2. It shows that when glycine buffer is at 5%, *B* is lowest and *S/B* is highest.

Under the optimum pH and buffer proportion conditions, the optimum concentrations of luminol and

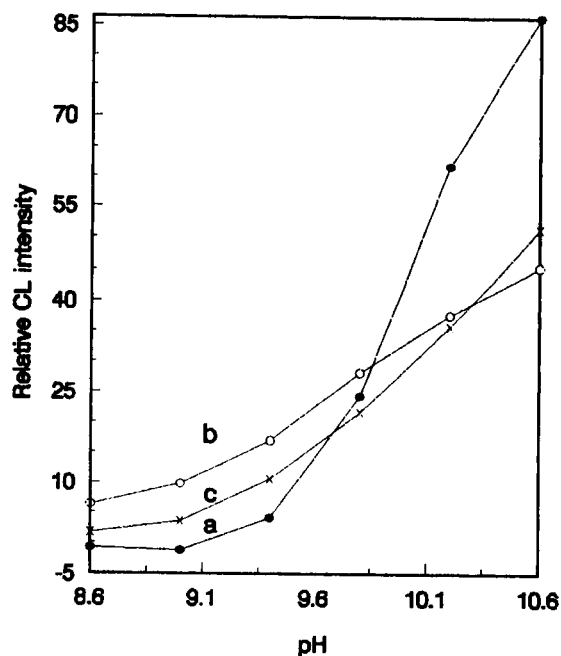


Fig. 1. CL intensity–pH profiles. Luminol,  $2 \times 10^{-4}$  M;  $H_2O_2$ ,  $10^{-2}$  M. The catalysts used were Mn-TPPA<sub>4</sub> (a), Mn-TPPA<sub>4</sub>/HSA (b) and Mn-TPPA<sub>4</sub>/BSA (c).

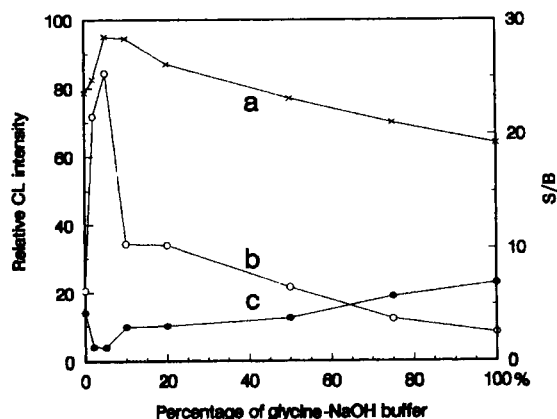


Fig. 2. Effect of buffer proportions on the CL intensity. Luminol,  $2 \times 10^{-4}$  M;  $H_2O_2$ ,  $10^{-2}$  M. (a) HSA enhanced CL intensity (S), (c) background signal (B), (b) S/B.

$H_2O_2$  of the enhanced CL reaction were tested by fixing one concentration and varying the other as described in the procedure. The values obtained were  $2.5 \times 10^{-4}$  M and  $2 \times 10^{-2}$  M, respectively.

### 3.2. Nature of the albumin enhanced CL reaction

There are several factors which can result in the enhancement of CL: (1) the rate of the reaction leading to the formation of the light-emitter, (2) the CL excitation efficiency, (3) the fluorescence quantum yield of the emitter, and (4) some combination of these factors [25]. In the present enhanced CL reaction, factor (1) has a substantial effect on the enhancement of its CL emission. Coordination and hydrophobic interactions between M-P and albumin make the M-P behave like the heme prosthetic group in peroxidase which is much more efficient for  $H_2O_2$  decomposition and resulted in the acceleration of the light-emitter formation of the CL reaction.

Table 2  
Effect of immunoreaction on albumin enhanced CL reaction

Mn-TPPA <sub>4</sub> (M)	$2 \times 10^{-7}$	$2 \times 10^{-7}$	$2 \times 10^{-7}$	$2 \times 10^{-7}$	$2 \times 10^{-7}$	$2 \times 10^{-7}$
BSA ( $\mu\text{g/ml}$ )	0	10	10	10	10	10
Anti-BSA <sup>a</sup>	0	0	1:400	1:300	1:200	1:100
$I_{CL}$ (arb. units)	3.0	25.0	12.5	3.2	18.5	16.0

Luminol,  $2.5 \times 10^{-4}$  M;  $H_2O_2$ ,  $1 \times 10^{-2}$  M; Mn-TPPA<sub>4</sub>,  $2 \times 10^{-7}$  M. The immunoreactions were carried out in 0.01 M PBS (pH 7.5) at 37°C for 30 min. The results obtained are the average of three measurements.

<sup>a</sup> Dilution of anti-BSA.

### 3.3. Coordination effect

A fifth coordinating ligand, histidine (His), is often necessary for M-P to function as peroxidase model. Mikros et al. [26] have reported that at pH 7, His was bound to M-P exclusively through imidazole N-3, as the fifth ligand for the metal. A heme peptide has a His residue (His 18 in the original horse heart cytochrome c) coordinated to Fe(II) of the heme as the fifth ligand, as a result of which the monomeric heme is in a high spin [27] or intermediate spin state [27,28] at neutral pH. These heme peptides exhibit peroxidase activity. In HSA and BSA, there are three His residues on their antigenic determination sites [29], and they can coordinate to M-P easily at neutral pH. This geometry allows the porphyrin macrocycle to interact with protein by stacking interaction which leaves the sixth coordination site available for  $H_2O_2$ . To verify this point, interactions between HSA, BSA, RSA, OVA, anti-BSA, anti-AFP (10  $\mu\text{g/ml}$ ) and Mn-TPPA<sub>4</sub> ( $2 \times 10^{-7}$  M) were evaluated in the catalytic luminol CL system under the selected reaction conditions. HSA, BSA and RSA enhance the CL intensity to different degrees (25, 7.6 and 3.4 fold, respectively), but no enhancement effect was found for OVA, anti-BSA and anti-AFP.

The coordination effect was further confirmed by an immunoreaction between the BSA/M-P complex and anti-BSA. If the coordination interaction between BSA and M-P was occurring, the active site of the BSA/M-P complex for combination with the substrate ( $H_2O_2$ ) was the sixth coordination site of M-P. When an immunoreaction occurs, this coordination site will be covered, and the catalytic activity of M-P is expected to be inhibited. The selection of the optimum antibody concentration for the immunoreaction was summarized in Table 2. As is indicated, at the optimum antibody concentration (1:300), the enhanced CL reaction was almost completely inhibited.

### 3.4. Hydrophobic effect

In addition to the coordination interaction between M-P and albumin mentioned above, there is also a hydrophobic interaction between albumin and M-P in the present CL system. Karatani [30] has reported that the luminol CL emission can be strongly enhanced by increasing the concentration of water-soluble polymers (WSPs) such as BSA. The enhancement effect was explained in terms of the binding of the monoanions of luminol to the hydrophobic regions of WSPs, and the WSPs offer hydrophobic and basic micro-environments well suited to the CL reaction. If the enhancement effect of albumin on the M-P catalyzed luminol reaction is also due to these reasons, one might have expected that the degree of enhancement by a certain protein is only related to the CL reagent, not to the catalyst. To clarify this point, the effect of 10  $\mu\text{g/ml}$  albumin (HSA was used as the model protein) on  $2 \times 10^{-7}$  M Mn-TMPyP (cationic P), Mn-TPPS<sub>4</sub> (anionic P) and Mn-TPPA<sub>4</sub> (non-ionic P) catalyzed CL reactions were examined under the same reaction conditions. Only the Mn-TPPA<sub>4</sub> catalyzed CL reaction was drastically enhanced (25 fold), and no enhancement effect occurs in the Mn-TPPS<sub>4</sub> and Mn-TMPyP catalyzed CL reactions. In addition, Karatani [30] has also reported that either under neutral or weakly alkaline conditions (0.1 M Na<sub>2</sub>CO<sub>3</sub>), the microenvironment of BSA was highly effective in producing the luminol CL emission. In the present enhanced luminol CL reaction, the effects of pH on the CL emission were obviously different for the different catalysts as shown in Fig. 1. These results indicate clearly that the enhancement effect in the present CL system is not due to the hydrophobicity of the protein thus providing a favourable microenvironment for efficient light emission, but due to the hydrophobicity of the protein which gives the M-P high catalytic activity, like hematin in peroxidase.

As further assurance that the hydrophobic interaction was occurring, the effects of HSA and BSA on the Mn-TPPA<sub>4</sub>/luminol/H<sub>2</sub>O<sub>2</sub> CL system were compared. HSA has a greater enhancing effect than BSA (Table 1). This suggests that HSA has a higher binding affinity to M-P than BSA, which agrees with previous observations [31].

Table 3

Effect of selected potential interfering compounds on the determination of 10  $\mu\text{g/ml}$  HSA under optimal conditions

Interference added	Max. tolerance conc. (M) <sup>a</sup>
Na <sup>+</sup> , Cl <sup>-</sup>	$1 \times 10^{-2}$
K <sup>+</sup> , Mg <sup>2+</sup> , SO <sub>4</sub> <sup>2-</sup>	$5 \times 10^{-3}$
NH <sub>4</sub> <sup>+</sup>	$1 \times 10^{-3}$
CO <sub>3</sub> <sup>2-</sup>	$6 \times 10^{-4}$
Glucose	$2 \times 10^{-4}$
Hb	250 <sup>b</sup>

<sup>a</sup> Maximum concentration causing a relative error <5%.

<sup>b</sup> ng/ml.

### 3.5. Analytical applications

After establishing the effect of the serum albumin on the M-P catalyzed luminol CL reaction, a brief study of the feasibility of utilizing the phenomenon as a means of determination of serum albumin was conducted. An interference study was undertaken to determine if the albumin enhanced CL reaction was prone to interference from other components in serum sample. The results are listed in Table 3. When added at levels higher than those given, all the interferences caused a positive error. The interference of carbonate was mainly due to the pH change of the Mn-TPPA<sub>4</sub>/HSA solution (0.01 M PBS, pH 7.5). As expected, hemoglobin (Hb) interferes to a significant extent because the present CL reaction conditions are suitable for Hb to act as a catalyst.

As can be seen from the discussion, the enhancement by albumin of the CL reaction is due to the hydrophobic and coordination interactions between M-P and albumin. Therefore, the concentration of M-P will be a critical factor, influencing the working range for albumin determination. Fig. 3 shows the effect of the concentration of Mn-TPPA<sub>4</sub> on the calibration graph for HSA under optimum conditions. The best sensitivity and wide working range (0.5–250  $\mu\text{g/ml}$ ) were obtained with  $6 \times 10^{-7}$  M Mn-TPPA<sub>4</sub>. When the Mn-TPPA<sub>4</sub> concentration was only  $8 \times 10^{-8}$  M, large amounts of protein will decrease the CL. This can be explained in terms of both the axial coordination sites of M-P being occupied by the protein molecules just as previously reported [8,9].

At  $6 \times 10^{-7}$  M Mn-TPPA<sub>4</sub>, calibration graphs for BSA and RSA were also examined; the working ranges

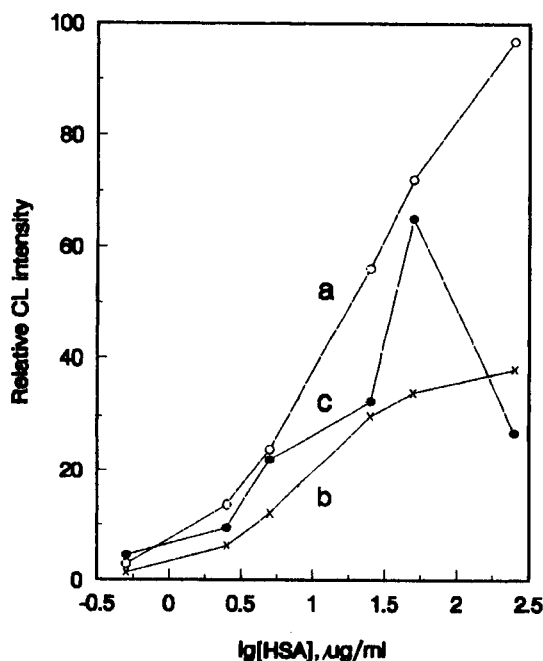


Fig. 3. Effect of Mn-TPPA<sub>4</sub> concentration on HSA working curve. The concentration of Mn-TPPA<sub>4</sub> is (a)  $8 \times 10^{-8}$  M, (b)  $2 \times 10^{-7}$  M and (c)  $6 \times 10^{-7}$  M. PMT voltages were  $-470$ ,  $-400$  and  $-300$  V, respectively.

for BSA and RSA were  $2.5$ – $250$   $\mu\text{g/ml}$  and  $5$ – $250$   $\mu\text{g/ml}$ , respectively. Detection limits ( $S/B > 3$ ) of HSA, BSA and RSA were  $85$ ,  $147$  and  $727$   $\text{ng/ml}$ , respectively. The relative standard deviation was  $2.2\%$  for the determination of  $10$   $\mu\text{g/ml}$  HSA ( $n = 11$ ).

## References

- [1] B. Morgan and D. Dolphin, *Struct. Bonding*, 64 (1987) 115.
- [2] T.G. Taylor and F. Xu, *J. Am. Chem. Soc.*, 109 (1987) 6201.
- [3] D. Mansuy, *Pure Appl. Chem.*, 59 (1987) 759.
- [4] P.A. Adams, in J. Everse, K.E. Everse and M.B. Grisham (Eds.), *Peroxidase Chem. Biol.*, Vol. 2, CRC Press, Boca Raton, FL, 1991, pp. 171–200.
- [5] C.-H. Lee, B. Garcia and T.C. Bruce, *J. Am. Chem. Soc.*, 112 (1990) 6434.
- [6] S. Benfis, A. Maiocchi, A. Moggi, F. Montanari and S. Quici, *J. Chem. Soc., Chem. Commun.*, (1990) 1794.
- [7] D.A. Baldwin, H.M. Marques and J.M. Pratt, *J. Inorg. Biochem.*, 30 (1987) 203.
- [8] F. Wang and Y.X. Ci, *Analyst*, 116 (1991) 297.
- [9] Y.X. Ci, J.K. Tie, Q.W. Wang and W.B. Chang, *Anal. Chim. Acta*, 269 (1992) 109.
- [10] T. Saito, S. Nakashima, M. Mifune, J. Odo, Y. Tanaka, M. Chikuma and H. Tanaka, *Anal. Chim. Acta*, 172 (1985) 285.
- [11] T. Saito, M. Mifune, S. Nakashima, Y. Tanaka, M. Chikuma and H. Tanaka, *Chem. Pharm. Bull.*, 34 (1986) 5016.
- [12] A. Wang, X.W. Wu, S.S. Sun and Y.X. Ci, *Acta Sci. Natr. Pek. Univ.*, 28 (1992) 399.
- [13] Y.X. Ci, L. Chen and W.B. Chang, *Microchem. J.*, 45 (1992) 72.
- [14] Z.F. Zhang and P.K. Dasgupta, *Anal. Chem.*, 64 (1992) 517.
- [15] T. Hara, M. Toriyawa and K. Tsukagoshi, *Bull. Chem. Soc. Jpn.*, 56 (1983) 2267.
- [16] Y.X. Ci, H.B. He, W.B. Chang and J.S. Liu, *Anal. Chim. Acta*, 237 (1990) 497.
- [17] Y. Ikariyama, S. Suzuki and M. Aizawa, *Anal. Chem.*, 54 (1982) 1126.
- [18] M.E. Wilson and G.M. Whiteside, *J. Am. Chem. Soc.*, 100 (1978) 306.
- [19] B.L. Iverson and R.A. Lerner, *Science*, 243 (1989) 1184.
- [20] K. Ohkubo, H. Ishida and T. Sagawa, *J. Mol. Catal.*, 53 (1989) L5.
- [21] T. Sagawa, H. Ishida, K. Urabe and K. Ohkubo, *Chem. Lett.*, (1991) 2083.
- [22] K. Yoshinaga, H. Itoh and T. Kito, *Polym. J.*, 23 (1991) 65.
- [23] E.A. Kabat, Kabat and Mayer's *Exp. Immunochem.*, 2nd edn., Part III, Charles C. Thomas, Springfield, 1961, pp. 733–738.
- [24] H.A. Neufeld, C.J. Conklin and R.D. Towner, *Anal. Biochem.*, 12 (1965) 303.
- [25] W.L. Hinze, T.E. Riehl, H.N. Singh and Y. Baba, *Anal. Chem.* 56 (1984) 2180.
- [26] E. Mikros, F. Gaudemer and A. Gaudemer, *Inorg. Chem.*, 30 (1991) 1805.
- [27] D.A. Baldwin, H.M. Marques and J.M. Pratt, *J. Inorg. Biochem.*, 27 (1986) 245.
- [28] J.-S. Wang and H.E. Van Wart, *J. Phys. Chem.*, 93 (1989) 7925.
- [29] M.Z. Atassi, in M.Z. Atassi, C.J. Van Oss, D.R. Absolom, (Eds.), *Molecular Immunology*, Marcel Dekker, New York, 1984, pp. 15–51.
- [30] H. Karatani, *Bull. Chem. Soc. Jpn.*, 60 (1987) 2023.
- [31] M. Rotenberg and R. Margalit, *Biochem. J.*, 229 (1985) 197.

# Analysis and characterisation of nitroglycerine based explosives by proton magnetic resonance spectrometry

D. Thorburn Burns <sup>\*,a</sup>, Robert J Lewis <sup>b</sup>

<sup>a</sup> Department of Analytical Chemistry, The Queen's University of Belfast, Belfast BT9 5AG, UK

<sup>b</sup> Northern Ireland Forensic Science Laboratory, Carrickfergus, Co Antrim BT38 8PL, UK

Received 18 May 1994

---

## Abstract

It has been shown that by using 500 MHz <sup>1</sup>H NMR it is possible, without prior separation, to quantify individual nitroaromatic compounds present in commercial nitroglycerine based explosives (gelnites). Patterns within the quantitative data provide a good degree of sample batch characterisation; typing of the explosive is achieved via total nitroaromatic content.

*Keywords:* Nuclear magnetic resonance spectrometry; Explosives; Nitroglycerine; Nitroaromatic compounds

---

## 1. Introduction

Although excellent trace methods are available for explosive residue analysis it is now not acceptable to examine bulk explosive material in areas dedicated to trace analysis. Relatively insensitive methods of analysis, provided that they are highly selective, are potentially useful and appropriate for the examination of bulk explosives.

Nuclear magnetic resonance (NMR) spectrometry has long been recognised as a powerful tool for structural analysis, however it has been unable to compete with the chromatographic methods commonly used by forensic science services for the examination of explosive residues. Hence there is only a limited amount of published material on NMR in a forensic context [1–9] essentially due to lack of sensitivity. Chromatographic analysis of explosives generally requires more

than one separation system in order to confirm a component of an explosive material. Typically gas chromatography with electron capture (GC-ECD) or thermal energy analyser (GC-TEA) detection, or liquid chromatography with electrochemical detection (LC-ED) is used for the initial screening of samples prior to confirmation using further systems. Sub-nanogram levels of explosives have been reported using the aforementioned techniques and indeed picogram levels have been detected by GC-TEA under favourable conditions [9–12].

The use of <sup>1</sup>H NMR for the examination of bulk samples of explosives, where sensitivity is not a key factor, is shown herein to be a valuable forensic tool as illustrated by the examination of commercial gelignites. The particular products examined were, Frangex, Frangex No. 1, Opencast Gelignite and Plaster Gelatine as produced by Irish Industrial Explosives. Common to each of these explosive types is a mixture of nitroaromatic compounds composed mainly of isomers of dinitrotoluene with varying amounts of mononitrotoluenes

---

\* Corresponding author.



and dinitroethylbenzenes. The overall amount of the nitroaromatic components in each explosive type varies from 2–10%, the particular value of which allows an explosive sample to be typed.

The distribution of compounds within the total nitroaromatic content has been found to permit a degree of batch characterisation. The overall procedure is simple as it requires no chromatographic separation, has minimal sample clean-up (filtration of sample solution to remove binder) is fast (spectroscopic scan time is 3.5 s, a 25 mg explosive sample requires 32 scans – total analysis time less than 2 min) and gives reliable estimates of individual nitroaromatic compound content.

## 2. Experimental

### 2.1. Apparatus

NMR spectra were obtained over the range 0–10 ppm using a General Electric GN Omega 500 spectrometer and glass sample tubes (5 mm o.d.).

### 2.2. Materials and reagents

#### *Nitro compounds*

The reference compounds were obtained commercially as indicated, apart from 2,5-dinitrotoluene which was prepared by selective synthesis [13]. 2,3-Dinitrotoluene (99%), 2,4-dinitrotoluene (97%), 2,6-dinitrotoluene (98%) and 3,4-dinitrotoluene (99%) were obtained from Aldrich. 2-Nitrotoluene and 3-nitrotoluene (both GPR Grade) were purchased from BDH; toluene (99%) from Fisons; ethyleneglycol dinitrate (20% w/w in kieselgur), nitroglycerine (20% w/w in kieselgur) and 2,4-dinitroethylbenzene were obtained from the Defence Research Agency.

#### *Reagents*

All other reagents were of analytical grade.

#### *Samples*

Samples were obtained from Irish Industrial Explosives over a period of time, when available, the date of manufacture is indicated.

#### *Type*

(i) Opencast Gelignite	1985
(ii) Frangex	Feb. 1, 1991
(iii) Plaster Gelatine	Feb. 1, 1991
(iv) Frangex	Sept. 12, 1991
(v) Frangex No 1	Sept. 26, 1991
(vi) Frangex	Jan. 22, 1993
(vii) Frangex	Jan. 19, 1994

#### *Date of manufacture*

Material recovered from four terrorist related incidents (A–D) were also examined.

### 2.3. Procedures

#### *Reference compounds*

1–5 mg of each compound was dissolved in 1.0 ml of deuteriochloroform containing 0.1% w/v tetramethylsilane (TMS) and the  $^1\text{H}$  NMR spectra were recorded.

#### *Samples of explosives*

An accurately weighed sample of about 0.250 g was placed in a 10-ml volumetric flask and made up to the volume with deuteriochloroform containing 0.1% w/v TMS and 0.1% w/v toluene (internal standard for quantitative work). Each flask was placed in an ultrasonic bath for 5 min to facilitate dissolution. The samples were filtered using a Gelman Acrodisc syringe filter (0.45  $\mu\text{m}$ ) prior to placing 1 ml in NMR sample tubes (5 mm o.d.) and the  $^1\text{H}$  NMR spectra were recorded.

## 3. Results

### 3.1. Qualitative and semi-quantitative studies

#### *Reference compounds*

The  $^1\text{H}$  NMR spectra recorded for each of the known compounds served as a basic reference library. All the compounds appeared to be spectroscopically pure except for 2,4-dinitrotoluene which contained a trace of 2,6-dinitrotoluene.

Table 1  
Methyl resonance of toluene and nitrotoluene reference compounds

Compound	Chemical shift (ppm)
Toluene	2.356
2,3-Dinitrotoluene	2.437
2,4-Dinitrotoluene	2.741
2,5-Dinitrotoluene	2.695
2,6-Dinitrotoluene	2.592
3,4-Dinitrotoluene	2.548
2-Nitrotoluene	2.607
3-Nitrotoluene	2.473
2,4,6-Trinitrotoluene	2.715

### Nitrotoluenes

The resonances attributable to the protons of the methyl substituents of each dinitrotoluene and mononitrotoluene isomer along with 2,4,6-trinitrotoluene and toluene were completely resolved in admixtures (Table 1). Hence it is possible to identify any of these compounds from the spectra recorded between 2–3 ppm. By using toluene as an internal standard, quantitative results were readily achieved. Aromatic ring protons resonate between 7.2–8.9 ppm giving complex patterns which are also well resolved, providing additional confirmation if needed.

### 2,4-Dinitroethylbenzene

The characteristic triplet and quartet resonances attributable to the ethyl substituent are located at 1.335–1.365 ppm and 3.012–3.057 ppm, respectively ( $J=7.47$  Hz). The quartet for the 2,4-isomer is well resolved from the 2,6-isomer, however, the triplets overlap. Aromatic ring protons resonate at 7.6–8.8 ppm and were well resolved.

Table 2  
Nitroaromatic compounds associated with commercially obtained samples

Sample and date of manufacture	Dinitrotoluene isomers						Dinitroethyl benzene	<i>ortho</i> -Nitrotoluene	<i>meta</i> -Nitrotoluene
	2,3-	2,4-	2,5-	2,6-	3,4-	3,5-			
(i) Open Gel, 1985	/	/	/	/	/	t	–	t	–
(ii) Frangex, Feb. 1, 1991	/	/	/	t	/	t	–	–	–
(iii) Plas. Gel., Feb. 1, 1991	/	/	/	t	/	t	–	–	–
(iv) Frangex, Sept. 12, 1991	/	/	/	t	/	t	–	–	–
(v) Frangex No. 1, Sept. 26, 1991	t	/	–	/	t	–	/	–	–
(vi) Frangex, Jan. 22, 1992	/	/	/	t	/	t	–	–	–
(vii) Frangex, Jan. 19, 1994	/	/	/	/	/	t	–	t	t

Key: / = >7% of total nitroaromatic compounds present; t = <3.5% of total nitroaromatic compounds present; – = indistinct from baseline.

### Nitroesters

(i) The four equivalent protons of ethyleneglycol dinitrate produce a single resonance at 4.752 ppm.

(ii) Spin–spin splitting due to coupling between the geminal and vicinal protons of nitroglycerine produces the highly characteristic resonance pattern between 4.6–4.9 ppm. The methine proton resonates at 5.5 ppm.

### Explosive samples

<sup>1</sup>H NMR spectra were recorded for each of the seven commercial samples of explosives and also for the samples recovered from four separate terrorist related incidents.

### Commercially obtained samples

All of the samples examined were found to contain nitroglycerine, ethyleneglycol dinitrate and a variable series of nitroaromatic compounds as detailed in Table 2.

Upon closer inspection of the spectra obtained from samples (ii), (iii), (iv) and (vi), which contained only the six dinitrotoluene isomers, variations in the relative methyl peak heights were noted. The dinitrotoluene isomer relative peak height ratios for these samples are shown in Table 3.

The isomer ratios for samples (ii), (iii) and (vi) are seen to be similar, however, that for sample (iv) differs significantly. It can be concluded from these results (Tables 2 and 3) that the nitroaromatic components present in these explosives are of importance in characterising samples.

Table 3

Relative methyl peak heights for samples containing only DNT isomers

Sample	Dinitrotoluene isomers					
	2,3-	2,4-	2,5-	2,6-	3,4-	3,5-
(ii) Frangex, Feb. 1, 1991	22.4	27.5	8.5	2.5	37.9	1.3
(iii) Plas. Gel., Feb. 1, 1991	23.3	26.5	8.2	2.4	38.4	1.3
(iv) Frangex, Sept. 12, 1991	19.9	34.5	7.4	2.9	33.6	1.5
(vi) Frangex, Jan. 22, 1992	22.7	27.2	8.2	2.5	37.8	1.7

Table 4

Nitroaromatic compounds associated with terrorist samples

Sample	Dinitrotoluene isomers								
	2,3-	2,4-	2,5-	2,6-	3,4-	3,5-	2,4-DNE B	<i>o</i> -NT	<i>m</i> -NT
A	/	/	t	/	/	t	/	/	–
B	t	/	t	/	/	t	/	/	–
C	/	/	/	/	/	t	–	–	–
D	/	/	/	/	/	t	–	–	–

Key to symbols as in Table 2.

Table 5

Relative methyl peak heights for samples C and D containing only DNT isomers

Sample	Dinitrotoluene isomers					
	2,3-	2,4-	2,5-	2,6-	3,4-	3,5-
C	22.8	26.7	8.3	2.5	38.5	1.2
D	23.4	27.1	8.3	2.4	37.6	1.2

Table 6

Analysis of a Frangex sample (Feb. 1, 1991)

DNT isomer	Chemical shift (ppm)	Peak height
2,4-	2.737	3.84
2,5-	2.693	1.17
3,4-	2.544	5.51
2,3-	2.434	3.36
2,6-	2.588	0.33
3,5-	2.642	0.11

 $W_{\text{DNT}} = 1.59695 \times 10^{-3}$  g, thus DNT = 4.0%.

### Terrorist (contraband) samples

All four samples examined were found to contain nitroglycerine, ethyleneglycol dinitrate and, similarly

to the commercial samples, a variable series of nitroaromatic compounds, identified from the upfield resonances observed between 1.3–3.2 ppm. The results are summarised in Table 4.

Samples A and B display similarities in their overall nitroaromatic make-up which includes the six dinitrotoluene isomers, 2,4-dinitroethylbenzene and 2-nitrotoluene. Samples C and D were similar to each other but distinct from A and B, containing only the six dinitrotoluene isomers. Further similarities between samples C and D were noted from the relative methyl peak heights of the dinitrotoluene isomers for both samples (see Table 5).

### 3.2. Quantitative analysis [14]

When evaluating contraband gelignite samples it is necessary to determine the total dinitrotoluene content to attribute a particular explosive type to a sample. Using toluene as the internal standard, the dinitrotoluene isomers associated with nitroglycerine based explosives may be determined from the peak heights of the methyl resonances and the amount of toluene present as follows:

$$W_{\text{DNT}} = \frac{W_{\text{TOL}} I_{\text{DNT}} M_{\text{DNT}}}{I_{\text{TOL}} M_{\text{TOL}}}$$

where  $W_{\text{DNT}}$  = weight (g) of dinitrotoluene isomers,  $W_{\text{TOL}}$  = weight (g) of toluene,  $I_{\text{DNT}}$  = sum of the peak heights of the methyl resonances of DNT isomers,  $I_{\text{TOL}}$  = peak height of methyl resonance of toluene,  $M_{\text{DNT}}$  = formula weight of dinitrotoluene,  $M_{\text{TOL}}$  = formula weight of toluene.

Results for a typical analysis (Table 6) are illustrated using 0.2243 g of Frangex (Feb. 1, 1991) in deuteriochloroform (10 ml) containing 0.0111 g of toluene. The spectrum for a 1.0 ml aliquot was recorded.

Quantitative determination was also obtained by GC-FID which reported the total DNT content as 4.1%.

## 4. Conclusions

Unequivocal identification of the nitroesters nitroglycerine and ethyleneglycol dinitrate, together with the individual nitroaromatic compounds associated with nitroglycerine based explosives is shown to be

readily achievable using a direct  $^1\text{H}$  NMR procedure.

From the limited number of commercial samples examined it is possible to identify the use of four different batches of material based on variation of nitroaromatic isomer content of the commercial so called "dinitrotoluene" used in manufacture. It is thus suggested that a degree of characterisation of contraband nitroglycerine based explosives may be possible. Samples (C) and (D) recovered from terrorist incidents show a striking resemblance to the directly obtained commercial samples produced on Feb. 1, 1991 and Jan. 22, 1992 (see Tables 3 and 5).

Although the degree of characterisation is speculative, being based on a limited database, further investigation of this class of explosive, focussing on the nitroaromatic compounds, may provide a means for attributing a particular batch type and possibly determining approximate dates of manufacture of contraband explosives. An important aspect will be to determine the batch to batch variation of the commercial "dinitrotoluene". Atypical batches and their products e.g. (v) (Frangex, Sept. 26, 1991) are readily identified.

### Acknowledgements

The authors wish to express their appreciation to the Director of the Northern Ireland Forensic Science Laboratory, Mr R.A. Hall, for his encouragement and assis-

tance in this work, and to Mr R. Murphy for his assistance with the  $^1\text{H}$  NMR analyses. We are indebted to the Irish Industrial Explosives (Co Meath, Ireland) and the Defence Research Agency (Kent) for providing us with samples of explosives.

### References

- [1] Y. Bamberger, Y. Margalit and S. Zitrin, in Proc. 3rd Int. Symp. Analysis and Detection of Explosives, 10–13 July, Mannheim, 1989, pp. 24–1.
- [2] M. Kasier, in Proc. 3rd Int. Symp. Analysis and Detection of Explosives, 10–13 July, Mannheim, 1989, pp. 28–1.
- [3] Y. Margalit, S. Abramovich-Bar, Y. Bamberger, S. Levy and S. Zitrin, *J. Energ. Mater.*, 4 (1986) 263.
- [4] J. Yinon and S. Zitrin, *Modern Methods and Applications in Analysis of Explosives*, Wiley, New York, 1993, pp. 203–204.
- [5] H.D. Schiele and G. Vordermaier, *Arch. Kriminol.*, 169 (1982) 155.
- [6] A. Alm, O. Dalman, I. Froten-Lindgren, F. Hulteen, T. Karlsson and M. Kowalska, FOA Report C 20267-D1, National Defense Research Institute, Stockholm, 1978.
- [7] D.G. Gehring and G.S. Reddy, *Anal. Chem.*, 40 (1968) 792.
- [8] R.E. Meyers and J.A. Meyers, in Proc. 1st Int. Symp. Analysis and Detection of Explosives, FBI Academy, Quantico VA, 1983, pp. 93–106.
- [9] A.D. Beveridge, *Forensic Sci. Rev.*, 4 (1992) 17.
- [10] J.M.F. Douse, *J. Chromatogr.*, 328 (1985) 155.
- [11] J.M.F. Douse, *J. Chromatogr.*, 256 (1983) 359.
- [12] D.H. Fine, W.C. Yu, E.U. Coff, E.C. Bender and D.J. Reutter, *J. Forensic Sci.*, 29 (1984) 732.
- [13] H.H. Hodgson and F. Heyworth, *J. Chem. Soc.*, (1949) 1624.
- [14] D.M. Rackhan, *Talanta*, 23 (1976) 269.

# Kinetic analysis of aluminum complex formation with different soil fulvic acids

Brian J. Plankey<sup>a</sup>, Howard H. Patterson<sup>b,\*</sup>, Christopher S. Cronan<sup>c</sup>

<sup>a</sup> Department of Chemistry, Feather River College, Quincy, CA 95971, USA

<sup>b</sup> Department of Chemistry, University of Maine, Orono, ME 04469, USA

<sup>c</sup> Department of Plant Biology and Pathology, University of Maine, Orono, ME 04469, USA

Received 7 June 1994

## Abstract

A fluorescence technique was used to investigate the complex formation kinetics of aluminum with fulvic acids isolated from different forest soil environments. In the pH range of 2.4–3.6, all of the fulvic acids were found to contain two kinetically distinguishable components, which define two types of average aluminum binding sites. Both of these average sites on all of the fulvic acids conformed to a bidentate chelating binding site kinetic analysis, from which average rate and equilibrium parameters were obtained. Evidence indicated that the difference in reaction rate between the two types of aluminum binding sites on the fulvic acids was due to a steric strain, whereby aluminum was repelled from the slower reacting sites. In comparing this study with a similar kinetic study carried out in acetate buffered solutions, it was found that the presence of buffer changed both the overall mechanism by which aluminum reacted with fulvic acid, and the nature of the sites on fulvic acid that bind aluminum.

**Keywords:** Fluorimetry; Fulvic acids; Aluminum complexation; Kinetic analysis

## 1. Introduction

It is widely recognized that fulvic acids exert important influences on acid–base chemistry and chemical speciation in soil and surface waters, metal transport, soil weathering, and metal toxicity [1]. Because of this, there have been increasing efforts to estimate the thermodynamic parameters and to model the geochemical behavior of fulvic acid and metal fulvate complexes [2–5].

In our own previous research, we have examined the kinetics of aluminum complexation with a single soil fulvic acid as a function of pH in the absence and presence of fluoride ion [6,7], and have investigated

the equilibrium behavior of aluminum complexation with three molecular weight fractions of a coniferous soil fulvic acid used in this study [8]. In this report, we present a kinetic analysis of aluminum complex formation with three different fulvic acids isolated from contrasting northern and southern forest soils in order to determine the extent to which fulvic acids isolated from different soils and bioclimatic regions vary in rate and extent of binding to aluminum. A fluorescence spectrophotometric analytical technique was used to monitor the course of the complexation reactions.

The objectives of the investigation were (i) to determine the rate of aluminum–fulvic acid complexation as a function of pH for all of the fulvic acids, (ii) to identify a mechanism for each reaction consistent with the experimental data, and (iii) to compare the result-

\* Corresponding author.

ing kinetic and equilibrium parameters in order to determine if fulvic acids differ significantly in aluminum binding behavior.

## 2. Experimental

### 2.1. Materials

The three fulvic acid samples were isolated from soils beneath hardwood and coniferous forest stands located in the Pancake-Hall watershed in the west-central Adirondack Mountains of New York, and in the Camp Branch watershed on the Cumberland Plateau of eastern Tennessee. Both sites have been described in detail elsewhere [9]. The northern soil fulvic acids were isolated from the O horizon of Spodosol soils beneath mixed northern hardwood (NHFA) and red spruce (NCFA) forest canopies. The pH of soil solutions at both of the northern sites ranged from 3.6 to 4.8. Soluble aluminum in soil solutions from both northern sites was 25 to 60  $\mu\text{M}$ .

The southern soil fulvic acid (SHFA) was isolated from O plus A horizons of an Ultisol soil profile beneath a mixed hardwoods forest canopy. Soil solutions from the southern site yielded soluble aluminum concentrations from 2 to 7  $\mu\text{M}$ , and pH values between 4.4 and 5.2. All three field soil samples were sieved through a 6 mm stainless steel mesh and were stored at 5°C until extraction.

Each soil sample was extracted for 3 h at 23–25°C on a shaker using a 1:10 ratio of soil to distilled water. The resulting slurry was centrifuged at 8000 rpm, the decantate was pressure filtered through a Gelman A/E glass fiber filter, and the filtrate was centrifuged a second time. The extracted soil solution was then acidified to pH 1 with concentrated HCl in order to precipitate humic acid. After 12 h of settling, the soluble fulvic acid solution was separated from the insoluble humic acids by centrifugation and decantation.

The fulvic acids in each sample were concentrated and purified by the XAD-8 adsorption chromatographic method of Leenheer [10]. Cation exchange chromatography using acid-washed Rexyn 101 resin was used to produce fulvic acids in fully protonated form. Finally, the fulvic acid samples were isolated by lyophilization and stored in a desiccator in the dark. Gen-

Table 1  
General characteristics of the three fulvic acids

Source forest cover type	NHFA <sup>a</sup>	NCFA	SHFA
	Northern hardwoods	Red spruce	Southern hardwoods
Fulvic acid, %carbon	45.3	47.9	47.2
Carboxyl content, mmol/g C	8.9	8.3	10.4
Molar ratio of COOH to C	0.11	0.10	0.13

<sup>a</sup>Abbreviations stand for Northern hardwood fulvic acid, Northern conifer fulvic acid, and Southern hardwood fulvic acid.

eral characteristics of the three fulvic acids are shown in Table 1.

The residual metal content of each fulvic acid was determined using plasma emission spectroscopy. For all three fulvic acids, the concentrations of Al, Ca, Mn and Fe were each less than or equal to 0.01% on a dry weight basis. The presence of  $\text{Cl}^-$ ,  $\text{NO}_3^-$  and  $\text{SO}_4^{2-}$  was checked for each fulvic acid sample using ion chromatography and was found to be below detection limits.

Aluminum solutions were prepared from reagent grade  $\text{Al}(\text{NO}_3)_3 \cdot 9\text{H}_2\text{O}$ . Initial aluminum concentrations varied between  $1.8 \times 10^{-3}$  M and  $3.6 \times 10^{-3}$  M. The initial fulvic acid concentration was always 5.05 mg/l. Although the fulvic acid molecular weights were not determined, the aluminum concentration was almost certainly always large enough for pseudo-first-order kinetics to be in effect, i.e., at least a ten-fold excess of aluminum [11]. For example, at the lowest initial aluminum concentration of  $1.8 \times 10^{-3}$  M, in order for the initial concentration of aluminum to be less than ten times the initial concentration of fulvic acid, the molecular weight of fulvic acid would have to be less than 28.

In all reactions, the pH was adjusted to the desired value by the addition of  $\text{HNO}_3$ . The ionic strength was maintained at 0.1 M by adding NaCl to each solution. It has been shown that chloride ion does not complex aluminum [12,13]. The reaction of each of the three fulvic acids with aqueous aluminum was studied at four different pH values ranging from approximately 2.4 to 3.6. Solution pH was determined with a Corning Semi-

Micro Combination Electrode connected to a Model 701A Orion digital pH meter. Standard buffers were used for reference with no corrections made for liquid junction potential differences. The concentration of  $H^+$  was taken as  $[H^+] = 10^{-pH}/\gamma_{H^+}$ , with  $\gamma_{H^+} = 0.78$  calculated from the Davies equation [14].

Concentrations were determined as molarities rather than as activities. However, since the ionic strength was constant in all solutions, the molarity of each species differed from its activity by only a proportionality constant dependent on the charges of the species.

## 2.2. Kinetic procedure

A fluorometric method was used to follow the course of the reactions of aluminum with the fulvic acid samples. This technique has been used in our earlier kinetic studies [6], and is based on the observation that fulvic acid fluorescence intensities increase upon binding to aluminum. In this stopped-flow method, the aluminum and fulvic acid solutions were mixed, and the fluorescence intensity was monitored as a function of time. Wavelengths of excitation and emission were 350 nm and 400 nm, respectively. The method has been described in detail in an earlier paper [6]. During the course of the reactions reported here, and in solutions that were stored for several weeks, there was never any sign of coagulation or precipitation, either by visual examination or by light scattering at 350 nm.

## 3. Results and discussion

### 3.1. Treatment of data

Pseudo-first-order kinetic plots of  $\ln(I_\infty - I_t)$  were made for all kinetic runs, where  $I_t$  is the intensity of fluorescence at any time  $t$  and  $I_\infty$  is the infinite time fluorescence intensity. The reactions followed pseudo-first-order kinetics because  $[Al^{3+}]$  was always large compared to the fulvic acid concentration. All of the pseudo-first-order kinetic plots consisted of two linear segments with different slopes. This is in accord with our previous study [6] and several other earlier studies of metal fulvic acid interactions that have indicated two general types of metal binding sites on fulvic acid [15–19].

The plots for all three fulvic acids indicate two first order reactions in which the observed rate parameters are separated by nearly an order of magnitude or more [20]. The intensity vs. time data are then consistent with the expression

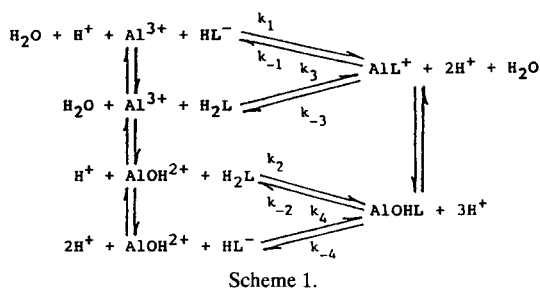
$$I_t = A[1 - e^{-k_{\text{obsd1}} t}] + B[1 - e^{-k_{\text{obsd2}} t}] + X \quad (1)$$

where  $I_t$  is the fluorescence intensity at time  $t$ ,  $k_{\text{obsd1}}$  and  $k_{\text{obsd2}}$  are observed pseudo-first-order rate parameters of the two reactions,  $X$  is a time-independent term including blank and fast reacting components, and  $A$  and  $B$  are constants [15]. The intensity vs. time data can be fit to Eq. 1 satisfactorily by nonlinear regression as described in a previous paper [6]. This nonlinear least squares treatment yielded two observed rate parameters,  $k_{\text{obsd1}}$  and  $k_{\text{obsd2}}$ . Each was the average of at least five runs.

Fulvic acids are operationally defined [21] and are in reality complex mixtures [15]. Eq. 1 (from which  $k_{\text{obsd1}}$  and  $k_{\text{obsd2}}$  were obtained for our three fulvic acids) is thus an approximation [19], because each fulvic acid has a distribution of different binding sites [15,19]. While no two binding sites on any fulvic acid are necessarily chemically identical [16,22], the two straight-line segments of the kinetic plots indicated that there are two kinetically distinguishable components of each fulvic acid. The  $k_{\text{obsd1}}$  and  $k_{\text{obsd2}}$  values are thus average values over two kinetically distinguishable parts of all the aluminum binding sites on each fulvic acid.

A further consequence of the complex mixture nature of fulvic acid is that an increased strength of metal binding occurs with decreasing metal to ligand ratios [23]. Therefore, aluminum–fulvic acid rate and equilibrium parameters are not constants; they depend, among other things, on the degree of metal coverage. For this reason, some researchers have argued that fulvic acid complexation cannot be understood in terms of simple monomeric ligand models [16,23,24]. We believe, however, that if the individual binding sites on fulvic acid are sufficiently alike to show only two kinetically distinguishable components, then a monomeric kinetic analysis for those two types of average aluminum binding sites is an appropriate model for aluminum–fulvic acid complexation [6].

As was done in an earlier paper [6], the  $k_{\text{obsd1}}$  and  $k_{\text{obsd2}}$  values for each fulvic acid were analyzed using an aluminum–salicylic acid kinetic model [14]. Since



this method has been described in detail [6,14], only an abbreviated explanation will be presented here. In using this model, we have assumed that chelating sites, similar to salicylic acid (2-hydroxybenzoic acid), are present in fulvic acids [6,15,16,22]. If this assumption is correct and these chelating sites are the aluminum binding sites on fulvic acids, then the mechanism for the reaction of aluminum with salicylic acid is the same as the mechanism for the reaction of aluminum with fulvic acid, even though fulvic acids contain more complex binding sites than simple monomeric salicylic acid.

Accordingly, we tested Scheme 1 for the reaction of aluminum with chelating sites on our fulvic acids [14,25,26]. In this Scheme 1, a deprotonated chelating site on fulvic acid has been designated as  $\text{HL}^-$  and  $\text{H}_2\text{L}$  represents a fully protonated site, in analogy with the aluminum–salicylic acid reaction [14], and an earlier aluminum–fulvic acid kinetic study [6]. Coordinated waters have been omitted for simplicity.

The relationship between the observed rate parameters and the rate and equilibrium parameters in reaction Scheme 1 is as follows. For both  $k_{\text{obsd1}}$  and  $k_{\text{obsd2}}$ , because all of the forward and reverse reactions are pseudo first order, at constant  $[\text{H}^+]$ ,  $k_{\text{obsd}}$  is a linear function of the total aluminum concentration,  $[\text{Al(III)}]$ :

$$k_{\text{obsd}} = k_f[\text{Al(III)}] + k_r[\text{H}^+] \quad (2)$$

where  $k_f$  and  $k_r$  are the forward and reverse rate parameters for the overall forward and reverse reactions, respectively [6,14]. An apparent equilibrium constant  $K_{\text{app}}$  can be defined as the formation parameter of the  $\text{AIL}^+$  complex from total aluminum and total ligand, and it can be shown that [14]

$$K_{\text{app}} = k_f/k_r \quad (3)$$

The  $k_{\text{obsd1}}$  and  $k_{\text{obsd2}}$  values for each fulvic acid along with Eqs. 2 and 3 were used to obtain  $K_{\text{app}}$  values for

the reaction of aluminum with both components of each fulvic acid. The  $K_{\text{app}}$  values so obtained were used in the analysis that follows (see Eq. 6). A typical  $k_{\text{obsd}}$  vs.  $[\text{Al(III)}]$  plot at constant  $[\text{H}^+]$  is shown in Fig. 1. We decided to use only three different aluminum concentrations for these plots because we desired to keep the aluminum-to-fulvic acid ratio as constant as possible so that the fulvic acid binding sites were as uniform as possible.

From reaction Scheme 1, the reported reaction of aluminum with salicylic acid [14], and our earlier aluminum fulvic acid study [6], the formation parameter for the aluminum–fulvic acid complex between  $\text{Al}^{3+}$  and a deprotonated chelating site of fulvic acid is

$$K_1 = k_1/k_{-1} = [\text{AIL}^+][\text{H}^+]/[\text{Al}^{3+}][\text{HL}^-] \quad (4)$$

Assuming that the fulvic acid binding sites are chelating sites, and that only the ligand species  $\text{H}_2\text{L}$  and  $\text{HL}^-$  are present at the low pH values of this study [6,26], then

$$K_{\text{app}} = [\text{AIL}^+][\text{H}^+]/([\text{Al}^{3+}] + [\text{AlOH}^{2+}]) \times ([\text{H}_2\text{L} + \text{HL}^-]) \quad (5)$$

Substituting the hydrolysis constant of aluminum,  $K_{\text{AlOH}}$ , and the first acid dissociation parameter of the supposed chelating group on fulvic acid,  $K_{\text{HL}}$ , and rearranging yields Eq. 6 [6].

$$\frac{[\text{H}^+]}{K_{\text{app}}([\text{H}^+] + K_{\text{AlOH}})} = \frac{1}{K_1} + \frac{[\text{H}^+]}{K_1 K_{\text{HL}}} \quad (6)$$

Eq. 6 was tested for both the fast reacting and slow reacting kinetically distinguishable component of each

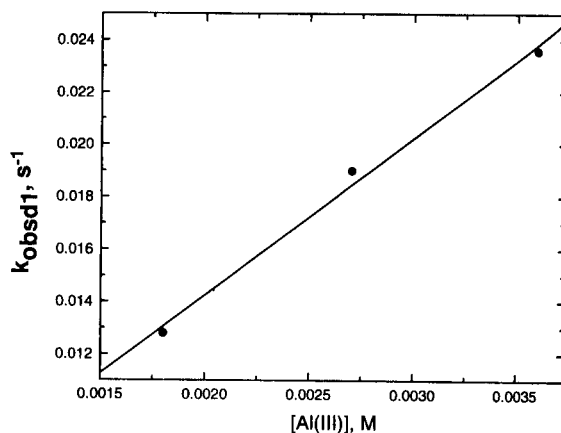


Fig. 1. Observed rate constant  $k_{\text{obsd1}}$  of NHFA as a function of total aluminum concentration at pH 2.44 and 25°C.



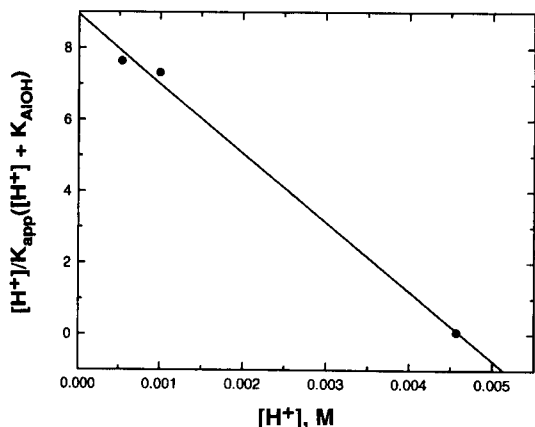


Fig. 2. Kinetic results of  $[H^+]/K_{app}([H^+] + K_{AlOH})$  as a function of  $[H^+]$  for the fast reacting component of NHFA at 25°C.

fulvic acid by plotting the left-hand side vs.  $[H^+]$ . The hydrolysis constant of aluminum at ionic strength 0.10 M,  $K_{AlOH} = 3.55 \times 10^{-6}$  M, was obtained from the literature [14]. While these plots gave good straight lines, such as in Fig. 2 for the fast reacting component of NHFA, the slopes were negative.

In both the aluminum–salicylic acid kinetic study [14] and in our previous kinetic study of the complexation of aluminum with fulvic acid (which was carried out with acetate buffer present) the  $[H^+]/K_{app}([H^+] + K_{AlOH})$  vs.  $[H^+]$  plots gave positive slopes [6].

A possible reason for this behavior is that the reaction path is different than reaction Scheme 1 in the absence of buffer. For example, if we assume that the concentration of  $L^{2-}$  is not small in the absence of buffer, and that instead the concentration of  $H_2L$  is negligible, then the reaction scheme in unbuffered solutions is shown in Scheme 2.

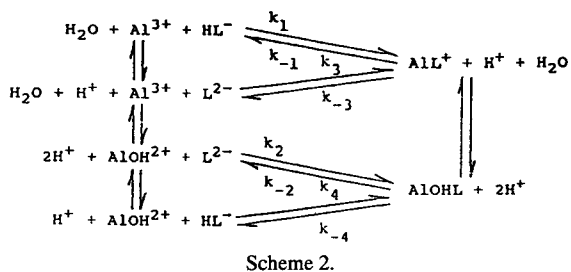
The expression for the apparent equilibrium parameter,  $K_{app}$ , is then

$$K_{app} = \frac{[AlL^+][H^+]}{([Al^{3+}] + [AlOH^{2+}]) \times ([HL^-] + [L^{2-}])} \quad (7)$$

and rearrangement yields

$$\frac{[H^+]}{K_{app}([H^+] + K_{AlOH})} = \frac{1}{K_1} + \frac{K_{HL2}}{K_1[H^+]} \quad (8)$$

where  $K_{HL2}$  is the second acid dissociation parameter of the supposed chelating group on fulvic acid.



Eq. 8 was tested for both the fast reacting and slow reacting component of each fulvic acid by plotting the left-hand side vs.  $1/[H^+]$ . All of these plots for NHFA, NCFA, and SHFA were linear with positive slopes (see Fig. 3, for example). The pH range was not extended because these plots would not remain linear at higher pH due to the increase in rate from more highly hydrolyzed species of Al(III) such as  $Al(OH)_2^+$  [6,14,25,26]. Again, however, because all six plots gave good straight lines, three points were deemed sufficient for these  $[H^+]/K_{app}([H^+] + K_{AlOH})$  vs.  $1/[H^+]$  plots.

One of the  $[H^+]/K_{app}([H^+] + K_{AlOH})$  vs.  $1/[H^+]$  plots is shown in Fig. 3. From the slopes and intercepts of these plots were obtained  $K_{HL2}$ ,  $K_1$ , and  $K_3 (= K_1/K_{HL2})$  values for both the fast reacting and slow reacting components of NHFA, NCFA, and SHFA. These values are shown in Table 2.

Assuming that the protolytic equilibria represented by the vertical arrows in Scheme 2 are rapid in comparison to complex formation [14,25], the following equation can be derived for both components of each fulvic acid [6].

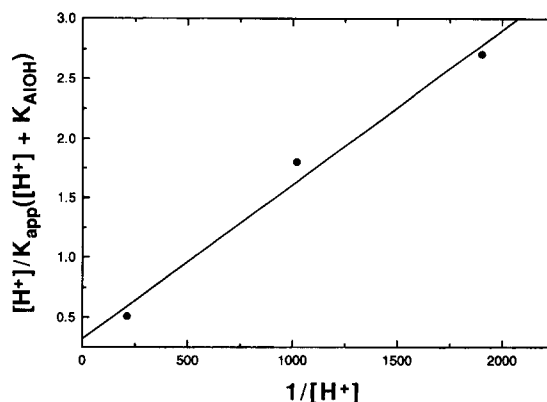


Fig. 3. Kinetic results of  $[H^+]/K_{app}([H^+] + K_{AlOH})$  as a function of  $1/[H^+]$  for the fast reacting component of SHFA at 25°C.

Table 2

Equilibrium parameter values for reaction of Al(III) with fulvic acids at 25°C

Fast reacting component	Slow reacting component
<b>NHFA</b>	
$K_{1,\text{site1}} = 2.36$	$K_{1,\text{site2}} = 0.239$
$K_{3,\text{site1}} = 2.23 \times 10^2$	$K_{3,\text{site2}} = 7.18 \times 10^1$
$K_{\text{HL2,site1}} = 1.06 \times 10^{-2}$	$K_{\text{HL2,site2}} = 3.33 \times 10^{-3}$
<b>NCFA</b>	
$K_{1,\text{site1}} = 10.7$	$K_{1,\text{site2}} = 1.78$
$K_{3,\text{site1}} = 2.80 \times 10^3$	$K_{3,\text{site2}} = 6.62 \times 10^2$
$K_{\text{HL2,site1}} = 3.82 \times 10^{-3}$	$K_{\text{HL2,site2}} = 2.69 \times 10^{-3}$
<b>SHFA</b>	
$K_{1,\text{site1}} = 3.14$	$K_{1,\text{site2}} = 0.715$
$K_{3,\text{site1}} = 7.73 \times 10^2$	$K_{3,\text{site2}} = 6.06 \times 10^2$
$K_{\text{HL2,site1}} = 4.06 \times 10^{-3}$	$K_{\text{HL2,site2}} = 1.18 \times 10^{-3}$

$$k_{\text{f}}K_1[\text{H}^+]/K_{\text{HL2}}K_{\text{app}} = k_1[\text{H}^+]/K_{\text{HL2}} + k_2K_{\text{AlOH}}/[\text{H}^+] + k_3 + k_4K_{\text{AlOH}}/K_{\text{HL2}} \quad (9)$$

Fig. 4 is a plot of the left side of Eq. 9 vs.  $1/[\text{H}^+]$  calculated with the  $k_{\text{obsd1}}$  values of the fast reacting component of SHFA. A good straight line was obtained, indicating that the  $k_1[\text{H}^+]/K_{\text{HL2}}$  term was very small or zero. The left side of Eq. 9 calculated with the  $k_{\text{obsd2}}$  values of the slow reacting component of SHFA also gave a straight line plot vs.  $1/[\text{H}^+]$  as did similar plots using both the  $k_{\text{obsd1}}$  and  $k_{\text{obsd2}}$  values of NHFA and NCFA. This indicates that, in all cases, the reaction of  $\text{Al}^{3+}$  with  $\text{HL}^-$  is so slow that it does not contribute to the overall rate of reaction.

### 3.2. Equilibrium parameters

Three equilibrium parameters were obtained for each kinetically distinguishable component of each fulvic acid. Assuming that the two kinetically distinguishable components of the fulvic acids arise from two different types of binding sites on each fulvic acid, we have labeled these parameters  $K_{\text{HL2,site1}}$ ,  $K_{1,\text{site1}}$  and  $K_{3,\text{site1}}$  for the fast reacting component, and  $K_{\text{HL2,site2}}$ ,  $K_{1,\text{site2}}$  and  $K_{3,\text{site2}}$  for the slow reacting component, as shown in Table 2. The  $K_{\text{HL2}}$  parameters are the second acid dissociation parameters for the fulvic acid aluminum binding sites, i.e.,  $K_{\text{HL2}}$  is the equilibrium parameter for the equilibrium



We can see that the  $K_{\text{HL2,site1}}$  and  $K_{\text{HL2,site2}}$  values for any given fulvic acid are not very different. This indicates that both types of binding sites are probably structurally quite similar. For example, they both could be salicylic acid type sites, as suggested by others [15,16,18,22], that differ only by virtue of the effects of different nearby functional groups. However, the large value of  $K_{\text{HL2}}$  seems to preclude such an assumption.  $K_{\text{HL2}}$  for salicylic acid is only about  $5 \times 10^{-14}$ .

In our earlier paper on the reaction of fulvic acid with aluminum in the presence of acetate buffer, we obtained values for the *first* acid dissociation parameter of fulvic acid, which were comparable to the first acid dissociation constant of salicylic acid and substituted salicylic acids [6]. Based on results from this study, we are forced to conclude that in the absence of buffer, not only is the mechanism changed, but the aluminum binding sites on fulvic acid are different as well.

One way to explain the change in binding sites is that in the presence of buffer, the stronger acid sites on fulvic acid are tied up by hydrogen bonding interactions with the buffer [27], and are thus not available to bind with aluminum. The acetate buffer concentration was at least 500 times the fulvic acid concentration in all of the buffered kinetic runs, and so there was always a large excess of buffer molecules to form hydrogen bonds with the deprotonated stronger acid sites on fulvic acid.

We still must explain why, in the absence of buffer, the acid dissociation parameter values were greater than those commonly measured for fulvic acid. For exam-

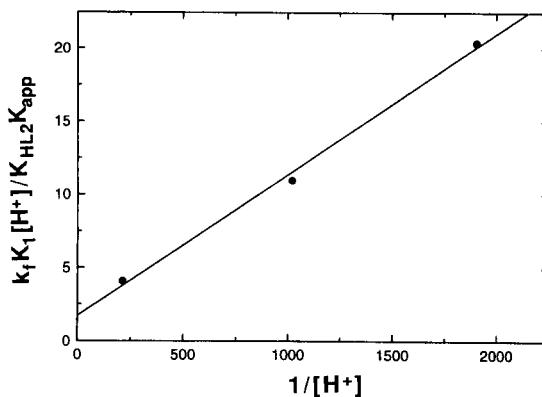


Fig. 4.  $k_{\text{f}}K_1[\text{H}^+]/K_{\text{HL2}}K_{\text{app}}$  as a function of  $1/[\text{H}^+]$  from  $k_{\text{obsd1}}$  values of SHFA at 25°C.

ple, over the range of pH used in this study, the value of the acid dissociation parameter for a Canadian soil fulvic acid ranged approximately from  $2.9 \times 10^{-3}$  to  $4.7 \times 10^{-3}$ , and from  $2.7 \times 10^{-5}$  to  $3.2 \times 10^{-5}$  for two different types of sites called type I and type II carboxyl groups [28]. We can also compare the  $K_{HL2}$  values obtained from the present kinetic analysis with the  $K_a$  values, the acid dissociation equilibrium constant values, for the same fulvic acids estimated by potentiometric titration in an earlier study [29]. The  $K_a$  values obtained in that study for NHFA, NCFA and SHFA were  $1.10 \times 10^{-4}$ ,  $7.24 \times 10^{-5}$  and  $1.51 \times 10^{-4}$ , respectively. These values are smaller still, apparently because of the monoprotic single-site model employed [29].

Thus, the model chosen to represent the complex fulvic acid molecule will to some extent determine the value of acid dissociation parameters obtained. But more importantly, in both of the earlier studies just cited, the measured acid dissociation parameters were average values over all of the proton binding sites in the molecule. In contrast, the  $K_{HL2}$  values determined in the present kinetic study are average values over the sites that bind both aluminum and protons. The inference is, then, that not all of the proton binding sites are available to aluminum, and, in the absence of buffer the aluminum binding sites are the strongly acidic sites. The reason why aluminum is excluded from some of the proton binding sites is possibly because of steric strain. The large hydrated aluminum ion simply may not fit into some of the sites where  $H^+$  ions can bind. According to Marcus [30], the volume of a hydrated  $Al^{3+}$  ion is  $102 \text{ \AA}^3$  while the volume of a hydrated  $H^+$  ion is only  $10.6 \text{ \AA}^3$ .

The three fulvic acids vary in their aluminum binding ability, as shown by the difference in the  $K_1$  and  $K_3$  equilibrium parameter values. In fact, both the variation among the three fulvic acids in the fast reacting site, as well as the variance between the fast reacting site and the slow reacting site for any given fulvic acid is greater than the corresponding variance in proton binding at these sites.

This rather large difference in the  $K_1$  and  $K_3$  values can again be explained in terms of steric strain. Both the smaller values of  $K_{1,site2}$  as compared to  $K_{1,site1}$ , and the smaller values of  $K_{3,site2}$  as compared to  $K_{3,site1}$ , may be due to the fact that the large hydrated aluminum ion does not fit as well into the slow reacting sites. This

could also explain the difference among the  $K_{1,site1}$  values and the  $K_{3,site1}$  values, as well as the difference among the  $K_{1,site2}$  values and the  $K_{3,site2}$  values. These differences appear to be larger than can be accounted for by the effects of different nearby functional groups. The much smaller hydrogen ion may have no trouble either entering or leaving either type site and the variation in the  $K_{HL2}$  values is smaller and can be accounted for by the effects of different nearby functional groups.

As was the case with the fulvic acid dissociation parameters, the model chosen to represent the aluminum–fulvic acid complex will also determine the measured value of the equilibrium parameter for complex formation. In an earlier study using NCFA [8], average aluminum–fulvic acid stability constants were much larger than the values of  $K_1$  and  $K_3$  found in this study. This is not uncommon for metal–fulvic acid complexes. An example will illustrate this point. Gamble and Schnitzer [22] have recalculated equilibrium parameter values for metal–fulvic acid complexation using the data of an earlier paper by Schnitzer and Hansen [31]. Using the same data, but choosing a different model for  $Cu^{2+}$ –fulvic acid complexation, for example, the recalculated equilibrium parameter value was 23 as compared to the original value of about 50,000.

In addition to the different way in which we have defined equilibrium parameters in the present study as compared to the earlier study which yielded greater equilibrium parameter values for NCFA [8], in this study the pH was lower, the ionic strength was higher, and the  $Al^{3+}$ -to-fulvic acid ratio was greater, all of which would yield smaller equilibrium parameter values [5,31,16], as observed.

### 3.3. Rate parameters

The slopes of the straight line plots of the left hand side of Eq. 9 vs.  $1/[H^+]$  for each component of each fulvic acid yielded the  $k_2$  values shown in Table 3. As was the case with the equilibrium parameters, the smaller values of  $k_2$  for the slower reacting sites can be explained by steric strain.

The two terms of the intercept of the plots of the left hand side of Eq. 9 vs.  $1/[H^+]$ ,  $k_3 + k_4 K_{AlOH}/K_{HL2}$ , cannot be separated because the reactions with forward rate parameters  $k_3$  and  $k_4$  have the same pH dependence. Assuming that  $k_4 K_{AlOH}/K_{HL2}$  is very small or zero and the total intercept of these plots is equal to  $k_3$ , yielded

Table 3  
Rate parameter values for reaction of Al(III) with fulvic acids at 25°C

Fast reacting component	Slow reacting component
<b>NHFA</b>	
$k_2 = 1.32 \times 10^3 \text{ M}^{-1} \text{ s}^{-1}$	$k_2 = 63.4 \text{ M}^{-1} \text{ s}^{-1}$
$k_3 = 3.32 \text{ M}^{-1} \text{ s}^{-1}$ (UL)	$k_3 = 0.116 \text{ M}^{-1} \text{ s}^{-1}$ (UL)
$k_{-3} = 1.49 \times 10^{-2} \text{ M}^{-1} \text{ s}^{-1}$ (UL)	$k_{-3} = 1.91 \times 10^{-4} \text{ M}^{-1} \text{ s}^{-1}$ (UL)
$k_4 = 9.91 \times 10^3 \text{ M}^{-1} \text{ s}^{-1}$ (UL)	$k_4 = 1.09 \times 10^2 \text{ M}^{-1} \text{ s}^{-1}$ (UL)
<b>NCFA</b>	
$k_2 = 3.00 \times 10^3 \text{ M}^{-1} \text{ s}^{-1}$	$k_2 = 2.44 \times 10^2 \text{ M}^{-1} \text{ s}^{-1}$
$k_3 = 8.72 \text{ M}^{-1} \text{ s}^{-1}$ (UL)	$k_3 = 0.494 \text{ M}^{-1} \text{ s}^{-1}$ (UL)
$k_{-3} = 3.11 \times 10^{-3} \text{ M}^{-1} \text{ s}^{-1}$ (UL)	$k_{-3} = 7.46 \times 10^{-4} \text{ M}^{-1} \text{ s}^{-1}$ (UL)
$k_4 = 9.38 \times 10^3 \text{ M}^{-1} \text{ s}^{-1}$ (UL)	$k_4 = 3.74 \times 10^2 \text{ M}^{-1} \text{ s}^{-1}$ (UL)
<b>SHFA</b>	
$k_2 = 2.72 \times 10^3 \text{ M}^{-1} \text{ s}^{-1}$	$k_2 = 1.57 \times 10^2 \text{ M}^{-1} \text{ s}^{-1}$
$k_3 = 1.72 \text{ M}^{-1} \text{ s}^{-1}$ (UL)	$k_3 = 0.659 \text{ M}^{-1} \text{ s}^{-1}$ (UL)
$k_{-3} = 2.23 \times 10^{-3} \text{ M}^{-1} \text{ s}^{-1}$ (UL)	$k_{-3} = 9.18 \times 10^{-3} \text{ M}^{-1} \text{ s}^{-1}$ (UL)
$k_4 = 1.97 \times 10^3 \text{ M}^{-1} \text{ s}^{-1}$ (UL)	$k_4 = 2.19 \times 10^2 \text{ M}^{-1} \text{ s}^{-1}$ (UL)

(UL) indicates upper limit value.

an upper limit for  $k_3$ , and in the same way, an upper limit for  $k_4$  was calculated. These upper limit values for  $k_3$  and  $k_4$  are also shown in Table 3. From the  $K_3$  equilibrium parameters and the upper limit  $k_3$  values were calculated upper limit  $k_{-3}$  values and these are shown in Table 3 as well. The rate parameter values for the slow reacting component are all smaller than the corresponding fast reacting component values, again possibly because of steric strain.

In an earlier comparative study of the potentiometrically measurable acidity of three different fulvic acids alone and then in the presence of Cu(II) and Eu(III) ions, two of the fulvic acids showed a 50% increase in proton release in the presence of Cu(II) ions while the third fulvic acid showed only a 25% increase in proton release upon addition of Cu(II) ions [32]. The authors attributed the extra proton release from the first two fulvic acids to the greater "accessibility" of Cu(II) binding sites on these two fulvic acids. In other words, the absence of steric strain. In that earlier study, when Eu(III) was the added metal ion, all three fulvic acids showed a 25% increase in proton release as compared to the free fulvic acid. Thus, it appears that the sterically strained (slow reacting) site is not accessible to the larger Eu(III) ion at all.

### 3.4. Comparison of fulvic acids

Comparison of the equilibrium parameter values of the fast reaction sites in Table 2 showed that the fulvic acids with the more weakly acidic sites contained the stronger aluminum binding sites. For example, among the three fulvic acids NCFA had the smallest  $K_{\text{HL2,site1}}$  value, but the largest values of  $K_{1,\text{site1}}$  and  $K_{3,\text{site1}}$ . This indicates that for the fast reacting component the stronger proton binding sites are also the stronger aluminum binding sites. A similar correlation was not observed for the slow reacting component. NCFA has the second largest  $K_{\text{HL2,site2}}$  value while  $K_{1,\text{site2}}$  and  $K_{3,\text{site2}}$  values are largest among the three fulvic acids. One would expect such an observation if the slow reacting sites on NCFA are less sterically strained than the slow reacting sites on SHFA, for example. SHFA had the smallest value of  $K_{\text{HL2,site2}}$ , yet smaller values of  $K_{1,\text{site2}}$  and  $K_{3,\text{site2}}$  than NCFA.

NCFA also gave the largest rate and equilibrium parameter values for the slow reacting component of any of our fulvic acids, indicating that these slow reacting sites were most accessible in NCFA. On the basis of the two observations just discussed, the slow reacting sites on NCFA are more accessible than the slow reacting sites on SHFA.

Besides comparisons of the site from which a fulvic acid was isolated and its chemical behavior, we can make some generalized statements about the aluminum and proton binding behavior of these fulvic acids. The hardwood fulvic acids NHFA and SHFA, in general, yielded smaller values for both rate and equilibrium parameters for aluminum binding than did the coniferous fulvic acid, NCFA. At the same time the two hardwood fulvic acids yielded larger values of  $K_{\text{HL2}}$  than did the coniferous fulvic acid. Thus, the coniferous fulvic acid binds both hydrogen and aluminum ions more strongly than do the hardwood fulvic acids.

It is obvious from this study that these three fulvic acids vary considerably in their aluminum binding behavior. The variation in the aluminum binding equilibrium parameters (the  $K_1$  and  $K_3$  values) among the three fulvic acids averaged more than 800% for both the fast reacting component and the slow reacting component. Variation in the proton binding equilibrium parameters (the  $K_{\text{HL2}}$  values) was not as pronounced as the variation in the aluminum binding equilibrium parameters. The average difference in the  $K_{\text{HL2}}$  values

among the three fulvic acids was only about 280%.

Finally, we note a recent study which has suggested that, because the carboxyl acidity of XAD resin extracts of aquatic dissolved organic matter are very uniform, XAD extracts are biased and cannot provide information that would differentiate between samples [33]. While we also find relative uniformity in the proton binding behavior of our XAD extracted fulvic acids, the aluminum binding behavior is not uniform from sample to sample, and on this basis we *can* differentiate between our three fulvic acid samples.

### 3.5. Conclusion

The fulvic acids in this study are quite different in their aluminum binding behavior, but not greatly different in their proton binding behavior at those same binding sites. We believe that this is due to steric strain whereby some of the fulvic acid sites are not accessible to aluminum because of the relatively large size of the hydrated aluminum ion. This steric strain is also responsible for the existence of a slow reacting component in these fulvic acids. All of the aluminum binding sites on fulvic acid are apparently structurally similar, but the slower reacting sites are less accessible to aluminum because of steric repulsion.

The present study can be compared to an earlier kinetic study of the reaction of aluminum with fulvic acid in acetate buffered solutions [6]. In the absence of buffer, aluminum complexed only the more strongly acidic sites on the fulvic acids. When buffer was present, however, the strong acid sites were apparently tied up by hydrogen bonding to the buffer. This forced aluminum to bind to less acidic sites on fulvic acid, with the result that the overall mechanism was changed by the buffer. When buffer was present the fulvic acid aluminum binding sites were apparently salicylic acid type sites [6]. However, in the absence of buffer the aluminum binding sites were different, and considerably more acidic than salicylic acid type sites.

This study illustrates the valuable information that can be obtained about the complexation of aluminum by fulvic acid in a kinetic analysis. Such details about the mechanism of the reaction are not available from equilibrium studies, and yet are clearly vital to a full understanding of aluminum–fulvic acid interactions in natural systems.

### Acknowledgements

This work was supported by the U.S. National Science Foundation (Grant BSR 8807826) and by the Faculty Research Committee (Grant No. 677), Idaho State University, Pocatello, Idaho.

### References

- [1] G.R. Aiken, D.M. McKnight, R.L. Wershaw and B. MacCarthy (Eds.), *Humic Substances in Soil, Sediment, and Water*, Wiley, New York, 1985.
- [2] B.G. Oliver, E.M. Thurman and R.L. Malcolm, *Geochim. Cosmochim. Acta*, 47 (1983) 2031.
- [3] E.M. Perdue, J.H. Reuter and R.C. Parrish, *Geochim. Cosmochim. Acta*, 48 (1984) 1257.
- [4] E. Tipping, M.M. Reddy and M.A. Hurley, *Environ. Sci. Technol.*, 24 (1990) 1700.
- [5] B.A. Browne and C.T. Driscoll, *Environ. Sci. Technol.*, 27 (1993) 915.
- [6] B.J. Plankey and H.H. Patterson, *Environ. Sci. Technol.*, 21 (1987) 595.
- [7] B.J. Plankey and H.H. Patterson, *Environ. Sci. Technol.*, 22 (1988) 1454.
- [8] S. Lakshman, R. Mills, H. Patterson and C. Cronan, *Anal. Chim. Acta*, 282 (1993) 101.
- [9] C.S. Cronan, C.T. Driscoll, R.M. Newton, J.M. Kelly, C.L. Schofield and R.J. Bartlett, *Water Resour. Res.*, 26 (1990) 1413.
- [10] J.A. Leenheer, *Environ. Sci. Technol.*, 15 (1981) 578.
- [11] J.H. Espensen, *Chemical Kinetics and Reaction Mechanisms*, McGraw-Hill, New York, 1981, pp. 12–15.
- [12] L.P. Holmes, D.L. Cole and E.M. Eyring, *Phys. Chem.*, 72 (1968) 301.
- [13] C.R. Frink and M. Peech, *Inorg. Chem.*, 2 (1963) 473.
- [14] B. Perlmuter-Hayman and E. Tapuhi, *Inorg. Chem.*, 16 (1977) 2742.
- [15] M.K.S. Mak and C.H. Langford, *Can. J. Chem.*, 60 (1982) 2023.
- [16] D.S. Gamble, A.W. Underdown and C.H. Langford, *Anal. Chem.*, 52 (1980) 1901.
- [17] D.S. Gamble, M. Schnitzer and I. Hoffman, *Can. J. Chem.*, 48 (1970) 3197.
- [18] W.T. Bresnahan, C.L. Grant and J.H. Weber, *Anal. Chem.*, 50 (1978) 1675.
- [19] C.H. Langford and M.K.S. Mak, *Comments Inorg. Chem.*, 2 (1983) 127.
- [20] M.K.S. Mak, C.H. Langford, *Inorg. Chim. Acta*, 70 (1983) 237.
- [21] S.E. Cabaniss and M.S. Shuman, *Geochim. Cosmochim. Acta*, 52 (1988) 195.
- [22] D.S. Gamble and M. Schnitzer, in P.C. Singer (Ed.), *Trace Metals and Metal-Organic Interactions in Natural Waters*, Ann Arbor Science, Ann Arbor, MI, 1974, Chap. 9.

- [23] E.M. Perdue and C.R. Lytle, *Environ. Sci. Technol.*, 17 (1983) 654.
- [24] M.S. Shuman, G.J. Collins, P.J. Fitzgerald and D.L. Olsen, in F.R. Christman and E.T. Gjessing (Eds.), *Aquatic and Terrestrial Humic Materials*, Ann Arbor Science, Ann Arbor, MI, 1983, Chap. 17.
- [25] F. Secco and M. Venturini, *Chem. Inorg.*, 14 (1975) 1978.
- [26] B. Perlmutter-Hayman and E. Tapuhi, *Inorg. Chem.*, 18 (1979) 875.
- [27] J. Buffle, *Complexation Reactions in Aquatic Systems: An Analytical Approach*, Halsted Press, New York, 1988, p. 312.
- [28] D.S. Gamble, *Can. J. Chem.*, 48 (1970) 2662.
- [29] H.H. Patterson, C.S. Cronan, S. Lakshman, B.J. Plankey and T.A. Taylor, *Sci. Total Environ.*, 113 (1992) 179.
- [30] Y. Marcus, *Ion Solvation*, Wiley, New York, 1985, p. 100.
- [31] M. Schnitzer and E.H. Hansen, *Soil Sci.*, 109 (1970) 333.
- [32] J. Ephraim, S. Alegret, A. Mathuthu, M. Bicking, R.L. Malcolm and J.A. Marinsky, *Environ. Sci. Technol.*, 20 (1986) 354.
- [33] M.S. Shuman, in E.M. Perdue and E.T. Gjessing (Eds.), *Organic Acids in Aquatic Ecosystems*, Wiley, New York, 1990, pp. 97–109.



ELSEVIER

Analytica Chimica Acta 300 (1995) 237–241

ANALYTICA  
CHIMICA  
ACTA

# Simple, rapid and sensitive spectrofluorimetric determination of diflunisal in serum and urine based on its ternary complex with terbium and EDTA

Pinelopi C. Ioannou \*, Evriklia S. Lianidou, Dimitrios G. Konstantianos

*University of Athens, Laboratory of Analytical Chemistry, Panepistimiopolis, Zografou, 157 71 Athens, Greece*

Received 6 June 1994; revised manuscript received 17 August 1994

## Abstract

A very simple, rapid and highly sensitive fluorimetric method for the determination of diflunisal in serum and urine is described. The method is based on the formation of a ternary complex between diflunisal,  $Tb^{3+}$  and EDTA in alkaline aqueous solutions. This complex exhibits very intense terbium ion luminescence with a main emission maximum at 546 nm when excited at 284 nm. Optimum conditions for the complex formation have been investigated. The detection limit for diflunisal is  $2.4 \mu g l^{-1}$ , while the range of application is  $0.01$ – $6.00 mg l^{-1}$ . The method has been successfully applied for the determination of diflunisal in untreated human serum and urine samples. Analytical recoveries from serum and urine samples spiked with diflunisal were in the ranges of 96.8–101.2% and 98.0–102.0%, respectively.

*Keywords:* Fluorimetry; Diflunisal; Serum; Terbium; Urine

## 1. Introduction

Diflunisal (DIF, 2,4-difluoro-4-hydroxy-3-biphenylcarboxylic acid) is a derivative of salicylic acid with similar analgesic and anti-inflammatory properties to aspirin. Different methods for the determination of DIF have been reported. The proposed methods for monitoring diflunisal in biological fluids are liquid chromatography (LC) [1], gas-liquid chromatography [2] and fluorimetry [3]. These methods are time-consuming and require removal of proteins prior to the measurement. Fluorimetric methods for the determination of DIF are based on its intrinsic fluorescence in various solvents. A method for the simultaneous determination of diflunisal and salicylic acid in serum based

on their intrinsic fluorescence in chloroform-acetic acid solutions has also been reported [4].

Fluorescent europium and terbium chelates are characterized by unique spectroscopic properties such as line emission spectra, large Stoke's shift and long-lived fluorescence [5]. When excited at wavelengths absorbed by an organic ligand, these complexes emit characteristic lanthanide ion line emission spectra. This is due to an intramolecular energy transfer through the excited triplet state of the ligand to the emitting level of the lanthanide ion. Several very important applications of europium and terbium complexes have already been reported [6] with the most attractive ones being their use as fluorescent labels for highly sensitive time-resolved fluorescence immunoassays and nucleic acid hybridization assays [7,8]. Another area with interesting applications is the fluorimetric determination of

\* Corresponding author.

organic molecules capable of transferring their triplet energy to lanthanide ions either via complexation or by intermolecular energy transfer regulated by diffusion processes. These methods are known as lanthanide-sensitized luminescence and are applicable to many aromatic aldehydes and ketones and a variety of biologically important compounds [6].

Terbium ions form strongly fluorescent ternary complexes with aminopolycarboxylic acids such as EDTA and phenol derivatives such as salicylic and sulfosalicylic acids [9,10]. A method for the determination of salicylate in plasma based on its ternary complex with terbium and EDTA has been reported [11]. Diflunisal also forms a fluorescent ternary complex with terbium and EDTA. This complex has already been applied for the development of a highly sensitive enzyme-amplified lanthanide immunoassay (EALL) [12].

Here, we report a very simple, rapid and sensitive fluorimetric method for the determination of diflunisal based on its ternary complex with terbium and EDTA. Optimum conditions for the complex formation have been investigated. The method has successfully been applied for the determination of diflunisal in human serum and urine samples without any pretreatment. Because of its simplicity and high sensitivity this method is advantageous for therapeutic drug monitoring and drug abuse screening of diflunisal in biological fluids.

## 2. Experimental

### 2.1. Apparatus

A Model 512 fluorescence spectrophotometer (Perkin-Elmer, Norwalk, CT), equipped with a 150-W xenon lamp and a magnetic stirrer under the cell holder was used. Instrument settings were as follows: energy mode; excitation wavelength 284 nm, with a bandwidth of 20 nm; emission wavelength 546 nm, with a bandwidth of 20 nm. A constant temperature of 25.0°C in the 1.000 cm (pathlength) sample cell was maintained with a thermostated water bath.

### 2.2. Reagents

All solutions were prepared in deionised distilled water from reagent grade materials, unless otherwise stated.

Aqueous stock solution of DIF (Sigma) containing 500 mg l<sup>-1</sup> was prepared at pH 12.0. This solution was stable for at least 1 month at room temperature. Working standard solutions of diflunisal were prepared by appropriate dilution. A terbium solution, 0.01 mol l<sup>-1</sup>, was prepared by dissolving the appropriate amount of terbium oxide (Merck) in concentrated nitric acid, evaporating to dryness and dissolving the residue in 0.01 mol l<sup>-1</sup> hydrochloric acid. An EDTA solution of 0.01 mol l<sup>-1</sup> and a CAPS (3-[cyclohexylamino]-1-propanesulfonic acid) (Sigma) buffer solution, 0.1 mol l<sup>-1</sup> of pH 12.7 were prepared. A working solution containing terbium and EDTA at a final concentration of 1.0 × 10<sup>-3</sup> mol l<sup>-1</sup> was prepared by mixing the appropriate volumes of terbium and EDTA solutions and diluting with CAPS buffer (final concentration of CAPS, 0.08 mol l<sup>-1</sup>). This working solution was used as a single reagent for the measurements.

### 2.3. Procedure

Transfer 10 μl of the sample (serum or urine) or aqueous standard into the cuvette, add 2.0 ml of the mixed Tb-EDTA reagent and start the stirrer. Measure the fluorescence intensity versus a reagent blank in which 10 μl of water is substituted for standard or sample. Calculate the unknown concentration, C<sub>DIF</sub>, from the calibration graph. Calculate the concentration of DIF in serum, C<sub>DIF,s</sub>, and urine, C<sub>DIF,u</sub>, from Eqs. 1 and 2, respectively:

$$C_{\text{DIF},s} = 1.80C_{\text{DIF}} \quad (1)$$

$$C_{\text{DIF},u} = 1.32C_{\text{DIF}} \quad (2)$$

where 1.80 and 1.32 are correction factors and their values depend on the actual dilution factors (200-fold according to the above procedure) of serum and urine samples.

## 3. Results and discussion

Aqueous alkaline solution of diflunisal show an intense intrinsic fluorescence with excitation maxima at 272 and 310 nm and an emission maximum at 420 nm [4]. In the presence of the Tb-EDTA mixture a strongly fluorescent ternary complex is formed in alkaline aqueous solution with excitation maxima shifted



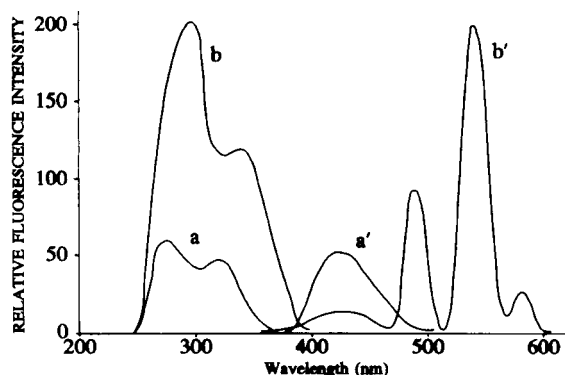


Fig. 1. Fluorescence excitation (a,b) and emission spectra (a',b') of: aqueous solutions (pH 12.6) of diflunisal,  $C = 4.0 \times 10^{-6}$  mol  $l^{-1}$ ,  $\lambda_{ex} = 272$  nm,  $\lambda_{em} = 420$  nm (a,a') and of the DIF-Tb-EDTA ternary complex,  $C_{Tb-EDTA} = 1.0 \times 10^{-3}$  mol  $l^{-1}$ ,  $\lambda_{ex} = 284$  nm,  $\lambda_{em} = 546$  nm (b,b').

towards longer wavelengths with respect to those for diflunisal ( $\lambda_{ex} = 284$  and 336 nm) and a narrow line terbium ion luminescence spectrum with maxima at 488, 547 and 596 nm (Fig. 1). The main emission band at 547 nm was selected for the measurements with excitation at 284 nm.

### 3.1. Optimum conditions for DIF-Tb-EDTA ternary complex formation

#### Effect of pH

The fluorescence intensity of diflunisal solutions in the presence of excess Tb-EDTA mixture was measured over a pH range from 9.0 to 13.5, by using Tris buffer and adjusting the pH with hydrochloric acid and sodium hydroxide solutions. The maximum fluorescence intensity was observed at a pH between 12.5 and 13.0 (Fig. 2). Among several buffer systems tested (Tris, CAPS, 2-amino-2-methyl-1-propanol (AMP), glycine, borate), a CAPS buffer solution at a concentration of 0.08 mol  $l^{-1}$  was found to be the most suitable for this pH range.

#### Reagent excess and stability of the complex

The effect of Tb-EDTA mixture excess on the fluorescence intensity of the ternary complex was investigated. The maximum fluorescence signal of the complex is observed at about 500-fold molar excess of Tb-EDTA (1:1) mixture (Fig. 3, curve a), while the intrinsic fluorescence of diflunisal practically disappeared (Fig. 3, curve b). It was found that a concen-

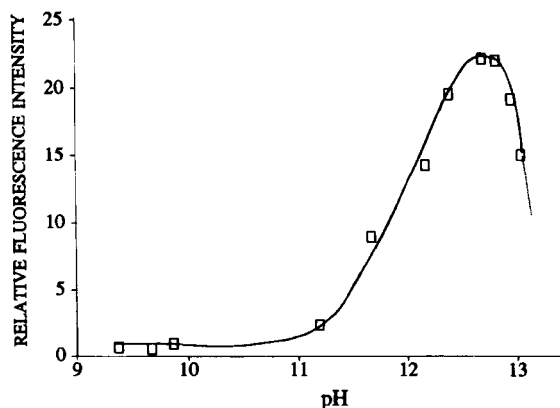


Fig. 2. Effect of pH on the fluorescence signal of the DIF-Tb-EDTA ternary complex ( $\lambda_{ex} = 284$  nm,  $\lambda_{em} = 546$  nm,  $C_{DIF} = 4.0 \times 10^{-7}$  mol  $l^{-1}$ ,  $C_{Tb-EDTA} = 1.0 \times 10^{-3}$  mol  $l^{-1}$ ).

tration of  $1.0 \times 10^{-3}$  mol  $l^{-1}$  of Tb-EDTA mixture is sufficient for the analytical range of application for diflunisal and was selected for the analytical procedure. The ternary complex is formed immediately when diflunisal is added to the alkaline Tb-EDTA solution. The fluorescence signal remains constant for at least 24 h if there are no changes in pH.

### 3.2. General analytical characteristics

The fluorescence signal was linearly related to the concentration of diflunisal in the range of 0.01–6.00  $\mu g$   $ml^{-1}$ . Pearson's correlation coefficient ( $r$ ) for the standard calibration graph was 0.9991. The detection limit was found to be 2.4 ng  $ml^{-1}$ . To test the precision,

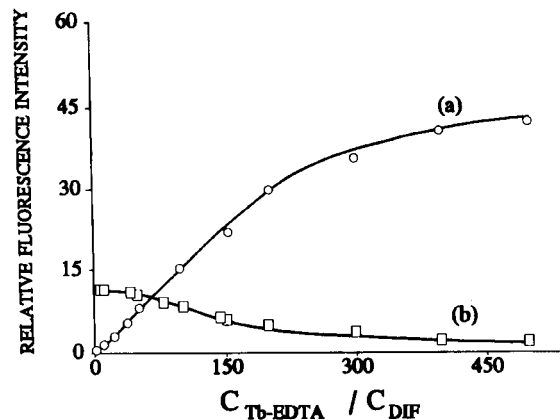


Fig. 3. Effect of the molar excess of Tb-EDTA mixture on: (a) the analytical signal of the DIF-Tb-EDTA ternary complex ( $\lambda_{ex} = 284$  nm,  $\lambda_{em} = 546$  nm) and (b), on the intrinsic fluorescence of diflunisal ( $\lambda_{ex} = 272$  nm,  $\lambda_{em} = 420$  nm).

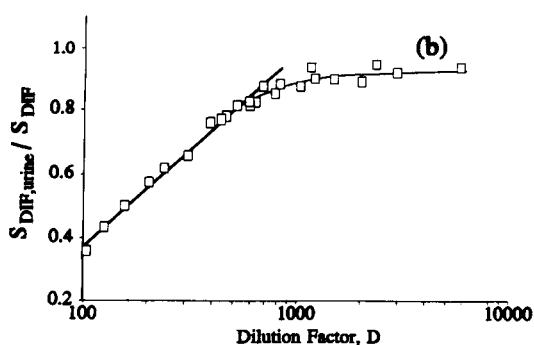
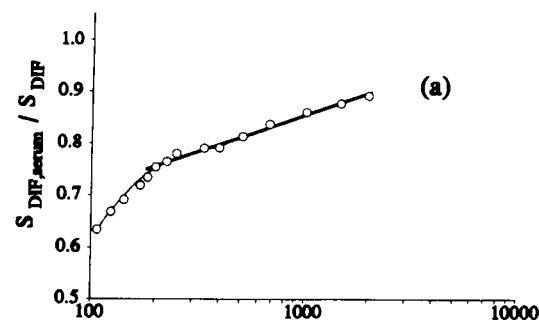


Fig. 4. Effect of the dilution factor,  $D$ , of serum (a) and urine (b) samples on the slope of the calibration graph for diflunisal.

three series of samples covering the range of interest for DIF ( $0.05$ ,  $0.50$  and  $5.00 \mu\text{g ml}^{-1}$ ) were analysed and the corresponding R.S.D. (%) values were found to be  $8.5$ ,  $3.0$  and  $2.0$ , respectively ( $n=9$ ).

### 3.3. Determination of diflunisal added to serum and urine samples

For measuring diflunisal in serum and urine, untreated samples were used. The fluorescence signals

Table 1  
Analytical recovery of DIF added to serum samples

Concentration added ( $\mu\text{g ml}^{-1}$ )	Concentration found <sup>a</sup> ( $\mu\text{g ml}^{-1}$ )	Recovery $\pm$ S.D. (%)
5.0	4.95	$99 \pm 2$
10.0	9.68	$97 \pm 2$
20.0	19.60	$98 \pm 3$
50.0	48.80	$98 \pm 1$
100.0	101.30	$101 \pm 3$
Mean		$98.6$

<sup>a</sup> Mean of four measurements at different dilutions for each sample (1000-, 340-, 200- and 150-fold dilutions).

Table 2  
Analytical recovery of DIF added to urine samples

Concentration added ( $\mu\text{g ml}^{-1}$ )	Concentration found <sup>a</sup> ( $\mu\text{g ml}^{-1}$ )	Recovery $\pm$ S.D. (%)
3.0	3.10	$103 \pm 4$
6.0	5.96	$99 \pm 1$
10.0	9.80	$98 \pm 4$
20.0	19.70	$98 \pm 2$
40.0	40.60	$101 \pm 2$
100.0	99.40	$99 \pm 5$
Mean		$99.7$

<sup>a</sup> Mean of three measurements (200-fold dilution).

obtained for serum and urine samples spiked with diflunisal were lower than those obtained with the corresponding DIF aqueous standards, depending on the dilution factor of the sample. To choose the better procedure for measuring DIF in serum and urine (direct calibration or standard addition), a detailed study of the effect of the dilution factor of the sample ( $D$ ) on the slope of DIF calibration graphs was carried out (Fig. 4). As can be seen from Fig. 4a, the slope of the calibration graph linearly increased with the logarithm of the dilution factor between 200 and 1100 for serum according to Eq. 3. For higher dilutions the slope of the calibration graph in serum practically reaches that of aqueous standard solutions. For urine samples (Fig. 4b) the slope of the calibration graph increased linearly with the logarithm of the dilution factor between 150 and 700 according to Eq. 4, reaching that of aqueous standards at higher dilutions ( $> 700$ ).

$$\begin{aligned} \text{Slope}_{\text{DIF,s}} / \text{Slope}_{\text{DIF}} \\ = 0.152 (\pm 0.01) \log D + 0.407 (\pm 0.027) \\ (r=0.9950) \end{aligned} \quad (3)$$

$$\begin{aligned} \text{Slope}_{\text{DIF,u}} / \text{Slope}_{\text{DIF}} \\ = 0.592 (\pm 0.023) \log D - 0.806 (\pm 0.056) \\ (r=0.9930) \end{aligned} \quad (4)$$

Thus, diflunisal added to serum and urine can be quantified by using: (i) the standard additions technique or (ii) a direct calibration graph and applying the correction as dictated by Eqs. 1 and 2. In this study, the second approach was used. Analytical recovery experiments on serum and urine samples spiked with DIF (using different dilution factors for each sample)

are shown in Tables 1 and 2, respectively. The concentrations selected are typical for DIF concentration levels in human serum and urine for 50 h after a single 750 mg oral dose [13,14].

### 3.4. Interference studies

The absence of detectable blanks in diflunisal-free serum and urine indicates that the constituents of the biological samples do not interfere with the fluorescence measurements. Interference from other drugs was tested by analysing serum and urine samples spiked with DIF where amounts of the drug under investigation were also added. None of the drugs tested (naproxen, indomethacin, amitriptyline, phenacetin, caffeine, antipyrine, theophylline) interfered with the determination of DIF even at concentrations higher than those achieved therapeutically. The only interference occurs from salicylic acid which also forms a ternary complex with Tb–EDTA at mass ratios (salicylic acid/diflunisal) > 0.3. This interference could be avoided by using synchronous scanning second-derivative fluorescence spectrometry (SDSFS) for measurements. Preliminary experiments have shown that, by using SDSFS, it is possible to determine simultaneously diflunisal and salicylic acid without any preliminary separation step. This work is in progress.

### 4. Conclusions

The present method for the determination of diflunisal is highly sensitive with detection limits 5 and 70 times lower than those obtained by the previously reported fluorimetric [4] and LC [1] methods, respectively. The method is very simple and rapid; it allows

the determination of diflunisal in biological fluids without any preliminary steps, and requires only a small sample volume (10  $\mu$ l). Moreover, the method can be easily adopted to LC or flow-injection techniques.

### Acknowledgements

We gratefully acknowledge support from the Ministry of Industry, Energy and Technology, General Secretariat of Research and Technology of Greece.

### References

- [1] M. Schwartz, R. Chion, R.J. Stubbs and W.F. Bayne, *J. Chromatogr.*, 380 (1986) 420.
- [2] D.J. Tocco, G.O. Breault, A.G. Zacchei, S.L. Steelman and C.V. Perrier, *Drug Metab. Dispos.*, 3 (1975) 453.
- [3] M. Balali-Mood, L.S. King and L.F. Prescott, *J. Chromatogr.*, 229 (1982) 234.
- [4] D.G. Konstantianos and P.C. Ioannou, *Eur. J. Pharm. Sci.*, 1 (1994) 209.
- [5] J.C.G. Bunzli and G.R. Choppin (Eds.), *Lanthanide probes in Life, Chemical and Earth Sciences, Theory and Practice*, Elsevier, Amsterdam, 1989.
- [6] J. Georges, *Analyst*, 118 (1993) 1481.
- [7] E.P. Diamandis and T.K. Christopoulos, *Anal. Chem.*, 62 (1990) 1149A.
- [8] E.F.G. Templeton, H.E. Wong, R.A. Evangelista, T. Granger and A. Pollak, *Clin. Chem.*, 37 (1991) 1506.
- [9] N.S. Poluektov, L.A. Alakaeva and M.A. Tischenko, *Zh. Anal. Khim.*, 28 (1973) 1621.
- [10] R.M. Dagnall, R. Smith and T.S. West, *Analyst*, 92 (1967) 358.
- [11] M.P. Bailey and B.F. Rocks, *Anal. Chim. Acta*, 201 (1987) 335.
- [12] H. Yu and E.P. Diamandis, *Clin. Chem.*, 39 (1993) 2108.
- [13] J.E. Ray and R.O. Day, *J. Pharm. Sci.*, 72 (1983) 1403.
- [14] C. Midskov, *J. Chromatogr.*, 278 (1983) 439.



ELSEVIER

Analytica Chimica Acta 300 (1995) 243–251

ANALYTICA  
CHIMICA  
ACTA

# 2-(5-Hydrazinocarbonyl-2-thienyl)-5,6-methylenedioxybenzofuran and 2-(5-hydrazinocarbonyl-2-furyl)-5,6-methylenedioxybenzofuran as novel fluorescence derivatisation reagents for carboxylic acids in liquid chromatography

Mikihiko Saito, Tamano Ushijima, Kazumi Sasamoto \*, Kenshi Yakata, Yosuke Ohkura, Keiyu Ueno

*Dojindo Laboratories, Tabaru 2025-5, Mashiki-machi, Kumamoto 861-22, Japan*

Received 7 March 1994; revised manuscript received 25 August 1994

## Abstract

The new acid hydrazides, 2-(5-hydrazinocarbonyl-2-thienyl)-5,6-methylenedioxybenzofuran (TMBH) and 2-(5-hydrazinocarbonyl-2-furyl)-5,6-methylenedioxybenzofuran (FMBH), were synthesized as precolumn fluorescence derivatisation reagents for carboxylic acids in liquid chromatography. These compounds readily react with carboxylic acids in the presence of a coupling reagent under mild conditions in aqueous solution to give fluorescent derivatives. The detection limits of lauric acid were both 0.1 pmol per 10  $\mu$ l injection volume at a signal-to-noise ratio of 3. The methods in which these compounds are used were applied to the assay of a standard mixture of prostaglandins (25  $\mu$ M) and prostaglandins in a human seminal fluid.

*Keywords:* Fluorimetry; Liquid chromatography; Fluorescence derivatisation reagents; Carboxylic acids; Thiophenyl benzofuran; Furyl benzofuran; Acid hydrazides; Prostaglandins

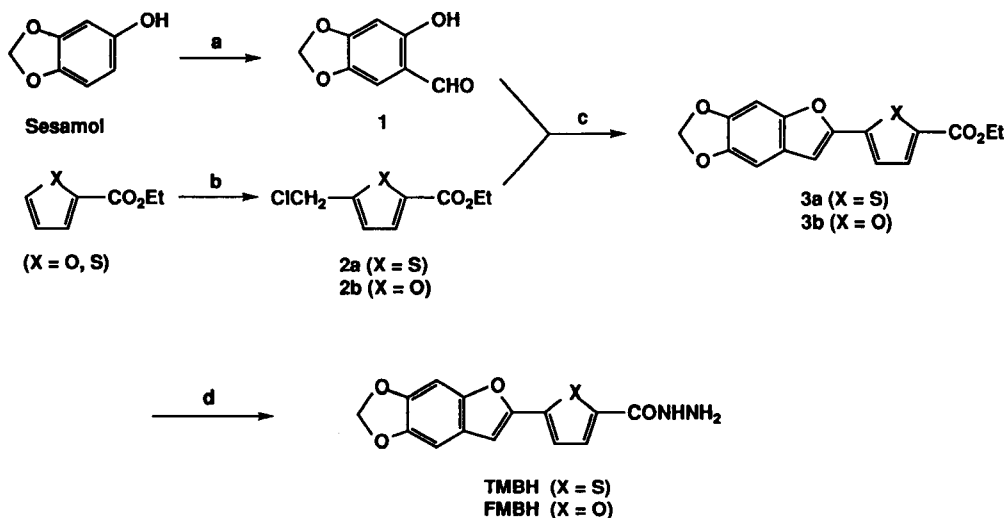
## 1. Introduction

Fatty acids like arachidonic acid are known to be of physiological importance. The quantification of these fatty acids, normally found in small quantities in biological samples, requires a sensitive and selective detection technique. Although numerous fluorescence derivatisation reagents for the liquid chromatographic (LC) determination of fatty acids have been reported [1,2], most of the reagents often require harsh reaction conditions and prolonged reaction times due to the

weak nucleophilicity of carboxyl functionalities. These problems, however, can be circumvented by using acid hydrazides such as 6,7-dimethoxy-1-methyl-2(1*H*)-quinoxalinone-3-propionylcarboxylic acid hydrazide (DMEQ-hydrazide) [3,4] and 4-(5,6-dimethoxy-2-benzimidazolyl)benzohydrazide [5]. These acid hydrazides permit derivatisation under relatively mild conditions in aqueous solution employing a condensation reagent such as 1-ethyl-3-(3-dimethylamino-propyl)carbodiimide (EDC).

In a preceding paper [6], a precolumn fluorescence derivatisation reagent for carboxylic acids, 2-(5-hydra-

\* Corresponding author.



Reagents and conditions: a)  $\text{POCl}_3$ , DMF, 20 °C, 16 h; b)  $(\text{CH}_2\text{O})_n$ ,  $\text{ZnCl}_2$ , HCl, 30 °C, 4 h; c)  $\text{K}_2\text{CO}_3$ , DMF, 110 °C, 16 h; d)  $\text{NH}_2\text{NH}_2$ , DMF, 70 °C, 1 h.

Scheme 1.

zinocarbonyl-2-oxazolyl)-5,6-methylenedioxybenzofuran (OMBH), was described, whose fluorogenic structural unit was 2-oxazolylbenzofuran bearing a methylenedioxy group to enhance its fluorescence. The fluorogenic moiety has been successfully used in a fluorescence derivatisation reagent, 2-(5-chlorocarbonyl-2-oxazolyl)-5,6-methylenedioxybenzofuran, for the LC determination of alcohols [7–9].

To investigate the effect of the oxazolyl portion of OMBH on the sensitivity and/or separation in LC analyses of fatty acids, we have synthesized two analogous acid hydrazides, 2-(5-hydrazinocarbonyl-2-thienyl)-5,6-methylenedioxybenzofuran (TMBH) and 2-(5-hydrazinocarbonyl-2-furyl)-5,6-methylenedioxybenzofuran (FMBH), that replace the oxazolyl portion with a thienyl or furyl group, respectively (Scheme 1), and the results of this study are reported here.

## 2. Experimental

### 2.1. Apparatus

Fluorescence spectra were measured on a Hitachi 650-60 spectrometer in  $10 \times 10$  mm quartz cells; spectral bandwidths of 10 nm were used in both the

excitation and emission monochromators. Proton nuclear magnetic resonance ( $^1\text{H}$  NMR) spectra were obtained on a Bruker AC-200P spectrometer operating at 200 MHz using tetramethylsilane as an internal standard. The splitting patterns were designated as follows: s, singlet; d, doublet; t, triplet; q, quartet. Infrared spectra were taken in, unless otherwise noted, KBr disks on a Hitachi 270-30 spectrometer. Fast atom bombardment mass spectra (FAB-MS) were measured on a Jeol JMS-AX 505W mass spectrometer using 2-nitrobenzyl alcohol as the matrix. Uncorrected melting points were obtained on a Yamato MP-21 melting point apparatus. LC analyses were performed with a Shimadzu LC-4A liquid chromatograph equipped with a RF-530 fluorescence detector (with a  $1\text{-}\mu\text{l}$  flow cell) operating at an excitation wavelength of 373 nm (for TMBH) or 362 nm (for FMBH) and an emission wavelength of 483 nm (for TMBH) or 462 nm (for FMBH). The column was a Wakosil ODS-II 5C18 HG ( $250 \times 4$  mm i.d.; particle size  $5\ \mu\text{m}$ ) and the temperature was 40 °C. The mobile phase was aqueous acetonitrile at a flow rate of  $1.0\ \text{ml}\ \text{min}^{-1}$ .

### 2.2. Chemicals

All chemicals were of analytical-reagent grade. Caprylic ( $\text{C}_8$ ), capric ( $\text{C}_{10}$ ), lauric ( $\text{C}_{12}$ ), myristic ( $\text{C}_{14}$ ),

palmitic (C<sub>16</sub>) and stearic (C<sub>18</sub>) acid were purchased from Wako (Osaka) and margaric (C<sub>17</sub>) acid was from Tokyo Chemical Ind. (Tokyo); all the acids were used without purification. Prostaglandins E<sub>1</sub>, E<sub>2</sub>, F<sub>1α</sub> and F<sub>2α</sub> were purchased from Sigma (St. Louis, MO). Stock solutions of the C<sub>8</sub>–C<sub>18</sub> acids (1 × 10<sup>-4</sup> M) were prepared in *N,N*-dimethylformamide (DMF) and diluted with water to give required concentrations prior to use.

### 2.3. Syntheses (Scheme 1)

#### 2-Hydroxy-4,5-methylenedioxy benzaldehyde (**1**) [10]

Freshly distilled phosphorus oxychloride (153 g, 1.0 mol) was slowly added to anhydrous DMF (73 g, 1.0 mol) with stirring at room temperature. Sesamol (125 g, 0.91 mol) was added to this solution portionwise over 4 h and then the mixture was stirred at room temperature overnight. The reaction mixture was poured onto ice water resulting in precipitation. The solids formed were collected and taken up into diethyl ether, washed with water, dried (MgSO<sub>4</sub>), and concentrated. Recrystallization of the residue from ethanol gave 124.1 g (39%) of aldehyde **1** as a slightly yellow crystalline solid (m.p. 125–126°C). <sup>1</sup>H NMR (CDCl<sub>3</sub>) δ (ppm): 6.07 (s, 2H, CH<sub>2</sub>), 6.57 (s, 1H, Ar), 7.08 (s, 1H, Ar), 9.99 (s, 1H, CHO), 11.01 (s, 1H, OH). IR (cm<sup>-1</sup>): 3080 (OH), 1655, 1620, 1485. FAB-MS: *m/z* = 167 [M + 1]<sup>+</sup>.

#### 5-Chloromethyl thiophene-2-carboxylic acid ethyl ester (**2a**) [11]

Hydrogen chloride gas was introduced to a stirred chloroform solution (50 ml) containing 2-thiophene carboxylic acid ethyl ester (15.6 g, 0.1 mol), paraformaldehyde (4.5 g) and zinc chloride (3.4 g, 25 mmol) at ca. 30°C over 4 h. The reaction mixture was poured onto ice water and extracted with chloroform (50 ml). The chloroform layer was washed with water (3 times), aqueous NaHCO<sub>3</sub> (2 times), and dried (Na<sub>2</sub>SO<sub>4</sub>). After the solvent was stripped off, the crude product was distilled in vacuo (86–94°C at 0.15 mmHg) to yield 11.0 g (54%) of compound **2a** as a colorless oil. <sup>1</sup>H NMR (CDCl<sub>3</sub>) δ (ppm): 1.32 (t, 3H, *J* = 7.1 Hz, Et), 4.31 (q, 2H, *J* = 7.1 Hz, Et), 5.07 (s, 2H, CH<sub>2</sub>Cl), 7.27 (d, 1H, *J* = 3.9 Hz, thiophene H-3), 7.67 (d, 1H, *J* = 3.8 Hz, thiophene H-4). IR (neat, cm<sup>-1</sup>): 3010, 1730 (ester), 1275, 1105. FAB-MS: *m/z* = 204 [M]<sup>+</sup>, 169 [M - 35]<sup>+</sup>.

#### 2-(5-Ethoxycarbonyl-2-thienyl)-5,6-methylenedioxybenzofuran (**3a**)

A mixture containing aldehyde **1** (3.0 g, 18.0 mmol), compound **2a** (3.68 g, 18.0 mmol) and K<sub>2</sub>CO<sub>3</sub> (2.49 g, 18.0 mmol) in anhydrous DMF (100 ml) was heated at 110°C for 16 h. The reaction mixture was filtered and the filtrate was concentrated in vacuo to give a colored residue. Chromatography on silica gel (CHCl<sub>3</sub>), followed by recrystallization from CHCl<sub>3</sub>-hexane (1:3, v/v), afforded 4.23 g (53%) of compound **3a** as a yellow crystalline solid (m.p. 124–126°C). <sup>1</sup>H NMR (CDCl<sub>3</sub>) δ (ppm): 1.39 (t, 3H, *J* = 7.1 Hz, Et), 4.37 (q, 2H, *J* = 7.1 Hz, Et), 6.01 (s, 2H, -OCH<sub>2</sub>O-), 6.69 (s, 1H, benzofuran H-4/H-7), 6.93 (s, 1H, benzofuran H-4/H-7), 6.99 (s, 1H, benzofuran H-3), 7.33 (d, 1H, *J* = 4.0 Hz, thiophene H-3), 7.74 (d, 1H, *J* = 3.9 Hz, thiophene H-4). IR (cm<sup>-1</sup>): 3500, 1720 (ester). FAB-MS: *m/z* = 316 [M]<sup>+</sup>. Fluorescence emission maximum (λ<sub>em</sub>) = 484 nm and excitation maximum (λ<sub>ex</sub>) = 383 nm in methanol.

#### 2-(5-Hydrazinocarbonyl-2-thienyl)-5,6-methylenedioxybenzofuran (TMBH)

A DMF solution (15 ml) containing compound **3a** (1.5 g, 4.78 mmol) and hydrazine hydrate (1.2 g, 23.5 mmol) was heated at 70°C for 1 h. Hydrazine hydrate (10 g) was further added resulting in precipitation of the product as crystalline solids. The reaction mixture was diluted with water (20 ml); the precipitates were collected, washed with methanol and dried in vacuo to afford 1.34 g (86%) of TMBH as a yellow powder (m.p. 262–263°C). <sup>1</sup>H NMR (DMSO-d<sub>6</sub>) δ (ppm): 4.51 (br, 2H, NH<sub>2</sub>), 6.07 (s, 2H, -OCH<sub>2</sub>O-), 7.13 (s, 1H, benzofuran), 7.23 (s, 1H, benzofuran), 7.32 (s, 1H, benzofuran), 7.50 (d, 1H, *J* = 3.9 Hz, thiophene H-3), 7.71 (d, 1H, *J* = 4.0 Hz, thiophene H-4), 9.86 (br, 1H, CONH). IR (cm<sup>-1</sup>): 3330, 3225, 3025, 2920, 1605, 1475, 1325. FAB-MS: *m/z* = 303 [M + 1]<sup>+</sup>. Anal. Calcd. for C<sub>14</sub>H<sub>10</sub>N<sub>2</sub>O<sub>4</sub>S: C, 55.63; H, 3.33; N, 9.27. Found: C, 55.79; H, 3.38; N, 9.23.

#### 5-Chloromethyl furyl-2-carboxylic acid methyl ester (**2b**) [11]

This compound was synthesized in the same manner as described for compound **2a** in 55% yield as a colorless oil (distilled at 108°C and 4 mmHg). <sup>1</sup>H NMR (CDCl<sub>3</sub>) δ (ppm): 3.90 (s, 3H, Me), 4.60 (s, 2H,

CH<sub>2</sub>Cl), 6.49 (d, 1H, *J* = 3.5 Hz, furan H-3), 7.13 (d, 1H, *J* = 3.5 Hz, furan H-4). IR (neat, cm<sup>-1</sup>): 3145, 2960, 1738 (ester), 1310, 1217. FAB-MS: *m/z* = 175 [M + 1]<sup>+</sup>.

#### 2-(5-Methoxycarbonyl-2-furyl)-5,6-methylenedioxybenzofuran (3b)

This compound was synthesized in the same manner as described for compound 3a in 39% yield as a slight yellow crystalline solid (m.p. 195–198°C). <sup>1</sup>H NMR (CDCl<sub>3</sub>) δ (ppm): 3.93 (s, 3H, Me), 6.01 (s, 2H, –OCH<sub>2</sub>O–), 6.76 (d, 1H, *J* = 3.4 Hz, furan H-3), 6.95 (s, 1H, benzofuran), 6.99 (s, 1H, benzofuran), 7.06 (s, 1H, benzofuran), 7.26 (d, 1H, *J* = 3.4 Hz, furan H-4). IR (cm<sup>-1</sup>): 3160, 1735 (ester), 1320. FAB-MS: *m/z* = 300 [M]<sup>+</sup>. Fluorescence: λ<sub>em</sub> = 462 nm and λ<sub>ex</sub> = 362 nm in methanol.

#### 2-(5-Hydrazinocarbonyl-2-furyl)-5,6-methylenedioxybenzofuran (FMBH)

This compound was synthesized from compound 3b in the same manner as for TMBH in 60% yield as light yellow powder (m.p. 261–262°C). <sup>1</sup>H NMR (DMSO-d<sub>6</sub>) δ (ppm): 4.51 (br, 2H, NH<sub>2</sub>), 6.08 (s, 2H, –OCH<sub>2</sub>O–), 6.92 (d, 2H, *J* = 3.6 Hz, furan H-3), 7.20 (s, 1H, benzofuran), 7.21 (d, 1H, *J* = 3.6 Hz, furan H-4), 7.24 (s, 1H, benzofuran), 7.32 (s, 1H, benzofuran), 9.80 (br, 1H, CONH). IR (cm<sup>-1</sup>): 3300, 1670, 1320. FAB-MS: *m/z* = 287 [M + 1]<sup>+</sup>. Anal. Calcd. for C<sub>14</sub>H<sub>10</sub>N<sub>2</sub>O<sub>5</sub>: C, 58.75; H, 3.52; N, 9.75. Found: C, 58.85; H, 3.58; N, 9.74.

#### 2.4. Procedure for preparing a sample solution of seminal fluid

Human seminal fluid specimen was obtained from a healthy volunteer in our laboratory. A 50-μl portion of the fluid was immediately mixed with 0.5 ml of dilute hydrochloric acid (pH 3.0) and 0.5 ml of ethyl acetate; the solution was vortexed and the ethyl acetate layer was separated. Ethyl acetate was evaporated under vacuum to give a residue which was then dissolved with 0.2 ml of water. The solution was transferred to a Toyopak-ODS column. PGs were eluted with 0.2 ml of methanol and derivatised as described below.

Table 1

Relative fluorescence intensities (RFI) of FMBH, TMBH and their lauric acid derivatives<sup>a</sup>

Compound	λ <sub>ex</sub> (nm)	λ <sub>em</sub> (nm)	RFI
FMBH	362	432	1
TMBH	375	458	1.8
FMBH-C <sub>12</sub> <sup>b</sup>	363	439	23.4
TMBH-C <sub>12</sub> <sup>c</sup>	376	468	24.8

<sup>a</sup> 10<sup>-6</sup> M in acetonitrile.

<sup>b</sup> FMBH-derivatised lauric acid.

<sup>c</sup> TMBH-derivatised lauric acid.

#### 2.5. Derivatisation procedure

100 μl of EDC in water (100 mM), 100 μl of 1% (v/v) aqueous pyridine, and 100 μl of TMBH in DMF (15 mM) were sequentially added to 100 μl of a mixture of the C<sub>8</sub>–C<sub>18</sub> acid (0.1 mM each). The mixture was incubated at 37°C for 60 min and a 10-μl aliquot of the reaction mixture was injected into the chromatograph.

### 3. Results and discussion

#### 3.1. Syntheses and fluorescence properties

The acid hydrazides TMBH and FMBH were synthesized from the corresponding 2-thiophene or 2-furan carboxylic acid ester in 25% or 13% overall yield, respectively, by a base-catalyzed condensation reaction [12] of aldehyde 1 with thiophene 2a or furan 2b as the key step, as outlined in Scheme 1. The fluorescence λ<sub>em</sub> value of TMBH in acetonitrile or methanol is 458 nm (λ<sub>ex</sub> = 375 nm) or 468 nm (λ<sub>ex</sub> = 371 nm), respectively; these wavelengths are longer than those of FMBH in the same solvent (λ<sub>em</sub> = 432 nm in acetonitrile at λ<sub>ex</sub> = 362 nm). The fluorescence intensity of TMBH is 1.8 or 1.5 times higher in acetonitrile or methanol than those of FMBH, respectively. The fluorescence intensities of TMBH and FMBH were greatly enhanced in their fatty acid derivatives, in which TMBH- and FMBH-derivatised lauric acid gave almost equal intensities (Table 1). Upon addition of water, both λ<sub>em</sub> of TMBH and FMBH are red-shifted (e.g., to 487 nm for TMBH and 463 nm for FMBH, respectively, in 50% (v/v) aqueous acetonitrile) and

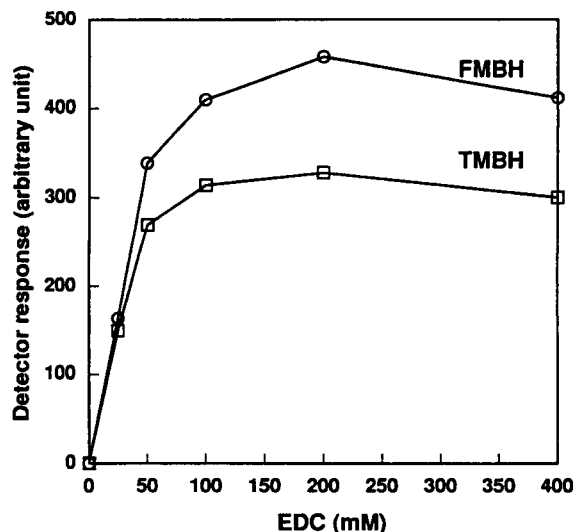


Fig. 1. Effect of EDC concentration on the derivatisation reactions of lauric acid using TMBH or FMBH. The conditions were detailed in the Experimental section.

the intensities are decreased. It is also observed with OMBH although the difference in  $\lambda_{em}$  is much smaller [6].

### 3.2. Derivatisation

Derivatisation is based on the reaction between carboxylic acids ( $\text{RCO}_2\text{H}$ ) and acid hydrazides

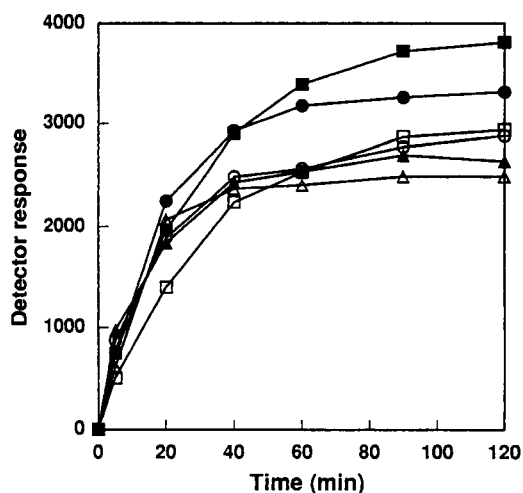


Fig. 2. Effect of reaction time and temperature on the derivatisation of lauric acid. Derivatisations were carried out using TMBH at 21°C (□), 37°C (○) or 50°C (△) and FMBH at 21°C (■), 37°C (●) or 50°C (▲), under the conditions described in the Experimental section.

( $\text{R}'\text{CONHNH}_2$ ) under basic conditions with the aid of EDC, a condensation reagent, to produce compounds of formulae  $\text{RCONH-NHCOR}'$ . Using lauric acid as a representative model, the reaction conditions for TMBH and FMBH were optimized as to the concentrations of the acid hydrazides, EDC and pyridine, and the reaction time and the temperature. The solutions of TMBH and FMBH were prepared from DMF which gave the most intense fluorescent peak among various solvents tested.

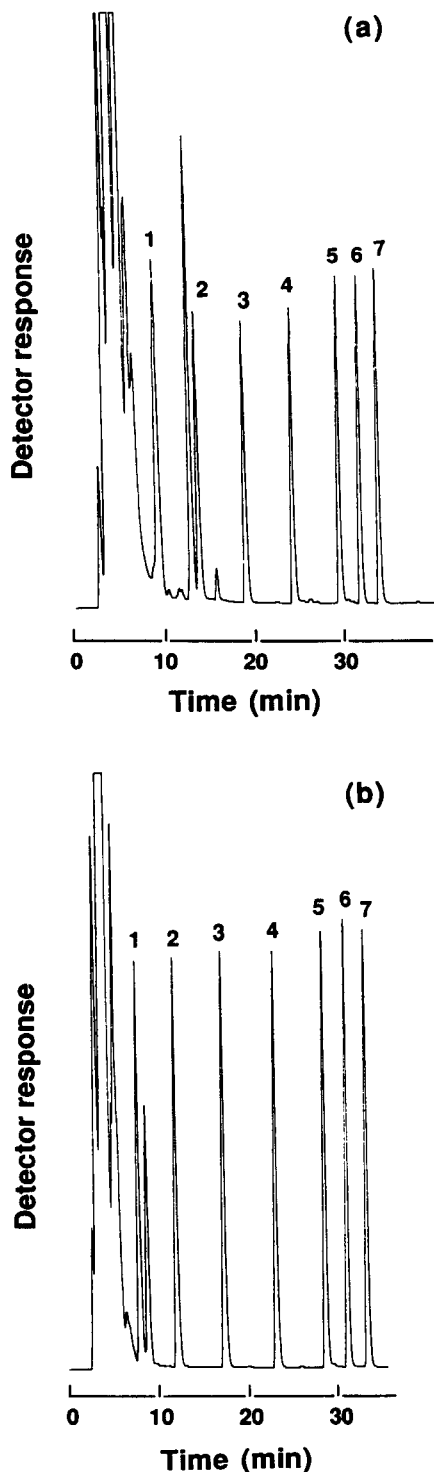
When a DMF solution (100  $\mu\text{l}$ ) of TMBH at various concentrations (0–20 mM) was used to derivatise 0.1 mM lauric acid in methanol (100  $\mu\text{l}$ ) in the presence of both 100 mM EDC (100  $\mu\text{l}$ ) and 20% (v/v) aqueous pyridine (100  $\mu\text{l}$ ) at 37°C for 30 min, the peak height of the TMBH-derivative of the acid increased with increasing concentration of TMBH and became maximum at concentrations higher than 10 mM. TMBH at concentrations higher than 20 mM in DMF tended to precipitate in the reaction medium. A similar profile was observed for FMBH with respect to the relationship between the fluorescent peak height of the derivatised acid and the concentration of the acid hydrazide; DMF solutions of TMBH and FMBH at 15 mM were used in the following experiments.

Fig. 1 shows the effects of EDC concentrations on the peak heights of TMBH- or FMBH-derivatives of lauric acid. A 100- $\mu\text{l}$  portion of 0.1 mM lauric acid was derivatised with 10 mM TMBH or FMBH (both 100  $\mu\text{l}$ ) in the presence of various concentrations of EDC (100  $\mu\text{l}$ ) and 1% (v/v) pyridine in methanol (100  $\mu\text{l}$ ) at 37°C for 60 min. Both TMBH and FMBH gave similar curves as indicated in the figure, in which the maximum fluorescence intensities were obtained at the EDC concentration of ca. 100 mM. A 100 mM EDC solution was therefore used as optimum for TMBH and FMBH in the following procedure.

The concentration of pyridine was varied from 0 to 10% (v/v) while the concentrations of the other reagents remained as above. Fluorescent peak heights of both TMBH- and FMBH-derivatives of the acid increased with increasing concentration of pyridine and reached the maximum and constant at 1.0% (v/v); the concentration at 1.0% (v/v) was employed as optimum for both acid hydrazides.

Fig. 2 demonstrates how the reaction time and temperature affect the fluorescence intensities of the derivatives of the acid under the conditions optimized as





above. Since both derivatisation reactions with TMBH and FMBH appeared to be complete within 60 min at 37°C or higher, the derivatisations were carried out at 37°C for 60 min as a standard protocol. The figure also suggests that the yield of the derivatisation reaction using FMBH is higher than that using TMBH, because FMBH gives higher fluorescence intensities than TMBH while FMBH- and TMBH-derivatised fatty acids have similar fluorescence intensities. The derivatives of the acid were stable for days at room temperature. We also tested  $\alpha$ -ketoglutaric acid and 18 different amino acids and confirmed that no fluorescent products were produced by these derivatisation procedures.

### 3.3. Separation of carboxylic acids

The typical chromatograms of a mixture of  $C_8$ – $C_{18}$  acids derivatised with TMBH and FMBH under the optimized conditions are shown in Fig. 3. In both cases, all peaks, well separated by a linear gradient elution of aqueous acetonitrile of 60 to 100% (v/v) over 40 min, were eluted within 35 min in response to the hydrophobicities of their peak components. Among other solvents tested, acetonitrile gave the best separation of the derivatised acids. Increasing the acetonitrile content in the mobile phase did not affect the fluorescence detection although the fluorescence intensities of TMBH and FMBH are decreased upon addition of water.

The precision was determined by performing ten separate analyses using a standard mixture of  $C_8$ – $C_{18}$  acids (1  $\mu$ M each). The within-run coefficient of variation (C.V.) values were less than 5% for any of the acids examined. The linearity of the fluorescence peak heights to the amount of fatty acids was examined for TMBH and FMBH using a mixture of  $C_8$ – $C_{18}$  acids of varying concentrations (1.25–250  $\mu$ M each). The peak heights of TMBH- and FMBH-derivatives of myristic acid ( $C_{14}$ ) were shown relative to those of capric acid ( $C_{10}$ ; 250  $\mu$ M) which was employed as the internal

Fig. 3. Chromatograms of the  $C_8$ – $C_{18}$  acids. Derivatisation and LC conditions of the acid mixture (0.25 nmol each per 10- $\mu$ l injection volume) were described in the Experimental section. (a) TMBH-derivatives and (b) FMBH-derivatives of carboxylic acids. Peaks: 1,  $C_8$ ; 2,  $C_{10}$ ; 3,  $C_{12}$ ; 4,  $C_{14}$ ; 5,  $C_{16}$ ; 6,  $C_{17}$ ; 7,  $C_{18}$ ; others, reagent blank.

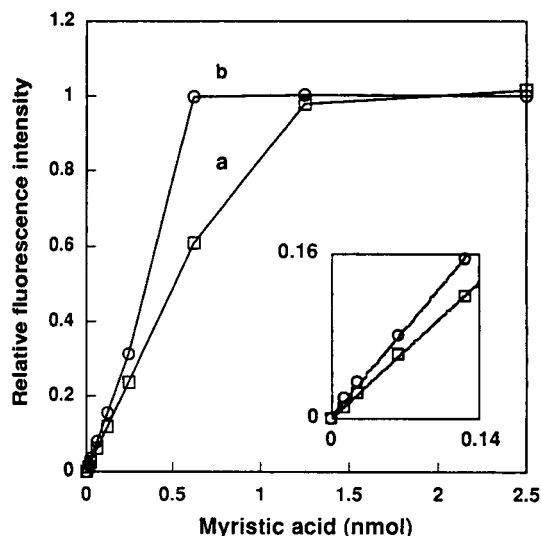


Fig. 4. Linearity of the relative fluorescence intensity to the amount of myristic acid ( $C_{14}$ ) in the derivatisation with TMBH (a) or FMBH (b). The derivatisation was performed as described in the Experimental section with TMBH (2.5 mM), EDC (25 mM), pyridine (0.25%), capric acid (250  $\mu$ M) as an internal standard, and a standard mixture of  $C_8$ – $C_{18}$  acids (1.25–250  $\mu$ M each). The relative fluorescence intensity is shown as the ratio of peak height of myristic ( $C_{14}$ ) to that of capric ( $C_{10}$ ) acid.

standard (Fig. 4). Linearity was observed for both cases using TMBH and FMBH in the range of 12.5 pmol to 0.6 nmol per 10- $\mu$ l injection volume ( $r = 0.999$  and  $0.996$  for TMBH and FMBH, respectively); the detection limit was 1–2 pmol at a signal-to-noise ( $S/N$ ) ratio of 3 in both cases. The fatty acids other than myristic acid showed a similar linearity and detection limits (data not given). These data also confirm that the yield of the derivatisation reaction using FMBH is greater than that using TMBH as described above.

The limits of detection were determined for the fatty acids under these conditions. All the acids of the concentrations as low as 0.1 pmol in a 10- $\mu$ l injection volume were detectable at  $S/N = 3$  either by TMBH and FMBH. The sensitivities of TMBH and FMBH for the fatty acids were equal to that of OMBH and were lower than DMEQ-hydrazide. The detection limit of 3–6 fmol for an injection volume of 10  $\mu$ l ( $S/N = 3$ ) was reported by Yamaguchi et al. [3] for the fatty acids using DMEQ-hydrazide. The major limiting factor to the detection sensitivities of TMBH and FMBH was that fluorescent by-products appeared near the acid peaks in the chromatogram. The advantage of these reagents relative to DMEQ-hydrazide is that they allow

slightly better separation with smaller retention times of the fatty acid mixture, particularly of those having a longer alkyl group ( $C_{16}$ – $C_{18}$ ), although the chromatographic conditions are not identical [3].

Derivatisation of a mixture of prostaglandins (PGs)  $F_{1\alpha}$ ,  $F_{2\alpha}$ ,  $E_1$  and  $E_2$  was undertaken using these acid hydrazides (Fig. 5). Isocratic elution with 34% (v/v) aqueous acetonitrile of the TMBH-derivatives of PGs gave four individual peaks although  $PGE_1$  and  $PGE_2$  were not well separated (Fig. 5a). The peaks for  $PGE_1$  and  $PGE_2$  overlapped when 35% (v/v) acetonitrile was used in the mobile phase, whereas none of the derivatised PGs were eluted within 150 min with 32% (v/v) aqueous acetonitrile. In contrast to TMBH, the resolution of  $PGE_1$  and  $PGE_2$  was improved with smaller retention times in the derivatisation with FMBH although the peaks for  $PGF_{1\alpha}$  and  $PGF_{2\alpha}$  overlapped with isocratic elution of 34% (v/v) acetonitrile (Fig. 5b). The FMBH-derivatives of  $PGF_{1\alpha}$  and  $PGF_{2\alpha}$  were not resolved even by elution with acetonitrile percentages < 32% (v/v), and increasing the acetonitrile content in the mobile phase resulted in poorer separation of  $PGE_1$  and  $PGE_2$ . For TMBH and FMBH, addition of methanol (e.g., 1%, v/v) did not affect the separation while it tended to retard the elutions. Both retention times of TMBH- and FMBH-derivatised PGs were larger than those of OMBH-derivatised PGs because of the greater hydrophilicity of thiophene and furan compared to oxazole, to which the poorer separation of PGs may be attributed. The within-run precision was calculated by repeated determinations ( $n = 10$ ) using this PG mixture. The C.V. value for any of the PGs did not exceed 5%.

An analysis of PGs in a human seminal fluid using FMBH was performed because FMBH gave better separation of  $PGE_1$  and  $PGE_2$  than TMBH. PGs were extracted with ethyl acetate as described in Ref. [13]. Fig. 6 shows the chromatogram obtained with the seminal fluid. The most remarkable peaks are  $PGE_1$  and  $PGE_2$ ; it is in agreement with the results reported by Yamaguchi et al. [13] for human seminal fluids. These peaks were identified by co-chromatography with the authentic PGs.  $PGF_{1\alpha}$  and  $PGF_{2\alpha}$  were not detected under these conditions. TMBH gave a similar chromatogram to FMBH with a slightly poor separation (data not shown).

In summary, two new acid hydrazides, TMBH and FMBH, for precolumn fluorescence labelling of fatty

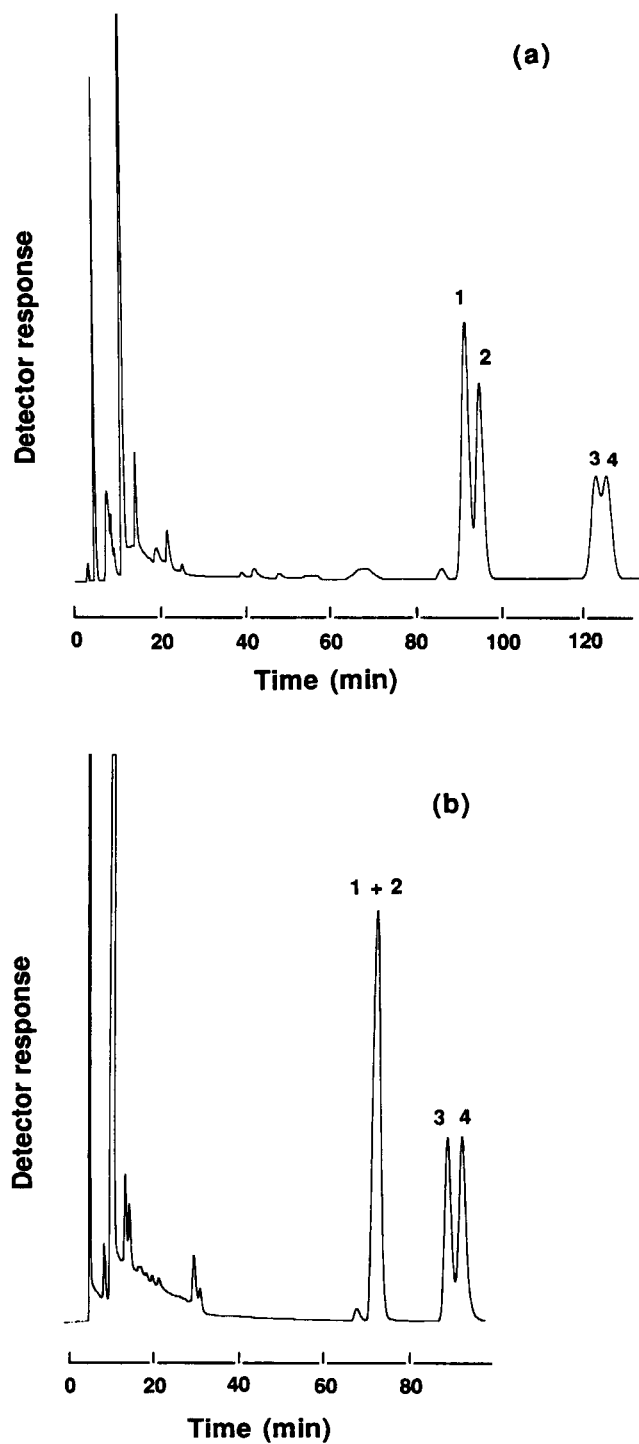


Fig. 5. Chromatograms of prostaglandins. Derivatisation and LC conditions of a PG mixture (0.25 nmol each per 10- $\mu$ l injection volume) were described in the Experimental section. (a) TMBH-derivatives and (b) FMBH-derivatives of PGs. Peaks: 1, PGF<sub>1 $\alpha$</sub> ; 2, PGF<sub>2 $\alpha$</sub> ; 3, PGE<sub>2</sub>; 4, PGE<sub>1</sub>; others, reagent blank.

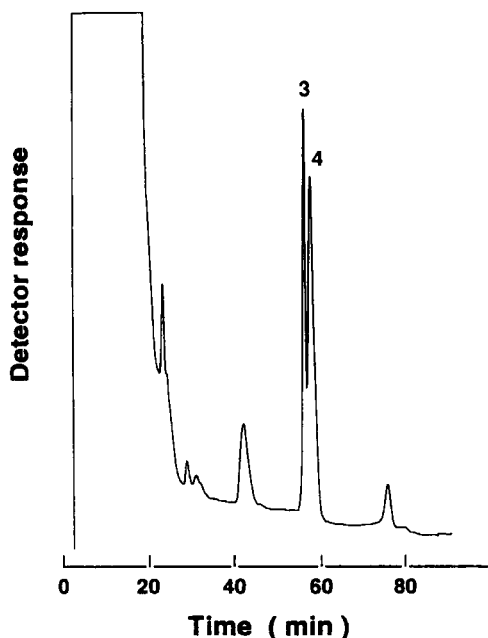


Fig. 6. Chromatograms obtained with a human seminal fluid. A portion (100  $\mu$ l) of the fluid was derivatised with FMBH as described in the Experimental section. LC conditions were identical to those for the standard PG mixture in Fig. 5. See Fig. 5 for peak identification. Other peaks except the reagent blank are not identified.

acids were synthesized and proved to be useful for the determination of fatty acids. TMBH and FMBH react with fatty acids under mild aqueous conditions and this is important for labelling biogenic compounds such as prostaglandins. Compared to OMBH, both TMBH and FMBH were found to have the same sensitivity for fatty acids with greater retention times of the derivatised acids in reversed-phase chromatography. However, TMBH and FMBH can be prepared in fewer synthetic steps and therefore in higher yield (or, at less costs), compared to OMBH.

A number of precolumn derivatisation methods have been reported for the assay of PGs with fluorescence

detection [1]. Among them, the methods utilizing *p*-(9-anthroyloxy)phenacyl bromide [14] and 3-bromomethyl-6,7-dimethoxy-1-methyl-2(1*H*)-quinoxalinone [13] are extremely sensitive to permit determination of PGs at fmol levels. Since TMBH and FMBH were proved to be potentially applicable to the assay of endogenous PGs in biological samples, we are currently establishing a sensitive and selective method to quantify fatty acids including PGs using these compounds.

## References

- [1] Y. Ohkura, *Anal. Sci.*, 5 (1989) 371.
- [2] Y. Ohkura and H. Nohta, in J.C. Giddings, E. Grushka and P.R. Brown (Eds.), *Advances in Chromatography*, Vol. 29, Marcel Dekker, New York, 1989, pp. 221–258.
- [3] M. Yamaguchi, T. Iwata, K. Inoue, S. Hara and M. Nakamura, *Analyst*, 115 (1990) 1363.
- [4] T. Iwata, K. Inoue, M. Nakamura and M. Yamaguchi, *Biomed. Chromatogr.*, 6 (1992) 120.
- [5] T. Iwata, M. Nakamura and M. Yamaguchi, *Anal. Sci.*, 8 (1992) 889.
- [6] M. Saito, Y. Chiyoda, T. Ushijima, K. Sasamoto and Y. Ohkura, *Anal. Sci.*, 10 (1994) 679.
- [7] H. Nagaoka, H. Nohta, Y. Kaetsu, M. Saito and Y. Ohkura, *Anal. Sci.*, 5 (1989) 525.
- [8] H. Nagaoka, H. Nohta, M. Saito and Y. Ohkura, *Anal. Sci.*, 8 (1992) 345.
- [9] H. Nagaoka, H. Nohta, M. Saito and Y. Ohkura, *Anal. Sci.*, 8 (1992) 565.
- [10] F. Kenji and M. Nakayama, *Bull. Chem. Soc. Jpn.*, 35 (1962) 1321.
- [11] R. Lukes, M. Janda and K. Kefurt, *Collect. Czech. Chem. Commun.*, 25 (1960) 1058.
- [12] O. Dann, G. Bergen, E. Dermant and G. Voltz, *Justus Liebigs Ann. Chem.*, 749 (1971) 68.
- [13] M. Yamaguchi, K. Fukuda, S. Hara, M. Nakamura and Y. Ohkura, *J. Chromatogr.*, 380 (1986) 257.
- [14] C.E. Morreal, D.K. Sinha, C.J. White and D.T. Nemoto, *J. Chromatogr.*, 345 (1985) 380.

## Fluorescence reaction and complexation equilibria between norfloxacin and aluminium(III) ion in chloride medium

Predrag T. Djurdjevic<sup>a,\*</sup>, Milena Jelicic-Stankov<sup>b</sup>, Dejan Stankov<sup>c</sup>

<sup>a</sup> Faculty of Science, University of Kragujevac, P.O. Box 60, 34000 Kragujevac, Yugoslavia

<sup>b</sup> Faculty of Pharmacy, University of Belgrade, 11221 Belgrade, Yugoslavia

<sup>c</sup> General Hospital "Dr. Dragisa Misovic", 11000 Belgrade, Yugoslavia

Received 4 May 1994; revised manuscript received 1 August 1994

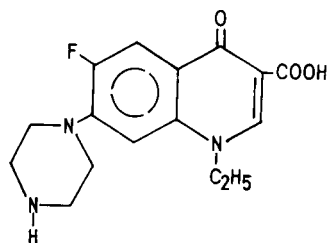
### Abstract

Norfloxacin, 1-ethyl-6-fluoro-1,4-dihydro-4-oxo-7-(1-piperazinyl)-3-quinoline carboxylic acid (NORH), reacts with aluminium(III) ion forming the strongly fluorescent complex  $[Al(HNOR)]^{3+}$ , in slightly acidic medium. The complex shows maximum emission at 440 nm with excitation at 320 nm. The fluorescence intensity is enhanced upon addition of 0.5% sodium dodecylsulphate. Fluorescence properties of the Al–NOR complex were used for the direct determination of trace amounts of NOR in serum. The linear dependence of fluorescence intensity on NOR concentration, at a NOR to Al concentration ratio of 1:10, was found in the concentration range 0.001–2  $\mu\text{g/ml}$  NOR with a detection limit of 0.1 ng/ml. The ability of aluminium(III) ion to form complexes with NOR was investigated by titrations in 0.1 M LiCl medium, using a glass electrode, at 298 K, in the concentration range:  $2 \times 10^{-4} \leq [Al] \leq 8 \times 10^{-4}$ ;  $5 \times 10^{-4} \leq [NOR] \leq 9 \times 10^{-4}$  mol/dm<sup>3</sup>;  $2.8 \leq \text{pH} \leq 8.3$ . The experimental data were explained by the following complexes and their respective stability constants,  $\log(\beta \pm \sigma)$ :  $[Al(HNOR)]$ , (14.60  $\pm$  0.05);  $[Al(NOR)]$ , (8.83  $\pm$  0.08);  $[Al(OH)_3(NOR)]$ , (–14.9  $\pm$  0.1), as well as several pure hydrolytic complexes of  $Al^{3+}$ . The structure of the  $[Al(HNOR)]$  complex is discussed, with respect to its fluorescence properties.

**Keywords:** Fluorimetry; Aluminium; Potentiometry; Norfloxacin

### 1. Introduction

Norfloxacin, 1-ethyl-6-fluoro-1,4-dihydro-4-oxo-7-(1-piperazinyl)-3-quinoline carboxylic acid (NORH)



\* Corresponding author.

is a broad spectrum antibiotic active against many gram-positive and gram-negative bacteria. It finds widespread use in the treatment of urinary infections with a good penetration in the infected sites. NORH (abbreviations: NORH-neutral acid, HNORH<sup>+</sup>-protonated acid at imino group of piperazinyl substituent, NOR-acid anion) is a strongly fluorescent compound and this property was used in our previous work [1] for its direct determination in the serum and pharmaceutical formulations. Pharmacokinetic studies [2,3] of NOR in plasma and body organs show a wide range of concentrations, from as low as 0.002 to 2 mg/l. There were also a few observations [4,5] that during

the parallel therapy with aluminium and magnesium containing antacids, the peak concentration of the NOR analogue, ciprofloxacin, in plasma, was significantly decreased. This effect suggests the formation of complex compound(s) between metal ions and antibiotic. The complexation reactions may be also expected in NOR–Al<sup>3+</sup> solutions. In an attempt to study the possible interactions between NOR and Al<sup>3+</sup> we noticed that the fluorescence intensity of NOR was greatly enhanced upon addition of Al. The effect observed, may thus, serve to improve the sensitivity of determination and limit of detection of NOR in serum.

The objective of the present work was, therefore, to develop the fast and direct method of fluorimetric determination of NOR in serum, utilizing its fluorescence reaction with Al<sup>3+</sup>. Study of complexation equilibria in vitro was undertaken to find the best complex formation model as well as the stability constants of the species formed in solution.

## 2. Experimental

### 2.1. Reagents

All reagents were of analytical purity grade. Water was doubly distilled. Norfloxacin standard, purity 100%, was a product of Sigma. Sodium dodecylsulphate (SDS) was purchased from Serva (a 2% solution in water was used). All other reagents were products of Merck. Stock solution of aluminium(III) chloride (0.0197 M) was analyzed by precipitation with ammonia and with EDTA complexometric titrations. Excess HCl in the stock solution of AlCl<sub>3</sub> (0.0053 M) was determined potentiometrically with standard NaOH, using a Gran plot. Working solutions of lower concentrations were made by dilution with water and addition of electrolyte and HCl, as necessary. Stock solutions of HCl, NaOH and LiCl were made and analyzed as described previously [6].

Buffer solutions of the required pH were made from citric acid and NaOH, according to Perrin and Dempsey [7]. For pH meter calibration freshly prepared potassium hydrogenphthalate and phosphate buffers were used.

### 2.2. Apparatus

Fluorescence measurements were made on Aminco SPF-500C spectrofluorimeter, equipped with a 300 W Xenon lamp and 1.0×1.0 cm quartz cells. The slit width was set to 2.5 nm on both the excitation and emission monochromators. To ensure reproducible experimental conditions spectrofluorimeter performance was checked daily using quinine sulphate solution (4 g/l quinine in 0.5 M H<sub>2</sub>SO<sub>4</sub>). UV spectra were taken on an LKB Ultrospec II beam-ratio spectrophotometer. Potentiometric titrations were performed by using a Tacussel Model 20,000 pH meter with a precision ±0.001 pH units and equipped with an TC-100 combined electrode. Standard solution of 0.1 M NaOH was added by a Metrohm Dosimat Model 665 with a Model 552 exchange unit.

## 3. Procedure

### 3.1. Spectrofluorimetric measurements

#### Calibration graph

Stock solution of NOR ( $1.0 \times 10^{-3}$  M) was prepared by dissolving NOR standard in water. Different portions of 0.5 μl–0.1 ml were transferred into 10-ml volumetric flasks, using a Hamilton syringe, and in each flask 2.00 ml of citrate buffer (pH 3.502), 2.5 ml 2% solution of SDS and 0.3 ml of working solution ( $1.0 \times 10^{-3}$  M) of AlCl<sub>3</sub> were added. After dilution to the mark with water and thorough mixing, the fluorescence intensity of each solution was measured at 440 nm with excitation at 320 nm.

#### Calibration graph and procedure for serum

A human pool serum was mixed with a standard solution of NOR, with a concentration of the drug in the 0.1–200.0 μg/ml range. A 0.1 ml aliquot of the prepared solution was diluted with 2.5 ml 2% SDS solution, 2.00 ml citrate buffer, 0.3 ml working solution of AlCl<sub>3</sub> and water, to 10 ml. Blank values were obtained by diluting the same volume of the serum, but without NOR. Fluorescence was measured at  $\lambda_{em}/\lambda_{ex} = 440/320$  nm.

### Analytical recovery

Seven different concentrations of NOR were added to human serum to get concentrations of 0.5–100.0  $\mu\text{g}/\text{ml}$  of NOR. These samples were treated according to the procedure for the calibration graph.

### 3.2. Spectrophotometric measurements

Spectra of NOR ( $4 \times 10^{-5}$  M) in the pH range 1.300–12.620 (10 spectra) in 0.1 M LiCl ionic medium, at 298 K were taken in the wavelength range 220–400 nm using the solutions of the same composition but without NOR as a blank. Spectra of the mixtures of NOR ( $6.0 \times 10^{-5}$  M) and  $\text{Al}^{3+}$  ( $2.0 \times 10^{-5}$  M) in the pH range 4.00–7.00, and wavelength range 300–400 nm were taken at 298 K using corresponding Al-free solutions as a reagent blank. The pH of all solutions was adjusted by the addition of 0.1 M HCl or 0.1 M NaOH. Solutions were left for 0.5 h before scanning.

### 3.3. Potentiometric measurements

All potentiometric measurements of the solutions were performed in a double-walled glass vessel at 298 K. The temperature was controlled by circulation of water through the jacket from a VEB Medingen Prufgerate Model E3E ultrathermostat bath, and maintained at  $\pm 0.1$  K. Purified nitrogen gas was bubbled through the solution to keep an inert atmosphere.

The pH meter was adjusted with phthalate and phosphate buffers. Calibration of the electrode system in terms of hydrogen ion concentration was performed according to the procedure of Irving et al. [8]. A check of electrode performance (slope of response,  $K_w$ ) was made as described earlier [6].

Test solutions were magnetically stirred. NaOH was added stepwise and pH readings were recorded every minute until stable values, within  $\pm 0.002$  pH units, were obtained. The maximum allowable equilibration time was 20 min. If, within this period, a stable value was not obtained, the next portion of base was added.

## 4. Results

NOR presents a strong fluorescence in an acidic (0.1 M HCl) solution with a maximum emission at 455 nm

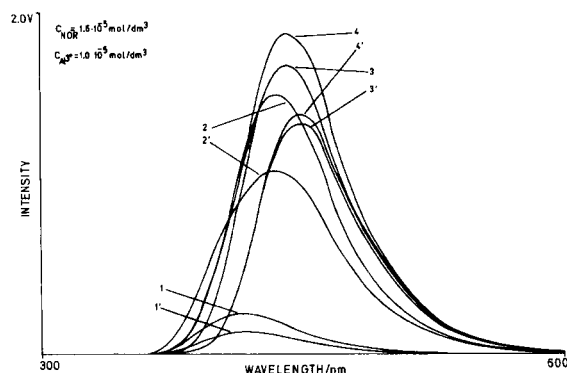


Fig. 1. Fluorescence emission spectra of NOR- $\text{Al}^{3+}$  solutions at 320 nm excitation.  $[\text{NOR}] = 1.6 \times 10^{-5}$ ,  $[\text{Al}] = 1 \times 10^{-5}$  mol/dm<sup>3</sup>, pH values: (1,1') = 8.50, (2,2') = 5.40, (3,3') = 4.00, (4,4') = 3.53. Numbers refer to NOR +  $\text{Al}^{3+}$  solutions, while primed numbers refer to solutions of pure NOR.

with excitation at 320 nm. Upon addition of  $\text{Al}^{3+}$ , the emission maximum significantly increases in intensity. Optimum concentration of  $\text{Al}^{3+}$ , for the determination of NOR in serum, was chosen by varying the concentration ratio of NOR to Al in the range 1:1 to 1:30.

The effect of acidity of the solution on the fluorescence properties was investigated by preparing the series of solutions with a NOR to Al concentration ratio of 2:1. The pH was adjusted by the addition of small amounts of 0.1 M HCl or 0.1 M NaOH. The obtained spectra are shown in Fig. 1. A maximum difference in intensity between the spectra of NOR and NOR + Al was found between pH 3–4.

The effect of SDS on fluorescence intensity was examined using solutions of the following composition:  $[\text{NOR}] = 2.0 \times 10^{-6}$  M,  $[\text{Al}] = 3.0 \times 10^{-5}$  M, pH 3.502. In one of these solutions 0.5% SDS was added. Fluorescence spectra of the two solutions at  $\lambda_{\text{ex}} = 320$  nm are shown in Fig. 2. It may be seen that in the presence of SDS fluorescence intensity increases approximately twice.

Spectrophotometric measurements were made on a series of solutions of NOR and NOR- $\text{Al}^{3+}$  in the pH range 4.00–7.00. These spectra are shown in Fig. 3. In a later case solutions of the same composition and pH with the exception of  $\text{Al}^{3+}$  were used as a reagent blank. It may be seen that the spectrum of the mixture exhibits a new peak at ca. 350 nm. The intensity and position of this peak vary upon changing the concentration ratio of NOR to Al, as well as the pH of solutions. With increasing concentration of NOR (pH 3.5,

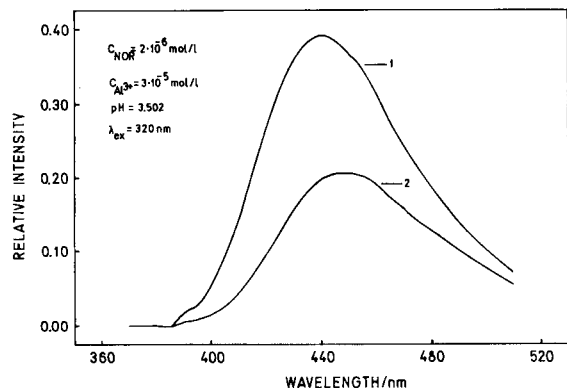


Fig. 2. Fluorescence emission spectra of NOR–Al<sup>3+</sup> solutions, with (curve 1) and without addition of 0.5% sodium dodecylsulphate (curve 2).

[Al] =  $2 \times 10^{-5}$  M) the absorbance, at 350 nm, increases up to a NOR to Al concentration ratio of 3:1 and then remains constant. The absorbance at 350 nm and constant concentrations of NOR and Al increases when increasing the pH to ca. 8.0.

Spectra of NOR were digitized at every 5 nm and subjected to mathematical analysis with the aid of the SQUAD program [9]. The sum:

$$S = \sum (A_{\text{obs}} - A_{\text{calc}})^2$$

was minimized, where  $A_{\text{obs}}$  is a measured absorbance and  $A_{\text{calc}}$  the calculated one using the formula:

$$A_{\text{calc}} = \sum \beta_n \cdot [\text{NOR}] \cdot [\text{H}]^n \cdot \epsilon_n$$

In this way the protonation constants of NOR:

$$\beta_1 = \frac{[\text{NORH}]}{[\text{NOR}] \cdot [\text{H}]} = 10^{8.60}$$

$$\beta_2 = \frac{[\text{HNORH}]}{[\text{H}]^2 \cdot [\text{NOR}]} = 10^{14.70}$$

were obtained. The standard deviation (S.D.) in calculated spectra was  $1 \times 10^{-3}$ , indicating a good fit of the data.

Preliminary treatment of the spectral data referring to NOR–Al solutions indicates the formation of several mononuclear complexes of the general composition NOR:Al = 1:1. The identity and stability of these complexes could not be calculated because of the relatively high instrumental noise and the disturbance by aluminium hydrolysis.

Potentiometric measurements were taken with the aim to establish the nature and stability constants of the

complexes formed in NOR–Al<sup>3+</sup> solutions. Protonation constants of NOR cannot be found in the literature and although the hydrolysis of aluminium has been extensively studied during the last several decades by many authors [10], it depends so much on particular experimental conditions [11] that it must be evaluated under exactly the same experimental conditions as for the complexation study. Therefore, protonation of NOR and hydrolysis of Al<sup>3+</sup> were studied separately.

Three titrations of NOR (1.18, 1.00 and 0.50 mmol/dm<sup>3</sup>) in 0.1 M LiCl medium at 298 K, were done with a total of 305 (V, pH) points. Excess HCl (4.0 mmol/dm<sup>3</sup>) was added in each solution. Potentiometric titrations of Al<sup>3+</sup> solutions were carried out under the same experimental conditions to find out the composition and stability of hydrolytic complexes of aluminium. The hydrolytic reaction of aluminium is extremely slow, nonetheless, pH readings were taken for 15–20 min after the addition of base, what was considered to be sufficient for the formation of hydrolytic species which form rapidly and may thus influence the complexation reaction of Al<sup>3+</sup>. The titrations were terminated as soon

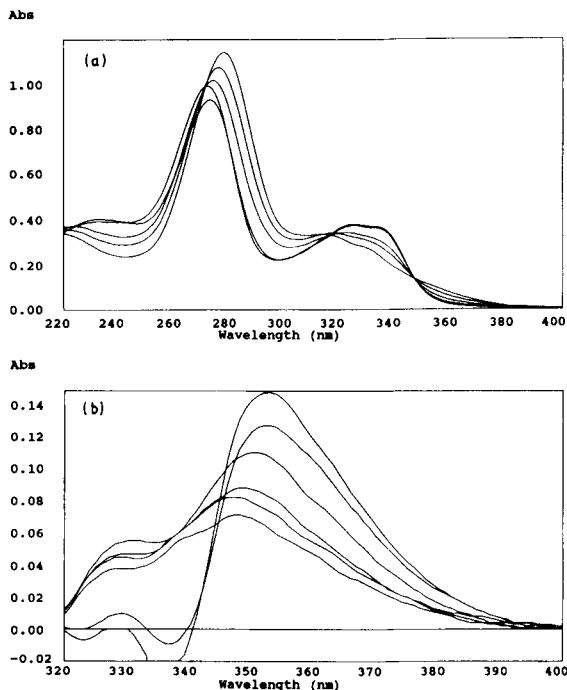


Fig. 3. UV spectra of NOR (a) and NOR + Al<sup>3+</sup> (b) solutions. pH interval for NOR solutions was 1.3–12.6 and that for NOR + Al<sup>3+</sup>, 4.0–7.0.



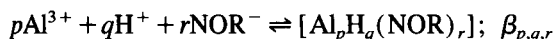
Table 1  
Summary of potentiometric titrations

Run	$10^{-4} \times C_{\text{Al}}$	$10^{-3} \times C_{\text{HCl}}$	$10^{-4} \times C_{\text{NOR}}$	$L/B$	pH range	$Z_{\text{max}}$	No.
1	1.97	0.065	5.00	2.54	3.089–8.260	5.67	48
2	3.94	0.13	9.00	2.28	2.828–8.375	5.05	80
3	7.90	0.25	9.00	1.14	2.760–8.160	3.71	85
4	4.94	1.10	5.50	1.11	2.973–8.347	1.88	85
5	3.95	2.00	–	–	3.091–4.270	0.234	33
6	12.0	2.30	–	–	2.992–4.292	0.117	13
7	23.5	2.70	–	–	3.001–4.380	0.266	31
8	98.5	5.10	–	–	3.096–3.926	0.055	38
9	4.0	2.00	–	–	3.012–4.426	0.257	36
10	47.5	3.40	–	–	3.039–4.242	0.179	20

All concentrations,  $C_x$ , are expressed in mol/dm<sup>3</sup>.  $Z$  is defined as  $Z = (h - H)/B$ , where  $h$  is the concentration of free hydrogen ion,  $H$  is the analytical concentration of hydrogen ion and  $B$  is total initial concentration of  $\text{Al}^{3+}$ .  $L$  = Total initial concentration of NOR. No. denotes total number of points included in the calculations.

as the first sign of turbidity appeared. The experimental data are summarized in Table 1.

For complexation investigation pH measurements at 298 K in 0.1 M LiCl medium were performed on solutions in which the total initial concentrations of  $\text{Al}^{3+}$  ranged between 0.2 and 0.8 mmol/dm<sup>3</sup> and that of NOR between 0.5–0.9 mmol/dm<sup>3</sup>, thus, the NOR to Al concentration ratio was varied from 1:1 to 2.5:1 (Table 1). Solutions remained clear up to a pH value of ca. 8.1, a slight opacity appeared beyond a pH value of 8.3. For the purpose of mathematical analysis in hydrolytic titrations, points between pH 3.5 and 4.2, and in complexation titrations between pH 3.0 and 8.0, were selected. In complexation data analysis three types of equilibria should be considered: (a) protonation of NOR, (b) hydrolysis of  $\text{Al}^{3+}$  ion and (c) general three-component equilibria:



which includes the case  $q = 0$ , i.e. the formation of pure Al–NOR complexes. Negative values of  $q$  represent hydroxo complexes. Upon evaluation of three-component equilibria (c), the binary models (a) and (b) were considered to be known.

Mathematical analysis of the experimental data was performed with the aid of a general least-squares program SUPERQUAD [12]. In the calculations the identity and stability of complexes which give the best fit to the experimental data, were determined by minimizing the error-squares sum of pH values:

$$U = \sum w_i (\text{pH}_{\text{obs}} - \text{pH}_{\text{calc}})^2$$

where  $w_i$  represents a statistical weight assigned to each point of the titration curve.  $\text{pH}_{\text{obs}}$  and  $\text{pH}_{\text{calc}}$  refer to the measured pH value and the calculated one, respectively, assuming the specific set of complexes and their stability constants. The pH was related to the potential  $E$  of the glass electrode through the relation:

$$E = E_0 - Q \cdot \text{pH}$$

where the constant  $E_0$  was arbitrarily set to 10 mV and refined during the calculations;  $Q$  is the slope of the glass electrode response, whose value was found to be 98.7% of the theoretical (Nernstian) one.

The best model was chosen using these criteria: (a) lowest value of  $U$ , (b) standard deviation in calculated stability constants less than 0.15 log units, (c) standard deviation in potential residuals, at  $\Delta\text{pH} = \pm 0.002$  pH units and  $\Delta V = \pm 0.0005$  ml, less than 3.0, (d) good-

Table 2  
Stability constants of the complexes formed in NOR– $\text{Al}^{3+}$  solutions, in 0.1 M LiCl medium at 298 K

Species	$\log(\beta \pm \sigma)$	$\log(\beta \pm \sigma)^a$	$\chi^2$	$s$
HNOR	$8.49 \pm 0.02$	$8.60 \pm 0.04$	11.0	1.80
HNORH <sup>+</sup>	$14.73 \pm 0.02$	$14.70 \pm 0.09$		
$[\text{Al}(\text{OH})]^{2+}$	$-5.62 \pm 0.10$			
$[\text{Al}(\text{OH})_2]^+$	$-9.74 \pm 0.02$		11.7	3.23
$[\text{Al}_3(\text{OH})_4]^{5+}$	$-13.7 \pm 0.11$			
$[\text{Al}(\text{HNOR})]^{3+}$	$14.60 \pm 0.05$			
$[\text{Al}(\text{NOR})]^{2+}$	$8.83 \pm 0.08$		14.8	3.90
$[\text{Al}(\text{OH})_3(\text{NOR})]^-$	$-14.85 \pm 0.11$			

<sup>a</sup> Spectrophotometric result.

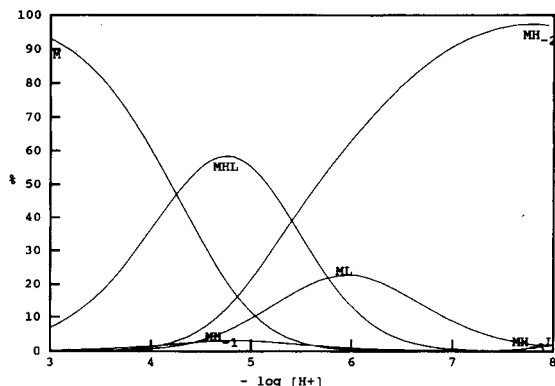


Fig. 4. Percent distribution of the species formed in NOR–Al<sup>3+</sup> solution, in 0.1 M LiCl ionic medium at 298 K. [Al] =  $5 \times 10^{-5}$ , [NOR] =  $1 \times 10^{-4}$  mol/dm<sup>3</sup>.

ness of fit statistics,  $\chi^2$  (Pearson's test), less than 12.6. In order to find the best model various complexes and combinations thereof were included in SUPERQUAD calculations.

In hydrolysis data treatment, the starting model comprised the "low" molecular weight complexes: (1, -1), (1, -2), (2, -1), (2, -2), (2, -4), (3, -3), (3, -4) and some oligomers found by Brown et al. [13]. All titration curves were treated together. In the first calculation cycle only the complexes (1, -1) and (1, -2) were accepted with rather high scatter of residuals, at pH > 4.0. In the next calculation cycle their stability constants were fixed and data points between pH 4.0 and 4.2 were treated separately. The best set of statistics was obtained with the complex (3, -4). Higher polynuclears were rejected. Results of calculation are summarized in Table 2. The stability constants obtained are in good agreement with the literature data [9].

In complexation data treatment, numerous species were selected to find the best model. More than 20 various models were tested. The data belonging to titration curves referring to one particular NOR to Al concentration ratio (2:1 or 1:1) were treated together. During the calculations analytical concentrations of the reagents along with the stability constants of the hydrolytic complexes of Al and protonation constants of NOR, were held constant, while  $E_0$  values were allowed to float.

It appeared that no acceptable fit of the whole titration curve can be obtained by one set of complexes. Therefore, first the points below pH ~ 4.5 were

included in calculations. A good fit was obtained with a single complex (1,1,1). This complex was included as non-refinable species and calculations were repeated this time including all the points up to pH ~ 8.0. At a NOR to Al concentration ratio of ca. 1:1 the complexes [Al(NOR)] and [Al(OH)<sub>3</sub>(NOR)] were accepted, while at a concentration ratio of ca. 2:1 besides these complexes the complex [Al(NOR)<sub>2</sub>] was also accepted. Inclusion of this complex in the model did not improve either the scatter of residuals or sample standard deviation, therefore its existence is doubtful. The complexes found and their respective stability constants are given in Table 2.

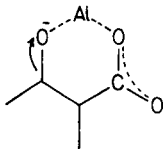
## 5. Discussion

Strong fluorescence of NOR in the presence of aluminium and SDS can be utilized for its direct determination in serum, without prior separation. The excitation at 320 nm was selected to minimize the serum emission. The emission at 440 nm was chosen for analysis. Excess Al<sup>3+</sup> must be added keeping in mind its binding to serum proteins, complexation with serum phosphate ion as well as with citrate ion from citrate buffer. According to the literature data [14,15] it may be estimated that roughly 20% of the available Al<sup>3+</sup> is bound to serum ions and proteins (albumin, transferrins) at pH < 4.0. Pharmacokinetic studies of 4-quinolone antibiotics (norfloxacin, ofloxacin, ciprofloxacin) [5,16,17], show that their binding affinity to serum albumin is low (they cannot displace bilirubin from albumin). At physiological pH, NOR is approximately 20–30% bound to serum albumin. Since its isoelectric point is 7.37 it largely exists in the form of cationic acid, at pH < 4.0. The isoelectric point of serum albumin is 4.8 [18] so that at pH < 4.0 it should be predominantly in the unionized or cationic form. Under these conditions the extent of NOR binding to serum albumin may be expected to be very low. It can further be decreased by the addition of SDS. The optimal Al to NOR concentration ratio was found to be 10–20:1 at pH 3.5 and a concentration of 0.5% SDS.

The fluorescence intensity was linearly proportional to the concentration of NOR in the concentration range 0.001–3.0  $\mu\text{g/ml}$ . The regression equation of the calibration line was:  $y = (5.77 \pm 0.02) \times 10^2 x + (2.1 \pm 0.1) \times 10^{-3}$  ( $n = 15$ ,  $r = 0.9999$ ,  $\sigma = 2.04 \times 10^{-3}$ )

where  $y$  = fluorescence intensity and  $x$  = concentration of NOR in  $\mu\text{g/ml}$ . For the determination of NOR in serum, the regression equation of the calibration line was:  $y = (5.81 \pm 0.02) \times 10^2 x + (3.5 \pm 0.1) \times 10^{-3}$  ( $n = 15$ ,  $r = 0.9999$ ,  $\sigma = 2.24 \times 10^{-3}$ ) in the concentration range 0.001–2.0  $\mu\text{g/ml}$ . The detection limit, defined after Miller [19] was 0.1 ng/ml. The analytical recovery was 99–101%. Using this method approximately 10 times lower concentrations of NOR can be determined in the presence of aluminium than in the absence of aluminium [1]. The detection limit was three times lower.

In order to explain the enhanced fluorescence of NOR in the presence of aluminium, one must first consider the species distribution diagram (Fig. 4.) It can be seen that at  $\text{pH} < 4.5$  the dominating complex is  $[\text{Al}(\text{HNOR})]$ . It is therefore reasonable to assume that strong fluorescence is due to this complex. Bearing in mind that  $\text{Al}^{3+}$  is a “hard” acid it may be supposed that it is bound to carbonyl and carboxylate oxygens of NOR:



thus, closing a six-membered ring. On the other hand the piperazinyl substituent has a natural chair conformation which is not favourable for fluorescence. Protonation of piperazinyl nitrogen stabilizes planar conformation, hence both binding effects of Al and protonation of the piperazinyl imino group lead to a stable planar structure and extended  $\pi$ -electron resonance, which enhances fluorescence properties.

The complex  $[\text{Al}(\text{NOR})]$  is probably formed, as indicated by Fig. 4, by protolytic dissociation of

$[\text{Al}(\text{HNOR})]$ . The complex  $[\text{Al}(\text{NOR})]$  is stable over a broad range of pH values and may possess a chelate structure. The mixed complex  $[\text{Al}(\text{OH})_3(\text{NOR})]$  may be formed by attaching an NOR ion to the  $\text{Al}(\text{OH})_3$  core.

## References

- [1] M. Stankov, D. Stankov, Z. Milicevic, D. Veselinovic and P. Djurdjevic, *Spectrosc. Lett.*, 26 (1993) 1709.
- [2] J.T. Smith, *Infection*, 14 (Suppl. 1) (1986) 3.
- [3] T. Bergan, A. Dalhoff and S.B. Thorsteinsson, *Ciprofloxacin, Proceedings of a Workshop held at the 14th International Congress of Chemotherapy, Kyoto, 1985*, p. 23.
- [4] H.C. Neu (Ed.), *Ciprofloxacin, Clinical Monograph*, ADIS Press, Manchester, 1988.
- [5] M. Neuman, *Clin. Pharmacokin.*, 14 (1988) 96.
- [6] M. Jelkic, D. Veselinovic and P. Djurdjevic, *Talanta*, 39 (1992) 665.
- [7] D.D. Perrin and B. Dempsey, *Buffers for pH and Metal Ion Control*, Chapman and Hall, London, 1974.
- [8] H. M. Irving, M.G. Miles and L.D. Pettit, *Anal. Chim. Acta*, 38 (1967) 475.
- [9] D.J. Leggett (Ed.), *Computational Methods for the Determination of Formation Constants*, Plenum, New York, 1985, pp. 159–220.
- [10] C.F. Baes and R.E. Mesmer, Jr., *The Hydrolysis of Cations*, Wiley, New York, 1976.
- [11] P. Djurdjevic and R. Jelic, *Z. Anorg. Allg. Chem.*, 575 (1989) 217.
- [12] P. Gans, A. Sabatini and A. Vacca, *J. Chem. Soc., Dalton Trans.*, (1985) 1195.
- [13] P. Brown, R. Sylva, G. Batley and J. Ellis, *J. Chem. Soc., Dalton Trans.*, (1985) 1967.
- [14] G.E. Jackson, *Polyhedron*, 9 (1990) 163.
- [15] W.R. Harris and J. Sheldon, *Inorg. Chem.*, 29 (1990) 119.
- [16] R. Wise, M.R. Lockley, M. Webberly and J. Dent, *Antimicrob. Agents Chemother.*, 26 (1984) 208.
- [17] R.H. Stutman, M.K. Parker and I.M. Marks, *Pediatrics*, 75 (1985) 294.
- [18] H.D. Jakubke and H. Jeschkeit, *Aminosäuren, Peptide, Proteine*, Akademie Verlag, Berlin, 1982.
- [19] J.N. Miller, *Analyst*, 116 (1991) 3.

## Instrument for Hadamard transform three-dimensional fluorescence microscope image analysis

Guanquan Chen <sup>a</sup>, Erwen Mei <sup>b,\*</sup>, Wenfang Gu <sup>b</sup>, Xiaobin Zeng <sup>b</sup>, Yun'e Zeng <sup>b</sup>

<sup>a</sup> Centre of Instrumental Analysis, Wuhan University, Wuhan, 430072, China

<sup>b</sup> Department of Chemistry, Wuhan University, Wuhan, 430072, China

Received 27 January 1994; revised manuscript received 1 August 1994

---

### Abstract

An instrument combining fluorescence microscopy with Hadamard transform multiplexed imaging was designed by which a three-dimensional Hadamard transform fluorescence microscopic cell image was obtained. The image can provide useful information including, simultaneously, the apparent dimensions and the shape of the analytical sample, the content and the distribution of some species in it.

*Keywords:* Image analysis; Fluorimetry; Microscopy; Hadamard transform

---

### 1. Introduction

The fluorescence microscope is a very important tool in cytobiology and clinical analysis [1–5]. It is often employed to observe the fluorescence intensity or distribution in cells or tissue, which can offer substantial information, including the apparent dimensions and shape of an analytical sample and the content and distribution of some species in it. All these are very useful in cytobiology and clinical medicine. For example, using this method, one can determine the content of DNA, free calcium, protein and some other species in cells [5–7] and quantitatively analyse the change in a cell's appearance and the distribution of some materials in it [4,8,9] by staining the cell with a fluorescence probe reagent. In general, the fluorescence microscope is often cou-

pled with a camera to obtain the image of an analytical sample. This is convenient to observe quantitatively the change in appearance of an analytical sample and the distribution of some species in it, but from the photograph it is difficult to obtain quantitative information on some trace materials in the sample.

The most effective method to determine trace materials in a cell is flow cytometry [10–14]. This can give a more precise content of DNA, free calcium, protein and some other materials in cells than other methods. One drawback with this instrument is that it cannot provide the image of an analytical sample, which is sometimes more important than other information in clinical medicine. Another disadvantage is this instrument cannot be used to analyse tissue samples.

Recently, good-quality inter-line transfer charge-coupled devices (CCDs) and frame grabbers have been used instead of the common camera to obtain microscopic images. The image can also offer some

---

\* Corresponding author. Present address: Centre of Instrumental Analysis, Wuhan University, Wuhan, 430072, China.

quantitative information, but this instrument is not suitable for analysing weak fluorescence signals owing to the limited sensitivity of CCDs. Hence it is necessary to develop an efficient and sensitive instrument that can provide simultaneously image information and relatively precise quantitative results for analytical samples.

Hadamard transform spectroscopy is one of the most important spectroscopic modulation techniques developed in the last 20 years. It has three advantages: Fellgett's advantage, by which an improvement in the signal-to-noise ratio can be obtained, the power distribution advantage and the multiplexed spatial imaging ability, which includes the source-encoded and signal-encoded image. In recent years, numerous publications have appeared that describe the application of these aspects in analytical chemistry [15–22]. Especially, Morris and co-workers [23–25] developed a method to combine the Raman microscope with the Hadamard transform technique and obtained an image with a resolution close to the diffraction-limited resolution of the microscope they used. However, we have found no reports on the technique of Hadamard transform multiplexed microscope fluorescence imaging.

In this study, we combined the Hadamard transform multiplexed image technique with a fluorescence microscope and successfully applied this system to obtain a three-dimensional Hadamard transform microscope fluorescence cell image. This image can offer much useful information, including cell apparent dimensions, shape and relative spatial positions on the slide, and one can also obtain some quantitative data including simultaneously the content of some species and their distribution in the cell. Because a sensitive photomultiplier was used in this experiment as a detector together with Fellgett's advantage arising from the Hadamard transform multiplexed imaging technique, very weak fluorescence signals can be detected that cannot even be recorded with a 0.02 lux sensitivity CCD camera device.

## 2. Theory

If a magnified fluorescence image signal is modulated by a Hadamard mask (signal-encoding image) on the focus square, the resulting fluorescence image

signal will be the sum of signals from each resolution element (pixel) of the image. Thus, for a mask consisting of opaque and transparent squares, the recorded signal generated by mask  $j$  is given by

$$Y_j = \sum_{i=1}^n S_{ij} X_i \quad (1)$$

where  $Y_j$  is the signal from the  $j$ th mask,  $S_{ij} = (S_{1j}, S_{2j}, \dots, S_{nj})$  is the vector of mask elements of the  $j$ th mask and  $X_i$  is the signal at position  $i$  on the image. The element  $S_{ij}$  has values 1 for each transparent square and 0 for each opaque square. For  $n$  resolution elements, the measurement process requires a sequence of at least  $n$  different masks. To recover all  $n$  signals,  $n$  measurements are necessary. These can be defined by  $n$  linear independent equations that completely define the system:

$$Y_1 = \sum_{i=1}^n S_{i1} X_i \quad (2.1)$$

$$Y_2 = \sum_{i=1}^n S_{i2} X_i \quad (2.2)$$

⋮

$$Y_n = \sum_{i=1}^n S_{in} X_i \quad (2.n)$$

In matrix notation, the set of Eqs. 2 may be written as

$$Y = S \cdot X \quad (3)$$

The system can be solved by calculating the inverse of matrix  $X$  according to the equation

$$X = S^{-1} \cdot Y \quad (4)$$

The matrix  $S^{-1}$  is computationally easy to generate, and is given by

$$S^{-1} = \frac{2}{n+1} \cdot W \quad (5)$$

where  $W$  is a matrix which has  $-1$ s where  $S^T$  has  $0$ s and  $+1$ s where  $S^T$  has  $+1$ s. Matrix  $S$  describes the configurations of the masks used for the encoding procedure and is called an  $S$ -matrix. It is derived from a Hadamard matrix, which contains elements  $+1$  and  $-1$  only.

The properties of  $S$  matrices and techniques for their generation have been discussed in detail [26]. An  $S$  matrix can be cyclic. A cyclic matrix has the

property that each row is generated from the previous row by shifting its elements one position to the left (or right) and placing the overflow in the position of the element that was first shifted. The advantage of using a cyclic matrix to configure the mask is that a single mask of  $2n - 1$  slits can be used to generate the configurations of all  $n$  individual masks. The mask is shifted incrementally at limiting aperture by a distance of one slit width. Each shift of the mask generates a row of the  $S$  matrix. Shifting the mask  $n - 1$  times generates the entire  $S$  matrix sequentially. We use a fast Hadamard transform (FHT) algorithm to solve Eq. 4 according to [26]. Finally, the image is recovered by placing every  $X_i$  in position  $i$ .

### 3. Experimental

Fig. 1 is a schematic diagram of the instrument of the Hadamard transform fluorescence microscope. The system consists of a research-grade fluorescence microscope (44XII, Shanghai Optical Instrument Factory), a monochromator (WDG30, Beijing Optical Instrument Factory), a Tatung 80386-based computer, a CCD video camera (Phillips) coupled with

an image interface card, a Hadamard transform device including a Hadamard mask, aperture, mechanical translation device which can move in two dimensions and stepper motor control electronics.

The fluorescence microscope is equipped with devices for epifluorescent illumination using a 150W mercury lamp as UV source. A halogen lamp is used as a transmission light source. All the objectives ( $2.5\times$ , N.A. 0.25;  $10\times$ , N.A. 0.25;  $40\times$ , N.A. 0.65;  $100\times$  (oil), N.A. 1.25) are achromatic.

A Tatung-80386-based computer was used for data acquisition, automatic control and inverse Hadamard transformation of the data. In this experiment, fast Hadamard transform (FHT) was employed to recover the image. All the software was written in turbo Pascal V. 5.5. In this experiment, all the experimental operations except sample preparing are controlled by computer.

A 0.02 lux sensitivity CCD video camera we used in the experiment isn't linear with fluorescence intensity owing to its automatic gain control electronics. By using the CCD camera and the image interface card, we can get a  $512\times 512$  or  $256\times 256$  pixels microscopic fluorescence image of analytical sample directly in vertical light system of this instrument. The image is used to compare with the

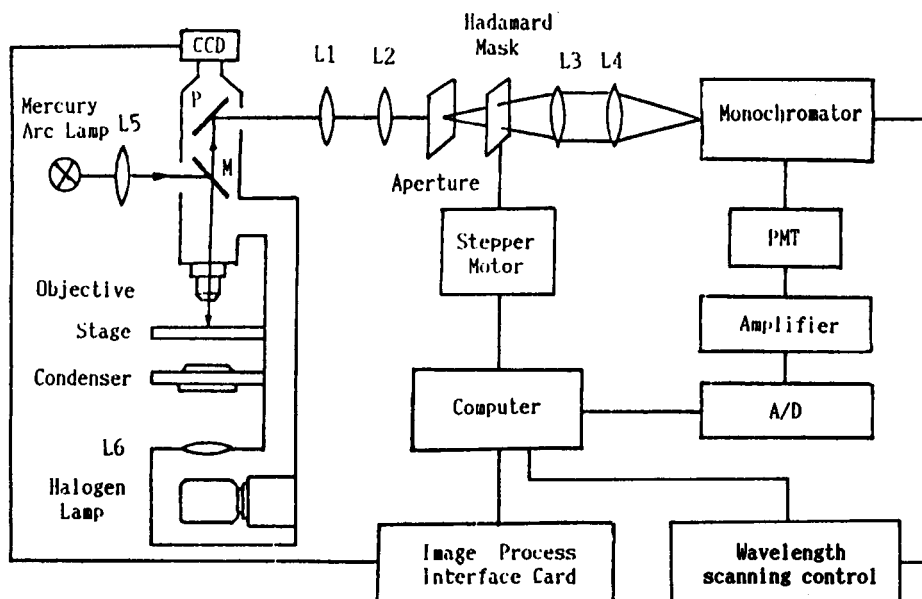


Fig. 1. Two-dimensional encoding Hadamard transform fluorescence microscope, M = dichroic beamsplitter; P = turning mirror.

Hadamard transform fluorescence image, from it, we can get more information and demonstrate the imaging ability of horizontal light system.

An uncooled photomultiplier tube (1P28, Hamamatsu), operated in the d.c. mode, was used as a detector. The signal from the PMT must be amplified before it is digitized by a 12-bit AD–DA interface card.

A 255-element cyclic Hadamard mask was used in this experiment. It was folded into a two-dimensional mask which includes a  $15 \times 17$  element array to obtain a  $15 \times 17$  pixels image. The unit resolution element was  $300 \mu\text{m} \times 300 \mu\text{m}$  square. The mask was fabricated photographically on a quartz glass plate. The aperture was a  $4.5 \text{ mm} \times 5.1 \text{ mm}$  transparent window which was also fabricated photographically on a quartz glass plate; it was fixed rigidly. The Hadamard mask was mounted on a translation stage positioned behind the fixed aperture. The translation stage which can move in  $X$ – $Y$  directions was mounted with two micrometer heads equipped with two stepper motors to control the two-dimensional movement of the mask. The deviation of the stepper motor movement was  $< 0.4 \mu\text{m}$  in the range of the stepper motor movement, which covered 16 mm. The stepper motor controlling electronics included two parts, a computer interface card used for sending the encoding cyclic pluse, and power amplifier electronics used for amplifying the power of encoding cyclic pluse running the stepper

motor because the power of the cyclic pluse from the computer interface card is too small to run it.

The monochromator was used for obtaining spectroscopic resolution in this instrument. This is useful when several fluorescence probe reagents are sometimes employed to tag a sample. In the common fluorescence microscope, the filters are often used to select a suitable fluorescence wavelength, so it is difficult to obtain a fine fluorescence emission spectrum of a complicated sample. In the present instrument, by monochromator scanning, this can easily be achieved.

An acridine orange-stained cell was used as an experimental sample. The cell sample was prepared according to the standard cytobiology method. All the reagents used in experiment were of general- or analytical-reagent grade.

#### 4. Results and discussion

In order to detect the imaging ability of this system and to adjust the initial position of Hadamard mask and optimum working conditions of this instrument, we first observed a transparent slit made with a razor blade in a piece of black paper. We used a halogen lamp as a transmission light source, using Kohler's principle of illumination for obtaining a uniform field (bright-field). Fig. 2 shows the image. Here the slit is clearly imaged. The  $X$  and  $Y$  dimen-

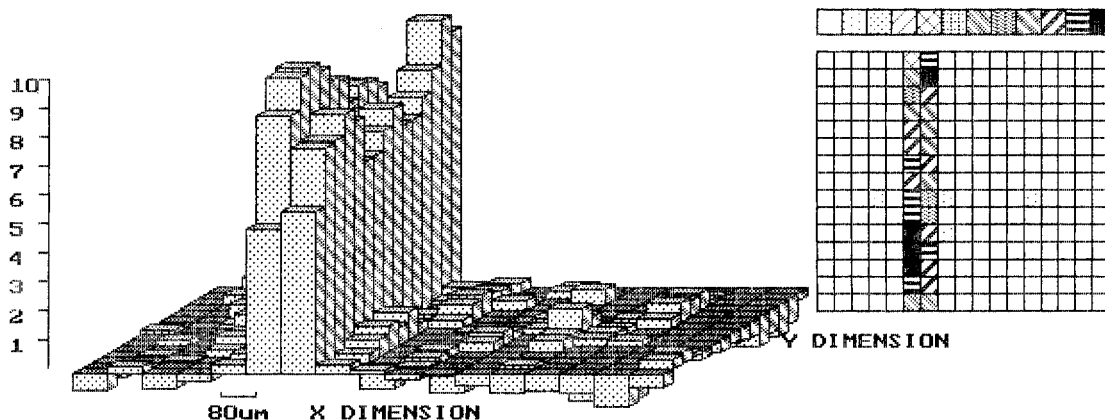


Fig. 2. Hadamard transform multiplexed three-dimensional microscope transmission light image of a slit in black paper, total intensity,  $2.079 \times 10^3$ ; maximum intensity, 90.55; mean intensity, 69.30; signal-to-noise ratio, 23.61.

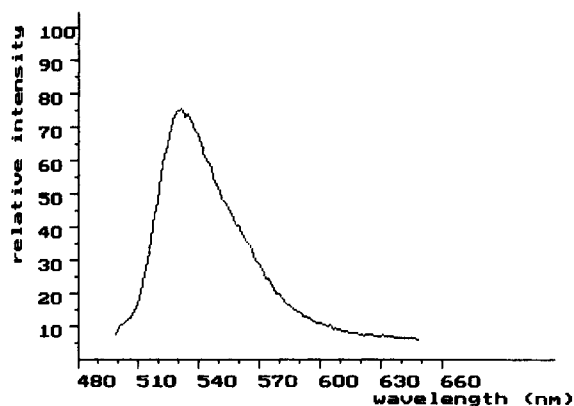


Fig. 3. Microscope fluorescence emission spectrum of acridine orange-stained *Campsis grandiflora* loose anther dust cell acquired by this instrument.

sions show the spatial position of the slit. The width of the slit is  $160\ \mu\text{m}$ , which agrees with that measured directly with the eyepiece scale. The relative intensity scale represents the transmission light intensity through the slit. The unequal height intensity is caused by three factors: the magnified image of the slit is not parallel to the row of the mask, with the result that the transmission light image of the slit cannot cover an equal area of the resolution elements in the two rows of the mask; the width of the slit is not completely uniform; and a non-ideal mask and the noise of the system. In general, the third factor always cause distortion of the image, but in this experiment the phenomenon is mainly caused by the

first and second factors. The relative intensity of some pixels in Fig. 2 shows negative signals, which are a characteristic artifact of Hadamard transform techniques. These arise primarily from the non-ideal mask and the noise, which generates apparent signals in regions that should be dark. The inverse transformation generates negative numbers at these points. The two-dimensional image beside the three-dimensional image is a vertical view of the three-dimensional image, in which the relative intensity scale is represented by a different fill pattern.

Fig. 2 demonstrates that with the Hadamard transform multiplexed imaging technique and the microscopic technique, we can obtain the three-dimensional image of a micro-sample with a detector (PMT), and the image can offer useful information including the apparent dimensions, the shape, the total transmission intensity and the transmission intensity distribution of an analytical sample.

Fig. 3 for an acridine orange-stained *Campsis grandiflora* loose anther dust cell, shows the microscope fluorescence emission spectrum obtained with this system. Fig. 3 shows that the maximum emission wavelength of this sample is 535 nm. We selected 535 nm as the wavelength for imaging cells.

Fig. 4 shows a Hadamard transform three-dimensional microscope fluorescence image of an anther dust cell, which provides useful information. The image shows the shape and the apparent dimensions of the cells. Also, from the image, one can obtain the total fluorescence intensity of the cell by accumulating all the pixels intensity covered by it, which is

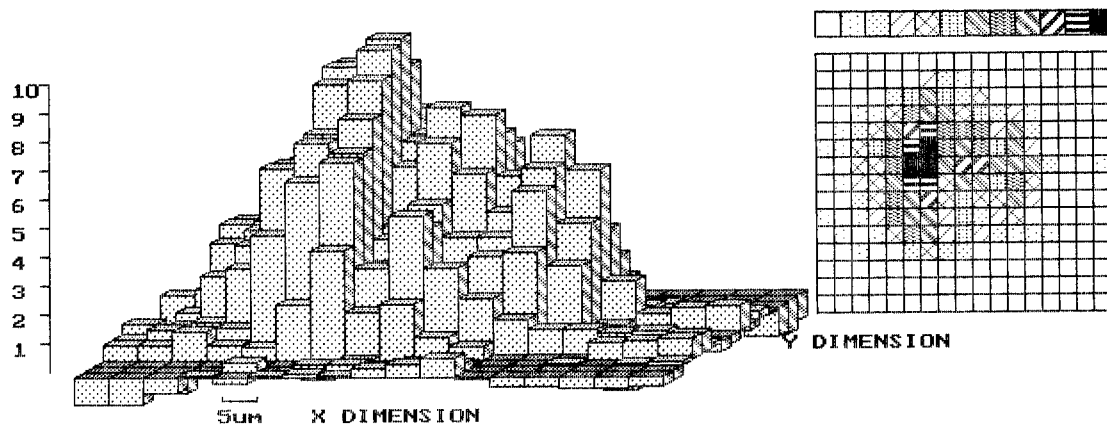


Fig. 4. Hadamard transform multiplexed three-dimensional microscope fluorescence image of an acridine orange-stained *Campsis grandiflora* loose anther dust cell measured at 535 nm.



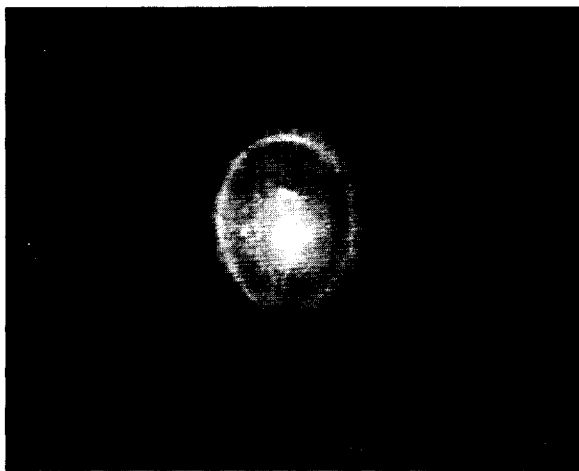


Fig. 5. Image acquired by CCD camera of an acridine orange-stained human breast cancer cell.

very useful, because it corresponds to the content of some species in the cell if a special fluorescence probe reagent is used to stain this species. Further, the image shows the distribution of cell fluorescence intensity, so that one can obtain the distribution image of some species in a cell. All this indicates that we can obtain simultaneously image and quantitative results for an analytical sample with this system.

In this experiment, one important problem encountered is fluorescence bleaching arising from the prolonged UV illumination. This is a more important factor than the non-ideal mask and the noise which can cause distortion of the fluorescence image. In

this experiment, the bleaching is related to the time of acquiring data (the time of illumination of the sample) and the magnifying power and numerical aperture (N.A.) of the objective used in the test when the same excitation source is used. In general, when we use a  $100\times$ , N.A. 1.25 objective, the bleaching of cell fluorescence is very rapid and when the last mask movement was finished (2 min were needed in this test) the fluorescence intensity had decreased to half of that at the beginning. It is certain that the true fluorescence image of the cell cannot be recovered. In this experiment we therefore only used a  $40\times$ , N.A. 0.65 objective, resulting in very slow bleaching of the cell fluorescence and only slight distortion of the Hadamard transform image. There are two ways to eliminate the effect of fluorescence bleaching in this experiment: shortening of the time of acquiring data, and calibrating the fluorescence bleaching by using a chemical kinetic model. In another paper, this problem will be discussed in detail and a method for calibrating it will be suggested.

In this experiment, one can also obtain the cell image with the CCD camera directly. Fig. 5 shows a microscope fluorescence image of a human breast cancer cell obtained with the CCD camera and Fig. 6 shows the Hadamard transform microscope fluorescence image of the same cell. Comparison of Figs. 5 and 6 shows that the Hadamard transform microscope fluorescence image can correctly show the fluorescence distribution of the analytical sample. As the CCD used in this experiment has automatic gain control electronics, is not linear with the fluores-

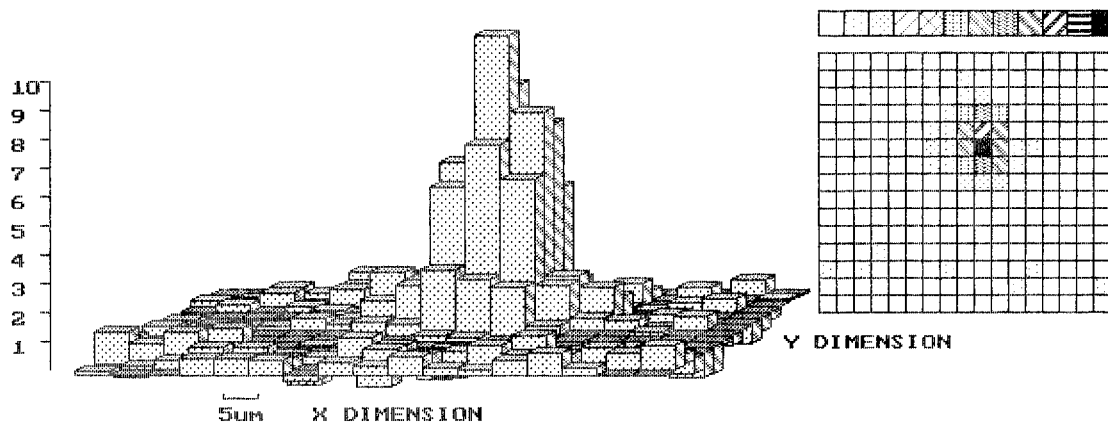


Fig. 6. Hadamard transform multiplexed three-dimensional microscope fluorescence image of the same cell as in Fig. 5 measured at 535 nm.

cence intensity and the image obtained is unsuitable for quantitative analysis, the CCD camera is only used to offer a higher fidelity image in this system. The disadvantage of the image obtained with the CCD camera for quantitative analysis is overcome by the Hadamard transform image, which can offer precise quantitative data. Because of the sensitive PMT used as a detector and the Fellgett's advantage arising from the Hadamard transform multiplexed technique, with a horizontal light system, one can image a very weak fluorescence signal that cannot be detected by 0.02 lux sensitivity CCD camera. This shows that the Hadamard transform microscope image analysis system is suitable for detecting weak signals.

## 5. Conclusion

This study has indicated that by using the Hadamard transform multiplexed imaging technique, one can obtain a three-dimensional microscope cell fluorescence image with one detector (PMT), and the image can simultaneously offer qualitative and quantitative information on cells. The analytical results show that this is a sensitive, effective and easy to operate method for analysing cells and other micro-samples.

## References

- [1] A.W. Coleman, M.J. Maguire and J.R. Coleman, *J. Histochem. Cytochem.*, 29 (1981) 959.
- [2] J.L. Bella and J. Gosalvez, *Biotechnol. Histochem.*, 66 (1991) 44.
- [3] V. Scali and F. Tinti, *Biotechnol. Histochem.*, 67 (1992) 356.
- [4] E.C. Lulai and W.C. Morgan, *Biotechnol. Histochem.*, 67 (1992) 185.
- [5] S. Sgorbati, E. Sparvoli, M. Levi and D. Chiatante, *Physiol. Plant.*, 75 (1984) 479.
- [6] D.B. Learn, S.J. Moloney and L.D. Giddens, *Biotechnol. Histochem.*, 67 (1992) 125.
- [7] P.P. Sanna, G.F. Jirikowski, G.A. Lewandowski and F.E. Bloom, *Biotechnol. Histochem.*, 67 (1992) 346.
- [8] M.H. Nathanson and A.D. Burgstahler, *Cell Calcium*, 13 (1992) 89.
- [9] J.S. Rotnes and J.G. Iversen, *Cell Calcium*, 13 (1992) 487.
- [10] N. Wang, B.G. Stenkvis and B. Tribukait, *Anal. Quant. Cytol. Histol.*, 14 (1992) 210.
- [11] G. Forsslund, A. Kreieberg, B. Nilsson and A. Zetterberg, *Anal. Quant. Cytol. Histol.*, 14 (1992) 153.
- [12] A. Pollack, H. Moulis, N.L. Block and G.L. Irvin, III, *Cytometry*, 5 (1984) 473.
- [13] J.L. Roti, R. Higashikubo, O.C. Blair and N. Uygur, *Cytometry*, 3 (1982) 91.
- [14] J.R. Krause and M.K. Blank, *Anal. Quant. Cytol. Histol.*, 14 (1992) 39.
- [15] T.J. Vickers, C.K. Mann and J. Zhu, *Appl. Spectrosc.*, 45 (1991) 42.
- [16] J.B. Park, T.W. Johnson, S.A. Dyer, B.K. Harms and R.A. Dyer, *Appl. Spectrosc.*, 44 (1990) 219.
- [17] D.C. Tilotta, R.M. Hammaker and W.G. Fateley, *Appl. Spectrosc.*, 41 (1987) 727.
- [18] E.R. Williams, S.Y. Loh and F.W. McLafferty, *Anal. Chem.*, 62 (1990) 698.
- [19] F.K. Fotiou and M.D. Morris, *Appl. Spectrosc.*, 40 (1986) 704.
- [20] F.K. Fotiou and M.D. Morris, *Anal. Chem.*, 59 (1987) 185.
- [21] F.K. Fotiou and M.D. Morris, *Anal. Chem.*, 59 (1987) 1446.
- [22] P.J. Treado and M.D. Morris, *Appl. Spectrosc.*, 42 (1988) 897.
- [23] P.J. Treado and M.D. Morris, *Appl. Spectrosc.*, 43 (1989) 190.
- [24] K.L. Liu, L.H. Chen, R.S. Sheng and M.D. Morris, *Appl. Spectrosc.*, 45 (1991) 1717.
- [25] A. Govil, D.M. Pallister, I-H. Chen and M.D. Morris, *Appl. Spectrosc.*, 45 (1991) 1604.
- [26] M. Harwit and N.J.A. Sloane, *Hadamard Transform Optics*, Academic Press, New York, 1980.

# Enzymatic–spectrophotometric determination of phytic acid with phytase from *Aspergillus ficuum*

J.G. March, A.I. Villacampa, F. Grases \*

Department of Chemistry, University of Balearic Islands, 07071 Palma de Mallorca, Spain

Received 16 May 1994

## Abstract

A method to determine phytic acid in the range 3–60  $\mu\text{M}$  based on the spectrophotometric determination of inorganic phosphate with vanadate and molybdate, after liberation by enzymatic hydrolysis of phytic acid with phytase from *Aspergillus ficuum* at pH 2.5 and 37°C is reported. The method has been applied successfully to determine phytic acid in wheat flour and in a pharmaceutical product.

**Keywords:** Enzymatic methods; Spectrophotometry; Phytic acid; *Aspergillus ficuum*

## 1. Introduction

Inositol hexakisphosphate, usually called phytic acid, is a natural compound of great interest in food chemistry and nutrition because of its role in metallic element and protein intestinal absorption and its beneficial action on some pathological processes such as calcium oxalate urolithiasis. Hence, the interest in its analytical determination is obvious.

As a consequence of the spectral characteristics of phytic acid, its instrumental determination (at  $\geq 0.15$  mM) has been mainly restricted to liquid chromatography with refractive index detection [1–6]. Some post-column reactions have also been investigated [7–10]. A phytic acid analysis based on total phosphorus determination by inductively coupled plasma atomic emission spectrometry (ICP-AES) have also been reported [11].

Recently, the hydrolysis of phytic acid catalysed by *Schwanniomyces castellii* phytase has been investi-

gated in the food industry as a process to decrease the phytate content of high fiber food. The rate and extent of the decrease of the phytic acid content allows a calibration plot for phytic acid determination to be achieved [12].

The aim of this paper is to report further on the analytical use of the enzymatic hydrolysis of phytic acid followed by the spectrophotometric determination of orthophosphate ions based on the formation of the yellow heteropolyanion with vanadate and molybdate [13].

## 2. Experimental

### 2.1. Reagents, solutions and apparatus

7 M Nitric acid, 0.02 M ammonium vanadate in 0.28 M  $\text{HNO}_3$  and 0.04 M ammonium molybdate ( $(\text{NH}_4)_6\text{Mo}_7\text{O}_{24} \cdot 4\text{H}_2\text{O}$ ) were purchased from Panreac. Crude phytase crude from *Aspergillus ficuum*, 4.1 units/mg

\* Corresponding author.

specific activity, was purchased from Sigma. Crude suspensions from 1 to 0.2 mg/ml were prepared in water with magnetic stirring until a homogeneous suspension was achieved. 1 Unit (U) liberates 1.0  $\mu\text{mol}$  of inorganic P from  $4.2 \times 10^{-2}$  M phytate per min at pH 2.5 and 37°C. Vitamin A acetate (retinyl acetate,  $\text{C}_{22}\text{H}_{32}\text{O}_2$ , 2900 U/mg) and vitamin E (DL- $\alpha$ -tocopherol,  $\text{C}_{29}\text{H}_{50}\text{O}_2$ , 1.1 U/mg) as an oily concentrate were from Fluka. Vitamin solutions were prepared in ethanol.

A chromatographic column was prepared with a strongly basic (50–100 mesh)  $\text{Cl}^-$  form Dowex 1X10 anion exchanger supplied by Fluka. The column was washed with 0.7 M NaCl and water before use.

Absorbance measurements were performed with a single beam spectrophotometer (Shimadzu UV-120-02) and disposable cells of 1 cm optical pathlength. pH measurements were performed with a 2002-Crison pH meter. A Perkin-Elmer Plasma 2000 emission spectrometer was used for total phosphorus determination.

## 2.2. Procedure

20 ml of solution containing phytic acid in the range 3–60  $\mu\text{M}$  were adjusted to pH 2.5 with 3 M HCl using a pH meter and thermostated at 37°C with water of constant temperature. A 1-ml portion of homogeneous phytase suspensions containing crude phytase (0.4 mg/ml) was added and the system was magnetically stirred for 60 min (incubation period). The reaction was terminated by addition of 3 ml of 7 M  $\text{HNO}_3$ . In order to determine free inorganic phosphate, 3 ml of ammonium vanadate and 3 ml of ammonium molybdate solutions were added; 2 ml of the final solution were filtered through a disposable 0.45- $\mu\text{m}$  filter syringe and the absorbance was measured at 400 nm against a reagent blank.

## 2.3. Treatment of real samples

The solid–liquid extraction of phytic acid was carried out with 3% sulphuric acid for 60 min. The sample was then centrifuged at 6000 rpm for 15 min and the supernatant filtered through a 0.45  $\mu\text{m}$  PTFE filter. The purification of the extract was accomplished by anion-exchange chromatography or by iron(III) phytate precipitation. When applying the chromatographic separation, 1 ml of sample filtrate was mixed with 1 ml

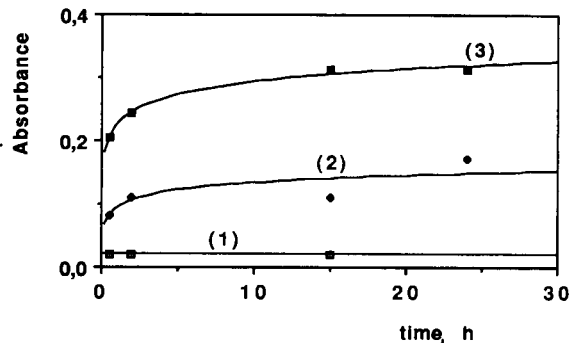


Fig. 1. Rate of phytic acid hydrolysis at different phytic acid initial concentrations: (1) 7.3  $\mu\text{M}$ , (2) 14.5  $\mu\text{M}$ , (3) 29.1  $\mu\text{M}$ . Hydrolysis pH and temperature, 2.5 and 37°C. Crude phytase, 49 mg/l.

of 0.11 M  $\text{Na}_2\text{EDTA}$ –0.75 M NaOH solution and transferred to the column. The eluate was discarded. The column was washed with water and 0.1 M NaCl. Finally the phytic acid was eluted with 2 M HCl. Phytate determination was carried out by the proposed enzymatic procedure, adjusting the pH to 2.5 with 4 M NaOH and considering the dilution of the sample when adjusting the pH.

When applying the iron(III) phytate precipitation, 5 ml of sample filtrate were mixed with 1 ml of 0.1 M  $\text{FeCl}_3$  in 3%  $\text{H}_2\text{SO}_4$ . The precipitate formed was separated by centrifugation (15 min at 6000 rpm) and washed with water. 1 ml of 1.5 M NaOH and 7 ml of water were added to the solid iron(III) salt in order to precipitate hydrated iron(III) oxide and liberate the phytate. After 30 min at 80°C the supernatant, containing the phytate, was separated by centrifugation and filtration. The determination of phytic acid was carried out as before. Total phosphorus analysis of purified extracts was also carried out by ICP-AES for comparative purposes [11].

## 3. Results and discussion

### 3.1. Study of the variables

The rate of inorganic orthophosphate liberation as a consequence of the enzymatic hydrolysis of phytic acid, corresponding to several initial phytic acid concentrations, is shown in Fig. 1. As can be seen, at 7.3  $\mu\text{M}$  the phytic acid hydrolysis was complete after 30 min, but, for higher phytic acid concentrations a longer time is necessary to reach the maximum concentration

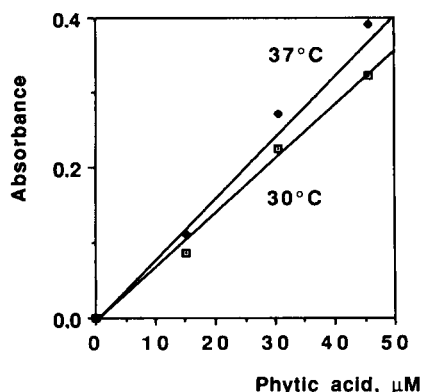


Fig. 2. Effect of temperature on the hydrolysis of phytic acid at several initial phytic acid concentrations. Hydrolysis pH and period, 2.5 and 60 min. Crude phytase, 49 mg/l.

of free phosphate. Considering that after 1 h of enzymatic hydrolysis, the absorbance became less dependent on time, 1 h was recommended when using this reaction for analytical purposes. The rate was also dependent on other variables such as temperature, pH during hydrolysis and amount of phytase. Fig. 2 shows the absorbance measurement for several phytic acid initial concentrations obtained at 30 and 37°C. As was expected, the hydrolysis was faster at 37°C and this temperature was chosen to study other variables

The influence of the pH on the enzymatic hydrolysis was studied at 30 and 60 min. In both cases the maximum enzyme activity was found at pH 2.5 (Fig. 3). As can be seen, the enzyme activity is strongly pH dependent.

The effect of amount of enzyme on the reaction has also been studied. Due to the incomplete phytic acid hydrolysis under the reported experimental conditions, the yield of the hydrolysis was dependent on the amount

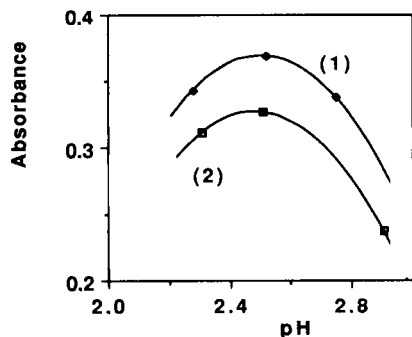


Fig. 3. Effect of pH on the hydrolysis of phytic acid. Hydrolysis period (1) 60 min, (2) 30 min. Phytic acid 45 μM. Crude phytase, 49 mg/l. Hydrolysis temperature, 37°C.

Table 1  
Yield of hydrolysis by several amounts of crude phytase (hydrolysis time, 60 min; hydrolysis pH, 2.5, initial phytic acid concentration, 45 μM)

Phytase crude (mg l <sup>-1</sup> )	Absorbance (400 nm)	Hydrolysis (%)
10	0.142	32
19	0.371	84
49	0.394	89

Results represent an average of three experiments. Assuming 100% hydrolysis, the absorbance would be 0.444.

of crude enzyme. The final sensitivity of the method depends on the amount of enzyme used. Table 1 summarises results obtained at three different phytase total activities. The yield of the hydrolysis has been calculated assuming the liberation of 6 mol of inorganic orthophosphate by 1 mol of phytic acid to be 100%. Considering the total liberation of 5 phosphate groups by phytic acid implies a 83.3% yield, and for 4.1 units of enzyme a higher yield has been observed, it can be concluded that under the reported experimental conditions, the enzyme used could catalyse the hydrolysis of the six phosphate groups of the phytic acid molecule.

### 3.2. Characteristics of the analytical method

Working as described with the proposed procedure a solution containing 45 μM phytic acid typically gave a 0.371 absorbance measurement, with a relative standard deviation of 1.5% (10 determinations). A linear calibration graph was obtained in the range 3–60 μM. The effects of several compounds of biological interest on the enzyme activity were also studied. The results obtained presented as tolerable amounts are summa-

Table 2  
Maximum tolerable concentrations of foreign species in the determination of 45 μM phytic acid

Species	Amount tolerated (μg/ml) <sup>a</sup>
Ethanol	10,000
Na <sup>+</sup> , Cl <sup>-</sup> , Ca <sup>2+</sup> , Zn <sup>2+</sup> , citrate	1000
Mg <sup>2+</sup> , Oxalate	100
Cu <sup>2+</sup>	50
Vitamin A acetate <sup>b</sup>	2
Vitamin E <sup>b</sup>	6

<sup>a</sup> Error ≤ 1.5%. <sup>b</sup> Solutions were prepared in ethanol.

Table 3  
Determination of phytic acid in real samples

	Purification by			
	Anion chromatography		Iron(III) precipitation	
	ICP	Enzymatic	ICP	Enzymatic
Lit-Stop® (mg phytic acid/tablet)	29.6	30.2	30.1	30.7
Wheat flour (mg phytic acid/g)	17.5	16.8	18.0	17.7

Lit-Stop®: Authex Lab., Marratxi, Balearic Islands, Spain. Phytic acid reported value: 30 mg per tablet.

rized in Table 2. It is worth mentioning that higher concentrations of foreign species always generated a negative error. None of the studied species can be considered necessary for phytase action, but some of them inhibited the phytase giving the negative error. Species reacting with phosphate at pH 2.5, e.g., Fe(III), must be absent. The effective inhibition of phytase by vitamin A and vitamin E should also be emphasized; 23 µg/ml (ppm) of vitamin A decreased the hydrolysis of phytic acid at 60 min by 35%; 46 ppm vitamin E causes a decrease of 59%.

### 3.3. Applications

In order to test the applicability of the proposed procedure it was applied to real samples: a pharmaceutical product (Lit-Stop®) and wheat flour. Real samples were also analysed using ICP-AES as reported by Plaami et al. [11]. Phytic acid from samples was extracted with 3% H<sub>2</sub>SO<sub>4</sub> and purified by anion-

exchange chromatography or iron(III) phytate precipitation and phytate dissolution with NaOH. The results are summarized in Table 3. Good agreement can be observed when comparing the two tested procedures to purify phytic acid and the two analytical procedures; the enzymatic method proposed in this paper and the one based on total phosphorus analysis by ICP-AES.

### Acknowledgements

Financial support by DGICYT (Grant PB 92-0429) is acknowledged. One of us (A.I.V.) was a fellow of the FPI program (Spain)

### References

- [1] B. Tangendjaja, K.A. Buckle and M. Wootton, *J. Chromatogr.*, 197 (1980) 274.
- [2] A.L. Camire and F.M. Clydesdale, *J. Food Sci.*, 47 (1982) 575.
- [3] B.E. Knuckless, D.D. Kuzmicky and A.A. Betschart, *J. Food Sci.*, 47 (1982) 1257.
- [4] E. Graf and F.R. Dintzis, *Anal. Biochem.*, 119 (1982) 413.
- [5] A.S. Sandberg and R. Ahderinne, *J. Food Sci.*, 51 (1986) 547.
- [6] J. Lehrfeld, *Cereal Chem.*, 66 (1989) 510.
- [7] J.J.L. Cilliers and P.J. Niekerk, *J. Agric. Food Chem.*, 34 (1986) 680.
- [8] G.W. Mayr, *Biochem. J.*, 254 (1988) 585.
- [9] K.D. Bos, C. Verbeek, C.H.P. Eeden, P. Slump and M.G.E. Wolters, *J. Agric. Food Chem.*, 39 (1991) 1770.
- [10] C.M. Clarkin, R.A. Minear, S. Kim and J.W. Elwood, *Environ. Sci. Technol.*, 26 (1992) 199.
- [11] S. Plaami and J. Kumpulainen, *J. Assoc. Off. Anal. Chem.*, 74 (1991) 32.
- [12] L. Segheilha, G. Moulin and P. Galzy, *J. Agric. Food Chem.*, 41 (1993) 2451.
- [13] Z. Marczenko, *Spectrophotometric Determination of Elements*, Wiley, New York, 1976.



ELSEVIER

Analytica Chimica Acta 300 (1995) 273–276

**ANALYTICA  
CHIMICA  
ACTA**

# Application of a mimetic enzyme for the enzyme immunoassay for $\alpha$ -1-fetoprotein

Yun-Xiang Ci \*, Yang Qin, Wen-Bao Chang, Yuan-Zong Li

*Department of Chemistry, Peking University, Beijing 100871, China*

Received 28 June 1993

## Abstract

A new mimetic enzyme immunoassay (MEIA) method for  $\alpha$ -1-fetoprotein (AFP) was developed using a mimetic enzyme Mn(III)-tetra(sulfophenyl)porphine (Mn-TPPS<sub>4</sub>) as a labelling reagent to catalyze the fluorescence reaction of 4-hydroxyphenylacetic acid (HPA) and hydrogen peroxide. In the sandwich assay standard AFP solution or AFP containing umbilical blood serum first reacts with antibody (anti-AFP) coated on a 40-well plate (polystyrene), and then further reacts with Mn-TPPS<sub>4</sub>-labelled anti-AFP; the Mn-TPPS<sub>4</sub> on the bound fraction, after removing the free fraction was determined by measuring the fluorescence intensity as a result of the reaction between HPA and H<sub>2</sub>O<sub>2</sub>, catalyzed by bound Mn-TPPS<sub>4</sub> and anti-AFP conjugate, which was proportional to the concentration of AFP. AFP in the range 0.01–10  $\mu$ g per well can be determined with a detection limit of 1 ng per well. The method has sufficient sensitivity to be applied to the determination of AFP in umbilical blood serum.

*Keywords:* Enzymatic methods; Immunoassay;  $\alpha$ -Fetoprotein; Manganese; Mimetic enzyme immunoassay

## 1. Introduction

Enzyme-antibody labels are very much used in immunochemistry; they play an important role in the diagnosis of infectious diseases. Among the different enzymes employed as markers in the heterogeneous enzyme immunoassay, alkaline phosphatase (AP), horseradish peroxidase (HRP) and galactosidase (Gal) are most commonly used. It is well known that natural substances having a porphine skeleton in their active centers, that is, peroxidase, heme and hematin [1–3], act as sensitive catalysts for the fluorescence and chemiluminescence reactions, and have been used in immunoassays [4,5]. Some synthesized metal complexes [6] instead of the above-mentioned natural sub-

stances have been used as catalysts in chemiluminescence immunoassay (CLIA) with the advantage of cheapness, reproducibility and easy labelling. Recently, we reported the use of a synthesized metal complex catalyst labelling reagent for fluoroimmunoassay of methotrexate. In this paper, Mn-TPPS<sub>4</sub>, which had been previously reported [7–9] to show the highest catalytic activity, was used for the analysis of AFP. It was determined by mimetic enzyme immunoassay using Mn-TPPS<sub>4</sub> as catalyst as follows: AFP from serum a sample first reacts with antibody (anti-AFP) coated on a polystyrene 40-well plate, and then further reacts with Mn-TPPS<sub>4</sub> labelled anti-AFP. The bound Mn-TPPS<sub>4</sub> labelled anti-AFP, after removing the free fraction, was detected by its ability to catalyze the formation of the fluorescent product from the reaction between hydrogen peroxide and hydroxypheny-

\* Corresponding author.

lactic acid. The fluorescence intensity is thus a measure of the concentration of AFP in the analytical sample.

## 2. Experimental

### 2.1. Materials

Mn–TPPS<sub>4</sub> was prepared in our laboratory. HPA was purchased from Sigma. AFP and anti-AFP were obtained from the Cancer Institute in Beijing (China), PCl<sub>5</sub> and H<sub>2</sub>O<sub>2</sub> (30%) were from Beijing Chemical Factory. H<sub>2</sub>O<sub>2</sub> (30%) was standardized by titration with standard KMnO<sub>4</sub>. The 40-well microtitre plate was a product of Qiujiu Biochemical Instruments Factory (Shanghai).

### 2.2. Instruments

The fluorescence spectra and relative fluorescence intensity were measured on a Hitachi 850 spectrofluorimeter with a 1-cm silica cell. The absorption spectra and absorbances were measured on a Shimadzu UV-300 apparatus.

### 2.3. Synthesis and characteristics of Mn–TPPS<sub>4</sub>–anti-AFP conjugate

Mn–TPPS<sub>4</sub> was prepared by the procedure described earlier [10] with a small modification. The synthesis was carried out by the reaction between TPPS<sub>4</sub> and 5% excess of manganese(II) acetate under reflux in aqueous solution. The product was purified on a cation-exchange resin column with acetone–water (1:1, v/v) as eluent.

Labelling of anti-AFP with Mn–TPPS<sub>4</sub> was carried out using PCl<sub>5</sub>. Mn–TPPS<sub>4</sub> and PCl<sub>5</sub> were ground in a mortar until the reaction was complete. After cooling, a small amount of dimethyl formamide (DMF) was added, which in turn, was added slowly to a neutral Na<sub>2</sub>CO<sub>3</sub>–NaHCO<sub>3</sub> (0.5 N) buffer and stirred for 1 h. During the reaction the pH should be maintained neutral to prevent deactivation of anti-AFP. After the reaction the solution was subjected to gel chromatography on a Sepharose G25 column by use of phosphate-buffered saline (PBS) as eluent; the portion of anti-AFP labelled with Mn–TPPS<sub>4</sub> was thus obtained.

Each concentration of the anti-AFP and the Mn–TPPS<sub>4</sub> in the labelled anti-AFP was determined by the use of absorbance calibration curves of Mn–TPPS<sub>4</sub> at 456 nm and anti-AFP at 595 nm after its reaction with Bio-Rad stainer (a protein assay kit containing Coomassie Brilliant Blue G-250), on the assumption that the absorbance of each constituent remained unchanged before and after labelling. It was concluded from the absorbance measurements that the mole ratio of Mn–TPPS<sub>4</sub> to anti-AFP was 20. The concentration of Mn–TPPS<sub>4</sub> and anti-AFP in Mn–TPPS<sub>4</sub>–anti-AFP conjugate were  $4 \times 10^{-4}$  M and 0.32 mg/ml, respectively.

### 2.4. Immunoassay (standard procedure)

A polystyrene 40-well microtitre plate was pre-treated with 50  $\mu$ l of 0.02% ovalbumin and was allowed to stand for one day. Then, the plate was washed with PBS–Tween 20 3 times and treated with 50  $\mu$ l of 0.2% glutaraldehyde in PBS buffer (pH 7.2) for 30 min at room temperature. The plate was washed with PBS–Tween 20 buffer 5 times and air-dried for 24 h.

100  $\mu$ l of anti-AFP in 0.05 N Na<sub>2</sub>CO<sub>3</sub>–NaHCO<sub>3</sub> buffer (pH 9.5) was used to coat the plate at 4°C overnight.

The plate was washed 3 times and blocked with 2% ovalbumin (100  $\mu$ l) for 1 h.

The plate well was washed 3 times with water and 100  $\mu$ l of unknown or standard AFP sample was transferred into the well and the reaction was allowed to proceed for 1 h.

The plate well was washed 3 times with water and 100  $\mu$ l of Mn–TPPS<sub>4</sub> labelled anti-AFP was added. The immunoassay reaction was allowed to proceed for 1 h.

This was followed by washing 3 times with water and addition of a suitable amount of HPA, H<sub>2</sub>O<sub>2</sub> and NaOH solutions (see below). After 13 min reaction the solution was diluted and the fluorescence intensity was measured with excitation and emission wavelengths of 322 and 425 nm, respectively. The optimal fluorescence reaction conditions are: reaction time, 13 min; HPA concentration, 0.024 M; H<sub>2</sub>O<sub>2</sub> concentration,  $1.86 \times 10^{-4}$  M; NaOH concentration, 0.05 M.



### 3. Results and discussions

#### 3.1. Optimization of coating concentration of anti-AFP

The polystyrene 40-well plate was incubated at 4°C overnight with anti-AFP, which was prediluted with Na<sub>2</sub>CO<sub>3</sub>–NaHCO<sub>3</sub> buffer to different concentrations, followed by incubation with standard AFP and Mn–TPPS<sub>4</sub> labelled anti-AFP. The experimental results showed that the optimal concentration for the coating solution ranged from 100 to 500 times dilution of the original anti-AFP solution.

#### 3.2. Optimization of the concentration of Mn–TPPS<sub>4</sub> labelled anti-AFP

The plate well was coated with a 1:200 dilution of antiserum and, in turn, was incubated with standard AFP and Mn–TPPS<sub>4</sub> labelled anti-AFP (0.32 mg/ml) prediluted to different concentrations. The 1:10 dilution of the original Mn–TPPS<sub>4</sub> labelled anti-AFP solution was optimal.

#### 3.3. Immunoassay of AFP in umbilical blood serum

Fig. 1 shows a calibration graph obtained by the sandwich method. According to this graph, AFP in the range 0.01–10.0 µg per well can be determined with a detection limit of 1 ng per well ( $S/N=3$ ). This method

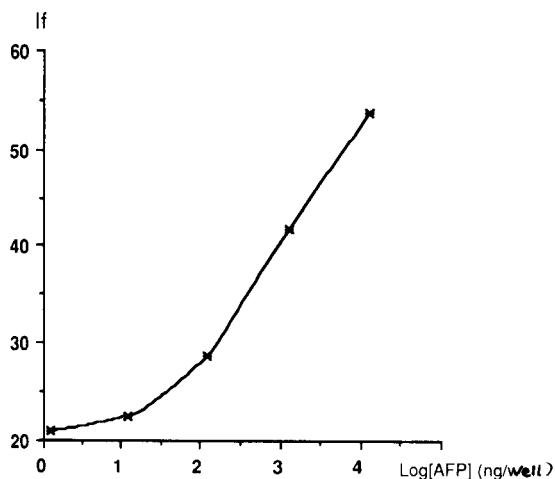


Fig. 1. Calibration graph for the determination of AFP. Conditions: anti-AFP, 1:100; Mn–TPPS<sub>4</sub> labelled anti-AFP, 1:10. If = Fluorescence intensity.

was used for the determination of AFP in the serum of umbilical blood provided by the Xiehe hospital (Beijing) to give a result of 50 µg/ml AFP. The result was in good agreement with the value determined by the radioimmunoassay method in the Hospital. The coefficient of variation ( $n=5$ ) within batch was 10% for the determination of 500 ng/ml AFP. Although the sensitivity of the method is insufficient for routine clinical purposes for cases where the concentration of AFP is very low, it may still be used in a few occasions where the AFP concentrations are high. For example, it may be used for monitoring AFP-producing liver tumours where the concentration of AFP is about 400 ng/ml and for the antenatal screening of birth abnormalities, in which the AFP level in maternal serum during normal pregnancy can reach 450–500 µg/ml and for an abnormal pregnancy the value may be 10 times higher than the normal value [11].

### 4. Conclusions

The synthesized manganese complex which functions as a catalyst for the fluorescence reaction between HPA and H<sub>2</sub>O<sub>2</sub> is useful and promising for immunoassay. The above method has the advantage of being sensitive enough for being used in some clinical assays, and can enable one to select the desired chemical structure of the labelling reagent since it is based on the use of the synthesized metal complex. In this sense, further exploiting of applications in the field of biochemical analysis is promising.

### Acknowledgements

This work was supported by the National Natural Science Foundation of China and the Ph.D Foundation for the National Education Committee of China. The authors are grateful to Prof. Zhenfu Fan and to The Cancer Institute of Beijing, for kindly providing the AFP samples used in this work.

### References

- [1] G.G. Guilbault and E. Hieserman, *Anal. Biochem.*, 26 (1968) 1.

- [2] G.G. Guilbault, *Handbook of Enzymatic Methods of Analysis*, Marcel Dekker, New York, 1976.
- [3] G.F. Zhang and P.K. Dasgupta, *Anal. Chem.*, 64 (1992) 517.
- [4] Y. Ikariyama and S. Suzuki, *Anal. Chem.*, 54 (1982) 1126.
- [5] H. Arakawa, M. Maeda and A. Tsuji, *Anal. Biochem.*, 97 (1979) 248.
- [6] T. Hara, K. Tsukagoshi, A. Arai and Y. Imashiro, *Bull. Chem. Soc. Jpn.*, 62 (1989) 2844.
- [7] Y.X. Ci and F. Wang, *Anal. Chim. Acta*, 233 (1990) 299.
- [8] F. Wang and Y.X. Ci, *Analyst*, 116 (1991) 297.
- [9] Y.X. Ci and F. Wang, *Talanta*, 37 (1990) 1133.
- [10] Y.X. Ci and F. Wang, *Fresenius' J. Anal. Chem.*, 339 (1991) 46.
- [11] G.H. Liu, G.L. Shi and Y.N. Shi, in *The Handbook for Commonly used Data in Medicine and Diagnosis Testing*, Shannxi Science Press, 1990, pp. 1044–1045.



ELSEVIER

Analytica Chimica Acta 300 (1995) 277-285

ANALYTICA  
CHIMICA  
ACTA

# On-line monitoring of D-lactic acid during a fermentation process using immobilized D-lactate dehydrogenase in a sequential injection analysis system <sup>☆</sup>

Hun-Chi Shu, Håkan Håkanson, Bo Mattiasson \*

*Department of Biotechnology, Chemical Center, Lund University, P.O. Box 124, S-221 00 Lund, Sweden*

Received 7 June 1994

## Abstract

A sequential injection analysis system (SIA) involving immobilized enzymes was set up to quantify D-lactic acid during fermentation processes. The analytical system is fully computerized and it operates by analysing aliquots removed from the bulk fermentation through a filtration setup. An assay cycle of 182 s includes 90 s of incubation time when the flow is stopped. The enzymes used in the analysis are D-lactate dehydrogenase co-immobilized together with L-alanine aminotransferase on porous glass. Cell free permeate was sampled from the permeate side of the filtration unit. The concentration of D-lactate was monitored during the entire fermentation processes. The data read were intermittently compared to off-line analysis. A good fit was obtained when comparing the results of the two ways of analysis used.

*Keywords:* D-Lactic acid; On-line monitoring; Fermentation; Sequential injection analysis (SIA)

## 1. Introduction

Lactic acid exists in two isomeric forms. When being produced chemically from fossil sources, racemic mixtures are often obtained. Several organisms produce lactic acid. In most cases, L-lactic acid is produced, but some microorganisms are also capable of producing the D-isomer. There is an important need to analyse for lactate in several sectors of society including in medicine for instance in dental care [1], in food science, and in the bioprocessing field, e.g., fermentation [2]. Lactic acid can also be used in plastic manufacture [3].

In the food industry, lactic acid is produced by bacterial fermentation and is essential for the manufacture of cheese, pickles, yoghurt, fermented meat products, and butter milk [4]. Furthermore, D-lactic acid is also an important freshness indicator for vacuum-packed chilled meat [5].

The analytical applications are many. In medicine, the level of L-lactate in blood gives an indication of the level of oxygenation in peripheral parts of the body. In food processing lactic acid gives a figure on the degree of acidification. Biotechnological production of lactate covers approximately 50% of the needs today. This fermentation is complicated by product inhibition and recovery problems which together negatively influence the economics of the fermentation process [4]. Several efforts to speed up the fermentation, to increase the volumetric productivity and to improve the yields have

\* Part of this paper was presented at *Biosensors for Food Analysis, RSC Food Chemistry Group Symposium, Leeds University, UK, April 11-12, 1994.*

\* Corresponding author.

been presented [6,7]. On-line monitoring of the fermentation process is such a step towards a better process monitoring and control and in a larger perspective towards a more economic production process. Analytical methods may handle either of the isomers or give an integrated value.

The methods to determine the D-lactic acid are mainly based on the use of D-specific lactate dehydrogenase (D-LDH) in flow-injection analysis (FIA) systems combined with a bioluminescence detector [8] or sequential injection analysis (SIA) system with a spectrophotometer as detector [9] or by liquid chromatography (LC) [10]. No method has been presented yet for quantification of D-lactic acid directly without chemical conversion.

A few methods have been published for on-line monitoring of L-lactic acid production during fermentation based on the use of lactate oxidase in a flow-injection system. [11,12] When D-lactate is to be monitored, lactate oxidase is not a suitable enzyme due to the lack of specificity for the D-isomer. Therefore, the cofactor dependent D-lactate dehydrogenase becomes the alternative choice. When the traditional FIA system was applied with immobilized D-LDH, the costly cofactor had to be supplied continuously and this consumption became a main drawback for this application. Some efforts have been made to reduce the expenses of the cofactor in FIA system [13,14]. Recently, a more simple system was demonstrated by using a SIA system integrated with a reactor with immobilized D-LDH. [9] The consumption of cofactor can be reduced substantially by providing the cofactor in the sequentially segmented mode of operation. The principle of the SIA system was first presented by Ruzicka et al. [15] and has been reviewed later [16]. In this work, a similar automatic SIA system was set up to monitor the production of D-lactic acid during a batch fermentation with *Lactobacillus delbrueckii* ATCC 9649. Sampling was done from the flux of a membrane filtration unit. The system is to be regarded as a model system for us to test this novel analytical system for on-line bioprocess monitoring.

## 2. Experimental

### 2.1. Chemicals

D-lactate dehydrogenase (E.C. 1.1.1.28) from *Leuconostoc mesenteroides* ssp. *cremoris* (specific activ-

ity, 350 and 430 U/mg, two batches of enzyme preparation) was prepared by affinity precipitation with Eudragit-Cibacron blue complex and DEAE cellulose ion exchange chromatography [17], L-alanine aminotransferase (glutamic-pyruvate transaminase, E.C. 2.6.1.2.; 76 U/mg protein) from porcine heart, D-lactic acid, NAD<sup>+</sup>, glutamic acid, and glycylglycine were purchased from Sigma (St. Louis, MO). The L-lactic acid and UV-enzymic kits for both D- and L-lactate were obtained from Boehringer (Mannheim). The silica beads were a generous gift from EKA Nobel (Surte, Sweden) with an average size of 41  $\mu\text{m}$ , a mean pore diameter of 200 Å and the specific surface area of 300 m<sup>2</sup>/g, according to the specifications given by supplier. All other chemicals were of analytical grade.

### 2.2. Immobilization of enzyme

Silica was modified with  $\gamma$ -aminopropyltriethoxysilane and later with glutaraldehyde following procedures described by Weetall [18]. D-LDH (550 U) dissolved in 400  $\mu\text{l}$  of 50 mM sodium phosphate buffer pH 7.0 was added to 0.5 g of aldehyde group containing silica. The mixture was left on a blood mixer at room temperature for coupling to take place. After 3 h, 110 U of L-alanine aminotransferase solution was added and coupling continued for another 2 h. Finally, 20 mg of sodium cyanoborohydride was added to reduce the Schiff's bonds formed between aldehyde groups and the enzymes in order to stabilize the coupling. The mixture was left for 1 h at room temperature and then overnight in a refrigerator. The preparation was then washed on a glass filter with 0.1 M phosphate buffer pH 7.0. and was packed in a column (30  $\times$  4 mm i.d.) with porous vyon discs at each end. The column was fitted with adapters for connection to the flow system to be used for analysis. The column, when not used, was stored in 0.1 M phosphate buffer pH 7.0 containing 0.02% sodium azide at 4°C. The blank reactor was prepared using the same procedure as above but no enzyme was added.

### 2.3. Microorganism and culture conditions

The microorganism used in the study was *Lactobacillus delbrueckii* ATCC 9649. The cells were maintained on MRS agar plate at 4°C and reinoculated weekly.

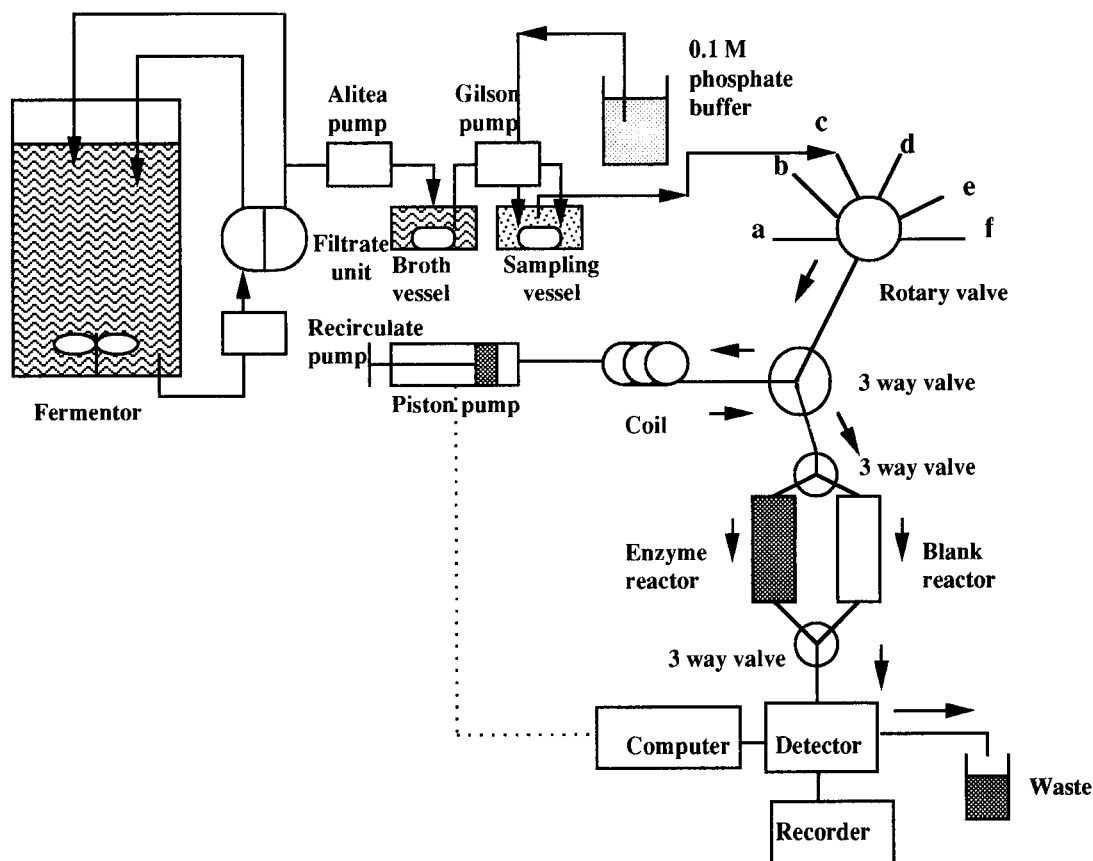


Fig. 1. Schematic representation of the sequential injection system and sampling unit.

#### 2.4. Media and growth condition

The medium used for this study had the following composition in g/l: glucose, 20; yeast extract, 15.0 (Difco, Detroit, MI); tryptone, 1.0 (Difco);  $\text{KH}_2\text{PO}_4$ , 1.0;  $\text{K}_2\text{HPO}_4$ , 1.0;  $\text{CH}_3\text{COONa} \cdot 3\text{H}_2\text{O}$ , 2.0; sodium citrate, 1.0; trace elements in mg/l:  $\text{MgSO}_4 \cdot 7\text{H}_2\text{O}$ , 100;  $\text{MnSO}_4 \cdot \text{H}_2\text{O}$ , 6.2;  $\text{FeSO}_4 \cdot 7\text{H}_2\text{O}$ , 4.0.

The cells were grown in a fermentor (Novaferm, Malmö) with an initial volume of 3 l. The inoculum used was 200 ml of 15 h culture of *L. delbrueckii*. The cultivation temperature was 37°C and the pH was maintained at 6.3 by titration with 3 M NaOH. The stirrer speed was kept at 150 rpm.

#### 2.5. Off-line analysis

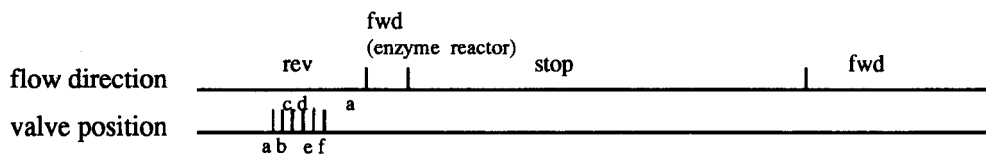
The sample of broth was taken regularly directly from the fermentor and the sampling vessel (see Fig. 1) during fermentation and kept in a freezer until anal-

ysis. Cell growth was monitored by measuring absorbance at 620 nm. Glucose was determined by a modification of the dinitrosalicylic method [19]. Cell free supernatants were prepared by centrifugation of samples and then, placed in 80°C water bath for 15 min to stop the enzymatic reaction before dilution. D- and L-lactic acid was measured by the Boehringer enzymatic kit, that measures the amount of NADH generated when incubating the sample with  $\text{NAD}^+$  and enzyme [20].

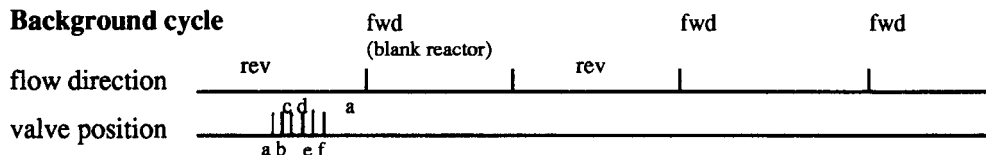
#### 2.6. On-line analysis

The schematic representation of the set-up including the SIA system and filtration sampling devices for on-line D-lactate analysis is shown in Fig. 1. A recirculation pump (Watson-Marlow 520S, Falmouth), a filtration unit with cellulose acetate filter (Sartorius; pore size, 0.2  $\mu\text{m}$ , surface area 63.6  $\text{cm}^2$ ), a filtrate pump (Alitea C-4, Uttran, Sweden) and a dilution

### Sample and calibration cycle



### Background cycle



Time →

### Sequence order, valve position: a-f

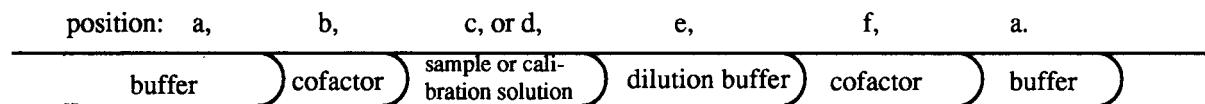


Fig. 2. Schematic representation of time lapses and sequential order of reagents in a measuring cycle (for details see text).

pump (Gilson, Minipuls 2). The broth from the fermenter was continuously circulated (1300 ml/min) through the filtration unit. The cell free permeate was pumped (69 ml/h) from the filtration unit to a small reservoir from which a continuous stream of the broth was pumped to a dilution unit where mixing with an equal volume of 0.1 M phosphate buffer pH 7.0 took place. The mixing of broth and buffer was done by pumping the broth and the buffer towards each other in identical tubings by the same pump up to the mixing point. The volume of the reservoir for filter broth was 0.8 ml. The overflow broth was removed by means of a pump operated at a high flow rate. Homogeneity in the sample was created by stirring with magnetic stirrer. The diluted sample was analysed using the SIA system. The time delay from fermenter to analysis is around 6 min. The SIA system was described earlier [9] and a little modification was made. It was constructed by a dual-piston, sinusoidal flow pump (Alitea AB, Uttran, Sweden); a six-port rotary valve (Cheminert 4162510, Valco instruments, Houston, TX); a three-way slider valve with pneumatic actuator (Rheodyne, 5300 and 5301, Cotati, CA); and a spectrophotometer (Shi-

madzu, UV-120-02, Kyoto) equipped with a 30  $\mu$ l dead volume and 10 mm light path flow-through cuvette (Hellma, Model 178.711, Müllheim/Boden) for absorbance measurements. NADH was monitored by measuring the absorbance at 340 nm. All the tubings connecting the different units were made of PTFE (0.8 mm i.d.). The holding coil, having a volume of 2 ml, served as a buffering volume to prevent the sample and the different reagents used from entering the syringe pump. A blank column without enzyme loading was used to correct for the blank absorbance from the broth. The on-line analysis is controlled by a program involving one blank cycle through the blank column and one calibration cycle per 5 sample cycles. The concentration of calibration solution is 5 mM. The time lapse of the measuring cycle of sample, calibration and the cycle of background with the sequence order is shown in Fig. 2. The total time for one analysis is 182 s including 90 s incubation time while the flow is stopped when the sample is in the column of immobilized enzyme. The blank absorbance was checked by a blank column with a similar measuring procedure as that for sample analysis (see Fig. 2). However, since no significant differ-

ence was observed in the reading while varying the length of incubation time when analysing samples in the blank reactor, the incubation time was omitted. The two reactors were washed for a short time in order to reduce any accumulation of material causing a background signal and to prevent clogging of the reactors. The measuring cycle is almost the same as previously used but with a modification for calibration solution aspiration and use of a blank column for background correction (for details see Ref. [9]). The principle of the SIA system is to suck the reagents into the system as small liquid segments in a desired order (Fig. 2). When all reagents have entered the system, a valve is switched, the flow is reversed and the reagents are forced through the reactor. In this case, the flow was stopped for a certain period in order to increase the conversion, and thus to improve the sensitivity of the analysis. The aspirated volume of wash/carrier buffer,  $\text{NAD}^+$ , sample or calibration, dilution buffer,  $\text{NAD}^+$ , and carrier buffer here are, 1.4, 0.2, 0.1, 0.1, 0.19 and 0.19 ml, respectively. During the whole study, the rate of pump setting was 20 rpm and the arc of cam was driven from 50 to 135 degree, corresponding to the syringe setting from 2.1 to 4.2 ml with an average flow rate of 3.2 ml/min. It is to be noted that the pump was stopped whenever the valve was being turned, in order to prevent the pressure from building up which would otherwise effect the reproducibility. Furthermore, for better reproducibility, the computer control is inevitable. The software is used to control the pump and valve movements in the measuring process and to handle the data from detector [20]. A micro-switch inside the pump was used to terminate the pumping processes in every analysis cycle (i.e., the starting position of every cycle is the same) to prevent any time errors from being accumulated during a long series of measurement.

The automated SIA is based on a personal computer with a four-channel digital input/output board (MetraByte, DAS-8PGA, Taunton, MA) which was used to expand the communication between the computer and the external devices. The valves and the pump are digitally monitored by computer via a driver circuit (Epipactis, Lund). These valves are activated by an electromagnetic valve (Festo, MZH-5/2-1.5-L-K, Esslingen). The pneumatic pressure was kept at about 7 bar. The analog output signals from the spectrophotometer were fed via a DC-amplifier to the computer by

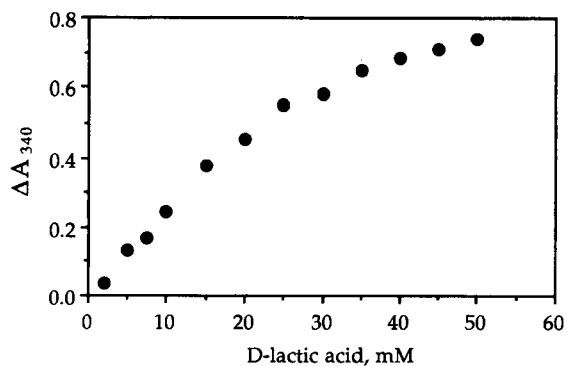


Fig. 3. Calibration curve of the on-line SIA system for D-lactate analysis; measuring conditions: 0.1 M glycylglycine with 0.07 M glutamate pH 10 and 4 mM  $\text{NAD}^+$ , 90 s incubation time.

which peak width and peak height were calculated and baseline could be adjusted automatically.

### 2.7. Measuring conditions

The conditions found optimal in our earlier study were applied here with 0.1 M of glycylglycine buffer including 70 mM glutamic acid as carrier buffer at pH 10, 4 mM  $\text{NAD}^+$  in glycylglycine buffer solution and 90 s incubation time.  $\text{NAD}^+$  solution was prepared fresh daily.

## 3. Results and discussion

Before applying the sensor system for fermentation monitoring, some calibration studies were performed.

### 3.1. Sensor calibration

A calibration curve of 2–50 mM D-lactic acid is shown in Fig. 3. A linear relationship between response and concentration was seen in the range from 2 to 25 mM which at higher concentrations levelled off. Substrate inhibition may be a reasonable explanation for this deviation. However by operating with a sequential enzyme reaction a much better sensitivity and operational range was achieved. The detection limit is around 1 mM which is higher than the original system due to the smaller amount of sample being used and a higher background of the samples of the fermentation broth.

During the on-line measuring, the response of the SIA system was found to slowly decrease. This was

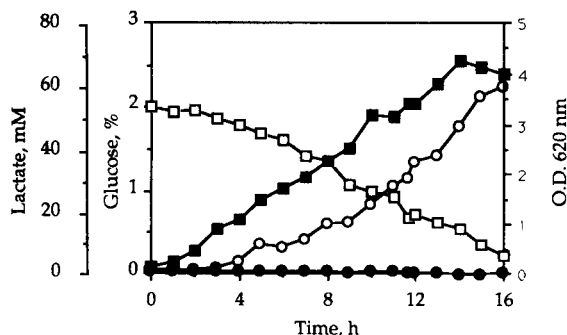


Fig. 4. Profile of the consumption of glucose (□), cell growth (■) and the D-lactate (○), L-lactate (●) production measured off-line by the Boehringer enzymatic kit during fermentation process.

interpreted as being mainly due to the inactivation of the enzyme sequence and partly because of the deactivation of the  $\text{NAD}^+$  cofactor in alkaline solution. To measure this decrease in response, a standard solution of D-lactate was used to calibrate the sensor throughout the fermentation. After an initial period of three assay cycles, we found that the decrease was quite constant with approximately 1% per hour. In addition, a slight increase of the background response was seen during the on-line monitoring as a result of the changes in the

broth during a fermentation process. Both the factors, the decrease in response of standard solution and the increase of background were taken into account when calculating the D-lactate concentration in the fermentation broth.

### 3.2. Cultivation of *L. delbrueckii*

A complete cultivation cycle of *L. delbrueckii* was followed by off line analysis. A profile of the glucose consumption, cell growth, and the concentration of the L- and D-form of lactic acid during fermentation is shown in Fig. 4. A maximal cell growth was seen after about 14 h. This corresponds to nearly total consumption of glucose and also maximal level, ca. 60 mM, of D-lactic acid in the broth. L-Lactic acid remained at very low concentration about 1 mM in the initial stages and decreased with time during the fermentation. *L. delbrueckii* ATCC 9649 produces mainly D-form of lactic acid.

### 3.3. On-line analysis

Typical SIA peaks registered during a fermentation in the time period of 400 to 600 min after inoculation

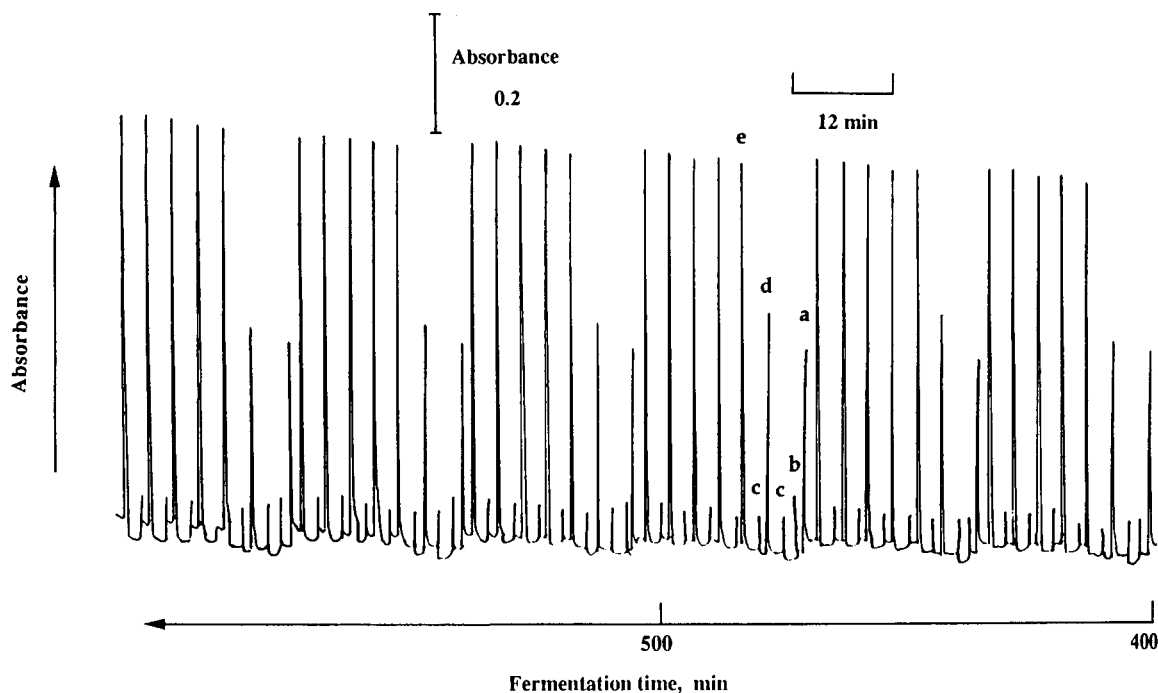


Fig. 5. 42 SIA sequential peaks in chart recorder acquired during the on-line monitoring of D-lactic acid production in *L. delbrueckii* ATCC 9649 batch fermentation at 400–600 min after inoculation, (a) background peak, (b) washing peak, (c) initial peak, (d) calibration peak, (e) sample peak.



were recorded on a chart recorder as shown in Fig. 5. The profile shows a background peak (a) generated by the background cycle together with two smaller overlapping ones (b) which were created by washing the enzyme and blank reactors respectively with buffer in the latter step of the background cycle. Then, also shown is a calibration peak (d) followed by a peak caused by improper mixing between adjacent liquid segments (c). The initial peak was caused by the mixture of leading  $\text{NAD}^+$  and the carrier buffer passing through detector. Five sample peaks (e) together also with the initial peak (c) then appeared later after the calibration peak (d). A steady increase of the response signal of sample peak was seen during the fermentation corresponding to the increase of D-lactate in the broth. A slight decrease of the calibration signal can also be observed. A very reproducible shape of the peaks can be seen and shows that the SIA system works properly.

In a preliminary study, non-diluted broth was used directly in the SIA system but the enzyme reactor was clogged after 11 h of operation (data not shown). If the broth was diluted twice, no significant clogging in the reactor was observed during 16 h of operation. However, a little pressure build-up still remained in the reactor because it took one or two seconds longer to expel all the washing buffer in the measuring cycle. Anyhow, it did not affect the SIA system because a spare time for washing step was made in programming to compensate for this effect. A 182 s time lapse is long enough to eliminate this problem.

Theoretically, it is easy to change the dilution ratio by modifying the amount of sample and the dilution solution within the aspiration step when too high a concentration of sample is introduced. However, in this study, we used a computer program developed for the another application [21] and the software for controlling of the pump and valve was not up-graded enough to be used for this purpose. Thus, the dilution procedure was instead made in the sampling system. Furthermore, one of the possible benefits to use the SIA system is that the flexibility to increase or to decrease the incubation time gives the method a larger dynamic range. Thus, SIA may be well suited to apply when monitoring processes involving large concentration changes during the cultivation. Such situations may appear, e.g., when recombinant microorganisms or high producing strains of bacteria are used. Thus, SIA has a potential that was not exploited here to manipulate the sampling volume

Table 1  
Comparison of SIA with the Boehringer enzymatic method for D-lactate analysis

Item	SIA	Boehringer test kit
Sampling	Automated	Manual
Sample pretreatment	Filtration and dilution	Centrifugation and dilution
Enzyme	D-LDH + ALT <sup>a</sup>	D-LDH + ALT
Detection	Spectrophotometer	Spectrophotometer
Analysis	On-line	Off-line
Reagent consumption	Enzyme and cofactor saving	Free form of enzyme
Time needed per sample	≈ 3 min	≈ 30 min
Note	Required sophisticated computer and software	–

<sup>a</sup> D-LDH + ALT = D-lactate dehydrogenase + L-alanine aminotransferase.

as a function of the previous reading. Hereby, the linear or the most precise and reproducible range can be kept in order to enhance the precision of the measurement. By fully exploiting the potential of SIA, extra dilution steps become superfluous and this will then reduce the need for equipment to perform the analysis. Anyway, in the study presented here, a less advanced computer program was used.

### 3.4. Comparison of the analysis systems

The advantages to use the SIA system compared with FIA have been discussed earlier [9]. A comparison of the on-line SIA method with the off-line Boehringer method is made in Table 1. Both methods are based on the same enzyme sequence, D-LDH and L-alanine aminotransferase (ALT) but in the former an immobilized preparation of enzyme is used in a small reactor and in the latter free enzymes are used. Besides convenience, higher throughput and less consumption of cofactor are the main advantages of the SIA system. Certainly, the on-line monitoring to acquire quick information of the fermentation is also a dramatic difference between two methods. The D-lactate concentration determined on-line with the SIA system was compared with the reading from the off-line sample from the dilution vessel determined by the Boehringer method. A fairly good agreement was obtained as seen in Fig. 6. D-lactic acid was produced slowly during the first 4 h and then

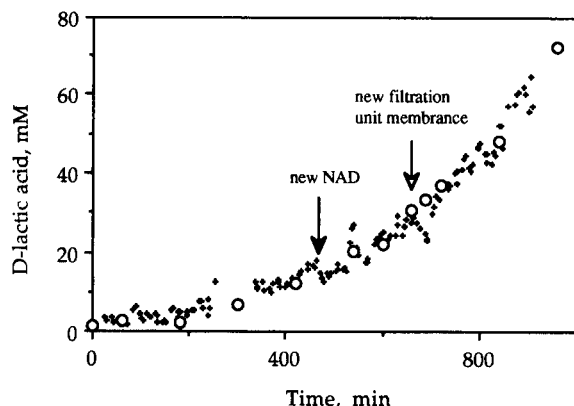


Fig. 6. D-Lactic acid content during fermentation as determined by on-line SIA system (+) and by off-line Boehringer enzymatic kit (O) sampling from the sampling vessel.

increased steadily until 14 h. The agreement between off-line samples from the sampling vessel and on-line data is better than when comparing with off-line data from the fermenter. Usually the concentration measured after correction for dilution is higher in the sampling vessel than that in the fermenter (Fig. 7). There are several possible explanations. Maybe more D-lactate was produced during the transport from the fermenter to the filtration unit or even inside the filtration unit. Cell mass accumulated at the surface of the membrane in the filtration unit as the process proceeded. However, there was no significant concentration decrease in lactate concentration monitored when a new membrane was introduced in the middle of the fermentation. Still another possibility involves further metabolism in the off-line sample where cells were still

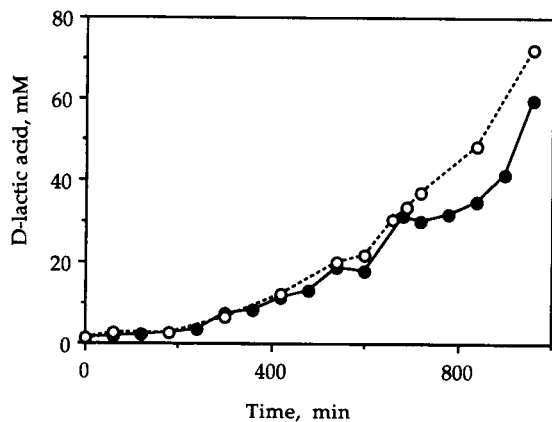


Fig. 7. D-Lactate concentration in off-line samples from the fermenter (●) and sampling vessel (○) determined by the Boehringer enzymatic kit method during fermentation process.

present during the period from sampling until analysis. If samples of undiluted broth were used in the system as in the preliminary study, a lower concentration of D-lactate (ca. 25–35%) in on-line system is observed than that in the off-line data when the broth concentration is higher than 25 mM (data not show). This is quite reasonable because the dilution ratio in off-line method is much larger than that in SIA system. The results clearly show that substrate inhibition takes place. Hence, a two times dilution was chosen in order to get a concentration of D-lactate from fermentation that suited the sensitivity of the analytical system. The present study has demonstrated that SIA may be a powerful and versatile technology for on-line monitoring during fermentation processes. A prerequisite is though that proper sampling and sample handling technology is used. The flow system is from many aspects ideal to meet such requirements.

#### 4. Conclusions

It is yet too early to make a fair comparison between the different on-line technologies since the optimization of the SIA system has not been done sufficiently and not enough cases have been evaluated. The present study shows clearly that SIA technology is promising to monitor D-lactic acid production on-line during the fermentation process.

#### Acknowledgements

The authors wish to thank Dr. Rajni Kaul for linguistic advice. Part of this work was supported by The National Swedish Board for Technical and Industrial Development (NUTEK) and The Swedish Agency for Research Cooperation with Developing Countries (SAREC). H.-C.S. was supported by The Educational Ministry of Taiwan.

#### References

- [1] S.A. Robrish, M.A. Curtis, S.A. Sharer and W.H. Bowen, *Anal. Biochem.*, 136 (1984) 503.
- [2] K. Buchta, in H.J. Rehm and G. Reed (Eds.), *Lactic acid. Biotechnology*, Vol. 3, Verlag Chemie, Weinheim, 1983 pp. 409–418.

- [3] E.S. Lipinsky and R.G. Sinclair, *Eng. Prog.*, 82 (1986) 26.
- [4] A. Demirci and A.L. Pometto, *J. Ind. Microbiol.*, 11 (1992) 23.
- [5] B.D. Pablo, M.A. Asensio, B. Sanz and J.A. Ordonez, *J. Appl. Bact.*, 66 (1989) 185.
- [6] V.M. Yabannavar and D.I.C. Wang, *Biotechnol. Bioeng.*, 37 (1991) 544.
- [7] T.B.V. Roy, H.W. Blanch and C.R. Wilke, *Biotechnol. Lett.*, 8 (1982) 483.
- [8] S. Girotti, S. Ghini, G. Carrea, R. Bovara, A. Roda and R. Budini, *Anal. Chim. Acta*, 255 (1991) 259.
- [9] H.-C. Shu, H. Håkanson and B. Mattiasson, *Anal. Chim. Acta*, 283 (1993) 727.
- [10] S. Ohmori and T.J. Iwamoto, *J. Chromatogr.*, 431 (1988) 239.
- [11] J. Nielsen, K. Nikolajsen, S. Benthin and J. Villadsen, *Anal. Chim. Acta*, 237 (1990) 165.
- [12] K. Schügerl, *Anal. Chim. Acta*, 213 (1988) 1.
- [13] W. Schuhmann, T. Becker, R. Betken, H.-L. Schmidt, M.B. Leible and A. Albrecht, Continuous determination of glucose and lactate in a mammalian cell culture fermentation process, *Proceedings of Biosensor and Flow Injection Analysis in Bioprocess Control 1992*, Freising, April 6–9, 1992.
- [14] A.M. Almuaibed and A. Townshend, *Anal. Chim. Acta*, 214 (1988) 161.
- [15] J. Ruzicka, G.D. Marshall and G.D. Christian, *Anal. Chem.*, 62 (1990) 1861.
- [16] J. Ruzicka and G.D. Marshall, *Anal. Chim. Acta*, 237 (1990) 329.
- [17] H.-C. Shu, G. Dong, R. Kaul and B. Mattiasson, *J. Biotechnol.*, 34 (1994) 1.
- [18] H.H. Weetall, *Methods Enzymol.*, 44 (1976) 134
- [19] G.L. Miller, *Anal. Chem.*, 31 (1954) 426.
- [20] K. Gawehn, in H.U. Bergmeyer (Ed.), *Methods of Enzymatic Analysis*, 3rd edn., Vol. VI, Verlag Chemie, Weinheim, 1984, pp. 588–592.
- [21] M. Nilsson, H. Håkanson and B. Mattiasson, *Proc. Control Qual.*, 4 (1992) 37.

# Microcalorimetric study of the enzymatic hydrolysis of starch: an $\alpha$ -amylase catalyzed reaction

G. Salieri<sup>a</sup>, G. Vinci<sup>b</sup>, M.L. Antonelli<sup>a,\*</sup>

<sup>a</sup> Department of Chemistry, University of Rome "La Sapienza", P. le Aldo Moro 5, 00185 Rome, Italy

<sup>b</sup> Institute of Merceology, University of Rome "La Sapienza", Via del Castro Laurenziano 9, 00161 Rome, Italy

Received 18 March 1994; revised manuscript received 2 August 1994

## Abstract

Microcalorimetric studies of enzyme activities have been made on the hydrolysis of starch catalyzed by  $\alpha$ -amylase. The best conditions for the hydrolysis of starch in the presence of  $\alpha$ -amylase have been pointed out and the  $\alpha$ -amylase activity was determined by isothermal batch microcalorimetry. The heat changes involved during the hydrolytic reaction can be related to the starch concentrations in a linear way and the heights of the calorimetric curves can be directly related to the amylase activities. Calibration curves were obtained. The new method for starch assay and  $\alpha$ -amylase activity determination is direct, simple, accurate and it needs no pretreatment of the sample or auxiliary reactions. The  $\alpha$ -amylase catalytic activity has also been investigated by microcalorimetry in the presence of some metal ions.

**Keywords:** Catalytic methods; Enzymatic methods; Enthalpimetry; Starch;  $\alpha$ -Amylase

## 1. Introduction

The enzymes belonging to the amylase class represent catalysts which can hydrolytically break the glucosidic bonds on the starch molecule and its derivatives [1]. In food industry these enzymes are largely employed, especially for the production of oven food products [2], glucose syrup [3], food-stuff products [4] and also alcohols and sugars [5]; moreover the amylolytic enzymes are used in paper and draper manufacture [6], for leavening the dough during bread-making [7], in malt saccharification [8] for brewing beer and in the detergents industry [9].

These hydrolytic enzymes act by breaking the glucosidic bonds of higher carbohydrates, by adding water molecules to them and by transforming the polymers

to lower-molecular-weight molecules (oligomers and/or monomers).

Nowadays the carbohydrases appear to be of great interest in food chemistry, because there are no alternative technologies for catalyzed hydrolysis [10].

$\alpha$ -Amylase is particularly capable to break the 1,4-glucosidic bonds of the starch molecule, so that the reaction products show the  $\alpha$ -D-configuration on the C<sub>1</sub> atom of D-glucose. These enzymes act on amylose and also on amylopectin (the two parts of the starch molecule). Therefore, in principle maltose, but also maltotriose and dextrans are produced in the presence of  $\alpha$ -amylases.

$\alpha$ -Amylases can be obtained from animal or microbial sources [2,11]. In the industrial field the enzymes coming from microorganisms (such as *Aspergillus oryzae*, *Bacillus amyloliquefaciens* or *Bacillus licheniformis*) are most commonly used [12,13].

\* Corresponding author.

In all cited applications many efforts are directed to the exact knowledge of the  $\alpha$ -amylase activity and also to its regulation, because the composition of the product mixture depends on the enzyme quantity [14] and moreover the different organoleptic peculiarities of food products are determined by the composition of the oligosaccharide mixture resulting from the enzymatic hydrolysis of starch [15].

The amylase activity has been determined by means of many analytical methods, but this variety causes sometimes confusion in relating the results obtained by different methods. The various methods differ from one another with regard to the analytical criteria, the detecting reaction, the instrumental techniques or in the choice of substrate [16,17].

Among the reported methods we can find the saccharogenic ones that are based upon the variation in the reducing power of the starch solution when its hydrolysis takes place; they are quite accurate but slow and affected by some matrix interferences [18]. Another kind of method exploits the decrease of the characteristic blue colour of the starch-iodine complex during the starch hydrolysis [19]; these methods are quite precise and fast, but they cannot be applied to high levels of activity and sometimes they do not give very accurate results.

Another class of enzymatic methods is represented by two groups: the first, classified as “chromogenic” [20], employs a complex formed by a dye with amylose or amylopectin as substrate; the second one, is an amylolytic reaction combined with other enzymatic reactions in cascade, in order to gain either the redox transformation of nicotinamide-adeninedinucleotide (spectrophotometric detection) [21] or the formation of oxygen peroxide, by means of glucosidase (electrochemical detection by means of biosensors) [22].

All these methods employ detection techniques that are very easy and fast, but often the final results are not reliable because of the accumulation of errors: too many reaction steps combined, many and tedious pre-treatments of the sample, interferences due to several reagents needed [23].

By examining the literature it appears that it is still necessary and useful to develop a new method for determining the amylase activity, which could be a reliable and direct method in order to minimize errors and to obtain accurate and unambiguous results.

Microcalorimetry seems to be a good answer to the above demand, because it allows the direct analysis of the enzymatic reactions and it permits to relate in a very simple way the heat change of reaction to the enzymatic activity or to the substrate concentration.

## 2. Experimental

### 2.1. Materials

All chemicals for the preparation of phosphate buffer and soluble starch solutions were commercial products of analytical grade.

$\alpha$ -Amylase lyophilized enzyme (Sigma, type II-A, from *Bacillus licheniformis*) was stored at  $-20^{\circ}\text{C}$  until used. Fresh solutions were prepared daily and stored at  $0^{\circ}\text{C}$ .

### 2.2. Apparatus

The microcalorimeter used was an isothermal batch instrument [24] of the heat conduction type (LKB Model 2107), equipped with two gold vessels of about 7 ml total volume, a multi-temperature cooling circulator (LKB Model 2209), a control unit (LKB Model 2107-350) and a potentiometric recorder (LKB Model 2210). Each vessel consists of a chamber divided into two compartments (2.5 and 4.5 ml) by an interior wall. The reactants are introduced into the two compartments separately. When the experiment starts the calorimetric drum is rotated, thereby the reactants are mixed and the reaction takes place.

All the equipment was housed in a thermostated room at  $25 \pm 1^{\circ}\text{C}$  and all measurements were made at  $30.00 \pm 0.01^{\circ}\text{C}$ . The calorimetric accuracy was checked by measuring the sucrose dilution heat [25] and the results were in agreement with the literature values within 0.5%.

A Metrohm Model 605 pH meter, equipped with a saturated calomel reference electrode (EA 404) and a glass electrode (EA 109) was used.

### 2.3. Calorimetric measurements

To establish the heat effect of dilution or other undesirable heat effects related to the main enzymatic reaction, preliminary experiments were performed. In the

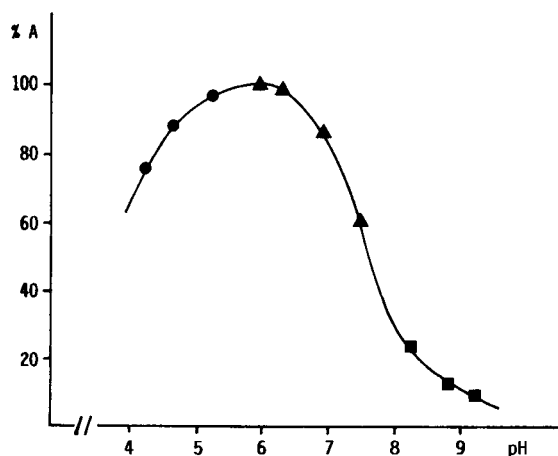


Fig. 1.  $\alpha$ -Amylase activity vs. pH. (●) Acetate buffer, (▲) phosphate buffer, (■) triethanolamine buffer.

case of substrate solutions only, some detectable heat quantity was recorded. In order to eliminate the substrate dilution heat, the experiments were carried out by filling the calorimeter in a differential way, so that all measurements were performed by filling the two compartments of the measuring vessel (detector 1) with 2 ml of enzyme solution and 2 ml of substrate solution, respectively. Meanwhile the reference vessel (detector 2) was filled with 2 ml of buffer and 2 ml of substrate solution.

The best pH conditions were tested by measuring the heat quantity that evolved in the pH 4–9 range obtained by means of three different buffer systems: acetate, phosphate and triethanolamine (Fig. 1).

Sodium and potassium phosphate buffer ( $7 \times 10^{-3}$  M) at pH 5.9 were chosen as the best system.

#### 2.4. Calibration curves

With particular regard to the kinetic conditions, the concentration ranges were suitably varied.

(1) Pseudo zero-order kinetics, with respect to the substrate [26], were obtained by an excess of substrate  $[S] \geq 10K_M$ , where  $[S]$  is the analytical concentration and  $K_M$  is the Michaelis-Menten constant for  $\alpha$ -amylase ( $K_M = 2.2$ – $3.4$  g/l) with the cited substrate [27].

The following conditions were established:  $[S] = 40$  g/l and  $[E]$  varying from 2 to 50 I.U./ml, where  $[E]$  is the  $\alpha$ -amylase activity (1 I.U. is the amount of enzyme which produces 1  $\mu$ mol of maltose in 1 min at  $30^\circ\text{C}$  in  $7 \times 10^{-3}$  M sodium and potassium phosphate

buffer at pH 5.9 using soluble starch as substrate). It must be noticed that this unit also accounts for the transferase activity.

The considered calorimetric quantity ( $\Delta_{\max}$ ) is the maximum deviation of the experimental curve (thermopile voltage vs. time) and the calibration curve was obtained by plotting  $\Delta_{\max}$  vs. enzymatic activity.

(2) Pseudo first-order conditions with respect to the substrate were established with an excess of enzyme. The operative conditions were:  $[E] = 300$  I.U./ml and  $[S]$  varying from 1 to 60 g/l.

The considered calorimetric quantity, in this case, is the area ( $A$ ) under the experimental curve (thermopile voltage vs. time).

The area ( $A_i$ ) of the calorimetric signal is directly proportional to the heat quantity ( $Q_i$ ) evolved during the hydrolysis of the substrate quantity ( $S_i$ ):

$$Q_i = \epsilon A_i \quad Q_i = \alpha [S_i]$$

where  $\epsilon$  is an instrumental constant and  $\alpha$  is the slope of the calibration curve ( $Q_i$  vs.  $[S_i]$ ).

All the experiments were run twice and the reported data (heights and areas) are the average values resulting from three measurements on the recorded curves.

All concentrations refer to the reagents in the calorimetric vessels before mixing.

Each analysis takes about 30 min, a large part of the time being necessary for equilibrating the temperature inside the calorimeter after filling.

### 3. Results and discussion

#### 3.1. $\alpha$ -Amylase activity

The calibration graph for measuring the amylase activity is shown in Fig. 2. The correlation between the enzymatic units and the calorimetric quantity ( $\Delta_{\max}$ ) is linear up to 35 I.U./ml; at higher activities a negative deviation is observed, probably due to a variation in the reaction kinetics. In fact the reaction goes from a zero order to a complex order kinetics at high levels of enzymatic units in the reaction batch.

In the linear range of the curve the kinetic order remains constant (pseudo zero-order due to the excess of substrate) the reaction rate is the sole factor responsible for the calorimetric output. Therefore, by increasing the amount of enzymatic units, the heat variations

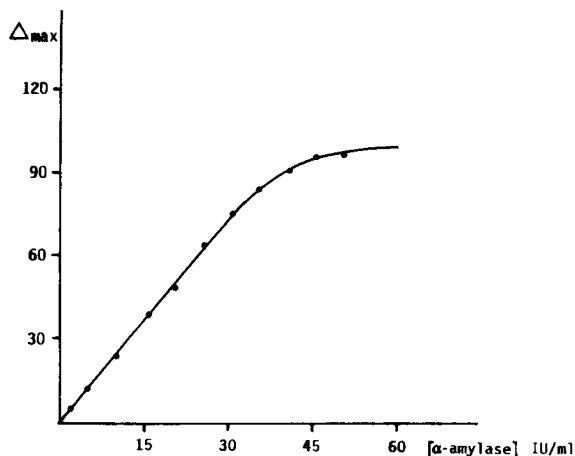


Fig. 2. Calibration curve for  $\alpha$ -amylase activity determination.  $T=30^{\circ}\text{C}$ , pH 5.9, phosphate buffer, [starch] = 40 g/l.

are high enough to be directly related to the amylase activity. The lower detectable limit of  $\alpha$ -amylase activity is 2 I.U./ml.

### 3.2. Substrate determination

The calibration graph useful for starch determination is plotted in the Fig. 3. The measured heat quantities ( $Q_i$ ) are directly proportional to the substrate concentration in the standard solutions and the relationship is linear in a wide range of concentrations.

At high molar levels of starch the negative deviation from linearity observed is caused by some problems due to precipitation phenomena occurring inside the calorimetric vessels during the equilibrating time. Moreover, inhibition from products could take place, because in the calorimetric methodology the reaction products remain in the vessel, while the enzymatic products are generally transformed by auxiliary reactions used in other analytical methods. Nevertheless, the reported method is suitable to analyze starch in the concentration range between 1 and 50 g/l.

### 3.3. Enzymatic catalysis in the presence of effectors

It is known that calcium ions stabilize the active form of the  $\alpha$ -amylase enzyme in the reaction medium [28]. At high temperature this phenomenon becomes more and more evident ( $65\text{--}75^{\circ}\text{C}$ ) [29]. Under the experimental conditions reported here ( $30^{\circ}\text{C}$ ) the stabilizing effect of  $\text{Ca}^{2+}$  ions was indeed weaker.

The presence of other metal ions (especially bivalent ones) exerts a relevant inhibition on the  $\alpha$ -amylase activity.

The effects of eight different ions have been studied with special regard to the amylase activity. The results are summarized in Fig. 4. From the graph relative to each metal ion, the inhibition trend can be deduced: in particular the ion quantity necessary for the beginning of the inhibition and for complete inhibition are determined.

As can be seen the ions can be divided into two classes according to their relative effects upon the  $\alpha$ -amylase efficiency. The first class inhibitors  $\text{Hg}^{2+}$ ,  $\text{Cu}^{2+}$ ,  $\text{Ag}^{+}$  and  $\text{Cd}^{2+}$  reach 100% inhibition at quite low concentration levels; the second class inhibitors  $\text{Zn}^{2+}$ ,  $\text{Mn}^{2+}$ ,  $\text{Co}^{2+}$  and  $\text{Ni}^{2+}$  show a lower inhibiting effect at higher concentration levels. In particular, our results have shown that the inhibitory effect could be ascribed to a direct interaction between the metal ion and the protein rather than to a complex formed by the ion and the substrate, in fact this is confirmed by the literature because similar effects have been noticed in the presence of the same ions with different substrates [28,30].

The inhibitory or stimulatory effects of several ions reported in the literature [28–31] are in general very different and sometimes contradictory. Our results do not completely agree with previously reported results either. In fact the sensitivity of the microcalorimetric technique allows to measure very small variations in the enzymatic efficiency [32] occurring in the presence

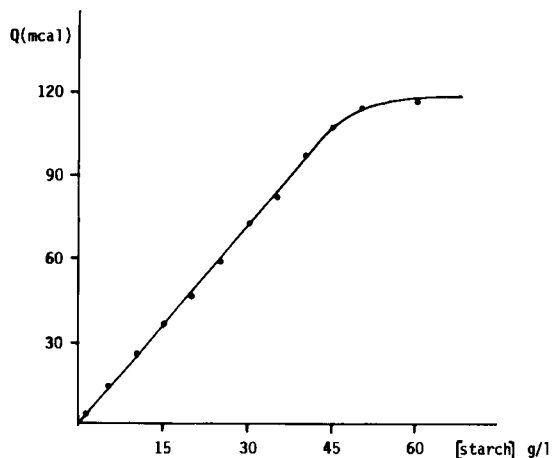


Fig. 3. Calibration curve for starch assay.  $T=30^{\circ}\text{C}$ , pH 5.9, phosphate buffer, [ $\alpha$ -amylase] = 300 I.U./ml.

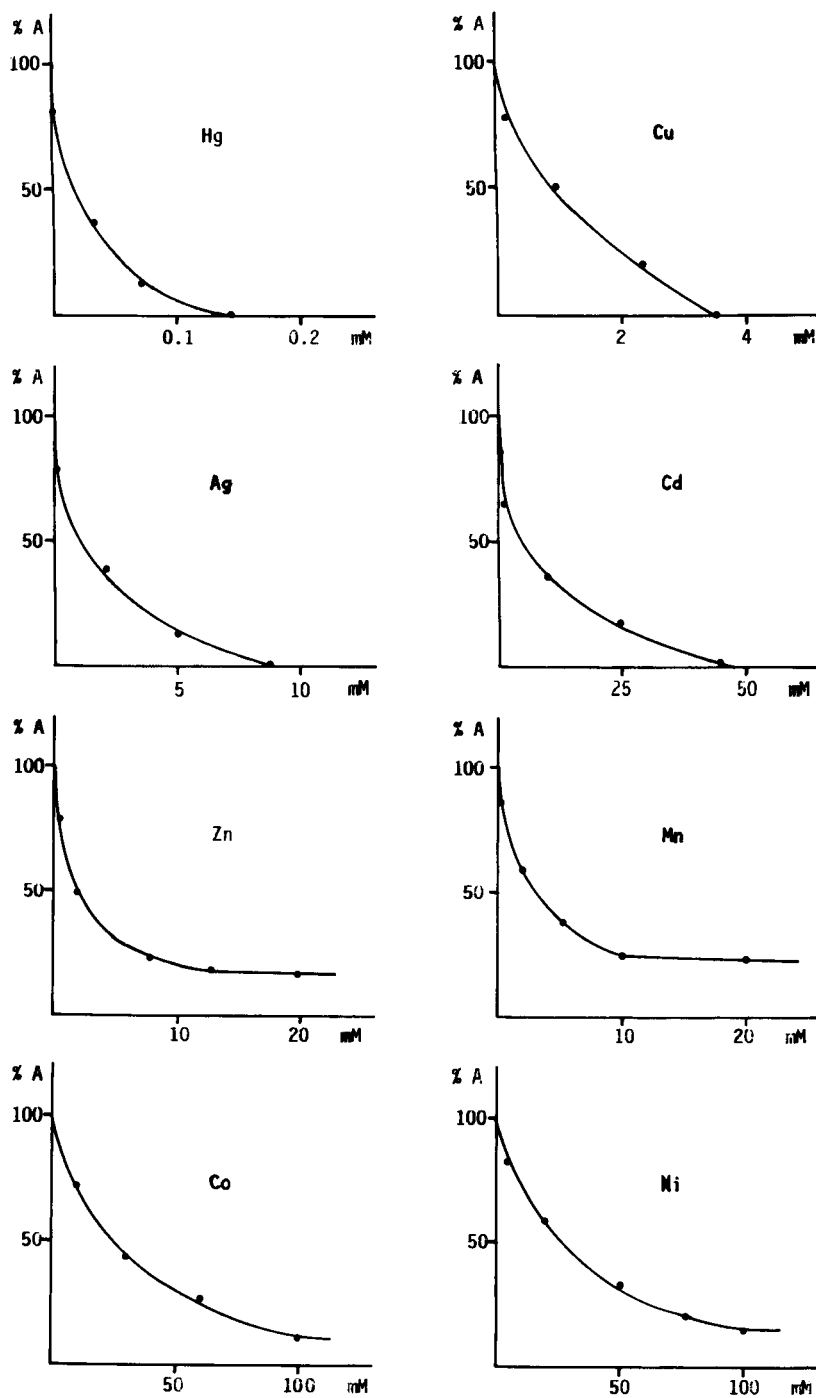


Fig. 4. Inhibition effects of metal ions upon the  $\alpha$ -amylase activity in the starch hydrolysis.  $T = 30^\circ\text{C}$ , pH 5.9, phosphate buffer, [starch] = 40 g/l, [ $\alpha$ -amylase] = 20 I.U./ml.

of very low concentrations of inhibitors. Maybe the direct relationship between concentration and signal of

the main enzymatic reaction, without other enzymatic auxiliary reactions, is the true cause of the fact that in



some cases higher ion levels have been found in the amylase inhibition with respect to those reported in the literature.

Moreover, it must be noticed that no interactions among the metal ions and the buffer ions can impair the calorimetric results, because the measurements are performed in a differential way. With respect to the inhibitory effect of some anions, such as citrate and oxalate [30] for example, we have found only a weak effect on the  $\alpha$ -amylase enzyme in the concentration range investigated ( $10^{-2}$ – $6 \times 10^{-1}$  M).

## References

- [1] M.V. Ramesh and B.K. Lonsane, *Biotechnol. Lett.*, 11 (1989) 649.
- [2] R.V. McAllister, *Adv. Carbohydr. Chem. Biochem.*, 36 (1979) 15.
- [3] T. Iwata and M. Ohnishi, *Starch/Staerke*, 42 (1990) 147.
- [4] R.M. Faulks and A.L. Bailey, *Food Chem.*, 36 (1990) 191.
- [5] T. Hoshino, *J. Ferm. Bioeng.*, 69 (1990) 228.
- [6] D. Wankhede, *Starch/Staerke*, 41 (1989) 123.
- [7] P. Colonna and J.L. Barry, *J. Cereal Sci.*, 11 (1990) 59.
- [8] V. Vlaev, *Chem. Eng. J.*, 44 (1990) 1351.
- [9] G. Jensen, *Tenside Superf. Deterg.*, 27 (1990) 30.
- [10] L.J. Denault and L.A. Underkofler, *Cereal Chem.*, 40 (1963) 618.
- [11] E.H. Fischer and E.A. Stein, *Enzymes*, 4 (1960) 313.
- [12] F.C. Mayer and J. Lerner, *J. Am. Chem. Soc.*, 81 (1959) 188.
- [13] S. Sen and P. Oriel, *Biotechnol. Lett.*, 11 (1989) 789.
- [14] E.J. Pyler, *The Baker Digest*, 2 (1969) 36.
- [15] A. Bourdet, *Am. Technol. Agr.*, 10 (1961) 301.
- [16] C. Larsen, *J. Clin. Chem. Clin. Biochem.*, 21 (1983) 45.
- [17] R. McCroskey, T. Chang, H. David and E. Winn, *Clin. Chem.*, 28 (1982) 1787.
- [18] K. Lorentz, *J. Clin. Chem. Clin. Biochem.*, 17 (1979) 499.
- [19] H.V. Street and J.R. Close, *Clin. Chim. Acta*, 1 (1956) 257.
- [20] M. Ceska, K. Birath and B. Brown, *Clin. Chim. Acta*, 26 (1969) 437.
- [21] W.H. Porter and R.E. Roberts, *Clin. Chem.*, 24 (1978) 1620.
- [22] G. Vinci, M.L. Antonelli, F. Botrè, G. Mele and G. Ruggieri, *Atti XVI Congresso Nazionale di Merceologia*, Pavia, 1–3 September, 1994.
- [23] L. Spandrio, *Analisi Biochimico Cliniche*, Piccin, Padova, 1991 p. 172.
- [24] P. Monk and I. Wadso, *Acta Chem. Scand.*, 22 (1968) 1842.
- [25] I. Wadso, *Acta Chem. Scand.*, 22 (1968) 927.
- [26] J.K. Grime, in J.K. Grime (Ed.), *Analytical Solution Calorimetry*, Wiley, New York, 1984, p. 312.
- [27] N.E. Welker and L.L. Campbell, *J. Bacteriol.*, 94 (1967) 1124.
- [28] T. Krishnan and A.K. Chandra, *Appl. Environ. Microbiol.*, 46 (1983) 430.
- [29] N. Ramasesh, K.R. Sreekantiah and V.S. Murthy, *Starch/Staerke*, 34 (1982) 274.
- [30] M.S.A. Safwat, S.A.Z. Mahmoud, R.M. Attia, M. Abd-El-Nasser and F.S. Ali, *Zentralbl. Mikrobiol.*, 138 (1983) 145.
- [31] S.A.Z. Mahmoud, S.M. Taha and R.M. Attia, *J. Bot. U.A.R.*, 11 (1968) 41.
- [32] M.L. Antonelli, V. Carunchio, M. Luciani and G. Vinci, *Thermochim. Acta*, 122 (1987) 95.

# Spectrophotometric determination of catecholamines with metaperiodate by flow-injection analysis

J.J. Berzas Nevado \*, J.M. Lemus Gallego, P. Buitrago Laguna

*Department of Analytical Chemistry and Food Technology, Universidad de Castilla-La Mancha, 13007 Ciudad Real, Spain*

Received 4 May 1994; revised manuscript received 1 August 1994

## Abstract

A flow-injection spectrophotometric method for the determination of adrenaline and isoprenaline, based on the reaction with metaperiodate, is described. The calibration graphs are linear up to  $2 \times 10^{-4}$  M. Flow injection allows the measurement of 120 samples per hour. The method was successfully applied to the determination of both catecholamines in pharmaceuticals.

**Keywords:** Flow injection; Spectrophotometry; Catecholamines; Metaperiodate

## 1. Introduction

Catecholamine drugs are now widely used in the treatment of bronchial asthma, hypertension, heart failure associated with organic heart disease, and cardiac surgery. The determination of catecholamines in biological fluids normally requires the use of trace analysis techniques, mainly chromatography with fluorimetric or electrochemical detection [1]. Catecholamines in pharmaceutical preparations are present in relatively large amounts, and increasing efforts have been directed towards the development of simple and reliable analytical methods.

To avoid interferences that may occur in the determination of 1,2-diphenolic drugs in formulations by direct measurements of the UV absorption, spectrophotometric methods, currently employed, involve the previous conversion of the drugs to coloured derivatives that permit absorbance measurements in the visible spectrum.

Several spectrophotometric methods have been commonly applied, as cited in the literature, and comprise derivatization reactions with organic reagents [2–9] and inorganic agents [10–16]. Some of these methods have been adapted to the stopped-flow technique and flow-injection analysis [17–20].

The purpose of the present investigation was to develop a simple, sensitive and rapid assay for catecholamines (adrenaline and isoprenaline) using a flow-injection system coupled to a colorimetric reaction. The method is based on the oxidation of catecholamine with sodium metaperiodate.

## 2. Experimental

### 2.1. Reagents

All solutions were prepared from analytical-reagent grade materials with distilled, deionized water. Adrenaline and isoprenaline stock solutions ( $1 \times 10^{-3}$  M) were prepared from Sigma product in 0.02 M acetic

\* Corresponding author.

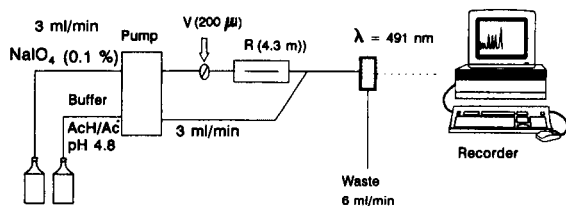


Fig. 1. Schematic diagram of the FI manifold used for the determination of catecholamines.

acid–acetate buffer solution, pH 4.8, and stored at 4°C in a dark bottle before use. Working solution were prepared daily from these solutions by diluting with Milli-Q water. The sodium metaperiodate reagent (0.1%), from Sigma product was prepared by dissolving 1 g in 1 l of distilled deionized water.

## 2.2. Apparatus

A Beckman Instruments DU-70 spectrophotometer connected to an IBM PS/2 and/or a Tandon 386 SX/20 SL II fitted with Beckman Data Leader Software [21] were used for all measurements and treatment of data.

A schematic diagram of the semi-automatic flow-injection analyzer used is shown in Fig. 1.

The flow manifold included a peristaltic pump (Minipuls 3 from Gilson) which pumped both reagent solution (buffer and metaperiodate) at the same flow rates through (polyethylene) flow tubes. The sample was injected into the carrier stream by an injection valve (Omnifit No. 1106) provided with a 200 µl loop. The absorbance peak of the resulting orange compound is followed using the spectrophotometer of the flow-injection analyzer, equipped with a 18 µl flow-cell (Hellma). Data were stored in the computer.

## 2.3. Procedure

### Continuous-flow

200 µl of sample solution containing adrenaline or isoprenaline was injected directly into the oxidant solution (0.1% NaIO<sub>4</sub>) carrier. The solution passed through a reactor (4.3 m length), and the buffer solution (0.05 M acetic acid–acetate buffer, pH 4.8) was added. The solution was carried to the flow cell, and the absorbance recorded.

The variation of absorbance was monitored at 491 nm throughout the reaction. Each solution was assayed

in triplicate. Sixty points per minute were measured. The FIA-graphs were stored in the computer, the graphs were smoothed using 7 experimental points [22] then the baseline was obtained with Data Leader Software, and for every peak the highest was obtained.

## Determination of catecholamines in pharmaceuticals

For solid formulations the official Universal Sampling Procedures were followed. From the final fine powder an accurately weighed portion was dissolved in buffer solution (0.02 M acetic acid–acetate buffer, pH 4.8), so that the concentration of the drugs was in the range of the calibration graphs. By using an ultrasonic bath or a mechanical shaker, the powder was completely disintegrated and the solution was either allowed to settle or it was filtered. For liquid formulations an appropriate dilution with acetate buffer solution (pH 4.8, 0.02 M) was all that was required, after which the procedure described above was carried out.

## 3. Results and discussion

Catecholamines in the presence of sodium metaperiodate are oxidized to the corresponding aminochromes. The absorption spectra of adrenaline and isoprenaline show an absorption maximum at 280 nm. Oxidation by metaperiodate yields two absorption

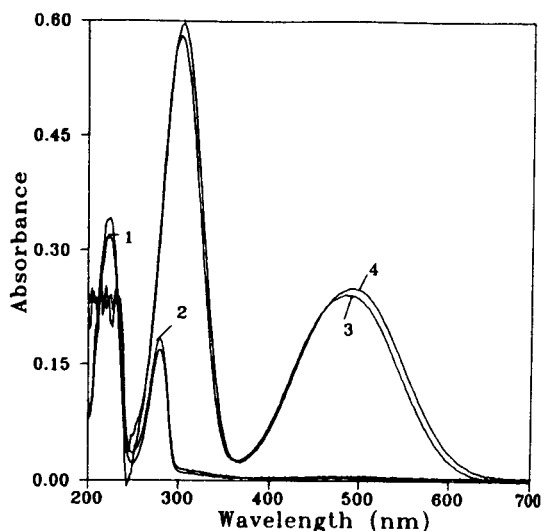


Fig. 2. Absorption spectra (pH 4.8, catecholamine concentration  $6 \times 10^{-5}$  M) of (1) adrenaline, (2) isoprenaline, (3) adrenaline with metaperiodate, (4) isoprenaline with metaperiodate.

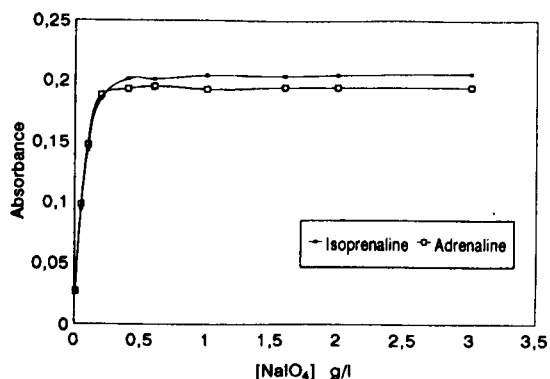


Fig. 3. Influence of metaperiodate concentration.  $\lambda = 491$  nm. Catecholamine concentration  $2 \times 10^{-4}$  M.

maxima at 303 and 491 nm, owing to the production of aminochrome derivatives (Fig. 2). The reaction in acetic medium is slow, but although the reaction sequence is complex the absorbance remains constant at least 30 min after preparation of the solution.

The conditions for the reaction between catecholamines and sodium metaperiodate were tested (temperature, time, order of addition, pH, oxidant concentration, etc.) and then an FI system was designed.

Others catecholamines (dopa, dopamine, methyl-dopa, etc.) interfere. Usually only one catecholamine is present in pharmaceutical preparations. The method may be suitable for adrenaline and isoprenaline determination in medicine. For biological fluids its applicability should be assessed carefully.

### 3.1. Effect of the reaction variables

Both the adrenaline and the isoprenaline system were optimized by changing each variable in turn while keeping all others unchanged. The variables studied were metaperiodate concentration, volume injected, length of the reactor, flow rate and temperature.

The reactants involved in the reaction were mixed in various sequences to determine their optimum distribution on the flow analysis system, the best results were obtained when they were mixed as follows: metaperiodate, catecholamine, buffer solution.

The effect of the concentration of sodium metaperiodate on the absorbance of isoprenaline and adrenaline ( $2 \times 10^{-4}$  M) is shown in Fig. 3. The peak height increased with the metaperiodate concentration up to 0.05 g/l, above which it remained virtually constant.

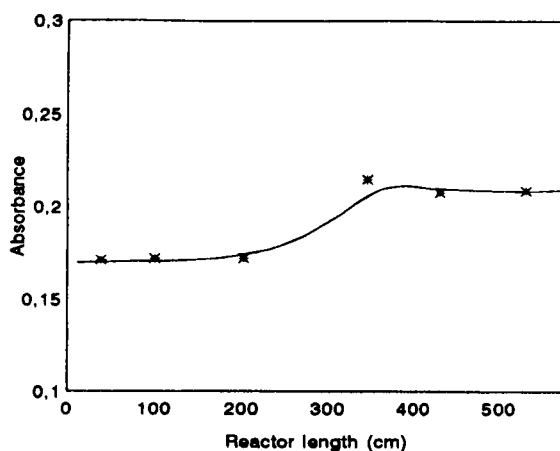


Fig. 4. Absorbance versus reactor length run at 491 nm. Isoprenaline concentration,  $2 \times 10^{-4}$  M.

A 0.1 g/l metaperiodate solution was used as carrier.

The volume injected was varied between 150 and 340  $\mu$ l; 200  $\mu$ l was selected as suitable.

Fig. 4 shows the influence of the length of the reactor on the peak height for isoprenaline, and similar results were obtained for adrenaline. A reactor of 430 cm was selected as appropriate.

Both reagent solutions had were pumped through the reactor at the same flow rates. The flow rate was varied between 1.25 and 4.25  $\text{ml min}^{-1}$ . The optimum flow rate value was 3  $\text{ml min}^{-1}$ .

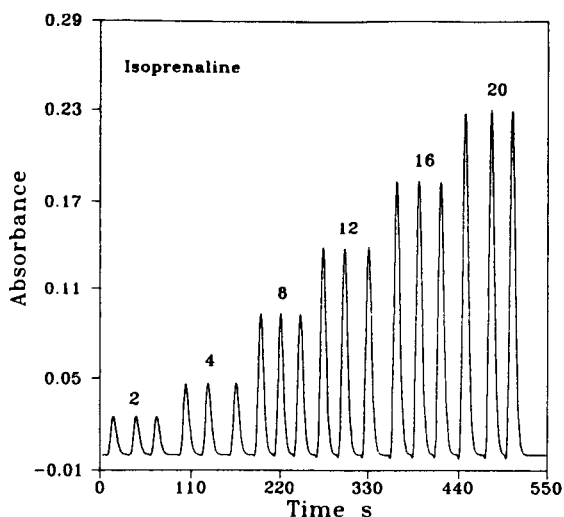


Fig. 5. Typical recorder output for a series of isoprenaline standards under the proposed conditions by de FI technique (numbers above the peak are concentrations in  $\text{M} \times 10^5$ ).

Table 1  
Parameters of the calibration graphs used for the determination of adrenaline and isoprenaline

Catecholamine	S.D. of the slope	S.D. of the intercept	Correlation coefficient	Detection limit (M)	Determination Limit (M)	R.S.D. (%) ( $n = 10$ )
Adrenaline	1.3	$1.6 \times 10^{-4}$	1.0000	$4 \times 10^{-7}$	$2 \times 10^{-6}$	0.435
Isoprenaline	7.3	$8.8 \times 10^{-4}$	0.9999	$8 \times 10^{-7}$	$3 \times 10^{-6}$	0.315

$$I_i = 2.20 \times 10^{-3} + 1146C_i, C_i = \text{isoprenaline concentration (M)}. I_a = 5.91 \times 10^{-3} + 1088C_a, C_a = \text{adrenaline concentration (M)}.$$

The effect of temperature on the system was studied in the range 20–85°C; the systems studied were not affected by temperature variations. Therefore room temperature was selected.

In the determination of the catecholamines a smoothing function based on the Savitzky and Golay algorithm [22] was used and 7 experimental points were considered to be the optimum number for the FI-graphs obtained.

Using the optimized FI scheme, calibration graphs were obtained for isoprenaline and adrenaline (Fig. 5). The useful working range was  $2 \times 10^{-5}$ – $2 \times 10^{-4}$  M, which is suitable for pharmaceutical analysis, although the method permits a linear range between  $5 \times 10^{-6}$  and  $1 \times 10^{-3}$  M.

The linearity of the calibration graphs was excellent. A relative standard deviation (R.S.D.) of less than 0.5 ( $n = 10$ ) was obtained. The sampling rate was 120 measurements  $h^{-1}$ . The results are summarized in Table 1.

### 3.2. Analysis of pharmaceutical preparations

The proposed method was satisfactorily applied to the determination of adrenaline and isoprenaline in pharmaceutical preparations. *Adrenaline*: adrenaline

hydrochloride, 1 mg/ml from Llorente SA (Spain). *Epixtasol*: this product contains adrenaline hydrochloride, 0.5 mg; vitamin P (rutin), 0.2 mg; naphazoline hydrochloride, 0.5 mg; antipyrine, 0.3 mg; and water, 1 g. The product has been made by Medical SA (Spain). *Frenal Compositum*: each pill with 20 mg Cromolyn Sodium; 0.1 mg isoprenaline sulphate; excipient lactose, from Sigma-tau SA (Spain).

The concentrations of the catecholamines were calculated by direct measurements using the appropriate calibration graph. For the standard additions method similar results were obtained.

Commercially available formulations were analyzed and the results obtained are summarized in Table 2. As can be seen, for all the formulations the assay results were in good agreement with values for the nominal contents. The results obtained for adrenaline and isoprenaline for each pharmaceutical are shown in Table 2.

### Acknowledgements

We gratefully acknowledge support from the DGI-CYT of the Ministerio de Educacion y Ciencia (Spain). Project PB 90-0397.

### References

- [1] A.J. Pesce and L.A. Kaplan, S. Bircher (Ed.), *Methods in Clinical Chemistry*, C.V. Mosby, St. Louis, MO, 1987, p. 944.
- [2] I.A. Biruk, V.V. Petrenko and B.P. Zorya, *Farm. Zh. (Kiev)*, 2 (1992) 57.
- [3] M.L. Iskander and H.A.A. Medien, *Microchem. J.*, 41 (1990) 172.
- [4] M.A. Korany, A.M. Wahbi and M.H. Abdel-Hay, *J. Pharm. Biomed. Anal.*, 2 (1994) 537.
- [5] S. Markovic and S. Amrain, *Pharmazie*, 45 (1990) 292.
- [6] M.E. El-Kommos, *Bull. Pharm. Sci.*, 10 (1987) 34.

Table 2  
Determination of adrenaline and isoprenaline in pharmaceutical preparations

Sample	Catecholamine	Nominal value (mg/l)	FIA method <sup>a</sup> found	S.D. <sup>a</sup>
Adrenaline	Adrenaline	1	1.057	0.1207
Epistaxol	Adrenaline	0.5	0.557	0.0045
Frenal Compositum	Isoprenaline	0.1 mg/pill	0.099	0.0084

<sup>a</sup> Average of three determinations.

- [7] A.N. Zakhari, F.B. Salem and M.S. Rizk, *Farmaco Ed.*, 42 (1987) 103.
- [8] M.Q. Al-Abachi, T.A. Al Ghabsha and N.A. Shahbaz, *Microchem. J.*, 31 (1985) 272.
- [9] O. Gerngross, K. Voss and H. Herfeld, *Ber. Dtsch. Chem. Ges.*, 66 (1933) 435.
- [10] F.B. Salem, *Anal. Lett.*, 26 (1993) 1959.
- [11] F.B. Salem, *Talanta*, 34 (1987) 810.
- [12] D.G. Sankar, C.S.P. Sastry and M.N. Reddy, *Indian Drugs*, 28 (1992) 272.
- [13] M.E. El-Kommos, M.A. Fardous and A.S. Khedr, *Talanta*, 37 (1990) 625.
- [14] M.E. El-Kommos, M.A. Fardous and A.S. Khedr, *J. Assoc. Off. Anal. Chem.*, 73 (1990) 516.
- [15] C.S.P. Sastry, R.K. Ekambareswara and U.V. Prasad, *Talanta*, 29 (1982) 917.
- [16] I.B. Prodromos, *Fresenius' J. Anal. Chem.*, 336 (1990) 124.
- [17] N. Rodriguez-López, J. Escibano and F. Garca-Casanovas, *Anal. Biochem.*, 216 (1994) 205.
- [18] M. Carmona, M. Silva and D. Pérez-Bendito, *Analyst*, 116 (1991) 1075.
- [19] C.A. Geogiou, M.A. Koupparis and T.P. Hadjiioannou, *Talanta*, 38 (1991) 689.
- [20] C.A. Geogiou and M.A. Koupparis, *Analyst*, 115 (1990) 309.
- [21] Beckman Instruments, *Spectroscopy*, 2 (1987) 16.
- [22] A. Savizky and M.J.E. Golay, *Anal. Chem.*, 34 (1964) 1627.



ELSEVIER

Analytica Chimica Acta 300 (1995) 299–305

ANALYTICA  
CHIMICA  
ACTA

# Spectrophotometric cell comprising parallel rotating and stationary bioreactors: application to the determination of glucose in serum samples

Julio Raba <sup>a</sup>, Shaofeng Li <sup>b</sup>, Horacio A. Mottola <sup>b,\*</sup>

<sup>a</sup> *Departamento de Química Analítica, Facultad de Química, Bioquímica y Farmacia, Universidad Nacional de San Luis, 5700 San Luis, Argentina*

<sup>b</sup> *Department of Chemistry, Oklahoma State University, Stillwater, OK 74078-0447, USA*

Received 3 May 1994; revised manuscript received 27 July 1994

## Abstract

A spectrophotometric cell comprising parallel bioreactors facing each other and containing immobilized enzyme preparations is described. The lower reactor rotates to minimize diffusional constraints, and the upper reactor is fixed to provide an integrated design for the realization of coupled enzyme-catalyzed reactions. The operating characteristics of the cell are illustrated with the determination of glucose using glucose oxidase [EC 1.1.3.4] and horseradish peroxidase [EC 1.11.1.7] as immobilized enzymes (horseradish peroxidase on the rotating reactor and glucose oxidase on the stationary one). The H<sub>2</sub>O<sub>2</sub> produced in the dissolved-oxygen oxidation of β-D-glucose enters into oxidative coupling in a reaction with *N,N*-dimethylaniline and 4-aminophenazone which is catalyzed by horseradish peroxidase; the absorbance of the colored complex formed provides the basis for monitoring. The cell was incorporated into a continuous-flow/stopped-flow/continuous-flow operation, and the determination was based on the rate of response under stopped-flow conditions. The overall approach was applied to the determination of glucose in standards of human serum and samples of bovine blood serum.

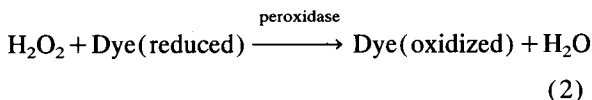
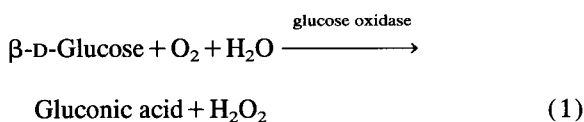
**Keywords:** Spectrophotometry; Bioreactors; Rotating bioreactor; Glucose

## 1. Introduction

The chemistry of enzyme-catalyzed reactions primarily dictates the approach to be used in monitoring the progress of the reaction [1]. In many instances, the main enzyme-catalyzed reaction is coupled with a second (indicator) reaction, and perhaps the most popular of these couplings uses an organic dye in the indicator

reaction. The dye reacts with a product (or the substrate) and the appearance, disappearance, or change in color is monitored spectrophotometrically. Reactions involving oxidases produce H<sub>2</sub>O<sub>2</sub> as one of the products, and the oxidizing power of this species is exploited in the indicator reaction. A very common scheme of this type is routinely applied in the determination of glucose using *o*-dianisidine (3,3'-dimethoxybenzidine) in the coupled indicator reaction:

\* Corresponding author.



The oxidized form of *o*-dianisidine, for instance, absorbs photons in the 460-nm region of the spectrum and permits the monitoring of the progress of the reaction. Implementation of this approach in continuous-flow systems is rather inefficient because of the use of immobilized enzyme preparations in the conventional manner of packed reactors. It has been shown recently, however, that parallel bioreactors facing each other and containing immobilized enzymes provide a convenient, tactical solution to on-line enzyme amplification by substrate cycling [2]. The coupling illustrated above with Eqs. 1 and 2 resembles the situation of coupled enzyme-catalyzed reactions encountered in enzyme amplification and, consequently, can be implemented similarly. Such implementation is illustrated in this paper, which also introduces the design and operating characteristics of a spectrophotometric cell comprising a dual bioreactor system with each reactor facing each other. In this design the lower reactor rotates (to minimize diffusional constraints) while the upper reactor is fixed. This permits efficient utilization of very minute amounts of each immobilized-enzyme preparation (1–2 mg, including inert support) and can conveniently be made part of a continuous-flow/stopped-flow/continuous-flow operation. Because of the extensive use of glucose determination (and the low cost of the enzymes involved) the general scheme illustrated by Eqs. 1 and 2 is used as model to show the implementation of rotation in a dual bioreactor with spectrophotometric monitoring in an integrated reactor/detection cell.

## 2. Experimental

### 2.1. Bioreactor/spectrophotometric cell

Fig. 1 shows details of the bioreactor/spectrophotometric cell. Located in the upper part of the flow cell is a film of double-sided tape (Scotch double-coated tape 665; 3M, St. Paul, MN) to which glucose oxidase

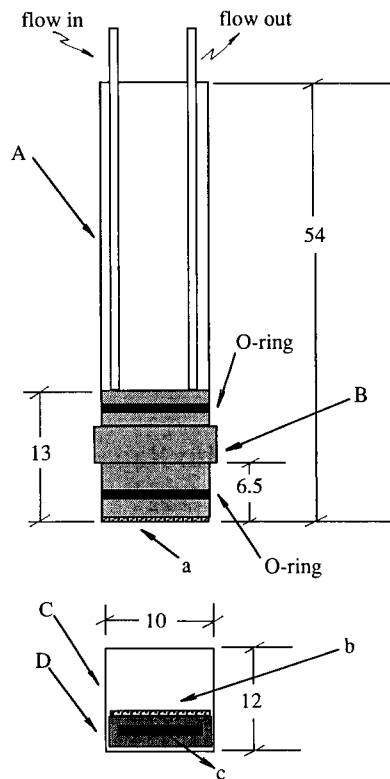


Fig. 1. Schematic representation of the dual bioreactor spectrophotometric cell. (A) Upper cell body (Plexiglass). (B) Intermediate cell body (black Delrin). (C) Lower cell body (borosilicate glass). (a) Fixed bioreactor (film with immobilized GOD). (D) Rotating bioreactor with (b) film with immobilized HRP. (c) Embedded miniature magnetic stirring bar. All measurements in millimeters.

[EC 1.1.3.4] (GOD) immobilized on controlled-pore glass was affixed [3]. The rotating disk, located at the bottom of the cell, contained an embedded micro magnetic stirring bar [3] and a double-sided tape onto which immobilized horseradish peroxidase [EC 1.11.1.7] (HRP) on controlled-pore glass was affixed. The magnetic stirrer and the variable transformer used to control the rotation velocity of the rotating disk, as well as the correspondence between the variable transformer setting and the revolutions-per-minute of the disk have been described earlier [3].

### 2.2. Continuous-flow system

A FIATron SHS-200 microprocessor-controlled solution handling unit (FIATron Systems, Milwaukee, WI) was used for pumping, sample introduction, and stopping of the flow. Fig. 2 illustrates schematically the



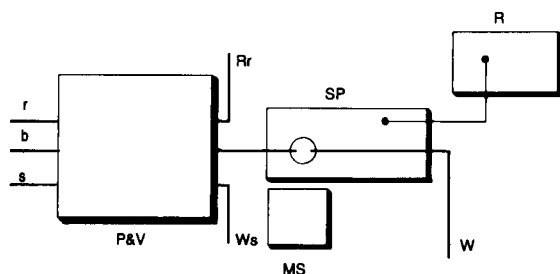


Fig. 2. Block diagram of continuous-flow system and detection arrangement; r and b represent the two intakes of reagents [phosphate buffer solution (0.10 M in total phosphate, pH 6.00), 3.00 mM in 4-aminophenazone and 3.93 mM in *N,N*-dimethylaniline] and carrier buffer solution (0.10 M in total phosphate, pH 6.00), respectively, and s the intake of sample. P and V represent the pump and valve unit (FIATron SHS-200). Ws = Excess sample recycled to the sample reservoir. W = Waste outlet line. Rr represents the line returning the excess reagents solution to the reagent reservoir. SP = Spectrophotometer (Spectronic 21, Bausch and Lomb, Rochester, NY). MS = Magnetic stirrer (custom made to rotate a magnet with a Dayton Model 3M247 motor from Dayton Electric, Chicago, IL); this magnetic stirrer was designed to generate no heat, a problem common with most commercially available stirrers. R = Strip-chart recorder (Model 7128A, Hewlett-Packard, San Diego, CA).

overall configuration of the continuous-flow setup. Tubing inside the FIATron unit was PTFE (0.50 mm i.d.); the pump tubing was Tygon (Fisher AccuRated, 1.0 mm i.d., Fisher Scientific, Pittsburgh, PA), and the rest of the tubing used was 1.0 mm i.d. PTFE (Cole Parmer, Chicago, IL). Table 1 gives the time intervals typically used in the continuous-flow/stopped-flow/continuous-flow operation programmed via the FIATron SHS-200. Individual components of the continuous-flow setup are specified in the legend to Fig. 2.

All pH measurements were made with an Orion Research (Cambridge, MA) Model 601A digital pH meter equipped with an epoxy-body combination electrode (Sensorex, Westminster, CA).

### 2.3. Reagents and solutions

The water used for solution preparation was deionized and further purified by distillation in a borosilicate glass still with a quartz immersion heater. All reagents used, except as noted, were of analytical grade. Glucose oxidase [EC 1.1.3.4] from *Aspergillus niger* (Type VII)  $1.25 \times 10^5$  I.U. per gram of solid and horseradish peroxidase [EC 1.11.1.7] (Type VI), 250–330 I.U. per mg of solid were purchased from Sigma (St. Louis,

MO). Anhydrous D-(+)-glucose (dextrose, corn sugar), *N,N*-dimethylaniline, 4-aminophenazone, Accutrol™ (normal and abnormal lyophilized preparation control standards), and the *o*-dianisidine glucose determination kit (Catalog No. 510-DA) were also from Sigma. Glutaraldehyde (25% aqueous solution) was from Aldrich (Milwaukee, WI). 3-Aminopropyl-modified controlled-pore glass, 1400 Å mean pore diameter and  $24 \text{ m}^2 \text{ g}^{-1}$  surface area, was from Electro-Nucleonics (Fairfield, NJ) and contained  $48.2 \mu\text{mol g}^{-1}$  of amino groups.

### 2.4. Enzyme immobilization

Glucose oxidase (10.0 mg of enzyme preparation in 0.50 ml of 0.10 M phosphate buffer, pH 7.00) and HRP (5 mg of enzyme preparation in 0.25 ml of 0.10 M phosphate buffer, pH 7.00) were immobilized as described earlier [3]. After washing with pH 7.00 phosphate buffer, the preparations were stored in the same buffer at 5°C between uses. The immobilized GOD and HRP preparations were perfectly stable for at least one month and two weeks of daily use, respectively.

### 2.5. Blood samples

Blood samples were taken from Angus x Hereford cattle via venipuncture. To each 10 ml of sample was added 1.25 mg of oxalic acid and the mixtures placed on ice. Upon arrival at the laboratory (and no more than 4 h after extraction), the samples were ultracentrifuged ( $3000 \times g$  for 20 min) in a Sorvall RC 3 ultracentrifuge (Du Pont, Wilmington, DE) and the plasma

Table 1  
Time intervals typically used in the continuous-flow/stopped-flow/continuous-flow operation as programmed via the SHS-200 unit

time interval (s)	Operating conditions	Pump
60	Carrier passed through system until sample introduction	ON
10	sample loading	ON
30	Sample transported by carrier to optimum position in reactor/detection cell	ON
90	Stopped flow cycle repeated for introduction of next sample	OFF

was decanted and stored at  $-20^{\circ}\text{C}$  until the determination of glucose.

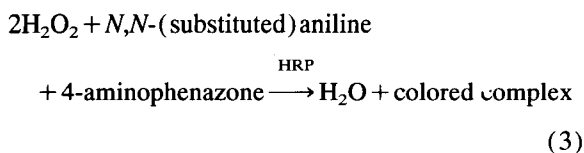
### 2.6. Procedure for the deproteinization of serum

To an aliquot of 0.20 ml of serum were added 1.80 ml of purified water and 1.0 ml of 0.60 M aqueous barium hydroxide. After mixing, 1.0 ml of 0.30 M zinc sulfate was added. After thorough mixing and 2 or more min of standing, the mixture was centrifuged. The supernatant liquid constituted a 1:20 protein-free solution ready for determination.

## 3. Results and discussion

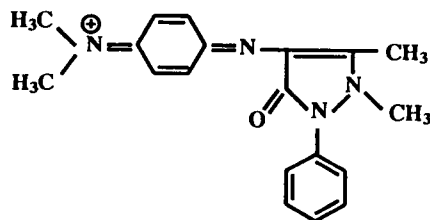
The advantages of bioreactor rotation to minimize or remove the problem associated with the slowing down of reactions in low-dimensional spaces, as is the case with immobilized reagents on porous surfaces, have been illustrated recently [3,4]. The virtues of operating with predominantly convective mass transfer to and from the biocatalyst (enzyme) immobilized on the reactor surface has been illustrated with electrochemical detection [3,4a,4c] and in chemiluminescence monitoring [4b]. More recently the implementation of two reactors for on-line coupling of two enzyme reactions has been reported [2]. In the assembly described here a miniature integrated double enzyme reactor/spectrophotometric cell of very simple construction and of wide adaptability to conventional spectrophotometers is described. The justification for the developmental efforts illustrated with this work is the recognition of the popularity enjoyed by colorimetric monitoring of enzyme-catalyzed reactions involving coupled systems.

Kabasakalian et al. [5] adapted the well known 4-aminoantipyrine method for arylamines [6] to the enzymatic determination of blood glucose. The chemistry involved in their method consists of coupling the reaction illustrated in Eq. 1 with:



an oxidative coupling reaction closely related to diazo

coupling. The colored complex shows a broad absorption band with maximum absorbance at 555 nm and a molar absorptivity of  $2.6 \times 10^4 \text{ M}^{-1} \text{ cm}^{-1}$  based on the probable structure illustrated below [6]:



Although *o*-dianisidine is the most used dye in the scheme of the reaction of Eq. 2, we ruled out its use because it is strongly adsorbed on the immobilized-enzyme-controlled pore glass film, impairing the biocatalytic action. 4-Aminophenazone, on the other hand, has been reported to be free of adsorption problems [7], and this was confirmed in this work. A significant advantage of the indicator reaction used here is the absence of carcinogenic reagents.

### 3.1. Effect of lower reactor rotation and continuous-flow/stopped-flow operation

As shown in Fig. 3, if the lower reactor is devoid of rotation, the response is lower because diffusional limitations control the enzyme-catalyzed reaction. Rotation of the lower reactor (with immobilized HRP), as expected [3], results in comparatively larger responses.

Under continuous-flow conditions (Fig. 4A) there is no noticeable response because the mean residence time in the reactor is not sufficient for the reaction responsible for color formation to proceed to levels of detectable absorbance with the instrumentation and flow conditions used here. Very low flow rate (detrimental with regard to dispersion) provides detectable signals; these, however, cannot compare with signals obtained by stopping the flow and rotating the lower reactor (Fig. 4B).

If the lower, rotating reactor contains immobilized GOD and the preparation containing immobilized HRP is affixed at the top of the cell, the response is about 90% lower than when the enzymes are placed in the opposite configuration (Fig. 5). This suggests that lowering the apparent Michaelis-Menten constant for the

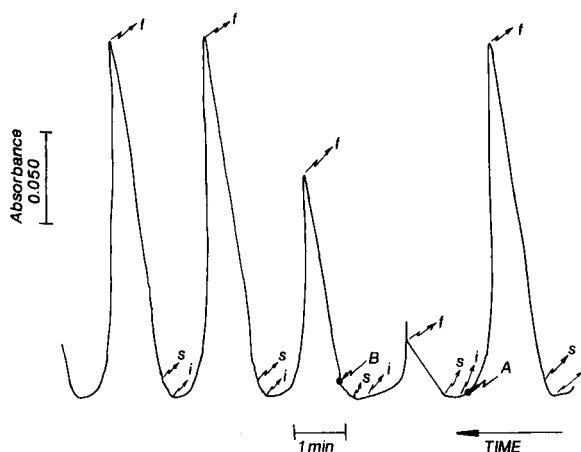


Fig. 3. Effect of reactor rotation under stopped flow. At A the rotation of the lower reactor was interrupted and at B the rotation was re-initiated (840 rpm). *i* = Injection, *s* = flow stopped, *f* = flow continued. Glucose concentration:  $1 \text{ mg ml}^{-1}$ . Flow rate:  $2.28 \text{ ml min}^{-1}$ . Sample size:  $73.3 \mu\text{l}$ .

reaction in Eq. 3 (overall this reaction is slower than reaction of Eq. 1, under the conditions used here) is more conducive to a more efficient utilization of bio-catalysts rather than lowering the value of the same constant for the reaction of Eq. 1.

### 3.2. Effect of cell volume and sample size

The volume of the cell was changed from 650 to  $330 \mu\text{l}$  by removing the O-rings between the upper and

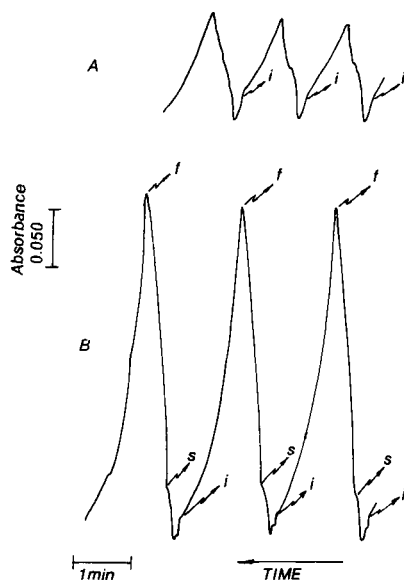


Fig. 4. Response under continuous flow (A), and under stopped flow (B). Glucose concentration:  $1 \text{ mg ml}^{-1}$ . Sample size,  $73.3 \text{ ml}$ . Rotation velocity, 840 rpm.

lower parts of the cell. As expected [3], the rate of response decreases with increasing cell volume because of the dilution effect favored by rotation and the absorbance response to bulk concentration. Consequently the smaller volume of  $330 \mu\text{l}$  (volume comprising the area between reactors) was used in all measurements.

Also as expected [3], the rate of response increased linearly with sample size. For convenience a sample size of  $73.3 \mu\text{l}$  was used to evaluate other parameters.

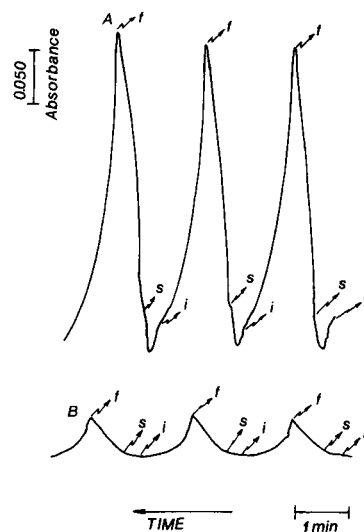


Fig. 5. Effect of inverting reactors: (A) glucose oxidase immobilized on the fixed reactor located in the upper part of the cell and horseradish peroxidase on the rotating reactor. (B) Glucose oxidase on the surface of the rotating reactor and horseradish peroxidase on the fixed reactor. Experimental conditions and meaning of *i*, *s*, and *f*, as in Fig. 3.

Table 2

Values of  $K_m'$  (Apparent Michaelis-Menten constant) for the GOD/HRP system (determination as discussed in the text, temperature  $20 \pm 1^\circ\text{C}$ )

Rotation velocity (rpm)	$K_m'$ (mM) <sup>a</sup>	Linear regression, S.D.
240	0.90	$\pm 0.07$
420	0.36	$\pm 0.08$
840	0.21	$\pm 0.05$
Free enzymes in solution <sup>b</sup>	5.22	$\pm 0.11$

<sup>a</sup> Each value of  $K_m'$  based on triplicate of six different substrate concentrations.

<sup>b</sup> Estimated by using the *o*-dianisidine glucose determination kit (Catalog No. 510-DA, Sigma, St. Louis, MO).

### 3.3. The apparent Michaelis-Menten constant

Table 2 summarizes the values of the apparent Michaelis-Menten constant,  $K_m'$ , for a given enzyme preparation and obtained at three different rotation velocities and stopping the flow for 90 s. The calculation of  $K_m'$  was performed under conditions in which  $[\text{Substrate}] \gg K_m'$  and the following applies assuming that the Briggs and Haldane scheme [8] is in operation:

$$(1/S) = (m/[\text{glucose}]) + n$$

where  $S$  = rate of response;  $K_m' = m/n$ . The apparent constant is then obtained from the slope and intercept of the  $1/S$  vs.  $1/[\text{glucose}]$  plot, a graphical approach similar to the Lineweaver-Burk plot.

As expected [3], the values of  $K_m'$  in Table 2 decrease as the velocity of rotation increases, and this confirms that rotation of the lower reactor minimizes the problem of diffusional limitations observed when using immobilized reagents.

### 3.4. Effect of pH and glucose concentration

The rate of response under stopped-flow conditions was practically independent of pH between pH 6.00 and 6.50 (Fig. 6). In the colorimetric determination using the same oxidative coupling reaction reported here [5], the recommended pH is 7.00; in our case, however, there was almost no response at this pH. The difference in pH profile is probably due to changes in properties of the biocatalysts as a result of immobilization. The pH used to evaluate other variables was

6.00 and provided by a phosphate buffer (0.10 M total phosphate).

A linear relation was observed between the rate of response and the glucose concentration in the range of 0.010 mM and 0.50 mM (rotation 840 rpm):

rate of response (at 555 nm)

$$= 1.16 + 51.89[C_{\text{glucose}}, \text{mM}]$$

The correlation coefficient for this type of plot was typically 0.9991, the standard deviations of slope and intercept were 0.91 and 0.18 respectively, the standard error of estimate was 0.318, and the limit of detection (based on  $3 \times$  sample standard deviation of blank readings) was ca.  $10 \mu\text{M}$ . The relative standard deviation for six successive measurements using a 0.070 mM glucose solution was typically 0.78%.

### 3.5. Determination of glucose in serum samples

Glucose was determined in two (normal and abnormal) serum standards (Accutrol<sup>TM</sup>) and in fifteen samples of bovine blood serum. The samples needed deproteinization because they arrived at the laboratory markedly colored and turbid. A volume of 0.50 ml of each sample (1:20 protein-free) was diluted to 5.00 ml with phosphate buffer (0.10 M total phosphate, pH 6.00). The resulting solution was intercalated into the flow system of Fig. 2 as "sample".

Although several chemical species (e.g., urate, ascorbate, bilirubin, and glutathione) interfere in the reaction involving HRP in the determination with *o*-dianisidine, such interferent action was not observed in the direct determination of glucose in blood serum. Fig.

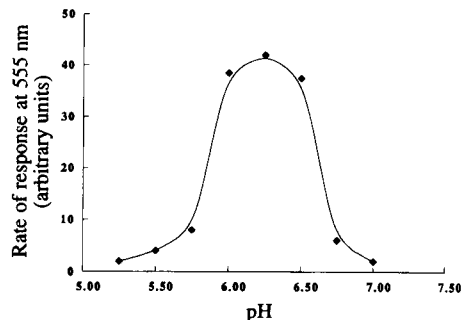


Fig. 6. Effect of pH. The rate of response corresponds to the integrated coupled system of immobilized GOD and HRP. Experimental conditions as described in text. Rotation velocity of HRP reactor: 840 rpm.

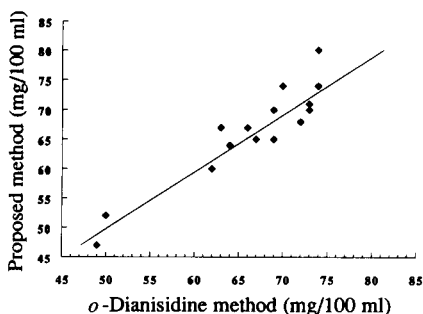


Fig. 7. Comparison of results obtained with the proposed method and with the *o*-dianisidine method. Results represent determinations in 16 serum samples (Pearson's correlation coefficient: 0.998; slope obtained by regression: 0.95, intercept: 3.2 mg 100 ml<sup>-1</sup>).

7 correlates results obtained by applying the *o*-dianisidine determination with the kit mentioned in the experimental section and by applying the method developed here. The Pearson's correlation coefficient was 0.998 and the standard error of the difference [9] was 1.08.

If the minimum measurement time of about 90 s is considered together with the transport time and a washing time of 30–60 s, the sum of these times gives a figure of about 24 for the number of samples which can be processed in 1 h.

#### 4. Conclusions

This article presents the implementation of chemical coupling of two enzyme-catalyzed reactions (main reaction and indicator reaction) in a specially designed flow through spectrophotometric cell. The cell comprises parallel bioreactors facing each other, with the lower reactor rotating and the upper fixed. The overall approach is shown to implement conveniently the chemical coupling utilizing very small amounts of biocatalyst (the immobilized proteinic material is about 1

ng) as a result of the imposed rotation to one of the reactors which minimizes diffusional limitations. The approach and cell are illustrated with the determination of glucose using glucose oxidase and peroxidase as immobilized enzymes, but it is open to any of the commonly used coupling of the main enzyme-catalyzed reaction with a second (indicator) reaction and spectrophotometric monitoring.

#### Acknowledgements

The authors wish to thank Jorge A. Vizcarra (Department of Animal Sciences, Oklahoma State University) for providing the samples of bovine blood. One of the authors (JR) acknowledges support in the form of a fellowship received from the Consejo Nacional de Investigaciones Científicas y Técnicas (CONICET) of Argentina.

#### References

- [1] H.A. Mottola, *Kinetic Aspects of Analytical Chemistry*, Wiley, New York, 1988, p. 63.
- [2] J. Raba and H.A. Mottola, *Anal. Biochem.*, 220 (1994) 297.
- [3] K. Matsumoto, J.J. Baeza Baeza and H.A. Mottola, *Anal. Chem.*, 65 (1993) 636.
- [4] (a) K. Matsumoto, J.J. Baeza Baeza and H.A. Mottola, *Anal. Chem.*, 65 (1993) 1658; (b) Zang-Hua Lan and H.A. Mottola, *Anal. Chim. Acta*, 293 (1994) 139; (c) J. Raba and H.A. Mottola, *Anal. Chem.*, 66 (1994) 1485.
- [5] P. Kabasakalian, S. Kalliney and A. Wescott, *Clin. Chem.*, 20 (1974) 606.
- [6] E. Eisenstaedt, *J. Org. Chem.*, 3 (1938) 153.
- [7] L. Gorton and L. Ögren, *Anal. Chim. Acta*, 130 (1981) 45.
- [8] G.E. Briggs and J.B.S. Haldane, *Biochem. J.*, 19 (1925) 338.
- [9] D.L. Massart, B.G.M. Vandeginste, S.N. Deming, Y. Michotte and L. Kaufman, *Chemometrics: A Textbook*, Elsevier, Amsterdam, 1988, p. 41.

## Kinetic spectrophotometric determination of hydrazine

A. Safavi \*, A.A. Ensafi

*Department of Chemistry, Faculty of Sciences, Shiraz University, Shiraz, Iran*

Received 13 September 1993; revised manuscript received 2 May 1994

### Abstract

A sensitive kinetic method for determining low levels of hydrazine has been described. The method is based on the measurement of the rate of the reaction between hydrazine and Mo(VI) in the presence of hydrochloric acid. The redox reaction was monitored spectrophotometrically at 710 nm. The variable-time and fixed-time methods were used. The calibration graph was linear for hydrazine concentrations of  $1.0 \times 10^{-4}$ – $1.4 \times 10^{-2}$  M, using the fixed-time method of analysis. The method is simple, rapid, precise, sensitive and widely applicable.

*Keywords:* Kinetic methods; Spectrophotometry; Hydrazine

### 1. Introduction

Hydrazine and its derivatives have found application in industry, agriculture and other fields including the manufacture of metal films, photographic chemicals, explosives, insecticides and blowing agents for plastic. On the other hand, hydrazine is a toxic material which must be treated with due respect. Thus, there has been an increasing demand for a highly sensitive method of determination of hydrazine in samples such as water, industrial and environmental materials.

Many methods have been proposed for the determination of hydrazine and its compounds. These include spectrophotometric [1,2], coulometric [3], amperometric [4–6], potentiometric [7] and titrimetric [8–10] methods as well as the measurement of

gases [11–13]. Various experimental hydrazine sensors have also been reported based on the detection of resistance change due to heat generated by catalytic oxidation of hydrazines [14], the measurement of currents with electrochemical oxidation of hydrazines [15,16] and construction of a polypyrrole film as the sensor [17]. Only a few kinetic methods for hydrazines are described in the literature. A kinetic potentiometric method has been described [18] for the determination of hydrazine, based on monitoring its reaction at 25°C and pH 9.0 with 1-fluoro-2,4-dinitrobenzene by means of a fluoride-selective electrode. Hydrazine was determined over the range of  $0.5$ – $8 \times 10^{-4}$  M, while another report [19] described the determination of  $2.0 \times 10^{-4}$ – $2.0 \times 10^{-3}$  M hydrazine using an iodide-selective electrode. Low levels of hydrazine ( $0.02$ – $30 \mu\text{g ml}^{-1}$ ) have been reported [20] to be determined using modular stopped flow/diode array detection system. Whereas some of these methods require special equipment, others demand carefully controlled condi-

\* Corresponding author.

tions and in some a complete report on selectivity is not available.

In the present investigation, a kinetic method is described for the determination of low levels of hydrazine. The method is simple, rapid and highly sensitive. It is also selective especially in the presence of large amounts of different types of organic compounds such as phenyl hydrazine, hydroxylamine, urea, acetaldehyde and formaldehyde.

## 2. Experimental

### 2.1. Reagents

Analytical reagent-grade chemicals and triply distilled water were used. Mo(VI) standard solutions (0.10 M) were prepared by dissolving 8.8276 g of  $(\text{NH}_4)_6\text{Mo}_7\text{O}_{24} \cdot 4\text{H}_2\text{O}$  (Merck) in about 300 ml of 0.010 M NaOH. The solution was neutralized by the addition of 0.10 M HCl and diluted to 500 ml with water in a volumetric flask.

A stock solution of hydrazine (0.50 M) (Merck) was prepared by dissolving hydrazine dihydrochloride (Merck) in water.

### 2.2. Apparatus

Absorption spectra were recorded on a Beckman DK.2A UV–visible recording spectrophotometer with 1-cm glass cells. A Perkin-Elmer Model 35 spectrophotometer with a 1-cm glass cell was used for absorbance measurements. All the solutions were previously heated to a working temperature of  $30 \pm 0.1^\circ\text{C}$  in a thermostated bath and this temperature was maintained in the reaction cell during the experiments.

### 2.3. Procedure

The reaction between hydrazine and Mo(VI) in the presence of HCl was followed spectrophotometrically by monitoring the absorbance change at 710 nm. Into a series of 10-ml volumetric flasks were added 1.0 ml of 1.0 M HCl followed by 5 ml of 0.10 M Mo(VI) solution. The solutions were kept at  $30^\circ\text{C}$  in a thermostated bath for 10–15 min. 2 ml of

hydrazine solution ( $> 1.0 \times 10^{-4}$  M) was added to initiate the reaction, and the solution was rapidly diluted to the mark with water. After mixing the solution, an appropriate volume was transferred to the spectrophotometric cell within 30 s to measure the absorbance. The time required for the absorbance to increase to 0.100 (or 1.00 for hydrazine concentrations  $> 4 \times 10^{-3}$  M) was measured (variable time method), or the absorbance change was recorded against water between 30 s and 3 min from initiation of the reaction (fixed time method). In both procedures, zero time was taken as the moment at which the last drop of hydrazine had been added and the solution was diluted to the mark with water. If higher concentrations of hydrazine ( $> 0.04$  M) have to be determined, the concentration of Mo(VI) should be decreased.

## 3. Results and discussion

A solution of Mo(VI) in the presence of  $\mu\text{g ml}^{-1}$  of hydrazine and HCl undergoes a rapid reaction. The redox reaction can be monitored by measuring the increase in absorbance of the solution ( $\lambda_{\text{max}} = 710$  nm) (Fig. 1). The variable-time and fixed-time methods were used for measuring the reaction rate. For the optimization of conditions, the variable time method was used.

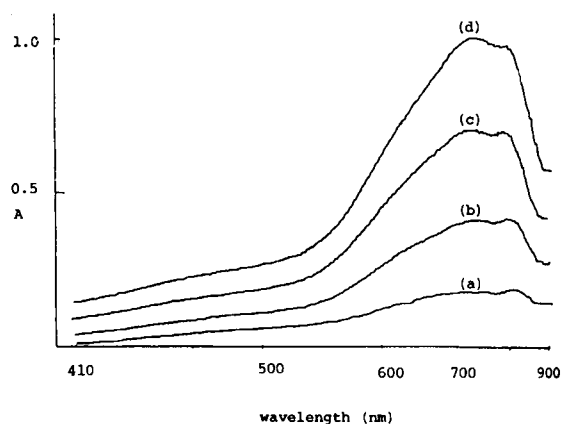


Fig. 1. Effect of time on the absorbance of the  $\text{N}_2\text{H}_4$ –Mo(VI)–HCl system. Time from addition of hydrazine: (a) 30 s; (b) 1.0 min; (c) 2.0 min; (d) 3.0 min.  $1 \times 10^{-3}$  M hydrazine.

### 3.1. Effect of variables

The influence of acidity and the concentration of Mo(VI) on the oxidation rate of hydrazine was studied at 30°C. The results showed that by increasing the concentration of hydrochloric acid, the reaction rate was increased while addition of a base to the reaction mixture caused a decrease in rate (Fig. 2). Thus 0.2 M HCl is recommended for use. Increasing the Mo(VI) concentration, resulted in an increase in the reaction rate, and 0.05 M Mo(VI) was selected for further studies.

Increasing the temperature from 15 to 45°C increased the reaction rate, (Fig. 3) but at the higher temperatures N<sub>2</sub> gas bubbles are formed. For this reason, 30° ± 0.1°C was selected for routine work.

The above study showed that the optimum conditions are 0.05 M Mo(VI), 0.2 M HCl, 30°C and 710 nm. For hydrazine concentrations up to 4.0 × 10<sup>-3</sup> M, the time required for the absorbance to reach a value of 0.100 was measured, while for higher concentrations, the time required for the absorbance to reach a value of 1.00 was measured. When the fixed-time method was used, a measuring time of 3 min was selected.

### 3.2. Analytical parameters

Calibration graphs were obtained by applying the variable time and fixed-time methods. When the variable time method was used, the calibration graph

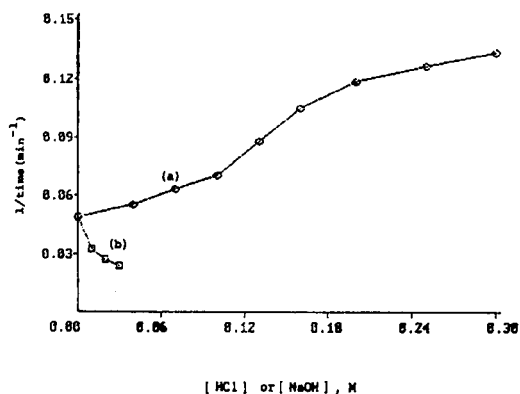


Fig. 2. Effect of (a) HCl concentration and (b) NaOH concentration on the reaction rate for 1 × 10<sup>-3</sup> M hydrazine.

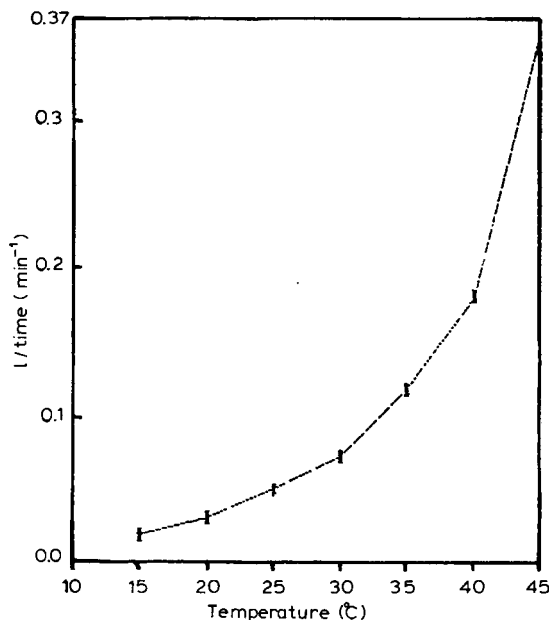


Fig. 3. Effect of temperature on the reaction rate.

of 1/time vs. hydrazine concentration was linear for hydrazine concentrations of 1.0 × 10<sup>-4</sup> M to 4.0 × 10<sup>-3</sup> M and 5.0 × 10<sup>-3</sup> M to 4.0 × 10<sup>-2</sup> M.

The equations for the calibration graphs are (time)<sup>-1</sup> (min<sup>-1</sup>) = 7.31 × 10<sup>-3</sup> + 2.04 × 10<sup>2</sup>C<sub>M</sub> with *r* = 0.994 for 1.0 × 10<sup>-4</sup>–4.0 × 10<sup>-3</sup> M hydrazine and (time)<sup>-1</sup> = 7.28 × 10<sup>-2</sup> + 11.8C<sub>M</sub> with *r* = 0.9937 for 5.0 × 10<sup>-3</sup>–4.0 × 10<sup>-2</sup> M hydrazine, respectively, where C<sub>M</sub> denotes the molar concentration of hydrazine. Higher concentrations of hydrazine (> 0.04 M) can be determined by the above method using lower concentrations of Mo(VI).

When the fixed-time method was used, the graph of increase in absorbance (Δ*A*) vs. hydrazine concentrations was linear for hydrazine concentrations of 1.0 × 10<sup>-4</sup>–1.4 × 10<sup>-2</sup> M. The equation for the calibration graph was Δ*A* = -84.7 × 10<sup>-4</sup> + 56.21C<sub>M</sub> with *r* = 0.9996.

The 2σ limit of detection [21] was 1 μg ml<sup>-1</sup> of hydrazine by the variable time method and 10 μg ml<sup>-1</sup> of hydrazine using the fixed-time method.

The accuracy and precision for the analysis of eight replicates of a series of samples containing various concentrations of hydrazine by the variable time method are shown in Table 1.



Table 1  
Precision and accuracy of the variable time method

Hydrazine present (M)	Hydrazine found (M)	R.S.D. (%) ( $n = 8$ )
$1.00 \times 10^{-3}$	$9.95 \times 10^{-4}$	4.1
$1.60 \times 10^{-3}$	$1.55 \times 10^{-3}$	5.7
$2.00 \times 10^{-3}$	$1.95 \times 10^{-3}$	4.8
$3.00 \times 10^{-3}$	$3.04 \times 10^{-3}$	6.1
0.0100	0.0104	2.1
0.0200	0.0184	2.2

### 3.3. Effects of foreign species

The effects of various compounds, cations and anions on the determination of  $1.0 \times 10^{-3}$  M hydrazine were studied by the variable time method. The results are summarized in Table 2. The tolerance limit was defined as the concentration of added species causing less than 3% relative error. Most ions and common species usually present with hydrazine compounds did not interfere with the determination. However, compounds which can reduce Mo(VI) could interfere with this determination.

### 3.4. Application to water samples

Hydrazine was determined after addition to drinking water and river water. Table 3 shows the results,

Table 2  
Effect of foreign species on the determination of 0.0010 M hydrazine

Species	Tolerance maximum level ( $\mu\text{g ml}^{-1}$ )
Hydroxylamine, phenyl hydrazine, urea	1000
Acetone, acetaldehyde	250
Methyl ethyl ketone	100
Formaldehyde	20
Al(III), Ni(II), Cu(II), Fe(II), Cd(II), Zn(II), Ca(II), Na(I), K(I), Mn(II)	1000
$\text{PO}_4^{3-}$ , $\text{NO}_3^-$ , $\text{I}^-$ , $\text{Br}^-$ , $\text{Cl}^-$	1000
$\text{HONH}_2\text{Cl}$	400
As(V)	500
Fe(III)	50
As(III)	10
Ascorbic acid	10

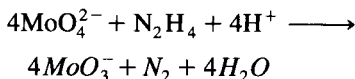
Table 3  
Determination of hydrazine added to water samples

Sample	Hydrazine concentration (molar)		Recovery
	Added	Found	
Drinking water	$1.00 \times 10^{-3}$	$9.8 \times 10^{-4}$	98.0
	$1.40 \times 10^{-3}$	$1.35 \times 10^{-3}$	96.4
	$1.80 \times 10^{-3}$	$1.74 \times 10^{-3}$	97.2
	$2.00 \times 10^{-3}$	$1.96 \times 10^{-3}$	98.0
	$6.00 \times 10^{-3}$	$6.0 \times 10^{-3}$	100.0
	River water	$1.00 \times 10^{-3}$	$9.6 \times 10^{-4}$
$1.40 \times 10^{-3}$		$1.34 \times 10^{-3}$	95.7
$1.80 \times 10^{-3}$		$1.73 \times 10^{-3}$	96.1
$2.0 \times 10^{-3}$		$1.94 \times 10^{-3}$	97.0
$6.0 \times 10^{-3}$		$5.9 \times 10^{-3}$	98.3

the recoveries being close to 100%, indicating that there are no interferents in such water samples.

### 3.5. Study of the reaction route

The reaction route was investigated by the study of the products of the reaction. Mo(VI) and hydrazine are colorless while the product of their reaction is blue, i.e., hydrazine reduces some Mo(VI) to Mo(V) in acidic media, thus forming molybdenum blue. In addition, at high concentrations of hydrazine in acidic media, after a time interval of about 10 min, evolution of nitrogen was detectable. Thus, the following mechanism for the reaction of Mo(VI) with hydrazine in acidic solutions is suggested to be:



## 4. Conclusions

This method can be used to determine hydrazine down to  $1 \times 10^{-4}$  M without the need for any preconcentration step. The method is very simple and more selective than most previously reported methods. The determination of hydrazine in the presence of hydroxylamine and phenylhydrazine is possible.

## Acknowledgement

The authors wish to express their gratitude to Shiraz University Research Council for their support of this work.

## References

- [1] A. Aleksundrov, P. Vasilevasuper and E. Kovacheva, *Mikrochim. Acta*, I (1968) 1007.
- [2] F. Dias, A.S. Olojola and B. Joselskis, *Talanta*, 26 (1979) 47.
- [3] L. Szebelledy and Z. Somogyi, *Z. Anal. Chem.*, 112 (1938) 391.
- [4] V.A. Khadeev and D. Mukhamed Zhanova, *Zavodsk. Lab.*, 36 (1970) 1443.
- [5] S.P. Mallelo and B.L. Khandelwal, *Mikrochim. Acta*, II (3–4) (1977) 245.
- [6] S. Ikeda, H. Sutake and Y. Kohri, *Chem. Lett.*, 6 (1984) 873.
- [7] W.R. McBride, R.A. Heny and S. Skolnik, *Anal. Chem.*, 23 (1951) 890.
- [8] V. Rajasekharan and C.G. Ramachandran, *Anal. Chim. Acta*, 57 (1971) 429.
- [9] C. Radhakrishnamurty and V.V.S. Dutt., *Analisis*, 2 (1973) 514 (*Anal. Abstr.*, 26 (1974) 822).
- [10] Y.A. Gawargious and A. Beseda, *Talanta*, 22 (1975) 757.
- [11] C.P. Lloyd and W.F. Pickering, *Talanta*, 16 (1969) 532.
- [12] S.S.M. Hasssan and M.T.M. Zaki, *Microchem. J.*, 15 (1970) 470.
- [13] S.S.M. Hassan, *Anal. Chim. Acta*, 54 (1971) 185; *Z. Anal. Chem.*, 255 (1971) 364.
- [14] E.F. Croomes and J.A. Murfree, *U.S. Pat.*, 915 706-78 (1980).
- [15] R.A. Saunders, J.J. De Corpo, B.J. Stammerjohn and R.J. Kautter, Report No. NRL-8199, Naval Research Laboratory, Washington, DC, 1978.
- [16] E.W. Schmidt, *Hydrazine and its Derivatives*, Wiley, New York, 1984, p. 448.
- [17] H.M. Ratcliffe, *Anal. Chim. Acta*, 239 (1990) 257.
- [18] E. Athanasion-Malaki and M.A. Koupparis, *Talanta*, 36 (1989) 431.
- [19] I.I. Koukli and A.C. Calokerinos, *Anal. Chim. Acta*, 192 (1987) 333.
- [20] M.C. Gutierrez, A. Gomez-Hens and D. Perez-Bendito, *Anal. Chim. Acta*, 225 (1989) 115.
- [21] J.C. Miller and J.N. Miller, *Statistics for Analytical Chemistry*, Ellis Horwood, Chichester, 1986.



ELSEVIER

Analytica Chimica Acta 300 (1995) 313–320

ANALYTICA  
CHIMICA  
ACTA

## Age estimation of old carpets based on cystine and cysteic acid content

János Csapó <sup>a,\*</sup>, Zsuzsanna Csapó-Kiss <sup>a</sup>, Truman G. Martin <sup>b</sup>, Staffan Folestad <sup>c</sup>,  
Owe Orwar <sup>c</sup>, Anna Tivesten <sup>c</sup>, Sándor Némethy <sup>d</sup>

<sup>a</sup> PANNON Agricultural University, Faculty of Animal Science, P.O. Box 16, Dénesmajor 2, H-7401 Kaposvár, Hungary

<sup>b</sup> Department of Animal Science, Purdue University, West Lafayette, IN 47907, USA

<sup>c</sup> Department of Analytical and Marine Chemistry, University of Göteborg and Chalmers University of Technology, S-412 96 Göteborg, Sweden

<sup>d</sup> Department of Marine Geology, University of Göteborg and Chalmers University of Technology, S-412 96 Göteborg, Sweden

Received 19 January 1994; revised manuscript received 8 August 1994

### Abstract

A method for the evaluation of the age of wool carpets and textiles was developed based on the age dependent alteration of amino acid composition of proteins. Samples of 23 wool carpets and textiles of known age, obtained from the Hungarian Museum of Industrial Arts and the Hungarian National Museum were analysed for amino acid content. Results were compared with data obtained for contemporary, untreated wool and wool carpet. The cysteic acid content of wool increases with age. The contemporary wool carpet contained 0.31 g of cysteic acid in 100 g of protein. Comparable figures were 1.87 g for a 550-year old carpet and 4.01–4.39 g for the 1600–1750 year old wool carpets. The cystine content decreased with age, the corresponding figures being 7.88, 3.12 and 1.19–0.97 g/100 g, respectively. Corresponding contents of methionine were 0.43, 0.21 and 0.20–0.00 g/100 g and for tyrosine 3.07, 2.11 and 0.20–0.00 g/100 g. Prediction equations were developed as linear regressions of the age of wool on cysteic acid, cystine and tyrosine contents. The 95% confidence intervals of estimates for two samples of unknown age were estimates plus or minus 30 and 38 years.

**Keywords:** Age estimation; Cysteic acid; Cystine; Methionine; Tyrosine; Wool

### 1. Introduction

Earlier publications [1,2] report on the investigation of racemization of amino acids, and it was found that samples whose protein contents were less than 2000–3000 years of age (mostly bones) were unsuitable for age determination using racemization. Examination of the amino acid composition of these samples revealed that the majority of cystine had decomposed or oxidised

to cysteic acid while tyrosine and methionine had all but disappeared from these ancient samples. Based on these findings, it was assumed that there must be a correlation between the age of the “recent” bone samples and their cystine, cysteic acid, methionine and tyrosine contents. After analysing some 50 bone samples, it was realised that the main protein constituent of bone (collagen) has a low concentration of sulphur-containing amino acids and that this method cannot be used for age estimation. Following this conclusion, the amino acid contents of various wool carpets and textiles

\* Corresponding author.

of known age were examined to investigate possible links between amino acid contents (cystine, cysteic acid, methionine, tyrosine) and age. In a review of publications found in archaeometry journals, no references to the use of amino acid composition for the determination of age were found.

The basis for using the amino acids for age determination is that the two sulphur containing amino acids are sensitive to oxidation both in the free state and when bound in peptide. Further, depending on environmental conditions, cystine may decompose into alanine, homocystine and glycine [3] or it may transform into homocysteine, homocystine and glycine [4]. Methionine may also be considerably degraded by being oxidised to methionine sulfone and sulfoxide [5]. In order to eliminate analytical problems due to the facts outlined above, a method was devised [6–8] for the determination of the two sulphur-containing amino acids in the oxidised state. This method has yielded considerably better results than determinations in the unoxidised state.

## 2. Experimental

### 2.1. *The analysed materials*

Samples of copt textiles and wool carpets of various ages were procured from the Hungarian National Museum and the Hungarian Museum of Industrial Arts. The samples are described in Tables 1 and 2. Taking care not to damage the textiles or carpets, portions of 20–100 mg were removed from the fabric for analysis. New wool of Hungarian merino sheep was obtained from our experimental farm. The new wool was untreated and was obtained directly from the sheep. The composition of the contemporary wool carpets was studied on carpets originating from the Domus Supermarket from the city of Kaposvár. The carpets were scratched with the fingernails until we collected ca. 2–3 g of sample per carpet.

The wool samples were treated in the following manner. After having cleaned the samples (both ancient and contemporary) from mechanical impurities, the wool fibres were washed three times with 40–60°C b.p. petroleum ether. During each washing the samples were left to soak in the ether for 20 min. Following this procedure, the samples were dried in a nitrogen current

(15 min), and then washed three times with distilled water. The samples were left to soak for 20 min during each washing cycle. Following washing with distilled water, the samples were dried again in a nitrogen current. The dry samples were stored in airtight containers until the time of analysis.

### 2.2. *Hydrolysis and processing of the hydrolysate*

Hydrolysis of the samples was performed in reusable Pyrex hydrolysis tubes (Pierce, Rockford, IL). The tubes had an internal diameter of 8 mm and could accommodate 8 ml of hydrolysing agent so that the liquid was not in contact with the PTFE sealing ring. In the case of contemporary wool and carpets, 20 mg samples were introduced into the hydrolysing tube. In the case of samples coming from ancient wool carpets minimal sample size was 6.2 mg. Prior to use, the Pyrex hydrolysing tubes were washed twice with 6 M hydrochloric acid and distilled water. After introducing the sample to be analysed, 5 ml of 6 M HCl was added and nitrogen was bubbled through the tubes with the aid of a glass capillary for 5 min. Immediately after bubbling, the tubes were sealed and hydrolysis was begun at 110°C. After hydrolysis, the tubes were allowed to cool to room temperature. After the tubes were opened, pH of the hydrolysate was adjusted to a value of 2.2, using 4 M NaOH. During pH adjustment, a salt/ice cooling mixture was used to maintain the temperature below 30°C. The resulting samples were diluted with a citrate buffer of pH 2.2. Samples were filtered and stored at –25°C until the time of analysis.

From preliminary experiments, it seemed that the normal period of 24 h was not sufficient for complete hydrolysis of wool proteins. After only 24 h of hydrolysis, there were several ninhydrin positive peaks which were difficult to assign, but appeared to be the result of incomplete hydrolysis. In a preliminary experiment wool samples were hydrolysed for 24, 48, 72, 96 and 120 h with 6 M HCl. The results were used to establish hydrolysis time for the main experiment.

### 2.3. *Analysis of amino acids*

Samples were analysed with the LKB 4101 (LKB Biochrom) automatic amino acid analyser. The amino acid standard and cysteic acid were obtained from Merck (Darmstadt). The analysis conditions were as

Table 1  
Wool threads of copt textiles and carpets from the Hungarian Applied Arts Museum

Sample No.	Inventory number	Nature of sample	Period (century AD)	Age of the sample (years)	Origin of the sample
1.1.	7436	cloth	3(?)	1750	unknown
1.2.	7429	cloth	4–5	1600	from Baron Weisenbach (blue)
1.3.	7429	cloth	4–5	1600	from Baron Weisenbach (red)
1.4.	7414	cloth	4–5	1600	Forrer collection
1.5.	7469	gobelin	4–5	1600	from Becker F.
1.6.	7441	gobelin	5	1550	Forrer collection
1.7.	7475	gobelin	5	1550	Forrer collection
1.8.	7475	gobelin	5	1550	Forrer Collection (flax fibre?)
1.9.	7434	decoration of cloth	5–6	1500	Forrer collection
1.10.	9013	cloth	6–8	1400	Forrer collection (imitation?)
1.11.	7417	decoration of cloth	6–8	1400	Forrer collection
1.12.	8642	gobelin	6–8	1400	Forrer collection
1.13.	7416	decoration of cloth	6–8	1400	from Szavai E.
1.14.	843161	cloth	10	1050	unknown
1.15.	14940	carpet	15	550	Anatolia
1.16.	13751	carpet	16–17	400	Anatolia
1.17.	5025	carpet	19	140	Turkmen
1.18.	15440	gobelin	unknown	unknown	unknown

follows. Ion-exchange column: length 55 cm, diameter 6 mm; temperature, 55°C for 30 min, and 70°C to the end of the analysis. Ion-exchange resin: Chromex UA-8. Buffer A: pH 3.28, 0.2 M [Na<sup>+</sup>], 25 min. Buffer B: pH 4.25, 0.2 M [Na<sup>+</sup>], 30 min. Buffer C: pH 6.45, 1.2 M [Na<sup>+</sup>], 55 min. Sodium hydroxide: 0.4 M, 10 min. Equilibration: buffer A, 30 min.

The flow rates of the buffers were 50 ml/h, and the flow rate of ninhydrin was 25 ml/h. The other parameters were those recommended by the manufacturer of the amino acid analyser for amino acid analysis. The analysis of amino acids was performed according to the method described previously [9].

#### 2.4. Preliminary comparison of modern and older wool samples

Five samples each of modern wool, modern carpet and 550 year old carpet were subjected to amino acid analysis. The complete amino acid profile was determined on each of these samples. The contrasts of means

$$\frac{\text{Wool} + \text{Modern Carpet}}{2} - \text{Old Carpet}$$

were tested by the *t*-test.

Table 2  
Carpets from the Hungarian National Museum

Sample No.	Inventory number	Nature of sample	Period (century AD)	Age of the samples (years)	Origin of the samples
2.19.	69/9158	carpet	end of 16	400	Transylvania
2.20.	19487	carpet	end of 17	300	from Teleki M.
2.21.	–	carpet	middle of 18	250	from China (Ningxia)
2.22.	–	carpet	beginning of 19	170	Anatolia, Balikesir
2.23.	–	carpet	from 1865	128	–
2.24.	–	carpet	2nd half of 19	120	Caucasus
2.25.	–	carpet	unknown	unknown	unknown

Table 3  
Amino acid composition (g amino acid/100 g protein) of wool samples of Hungarian Merino sheep after various hydrolysis times

Amino acids	Hydrolysis time (hours)				
	24 <sup>a</sup>	48 <sup>a</sup>	72 <sup>a</sup>	96 <sup>a</sup>	120 <sup>a</sup>
Cysteic acid	0.15	0.15	0.16	0.16	0.19
Aspartic acid (Asp)	7.3	7.4	8.0	8.3	8.3
Threonine (Thr)	6.2	5.9	6.0	6.1	6.2
Serine (Ser)	7.5	7.6	7.1	7.1	7.2
Glutamic acid (Glu)	11.3	12.7	15.0	15.4	15.5
Proline (Pro)	6.0	6.5	6.6	6.9	7.2
Glycine (Gly)	4.9	4.6	4.6	5.0	4.8
Alanine (Ala)	4.5	4.5	4.4	4.9	4.4
Cystine (Cys)	12.0	10.2	8.0	7.6	7.1
Valine (Val)	6.8	7.0	7.0	7.3	7.3
Methionine (Met)	0.4	0.5	0.4	0.3	0.4
Isoleucine (Ile)	3.3	3.6	3.7	3.5	3.2
Leucine (Leu)	7.8	8.2	8.2	7.9	8.4
Tyrosine (Tyr)	3.5	2.9	2.4	1.4	1.2
Phenylalanine (Phe)	4.2	4.2	4.0	4.0	4.1
Lysine (Lys)	3.5	3.2	3.2	3.3	3.5
Histidine (His)	0.8	0.8	0.8	0.8	0.8
Arginine (Arg)	7.7	7.7	7.8	7.8	8.1
Ammonia	2.3	2.4	2.2	2.2	2.3

<sup>a</sup> Number of the samples = 3.

### 2.5. Statistical analysis of the data

Based on the hypothesis that carpet age can be estimated from amino acid analysis, known age ( $y$ ) was regressed on cysteic acid, cystine, methionine and tyrosine contents and on the ratio cysteic acid/cystine. The accuracies of the functions were measured by correlation between predicted age ( $\hat{y}$ ) and actual age ( $y$ ) and by the standard deviation of the difference ( $y - \hat{y}$ ) designated as  $s_{y-x}$ .

## 3. Results and discussion

### 3.1. The influence of hydrolysis time on the amino acid composition of wool

The amino acid contents of the wool of Hungarian merino sheep, after being subjected to various hydrolysis times, are shown in Table 3. It may seem, from the data, that cystine is the only amino acid undergoing significant change as a result of changing hydrolysis times. However, regression analysis showed that there

were significant ( $P < .05$ ) increases in levels of aspartic acid, glutamic acid, proline and valine associated with increased hydrolysis time. Significant ( $P < .05$ ) decreases were seen for cystine and tyrosine. The very large decrease in cystine content (85% after 48 h, 72% after 72 h and 59% after 120 h) did not seem to be due to oxidation since cysteic acid content increased by only 27% in 120 h.

The trends of amino acids which changed with increased time of hydrolysis would suggest that as much as 72 h hydrolysis may be desirable. However, the ninhydrin positive peaks observed after 24 h were not observed after 48 h of hydrolysis. The decision was made to use 48 h hydrolysis in the remainder of this study.

### 3.2. Reliability of the analytical method

Considering the enormous difficulties encountered in obtaining samples and the high value of the material to be subjected to analysis, a preliminary trial was conducted to assess the reliability and accuracy of analytical methods. The amino acid compositions of contemporary wool, a contemporary wool carpet and a 550 year old wool carpet are shown in Table 4. Examining the amino acid compositions of contemporary wool and carpet, it is interesting to note that the fibres originating from the modern carpet contained twice as much cysteic acid and only 78% as much cystine as the virgin, untreated wool. The comparable differences with respect to the other amino acids were small. The situation changes substantially when we compare the composition of wool fibres from a 550 year old carpet with the mean composition of contemporary wool and carpet. The cysteic acid content of the ancient sample is strikingly higher than that in contemporary fibres (ca. 9 times). Also striking is the low cystine content, which is ca. one-third that of contemporary wools. The ancient wool fibre also contains more serine and glycine than contemporary samples. This may be correlated with the decomposition of cystine. Also worth mentioning are the lower tyrosine, methionine and lysine contents of the ancient wool. Another indicator of the partial decomposition of amino acids is the high ammonia content in the older carpet. With respect to the other amino acids, the three examined samples were very similar.

Table 4  
Amino acid composition of Hungarian Merino sheep's wool, modern wool carpet and 550 year old carpet samples

Amino acid content (g AA/100 g protein)	Wool <sup>a</sup>		Modern carpet <sup>a</sup>		Old carpet <sup>a,b</sup>	
	Mean	S.D.	Mean	S.D.	Mean	S.D.
Cysteic acid	0.150	0.009	0.312	0.026	1.854 <sup>c</sup>	0.212
Asp	7.36	0.34	7.44	0.39	7.74	0.68
Thr	5.93	0.31	6.11	0.29	5.75	0.34
Ser	7.55	0.27	7.77	0.34	8.93 <sup>c</sup>	0.43
Glu	12.53	0.29	12.12	0.27	12.80	0.31
Pro	6.43	0.25	6.44	0.37	6.45	0.62
Gly	4.68	0.21	5.23	0.19	5.46 <sup>c</sup>	0.28
Ala	4.52	0.19	4.84	0.20	5.19	0.34
Cys	10.18	0.27	7.90	0.26	3.09 <sup>c</sup>	0.27
Val	7.02	0.33	7.27	0.41	7.23	0.52
Met	0.47	0.04	0.43	0.05	0.21 <sup>c</sup>	0.07
Ile	3.73	0.21	3.91	0.28	3.66	0.24
Leu	8.10	0.39	8.37	0.41	8.07	0.43
Tyr	3.02	0.27	3.14	0.30	2.08 <sup>c</sup>	0.38
Phe	4.22	0.35	4.36	0.41	4.28	0.49
Lys	3.29	0.21	3.49	0.26	2.72 <sup>c</sup>	0.37
His	0.76	0.18	0.68	0.10	0.51	0.15
Arg	7.68	0.63	7.94	0.72	7.84	1.03
Ammonia	2.38	0.21	2.25	0.24	6.15 <sup>c</sup>	0.49

<sup>a</sup> Number of the samples = 5.

<sup>b</sup> Estimated age = 550 years.

<sup>c</sup> Significance of (wool + modern carpet/2) – old carpet has  $P > 0.99$ .

Comparison of the coefficients of variation (CV) for the three types of samples would indicate greater variability among samples of the older carpet than in the modern wools. However, virtually all of the increased CVs are associated with significant decreases in the means and relatively constant standard deviations. As a result, we can conclude that analytical precision is essentially equal for both type of samples.

### 3.3. Relationship of age of sample with cysteic acid, cystine, methionine and tyrosine contents

After the optimisation of hydrolysis time and the examination of reliability of the analytical method, samples obtained from the Hungarian Industrial Art Museum (Table 1) and the Hungarian National Museum (Table 2) were analysed. We often had only a few milligrams of fabric originating from ancient clothing or decorations. As a consequence, the data

shown in Table 5 for such materials are the result of a single analysis. In the case of carpet samples, adequate amounts of sample were available and the table shows the average result of duplicate determinations.

Data in Table 5 show that, as the age increased the cysteic acid content increased and the cystine content decreased (Fig. 1). When compared with contemporary wool, the cysteic acid contents were approximately 10, 20 and 30 times as great at 500, 1000 and 1700 years, respectively. The cystine content decreased to less than 50% in 120–140 years, to 35% in 500 years and to 10% in 1600–1700 years. The differences are even greater when expressed as a ratio of cysteic acid/cystine. The 1600–1700 year old samples had a ratio more than 100 times as great as that of modern carpets.

Both the methionine and tyrosine content decreased with age (Fig. 2). In the 1750 year old wool fibre and

Table 5  
Amino acid composition of wool carpets and wool threads of copt textiles of different ages

Sample No.	Age of the samples (years)	Amino acids (g amino acid/100 g protein)				
		Cysteic acid	Cys.	Cysteic acid/Cys.	Met.	Tyr.
1.1.	1750	4.39	0.97	4.48	0.00	0.00
1.2.	1600	4.30	1.03	4.17	0.00	0.00
1.3.	1600	4.27	1.21	3.53	0.02	0.15
1.4.	1600	4.33	1.10	3.93	0.02	0.20
1.5.	1600	4.01	1.19	3.37	0.01	0.20
1.6.	1550	3.99	1.22	3.27	0.03	0.30
1.7.	1550	3.97	1.33	2.98	0.03	0.38
1.8.	1550	3.82	1.19	3.21	0.02	0.54
1.9.	1500	3.93	1.22	3.22	0.03	0.53
1.10.	1400	3.81	1.53	2.49	0.03	0.75
1.11.	1400	3.54	1.50	2.36	0.04	0.77
1.12.	1400	3.72	1.54	2.42	0.04	0.73
1.13.	1400	3.65	1.43	2.55	0.05	0.89
1.14.	1050	3.12	1.78	1.75	0.15	1.33
1.15.	550	1.87	3.12	0.60	0.21	2.11
1.16.	400	1.49	3.21	0.46	0.28	2.32
2.19.	400	1.53	3.43	0.45	0.27	2.29
2.20.	300	1.32	3.82	0.35	0.31	2.31
2.21.	250	1.21	3.79	0.32	0.29	2.43
2.22.	170	1.19	4.15	0.29	0.33	2.37
1.17.	140	1.22	4.24	0.29	0.38	2.85
2.23.	128	1.03	4.20	0.25	0.40	2.59
2.24.	120	0.88	5.19	0.17	0.39	2.83
1.18.	unknown	1.92	3.24	0.59	0.24	1.99
2.25.	unknown	1.44	3.91	0.37	0.34	2.38

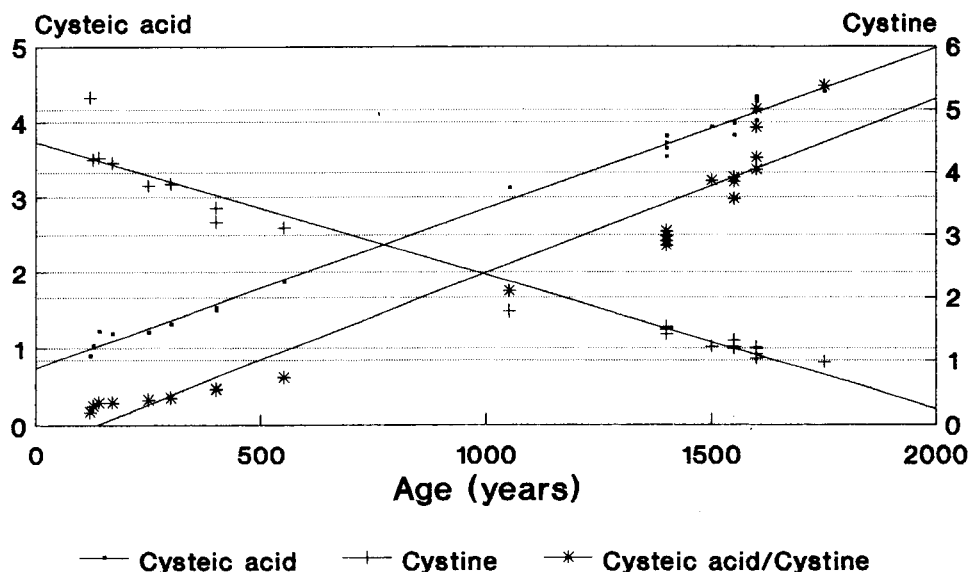


Fig. 1. Age estimation of wool based on cysteic acid and cystine content.

one of the 1600 year old wool fibres, we were unable to detect the presence of either tyrosine or methionine. The methionine content of the samples decreased to 85% of the original level in 100–140 years, to 55% in 400–500 years and to almost nil in 1600–1700 years. Tyrosine decreased 10–15% in 100–140 years, 30% in 400–500 years, and was almost completely decomposed at 1600–1700 years.

Regressions of age on amino acid content were based on analyses of the 23 samples having known ages

(Table 5) which were described in Tables 1 and 2. The amino acid contents of the modern carpet were not included in the estimation of regression due to curvilinearity introduced by including that sample. These curvilinear functions resulted in large differences between known age ( $y$ ) and predicted age ( $\hat{y}$ ) at the extreme ages. Since we cannot extrapolate regressions beyond the range of the data, equations developed in this study can be expected to apply to wool samples 120 to 1700 years of age.

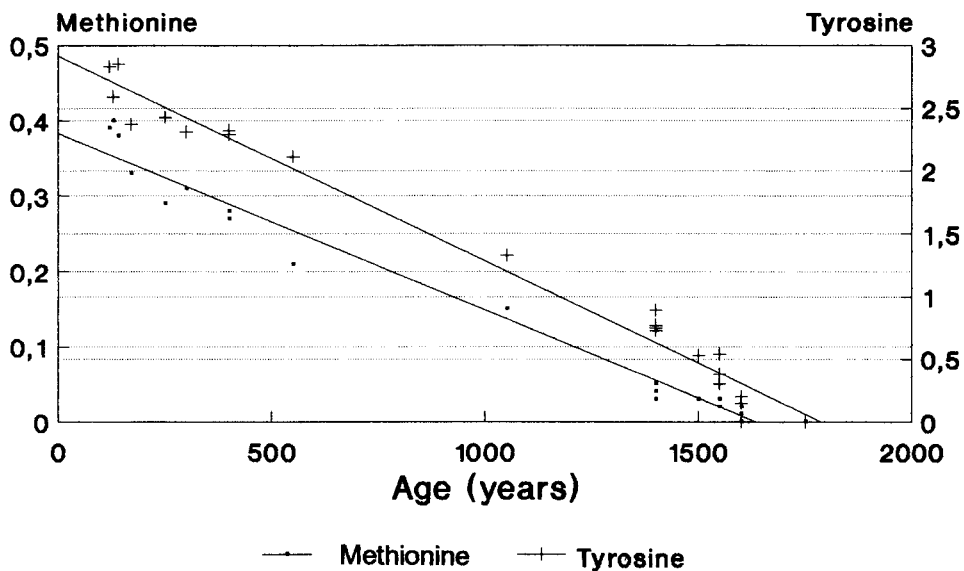


Fig. 2. Age estimation of wool based on methionine and tyrosine content.



Table 6

Equations, correlation coefficients ( $r_{xy}$ ) and errors of estimate ( $s_{y,x}$ ) for linear regressions of age on amino acid contents of wool carpets and wool threads of copt textiles of different ages

Independent variable	Equation ( $a + bx$ )	$r_{xy}$	$s_{y,x}$ (years)
Cysteic acid ( $x_1$ )	$\hat{y} = -335 + 467x_1$	0.996	55.3
Cystine ( $x_2$ )	$\hat{y} = 2068 - 453x_2$	-0.981	124.9
Tyrosine ( $x_3$ )	$\hat{y} = 1770 - 599x_3$	-0.988	100.4
Methionine ( $x_4$ )	$\hat{y} = 1539 - 3601x_4$	-0.855	334.5
Cysteic acid/cystine ( $x_5$ )	$\hat{y} = 366 + 401x_5$	0.974	146.1

Linear regression equations, correlations and standard errors of estimate ( $s_{y,x}$ ) for the regressions of age on amino acid contents are shown in Table 6. Based on the correlations and errors of estimate, cysteic acid content was the most accurate estimator followed by the tyrosine and cystine contents. The cysteic acid/cystine ratio was a less accurate predictor than either of the components of the ratio and the methionine content was clearly the least accurate predictor.

Correlations among the various amino acid contents were extremely high. Considering the three most accurate estimators, the correlation coefficients were -0.980 for cysteic acid and cystine, -0.990 for cysteic acid and tyrosine, and +0.970 for cystine and tyrosine. As a result of these high values between independent variables, very little could be gained by using multiple regression. However, the average of estimates based on cysteic acid, cystine and tyrosine was found to have a standard error of approximately the same size as that based on cysteic acid alone. Use of the average

of estimates allows compensation for errors of analysis for individual amino acids.

The standard error for a given estimate of age can be calculated for

$$s_{\hat{y}} = s_{y,x} \sqrt{\frac{1}{n} + \frac{(x - \bar{x})^2}{SSX}}$$

where  $n$  = number of observations on the sample (23 in this case),  $x$  = observed value of amino acid content in the unknown sample,  $\bar{x}$  = mean amino acid content of the 23 samples and  $SSX$  = sum of  $(x - \bar{x})^2$  for the 23 samples.

The standard error of the mean of three estimates

$$\left( \frac{\hat{y}_1 + \hat{y}_2 + \hat{y}_3}{3} \right)$$

can be calculated as

$$\sqrt{\frac{s_{\hat{y}_1}^2 + s_{\hat{y}_2}^2 + s_{\hat{y}_3}^2 + 2r_{x_1x_2}s_{\hat{y}_1}s_{\hat{y}_2} + 2r_{x_1x_3}s_{\hat{y}_1}s_{\hat{y}_3} + 2r_{x_2x_3}s_{\hat{y}_2}s_{\hat{y}_3}}{9}}$$

Confidence limits calculated as  $\hat{y} \pm (t_{21 \text{ d.f.}, 0.05}) (s_{\hat{y}})$  (d.f. = degrees of freedom) can be placed on each estimate. Standard errors and 95% confidence limits for estimates of age of samples 1.18 and 2.25 are shown in Table 7. Sample 1.18 estimates vary from 562 to 600 years and average 580 years. All four sets of confidence limits overlap, indicating that the estimates are not significantly different ( $P < 0.05$ ). It is 95% certain that sample 1.18 is between 550 and 610 years of age. Estimates for sample 2.25 range from 297 to 344 years and average 326 years. All confidence limits overlap, and

Table 7

Estimates and confidence limits for the ages of two carpets of unknown age

Sample No.	Amino acid	Content (g/100 g protein)	$\bar{x}$	SSX	$\hat{y}$ (years)	$s_{\hat{y}}$ (years)	95% C.L. <sup>a</sup> (years)	
							L.L.	U.L.
1.18.	Cysteic acid	1.92	2.90	39.70	562	14.4	532	592
	Cystine	3.24	2.32	41.03	600	31.6	534	666
	Tyrosine	1.99	1.26	23.70	578	25.8	524	632
	Mean	—	—	—	580	14.2	550	610
2.25.	Cysteic acid	1.44	2.90	39.70	337	17.2	301	373
	Cystine	3.91	2.32	41.03	297	40.5	213	381
	Tyrosine	2.38	1.26	23.70	344	31.2	279	409
	Mean	—	—	—	326	18.1	288	364

Lower and upper values of the 95% confidence limit.

it is 95% certain that the sample 2.25 is between 288 and 364 years of age.

Increasing the cysteic acid and decreasing the cystine and tyrosine contents associated with increasing the age of wool samples have been shown to provide an accurate basis for estimating the age of wool carpet or cloth. However, caution should be exercised in using the prediction equations presented in this paper. A different laboratory working with wool fabric of a different origin should analyse some samples of known age to either verify the applicability of these equations or to develop a set of equations appropriate for their samples.

### Acknowledgements

The financial support of the Hungarian Research Fund (OTKA T 6653) is gratefully acknowledged. S.

Folestad acknowledges support from the Swedish Natural Science Research Council.

### References

- [1] J. Csapó, Zs. Csapó-Kiss, L. Költő and I. Pap, *Archaeometry*, 90 (1990) 627.
- [2] J. Csapó, I. Pap and L. Költő, *Anthropologia Hungarica*, 1 (1988) 67.
- [3] T. Yoritaka and T. Ono, *Nagasaki Iggakai Zassi*, 29 (1954) 400.
- [4] K. Osono, I. Mukai and F. Tominaga, *Nagasaki Iggakai Zassi*, 39 (1955) 156.
- [5] A.J.P. Martin and R.L.M. Synge, *Adv. Protein Chem.*, 2 (1945) 1.
- [6] E. Schram, S. Moore and E.I. Bigwood, *J. Biol. Chem.*, 57 (1954) 33.
- [7] S. Moore, *J. Biol. Chem.*, 238 (1963) 235.
- [8] C.H.W. Hirs, *J. Biol. Chem.*, 219 (1956) 611.
- [9] J. Csapó, Zs. Csapó-Kiss and I. Tóth-Pósfai, *Acta Alimentaria*, 1 (1986) 3.

# Simultaneous determination of arsenic, antimony and selenium by gas-phase diode array molecular absorption spectrometry, after preconcentration in a cryogenic trap

Susana Cabredo Pinillos <sup>a</sup>, Jesús Sanz Asensio <sup>a,\*</sup>, Javier Galbán Bernal <sup>b</sup>

<sup>a</sup> Chemistry Department, Analytical Chemistry Section, University of La Rioja, 26001 Logroño, Spain

<sup>b</sup> Analytical Chemistry Department, Faculty of Sciences, University of Zaragoza, 50009 Zaragoza, Spain

Received 11 February 1994; revised manuscript received 20 July 1994

## Abstract

This paper describes a method for the simultaneous determination of As(III), Sb(III) and Se(IV) by combining hydride generation and gas phase molecular absorption spectrometry. A system for continuous hydride generation has been designed and developed, based on the use of a double process of gas–liquid separation, and optimal compromise operation conditions for the three compounds have been found. After generation, the hydrides are collected in a liquid nitrogen cryogenic trap, and then evaporated and driven to the flow cell of a diode array spectrophotometer, in which the transient signals over the 190–250 nm wavelength interval are measured. Under the recommended conditions (sample flow: 35 ml min<sup>-1</sup>, 0.5 M HCl; reductor flow: 4 ml min<sup>-1</sup> of 4% NaBH<sub>4</sub> solution) linear response ranges above 50 μg l<sup>-1</sup> for As(III), 30 μg l<sup>-1</sup> for Sb(III) and 200 μg l<sup>-1</sup> for Se(IV) are obtained with detection limits of 22 μg l<sup>-1</sup>, 15 μg l<sup>-1</sup> and 65 μg l<sup>-1</sup>, respectively. Multiwavelength linear regression equations were used for the simultaneous determination of the three elements in different synthetic samples, with good precision and accuracy and to study simultaneously the interference from different chemical species for the three compounds. Results were similar to those obtained by other techniques using hydride generation.

**Keywords:** Hydride generation; Antimony; Arsenic; Preconcentration; Selenium

## 1. Introduction

Hydride Generation (HG) has been widely used for many years [1] to determine elements which form hydrides; the great improvements in selectivity and sensitivity obtained justify investigations to develop the technique. These have produced continuous improvements such as electrochemical hydride generation [2] and new combinations with techniques like molecular chemiluminescence [3,4] or UV–visible molecular spectrometry (absorption [5–9], including

thermal lens [10], and emission [11]). One of the approaches that has been extensively developed is the adaptation of a preconcentration step to the generation process; initially, when acid–metal reductors were used, this step was necessary because hydride generation was slow, and nowadays it is still used to improve sensitivity. The preconcentration can be performed in two different ways: (a) at room temperature, through trapping and chemical reaction between the hydride and an organic reagent in solution, in which the hydride characteristics are lost, or (b) by physical preconcentration, so that it does not undergo chemical change.

\* Corresponding author.

In the first case, it is traditional to use organic solutions of spectrophotometric reagents to facilitate determination by molecular absorption spectrometry. Although Ag–diethyldithiocarbamate is the best reagent for determination of As and Sb [12], reagents are available for every element which generates a hydride. This kind of reaction is not necessary for determination by atomic spectrometric techniques and thus, for example Yamaya et al. [13] retained selenium hydride in a  $\text{HClO}_4\text{--KMnO}_4$  solution prior to Se(IV) determination by atomic absorption spectrometry (AAS).

In the second case, the devices used to collect hydrides can be of different types but, at present, the most widely used are cold traps, based on liquid nitrogen cooling. The generation and collection process with these devices can be performed in two different ways, continuously or discontinuously. If the continuous mode is used, two separated flows of reductor ( $\text{NaBH}_4$ ) and analyte (in acidic medium) are mixed; the generated hydride is separated from the liquid phase and preconcentrated in a liquid nitrogen trap, before determination of selenium [14], tin [15] or arsenic(III) and -(V) [16] by AAS.

If the discontinuous mode is used, the sample (acidic medium) is placed in a vessel and the reductor solution is added. The hydride is displaced with a carrier gas ( $\text{N}_2$  or He) and collected in a cold trap. This procedure has been used in the generation of volatiles that need a longer reaction time, such as organometallic hydrides in speciation studies. Thus, arsenic [17], antimony [18], inorganic and methyl species of selenium [19], and tin [20] and organo-germanium species [21] have been determined by atomic spectrometric techniques.

The introduction of diode-array detection systems in UV–visible spectrophotometers has resulted in important improvements in their analytical capability, increasing their use in more selective studies by liquid chromatography or the development of gas phase molecular absorption spectrometry (GPMAS). This last technique has been used in the determination of Sb [5], Se [6] and Ge [7], after hydride generation, and sulphide [22] and ammonium [23] by  $\text{H}_2\text{S}$  and  $\text{NH}_3$  generation. Its potential for speciation studies, (e.g., As(III) and As(V)) [24] or binary determinations of species (Bi and Se) [25] for which absorption spectra overlap, has been demonstrated. This paper shows that the use of hydride generation in a continuous mode, coupled to retention in liquid nitrogen, permits the use

of GPMAS for the simultaneous determination of As, Sb and Se down to trace levels. The mathematical data treatment permits determinations of these three elements, although their hydride absorption spectra show considerable overlap, with good precision and accuracy.

## 2. Experimental

### 2.1. Apparatus

All measurements were performed by using a Hewlett-Packard Model HP 8451A diode array spectrophotometer furnished with a quartz flow cell of 1 cm path length (Hellma 174 QS) and equipped with a HP98155A keyboard (Hewlett-Packard), a floppy disk drive for bulk data storage (Hewlett-Packard HP9121) and a graphics plotter (HP7475A).

For mathematical treatment a Hewlett-Packard Vectra microprocessor with Eureka<sup>®</sup> software was used.

Reagents were pumped using two peristaltic pumps, Masterflex Models 7518-10 and 7016-20 from Cole Palmer (Chicago, IL).

### 2.2. Reagents

All reagents used were of analytical grade quality. Doubly distilled water was used. Standard arsenic solution,  $1000 \text{ mg l}^{-1}$ , was prepared by dissolving  $\text{As}_2\text{O}_3$  (Merck) in 5 M NaOH, neutralizing with 5 M HCl and diluting to volume with 0.5 M HCl. Standard antimony solution,  $1000 \text{ mg l}^{-1}$ , was prepared by dissolving potassium antimony(III) oxide tartrate hydrate (extra pure, Merck) in water and acidifying to 0.5 M in HCl. Standard selenium solution,  $1000 \text{ mg l}^{-1}$ , was prepared by dissolving extra-pure selenium metal (Merck) (1 g) in the minimum volume of 60% w/v  $\text{HNO}_3$  and the solution was evaporated nearly to dryness. Doubly distilled water (2 ml) was added and the solution was evaporated nearly to dryness (this was repeated twice). The residue was subsequently diluted to 1 l with 10% v/v HCl. Working standards were prepared by serial dilution of the stock solution with distilled water immediately before use. A 4% w/v  $\text{NaBH}_4$  aqueous solution was prepared immediately before use (Merck). Solutions containing potential interferents were prepared from chloride or nitrate salts.

### 3. System description. Procedure

Fig. 1 shows a schematic representation of the system used. The solutions are mixed well in the mixer (1) and enter the first gas–liquid separator (2) where the nitrogen carrier gas (20 ml min<sup>-1</sup>) transfers the gaseous products into the water trap. The rest of the liquid goes to a second gas–liquid separator (3), through which N<sub>2</sub> gas is bubbled at 20 ml min<sup>-1</sup>. The gas flow from this separator is carried into the water trap too. The water trap (4) is full of Raschig rings, and is immersed in an ice and salt bath (approximately -10°C). Finally, hydrides are retained in a glass U-tube (5) which contains a small quantity of glass spheres (diameter 2 mm), immersed in liquid nitrogen (-196°C). The liquid nitrogen trap is vented to the atmosphere. The Raschig rings and the small glass spheres are silanized.

The U-tube hydride trap is fitted with a four-way valve. This can be closed to retain compounds for temporary storage. After generation and trapping of a volatile hydride for 5 min, the U-tube is closed and removed from the liquid nitrogen for 5 more min. It is then introduced into hot water (approximately 80°C) for 1 min, after which the hydrides are transported to the continuous flow cell and placed in the spectrophotometer, with a nitrogen flow of 2000 ml min<sup>-1</sup>.

To measure the transient signal, the spectrophotometer is programmed with a BASIC program that permits storage of molecular absorption spectra in the 190–250 nm range. The time interval between successive spectral plots is 0.2 s. All determinations of mixtures or standards are made at least in triplicate.

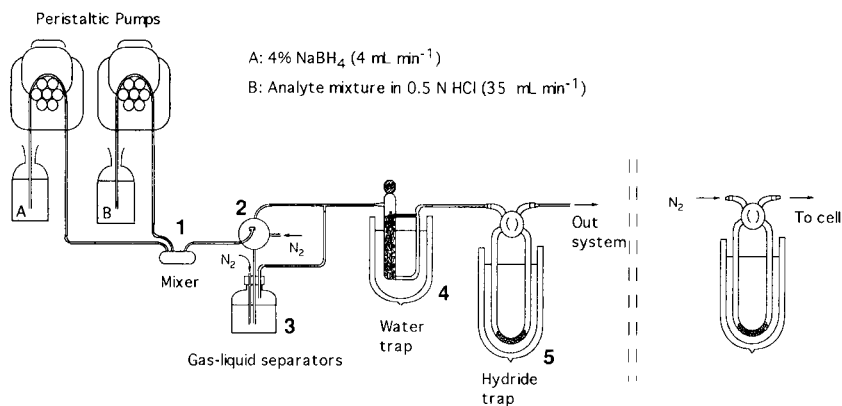


Fig. 1. Schematic diagram of the system (for explanation, see text).

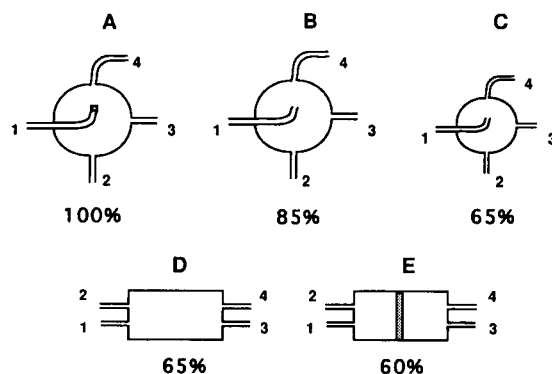


Fig. 2. Different gas–liquid separators used. (1) From mixer; (2) to waste; (3) nitrogen flow; (4) nitrogen + hydrides. Relative efficiencies for Se are shown.

To determine the As, Sb and Se contents in a mixture the maximum absorbance values for every wavelength from the 16 wavelength intervals between 190 and 220 nm (the spectral bandwidth of the spectrophotometer is 2 nm) are obtained. The computer then solves a series of simultaneous equations using the Eureka program.

### 4. Optimization of parameters

#### 4.1. Instrumental

Selenium requires more drastic experimental conditions than As or Sb to generate its hydride and has the lowest sensitivity. Due to these characteristics most of the optimization studies were performed on this element, but later, verifications with As and Sb were made.

### Gas–liquid separator

Different gas–liquid separators were designed in various sizes and types, as indicated in Fig. 2. This also shows the relative efficiency of the different separators compared to the spherical separator (A) with a porous glass tip. Besides giving a smaller efficiency, separator C resulted in too much water being transported with the hydrides. Cylindrical separators (D and E) were inconvenient to use.

In order to increase the separation effectiveness, the possibility of using two gas–liquid separators in series was studied, and different assays were made using different combinations of separators. The best results were obtained by coupling the spherical separator (A) with a bubbler (Fig. 1), which resulted in signal increases of 20% compared to the use of separator A alone.

### Water trap

During the separation step, part of the liquid is nebulized and carried with the hydrides. Prior to the hydride retention in a liquid nitrogen trap, this liquid must be eliminated to avoid both suppression of hydride revolatilization and the transfer of water into the flow cell. In previous studies a multitude of water retaining materials have been used (drierite, molecular sieves, magnesium perchlorate, sulphuric acid, calcium chloride, ice baths or dry ice–acetone baths); in this paper the first drying agent used was calcium chloride. This gave acceptable results but had to be replaced many times and can result in partial hydride retention. The best results were obtained using an ice–salt bath, which offers an adequate temperature to retain the water without keeping back the hydrides. This effect was observed when a dry ice–acetone bath (ca.  $-70^{\circ}\text{C}$ ) was used.

### Nitrogen flow

Nitrogen was used as carrier gas in two parts of the system. One flow carries the hydrides from the gas–liquid separators to the cryogenic trap and the other transfers them to the flow cell from the collector once they have been revolatilized.

Nitrogen flow rates in the separators (2 and 3) were studied between 20 and 100  $\text{ml min}^{-1}$  for both separators in as wide a range as possible of flow-rate combinations. The results obtained are summarized in the following points. (1) Independently of the absolute value, both flows have to be equal to avoid problems

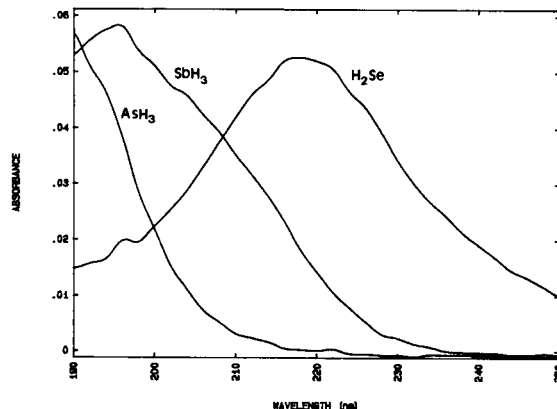


Fig. 3. Gas phase molecular absorption spectra of  $\text{AsH}_3$ ,  $\text{SbH}_3$  and  $\text{H}_2\text{Se}$ .

of the gas reverse movement into the corresponding liquid phases, which produces redissolved hydride and less separation effectiveness. (2) The flow must be the lowest possible; for instance, if the flow decreases from 100 to 20  $\text{ml min}^{-1}$  for every separator, the analytical signal increases by 400%. This is logical because the larger is the flow rate the lesser is the residence time of the hydride in the trap. (3) If the flow rate is  $< 20 \text{ ml min}^{-1}$  in every separator, nitrogen is retained in the cryogenic trap. This nitrogen is later revolatilized, escaping from the valve and allowing hydride escape.

With respect to the nitrogen flow that transfers the hydride to the flow cell, it was observed that, as the flow was increased from 50  $\text{ml min}^{-1}$ , bigger and more reproducible signals were obtained with an optimum of 2000  $\text{ml min}^{-1}$ . At 50  $\text{ml min}^{-1}$ , the signals gave a very good reproducibility but were smaller due to a hydride dilution effect in the carrier gas, as observed in previous studies [5–7].

### Other parameters

Another aspect of the system that was studied is the distance between the mixer and the separator. Many distances were assessed but no differences in signal were observed. Thus it was proposed to use the minimum possible distance (3–4 cm). An exhaustive study was also performed of the time necessary for hydride revolatilization. The results indicated: (1) a stabilization time of the U-tube at room temperature was necessary before introduction into the hot water bath (if not, thermal shock sometimes shattered the trap); 5 min is optimal since over longer periods the signal decreases; (2) heating the U-tube after the 5 min of

Table 1  
Variation of H<sub>2</sub>Se absorbance with NaBH<sub>4</sub> concentration

NaBH <sub>4</sub> conc. [% (w/v)]	Absorbance
2	0.0055
4	0.0094
6	0.0092
8	0.0081

stabilization was necessary; 1-min heating is optimal. If the measurement is performed without stabilization and heating, the signal decreases by ca. 50%.

#### 4.2. Chemical

Although the generation conditions of these hydrides and their determination by GPMAS have been studied in previous papers [5,6,23] it has always been by discontinuous procedures where a great amount of H<sub>2</sub> gas arrived with the generated hydrides in the measurement cell. When cryogenic retention is used, H<sub>2</sub> is removed, which can alter the molar absorptivities of the hydrides. Besides this in coupling hydride generation with another techniques (usually AAS), the generation conditions change depending upon whether a continuous or discontinuous method is used. It is therefore necessary to study the main chemical parameters that affect the generation yield, viz., the medium acidity and NaBH<sub>4</sub> concentration.

#### NaBH<sub>4</sub> concentration

As observed in Table 1, the greatest signal appears at 4 or 6% NaBH<sub>4</sub>. The decrease at larger concentrations is explained by the great quantity of hydrogen generated, which impedes the circulation of the carrier

Table 2  
Analytical characteristics

Element	Sensitivity (ml μg <sup>-1</sup> )	Lower limit (μg ml <sup>-1</sup> )	Detection limit (μg ml <sup>-1</sup> )	R.S.D. <sup>a</sup> (%)	R.S.D. <sup>b</sup> (%)
As	0.1020	0.050	0.022	10.5	3.6
Sb	0.1720	0.030	0.015	10.1	3.8
Se	0.0307	0.200	0.065	11.0	4.0

<sup>a</sup> Obtained for a concentration equal to a lower limit of the linear calibration range.

<sup>b</sup> Obtained for a concentration five times larger than the lower limit.

Table 3  
Results for simultaneous determinations

Mixture	Conc.	[As] (μg l <sup>-1</sup> )	[Sb] (μg l <sup>-1</sup> )	[Se] (μg l <sup>-1</sup> )
1	Real	50	50	500
	Found	32	59	620
2	Real	400	400	200
	Found	390	320	210
3	Real	200	200	2000
	Found	260	130	2000
4	Real	400	50	2000
	Found	400	59	2300
5	Real	2000	2000	5000
	Found	1700	1800	4500
6	Real	1000	50	500
	Found	800	61	510
7	Real	50	1000	500
	Found	37	1200	620

gas (N<sub>2</sub>) through the system. The pressure gauge controlling the nitrogen flow indicated a pressure loss.

#### Acid

The amount of acid necessary for hydride generation was studied. For hydrogen selenide, the signal was not significantly modified over the range 0.5 to 2 M HCl, but decreased slightly at smaller or larger acid concentrations.

#### 5. Analytical characteristics

Under the optimal instrumental and chemical conditions outlined in the Experimental section individual calibration studies were made for each element, using their wavelengths of maximum absorbance (Fig. 3) (190, 198 and 220 nm for As, Sb and Se, respectively). The sensitivity values obtained (slopes of calibration graphs) are indicated in Table 2. The same table gives the lower limits of the linear response range, the detection limits (based on twice the background standard deviation) and the reproducibility values (expressed as R.S.D.) obtained for two concentrations of each element, one the lower limit of the linear response range and the other to a selected higher concentration value.

The sensitivity was greater for As(III) and Sb(III) than for Se(IV); nevertheless these differences were not reflected in the detection limits, possibly because the maximum absorbance of Se(IV) appears in a spec-

Table 4  
Results for interference study

Species	As	Sb	Se
Ca, Mg, Sr, Ba, Cr, Mn	4000 <sup>a</sup>	4000 <sup>a</sup>	1000 <sup>a</sup>
Fe	4000 <sup>a</sup>	4000 <sup>a</sup>	500
Hg	4000 <sup>a</sup>	4000 <sup>a</sup>	1000 <sup>a</sup>
Te	1000	1000	250
Pb	1000	1000	50
Sn	100	100	100
Ge	50	4000 <sup>a</sup>	1000 <sup>a</sup>
Ni	40	40	5
Co	40	40	5
Cu	100	100	10
Bi	200	20	50
Cd	2000	2000	500
Al, Zn	4000 <sup>a</sup>	4000 <sup>a</sup>	1000 <sup>a</sup>

<sup>a</sup> Maximum ratio tested. Minimum ratio (w/w) giving 10% change in signal.

tral zone in which the baseline noise is smaller. The analytical parameters obtained are much better than those observed for discontinuous determinations.

## 6. Simultaneous determination

When a spectrophotometer with diode-array detector is used, simultaneous determination of the three hydrides in a mixture can be performed. The first procedure tested involved solving the following three equations with three unknown concentrations:

$$\text{Abs}_{190}^m = a_{190}^{\text{As}} [\text{As(III)}] + a_{190}^{\text{Sb}} [\text{Sb(III)}] + a_{190}^{\text{Se}} [\text{Se(IV)}]$$

$$\text{Abs}_{198}^m = a_{198}^{\text{As}} [\text{As(III)}] + a_{198}^{\text{Sb}} [\text{Sb(III)}] + a_{198}^{\text{Se}} [\text{Se(IV)}]$$

$$\text{Abs}_{220}^m = a_{220}^{\text{As}} [\text{As(III)}] + a_{220}^{\text{Sb}} [\text{Sb(III)}] + a_{220}^{\text{Se}} [\text{Se(IV)}]$$

where  $\text{Abs}_y^m$  is the measured absorbance of the mixture at each of the three wavelengths corresponding to the maximum absorbance of each hydride and  $a_x^y$  is the molar absorptivity of the individual hydride at the wavelength specified. The results obtained using this method on synthetic mixtures of As(III), Sb(III) and Se(IV) were quite imprecise and inaccurate, however.

In order to improve these results, a multi-wavelength method was applied. A system of  $n$  equations with three unknowns must be resolved, where  $n$  is the number of wavelengths used ( $n > 3$ ) and the three unknowns are the concentrations of As, Sb and Se in the mixture. Absorbance values for every wavelength were obtained using a BASIC program. This program permits (i) obtaining the molecular absorption spectra in the range 190–250 nm while the hydrides are passing through the flow cell, (ii) storage of the absorbance values for every wavelength covering all spectra and (iii) selection of the maximum absorbance values for every wavelength and the numerical order of the spectrum in which these values appear.

In all cases it was observed that the absorbance maxima occurred at the same time for all wavelengths. Because of this, the three hydrides are volatilized and carried to the cell at the same time, so the reproducibility of the results is good.

In order to solve the equations, a mathematical program (Eureka) using an iterative procedure was used. Different wavelength intervals were assessed, but the best results were obtained using all wavelengths between 190 and 220 nm (16 equations, because the spectral bandwidth of the spectrophotometer is 2 nm). In Table 3 the results obtained for several mixtures of As, Sb and Se are shown. All results are the average of three determinations and the R.S.D. values were, in all cases, < 5%. The concentrations found agreed reasonably with the known values although some problems remain.

## 7. Interference study

The proposed method for the simultaneous determination of the three elements as outlined above, allows the simultaneous study of interference effects on the three species. Solutions containing As, Sb and Se and the potential interferent element were prepared. Each of these solutions was subjected to the generation and determination procedure and the concentrations obtained by this method were compared with the known values to assess the extent of interference. Table 4 indicates the minimum w/w ratios at which the concentration obtained differs by 10% from the known value. All experiments were performed in triplicate.



## Acknowledgements

This work was supported by CICYT (project No. 541 A.783). S. Cabredo thanks the FPI grant to Instituto de Estudios Riojanos of La Rioja (Spain).

## References

- [1] J. Dedina, *Prog. Anal. Spectrosc.*, 6 (1983) 163.
- [2] Y. Lin, X. Wang, D. Yuan, P. Yang and B. Huang, *J. Anal. At. Spectrom.*, 7 (1992) 287.
- [3] K. Fujiwara, A. Kuramochi and H. Tsubota, *Anal. Sci.*, 6 (1990) 425.
- [4] K. Fujiwara, M. Uchida, M. Chen, Y. Kumamoto and T. Kumamaru, *Anal. Chem.*, 65 (1993) 1814.
- [5] J. Sanz, F. Gallarta, J. Galbán and J.R. Castillo, *Fresenius' Z. Anal. Chem.*, 330 (1988) 510.
- [6] J. Sanz, F. Gallarta, J. Galbán and J.R. Castillo, *Analyst*, 113 (1988) 1387.
- [7] J. Sanz, L.A. Ortega, J. Galbán and J.R. Castillo, *Microchem. J.*, 41 (1990) 29.
- [8] M.S. Cresser, *Lab. Pract.*, 27 (1978) 639; and references cited therein.
- [9] A. Syty, *Anal. Chem.*, 51 (1979) 911; and references cited therein.
- [10] M.A. Rius, G. Ramis, S. Cabredo and J. Galbán, *Quim. Anal. (Int.)*, 12 (1993) 7.
- [11] D.A. Stiles, A.C. Calokerinos and A. Townshend (Eds.), *Flame Chemiluminescence Analysis by Molecular Emission Cavity Detection*, Wiley, Chichester, 1994.
- [12] R. Merry and B. Zarcinas, *Analyst*, 105 (1980) 558.
- [13] K. Yamaya, T. Aoki and I. Kim, *Bunseki Kagaku*, 41 (1992) 263.
- [14] U. Ornemark, J. Pettersson and A. Olin, *Talanta*, 39 (1992) 1089.
- [15] P.N. Vijan and C.Y. Chan, *Anal. Chem.*, 48 (1976) 1788.
- [16] M. Burguera, J.L. Burguera, M.R. Brunetto, M. de la Guardia and A. Salvador, *Anal. Chim. Acta*, 261 (1992) 105.
- [17] M. Andreae, *Anal. Chem.*, 49 (1977) 820.
- [18] M. Andreae, J. Asmode, P. Foster and L. Van't Dack, *Anal. Chem.*, 53 (1981) 1766.
- [19] S. Jiang, H. Robberetch, J. Adams and D. Van den Berghe, *Toxicol. Environ. Chem.*, 6 (1983) 191.
- [20] O.F. Donard, S. Rapsomanikis and J.H. Weber, *Anal. Chem.*, 58 (1986) 772.
- [21] K. Jin, Y. Shibata and M. Morita, *Anal. Chem.*, 63 (1991) 986.
- [22] J. Sanz, S. Cabredo and J. Galbán, *Anal. Lett.*, 25 (1992) 2095.
- [23] J. Sanz, S. de Marcos, O. Muro and J. Galbán, *Mikrochim. Acta*, 110 (1993) 193.
- [24] J. Sanz, F. Gallarta and J. Galbán, *Anal. Chim. Acta*, 255 (1991) 113.
- [25] J. Sanz, S. de Marcos, J. Galbán and F. Gallarta, *Analisis*, 21 (1993) 27.

# Comparison of two methods for coating piezoelectric crystals

M. Teresa Gomes <sup>\*</sup>, Armando C. Duarte, João P. Oliveira

*Department of Chemistry, University of Aveiro, 3800 Aveiro, Portugal*

Received 15 April 1994; revised manuscript received 20 July 1994

## Abstract

Quartz piezoelectric crystals were coated with triethanolamine using two procedures: spray and syringe methods. The reproducibility of both coating methods was evaluated comparing the relative standard deviation of batches of four crystals coated by each of the procedures. The relative standard deviation obtained with the spray method is a hyperbolic function of the coating frequency and is, at least, three times lower than the one calculated from results of the syringe method, which is not frequency dependent. An explanation for the poorer reproducibility of the syringe method is given, based on the radial sensitivity theory and the non-uniformity of the coating distribution over the crystal, as evidenced by microscopic photographs.

*Keywords:* Quartz crystal microbalance; Coatings; Piezoelectric crystals

## 1. Introduction

Sauerbrey's [1] equation relating the change in the vibrational frequency of a piezoelectric quartz crystal with an addition of mass is widely used in the application of quartz crystal microbalances to the detection of gaseous compounds. However, the equation assumes that the mass added to a piezoelectric crystal is uniformly distributed like a rigidly elastic thin film. As in practice this is not true, calibration is always needed.

The crystals show greater mass sensitivity on the center of the electrodes: the sensitivity decreases monotonically with the radius, in a Gaussian manner [1–6] becoming, in the gas phase, negligible at and beyond the electrode boundary [4–6]. This is also true in liquids, although, due to field fringing, there is some sensitivity beyond the electrode edges [5,6]. As a result, the same amount of mass deposited can cause different frequency shifts depending on their location in the

active area of the crystal. Therefore, besides calibration, it is now clear that an analysis can only be performed with similar sensitivity if coating can be reproducible.

In order to apply a liquid coating there are several possibilities, the most common being: dropping, smearing, dipping, spraying [7], and spin coating. Dipping does not permit control over the deposition. Smearing is time consuming and as the control parameter is the frequency, it is possible to have different quantities of coating unevenly spread over the electrodes. Spin coating is not used very often. This paper reports the results obtained when using spraying and syringe dropping as different methods for coating piezoelectric crystals.

## 2. Experimental

### 2.1. Apparatus

The experimental setup is shown schematically in Fig. 1. The cell design consists of a pyrex cylinder with

<sup>\*</sup> Corresponding author.

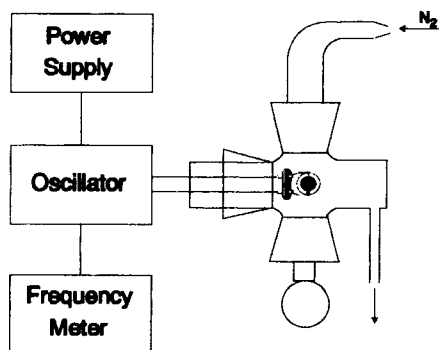


Fig. 1. Schematic diagram of the experimental apparatus.

a length of 9.0 cm and a diameter of 2.5 cm. One of the ends is fitted with a 14/20 female connector which permits the easy change of the crystal. The other end is sealed with a window to monitor the position of the crystal inside. Placed 4.5 cm from the window, and facing the crystal, there are two female 14/20 fittings positioned at 180° angles around the cell. These openings can be used for the introduction of gases, although in this experiment one opening not in use was sealed with 14/20 male stopper. The nitrogen is exhausted through a 6 mm glass tube placed near the window. The dry nitrogen flow was monitored by a calibrated variable area flow meter (Cole-Parmer).

The crystals used were 9 MHz AT cut, with silver plated electrodes (TXC). The crystal oscillator circuit based on TTL inverter gates and the 5 V power supply were both home made. The frequency was measured with a digital counter (Leader Model LDC-823A) with a range of 10 Hz to 250 MHz and a resolution of 0.1 Hz.

The spraying device design is shown schematically in Fig. 2. The spraying device consisted of a commercial air-brush (Badger Model 200), with a solution reservoir, a plate driven by a 10 rpm precision motor (Saia), and a calibrated variable area flowmeter (Cole-Parmer), to control the nitrogen flow. The air-brush had an internal mix geometry and the opening of the orifice was variable. The plate had four pairs of orifices and each one could hold a crystal upright. The plate was positioned in front of the air-brush and as it was rotating each of the crystals received a spray of solution. To prevent the rear face of the opposite crystals from being reached by the spray, the plate was divided into four chambers.

A 10  $\mu$ l Hamilton syringe (Model 701 RN) with a repeatability ( $z_{95\%} \times \sigma \times \sqrt{2}$ ) of  $0.070 \times 10^{-6}$  g for a  $3 \times 10^{-6}$  l delivery was used.

The observation of the surface of the crystal was carried out by a BH-2 optical microscope coupled to a CUE-2 image analyser, from Olympus.

## 2.2. Reagents

Triethanolamine (8377 Merck) was dissolved in acetone (p.a. 14, Merck), and the nitrogen was R grade from "ArLíquido".

## 2.3. Procedure

Triethanolamine was used as coating, based on the fact that it does not react with air and it is not volatile at room temperatures between 15 and 25°C. Even at 27°C and under a nitrogen flow of 500 ml min<sup>-1</sup> Che-

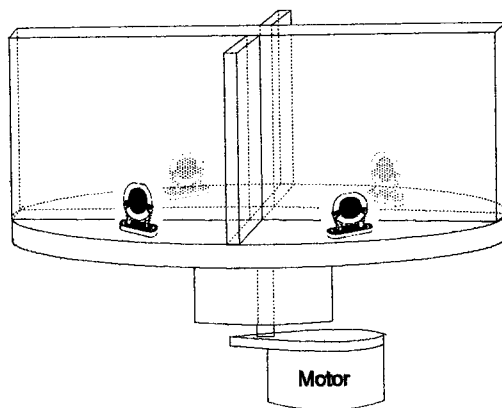
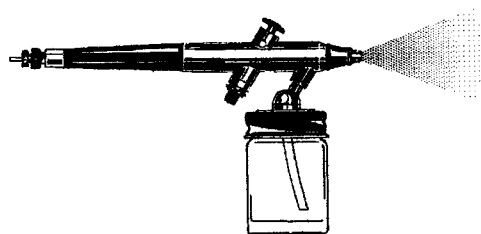


Fig. 2. Schematic arrangement of the spraying device and rotating plate.

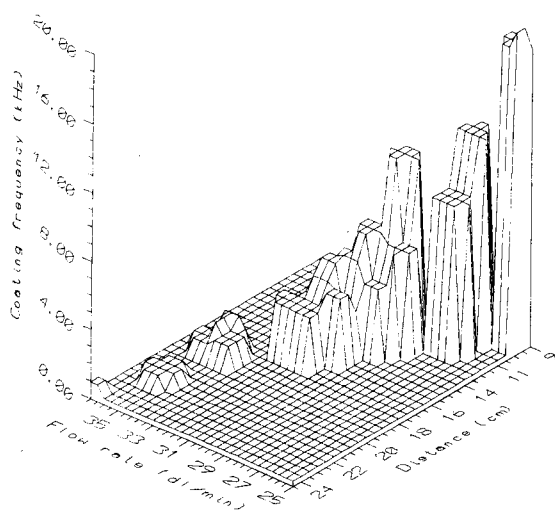


Fig. 3. Average decrease in frequency due to coating obtained with the spray method.

ney and Homolya [8] have shown that the loss of coating was negligible.

Although this compound is hygroscopic, this is not a severe problem as was experimentally confirmed with two coated crystals, with frequency decreases due to coating of 3.262 kHz and 2.660 kHz, respectively. When these coated crystals were exposed to the laboratory air for 30 min, the fluctuation in the frequency was found to be only 14 Hz and 10 Hz, respectively.

In both methods, and for each crystal, the oscillating frequency was measured under a nitrogen flow of 55 ml min<sup>-1</sup>, before and after coating. The frequency was recorded after evaporating the solvent in a nitrogen flow for 5 min. The experiments were carried out using batches of four crystals, and while the frequency of one was being monitored the others were kept in a desiccator.

Triethanolamine in acetone was used at very dilute solutions, respectively 2.0% m/v in the spray reservoir and from 0.15% m/v to 0.8% m/v with the syringe.

In the syringe coating method, four crystals were held with the faces as horizontal as possible, and a drop of the coating solution was applied with a microsyringe on the centre of the upper electrode.

In the spray method, the quantity of solution reaching each crystal and the dimension of the drops, can be controlled by several parameters. The opening of the spray orifice was held constant, but the flow, the distance from the air brush to the plate and the height of the air brush were varied. The concentration of the

solution and the number of times each crystal passes in front of the spray were held constant. The plate was allowed to make eight complete rotations, thus exposing each crystal eight times to the spray. At the beginning of each experiment the level of solution inside the air-brush reservoir was kept constant since such was noticed to be an important factor.

### 3. Results and discussion

The results obtained with the spray method are displayed in Fig. 3. Different frequency changes due to coating can be achieved by different combinations of the propeller gas flow to the spray, and the distances from the nozzle to the crystal in front of the spray plume. The level difference between the nozzle spray and the centre of the crystal was not varied more than 3.3% during the experiments. Each data point used for plotting Fig. 3 is an average of the individual frequency decrease due to coating of four crystals occupying four different positions at the plate and coated during its rotation.

Figs. 4 and 5 show the relative standard deviations for frequency changes due to coating of batches of four crystals, obtained respectively with the spray method and with the application of  $3 \times 10^{-6}$  l solutions of different concentrations with a syringe. A comparison of the two graphs shows that the relative standard deviation

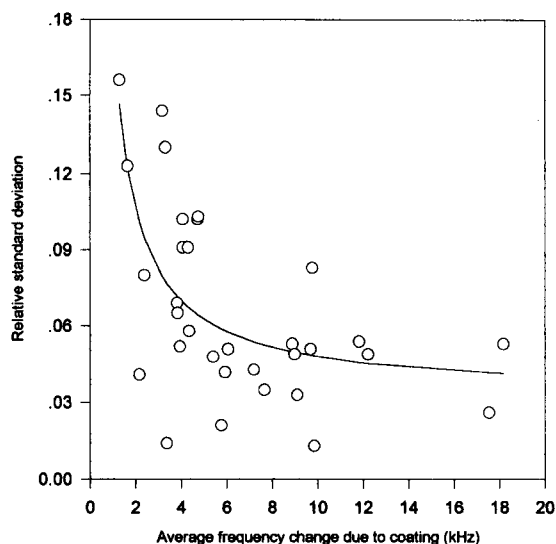


Fig. 4. Relative standard deviation of the frequency changes due to coating by the spray method.

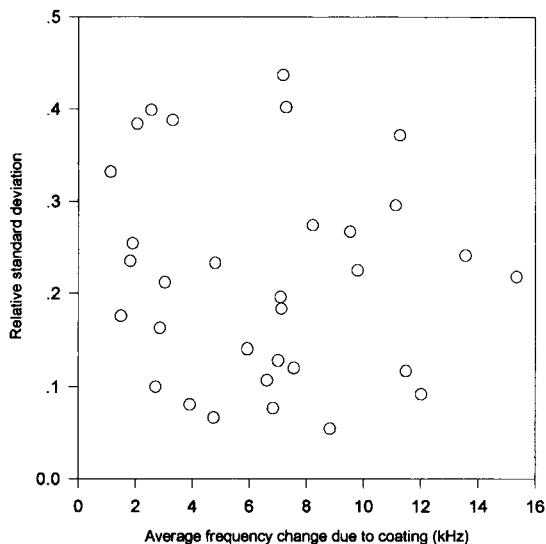


Fig. 5. Relative standard deviation of the frequency changes due to coating by the syringe method.

tion for results obtained with the spray method is, in general, much lower than the one obtained with the syringe coating.

The relative standard deviation decreases with the frequency change due to coating for the spray method, but no trend could be found for the syringe method. In the spray method the equation that describes the variation of the relative standard deviation (R.S.D.) with the frequency change due to coating ( $F$ )

( $R.S.D. = 0.034 + 0.14/F$ ) can be mainly attributed to the presence of electronic instrumental noise. In the mentioned equation, the constant can be related to white noise, and the second term can represent the contribution of pink noise.

In the syringe method, the electronic noise must be also present, but the observed variability must be associated to some other effect. This arises because there is a much higher variability associated to the syringe method. As can be seen from Fig. 6, the coating obtained with the spray method is uniformly distributed all over the crystal in the form of small drops, while during the delivery of the solution with the syringe the liquid spreads over the crystal, mainly in the electrode area, but neither always in the same way, nor occupying the same region or having the same area. The non-uniformity of the distribution of the amine over the crystal can be seen in Fig. 7.

The non-uniformity on coating distribution can explain the variation of the frequency changes due to coating, as can be shown in the radial distribution model of the crystal sensitivity displayed on Fig. 8. As the coated area of the crystal is larger with the spray method (Fig. 8A) than with the syringe method (Fig. 8B), a different arrangement of the small drops will not cause significant frequency changes. With the syringe method, as the size of the drops is bigger and very different, and as we compare different areas of the crystal, a slightly different position of the drops, mov-

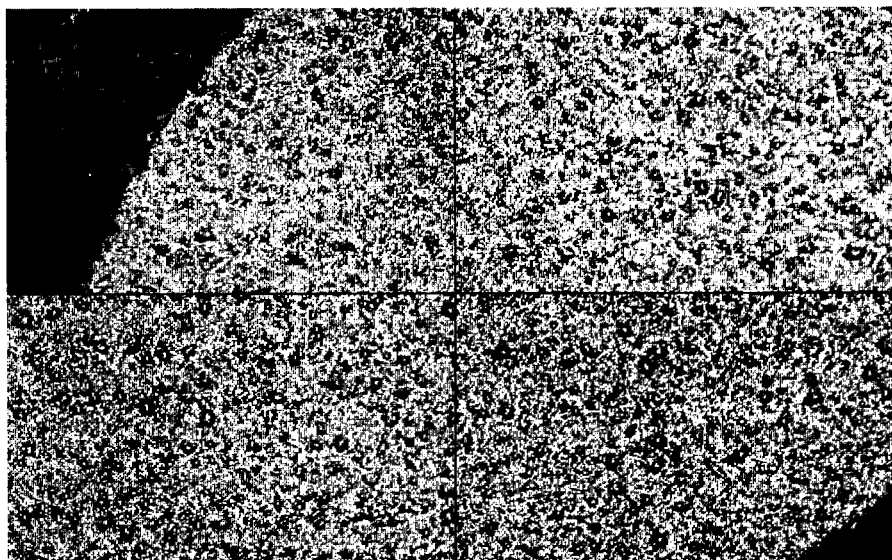


Fig. 6. Optical microscope images of four different areas of the crystal surface coated by the spray method (magnification  $50\times$ ).

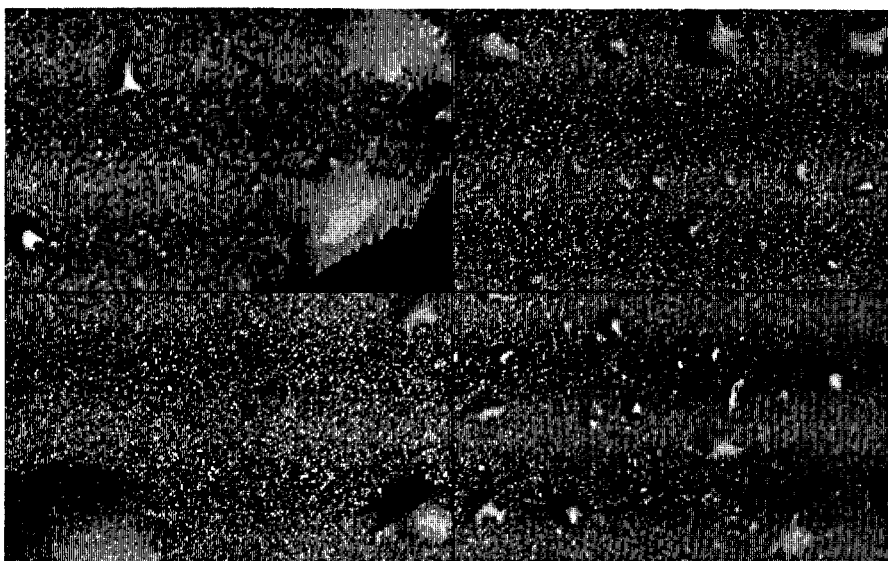


Fig. 7. Optical microscope images of four different areas of the crystal surface coated by the syringe method (magnification  $50\times$ ).

ing to areas of bigger or smaller sensitivity, could cause significant change in the decrease of the frequency due to coating.

It is apparent from the present study that the experimental data also indicate that when it is important to obtain crystals with the same sensitivity, as when they are used as sensors for quantitative analysis, where the interactions of the analyte with the coating should take

place, in different crystals, at points of equal mass sensitivity, the spray method should be used.

#### Acknowledgements

The authors thank the Chemical Engineering Department of the University of Coimbra for providing the microscope images.

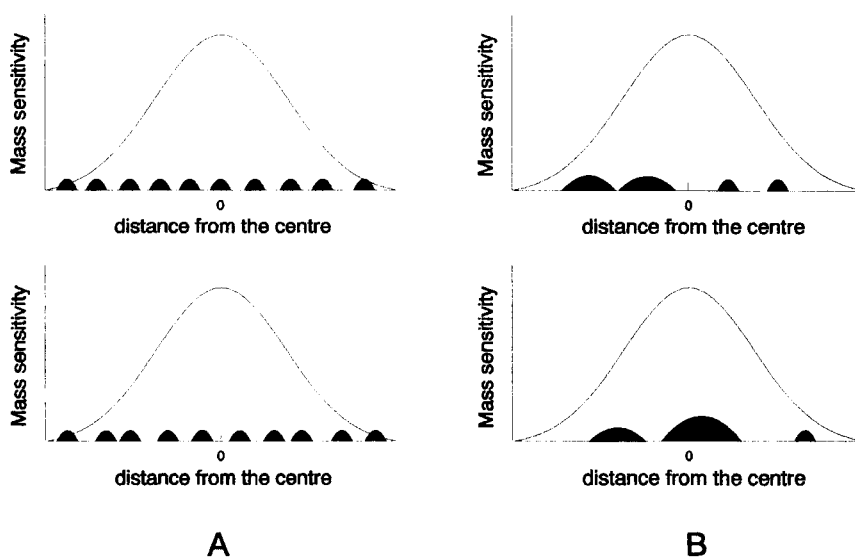


Fig. 8. Theoretical Gaussian mass sensitivity and hypothetical coating distribution of two crystals for the spray method (A), and syringe method (B).

**References**

- [1] G. Sauerbrey, *Z. Phys.*, 155 (1959) 206.
- [2] B.A. Martin and H.E. Hager, *J. Appl. Phys.*, 65 (1989) 2630.
- [3] D.M. Ullevig, J.F. Evans and M.G. Albrecht, *Anal. Chem.*, 54 (1982) 2341.
- [4] V.M. Bel'kov and L.M. Malinovskaya, *Zh. Anal. Khim.*, 39 (1984) 1614.
- [5] M.D. Ward and E.J. Delawski, *Anal. Chem.*, 63 (1991) 886.
- [6] A.C. Hillier and M.D. Ward, *Anal. Chem.*, 64 (1992) 2539.
- [7] J. Hlavay and G.G. Guilbault, *Anal. Chem.*, 49 (1977) 1890.
- [8] J.L. Cheney and J.B. Homolya, *Anal. Lett.*, 8 (1975) 175.



ELSEVIER

Analytica Chimica Acta 300 (1995) 335–340

---

---

**ANALYTICA  
CHIMICA  
ACTA**

---

---

## Book Reviews

Karel Eckschlager and Klaus Danzer, *Information Theory in Analytical Chemistry*, Vol. 128 in the Chemical Analysis Series, Wiley, New York, 1994 (ISBN 0-471-59507-1). xi + 275 pp. Price £54.00.

The nature of analytical chemistry, like almost all aspects of life, is being altered radically by the rate of development of computer technology and in particular, the ability to process vast amounts of information at incredibly fast speeds.

Traditionally, chemical analysis has consisted of sampling, sample preparation, analysis, and interpretation of results. Calibration consisted of making a standard curve and measuring the correlation coefficient to quantify the degree of linearity. Statistical analysis typically involved reporting the mean and standard deviation of several replicate analyses. Quite suddenly, it seems, we are confronted with multivariate analytical approaches which lead to more complex calibration designs, and instrumental methods which generate huge data sets which are often multi-dimensional in nature.

Clearly, the traditional analytical approach cannot be used in this emerging framework, and is being replaced with concepts from information technology, probability theory and advanced statistical methods. This book charts the impact of principles based on information theory on how analytical data is acquired, processed and interpreted. In the future, the value of an analyst's work will be gauged in terms of 'information profitability' measured in bits per currency unit.

The book covers aspects of chemometrics, optimisation of analytical strategy, quality assurance, signal processing, classification of analytical information, and the links between information theory and analytical chemistry in general. Specific topics include

identification of components, qualitative and quantitative analysis, multicomponent analysis, chemometrics and structure analysis. The spatial distribution of sample components is discussed both in terms of the 3-D structure of materials and molecules, and in terms of surface distribution in non-homogeneous (e.g., solid) samples. The book has a comprehensive index and references for further reading at the end of each chapter (mainly pre-1992).

It is not an easy book to read, and would be more suitable for specialist courses in areas such as chemometrics rather than for general undergraduate studies. In addition, the reproduction of some of the illustrations is very light. However, it should be on the shelf of anyone involved in research or teaching in analytical chemistry, and it will be an invaluable aid to those specialising in the impact of computer information technology on analytical chemistry.

Dermot Diamond

S.P. Maj, *The Use of Computers for Laboratory Automation*, The Royal Society of Chemistry, London, 1993 (ISBN 0-85186-744-8). xviii + 358 pp. Price £22.50.

This book is more about computers than laboratory automation. However, with its clear presentation and eminently readable style, it provides a valuable source of information on computing principles and computer architecture for those using computers.

Nine chapters cover the basics of computing and computers and include: Communicating with the Computer; Microprocessors; Memory Devices; Operating Systems; Input and Output Interfaces; Net-



working; Introduction to Data Processing; Software Engineering; and Laboratory Information Management Based Systems. A 'Bibliography' and 'Subject Index with Abbreviations' are included. The inclusion of abbreviations is very valuable although there are some abbreviations/acronyms omitted from the index either by unexplained design or default.

The sections relating to interfacing devices and LIMS focus on aspects of computing that are directly relevant to the laboratory environment and automation therein. At its modest price the book provides very good value for money and could be read to advantage by many whose daily work brings them in contact with computers. The book would be particularly helpful to those who want to communicate with computing specialists or need to understand the specifications of computing facilities provided with new laboratory equipment.

John D. Green

D.A. Stiles, A.C. Calokerinos and A. Townshend (Eds.), *Flame Chemiluminescence Analysis by Molecular Emission Cavity Detection*, Wiley, Chichester, 1994 (ISBN 0-471-94340-1). xiii + 205 pp. Price £50.00.

Molecular emission cavity analysis (MECA) is a flame chemiluminescence technique which is characterized by the use of a small cavity as the means for sample introduction into the flame and as the reaction space for all processes up to emission of radiation. The emitting species are restricted mainly to non-metals and metalloids, but gas generation systems or a great variety of derivatization reactions expand the technique to various analytical applications.

The contributors are all key researchers who have developed and improved this technique, and consequently, the contents of the monograph are substantial. The first chapter describes briefly the circumstances of the development of MECA. The chapter describing the introduction and basic principles is systematically written, and comparison with other techniques makes the advantages of this technique clear. Chapter 3 "Instrumentation and automation" describes the simplicity and the easy assembly of a

MECA instrument. These chapters are a good guide for many readers to understand the characteristics of the technique.

Chapters 4 to 7 comprehensively provide detailed analytical applications, such as emission spectra, interferences and their elimination, incorporation with other techniques and a great variety of derivatization reactions for indirect determination, which are useful for analytical chemists.

The contributors surely succeeded in describing the usefulness of the technique as a detector. The monograph would absorb even more interest of readers and would encourage and stimulate research in this field, if those areas of immaturity were emphasized a little more.

Koichi Nakajima

Z.B. Alfassi (Ed.), *Chemical Analysis by Nuclear Methods*, Wiley, Chichester, 1994 (ISBN 0-471-938343). xx + 556 pp. Price £90.00.

As the contents list of this book indicates, the term "nuclear analysis" embraces a remarkably wide range of methods and techniques used in analysis. In this respect the book differs from a number of other recent books in the field. It probably gives the most comprehensive survey of all these methods. Also the subdivision is different, since it is not focussed on applications, but subdivided in 5 major parts, describing the physical background, the analysis by means of neutron sources, particle accelerators, radioactive sources and finally the use of radiotracers. Chapters 1 to 5 (part 1) give a classical and concise description of interaction with matter, detection and production of radiation and isotopes and finally some basic principles of radiation protection. The major interest of the book, however, is in the following 15 chapters, each of which, typically, comprises 20 to 35 pages. The principles, the equipment and the applicability of a group of nuclear methods of analysis are summarized in a clear and surveyable way, generally not overloaded with complicated figures or numerical data. Not only the more classical methods are treated, such as activation analysis, particle induced X-ray emission, isotope dilution and radio-immunoassay, but also less applied and more recently

developed methods are discussed, such as analysis by positron annihilation, scattering of  $\alpha$ ,  $\beta$  and  $\gamma$  radiation for chemical analysis, nuclear microprobes, ion-backscattering and elastic recoil detection, thermalization, scattering and absorption of neutrons.

This book can surely be an excellent introduction to researchers or analysts, new to the field and looking for a nuclear technique to solve their analytical problems in nuclear physics, chemistry, material and environmental sciences, geology or biology.

R. Dams

H. Bennett and G. Oliver, *XRF analysis of Ceramics, Minerals and Allied Materials*, Wiley, Chichester, 1992 (ISBN 0-471-93457-7). 298 pp. Price US\$101.00.

This book is a precious edition of significant practical value for the many accredited laboratories around the world which use X-ray fluorescence as an analytical method and deal with the extremely difficult domain of analysing ceramics and related materials like minerals, rocks, glasses and slags. A wealth of information is provided for the solution of most of the practical problems in this field, both for direct analyses and for the common fused, cast bead method. A number of verified procedures are given in detail; they allow an extremely wide range of material types to be handled in a simple, accurate and rapid way. Background information about complementary techniques and processes is given as well.

The book is written in a very comprehensible way. The authors are experienced practical analysts with an excellent understanding of the importance of the analytical process itself. In summary, the book constitutes a valuable reference volume for all analysts involved with bulk-manufacture ceramic products and their raw materials.

Jasna Injuk

John A. Weil, James R. Bolton and John E. Wertz, *Electron Paramagnetic Resonance, Elementary Theory and Practical Applications*, Wiley, New York,

1994 (ISBN 0-471-57234-9). xxi + 568 pp. Price £66.00.

This monograph is intended to be an introduction and tutorial on electron paramagnetic resonance for students at senior undergraduate or postgraduate level either as a taught course text book or as a self-study guide. The treatment is comprehensive and in depth. Following an introduction to basic principles it deals in turn with magnetic interactions between particles, isotropic hyperfine effects, Zeeman energy and hyperfine anisotropies, systems with more than one unpaired electron, species in the gas phase, transition-group ions, interpretation of epr parameters, relaxation times, line widths and kinetic phenomena, time dependent excitation of spins, double resonance techniques and "other topics". This latter chapter is an all too brief applications area survey.

Appendices, 27% of the text, deal with what is regarded as necessary supporting material. These include mathematical operations, quantum mechanics of angular momentum, exact calculation of hyperfine interaction in the hydrogen atom, detailed discussion of instrumentation, technical performance and experimental conditions.

You will thus deduce this is not a book for the dilettante or for the faint of heart. It is a first class text for the serious student of the subject who, if they accept the challenge, will be led to acquire, as the authors put it so modestly, "a respectable understanding of the experiments, equipment and background".

An essential purchase for all tertiary level libraries whose readers take their chemistry seriously.

D. Thorburn Burns

Zbigniew Galus, *Fundamentals of Electrochemical Analysis*, Ellis Horwood, New York (ISBN 0-13-345281-6), and Polish Scientific Publishers PWN, Warsaw, 1994 (ISBN 83-01-11255-7). xiii + 606 pp. Price \$118.50.

This is the second (revised) edition of this book which first appeared in 1976. The nineteen chapters are primarily concerned with polarography, stationary electrode voltammetry, chronoamperometry and

chronocoulometry, rotating disc voltammetry, and chronopotentiometry.

The first chapter briefly describes the principles of the electroanalytical techniques. Chapter two discusses the structure of the electrode double layer and is followed by a chapter describing working electrode materials and their shapes. The transport of electroactive species to electrodes is the subject of chapter four and this is followed by a chapter on rates of electrode processes. Chapter six consists of 132 pages which describe the equations relating limiting current, peak current, or transition times to concentration, and other factors, under conditions where the rate of mass transport controls the electrode process. A similar discussion on electrode processes controlled by the rate of charge transfer follows in the next, smaller section. Chapter eight considers the full course of the curves recorded by the different electroanalytical techniques and describes methods for determining the kinetics of electrode processes. The application of the techniques to studies of electrode processes is described in the next seven chapters and includes: electrode processes preceded (CE) or followed (EC) by chemical reactions; catalytic processes; chemical reactions of second and higher orders; ECE processes; reactions of metal complexes; reactions of adsorbed species. The relative merits of the electroanalytical techniques for quantitative analysis are very briefly discussed in the next chapter, which is a new addition. Cyclic methods involved in studies on diffusion processes and kinetic reactions are treated in the next two chapters. The final chapter is new and covers the voltammetric behaviour and properties of microelectrodes and redox polymer electrodes.

As with the earlier edition, this book can be highly recommended to post-graduate students and research workers in electrochemistry who wish to investigate the nature of electrode reactions. However, it would not be suitable for the novice who wishes to use electroanalytical techniques to overcome problems in quantitative chemical analysis.

John P. Hart

R.N. Reeve, *Environmental Analysis*, Wiley, Chichester, 1994 [ISBN 0-471-953134-X (cloth), 0-471-

93833-S (paper)]. xx + 263 pp. Price £19.50/US\$31.50 (paper), £45.00/US\$72.50 (cloth).

This is the 32nd book in the *Analytical Chemistry by Open Learning* (ACOL) series which is designed for training, continuing-education and updating of all technical staff concerned with Analytical Chemistry. It follows the same format as earlier ACOL publications in that it is a self-learning text with numerous self assessment questions (and answers) throughout. A welcome addition to earlier texts is a reasonably good index but a more informative running header would also facilitate random access to particular sections of the book.

The text is well written for the audience that it is trying to satisfy, with an appropriate level of technical detail throughout and reference to other books in the ACOL series. There are eight chapters that take the reader logically through the need for environmental analysis, the transport of pollutants in the environment, the analysis of major constituents and trace pollutants in water, the analysis of soils, atmospheric analysis of gases and particulates and ultra-trace analysis. The last chapter refers exclusively to the determination of organic species in environmental matrices by mass spectrometric methods and, although worthwhile, could have been expanded to include aspects of inorganic ultra-trace analysis.

The diagrams are generally simple and clear and there are several brief but helpful tables including, e.g., a typical pretreatment scheme for soils, a diagram of pesticide dispersal, a table of EC maximum admissible concentrations and guide levels for substances in water intended for human consumption and chromatograms of commercial oils. There is also a section on units of measurement which is essential given the unfortunate preponderance of parts per million and related terms in the environmental literature. Expansion of this section to cover interconversion between units and, e.g., calculations for the preparation of standards would be a welcome addition.

There is a lack of modern textbooks coherently covering Environmental Analysis, a subject that is increasingly being taught as part of various Chemistry and Environmental Science courses. For that reason alone this text warrants approval. The fact that it covers the subject in a clear and logical

manner at a level appropriate for technicians and introductory undergraduate courses justifies a stronger recommendation.

Paul J. Worsfold

M. Lederer, *Chromatography for Inorganic Chemistry*, Wiley, Chichester, 1994 (ISBN 0-471-94286-3, paperback edn.). 221 pp. Price £17.95.

The book is based on the lecture material and notes delivered to advanced students on a number of university courses. This has resulted in a rather interesting style with a strong historical context to the material, which is understandable knowing the long pioneering work of the author in this area. I quite like this approach, not only for the surprise at finding out the amount of work that has been already done, but also as a useful source of ideas for future work. As the title suggests, the book deals primarily with the use of chromatography for the study of inorganic processes. However, although not focussing on analytical aspects, there is plenty of material to interest the analytical scientist. Clearly, a book this size cannot go into great detail and therefore it gives key examples of separations in the main areas of paper, thin layer and column chromatography, covering all the major sorption mechanisms. Except for a small chapter on gas chromatography the book predominately deals with liquid phase separations focussing on aqueous media. There is a section on electrophoresis which is of topical interest considering the recent developments in capillary separations. All in all a very readable and interesting book which I strongly recommend for the personal bookshelf of both the student and practitioner of inorganic separations.

P. Jones

A. Benninghoven, Y. Nihei, R. Shimiza and H.W. Werner, *Secondary Ion Mass Spectrometry. SIMS IX*, Wiley, Chichester, 1994 (ISBN 0-471-94218-9). xxiv + 983 pp. Price £120.00.

As with reports of previous SIMS conferences, this is a collection of summaries of the majority of

papers (> 200) presented at the Ninth International Conference on SIMS in Yokohama, Japan, November 7–12, 1993. Plenary lectures are allocated up to 7 pages, other presentations 4 pages, all presented in camera-ready format. The major sections are: fundamentals, quantification, instrumentation, post ionization, CsX<sup>+</sup>-SIMS, TOF-SIMS, surface analysis, combined techniques, imaging and focused ion beam, and applications (depth profiling and semiconductors, organic and biological materials, insulators and metals, geological materials and environmental problems). There is no subject index.

Irving W. Wainer (Ed.), *Drug Stereochemistry. Analytical Methods and Pharmacology*, Marcel Dekker, New York, 2nd edn., 1993 (ISBN 0-8247-8819-2). xvi + 425 pp. Price US\$165.00.

The continuing rapid growth in interest in the stereochemistry of drug molecules, especially from the analytical point of view the development of means of separating and/or identifying stereo-isomers, ensures a warm welcome for the second edition of a much appreciated text. Eighteen authors, including the editor, contribute to the chapters, which are grouped into “introductory” material, separation and preparation of stereochemically pure drugs (including competitive binding, chromatographic and enzymatic procedures), pharmacokinetic and pharmacodynamic differences between stereo-isomers, and overview (a new series of short chapters on regulatory, industrial and clinical aspects). Much of the information is new or has been rewritten, so that the new edition will be a constant companion to all working with chiral drug molecules.

C.C. Leznoff and A.B.P. Lever (Eds.), *Phthalocyanines. Properties and Applications*, Vol. 3, VCH, New York, 1993 (ISBN 1-56081-638-4). xi + 303 pp. Price DM198.00/£81.00.

Phthalocyanines are of great interest to a variety of chemists, including those analytical chemists interested in sensors. In this volume there are five articles: redox chemistry of metallophthalocyanines in solution (Lever et al.), electrochromism and dis-

play devices (Nicholson), molecular electronic devices (Simic-Glavaski), Raman spectra (Smith and Rospendowski) and absorption and magnetic circular dichroism of ring-oxidized and ring-reduced complexes (Stillmann). The book seems to be produced from the authors' camera-ready copy, giving a variation in presentation which perhaps could be avoided with today's computer technology.

B.E. Conway, J. O'M Bockris and R.E. White (Eds.), *Modern Aspects of Electrochemistry*, No. 26, Plenum, New York, 1994 (ISBN 0-306-44608-1). xiii + 340 pp. Price US\$89.60.

This volume contains six articles of similar length on very diverse topics, viz., phase transitions at the double layer at electrodes, electrochemistry and electrochemical catalysis in microemulsions, water electrolyzers and fuel cells, electrogalvanising, electroanalytical methods for  $\text{Al}_2\text{O}_3$  in molten cryolite and

electrochemical aspects of the environmental cracking of metals.

*IARC Monographs on the Evaluation of Carcinogenic Risks to Humans*, Vol. 57, *Occupational exposures of hairdressers and barbers and personal use of hair colourants; some hair dyes, cosmetic colourants, industrial dyestuffs and aromatic amines*, IARC, Lyon, 1993 (ISBN 92-832-1257-6). 427 pp. Vol. 58, *Beryllium, cadmium, mercury and exposures in the glass manufacturing industry 1993* (ISBN 92-832-1258-4). 444 pp. Price for each 75.00 SFr/US\$67.50 (SFr52.50 in developing countries).

The two volumes continue the provision of documentary information about the activities and substances given in the titles with regard to the production and properties of the materials, descriptions of studies of carcinogenic effects, details of exposure and copious references.



ELSEVIER

Analytica Chimica Acta 300 (1995) 341–343

**ANALYTICA  
CHIMICA  
ACTA**

## Author Index

- Antonelli, M.L., see Salieri, G. 287
- Bakken, G.A.  
— and Kalivas, J.H.  
Assessing chromatographic peak purity using condition index and singular value evolving profiles 173
- Berzas Nevado, J.J.  
—, Lemus Gallego, J.M. and Buitrago Laguna, P.  
Spectrophotometric determination of catecholamines with metaperiodate by flow-injection analysis 293
- Bielejewska, A.  
—, Koźbiał, M., Nowakowski, R., Duszczyk, K. and Sybil-ska, D.  
Studies on the behaviour of  $\alpha$ -,  $\beta$ - and  $\gamma$ -cyclodextrins and some derivatives under reversed-phase liquid chromatographic conditions 201
- Bilitewski, U., see Günther, A. 117
- Bloemendal, H.  
— and Satijn, M.  
Simple reversible staining of proteins transferred from polyacrylamide gels onto nitrocellulose membranes 1
- Bock, U., see Kullick, T. 25
- Bøwadt, S., see De Boer, J. 155
- Brinkman, U.A.Th., see De Boer, J. 155
- Buitrago Laguna, P., see Berzas Nevado, J.J. 293
- Burns, D.T.  
— and Lewis, R.J.  
Analysis and characterisation of nitroglycerine based explosives by proton magnetic resonance spectrometry 221
- Cabredo Pinillos, S.  
—, Sanz Asensio, J. and Galbán Bernal, J.  
Simultaneous determination of arsenic, antimony and selenium by gas-phase diode array molecular absorption spectrometry, after preconcentration in a cryogenic trap 321
- Cao, X.-L.  
—, Hewitt, C.N. and Waterhouse, K.S.  
Study of the responses of a gas chromatography–reduction gas detector system to gaseous hydrocarbons under different conditions 193
- Chang, C.-M.  
— and Huang, H.-J.  
Impedance analysis of the transport of counter ions at polypyrrole–Nafion composite electrodes 15
- Chang, W.-B., see Ci, Y.-X. 273
- Chang, W.-B., see Tie, J.-K. 215
- Chen, G.  
—, Mei, E., Gu, W., Zeng, X. and Zeng, Y.  
Instrument for Hadamard transform three-dimensional fluorescence microscope image analysis 261
- Chen, L., see Wang, J. 127
- Chen, Q., see Wang, J. 111
- Ci, Y.-X.  
—, Qin, Y., Chang, W.-B. and Li, Y.-Z.  
Application of a mimetic enzyme for the enzyme immunoassay for  $\alpha$ -1-fetoprotein 273
- Ci, Y.-X., see Tie, J.-K. 215
- Cronan, C.S., see Plankey, B.J. 227
- Csapó, J.  
—, Csapó-Kiss, Z., Martin, T.G., Folestad, S., Orwar, O., Tivesten, A. and Némethy, S.  
Age estimation of old carpets based on cystine and cysteic acid content 313
- Csapó-Kiss, Z., see Csapó, J. 313
- Dao, K.L., see Fung, Y.S. 207
- Dao, Q.T., see De Boer, J. 155
- De Boer, J.  
—, Dao, Q.T., Wester, P.G., Bøwadt, S. and Brinkman, U.A.Th.  
Determination of mono-*ortho* substituted chlorobiphenyls by multidimensional gas chromatography and their contribution to TCDD equivalents 155
- De Luca Rebello Wagener, A., see Erthal Santelli, R. 149
- Deng, J., see Liu, H. 65
- De Robertis, A.  
—, Di Giacomo, P. and Foti, C.  
Ion-selective electrode measurements for the determination of formation constants of alkali and alkaline earth metals with low-molecular-weight ligands 45
- Di Giacomo, P., see De Robertis, A. 45
- Djurdjevic, P.T.  
—, Jelkic-Stankov, M. and Stankov, D.  
Fluorescence reaction and complexation equilibria between norfloxacin and aluminium(III) ion in chloride medium 253
- Duarte, A.C., see Gomes, M.T. 329
- Duszczyk, K., see Bielejewska, A. 201

- Ensafi, A.A., see Safavi, A. 307
- Erthal Santelli, R.  
—, Salgado Lopes, P.R., Leme Santelli, R.C. and De Luca Rebello Wagener, A.  
Turbidimetric determination of sulphate in waters employing flow injection and lead sulphate formation 149
- Folestad, S., see Csapó, J. 313
- Foti, C., see De Robertis, A. 45
- Fung, Y.S.  
— and Dao, K.L.  
Ion chromatographic determination of traces of some oxoanions with direct spectrophotometric detection 207
- Galbán Bernal, J., see Cabredo Pinillos, S. 321
- Gartske, C.  
— and Huber, C.O.  
Amperometric determination of oxidizable solutes in water with a solution exchange technique 53
- Ghourchian, H.O.  
— and Kamo, N.  
Latex piezoelectric immunoassay: effect of interfacial properties 99
- Gomes, M.T.  
—, Duarte, A.C. and Oliveira, J.P.  
Comparison of two methods for coating piezoelectric crystals 329
- Grases, F., see March, J.G. 269
- Gu, W., see Chen, G. 261
- Günther, A.  
— and Bilitewski, U.  
Characterisation of inhibitors of acetylcholinesterase by an automated amperometric flow-injection system 117
- Håkanson, H., see Shu, H.-C. 277
- Hewitt, C.N., see Cao, X.-L. 193
- Higson, S.P.J.  
— and Vadgama, P.M.  
Diamond like carbon coated films for enzyme electrodes; characterization of biocompatibility and substrate diffusion limiting properties 77  
— and Vadgama, P.M.  
Diamond like carbon films for enzyme electrodes: characterisation of novel overlying permselective barriers 85
- Huang, H.-J., see Chang, C.-M. 15
- Huang, X.  
—, Pot, J.J. and Kok, W.Th.  
Electrochemical characteristics of conductive carbon cement as matrix for chemically modified electrodes 5
- Huber, C.O., see Gartske, C. 53
- Iijima, S., see Mizutani, F. 59
- Ioannou, P.C.  
—, Lianidou, E.S. and Konstantianos, D.G.  
Simple, rapid and sensitive spectrofluorimetric determination of diflunisal in serum and urine based on its ternary complex with terbium and EDTA 237
- Jelickic-Stankov, M., see Djurdjevic, P.T. 253
- Jiang, Z.-L.  
—, Liao, L.-X. and Liu, M.-D.  
Catalytic method for the determination of traces of tungsten by linear scan voltammetry 107
- Kalivas, J.H., see Bakken, G.A. 173
- Kamo, N., see Ghourchian, H.O. 99
- Kok, W.Th., see Huang, X. 5
- Konstantianos, D.G., see Ioannou, P.C. 237
- Koźbiał, M., see Bielejewska, A. 201
- Kriz, D.  
— and Mosbach, K.  
Competitive amperometric morphine sensor based on an agarose immobilised molecularly imprinted polymer 71
- Kullick, T.  
—, Bock, U., Schubert, J., Scheper, T. and Schügerl, K.  
Application of enzyme-field effect transistor sensor arrays as detectors in a flow-injection analysis system for simultaneous monitoring of medium components. Part II. Monitoring of cultivation processes 25
- Lahuerta Zamora, L.  
— and Martínez Calatayud, J.  
Continuous flow-injection-atomic absorption spectrometric method for the determination of Ondansetron 143
- Lau, O.-W.  
— and Mok, C.-S.  
Indirect conductimetric detection of amino acids after liquid chromatographic separation 183
- Leme Santelli, R.C., see Erthal Santelli, R. 149
- Lemus Gallego, J.M., see Berzas Nevado, J.J. 293
- Lewis, R.J., see Burns, D.T. 221
- Li, S., see Raba, J. 299
- Li, Y.-Z., see Ci, Y.-X. 273
- Lianidou, E.S., see Ioannou, P.C. 237
- Liao, L.-X., see Jiang, Z.-L. 107
- Liu, H.  
— and Deng, J.  
Amperometric glucose sensor using tetrathiafulvalene in Nafion gel as electron shuttle 65
- Liu, M.-D., see Jiang, Z.-L. 107
- Lund, W., see Zernichow, L. 167
- Malinowska, E.  
— and Meyerhoff, M.E.  
Role of axial ligation on potentiometric response of Co(III) tetraphenylporphyrin-doped polymeric membranes to nitrite ions 33
- March, J.G.  
—, Villacampa, A.I. and Grases, F.  
Enzymatic-spectrophotometric determination of phytic acid with phytase from *Aspergillus ficuum* 269
- Martin, T.G., see Csapó, J. 313
- Martínez Calatayud, J., see Lahuerta Zamora, L. 143
- Mattiasson, B., see Shu, H.-C. 277
- Mei, E., see Chen, G. 261

- Meyerhoff, M.E., see Malinowska, E. 33
- Mizutani, F.  
—, Yabuki, S. and Iijima, S.  
Amperometric glucose-sensing electrode based on carbon paste containing poly(ethylene glycol)-modified glucose oxidase and cobalt octaethoxyphthalocyanine 59
- Mok, C.-S., see Lau, O.-W. 183
- Mosbach, K., see Kriz, D. 71
- Mottola, H.A., see Raba, J. 299
- Némethy, S., see Csapó, J. 313
- Neshkova, M.  
— and Pancheva, E.  
Chalcogenide based all-solid-state thin electroplated ion-selective membrane for Hg(II) flow-injection determinations 133
- Nowakowski, R., see Bielejewska, A. 201
- Ohkura, Y., see Saito, M. 243
- Oliveira, J.P., see Gomes, M.T. 329
- Orwar, O., see Csapó, J. 313
- Pancheva, E., see Neshkova, M. 133
- Patterson, H.H., see Plankey, B.J. 227
- Pedrero, M., see Wang, J. 111
- Pingarrón, J.M., see Wang, J. 111
- Plankey, B.J.  
—, Patterson, H.H. and Cronan, C.S.  
Kinetic analysis of aluminum complex formation with different soil fulvic acids 227
- Pot, J.J., see Huang, X. 5
- Qin, Y., see Ci, Y.-X. 273
- Raba, J.  
—, Li, S. and Mottola, H.A.  
Spectrophotometric cell comprising parallel rotating and stationary bioreactors: application to the determination of glucose in serum samples 299
- Safavi, A.  
— and Ensafi, A.A.  
Kinetic spectrophotometric determination of hydrazine 307
- Saito, M.  
—, Ushijima, T., Sasamoto, K., Yakata, K., Ohkura, Y. and Ueno, K.  
2-(5-Hydrazinocarbonyl-2-thienyl)-5,6-methylenedioxybenzofuran and 2-(5-hydrazinocarbonyl-2-furyl)-5,6-methylenedioxybenzofuran as novel fluorescence derivatisation reagents for carboxylic acids in liquid chromatography 243
- Salgado Lopes, P.R., see Erthal Santelli, R. 149
- Salieri, G.  
—, Vinci, G. and Antonelli, M.L.  
Microcalorimetric study of the enzymatic hydrolysis of starch: an  $\alpha$ -amylase catalyzed reaction 287
- Sanz Asensio, J., see Cabredo Pinillos, S. 321
- Sasamoto, K., see Saito, M. 243
- Satijn, M., see Bloemendal, H. 1
- Scheper, T., see Kullick, T. 25
- Schubert, J., see Kullick, T. 25
- Schügerl, K., see Kullick, T. 25
- Shu, H.-C.  
—, Håkanson, H. and Mattiasson, B.  
On-line monitoring of D-lactic acid during a fermentation process using immobilized D-lactate dehydrogenase in a sequential injection analysis system 277
- Stankov, D., see Djurdjevic, P.T. 253
- Sybiliska, D., see Bielejewska, A. 201
- Tie, J.-K.  
—, Chang, W.-B. and Ci, Y.-X.  
Peroxidatic activity of metalloporphyrin binding to serum albumin: enhancement effect of serum albumin on metalloporphyrin catalyzed luminol chemiluminescence reaction 215
- Tivesten, A., see Csapó, J. 313
- Ueno, K., see Saito, M. 243
- Ushijima, T., see Saito, M. 243
- Vadgama, P.M., see Higson, S.P.J. 77, 85
- Villacampa, A.I., see March, J.G. 269
- Vinci, G., see Salieri, G. 287
- Wang, J.  
—, Chen, L. and Wu, H.  
Gradient flow-injection amperometry based on induced retention by the detector coating 127  
—, Chen, Q., Pedrero, M. and Pingarrón, J.M.  
Screen-printed amperometric biosensors for glucose and alcohols based on ruthenium-dispersed carbon inks 111
- Waterhouse, K.S., see Cao, X.-L. 193
- Wester, P.G., see De Boer, J. 155
- Wu, H., see Wang, J. 127
- Yabuki, S., see Mizutani, F. 59
- Yakata, K., see Saito, M. 243
- Yu, P.  
— and Zhou, D.  
Thin-film biosensor for the measurement of glucose concentration in human serum and urine 91
- Zeng, X., see Chen, G. 261
- Zeng, Y., see Chen, G. 261
- Zernichow, L.  
— and Lund, W.  
Size exclusion chromatography of aluminium species in natural waters 167
- Zhou, D., see Yu, P. 91



**PUBLICATION SCHEDULE FOR 1995**

	O'94	N'94	D'94	J	F	M	A	M	J	J	A	S
Anal. Chim. Acta	296/2 296/3 297/1-2	297/3 298/1 298/2	298/3 299/1 299/2	299/3 300/1-3 301/1-3	302/1 302/2-3 303/1	303/2-3 304/1 304/2	304/3 305/1-2 305/3	306/1 306/2 306/3				
Vib. Spec.		8/1		8/2		8/3		9/1		9/2		9/3

**INFORMATION FOR AUTHORS**

**Detailed "Instructions to Authors"** for *Analytica Chimica Acta* was published in Volume 289, No. 3, pp. 381-384. Free reprints of the "Instructions to Authors" of *Analytica Chimica Acta* and *Vibrational Spectroscopy* are available from the Editors or from: Elsevier Science B.V., P.O. Box 330, 1000 AH Amsterdam, The Netherlands. Telefax: (+31-20) 4852 459.

**Manuscripts.** The language of the journal is English. English linguistic improvement is provided as part of the normal editorial processing. Authors should submit three copies of the manuscript in clear double-spaced typing on one side of the paper only. *Vibrational Spectroscopy* also accepts papers in English only.

**Rapid publication letters.** Letters are short papers that describe innovative research. Criteria for letters are novelty, quality, significance, urgency and brevity. Submission data: max. of 2 printed pages (incl. Figs., Tables, Abstr., Refs.); short abstract (e.g., 3 lines); no proofs will be sent to the authors; submission on floppy disc; no revision will be possible.

**Abstract.** All papers, reviews and letters begin with an Abstract (50-250 words) which should comprise a factual account of the contents of the paper, with emphasis on new information.

**Figures.** Figures should be suitable for direct reproduction and as rich in contrast as possible. One original (or sharp glossy print) and two photostat (or other) copies are required. Attention should be given to line thickness, lettering (which should be kept to a minimum) and spacing on axes of graphs, to ensure suitability for reduction in size on printing. Axes of a graph should be clearly labelled, along the axes, outside the graph itself.

All figures should be numbered with Arabic numerals, and require descriptive legends which should be typed on a separate sheet of paper. Simple straight-line graphs are not acceptable, because they can readily be described in the text by means of an equation or a sentence. Claims of linearity should be supported by regression data that include slope, intercept, standard deviations of the slope and intercept, standard error and the number of data points; correlation coefficients are optional.

Photographs should be glossy prints and be as rich in contrast as possible; colour photographs cannot be accepted. Line diagrams are generally preferred to photographs of equipment. Computer outputs for reproduction as figures must be good quality on blank paper, and should preferably be submitted as glossy prints.

**Nomenclature, abbreviations and symbols.** In general, the recommendations of IUPAC should be followed, and attention should be given to the recommendations of the Analytical Chemistry Division in the journal *Pure and Applied Chemistry* (see also *IUPAC Compendium of Analytical Nomenclature, Definitive Rules, 1987*).

**References.** The references should be collected at the end of the paper, numbered in the order of their appearance in the text (not alphabetically) and typed on a separate sheet.

**Reprints.** Fifty reprints will be supplied free of charge. Additional reprints (minimum 100) can be ordered. An order form containing price quotations will be sent to the authors together with the proofs of their article.

**Papers dealing with vibrational spectroscopy** should be sent to: Dr J.G. Grasselli, 150 Greentree Road, Chagrin Falls, OH 44022, U.S.A. Telefax: (+1-216) 2473360 (Americas, Canada, Australia and New Zealand) or Dr J.H. van der Maas, Department of Analytical Molecular Spectrometry, Faculty of Chemistry, University of Utrecht, P.O. Box 80083, 3508 TB Utrecht, The Netherlands. Telefax: (+31-30) 518219 (all other countries).

© 1995, ELSEVIER SCIENCE B.V. All rights reserved.

0003-2670/95/\$09.50

No part of this publication may be reproduced, stored in a retrieval system or transmitted in any form or by any means, electronic, mechanical, photocopying, recording or otherwise, without the prior written permission of the publisher, Elsevier Science B.V., Copyright and Permissions Dept., P.O. Box 521, 1000 AM Amsterdam, The Netherlands.

Upon acceptance of an article by the journal, the author(s) will be asked to transfer copyright of the article to the publisher. The transfer will ensure the widest possible dissemination of information.

**Special regulations for readers in the U.S.A.**-This journal has been registered with the Copyright Clearance Center, Inc. Consent is given for copying of articles for personal or internal use, or for the personal use of specific clients. This consent is given on the condition that the copier pays through the Center the per-copy fee stated in the code on the first page of each article for copying beyond that permitted by Sections 107 or 108 of the US Copyright Law. The appropriate fee should be forwarded with a copy of the first page of the article to the Copyright Clearance Center, Inc., 222 Rosewood Drive, Danvers, MA 01923, U.S.A. If no code appears in an article, the author has not given broad consent to copy and permission to copy must be obtained directly from the author. The fee indicated on the first page of an article in this issue will apply retroactively to all articles published in the journal, regardless of the year of publication. This consent does not extend to other kinds of copying, such as for general distribution, resale, advertising and promotion purposes, or for creating new collective works. Special written permission must be obtained from the publisher for such copying.

No responsibility is assumed by the publisher for any injury and/or damage to persons or property as a matter of products liability, negligence or otherwise, or from any use or operation of any methods, products, instructions or ideas contained in the material herein.

Although all advertising material is expected to conform to ethical (medical) standards, inclusion in this publication does not constitute a guarantee or endorsement of the quality or value of such product or of the claims made of it by its manufacturer.

Ⓢ The paper used in this publication meets the requirements of ANSI/NISO 239.48-1992 (Permanence of Paper).

PRINTED IN THE NETHERLANDS

# ANALYTICA CHIMICA ACTA

---

INTERNATIONAL JOURNAL DEALING WITH EVERY BRANCH OF  
ANALYTICAL CHEMISTRY

REVUE INTERNATIONALE CONSACRÉE A TOUS LES DOMAINES  
DE LA CHIMIE ANALYTIQUE

INTERNATIONALE ZEITSCHRIFT FÜR ALLE GEBIETE DER  
ANALYTISCHEN CHEMIE

*Editor*

PAUL-E. WENGER (*Geneva*)

*Assistant Editors*

G. CHARLOT, *Paris* - C. DUVAL, *Paris* - F. FEIGL, *Rio de Janeiro*  
L. V. FLAMACHE, *Bruzelles* - R. FLATT, *Lausanne* - J. GILLIS, *Gand*  
T. P. HILDITCH, *Liverpool* - M. JEAN, *Paris* - C. J. VAN NIEUWENBURG, *Delft*  
A. OKÁČ, *Brno* - H. A. J. PIETERS, *Geleen* - N. STRAFFORD, *Manchester*  
R. VIOLLIER, *Basel* - F. WOKES, *London*

Vol. 1

1947

ELSEVIER PUBLISHING COMPANY, INC.

NEW YORK



AMSTERDAM

---

*Anal. Chim. Acta*, Vol. 1, p. 1—445, 1947